

AD-A062 408

KAMAN AVIDYNE BURLINGTON MASS

F/G 1/3

MEASUREMENTS OF BLAST PRESSURES ON A RIGID 65 DEG SWEEPBACK WIN--ETC(U)

JAN 78 J R RUETENIK, R F SMILEY

DNA001-76-C-0106

UNCLASSIFIED

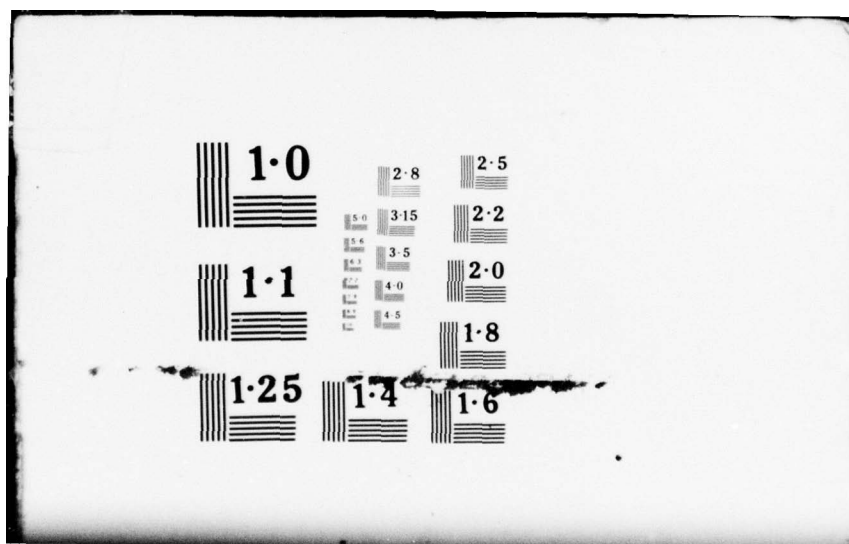
KA-TR-145

DNA-4504F

NL

1 OF 5
ADA
062408





(12) **LEVEL III**

AD-E300 387

(18) DNA 4504F

SBIE AD-E300 387

AD A062408

**MEASUREMENTS OF BLAST PRESSURES
ON A RIGID 65° SWEEPBACK WING AT
MACH 0.76 FROM ROCKET PROPELLED
SLED TESTS.**

Phase 2 Test Documentation.

Kaman AviDyne
83 Second Avenue
Burlington, Massachusetts 01803

(10) J. Ray / Rutenik
Robert F. / Smiley

(11) 24 January 1978

(12) 432 P.

(14) KA-TR-145

Final Report for Period January 1977 - December 1977

CONTRACT No/DNA 001-76-C-0106

(15) APPROVED FOR PUBLIC RELEASE;
DISTRIBUTION UNLIMITED.

(16) THIS WORK SPONSORED BY THE DEFENSE NUCLEAR AGENCY
UNDER RDT&E RMSS CODES B342076464 N99QAXAE51014
H2590D, B342077464 N99QAXAE50101 H2590D AND B342077464
N99QAXAE50101 H2590D.

62704 H
Prepared for
Director
DEFENSE NUCLEAR AGENCY
Washington, D. C. 20305

(17) E510
E5PL

DDC
RECEIVED
DEC 19 1978
B

78 11 08 013
194 970 mt

Destroy this report when it is no longer
needed. Do not return to sender.

PLEASE NOTIFY THE DEFENSE NUCLEAR AGENCY,
ATTN: TISI, WASHINGTON, D.C. 20305, IF
YOUR ADDRESS IS INCORRECT, IF YOU WISH TO
BE DELETED FROM THE DISTRIBUTION LIST, OR
IF THE ADDRESSEE IS NO LONGER EMPLOYED BY
YOUR ORGANIZATION.



UNCLASSIFIED

SECURITY CLASSIFICATION OF THIS PAGE (When Data Entered)

REPORT DOCUMENTATION PAGE		READ INSTRUCTIONS BEFORE COMPLETING FORM
1. REPORT NUMBER DNA 4504F ✓	2. GOVT ACCESSION NO.	3. RECIPIENT'S CATALOG NUMBER
4. TITLE (and Subtitle) MEASUREMENTS OF BLAST PRESSURES ON A RIGID 65° SWEEPBACK WING AT MACH 0.76 FROM ROCKET PROPELLED SLED TESTS Phase 2 Test Documentation A053468 / A062365		5. TYPE OF REPORT & PERIOD COVERED Final Report for Period January 1977—December 1977
7. AUTHOR(s) J. Ray Ruetenik Robert F. Smiley		6. PERFORMING ORG. REPORT NUMBER KA TR-145
9. PERFORMING ORGANIZATION NAME AND ADDRESS Kaman Avidyne 83 Second Avenue Burlington, Massachusetts 01803		8. CONTRACT OR GRANT NUMBER(s) DNA 001-76-C-0106 ✓
11. CONTROLLING OFFICE NAME AND ADDRESS Director Defense Nuclear Agency Washington, D.C. 20305		10. PROGRAM ELEMENT, PROJECT, TASK AREA & WORK UNIT NUMBERS NWED Subtasks N99QAXAE510-14 and N99QAXAE501-01
14. MONITORING AGENCY NAME & ADDRESS (if different from Controlling Office)		12. REPORT DATE 24 January 1978
		13. NUMBER OF PAGES 434
		15. SECURITY CLASS (of this report) UNCLASSIFIED
		15a. DECLASSIFICATION DOWNGRADING SCHEDULE
16. DISTRIBUTION STATEMENT (of this Report) Approved for public release; distribution unlimited.		
17. DISTRIBUTION STATEMENT (of the abstract entered in Block 20, if different from Report)		
18. SUPPLEMENTARY NOTES This work sponsored by the Defense Nuclear Agency under RDT&E RMSS Codes B342076464 N99QAXAE51014 H2590D, B342077464 N99QAXAE50101 H2590D and B342077464 N99QAXAE50101 H2590D.		
19. KEY WORDS (Continue on reverse side if necessary and identify by block number) Blast Explosives Subsonic Shock Aircraft Sled Test Wing Pressure Vortex Experimental Test Sweptback		
20. ABSTRACT (Continue on reverse side if necessary and identify by block number) Interaction of a blast wave with a highly sweptback wing model was measured in a series of two sled tests performed on the 50,788-foot tract at Holloman Air Force Base in June and August of 1977. These two tests were a continuation of the program of three tests carried out during the summer of 1976. The sled, traveling at Mach 0.76, was intercepted successively by blast waves produced from the sequential detonation of three charges of TNT.		

DD FORM 1 JAN 73 1473

EDITION OF 1 NOV 65 IS OBSOLETE

UNCLASSIFIED

SECURITY CLASSIFICATION OF THIS PAGE (When Data Entered)

UNCLASSIFIED

SECURITY CLASSIFICATION OF THIS PAGE(When Data Entered)

20. ABSTRACT (Continued)

The model consisted of a sting-mounted wing and fuselage combination. Wing properties were: 46.80-in. span, 18.95-in. mean chord, 2.47 aspect ratio, 0.29 taper ratio, 67 deg. leading edge sweepback, 64.8 deg. quarter-chord sweepback, and a 64A012 wing section. Blast induced loadings were measured at 20 locations on the wing for blast intercept overpressures of about 4 psi for blast intercept angles of about 50, 90 and 135 degrees from head-on.

In the first test blast intercepts from bursts 45 degrees out of the plane of airplane symmetry were simulated by mounting the model at a roll angle of 45 degrees. In the second test a 10,000 pound charge was employed for one burst for studying the effect of blast yield.

This report describes the tests and presents the reduced test data.

UNCLASSIFIED

SECURITY CLASSIFICATION OF THIS PAGE(When Data Entered)

PREFACE

This work was performed by the Avidyne Division of the Kaman Sciences Corporation for the Defense Nuclear Agency under Contract DNA 001-76-C-0106. MAJ David W. Garrison of the DNA Shock Physics Directorate served as technical monitor to July 31, 1977, and CAPT Michael Rafferty from August 1, 1977, through the remainder of the program.

Dr. J. Ray Ruetenik of Kaman Avidyne was the project leader under Dr. Norman P. Hobbs, Technical Director of KA. Mr. Robert F. Smiley performed engineering functions.

Appreciation is expressed to MAJ Garrison and CAPT Rafferty for their continuing interest and significant support of this program. Appreciation is also expressed to the Holloman Air Force Base Test Directorate personnel, particularly Mr. Floyd D. Amburgey of Track Operations for coordination of the test activities, Mr. Daniel J. Krupovage of Track Engineering for mechanical engineering functions and Mr. Joe Haden of Track Instrumentation for electronic and sled-instrumentation support. Appreciation is also expressed to Army Ballistics Research Laboratories personnel headed by Mr. George Teel for providing the blastline measurements.

ACCESSION for		
NTIS	Write Section	<input checked="" type="checkbox"/>
DDC	Buff Section	<input type="checkbox"/>
UNANNOUNCED		<input type="checkbox"/>
JUSTIFICATION		
BY		
DISTRIBUTION/AVAILABILITY CODES		
Dist.	AVAIL.	and/or SPECIAL
A		

CONVERSION FACTORS FOR U.S. CUSTOMARY
TO METRIC (SI) UNITS OF MEASUREMENT.

To Convert From	To	Multiply By
angstrom	meters (m)	1.000 000 X E -10
atmosphere (normal)	kilo pascal (kPa)	1.013 25 X E +2
bar	kilo pascal (kPa)	1.000 000 X E +2
barn	meter ² (m ²)	1.000 000 X E -28
British thermal unit (thermochemical)	joule (J)	1.054 350 X E +3
calorie (thermochemical)	joule (J)	4.184 000
cal (thermochemical)/cm ²	mega joule/m ² (MJ/m ²)	4.184 000 X E -2
curie	giga becquerel (GBq)*	3.700 000 X E +1
degree (angle)	radian (rad)	1.745 329 X E -2
degree Fahrenheit	degree kelvin (K)	$T_K = (T_F + 459.67)/1.8$
electron volt	joule (J)	1.602 19 X E -19
erg	joule (J)	1.000 000 X E -7
erg/second	watt (W)	1.000 000 X E -7
foot	meter (m)	3.048 000 X E -1
foot-pound-force	joule (J)	1.355 818
gallon (U.S. liquid)	meter ³ (m ³)	3.785 412 X E -3
inch	meter (m)	2.540 000 X E -2
jerk	joule (J)	1.000 000 X E +9
joule/kilogram (J/kg) (radiation dose absorbed)	Gray (Gy)**	1.000 000
kilotons	terajoules	4.183
kkip (1000 lbf)	newton (N)	4.448 222 X E +3
kip/inch ² (ksi)	kilo pascal (kPa)	6.894 757 X E +3
ktap	newton-second/m ² (N-s/m ²)	1.000 000 X E +2
micron	meter (m)	1.000 000 X E -6
mil	meter (m)	2.540 000 X E -5
mile (international)	meter (m)	1.609 344 X E +3
ounce	kilogram (kg)	2.834 952 X E -2
pound-force (lbf avoirdupois)	newton (N)	4.448 222
pound-force inch	newton-meter (N·m)	1.129 848 X E -1
pound-force/inch	newton/meter (N/m)	1.751 268 X E +2
pound-force/foot ²	kilo pascal (kPa)	4.788 026 X E -2
pound-force/inch ² (psi)	kilo pascal (kPa)	6.894 757
pound-mass (lbm avoirdupois)	kilogram (kg)	4.535 924 X E -1
pound-mass-foot ² (moment of inertia)	kilogram-meter ² (kg·m ²)	4.214 011 X E -2
pound-mass/foot ³	kilogram/meter ³ (kg/m ³)	1.601 846 X E +1
rad (radiation dose absorbed)	Gray (Gy)**	1.000 000 X E -2
roentgen	coulomb/kilogram (C/kg)	2.579 760 X E -4
shake	second (s)	1.000 000 X E -8
slug	kilogram (kg)	1.459 390 X E +1
torr (mm Hg, 0° C)	kilo pascal (kPa)	1.333 22 X E -1

*The becquerel (Bq) is the SI unit of radioactivity; 1 Bq = 1 event/s.

**The Gray (Gy) is the SI unit of absorbed radiation.

A more complete listing of conversions may be found in "Metric Practice Guide E 380-74," American Society for Testing and Materials.

TABLE OF CONTENTS

	<u>Page</u>
1. INTRODUCTION	9
2. TEST EQUIPMENT	11
2.1 HAFB Sled Track	11
2.2 General Test Arrangement.	11
2.3 Test Area	11
2.4 Sled.	15
2.5 Wing Model.	19
2.6 Explosives.	22
2.7 Blast-Line Pressure Measurements.	29
2.8 Wing Pressure Measurements.	29
2.9 Sled Velocity and Position Measurements	29
2.10 High Speed Photography.	29
2.11 Telemetry	34
2.12 Model Strength and Stiffness Tests.	34
2.12.1 Strength.	34
2.12.2 Deflection.	36
2.12.3 Frequencies	36
3. TEST SERIES.	39
3.1 Intercept Conditions.	39
3.2 Run 9B-A4	44
3.3 Run 9B-A5	44
4. TEST DATA.	47
4.1 A/D Data Processing	47
4.2 Data Presentation	47
4.3 Accuracy of Data.	49
5. BLAST VARIABLES AT SLED.	51
6. DISCUSSION	73
6.1 Motion of Tufts	73
7. CONCLUDING REMARKS	85
REFERENCES.	87
APPENDIX A Pressure and Acceleration Time Histories	89

78³ 11 08 013

LIST OF ILLUSTRATIONS

<u>Figure</u>		<u>Page</u>
1	Schematic of typical HAFB blast test arrangement . . .	10
2	Photograph of blast area for Run 9B-A5	12
3	View of blast-line probes for first intercept.	13
4	Oblique view of model in rolled position on sled . . .	16
5	Front view of unrolled model on sled	17
6	Front view of 45° rolled model on sled	18
7	Closeup view of pressure transducers on the sled . . .	20
8	Sketch of wing and fuselage model showing pressure measurement stations	23
9	Typical 1,000 pound charge	25
10	10,000 Pound Charge.	26
11	Firing box and burial hole	27
12	Control units for firing sets.	28
13	Sled velocity profiles	30
14	Intercept 1 area with grid board	32
15	Developmental tuft layout on model lower wing half, Run 9B-A4.	33
16	Sled telemetry system.	35
17	Blast flow conditions at the sled for Run 9B-A4, Intercept 1	55
18	Blast flow conditions at the sled for Run 9B-A4, Intercept 2	58
19	Blast flow conditions at the sled for Run 9B-A4, Intercept 3	61
20	Blast flow conditions at the sled for Run 9B-A5, Intercept 1	64
21	Blast flow conditions at the sled for Run 9B-A5, Intercept 2	67

LIST OF ILLUSTRATIONS (CONT'D)

<u>Figure</u>		<u>Page</u>
22	Blast flow conditions at the sled for Run 9B-A5, Intercept 3	70
23	Photographs of tufts on lower wing at second intercept of Run 9B-A5	74
24	Image motion camera photograph of tufts on lower wing 15 feet north of second intercept of Run 9B-A5.	83
25	Blast-Line overpressures, Run 9B-A4, Intercept 1 . .	90
26	Differential wing pressures, Run 9B-A4, Intercept 1.	94
27	Blastward and leeward wing pressures, Run 9B-A4, Intercept 1	130
28	Total Pressure at model, Run 9B-A4, Intercept 1. . .	136
29	Total Pressure at sled, Run 9B-A4, Intercept 1 . . .	138
30	Static pressure 1 at sled, Run 9B-A4, Intercept 1. .	140
31	Static pressure 2 at sled, Run 9B-A4, Intercept 1. .	142
32	Wing Acceleration, Run 9B-A4, Intercept 1.	144
33	Blast-line overpressures, Run 9B-A4, Intercept 2 . .	146
34	Differential wing pressures, Run 9B-A4, Intercept 2.	150
35	Blastward and leeward wing pressures, Run 9B-A4, Intercept 2	186
36	Total pressure at model, Run 9B-A4, Intercept 2. . .	192
37	Total pressure at sled, Run 9B-A4, Intercept 2 . . .	194
38	Static pressure 1 at sled, Run 9B-A4, Intercept 2. .	196
39	Static pressure 2 at sled, Run 9B-A4, Intercept 2. .	198
40	Wing acceleration, Run 9B-A4, Intercept 2	200
41	Blast-line overpressures, Run 9B-A4, Intercept 3 . .	202
42	Differential wing pressures, Run 9B-A4, Intercept 3.	204

LIST OF ILLUSTRATIONS (CONT'D)

<u>Figure</u>	<u>Page</u>
43	Blastward and leeward wing pressures, Run 9B-A4, Intercept 3 240
44	Total pressure at model, Run 9B-A4, Intercept 3. . . . 246
45	Total pressure at sled, Run 9B-A4, Intercept 3 248
46	Static pressure 1 at sled, Run 9B-A4, Intercept 3. . . 250
47	Static pressure 2 at sled, Run 9B-A4, Intercept 3. . . 252
48	Wing acceleration, Run 9B-A4, Intercept 3. 254
49	Blast-line overpressures, Run 9B-A5, Intercept 1 . . . 256
50	Differential wing pressures, Run 9B-A5, Intercept 1. . 260
51	Blastward and leeward wing pressures, Run 9B-A5, Intercept 1 296
52	Total pressure at model, Run 9B-A5, Intercept 1. . . . 304
53	Total pressure at sled, Run 9B-A5, Intercept 1 306
54	Static pressure 1 at sled, Run 9B-A5, Intercept 1. . . 308
55	Static pressure 2 at Sled, Run 9B-A5, Intercept 2. . . 310
56	Wing acceleration, Run 9B-A5, Intercept 1. 312
57	Blast-line overpressures, Run 9B-A5, Intercept 2 . . . 314
58	Differential wing pressures, Run 9B-A5, Intercept 2. . 318
59	Blastward and leeward wing pressures, Run 9B-A5, Intercept 2 354
60	Total pressure at model, Run 9B-A5, Intercept 2. . . . 362
61	Total pressure at sled, Run 9B-A5, Intercept 2 364
62	Static pressure 1 at sled, Run 9B-A5, Intercept 2. . . 366
63	Static pressure 2 at sled, Run 9B-A5, Intercept 2. . . 368

LIST OF ILLUSTRATIONS (CONCL'D)

<u>Figure</u>		<u>Page</u>
64	Wing acceleration, Run 9B-A5, Intercept 2	370
65	Blast-line overpressures, Run 9B-A5, Intercept 3. . .	372
66	Differential wing pressures, Run 9B-A5, Intercept 3 .	376
67	Blastward and leeward wing pressures, Run 9B-A5, Intercept 3.	412
68	Total pressure at model, Run 9B-A5, Intercept 3 . . .	420
69	Total pressure at sled, Run 9B-A5, Intercept 3. . . .	422
70	Static pressure 1 at sled, Run 9B-A5, Intercept 3 . .	424
71	Static pressure 2 at sled, Run 9B-A5, Intercept 3 . .	426
72	Wing acceleration, Run 9B-A5, Intercept 3	428

LIST OF TABLES

<u>Table</u>		<u>Page</u>
1	Blast-line stations for runs	14
2	Basic model data	21
3	Distribution of airloads measurement stations over instrumented (upper) wing	24
4	Sled, support and model modes.	37
5	General sled test conditions	40
6	Blast intercept conditions	41
7	Pressure measurements on the wing.	42
8	Comparison of intercept location estimates	43
9	Index of test data figures	48

SECTION 1

INTRODUCTION

A series of blast tests had been conducted at the 50,788-ft high speed sled track at the Holloman Air Force Base (HAFB) during the summer of 1976, described in Reference 1 and illustrated in Figure 1, for measuring blast-induced wing loadings on a high-sweepback wing at high subsonic speed. The objective of the tests reported here, which were conducted during June and August of 1977, was to examine the effect of other blast encounters on the wing loadings.

A total of six bursts were intercepted in the two sled runs. In the first run the burst centers were 45 degrees out of the plane of symmetry of the wing model to provide airloads data for a non-symmetrical blast intercept. In the second run, which involved symmetrical intercepts, a 10,000-pound charge of TNT was employed for the second burst, in place of the 1,000-pound TNT charges used for the other bursts, in order to examine the effect of charge yield on the wing loading.

A new connector was built for the model sting on the sled to provide for a selectable model roll orientation to achieve a selectable out-of-plane burst intercept angle. Measures were taken for the charge firing systems to ensure that the electromagnetic field radiated from each burst would not induce premature firing of any other charge. These are reported here.

Both sled runs were made at a nominal preintercept Mach number of 0.76 and Reynolds number based on mean chord of 7.0 million. The test model had a 46.80-in wing span and 18.95-in mean chord. Six separate TNT charges were detonated, five of 1,000 pounds and one of 10,000 pounds. Test results are reported for six blastwave intercepts, nominally 50, 90 and 135 degrees from head-on, at blast overpressures of about four psi.

The test techniques developed and used in the three test runs are described in Section 2 and Reference 1. The test conditions, test results and data analysis procedures are presented in Sections 3, 4 and 5, respectively. Test results on tuft measurements are discussed in Section 6 and concluding remarks are presented in Section 7.

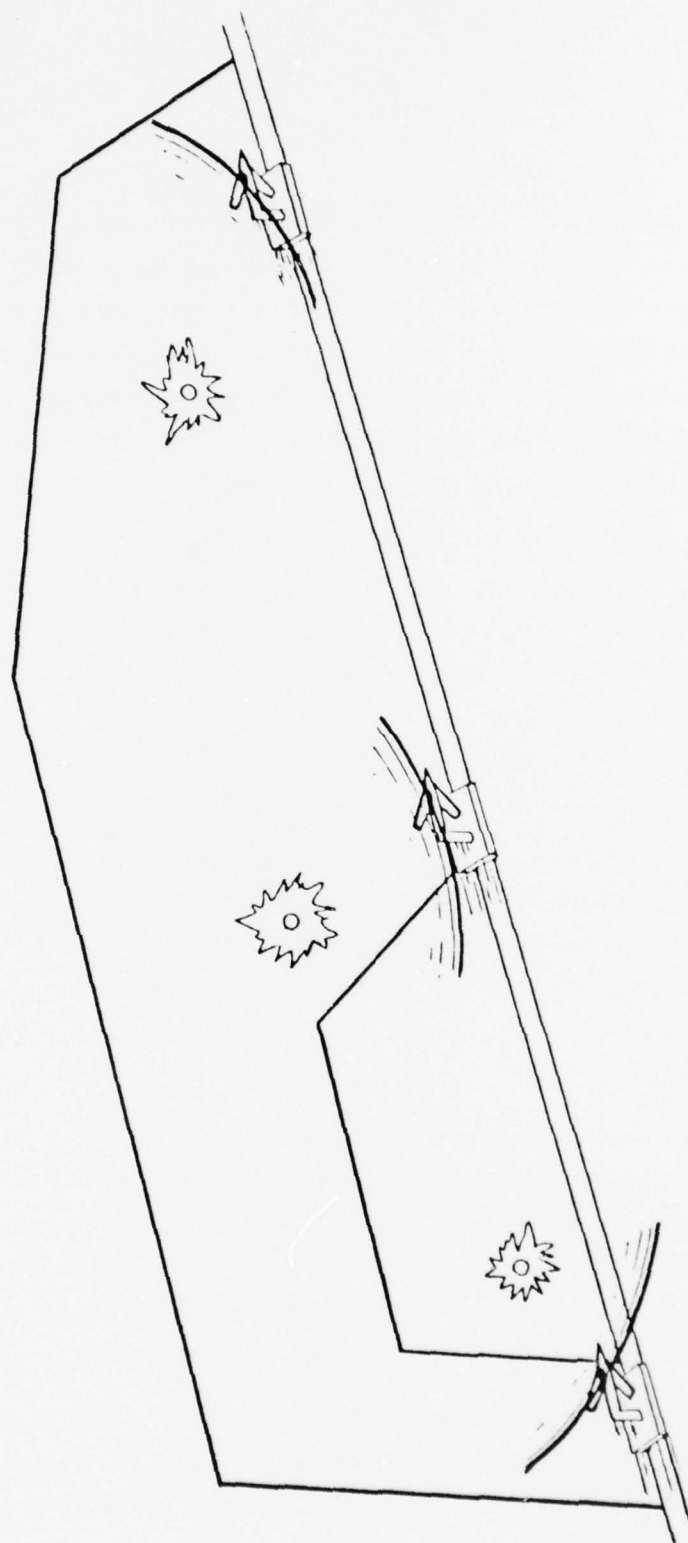


Figure 1. Schematic of typical HAFB blast test arrangement.

SECTION 2

TEST EQUIPMENT

2.1 HAFB SLED TRACK

The 50,788-ft high-speed track and associated general test equipment at HAFB are described generally in Reference 2. In the test procedure described here, the dual-rail sled employed ran from south to north. The sled was launched near the 10,500-ft station, entered the blast test area extending from about the 12,500-ft station to the 13,850-ft station, and then coasted out to about the 40,000-ft station.

2.2 GENERAL TEST ARRANGEMENT

A sketch of the overall test arrangement is shown in Figure 1. The moving sled enters the field of view from the left and progressively encounters the blast waves from the detonation of three separate TNT charges generally centered about 6 feet above ground level at various locations on the west side of the track, except for one charge in the second run which was stacked at the ground level.

2.3 TEST AREA

The ground surface in the test area is described in detail in Reference 1. A photograph of this area with explosive charges in place for Run 9B-A5 is given in Figure 2. The explosive charge locations for the three intercepts are indicated as 1, 2 and 3 in this figure. The sled moves from the upper left (south) to the lower right (north) in this view so the blast area is to the left of the sled. The test area extends 1250 feet along the track and 320 feet to the west from the track.

Four blast-line pressure probes were used to define the free-air blast profile for each of the three intercepts for each run, as can be seen for the first intercept location in Figure 3. The locations of the vertical struts supporting these pressures transducers, designated 1 to 12, in terms of track station (distance parallel to track) are given in Table 1. All struts were located laterally (perpendicular to track) 7.5 feet west of the track centerline. All transducers were

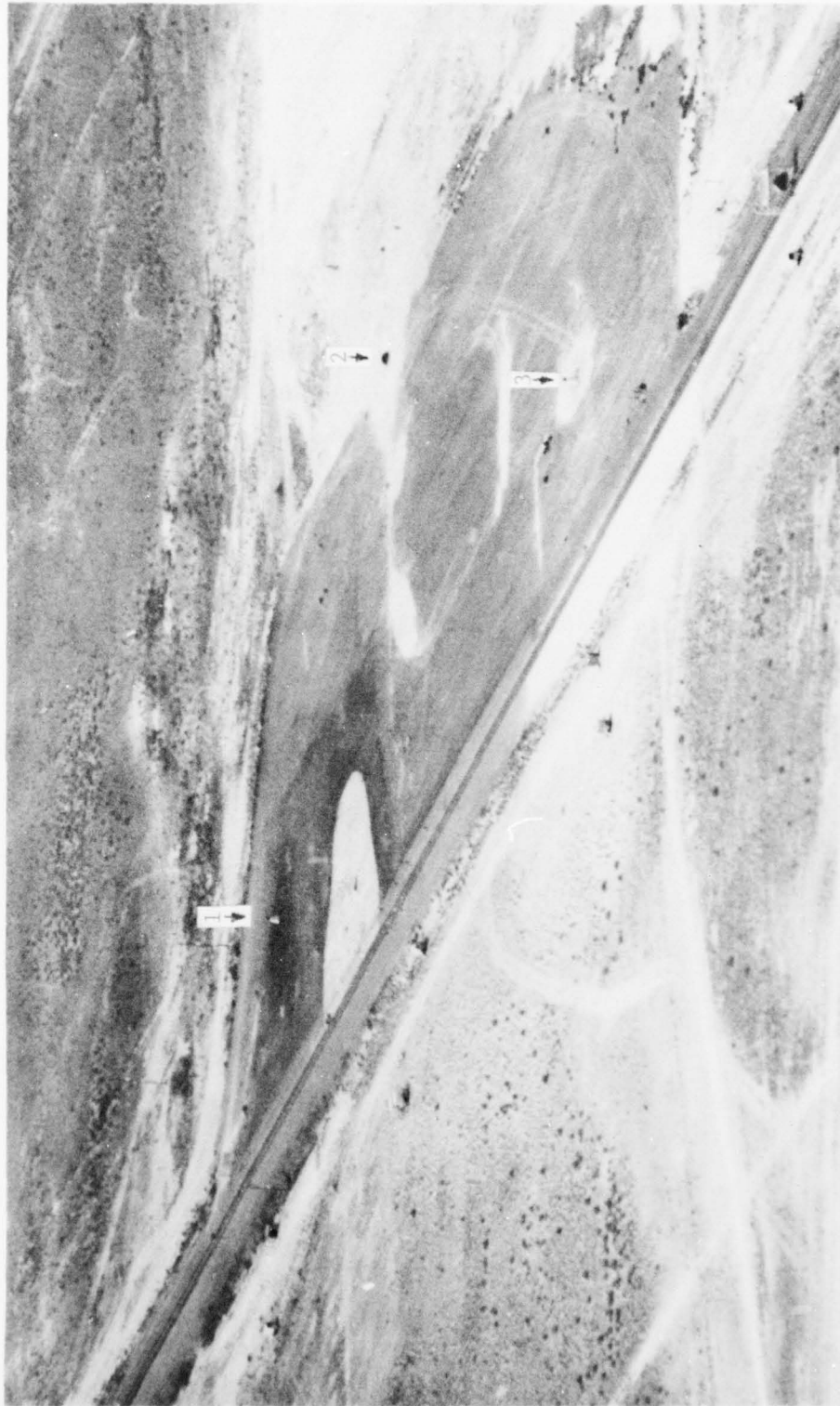


Figure 2. Photograph of blast area for Run 9B-A5.



Figure 3. View of blast-line probes for first intercept.

Table 1

BLAST-LINE STATIONS FOR RUNS

(Location of Blast-Line Probe Mount)

Intercept Station No.	TRACK STATION*			
	RUN 4		RUN 5	
	DIP	Mounts	DIP	Mounts
1	12744	12746.9 12752.6 12758.9 12772.0	12744	12746.9 12752.6 12758.9 12772.0
2	13180	13171.9 13187.9 13202.7 13225.7	13153	13133.9 13171.9 13202.7 13251.1
3	13730	13713.1 13738.3 13768.1 13813.5	13730	13713.1 13738.3 13768.1 13813.5

DIP - Desired Intercept Point

*All mount poles are located 4 feet west of west rail (7.5 feet west of track centerline).

located approximately 18 inches closer to the corresponding charge location than the supporting strut.

Screen boxes located adjacent to the west rail at designated locations were used to trigger the explosive firings and breakwires placed across the west rail at specified locations were used to provide a common time reference signal for checking time correlation of different recorders. They served as links in electrical circuits, which were either broken by the leading edge of the forward left slipper of the sled (for breakwires) or connected by knife-edge pairs mounted at the rear of the sled tied together electrically (for screen boxes). The trigger screen boxes were located between about 92 and 176 feet ahead of the desired intercept point (DIP) and the time reference breakwires were located between 9 and 21 feet ahead of the DIP.

Several grid boards with diagonal stripes were placed in the blast area to serve as backgrounds for photographic studies of sled and blast wave motions.

2.4 SLED

A modified HAFB dual rail rocket sled, designated as FDN 6326, was employed in these tests.

Photographs and descriptions of the sled and associated propulsion rocket motors are presented in Reference 1 and in Figure 4. The top surface of the sled is basically a thick blunt flat plate whose front and blastward edges are faired to minimize sled drag and distortion of the blast wave striking the model due to interference with the sides and lower parts of the sled structure.

The test model is mounted on the front of the sled by the vertical strut and horizontal sting attachment seen in Figure 4. The attachment of the vertical strut to the horizontal sting is by a bolted connection whereby the model can be set at various rotation angles (roll angles) about the sting axis. (This bolted connection replaced the rigid zero roll connection used in Reference 1). Figure 5 and 6 present front views

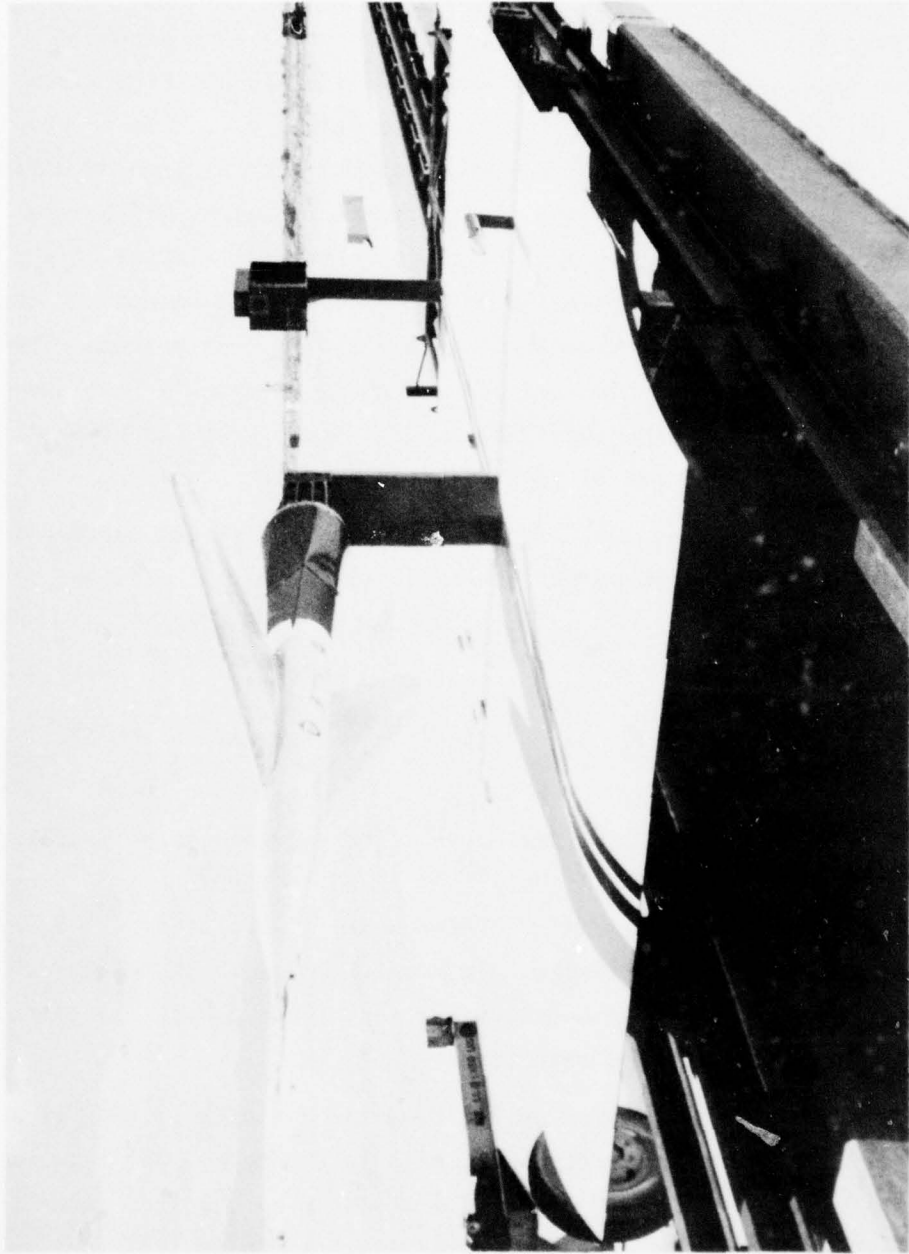


Figure 4. Oblique view of model in rolled position on sled.

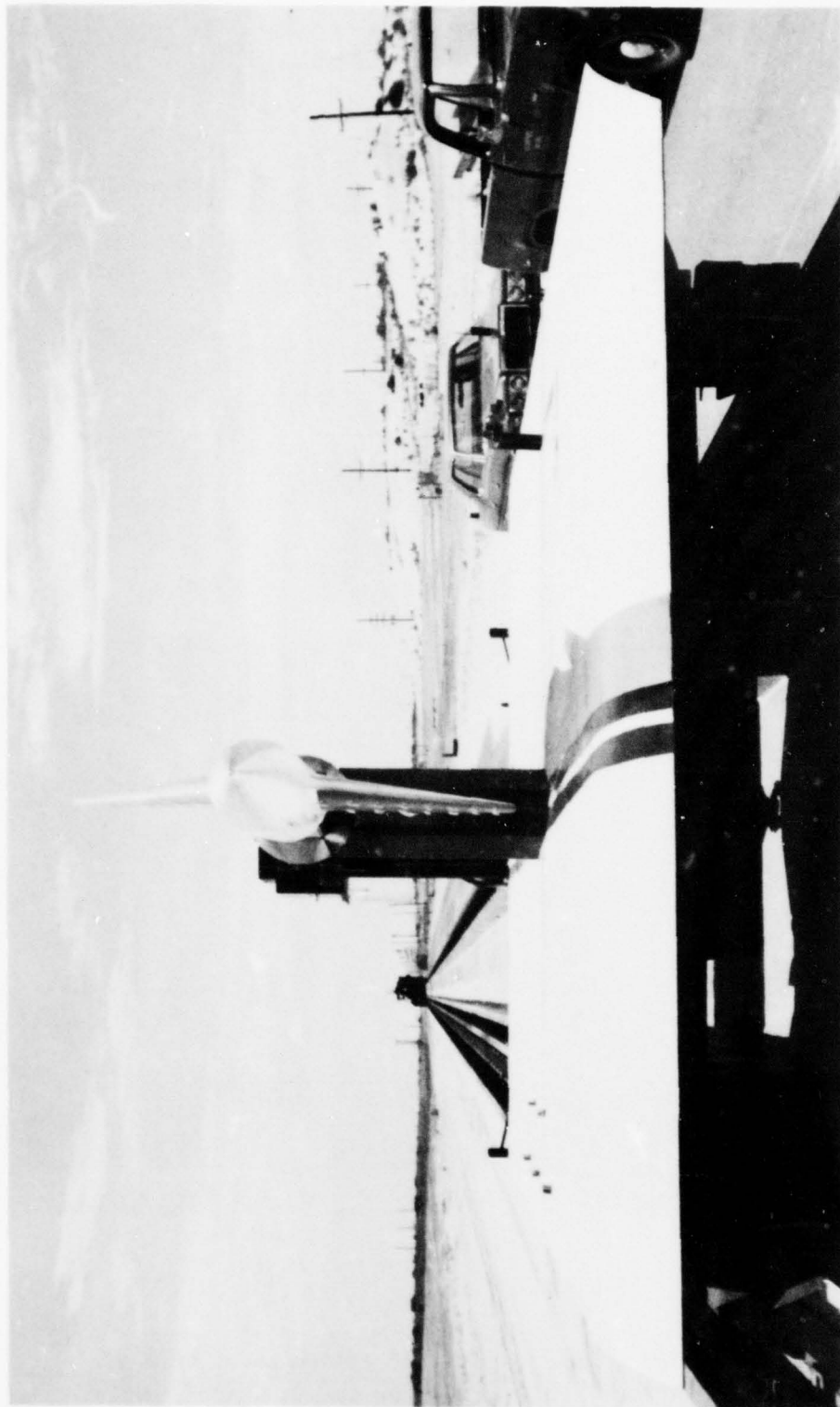


Figure 5. Front view of unrolled model on sled.

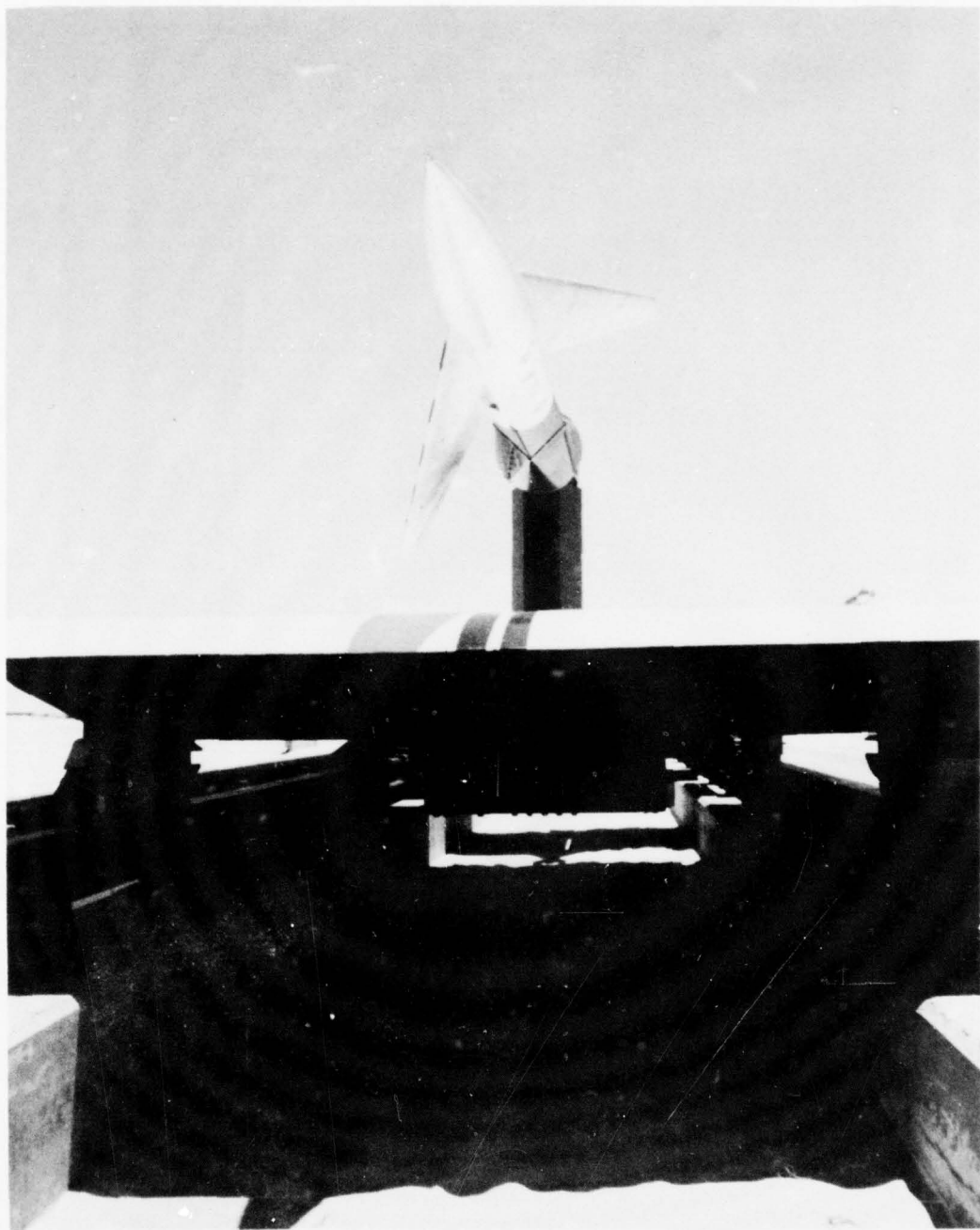


Figure 6. Front view of 45° rolled model on sled.

of the model on the sled in an unrolled (Run 9B-A5) and a 45° rolled (Run 9B-A4) position, respectively. The pitch angle of the model, for initial angle of attack, is achieved by a combination of wedge shimming between connector faces and rotation of the strut.

A pair of cameras aimed at the upper wing half are mounted on the sled bed in a box behind the model, as indicated in Figure 4.

The propulsion systems used to drive and maintain the sled at nearly constant speed are described in Reference 1. For all test intercepts, the sled speed after blast intercept did not vary more than about 3 fps from the intercept speed during the next 100 feet of travel, which is about the maximum distance of interest.

A pitot probe and two pressure transducers were located together on the blastward side of the upper surface of the sled, as indicated in Figures 4 and 7. The pitot probe was located above the surface of the sled about 6 inches. The two pressure transducers were mounted flush with the upper surface of the sled about 10 inches ahead of the pitot probe. These transducers were installed to provide a check on the accuracy of the blast pressures as obtained from the blast-line probes.

2.5 WING MODEL

The test model consisted of the swept wing model of Reference 1 with a nose and partial fuselage section, sting-mounted to the sled as shown in Figure 4. The model wing planform, fuselage and nose sections were constructed to simulate the basic features of the B-1 aircraft in its most sweptback position at 1/20 of full scale dimensions. Basic model data are listed in Table 2. Wing leading and trailing edge sweepback angles were 67° and 55° , respectively. The wing cross section (stream-wise) was made up as a 64A012 symmetrical airfoil.

The wing was mounted at angles of attack of 3.5° and 3.2° , for Runs 9B-A4 and 9B-A5, respectively, in a direction such that the pre-blast steady-state lift force was in the same direction as the blast-induced force. For Run 9B-A4 the model was rolled 45° , with the upper tip rolled toward the burst point.

The wing construction is described in Reference 1.

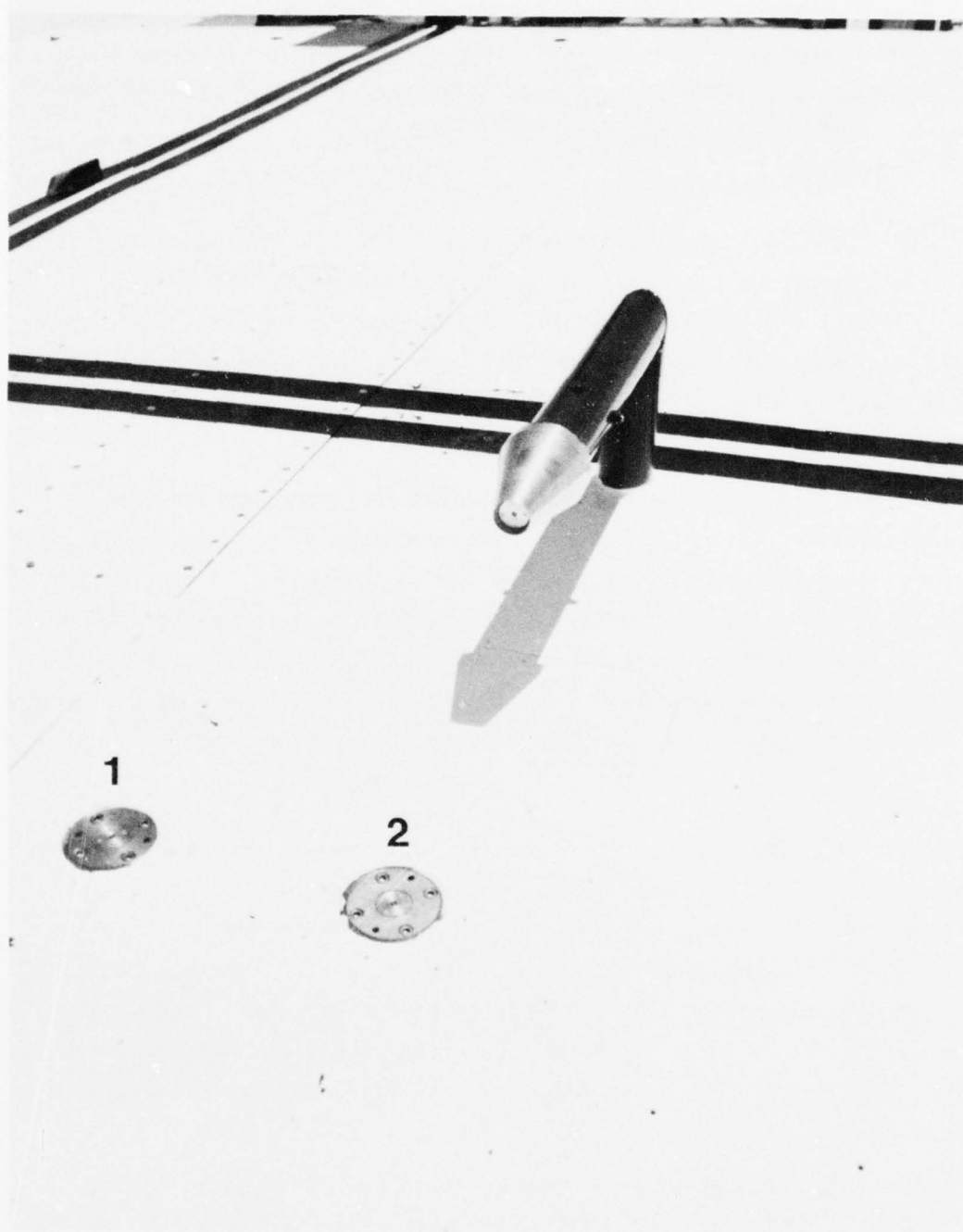


Figure 7. Closeup view of pressure transducers on the sled.

Table 2

BASIC MODEL DATA

Wing Span, b	46.80 in.
Wing Planform Area, S	6.16 ft ²
Aspect Ratio	2.47
Taper Ratio	0.29
Leading-Edge Sweepback	67.0 deg.
Quarter-Chord Sweepback	64.8 deg.
Trailing-Edge Sweepback	55.0 deg.
Mean Chord (S/b)	18.95 in.
Root Chord (at model centerline)	30.60 in.
Wing Section (streamwise)	64A012
Thickness Ratio (streamwise)	12%
Pressure Stations (Two transducers per station)	20
Fuselage Diameter	8 in.

Holes for twenty wing transducer locations were located as indicated in Figure 8 and Table 3. Two transducers were installed for each location to measure pressure differences between wing blastward and leeward surfaces. Also provision was made for one pressure transducer being located at the nose-tip of the fuselage for measurement of model total pressure at the sled. An accelerometer was mounted inside the left wing half near the 90 percent semi-span location for measurement of wing motion normal to the wing plane.

2.6 EXPLOSIVES

The explosives used for each firing consisted of either 1,000 or 10,000-lb charges of TNT, constructed and used as described in Reference 1. Figure 9 shows a typical pre-test view of a 1,000-lb TNT charge set up on a styrofoam pillar with center about 6 feet above the ground. Figure 10 shows the 10,000-lb charge.

The explosives were detonated by modified portable Reynolds Industries Exploding Bridgewire Firing Sets, using Reynolds Industries boosted RP-1 detonators. Each firing set was buried about one to two feet below the surface of the test area at a distance of 75 to 100 feet from the respective charge. A photograph of a firing box and burial hole is shown in Figure 11. Sand bags shown in the figure were placed over each hole for blast protection. The RG-22 triggering cables from the screenboxes at the track to the firing sets, for initiation of firing, were laid on the surface of the test area. The RG-58 firing cables from the firing sets to the charge detonators were laid above ground and fixed at the charges to prevent pull-away from the detonators.

The firing sets were connected to remote control units by means of RG-22B/U cables. Within the test area the cables were buried to a minimum depth of two feet for shielding from blast radiation. The control units were located at about track station 11,000, about 1500 feet south of the test area. A photograph of the control units mounted in their protective box is shown in Figure 12. The arming plugs at the control panel in the Alpha Blockhouse, at track station zero, were connected electrically to the control units.

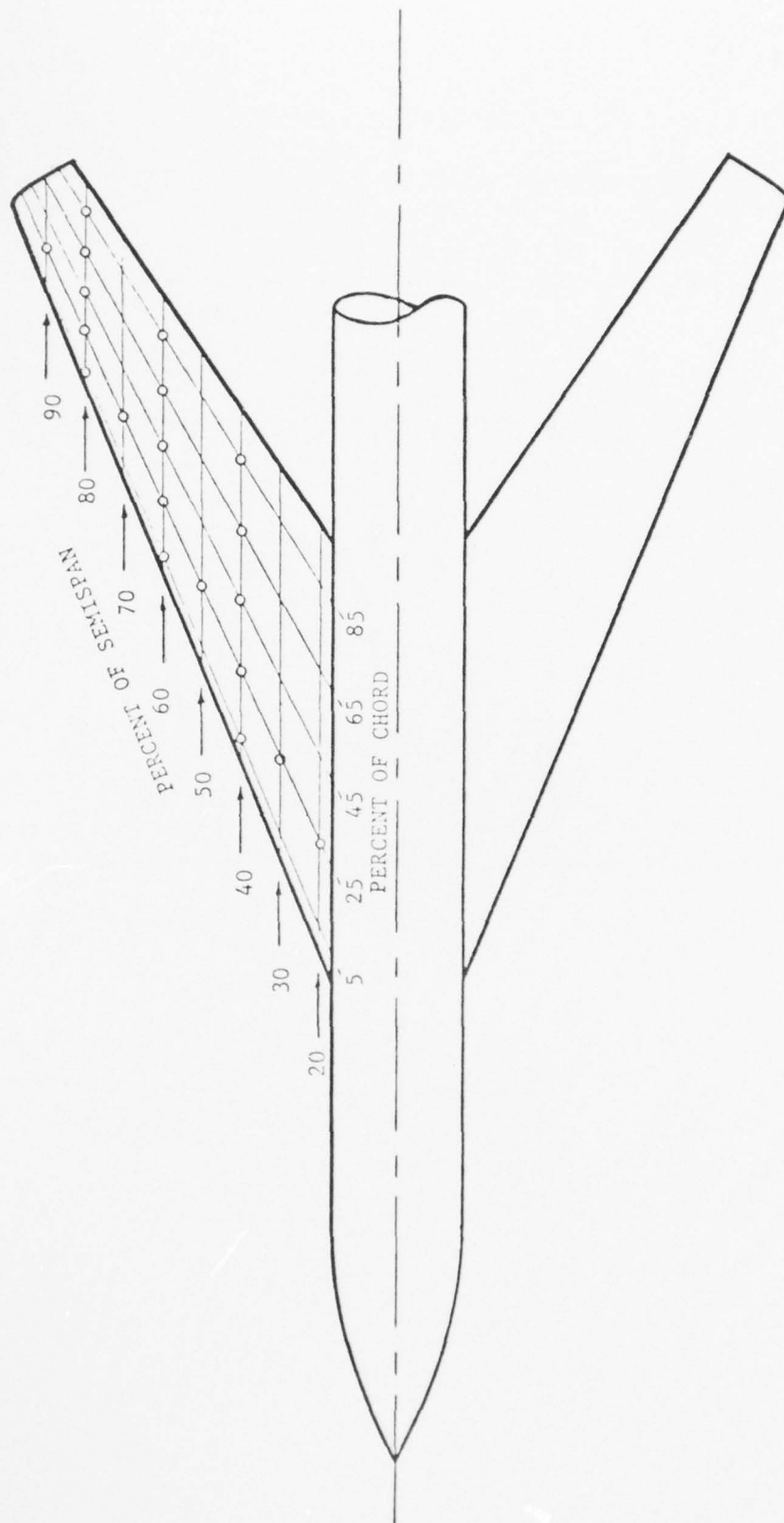


Figure 8. Sketch of wing and fuselage model showing pressure measurement stations.

Table 3

DISTRIBUTION OF AIRLOADS MEASUREMENT STATIONS OVER INSTRUMENTED (UPPER) WING.

Spanwise Locations (Percent of Semispan)	Chordwise Locations (Percent of Local Chord)				
	5	25	45	65	85
20		X			
30		X			
40	X	X	X	X	X
50		X			
60	X	X	X	X	X
70		X			
80	X	X	X	X	X
90		X			

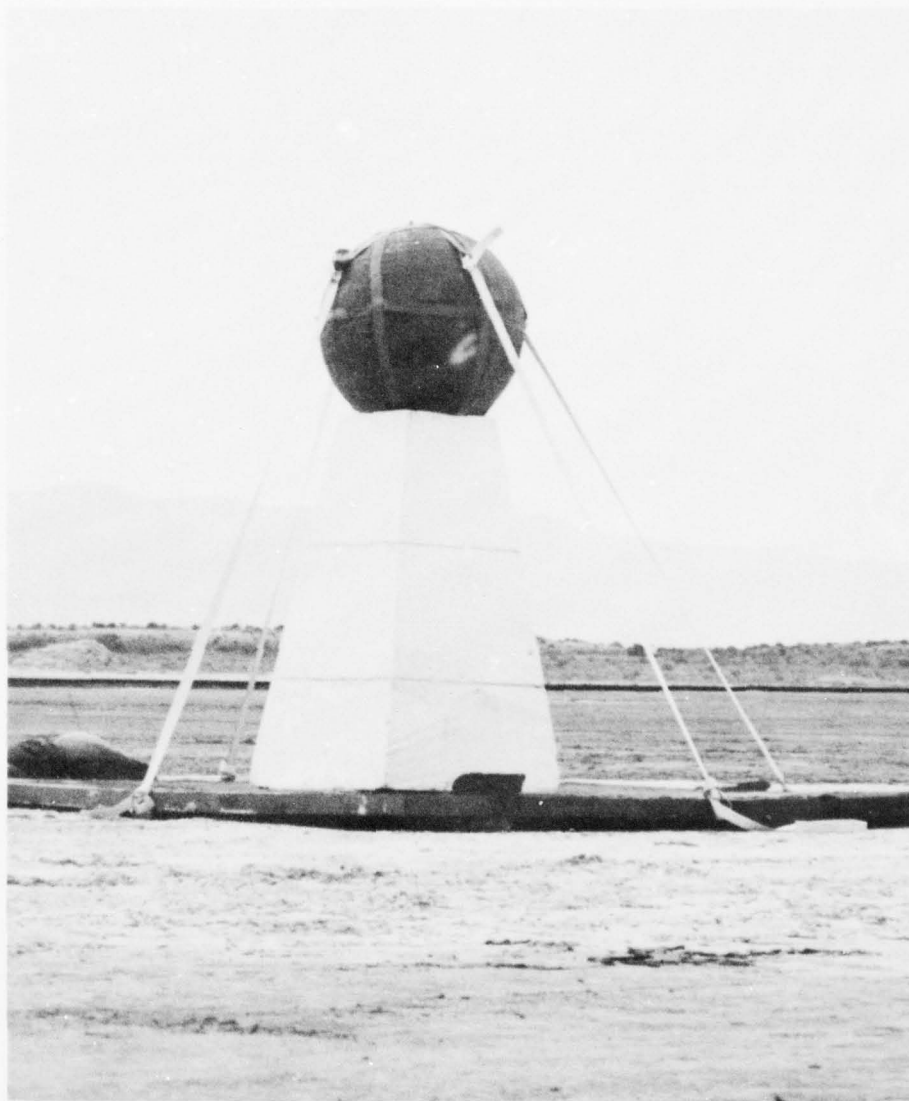


Figure 9. Typical 1,000 pound charge.



Figure 10. 10,000 pound charge.



Figure 11. Firing box and burial hole.



Figure 12. Control units for firing sets.

Extensive tests were performed on the firing sets to qualify them against premature firing from various signal sources and to achieve reliability of firing.

2.7 BLAST-LINE MEASUREMENTS

The blast-line probe system employed was the same as is described in Reference 1.

2.8 WING PRESSURE MEASUREMENTS

Pressures on the wing were measured using Kulite high performance pressure transducers of the XCQL-41-093-025 and XCQL-37-093-25D series. These transducers have a 25-psi range, 0.093-in diameter, low acceleration sensitivity and a 230 kHz natural frequency. All transducers were initially mounted with their surfaces flush with the wing surface, and remained nearly flush through the two test runs.

The transducer signals were generally connected in pairs electrically through differential amplifiers for measuring the difference in pressure between the blast-side and lee-side surfaces of the wing. The transducers were calibrated in this arrangement for matching of gains. Calibrations were carried out before and after each test.

The wing was shielded from the sun prior to sled firing to minimize solar heating. Polystyrene blocks were placed over the wing for this purpose. The blocks were pulled away from the model as the sled started down the track.

2.9 SLED VELOCITY AND POSITION MEASUREMENTS

Sled position and velocity were measured with the standard HAFB VMS system described in Reference 1.

Figure 13 presents time histories of sled velocity in the test area for the two runs made.

In addition to the above VMS measurements, independent measurements of sled position along the track were obtained for several times from the breakwire signals used to provide timing information (see Section 2.3).

2.10 HIGH-SPEED PHOTOGRAPHY

Various high-speed cameras running at speeds between 120 and 10,000 frames per second were employed in the two tests. At the first and third

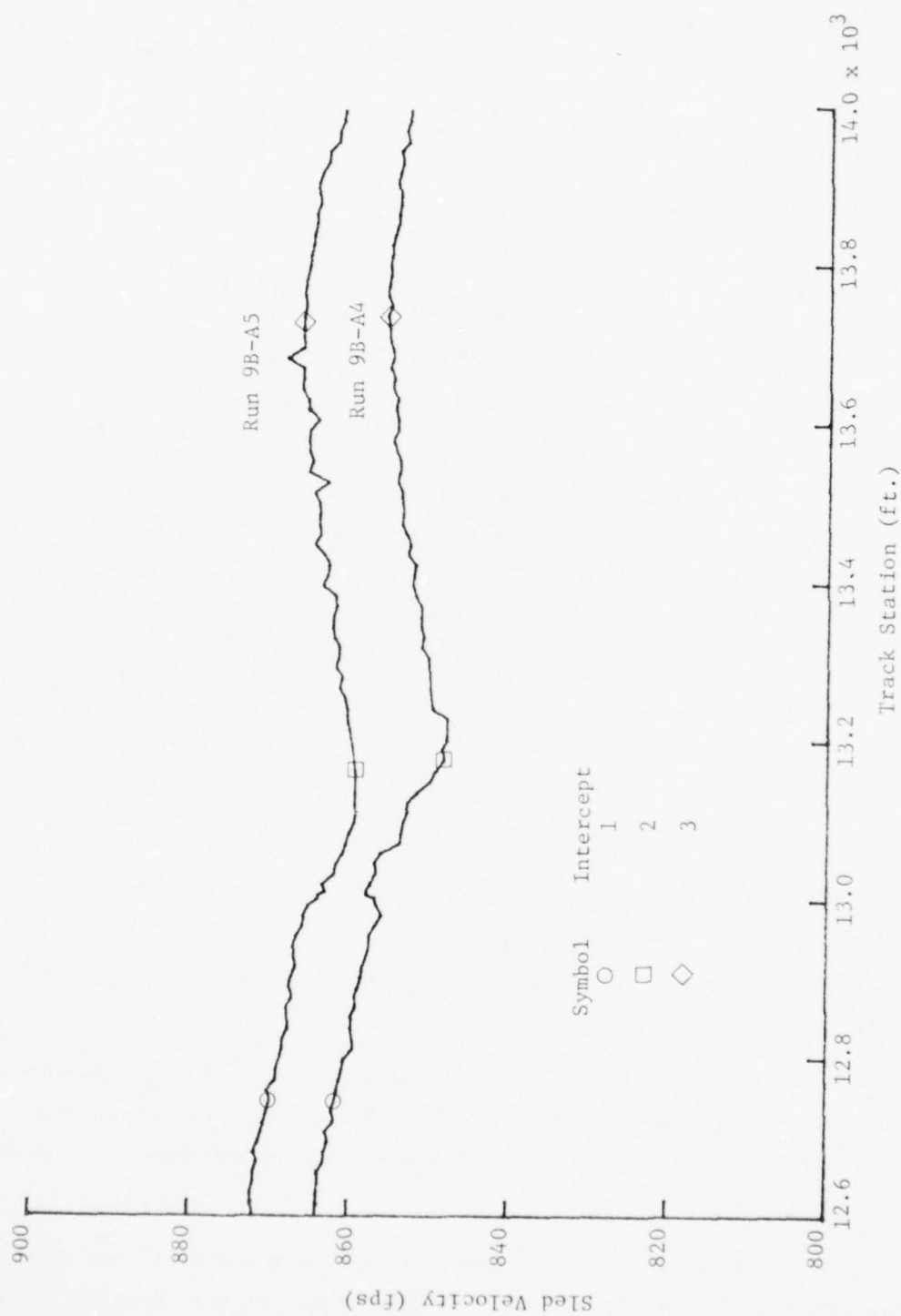


Figure 13. Sled velocity profiles

intercept areas, 4 x 16-ft. grid boards with parallel black and white stripes, Figure 14, were placed west of the track for observation of the blast shock intercept with the sled, using NOVA cameras at 10,000 frames per second. Two sled-borne 1000-fps cameras mounted in a box on the sled (Fig. 4) were used for monitoring lateral deformations of the wing model.

Various lower speed motion picture cameras were used for general surveillance of the run phenomena. Two were mounted over the track looking south for overall observation of the blast waves and sled. Additional tracking cameras, mounted on a building 1/2-mile east of the track were used for surveillance, as were also several cameras mounted in a helicopter about two miles east and 3500 feet above the track.

Tufts were mounted on the leeside of the lower wing semispan for observation of vortex motion. Cameras were located east of the track for viewing the second intercept. They were placed so as to observe the vortex motion before, during and after blast intercept.

In Run 9B-A4B various combinations of tufts and cameras, with color film, were used for development of the tuft-photography technique. Figure 15 shows the tufts after the run was completed. The tufts were of different material, colors, length, attachment methods and wing paint background. All the tufts remained attached. Some unravelled more than others and some were more flexible. There was a significant variation in detectability of the tufts as viewed from the test films.

A single Nova high-speed camera was located about 21 feet from the model in Run 9B-A4 viewing the second intercept area along about a 24 foot field of view at the model. A frame rate of 2500 fps was employed using color film. An image motion camera was located a few feet further north to obtain a stop-motion view of the model.

From the results of Run 9B-A4 and some laboratory tests, the photography technique used in Run 9B-A5 was developed. Two Nova high-speed cameras were located about 90 feet east of the track running at about 10,000 fps at the time of intercept. The field of view of one camera was centered on the desired blast intercept point, for viewing the tufts



Figure 14. Intercept 1 area with grid board.

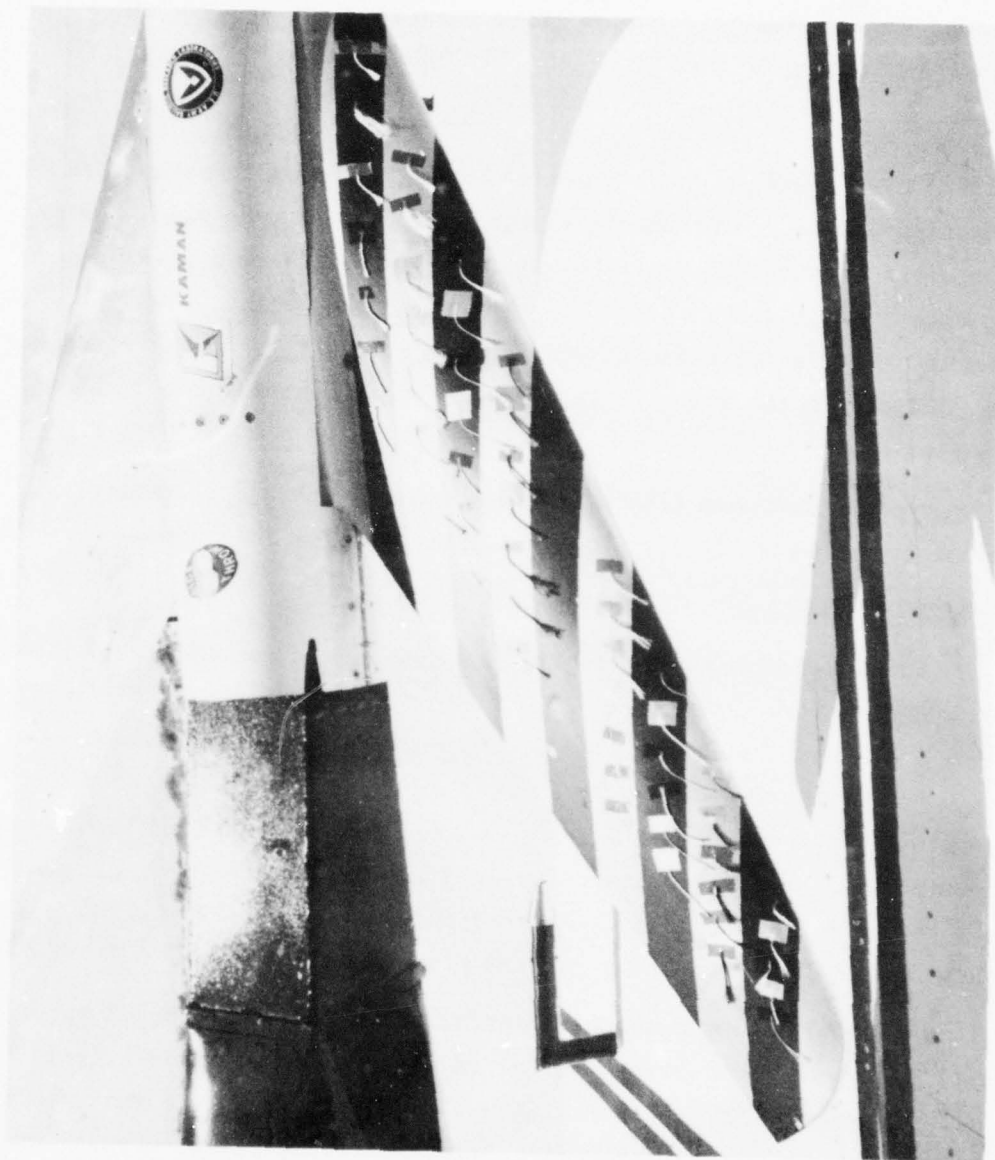


Figure 15. Developmental tuft layout on model lower wing half, Run 9B-A4.

prior to blast intercept and during the lift buildup period. The field of view of the other camera was centered 10 feet further north for observing the later stages of the vortex motion. The image motion camera viewed at five feet further north. The tuft photography results of this test were good, showing the tuft motion quite clearly. The results are discussed in Section 6.

2.11 TELEMETRY

All sled-borne transducer signals were telemetered from the sled to a HAFB ground receiving station. Six transmitters were used, operating at carrier RF frequencies near 800 MHz, with 4 transducer signals generally multiplexed in each transmitter at sub-carrier frequencies of 64, 96, 128 and 160 kHz, having a frequency response of 8 kHz for each transducer signal. Figure 16 shows the telemetry electronic system located below the surface of the sled.

The overall response time of the instrumentation and telemetry system to transient pressures is estimated to be about 0.1 milliseconds.

2.12 MODEL STRENGTH AND STIFFNESS TESTS

The model and its strut-sting support had been designed strengthwise to meet conservative design specifications of blast airloads. For stiffness the model and its support had been designed to keep the frequencies of the wing modes and the support lateral modes well separated from the frequencies of the sled lateral modes and to keep the model deflections and motion small so the resultant airloads produced by the deflections and motion would be negligible. These criteria were applied to the redesign of the sting connector for the present tests.

Loads and vibration tests were performed on the model, model-support and sled system at HAFB during the period of March 7 to 11, 1976, prior to the test program with the model at a 45-deg roll angle. A test report was prepared and distributed by HAFB, Reference 3. Critical results of those tests are reviewed here.

2.12.1 Strength

The loads test of the sting connector indicated design goals had been met.



Figure 16. Sled telemetry system.

2.12.2 Deflection

Deflections of the wing, wing box and sting were measured during the loads tests. The measured deflections were compared against the predictions of the NASTRAN code calculations performed by D. J. Krupovage, Reference 4. The sting pitch deflections were essentially the same as before the connector redesign and well within design objectives. Wing rotation due to sting torsional rotation was negligible.

2.12.3 Frequencies

Shake tests were performed with the sled mounted on rails in the laboratory. The shaker force was applied separately in both the lateral and the vertical direction relative to the track. Accelerations were measured normal to the wing plane, which was at the 45-deg roll angle. The lowest eleven frequencies measured in the tests are listed in Table 4, taken from Reference 4. The measured frequencies are compared there with results of the tests of March 1976, before the connector was added, and with the NASTRAN predictions of Reference 4.

The first nine modes have frequencies about equal to the values before the connector was added. The last two modes were lateral wing motion, i.e. normal to the wing plane, due to sting bending and wing rotation due to sting torsion. The two frequencies had been reduced from 70.70 and 79.84 to 56.2 and 58.1, respectively. The reductions are attributed to the addition of the connector, but the frequencies were still well above the lowest mode involving the wing, sting and strut of 25.6 Hz.

The first eight modes agreed reasonably well with the NASTRAN predictions of March 1977, but the remaining three did not. It is believed that this could be corrected by refinement of the modeling, but these modes were not believed to be significant, so it was not done.

Table 4

SLED, SUPPORT AND MODEL MODES

No.	90° Model Measured May 76	45° Model Measured Mar 77	Mode Shape Description	90° Model NASTRAN Calculated Nov. 75	90° NASTRAN Recalculated Mar. 77	45° NASTRAN Calculated Mar. 77
1	18.91	18.0	Vert - longeron & slipper beam bending	19.11	18.90	18.87
2	22.33	22.5	Lat - longeron bending	19.51	19.10	19.20
3	24.65	25.6	Vert - sting bending	26.55	24.59	24.80
4	26.654	30.8	Lat - strut, longeron and sting bending	26.61	26.00	26.04
5	34.57	34.0	(Ground plane)	Not modeled		
6	44.21	42.8	Lat - sting bending & strut base rocking	44.44	42.94	42.33
7	50.98	50.0	(Camera pod)	Not modeled		
8	58.61	59.2	Sting torsion	59.59	59.19	58.72
9	76.809	75.0	Sled rocking pitch plane	64.26	63.41	63.29
10	70.70	56.2	Lat wing & sting	67.44	66.84	66.55
11	79.84	58.1	Lat wing & sting	72.88	72.03	71.99

SECTION 3

TEST SERIES

3.1 INTERCEPT CONDITIONS

The test conditions for the runs and intercepts are tabulated in Tables 5 and 6. Table 5 gives general sled test conditions for each run, including atmospheric pressure, temperature and wind conditions and the nominal sled speed. Table 6 gives specific charge and blast intercept conditions for each blast intercept, including charge weight, sled intercept velocity, charge-sled intercept geometrical relationships, blast intercept angle (ϕ), incident blast intercept overpressure (Δp_s), and the peak angle of attack produced by the blast wave.

Sled-borne pressure transducer locations were the same for all runs, as given in Figure 8 and Table 3. For most locations only the differential pressures between the two surfaces of the (upper) wing were recorded. For a few locations individual pressures on the leeward or blastward side of the model were recorded as indicated in Table 7.

The reference point on the wing which is used to define the wing-blast intercept location is defined as that point where the wing 40 - percent chordline intersects the centerline of the model fuselage. The corresponding blast intercept time for this point can be easily determined from the observed blast arrival times at the two wing transducers closest to that reference point, which are at the 20 and 30 percent semispan locations.

The track station at blast intercept time for the model reference point was estimated by three essentially independent methods for each intercept, results of which are presented in Table 8.

The first estimate made (A) was based on the sled trajectory measurements described in Reference 1 and Section 2.9 and the blast intercept time as determined by the wing pressure transducers (t_1). The second estimate (B) was based on the timing breakwire location, the sled

Table 5

GENERAL SLED TEST CONDITIONS

Run No.	Date	Ambient Conditions						Nominal Sled Speed		Angle of Attack (deg)	Roll Angle (deg)
		Pressure	Temp. (°F)	Wind							
				(in. Hg)	(psia)	Dir. (deg)	Vel. (Kn)				
								(fps)	(Mach No.)		
9B-A4	6/9/77	25.75	12.59	86.6	-	<5	870	0.76	3.5	45	
9B-A5	8/10/77	25.90	12.67	79.9	-	<5			3.2	0	

Table 6
BLAST INTERCEPT CONDITIONS

Run No.	Intercept No.	Charge Weight (lbs)	Sled Velocity		Distance from Charge Station to Intercept Point (ft)			Intercept Angle (deg. from head-on)	Blast Shock Over-pressure (psi)	Blast Peak Angle of Attack (deg) ^b
			(fps)	(Mach)	Parallel ^a to Track	Perpendicular to Track	Radial Distance			
9B-A4	1	1000	862	.752	-102.9	122.6	160.1	50.0	4.36	14.0
	2	1000	848	.740	-3.1	160.0	160.0	88.9	4.10	18.9
	3	1000	855	.746	107.5	113.1	156.0	133.5	4.20	17.7
9B-A5	1	1000	870	.764	-101.7	122.6	159.3	50.3	4.34	13.6
	2	10,000	859	.754	0.3	339.2	339.2	90.1	3.82	17.4
	3	1000	866	.760	110.5	113.1	158.1	134.3	4.29	17.1

^a In direction of sled travel.

^b Includes pre-blast angle of attack.

Table 7

PRESSURE MEASUREMENTS ON THE WING

Transducer location, %semispan/%chord (Fig. 8)	Measurement recorded ^a during Run:	
	9B-A4	9B-A5
20/25	B	B
30/25	D, B, L	D, B, L
40/05	D	D
40/25	D	D
40/45	D	D
40/65	D	D
40/85	D	D
50/25	D	D
60/05	*	L
60/25	D	D
60/45	D	D
60/65	D	D
60/85	D	D
70/25	D	D
80/05	D	D
80/25	D	D
80/45	D	D
80/65	D	D
80/85	D	D
90/25	D	D

^aD for differential pressure, B for blastward pressure, L for leeward pressure, * for no reliable data obtained.

Table 8

COMPARISON OF INTERCEPT LOCATION ESTIMATES

Run No.	Intercept No.	Intercept Station Estimate (ft) *			
		A	B	C	av
9B-A4	1	0.5	-0.7	-0.1	-0.1
	2	-2.4	-3.6	-3.3	-3.1
	3	-5.1	-5.8	-6.0	-5.6
9B-A5	1	1.4	1.0	0.9	1.1
	2	0.6	0.2	0.2	0.3
	3	-2.3	-2.8	-2.7	-2.6

* Distance ahead of Desired Intercept Point in the direction of sled motion (see text, Sec. 3.1, for meaning of A, B, C, designations). The Track Station for the DIP is given in Table 1.

speed, the indicated time of wire breaking and the blast intercept time t_1 . The third method (C) was based on the location of the firing screen-box, the sled speed, the time of the detonation, and the blast intercept time t_1 . Values of intercept conditions obtained by these three methods differ somewhat due to the associated experimental uncertainties. It is recommended that the intercept conditions presented in Table 6, based on the average values presented in Table 8, be used for any calculations relevant to the test program.

3.2 RUN 9B-4

This test was performed to obtain blast intercepts for bursts out of the airplane plane of symmetry, resulting in nonsymmetrical intercepts. The intercepts were for three different intercept angles of 50° , 90° and 135° at a blast shock overpressure level of 4 psi, with the instrumented wing rolled 45° toward the blast. Weather conditions were good with the temperature 86.6 deg. F. and a wind of less than 5 knots. This run was successful in that all three charges detonated as scheduled, all three intercepts occurred at the scheduled intercept angles and overpressure levels, and the intercept sled speed was close to the planned value of Mach 0.76. Useful pressure data were obtained from all but one sled-borne pressure transducer locations and from all but two of the twelve blast-line transducers.

3.3 RUN 9B-A5

This test was performed to obtain symmetrical blast intercepts as in the 1976 series, at a 4-psi overpressure level for blast intercept angles of 50° , 90° and 135° with an unrolled wing. Weather conditions were very good. The temperature was 79.9 deg. F and there was essentially no wind. The second intercept condition was intended to be the same as that for Run 9B-A2 of the previous series (Ref. 1) except having a longer blast duration for examination of the effect of yield. The burst was produced by a 10,000 lb. TNT charge as compared to 1000 lb. charges for all other intercepts.

This run was successful in that the desired sled speed, intercept angle and intercept pressure levels were obtained and all wing transducer locations and all blast-line pressure transducers produced useful data.

SECTION 4

TEST DATA

4.1 A/D DATA PROCESSING

Seven types of event data were obtained as a function of time during a run:

1. Sled position and velocity.
2. Blast-line pressure.
3. Total pressure at the model and at the sled.
4. Static pressure at the sled.
5. Wing pressure.
6. Wing acceleration.
7. Lateral bending moment at the sting root.

All data were processed to digital form by WSMR and were provided to KA as tabular data. In addition Items 2 to 7 were provided in graphical form and on magnetic tapes.

The sled-borne transducer data (items 2 to 6) were taken from the analog tapes at 0.05 millisecond intervals for about 20,000 times per run.

4.2 DATA PRESENTATION

Graphical time history plots of most of the measured blast-line and sled-borne transducer measurements are presented in this report according to the index of figures given in Table 9.

Time histories of blast-line pressures, blastward and leeward wing pressures, total pressure at the model and at the sled, static pressure at the sled, and model acceleration are presented in Appendix A.

In all figures presenting time histories of sled transducer pressures, transducer locations are identified by a four digit code, e.g., 60/05, where the first two digits (60) give the spanwise distance from the model centerline as a percent of the semi-span (e.g., 60%) and the

Table 9
INDEX OF TEST DATA FIGURES

Run Number	Intercept Number	Figure Number						
		Blast-Line Pressures	Wing Pressures		Total Pressure		Sled Static Pressure %	
			Differ-entail	Blastward/Leeward	At Model	At Sled	1	2
9B-A4	1	25	26	27	28	29	30	31
	2	33	34	35	36	37	38	39
	3	41	42	43	44	45	46	47
9B-A5	1	49	50	51	52	53	54	55
	2	57	58	59	60	61	62	63
	3	65	66	67	68	69	70	71
								72

* See Figure 7 for number designations

last two digits (05) give the percentage chordwise distance from the leading edge of the wing.

4.3 ACCURACY OF DATA

Data accuracy and interference corrections for the blast-line data are discussed generally in Reference 1.

SECTION 5

BLAST VARIABLES AT SLED

In order to utilize the blast-line pressure data presented in Section 4 for the comparison of experimental and theoretical wing pressures, it is necessary to interpolate or extrapolate the experimental blast-line pressures to obtain the blast pressure time history at the sled as a function of time, and to also estimate the corresponding blast density and velocity time histories as well. The blast pressures at the sled were generally obtained as indicated below and the corresponding densities and velocities were obtained by using the method described in Reference 5, as discussed in Appendix B of Reference 1. The resulting time histories of pressure, density and velocity at the sled are presented in Figures 17 to 22.

For each blast line transducer time history, a corresponding time history of the blast overpressure at the sled was determined by assuming that the shapes of the overpressure time histories at a blast line transducer location and at the sled location are the same, if the overpressure is expressed as a fraction of the shock overpressure at the location and the time is expressed as a fraction of the positive duration of the blast wave, or

$$\Delta p / \Delta p_s = f(\Delta t / t_{\Delta p+}) \quad (1)$$

where

Δp_s is the shock overpressure

Δp is the overpressure at time t

Δt is time after shock arrival ($t - t_s$)

t is time

t_s is shock arrival time

$t_{\Delta p+}$ is the positive duration time of the overpressure, as determined theoretically from Brode's analysis (Fig. 36 of Reference 6).

$f(\Delta t/t_{\Delta p+})$ is the experimental variation of $\Delta p/\Delta p_s$ with $\Delta t/t_{\Delta p+}$ as obtained from a blast line transducer, after fairing out some obvious interference pulses and noise.

The shock overpressure corresponding to any position of the sled was interpolated or extrapolated from the corresponding blast line transducer value with the equation

$$\Delta p_s(r_r) = \Delta p_s(r_b) [\Delta p_s(r_r)^*/\Delta p_s(r_b)^*] \quad (2)$$

where

r_b designates the radius from the burst point to the blast line transducer.

r_r designates the instantaneous radius from the burst point to the model reference point, as determined from the problem geometry and the experimental sled trajectory.

$\Delta p_s(r)$ designates the shock overpressure at a point at a radial distance r from the burst.

$\Delta p_s(r_b)$ is the experimental shock overpressure at the blast line transducer

and the $*$'s designate theoretical values as obtained from Brode's theory (Reference 6), using the curves presented in Reference 5.

Using the above equations, overpressure time histories at the sled were calculated for each intercept for all of the blast line transducers for which useful data were obtained. Then all time histories obtained for each intercept were averaged to obtain a best estimate of the true

time history for that intercept. The following weighted average equation was used for this purpose for intercepts 2 and 3 of Runs 9B-A4 and 9B-A5.

$$p = \frac{w_1 p_1 + w_2 p_2 + \dots + w_n p_n}{w_1 + w_2 + \dots + w_n} \quad (3)$$

where

p is the weighted average pressure at any time

p_i is the pressure estimate from the i -th transducer

n is the number of transducers

w_i is a weighting factor given by

$$w = A(\Delta\theta) \times B \quad (4)$$

$$A(\Delta\theta) = 0.1 + 0.9 \exp(-(\Delta\theta/7.5^\circ)^2) \quad (5)$$

$$B = \exp[-20(\Delta p_{s, \text{sled}}^* / \Delta p_{s, \text{blast line}}^* - 1)^2] \quad (6)$$

$\Delta\theta$ is the circumferential angle between a ray from the burst to the blast line transducer and a ray from the burst to the sled reference point.

The factor $A(\Delta\theta)$ gives maximum weight to blast line transducers lying on a radial line between the burst and the sled and the factor B gives maximum weight to transducers located at the same radial distance from the blast as the sled. The particular expressions for these two weighting factors A and B given above, while somewhat arbitrary, were considered satisfactory in Reference 1 since several other choices of weighting factors gave about the same end results. However, for intercepts 1 of both Runs 9B-A4 and 9B-A5 the above procedure gave unrealistic results because of an apparent significant deviation of the blast-line pressure signals from an axisymmetrical pattern. Consequently, for these two intercepts it was found to be more realistic to interpolate or extrapolate the test data by a slightly different procedure using only the transducers located nearest to the sled at any particular time.

The time histories of the blast overpressure at the sled obtained by the above procedure for all intercepts are shown in the first parts of Figures 17 to 22. These time histories cover the time period from initial shock arrival up to the time of second shock arrival.

The corresponding time histories of blast density and velocity, as obtained as described in Appendix B of Reference 1, are also presented in Figures 17 to 22.

In order to provide an independent check on the reliability of the blast conditions at the sled as determined above, these above pressures and total pressures derived from these pressures and velocities were compared with the corresponding direct measurements of static and total pressure measurements made on the sled.

For Run 9B-A4, total pressure time histories as calculated from the data in Figures 17 to 22 were found to be in good agreement with the direct measurements of total pressure on the model. Differences were generally in the noise level and were usually well under 1 psi. The directly measured time histories of total and static pressures on the sled were also in fair agreement with the calculated values but were sometimes larger and noisier, probably due to the lower physical location of these transducers (than for the model total pressure probe) where they are more subject to track and sled interference effects.

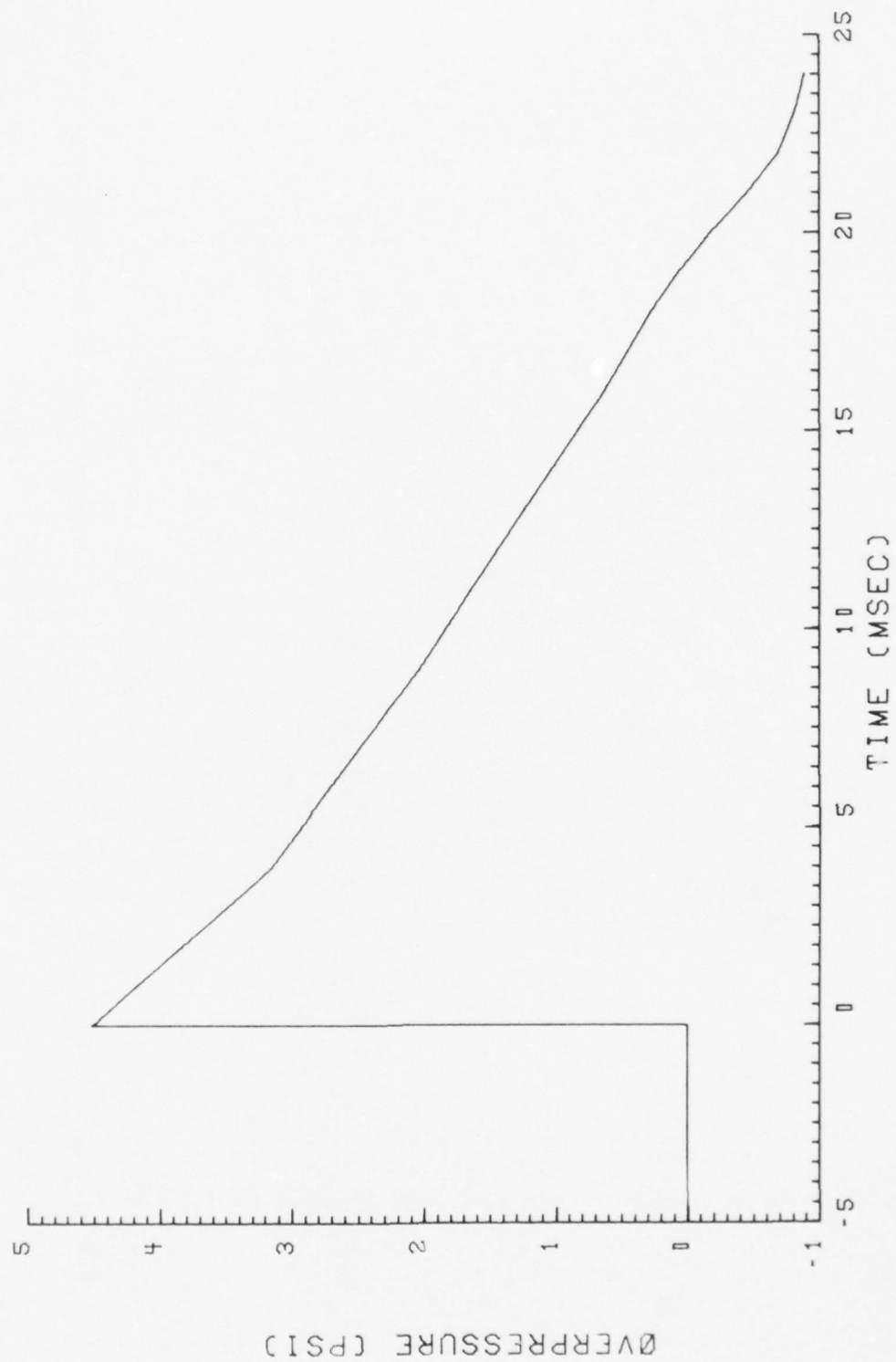


Figure 17. Blast flow conditions at the sled for Run 9B-A4, Intercept 1.

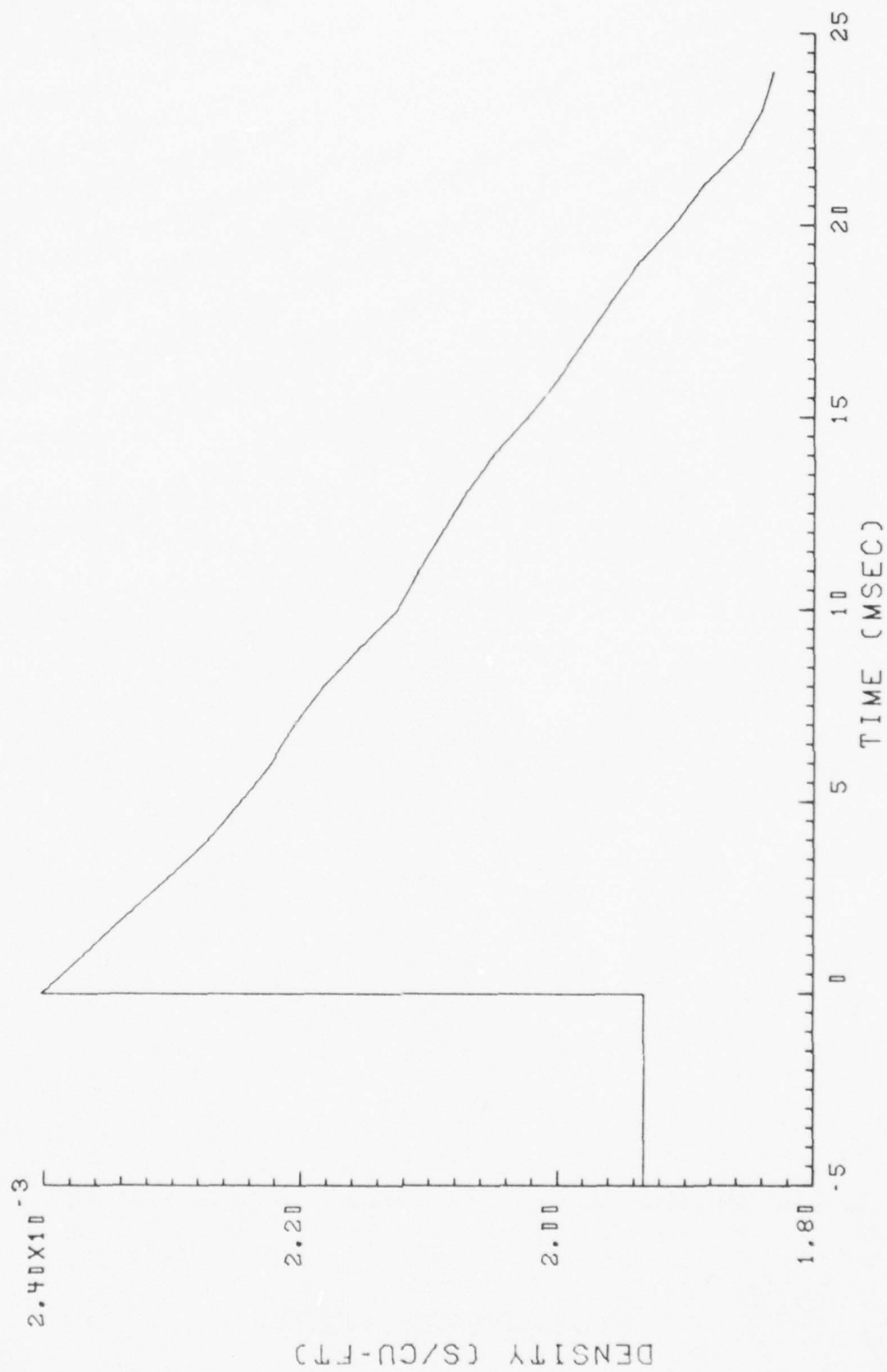


Figure 17. Continued

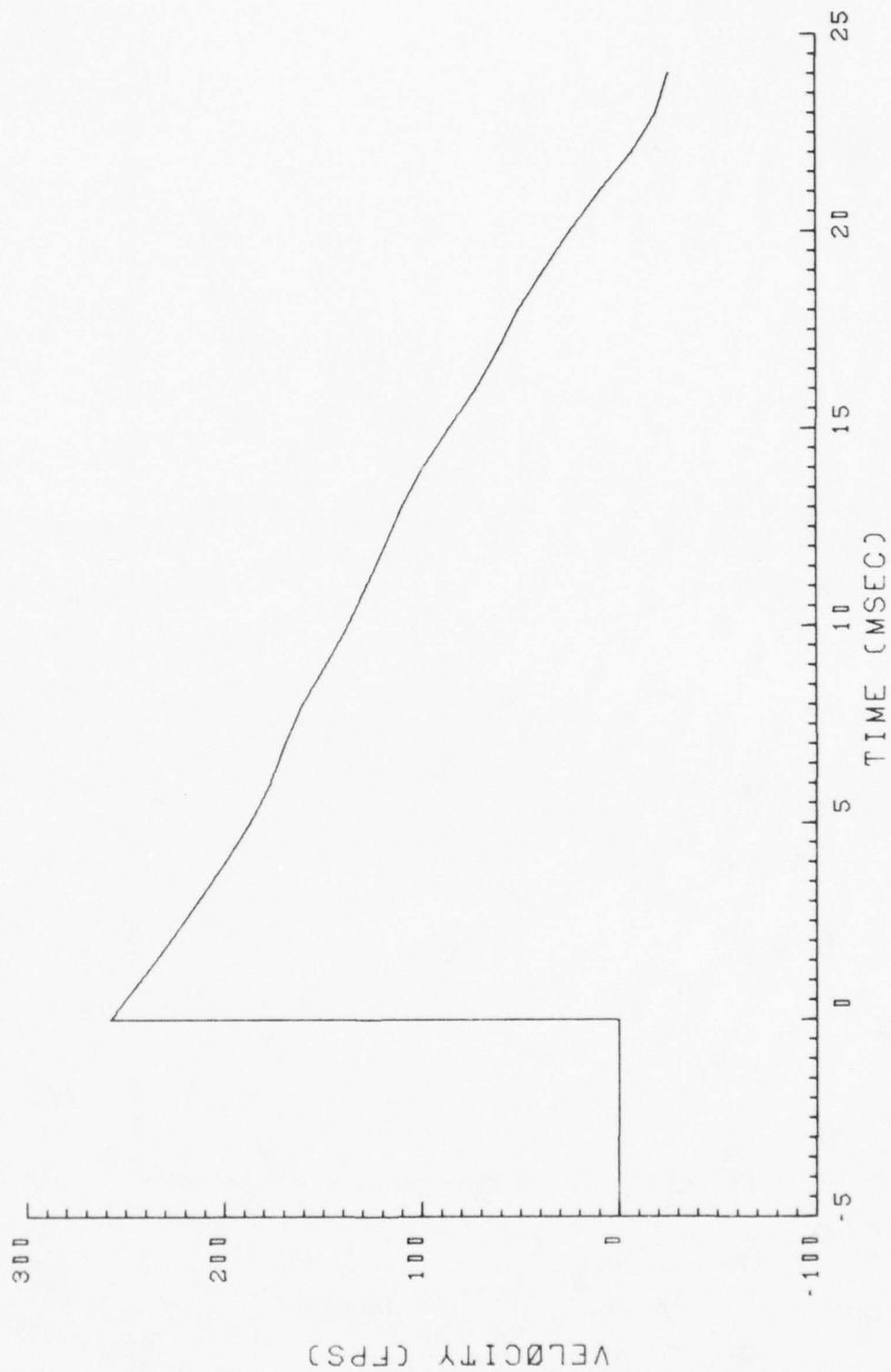


Figure 17. Concluded.

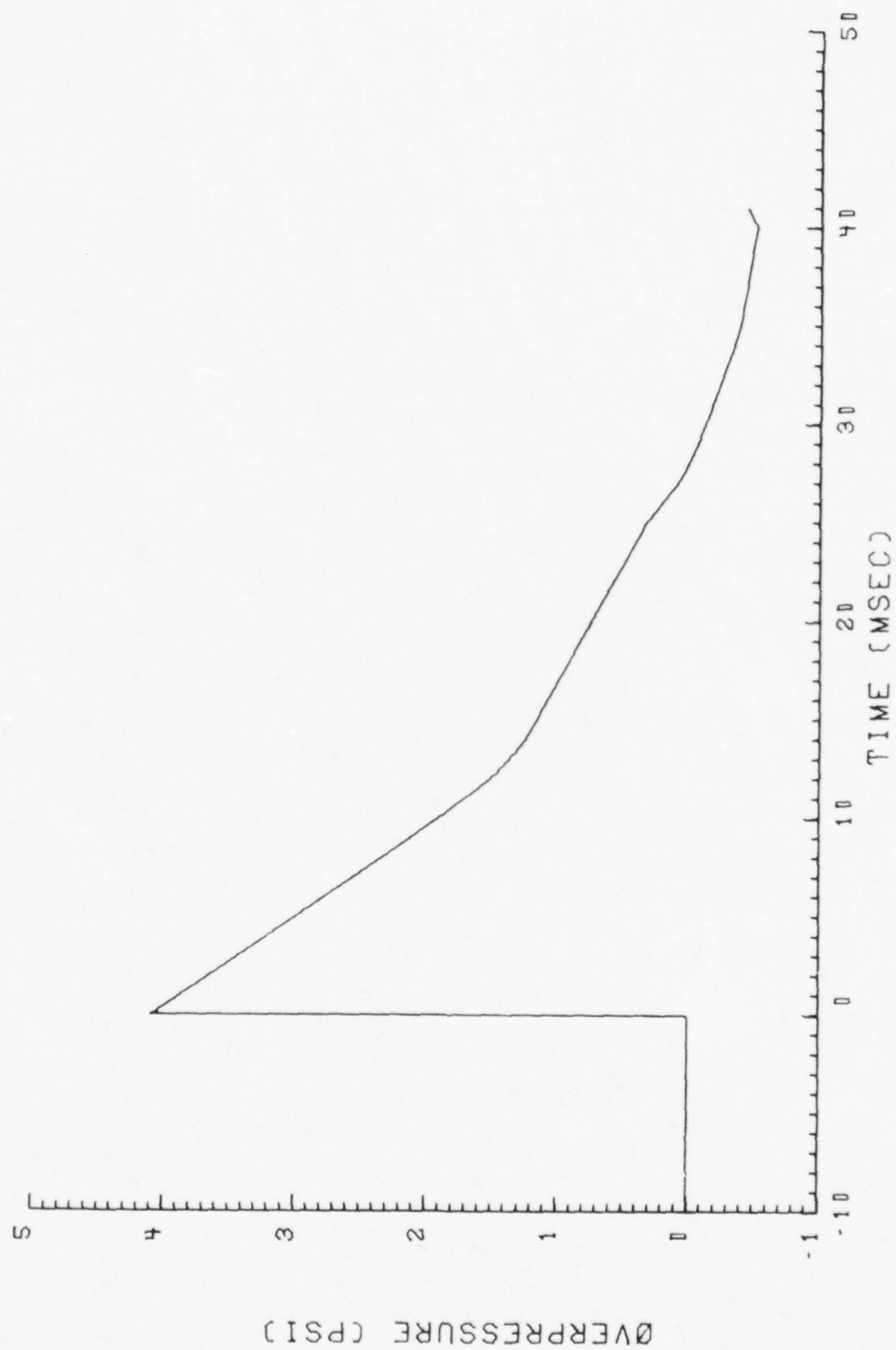


Figure 18. Blast flow conditions at the sled for Run 9B-A4, Intercept 2.

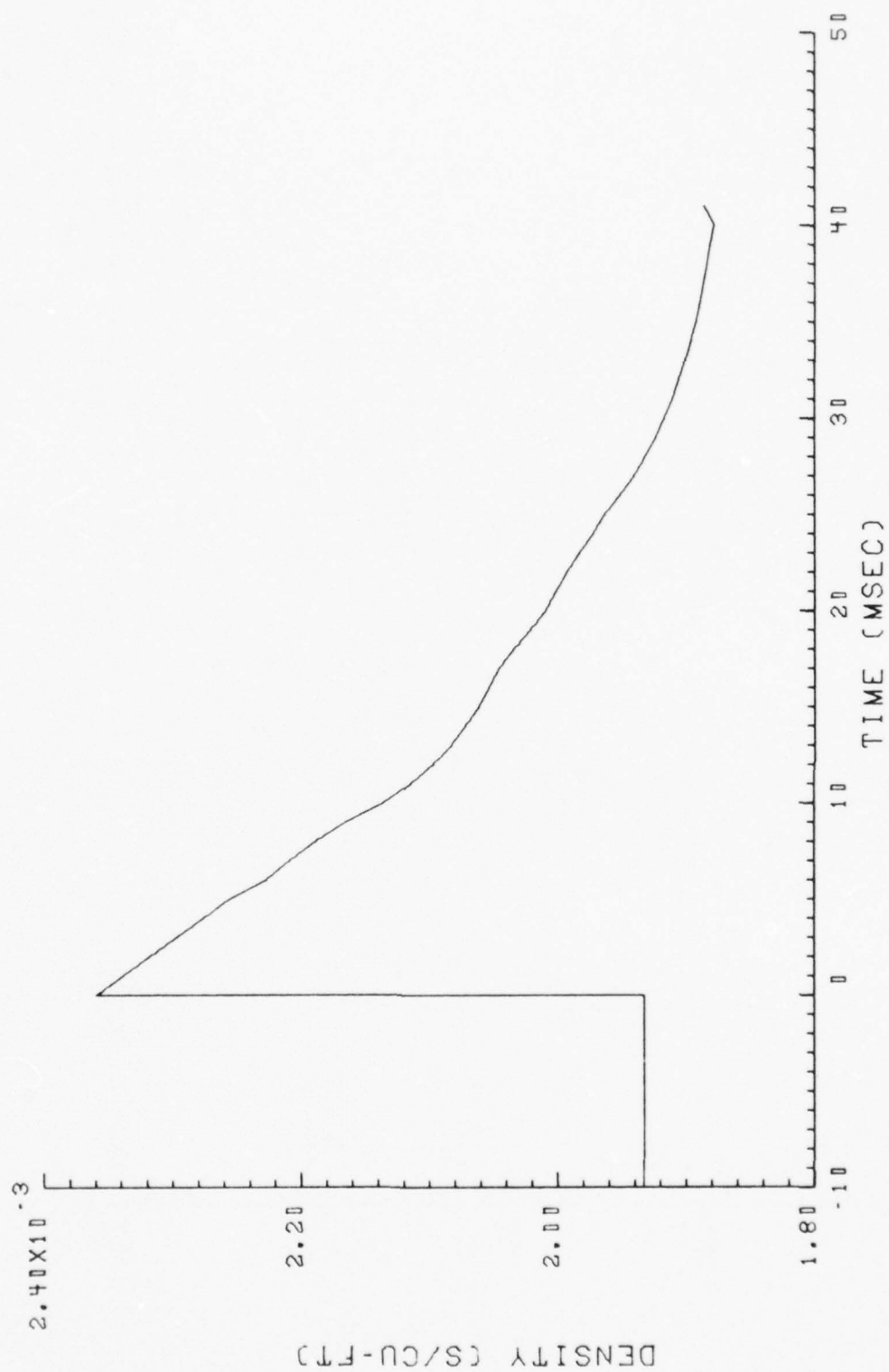


Figure 18. Continued.

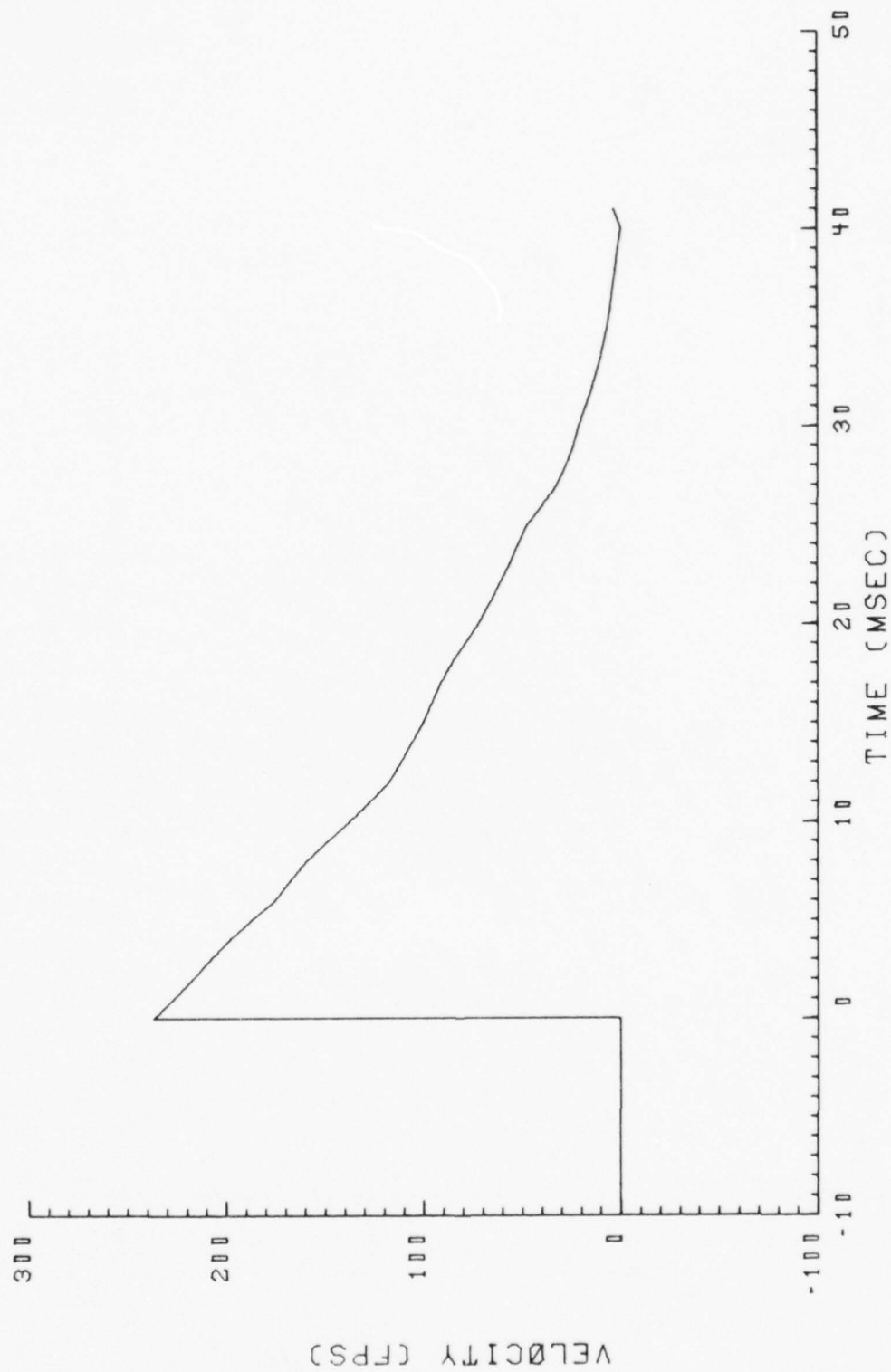


Figure 18. Concluded.

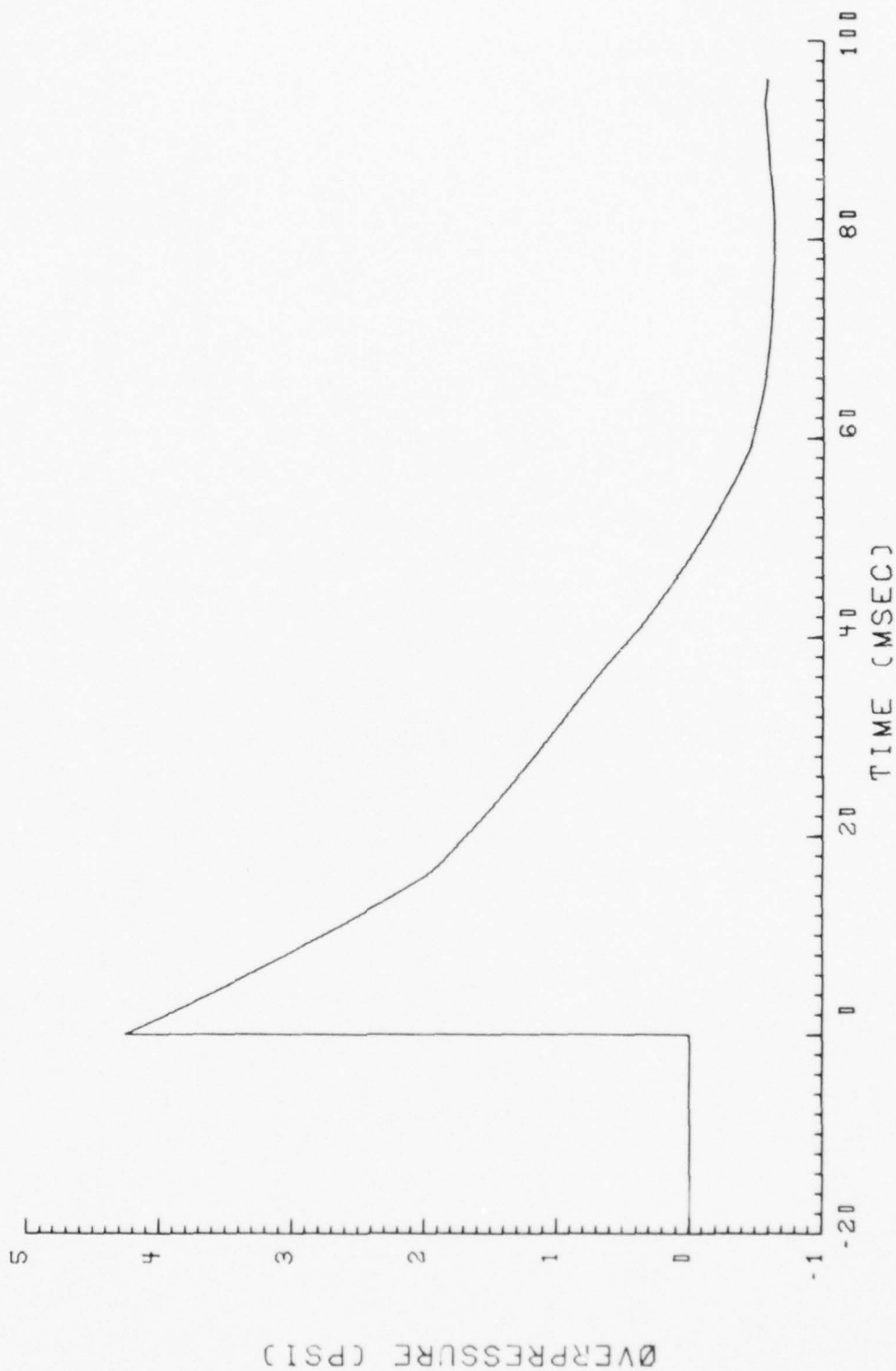


Figure 19. Blast flow conditions at the sled for Run 9B-A4, Intercept 3.

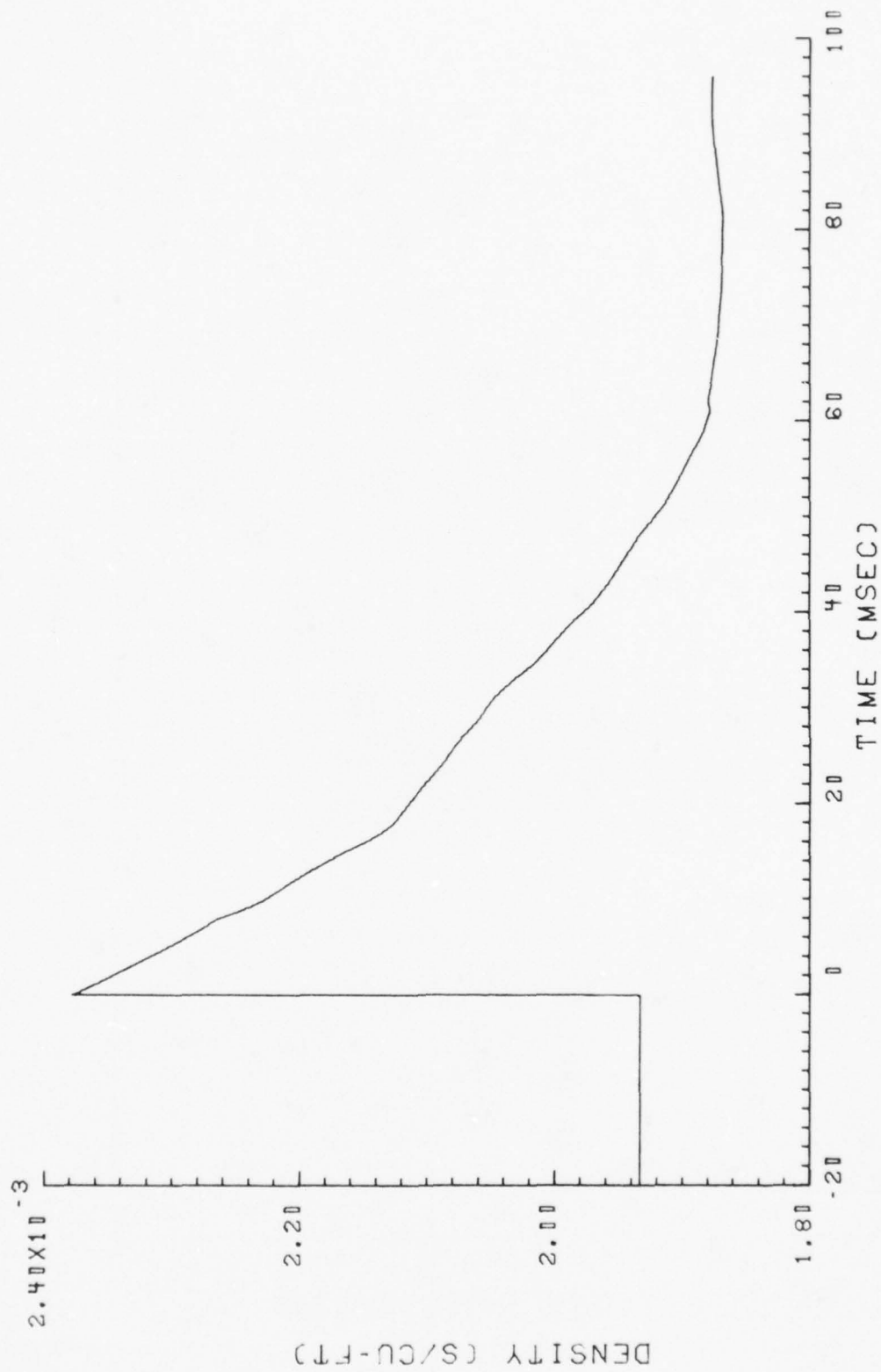


Figure 19. Continued

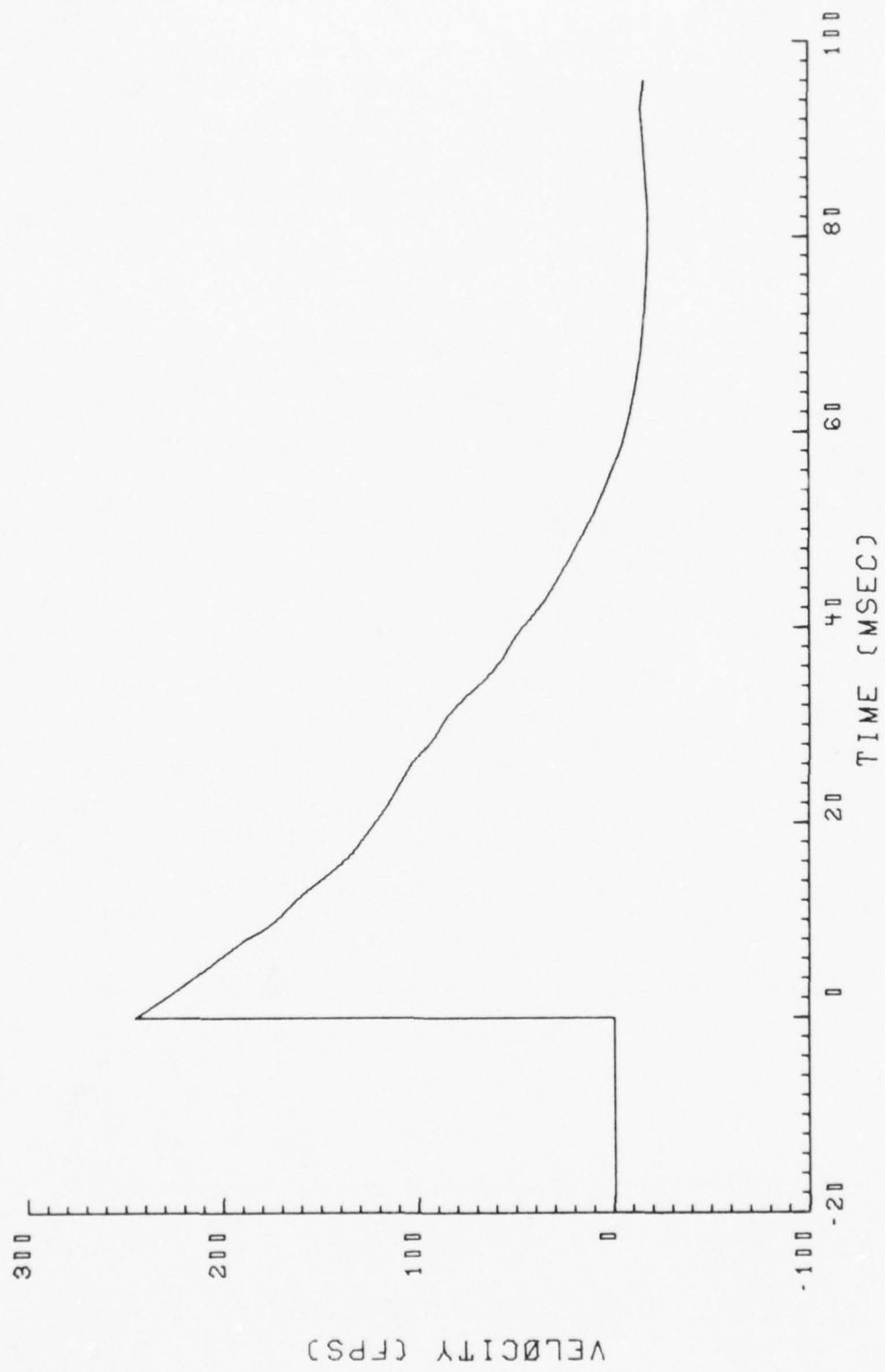


Figure 19. Concluded

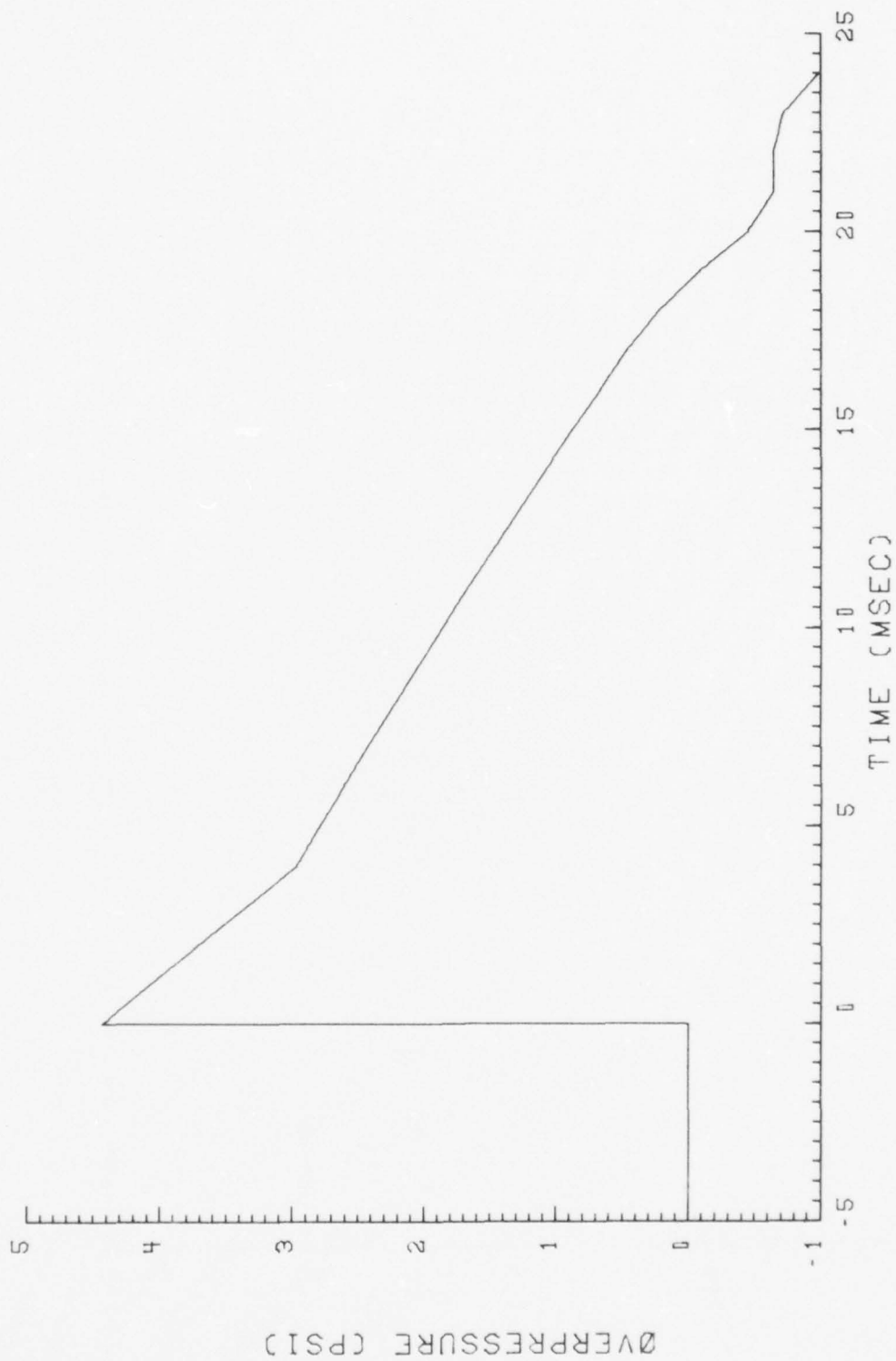


Figure 20. Blast flow conditions at the sled for run 9B-A5, Intercept 1

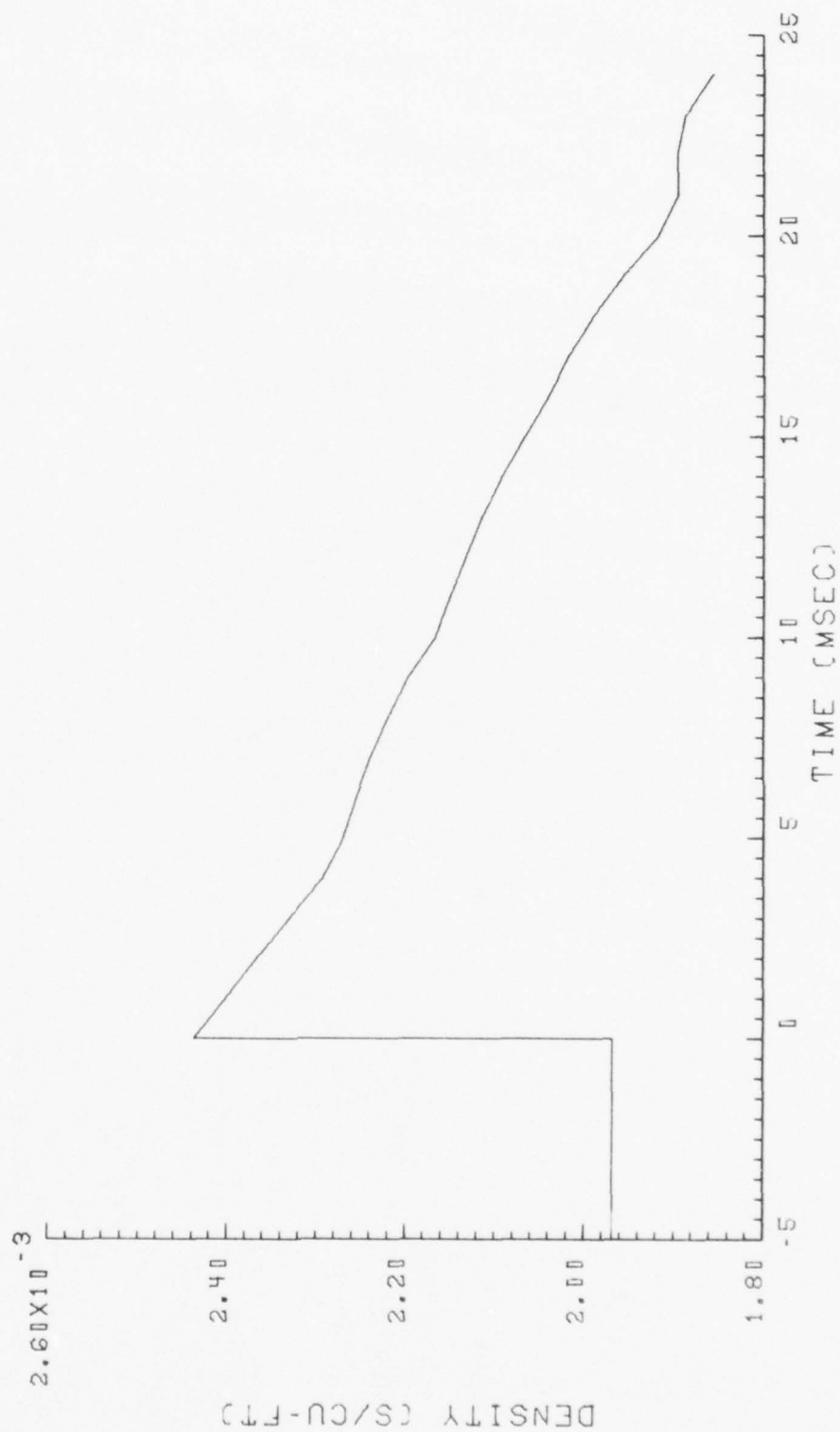


Figure 20. Continued

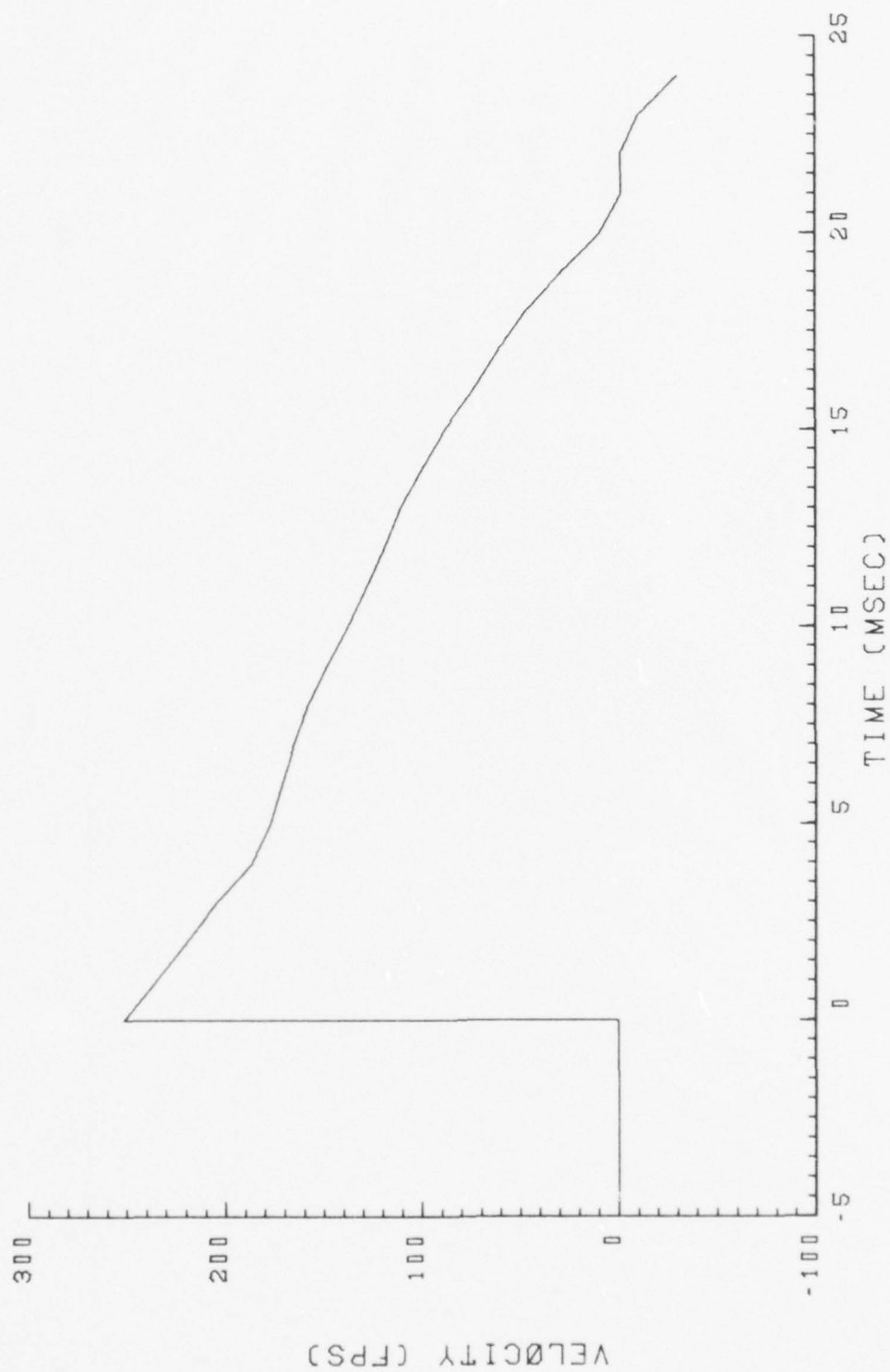


Figure 20. Concluded.

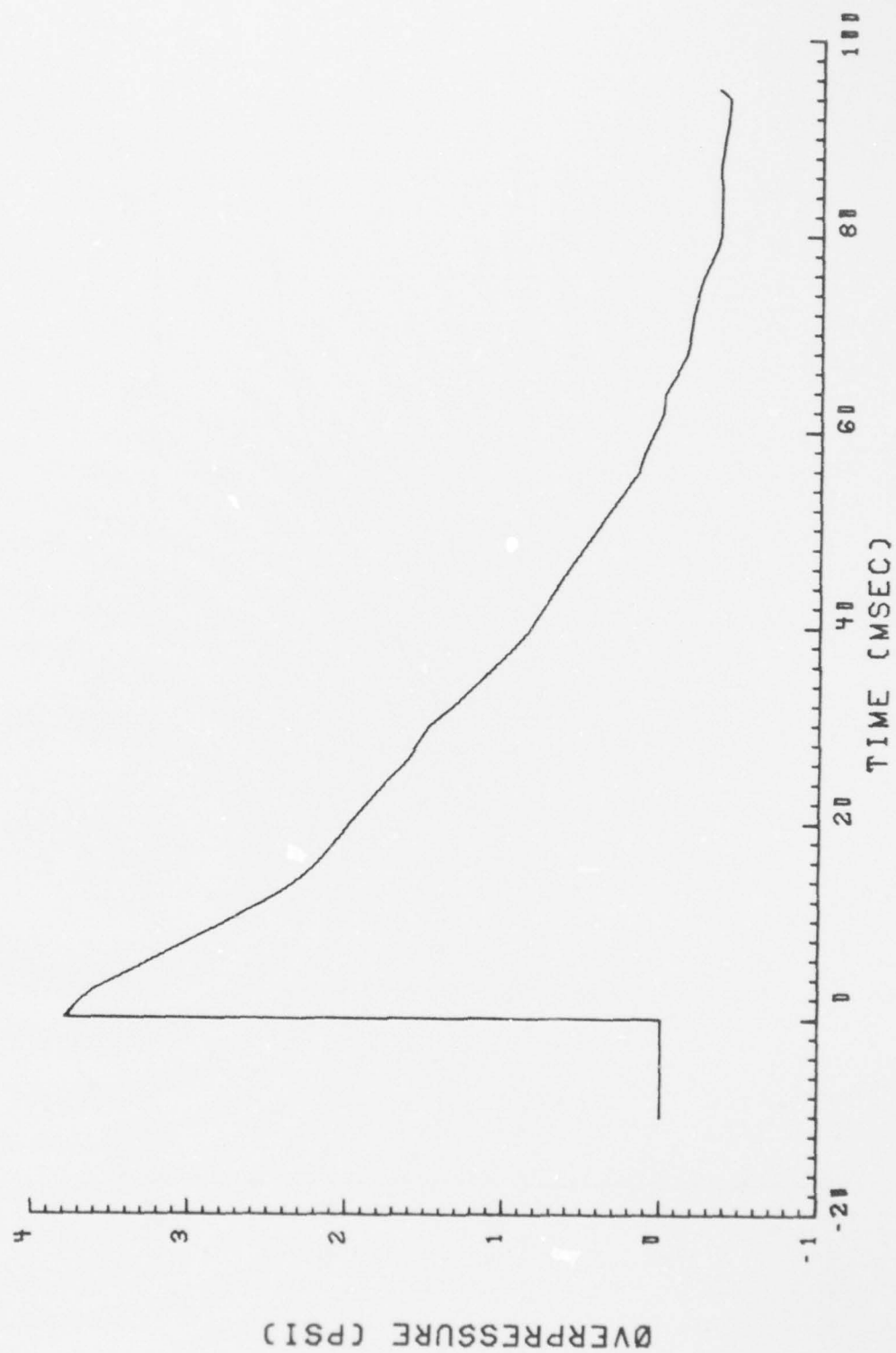


Figure 21. Blast flow conditions at the sled for Run 9B-A5, Intercept 2.

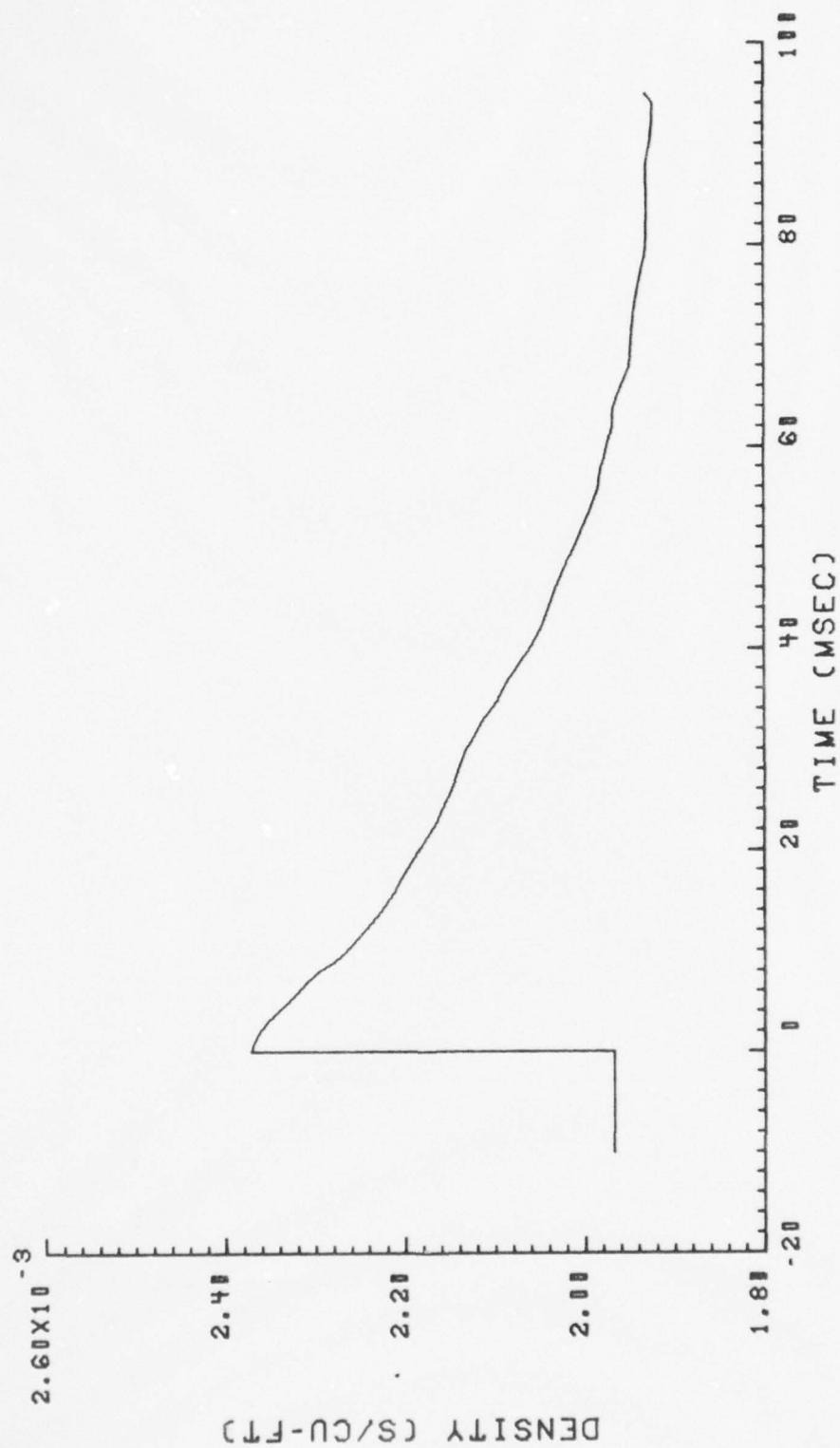


Figure 21. Continued.

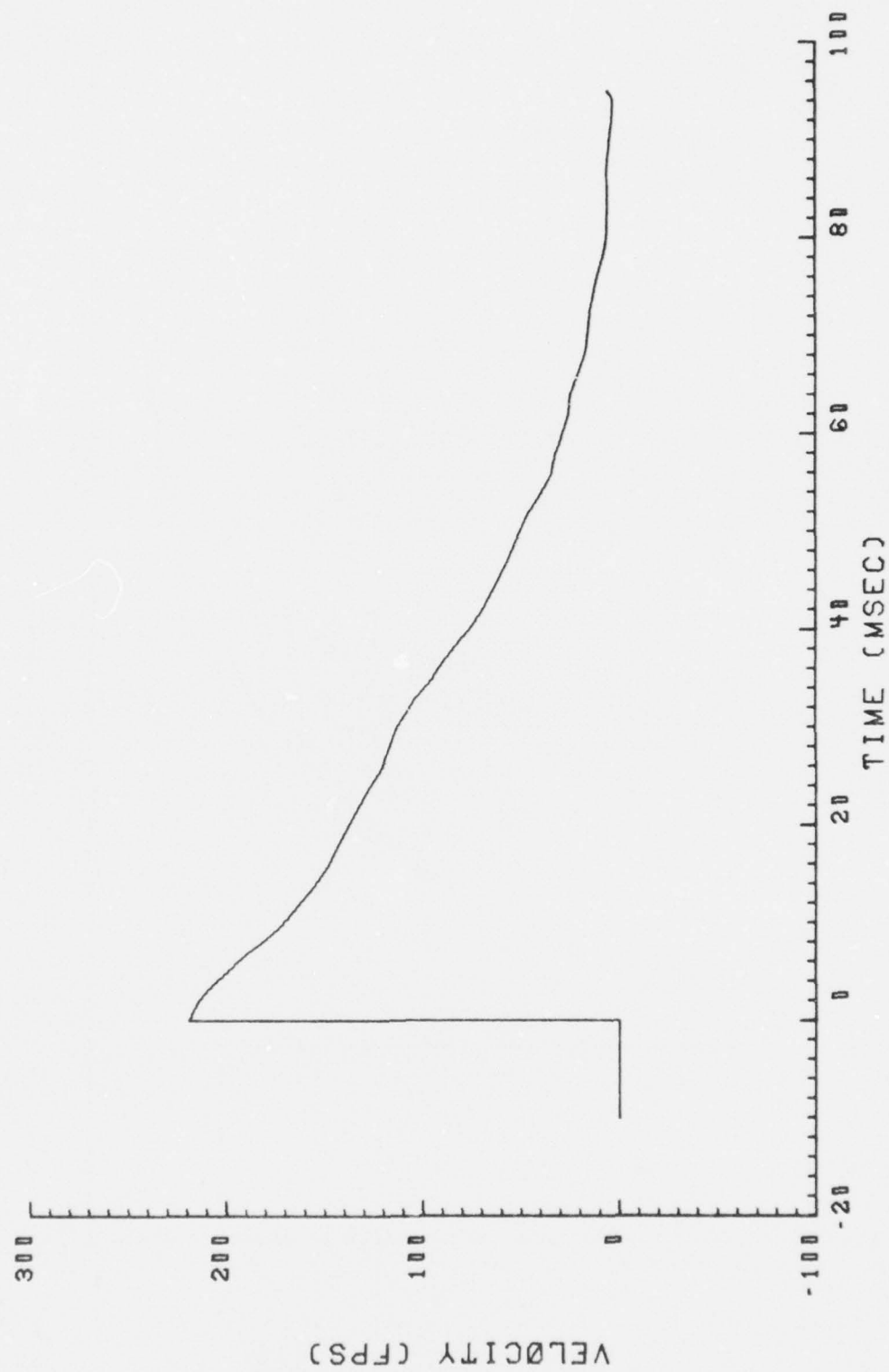


Figure 21. Concluded.

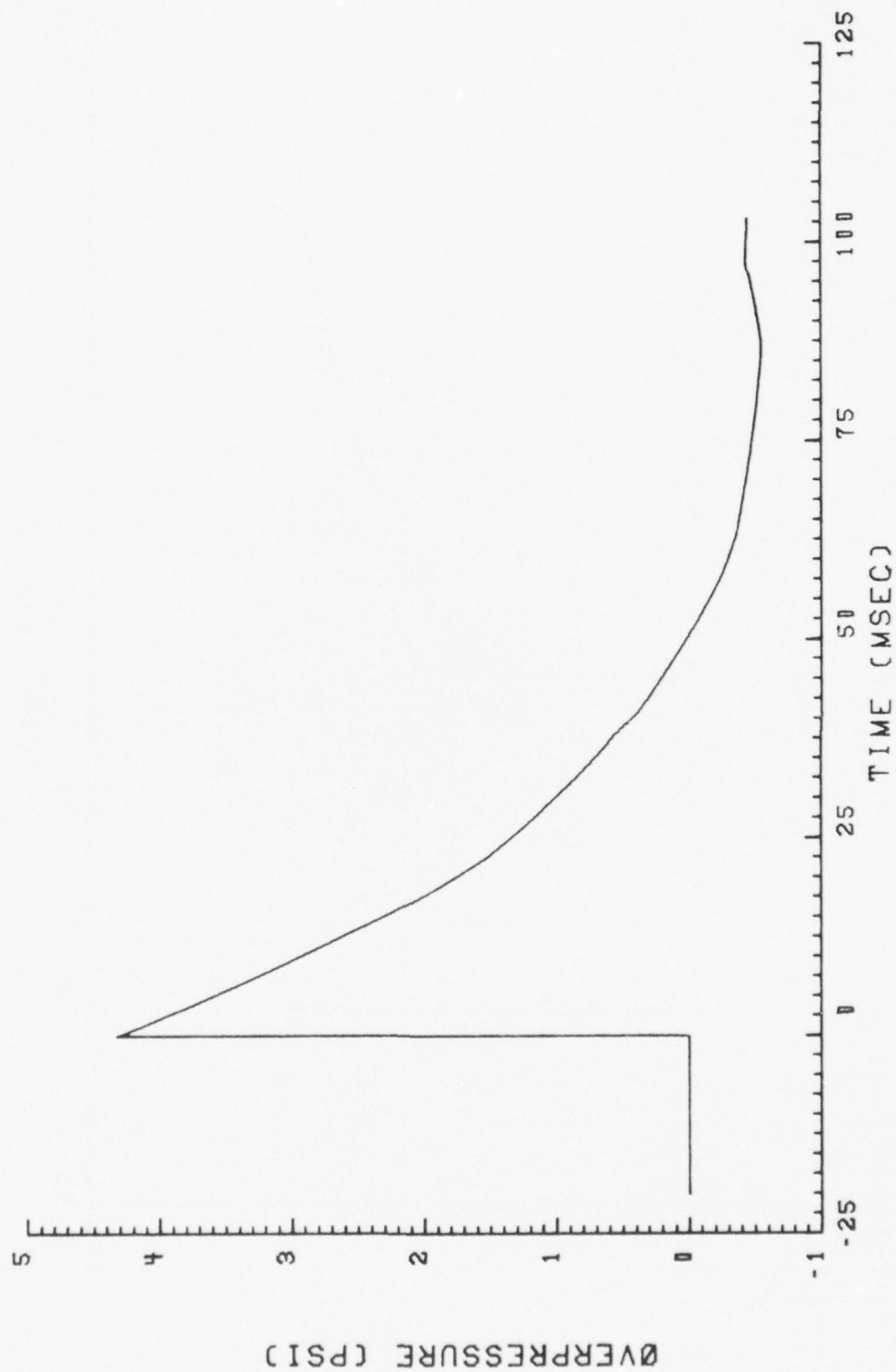


Figure 22. Blast flow conditions at the sled for Run 9B-A5, Intercept 3.

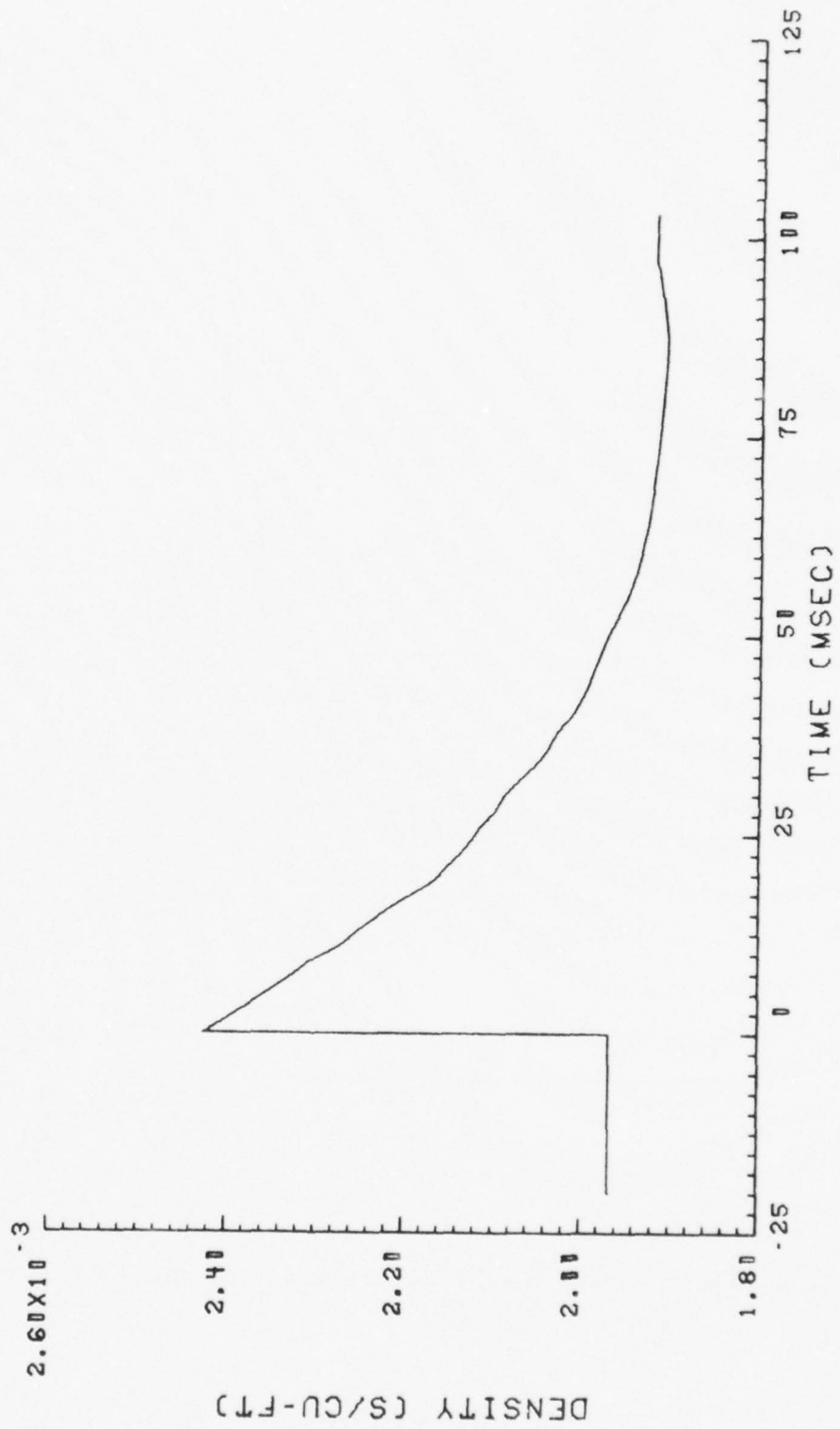


Figure 22. Continued

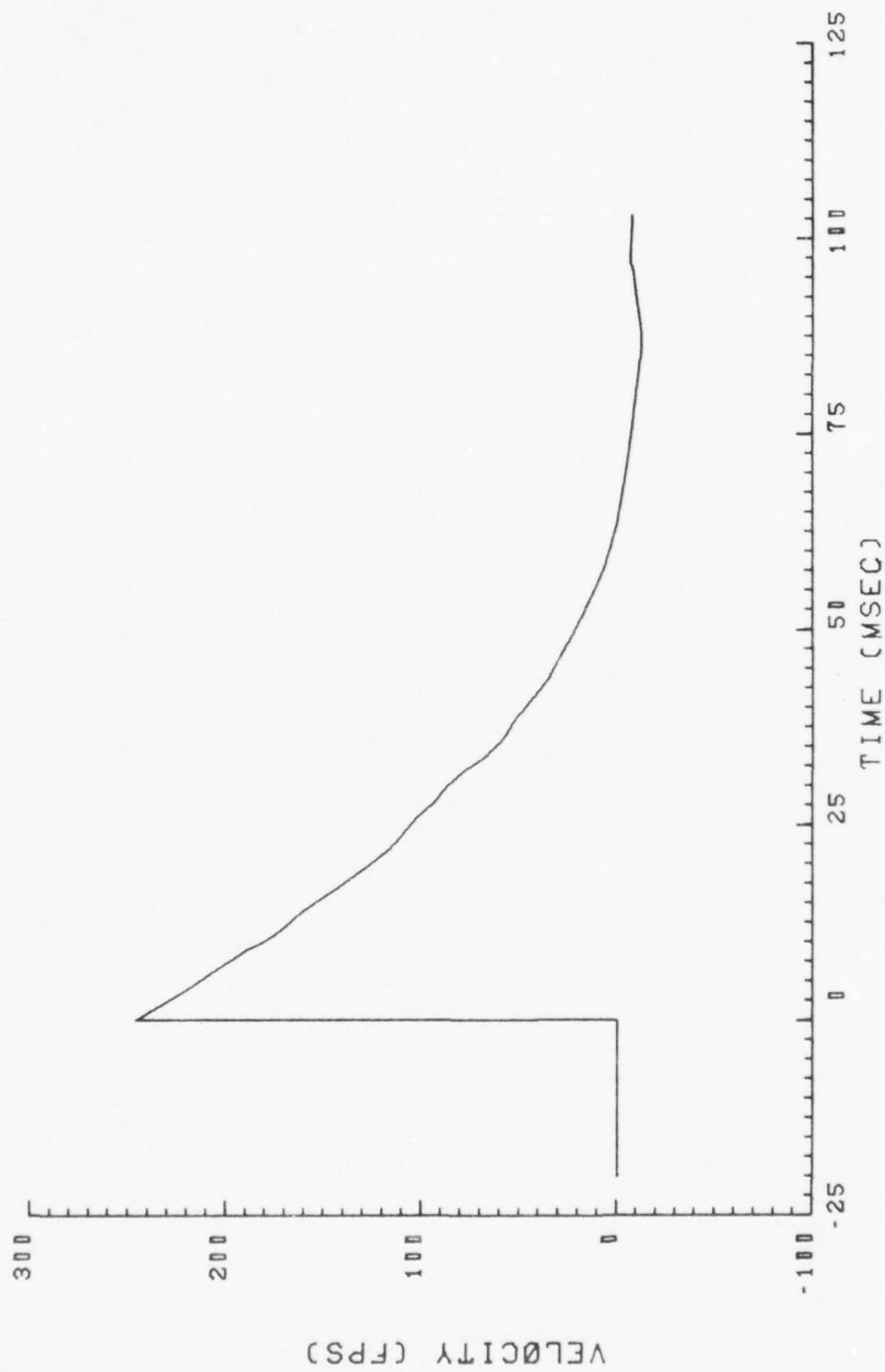


Figure 22. Concluded

SECTION 6

DISCUSSION

The objective of this report is to document the Phase 2 sled test results and to lay a foundation for correlations of these data with theoretical calculations based on the VIBRA-6 or other blast vulnerability codes. It is planned to discuss the obtained pressure data in detail in a subsequent volume, in which the test data will be compared with predictions of the VIBRA-6 code. The discussion in this section deals only with the tuft photographs obtained during the tests.

6.1 MOTION OF TUFTS

Two 35-mm cameras and an image motion camera (IMC) were used for viewing the tuft motion before and after the intercept of the second blast wave of Run 9B-A5. The FX-2 35-mm camera was located so its field of view was centered at the desired intercept point, track station 13153. The FX-3 35-mm camera was located so its field of view was centered 10 feet further north, track station 13163, that is, 10 feet further along the track in the direction of sled travel. The IMC camera views the sled through essentially a vertical slit, which viewed the sled 5 feet further north, track station 13168.

A 14-frame sequence of the film from the FX-2 camera is presented in Figure 23a through c. The nominal frame rate of the two FX cameras was 2500 fps. The five frames in Figure 23a and the first frame of Figure 23b indicate the flow prior to blast intercept. The first indication of the blast intercept is in Figure 23b, frame 7, where the tufts near the leading edge of the two most outboard rows of tufts are yanked so as to essentially align with the leading edge. In the next frame this effect shows up over a larger portion of the three most outboard rows of tufts and along the remainder of the leading edge. The tufts, except near the root, continue to swing around toward the forward direction through the remainder of the frames of the FX-2 camera, Figure 23a-c.

FIGURE 23.

PHOTOGRAPHS OF TUFTS ON LOWER WING
AT
SECOND INTERCEPT OF RUN 9B-A5.

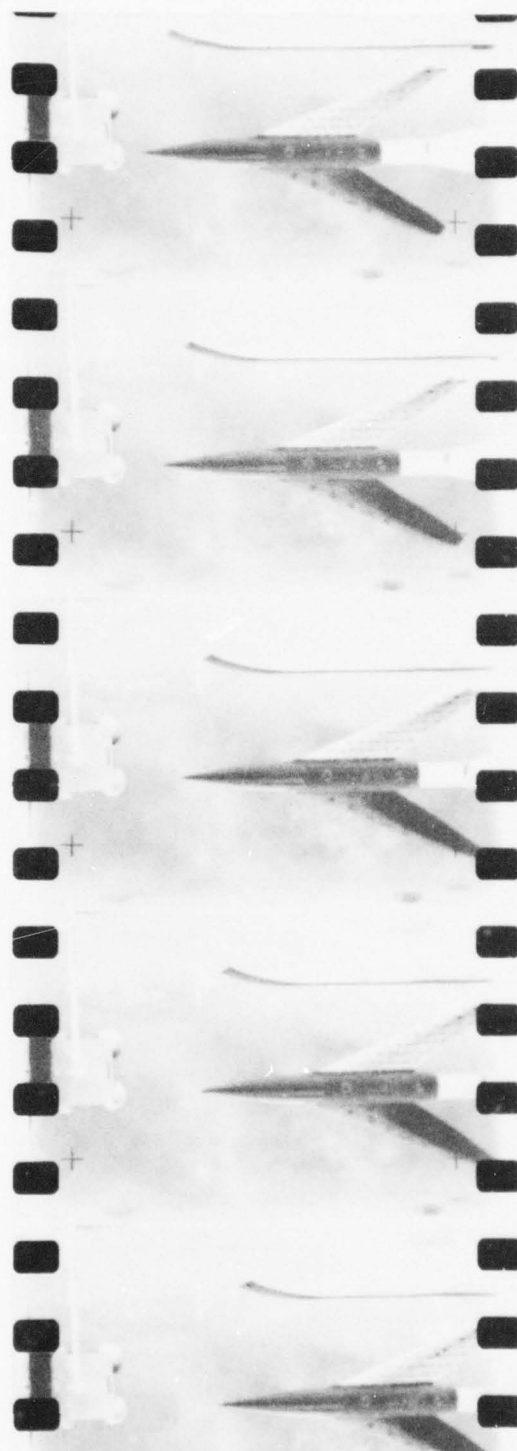


Figure 23a. Frames 1-5 of camera FX-2

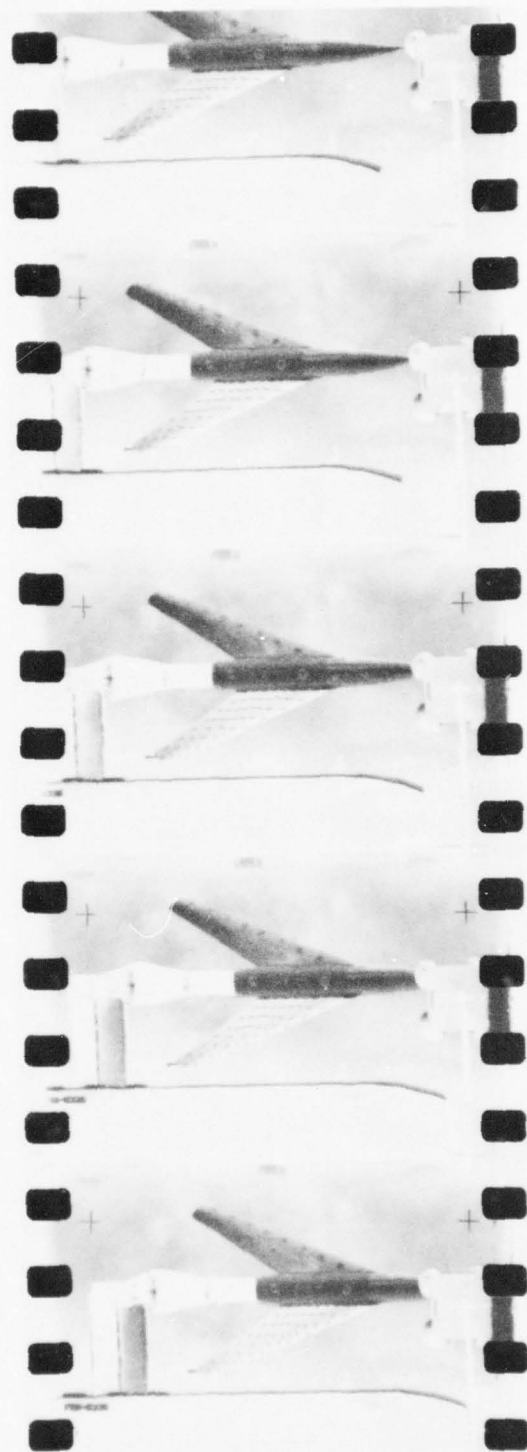


Figure 23b. Frames 6-10 of camera FX-2

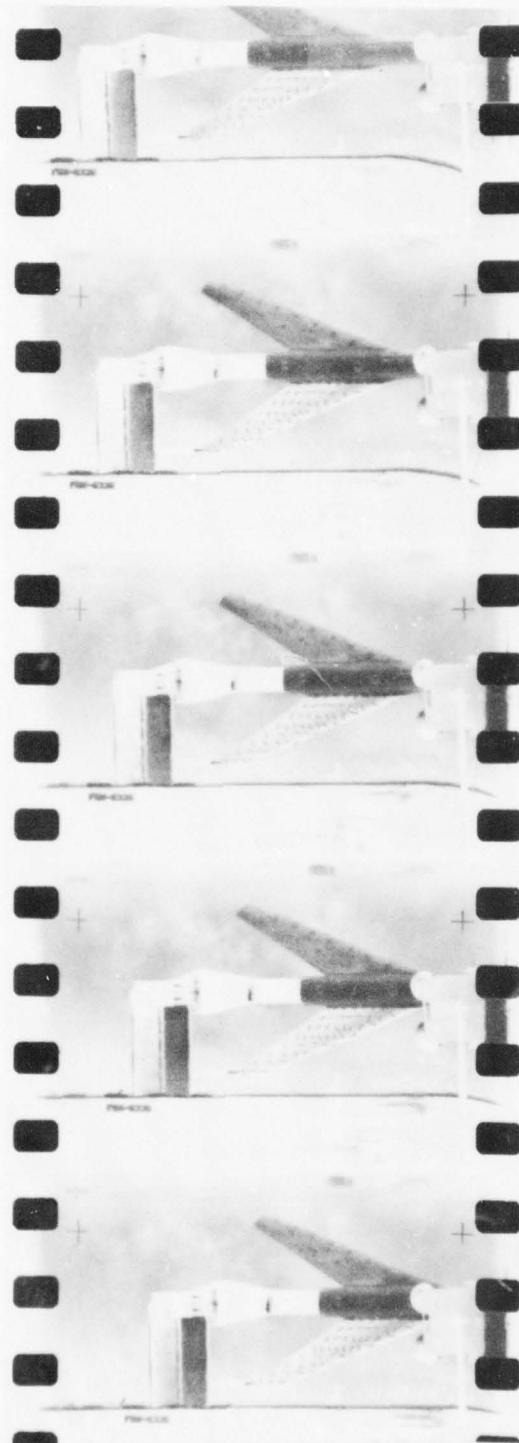


Figure 23c. Frames 10-14 of camers FX-2

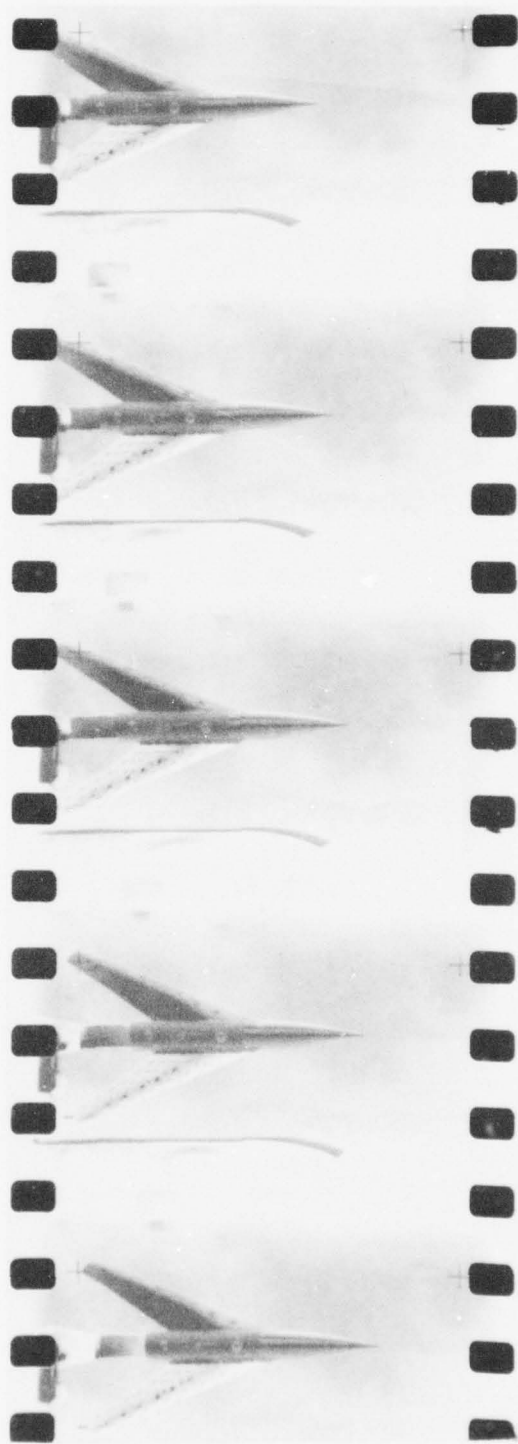


Figure 23d. Frames 1-5 of camera FX-3

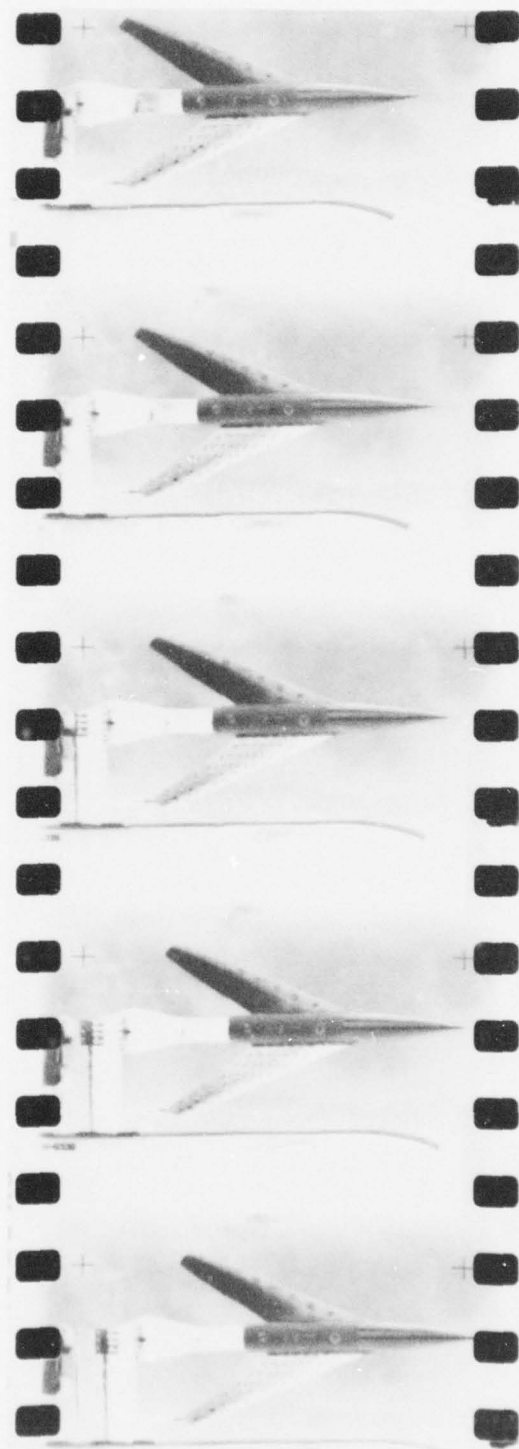


Figure 23e. Frames 7-11 of camera FX-3

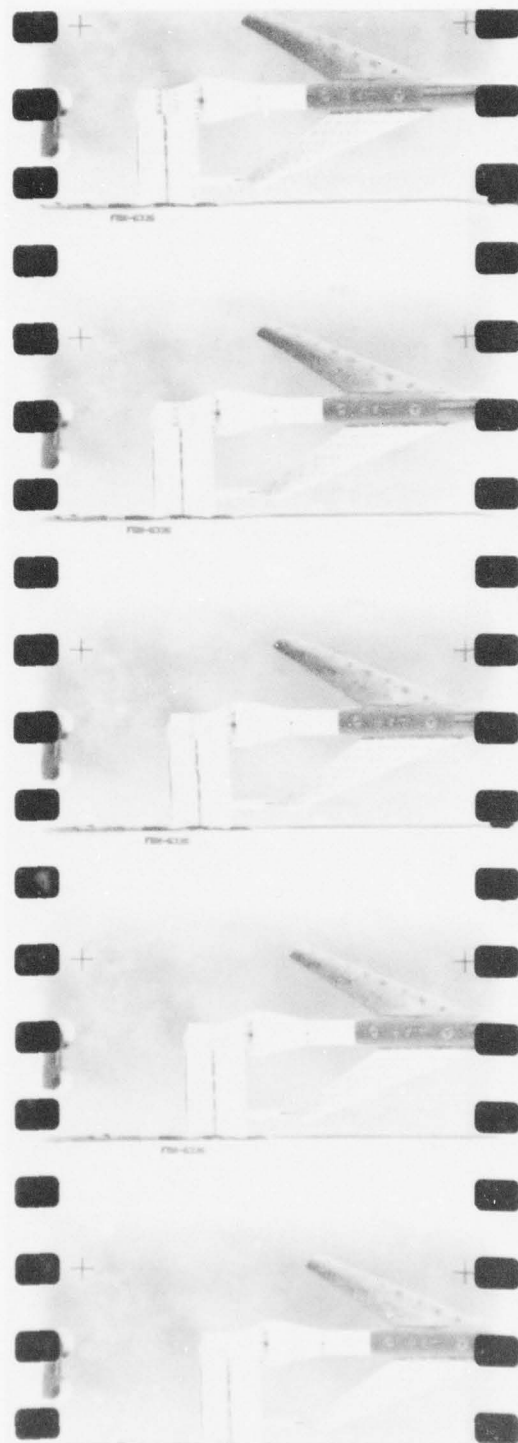


Figure 23f. Frames 15-19 of camera FX-3

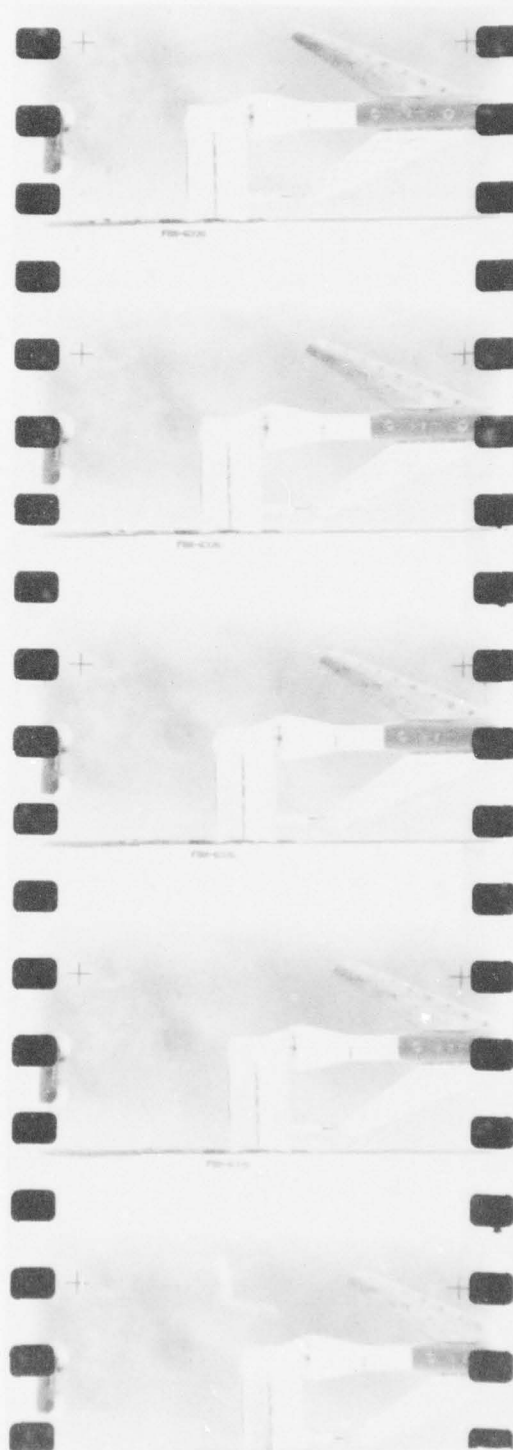


Figure 23g. Frames 18-22 of camera FX-3

The rotation of the tufts from the rearward direction prior to blast intercept to the forward direction following intercept is confirmation of the vortex that is formed on the leeward surface of the wing due to the blast wave. The intercept period observed by the FX-2 frames shown here is about 3.2 milliseconds for the nominal camera rate of 2500 fps, which is the period when the vortex appears to form at the leading edge and starts to move rearward according to the differential pressure records.

The FX-3 camera Figure 23d, picks up the wing about 5 milliseconds later. The tufts appear to indicate the vortex has a high sweep angle. Forward of the apparent vortex location outboard on the wing the tufts have the rather random orientation characteristic of flow ahead of such a vortex. The FX-3 frames, Fig. 23d-g, extend over a nominal period of about 8.8 milliseconds, so the last frame is about 17 milliseconds after blast intercept. At this time the vortex is not expected to have started to return toward the leading edge.

The photograph of the image motion camera is shown in Figure 24. This is a moving-focal plane picture so it is equivalent, as mentioned, to a view through a vertical slit. This view is taken about 17 milliseconds after blast intercept. At this time the vortex may have started moving forward, but it is expected to be near the most rearward position. The tuft pattern is similar to that from the FX-3 camera.

These tuft motions confirm the presence of the vortex on the leeward side of the wing following blast intercept for this near 90° intercept angle as was indicated by the time histories of the differential pressure measurements.

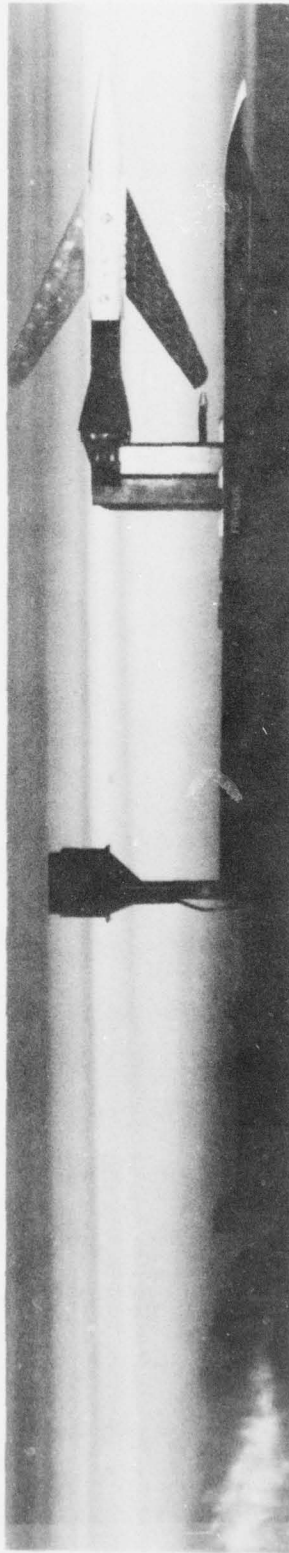


Figure 24. Image motion camera photograph of tufts on lower wing 15 feet north of second intercept of Run 9B-A5.

SECTION 7

CONCLUDING REMARKS

Blast loadings have been measured on a rigid 65 deg-sweepback wing at Mach 0.76 in two sled runs. In Run 9B-A4 the wing was rolled 45 degrees to achieve a blast intercept from the left side of the model. In Run 9B-A5 all intercepts were symmetrical. A 10,000-lb charge of TNT was used in one intercept of this second run compared with 1,000-lb charges of TNT for other intercepts to examine blast duration effects. All intercepts had about a 4-psi shock overpressure.

The effect of a strong leading-edge vortex was evident on the loadings, particularly for peak blast induced angles of attack greater than 10 degrees, so tufts were mounted on the leeward side of the wing and photographed during the tests. The tuft pictures did verify the presence of the vortex and showed its marked influence on the flow direction at the wing surface.

The objective of this report is to describe the tests and present the test data. The VIBRA-6 code predictions are to be compared with the measured blast loadings in a separate report. The blast properties at the model have been determined and presented for both runs. The loading data for the wing have been verified for Run 9B-A4; the data from Run 9B-A5 were received too late for more than a first pass validation.

In light of the results obtained in these tests it is recommended that similar blast loading tests be conducted with a low-sweep rigid wing and with a flexible wing. It is expected that the results from all of these tests could essentially provide the data base required for validation of methods for prediction of blast airloads on wings of current military fixed-wing aircraft of interest.

REFERENCES

1. Ruetenik, J.R., and Smiley, R.F., Measurements of Blast Pressures on a Rigid 65° Sweptback Wing at Mach 0.76 from Rocket Propelled Sled Tests, Vol. I - Test Documentation, Kaman Avidyne Report TR-137, Vol. I, U.S. Defense Nuclear Agency, Report No. 4400F-1, 20 June 1977.
2. Holloman Track Capabilities, MDC-TDR-62-9, HAFB, September 1962.
3. Valle, Joe, Jr., Test Event Report, Aircraft Blast Interaction Test, Job Order No. 921DST01, Central Inertial Guidance Facility, Hdq. 6585th Test Group, Environmental Test Section, HAFB, NM, 15 March 1977.
4. Krupovage, D.J., Mode Shapes and NASTRAN Plots, 6585TH Test Group, HAFB, 28 March 1977, unpublished.
5. Ruetenik, J.R., and Lewis, S.D., Computation of Blast Properties for Spherical TNT or Pentolite from Measured Pressure Histories, AFFDL-TR-66-47, October 1966.
6. Brode, H.L., A Calculation of the Blast Wave from a Spherical Charge of TNT, RAND RM-1965, August 1957. (AD 144302).

APPENDIX A

PRESSURE AND ACCELERATION TIME HISTORIES

This appendix presents time histories of most of the measured blast-line and sled-borne transducer measurements obtained during the present test program, arranged as indicated in Table 9.

Material is presented here according to the chronological order of intercepts as indicated in Table 6. For each intercept blast-line pressures are presented first, followed by differential, blastward and leeward wing pressures, total pressure at the model and at the sled, static pressure at the sled, and wing acceleration.

The reference time for the origin of the time scale in each figure is indicated at the bottom of the figure in the form $T_0 = X-Y-Z$ where X designates hours, Y designates minutes and Z designates seconds. For Run 9B-A4, the reference times (T_0) for the blast line data are based on a nominal time standard which is different from the true time standard used for the rest of the data; examination of the test data indicates that true T_0 values may be obtained for the 9B-A4 blast line plots by subtracting 1-5-47.304 from the indicated T_0 values.

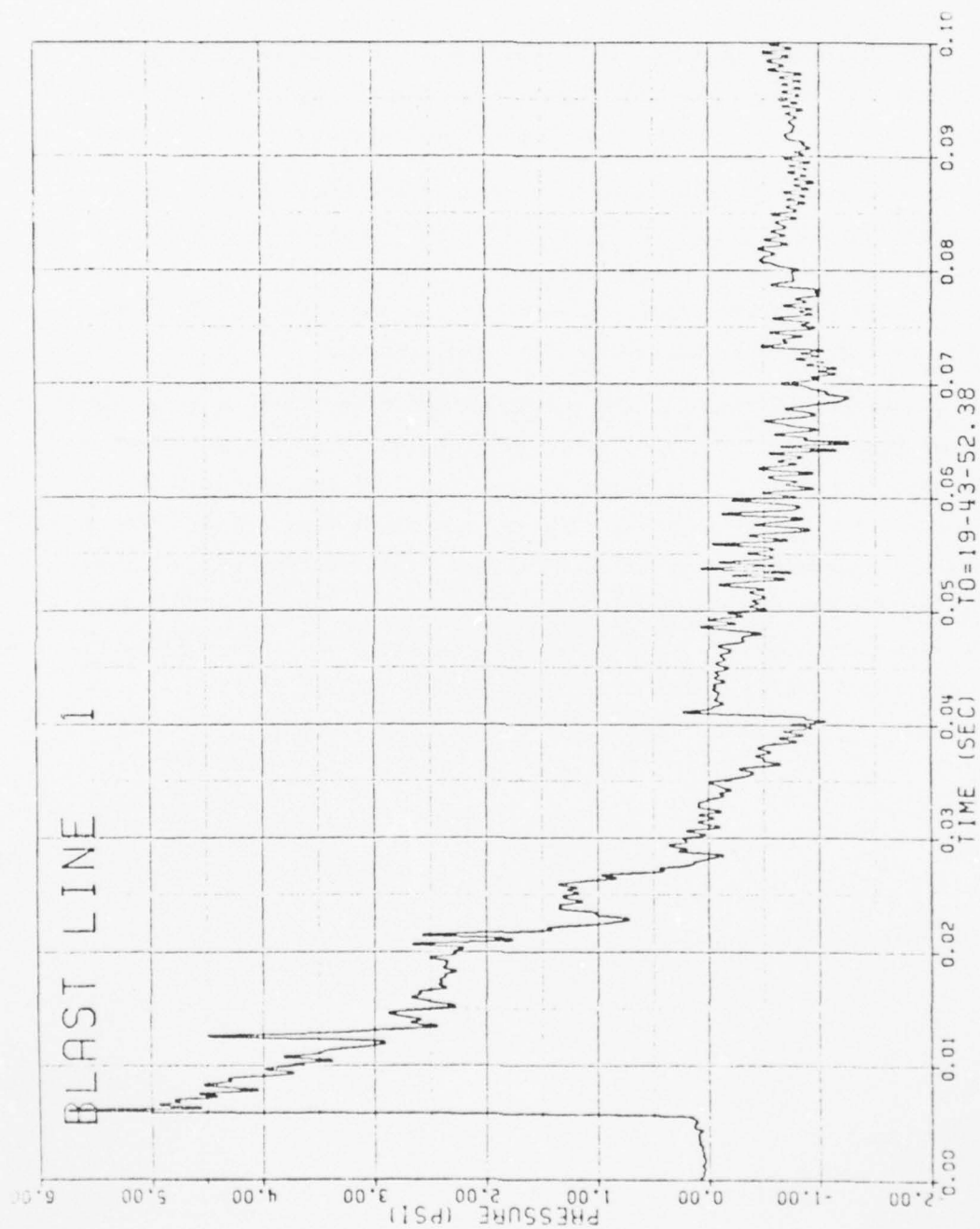


Figure 25. Blast-Line Overpressures, Run 9B-A4, Intercept 1.

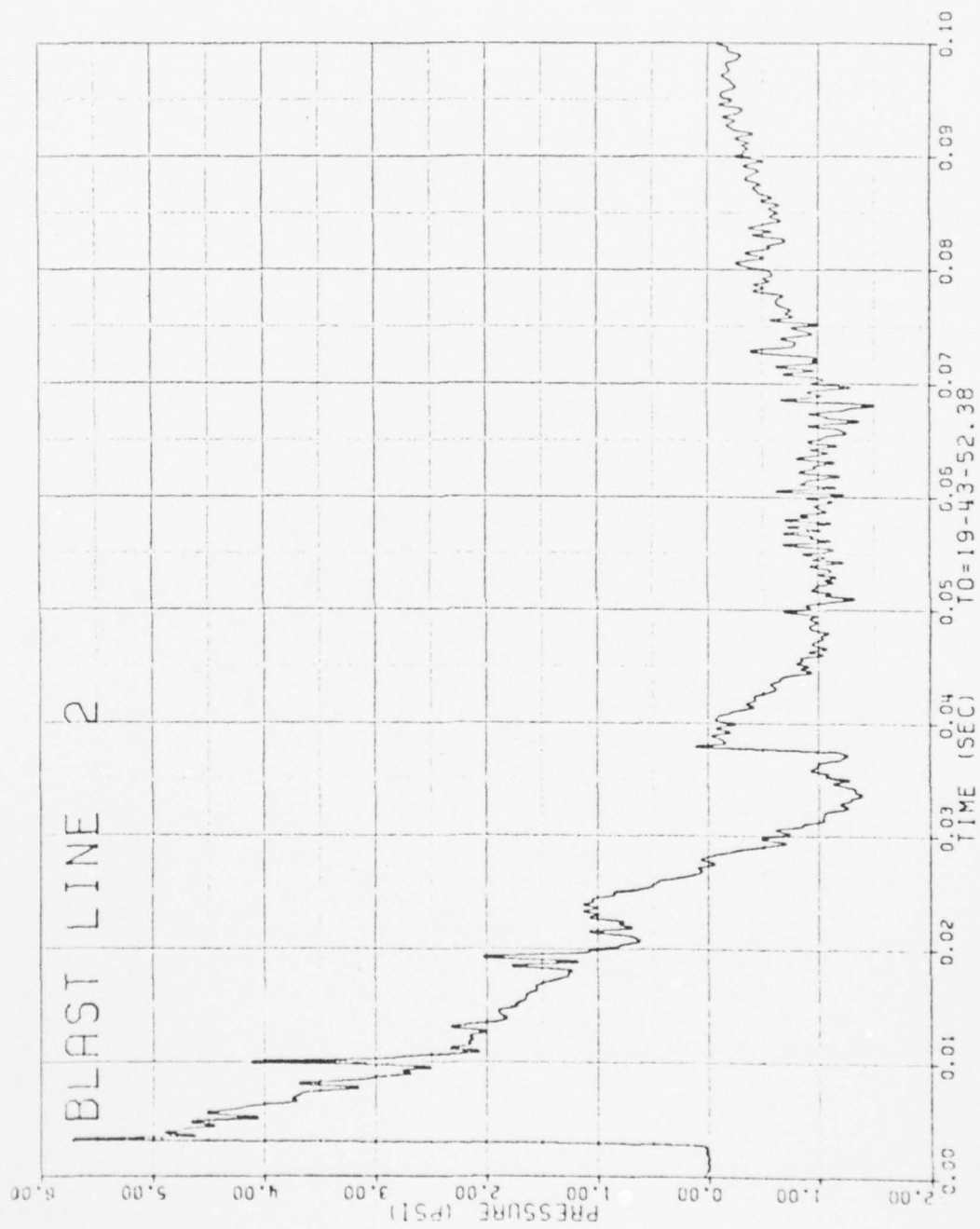


Figure 25. Continued

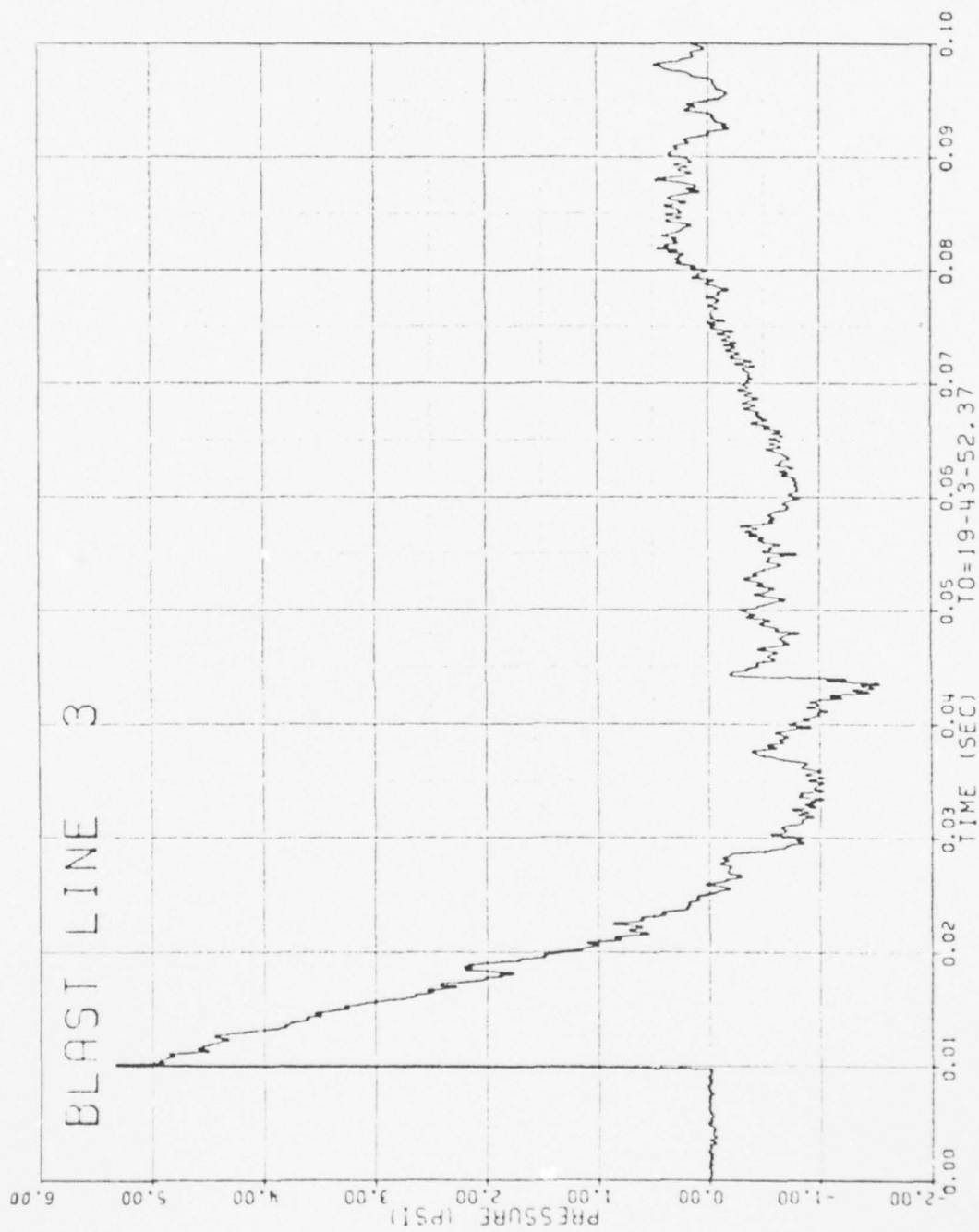


Figure 25. Continued

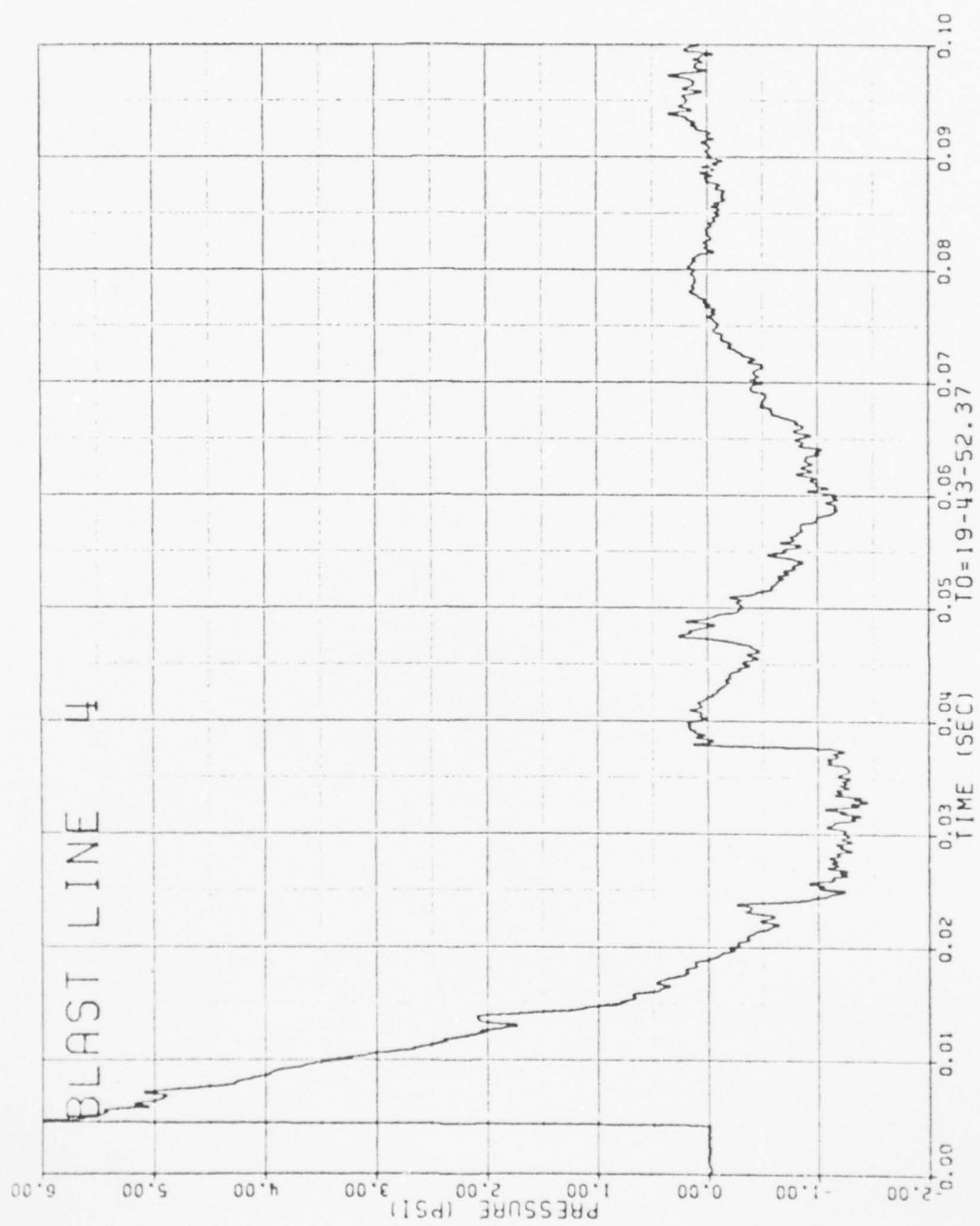


Figure 25. Concluded

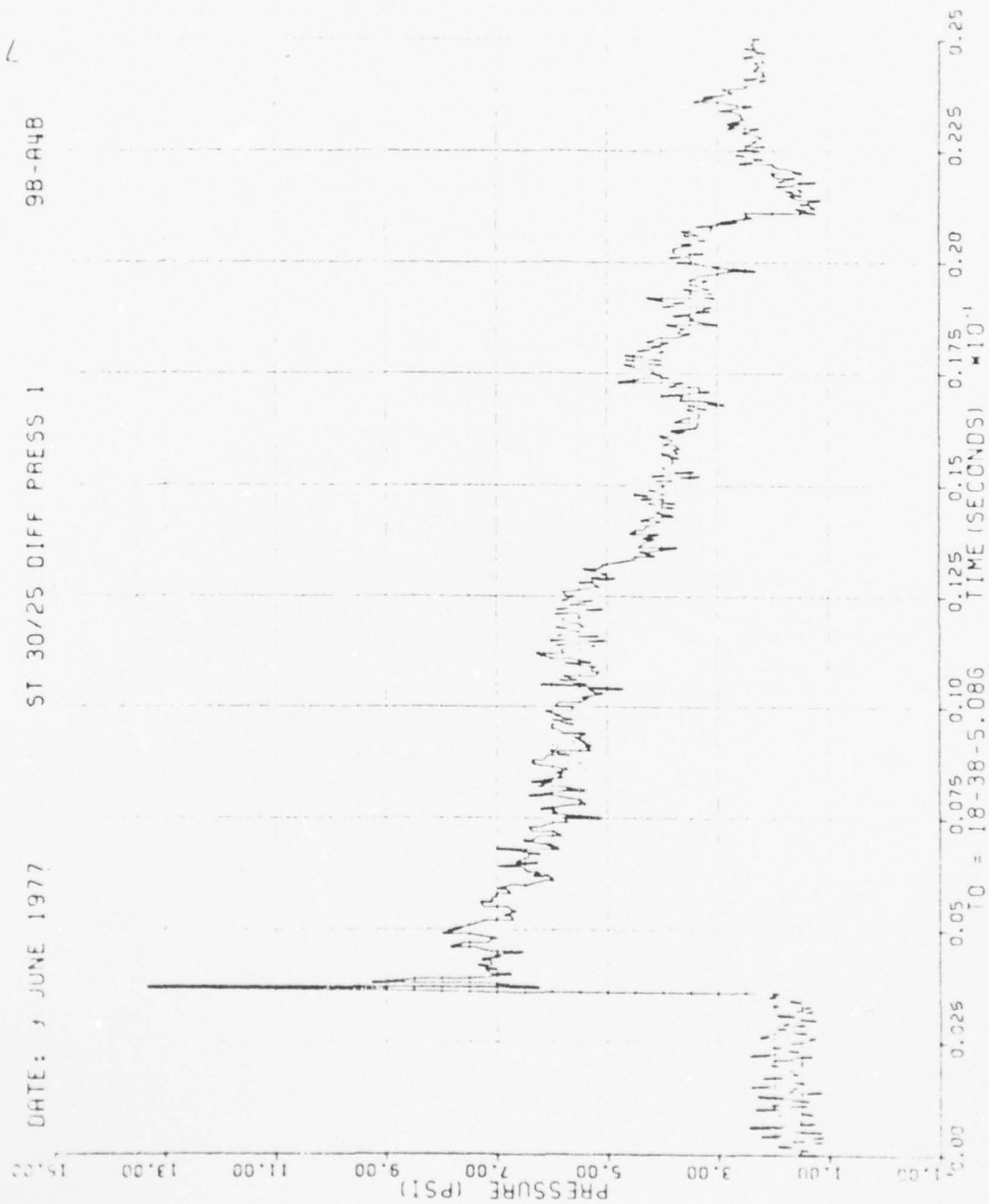


Figure 26. Differential Wing Pressures, Run 9B-A4, Intercept 1.

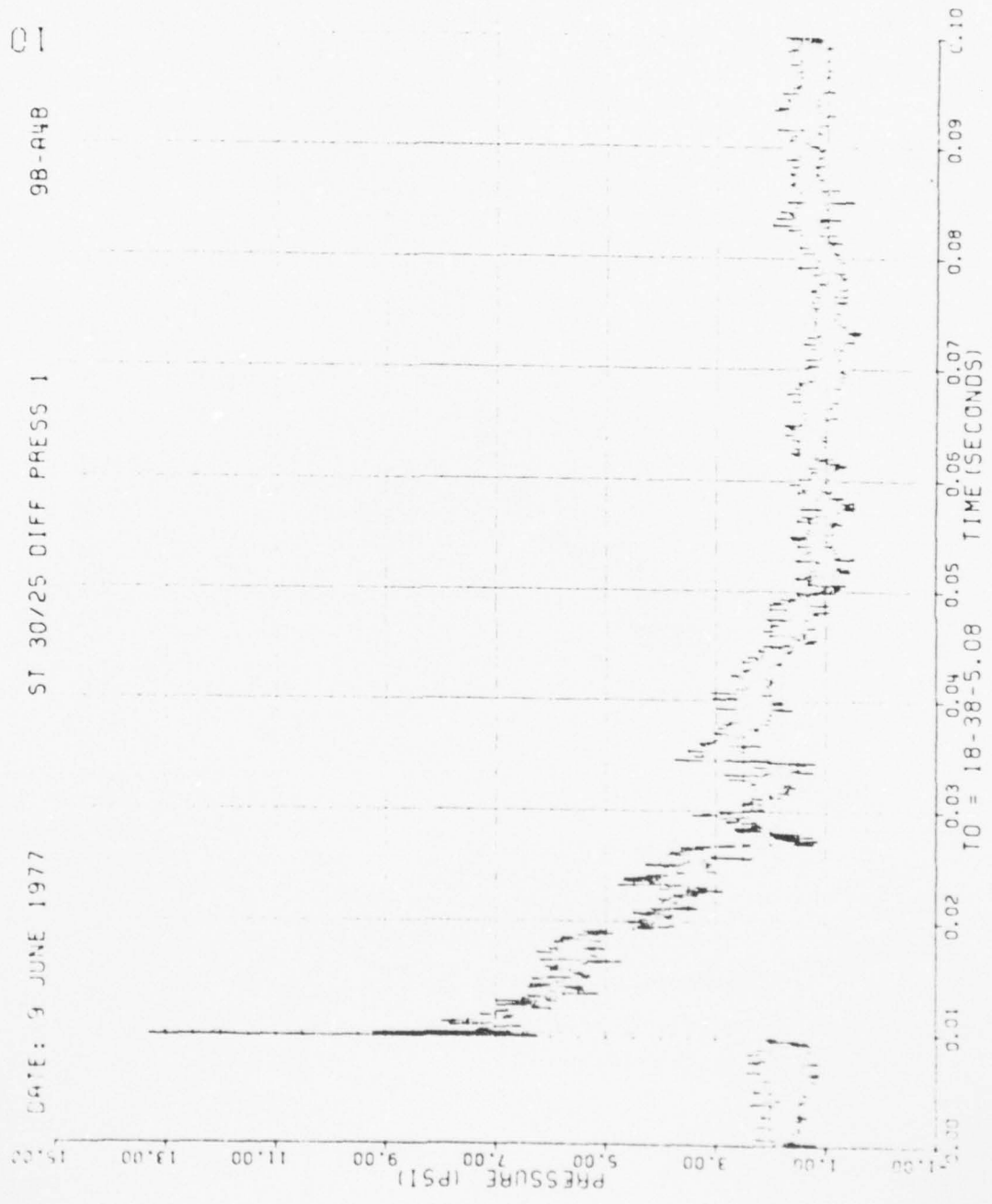


Figure 26. Continued

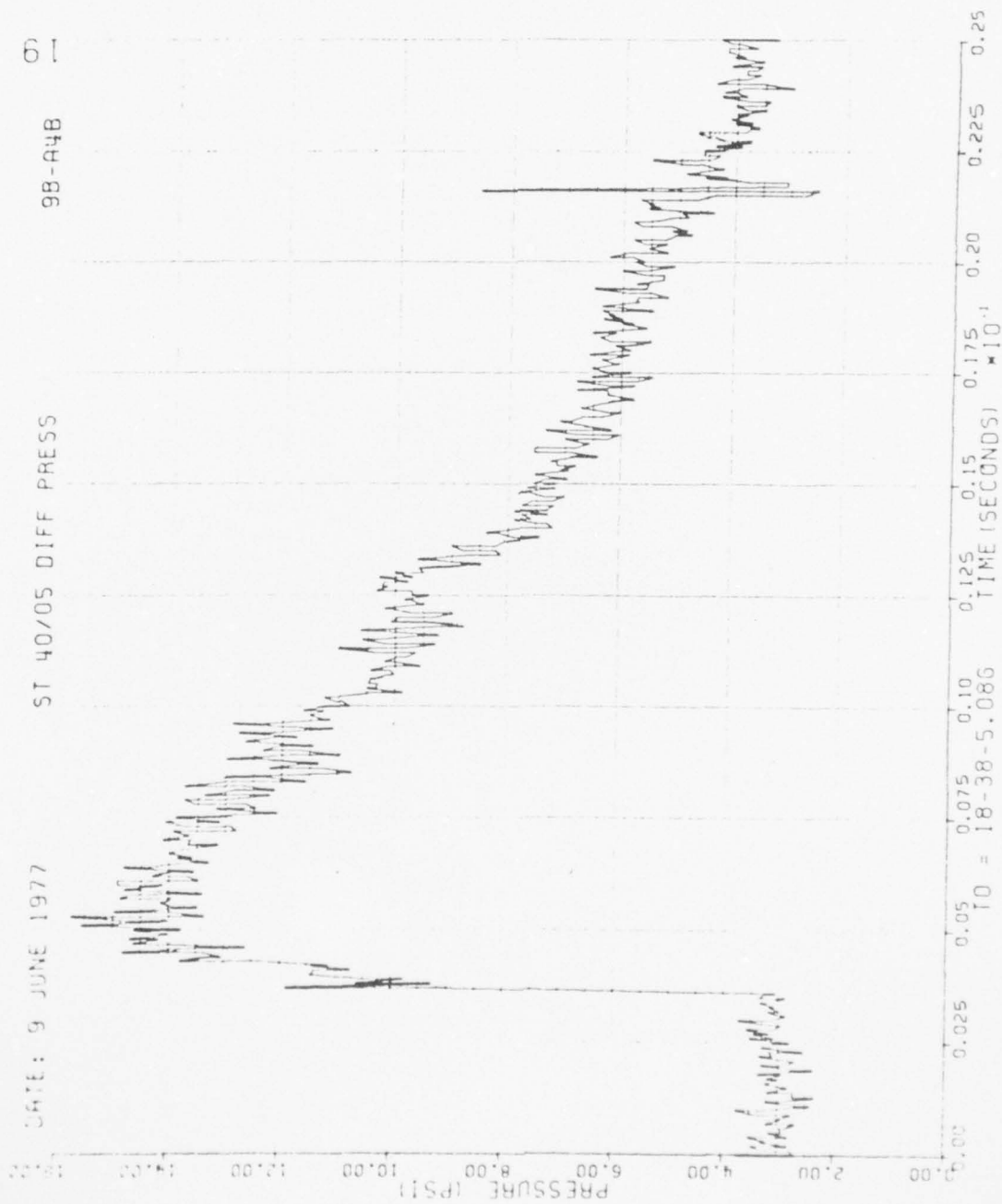


Figure 26. Continued

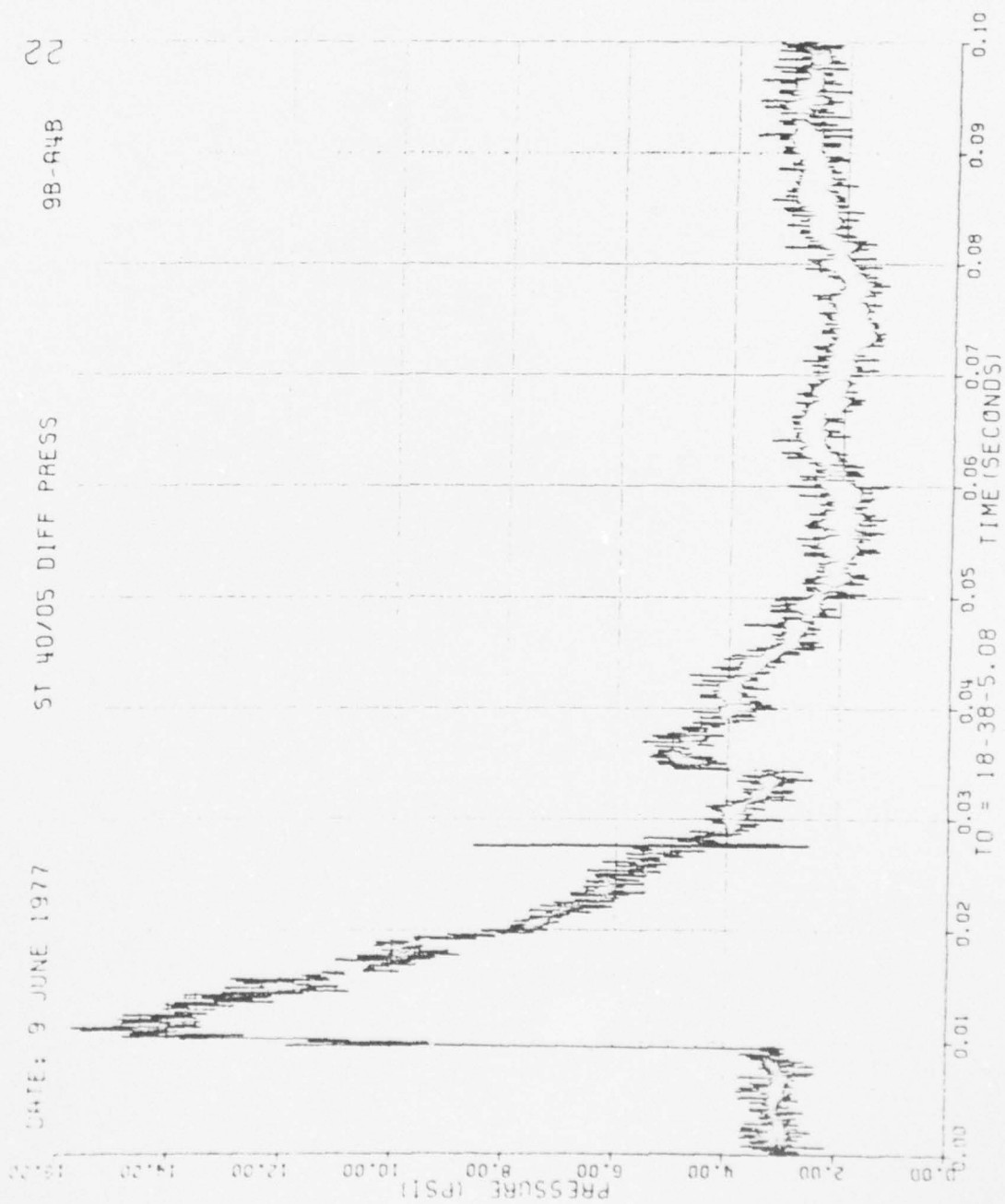


Figure 26. Continued

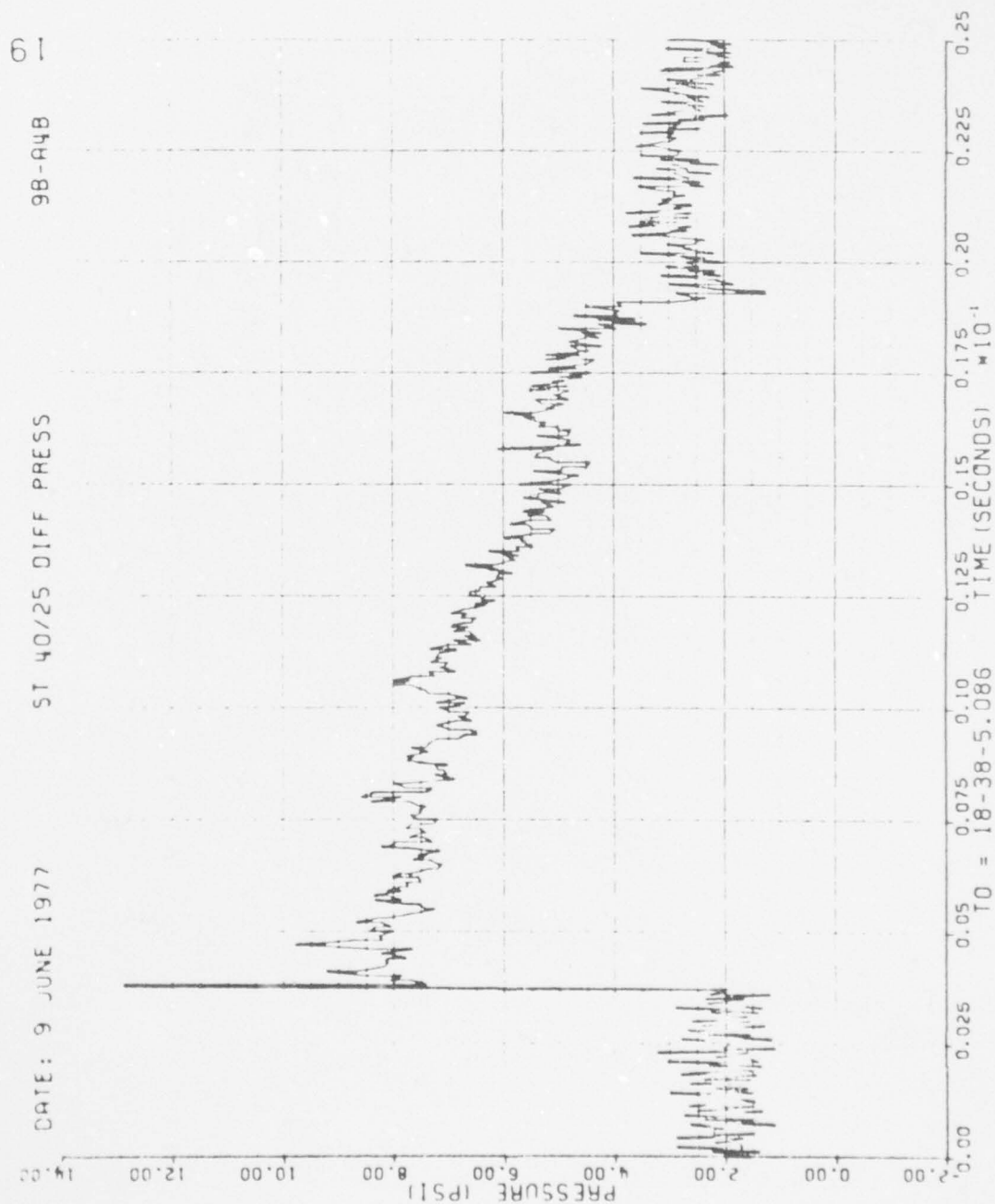


Figure 26. Continued

AD-A062 408

KAMAN AVIDYNE BURLINGTON MASS

F/G 1/3

MEASUREMENTS OF BLAST PRESSURES ON A RIGID 65 DEG SWEEPBACK WIN--ETC(U)

JAN 78 J R RUETENIK, R F SMILEY

DNA001-76-C-0106

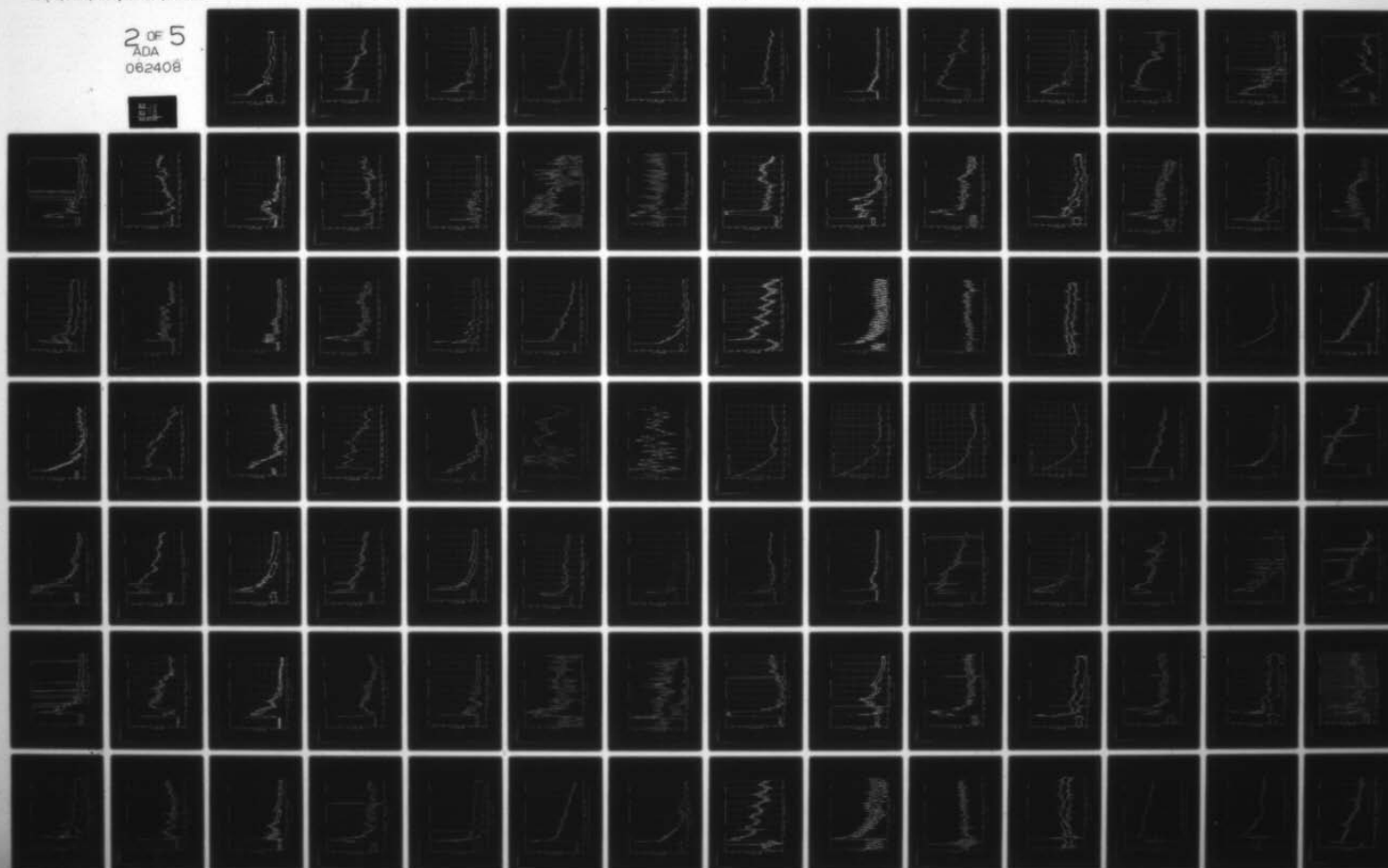
UNCLASSIFIED

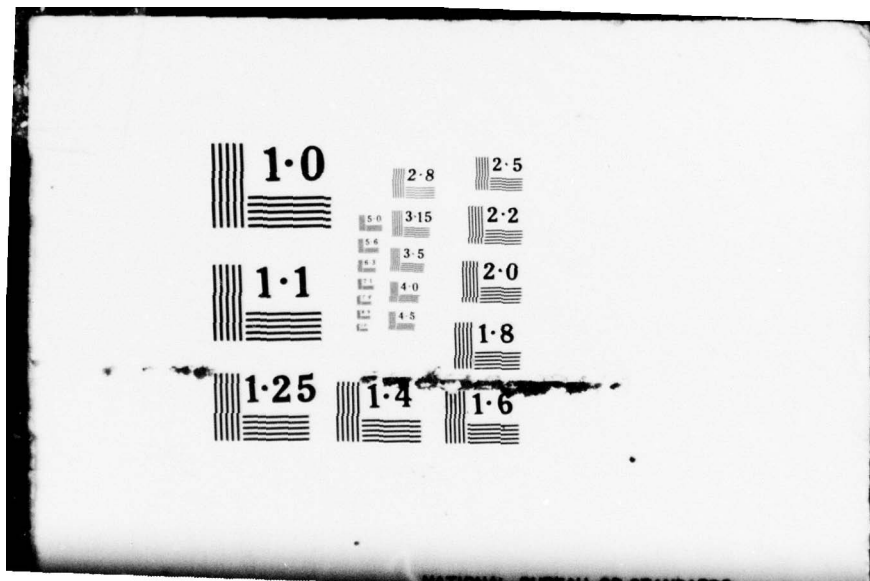
KA-TR-145

DNA-4504F

NL

2 OF 5
ADA
062408





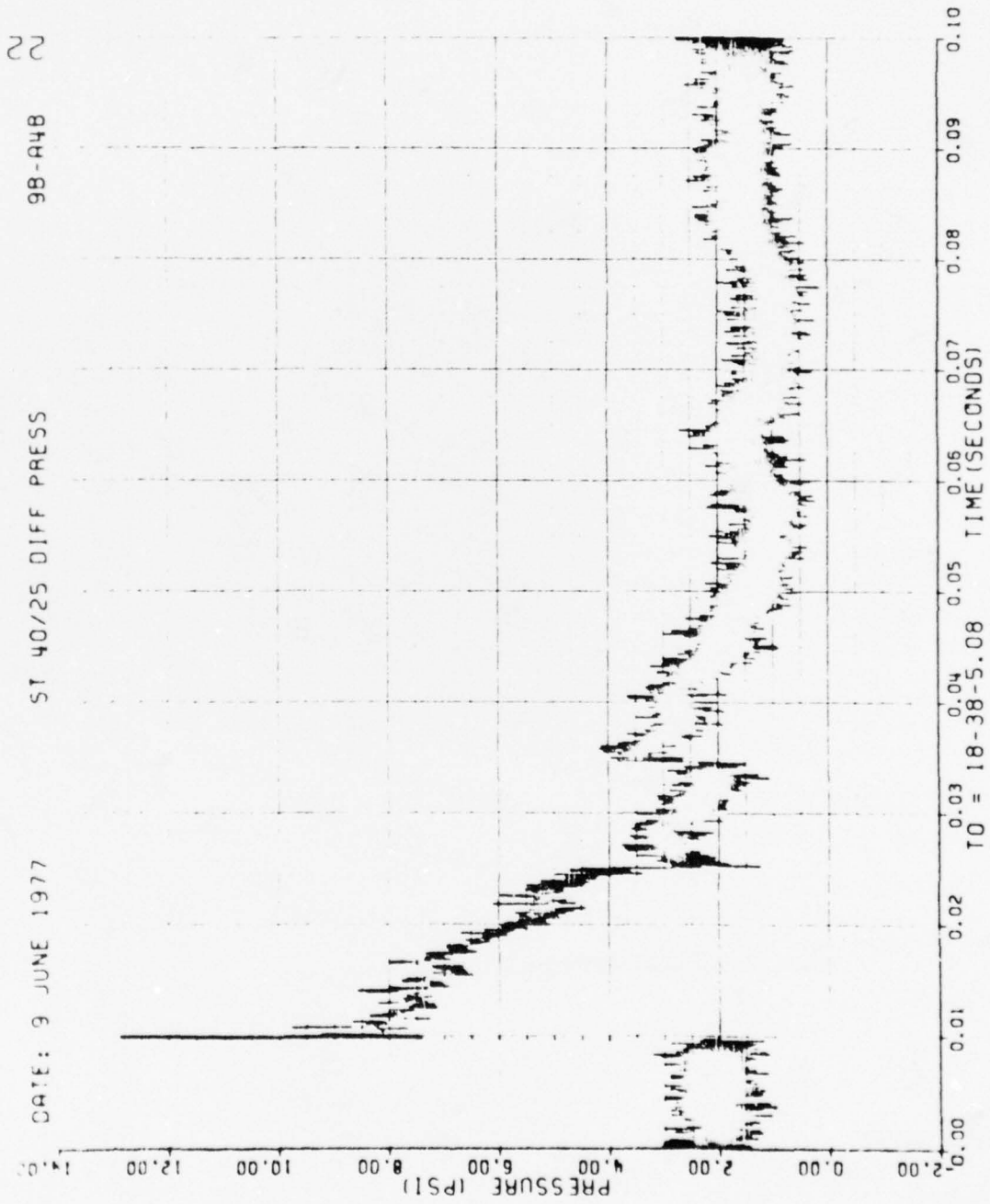


Figure 26. Continued

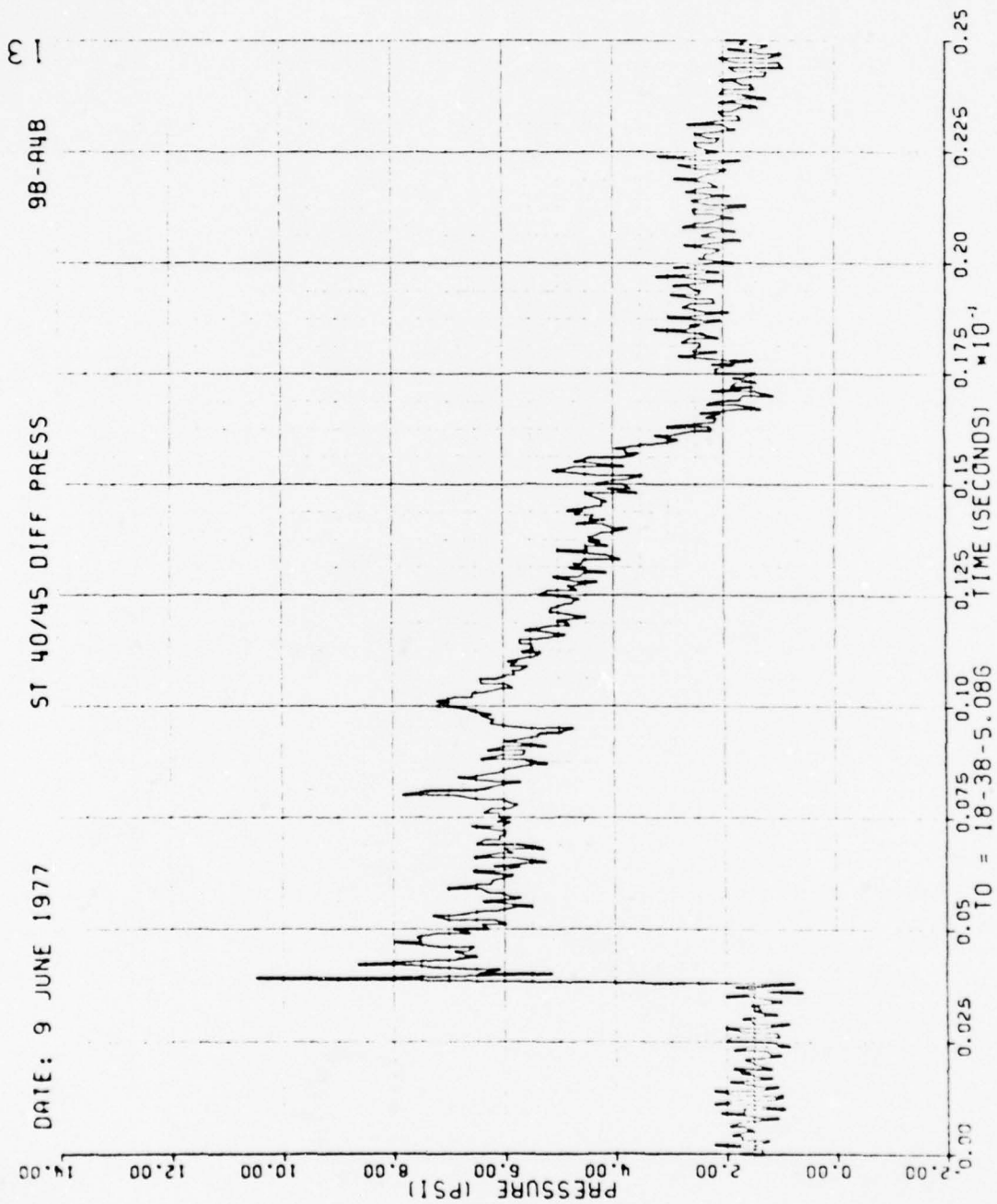


Figure 26. Continued

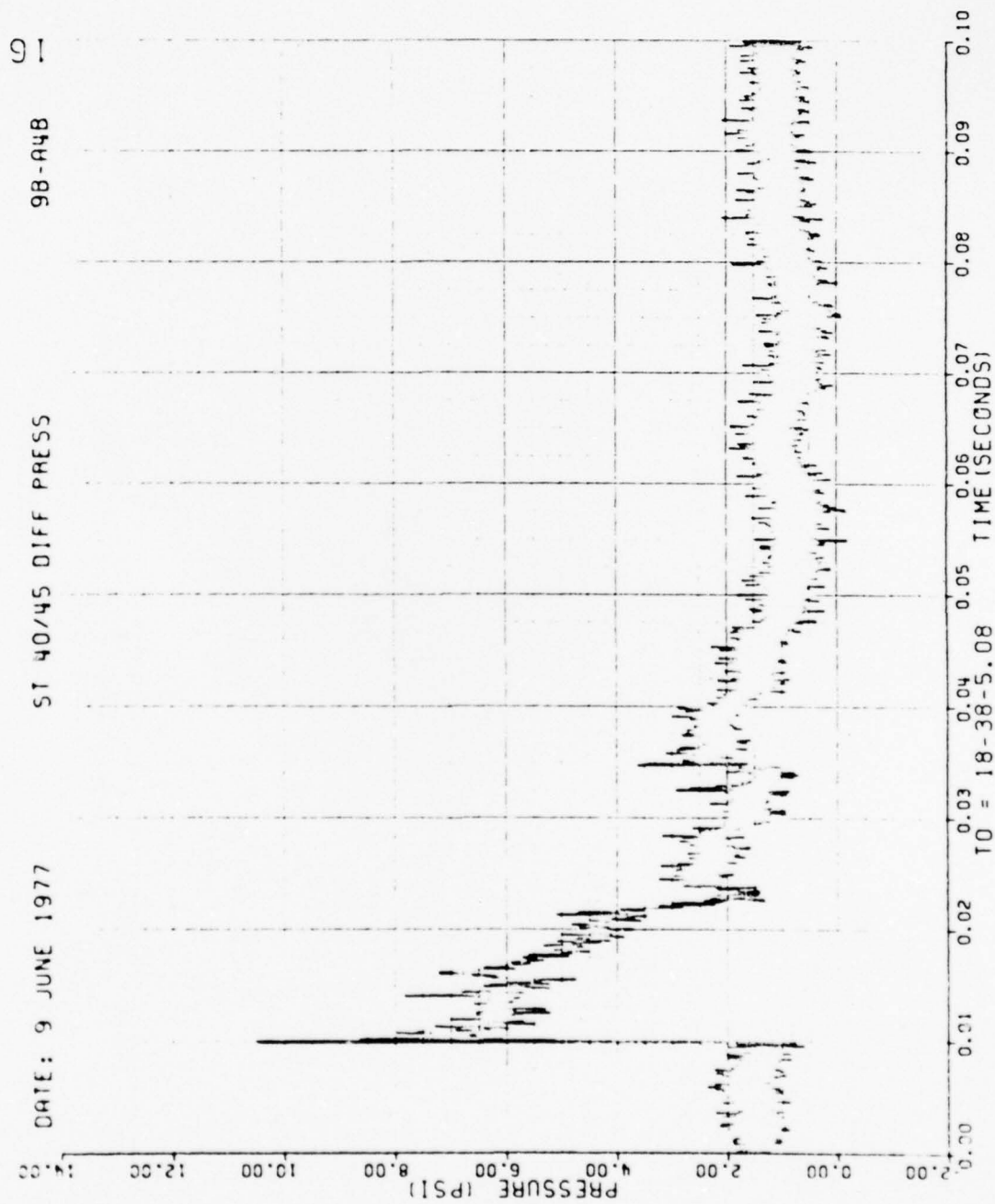


Figure 26. Continued

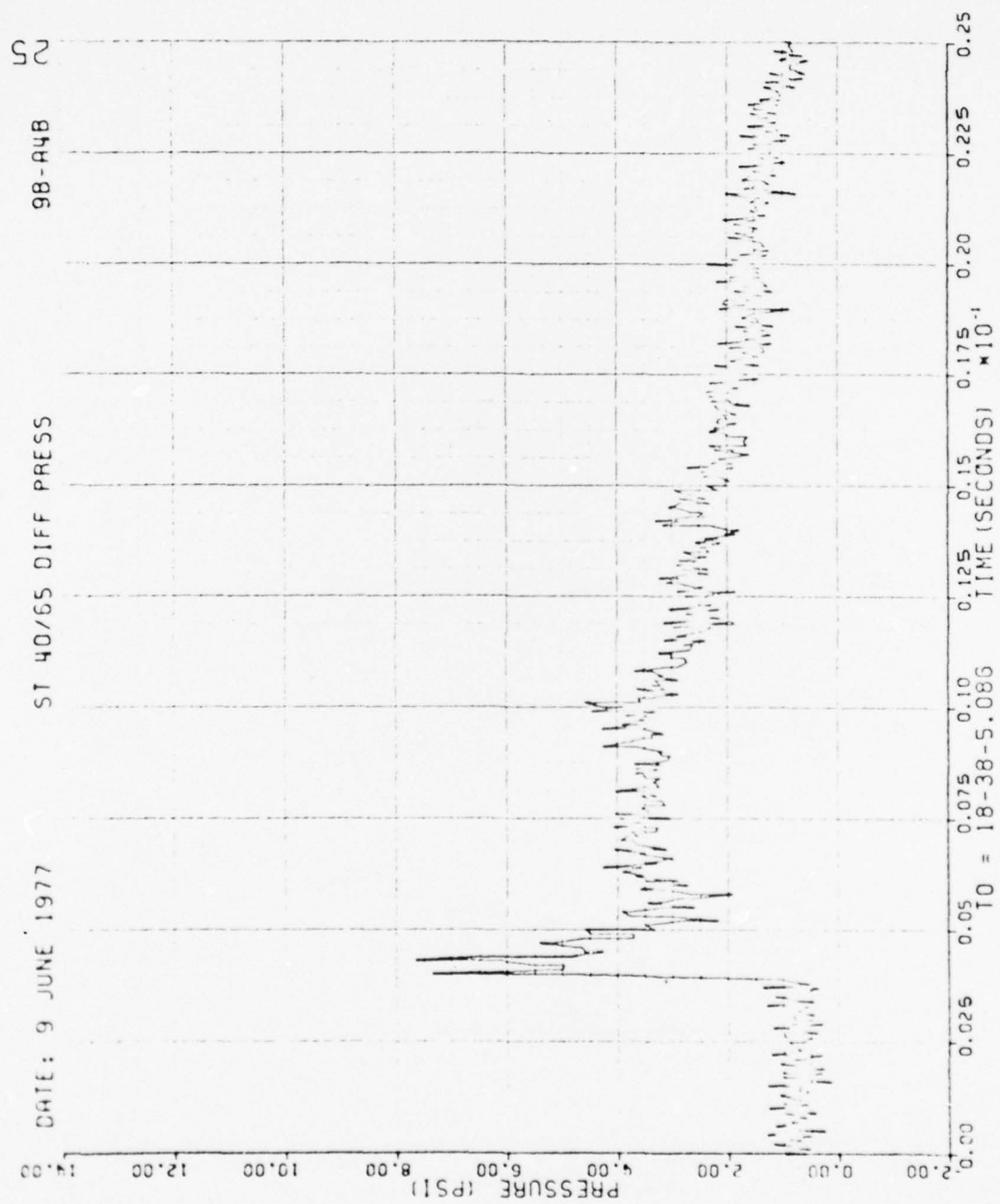


Figure 26. Continued

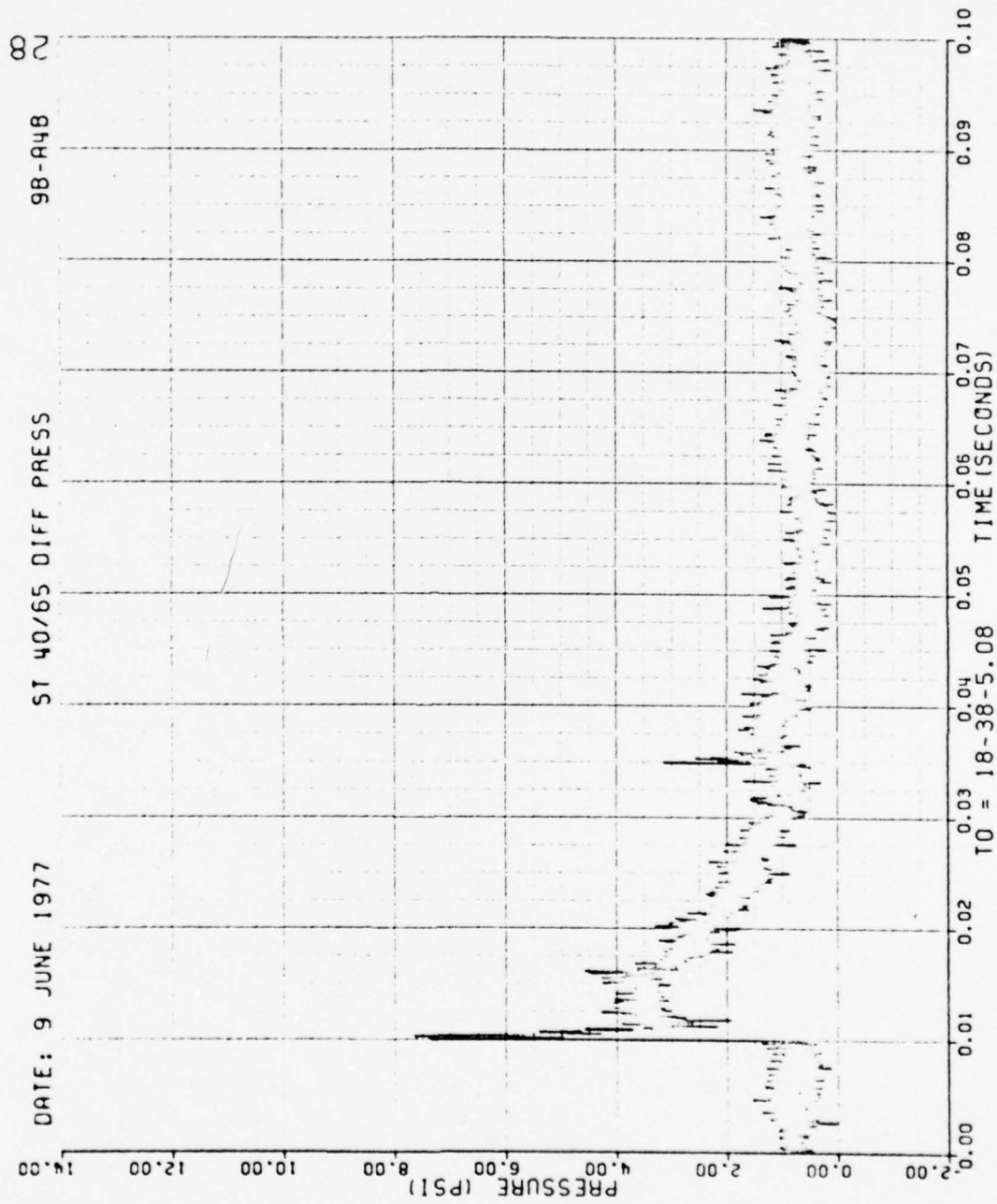


Figure 26. Continued

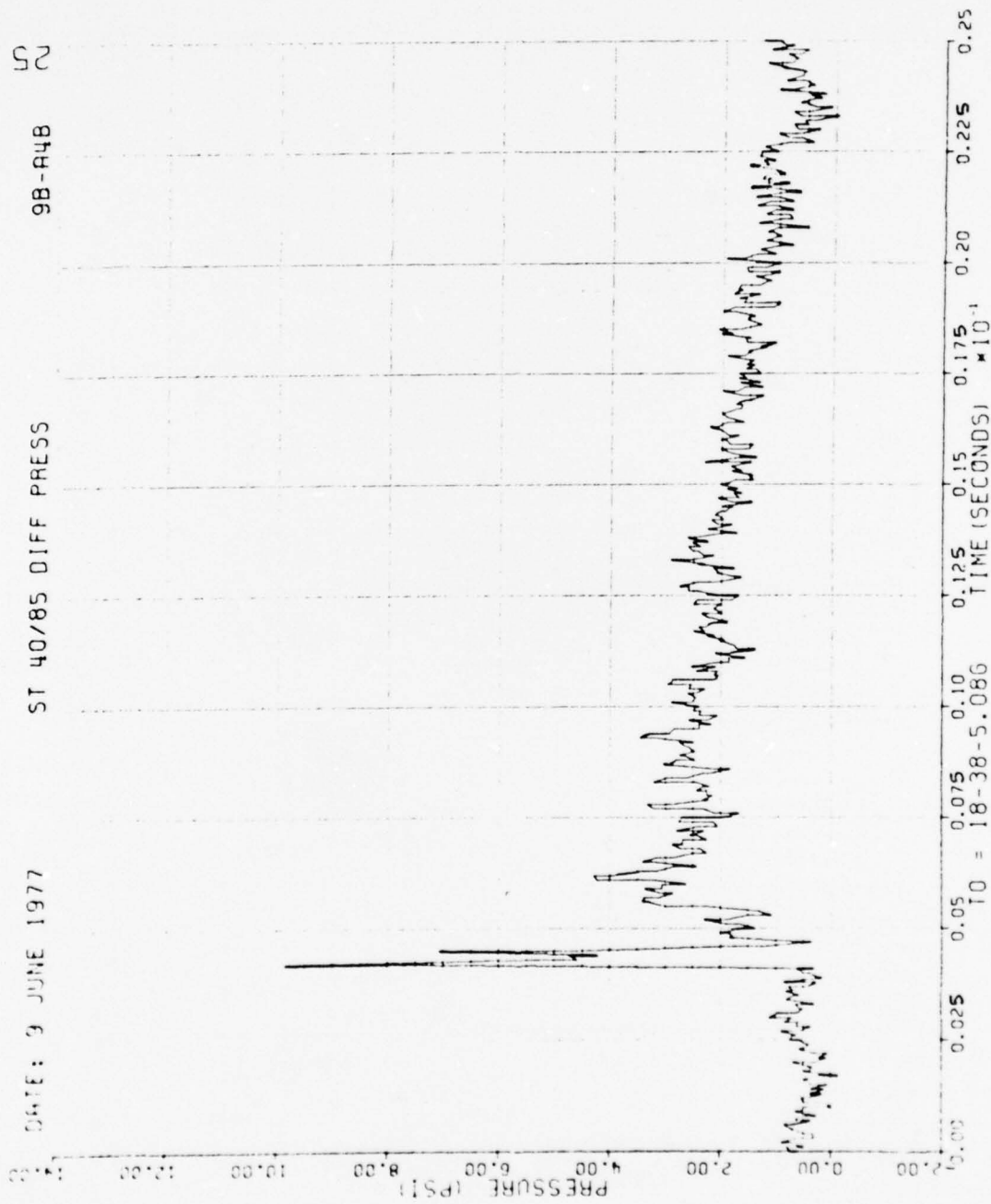


Figure 26. Continued

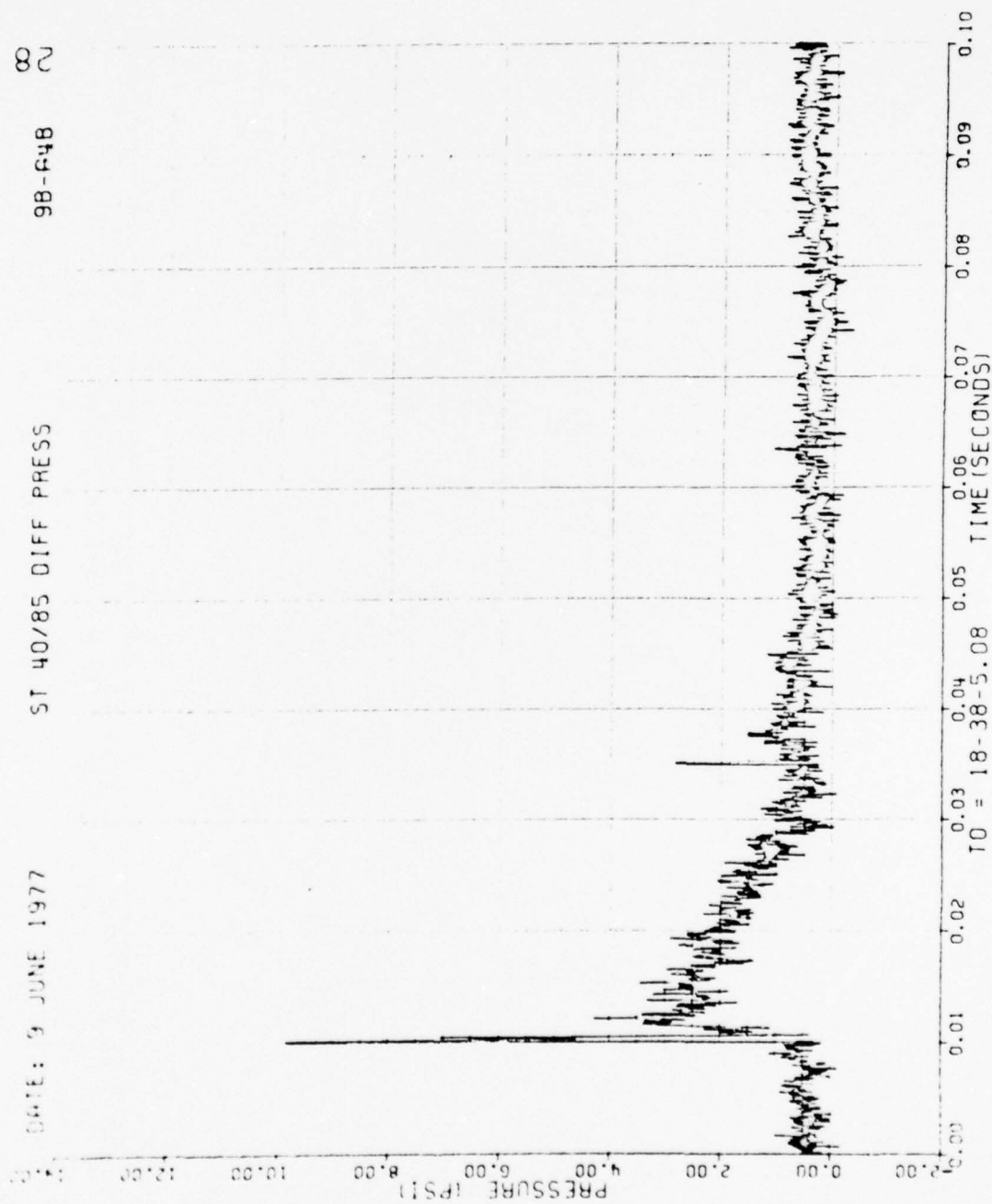


Figure 26. Continued

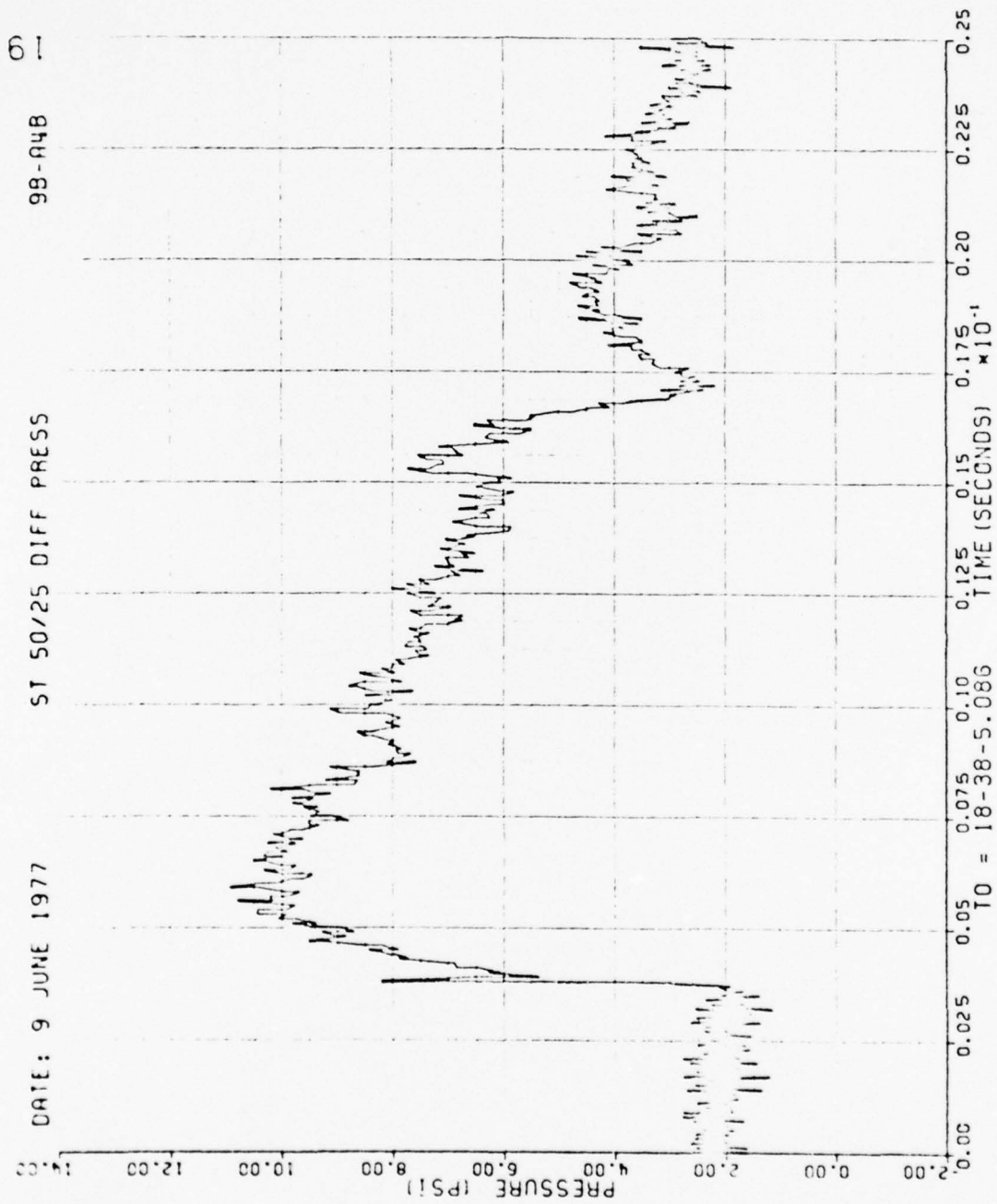


Figure 26. Continued

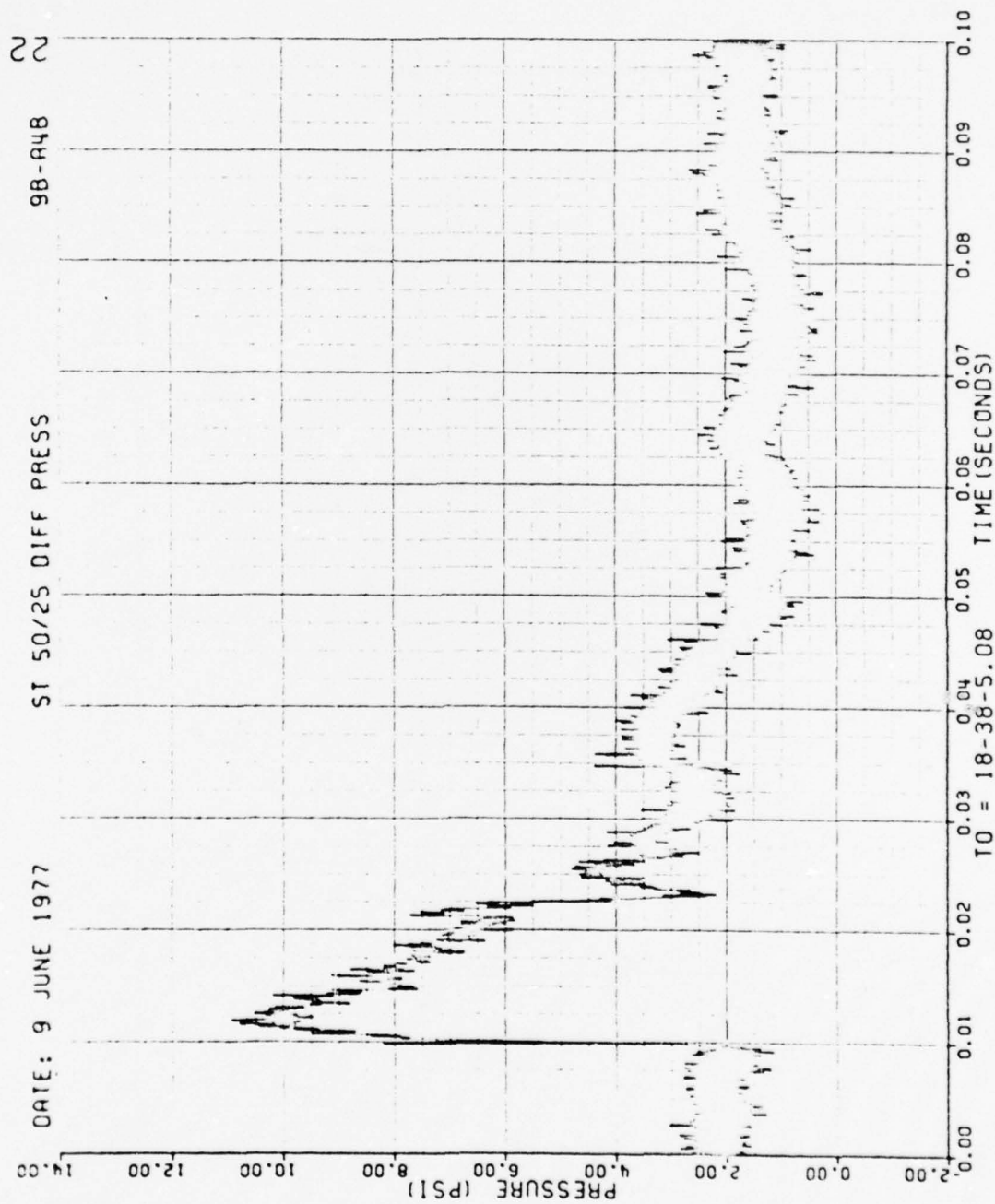


Figure 26. Continued

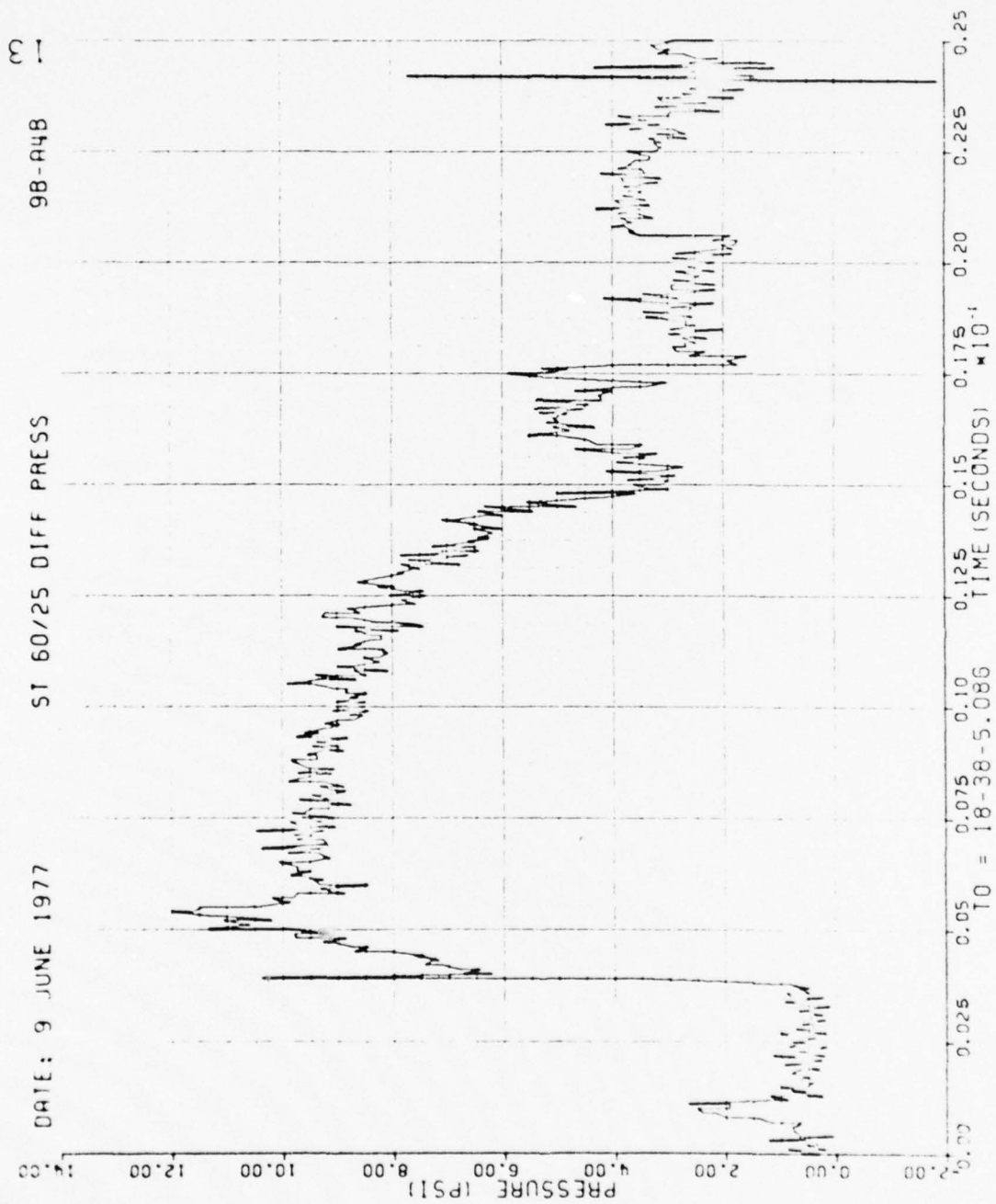


Figure 26. Continued

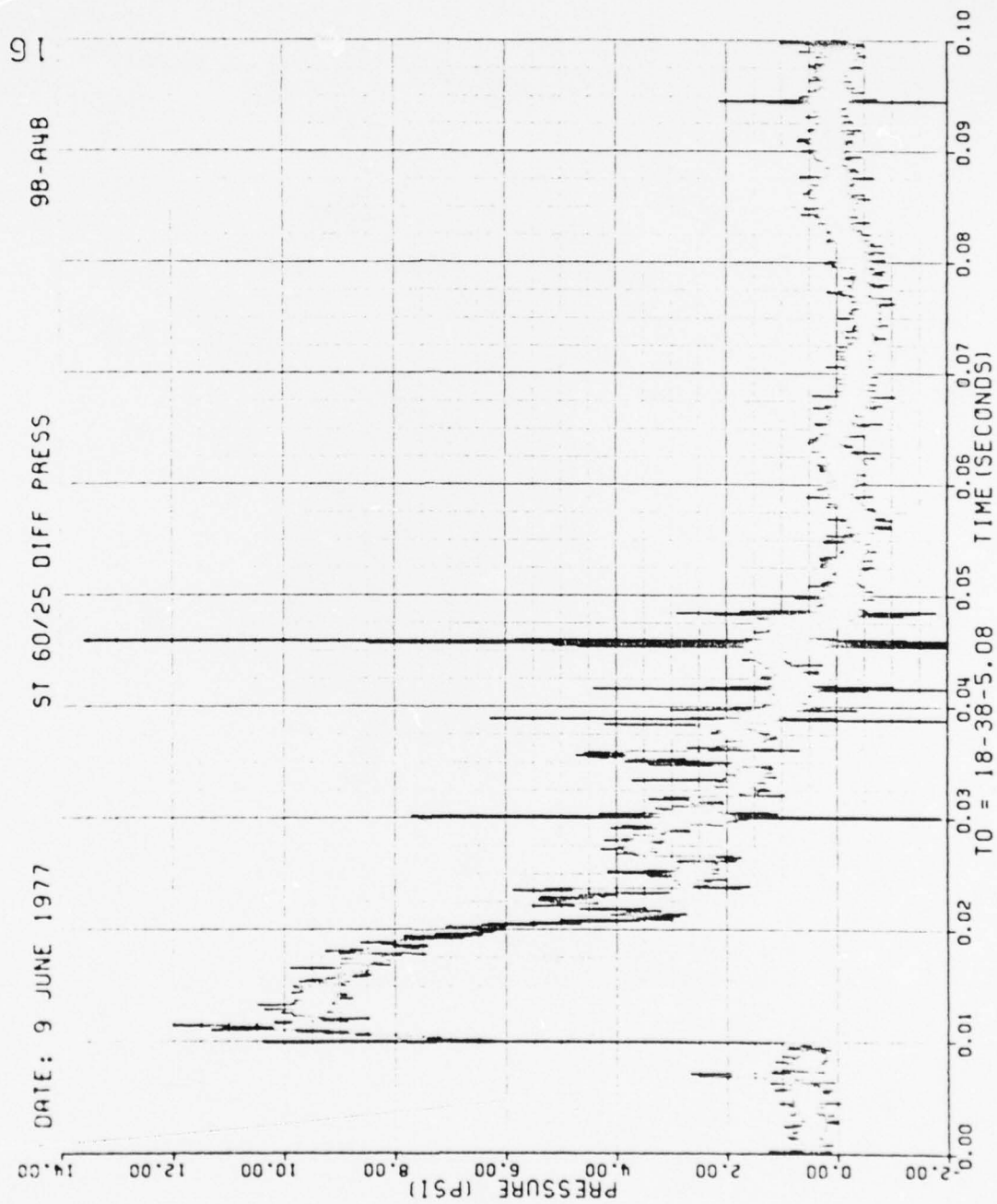


Figure 26. Continued

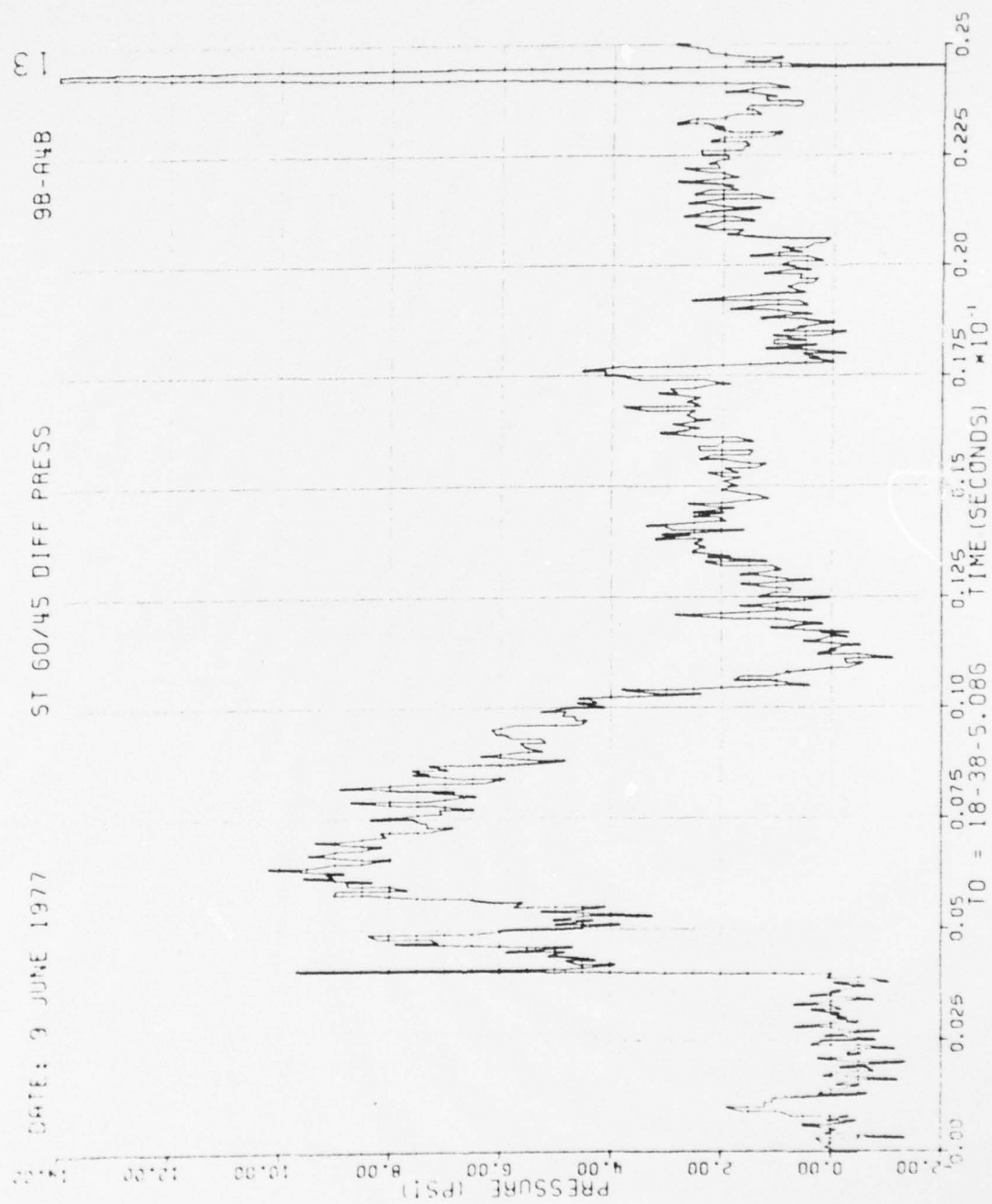


Figure 26. Continued

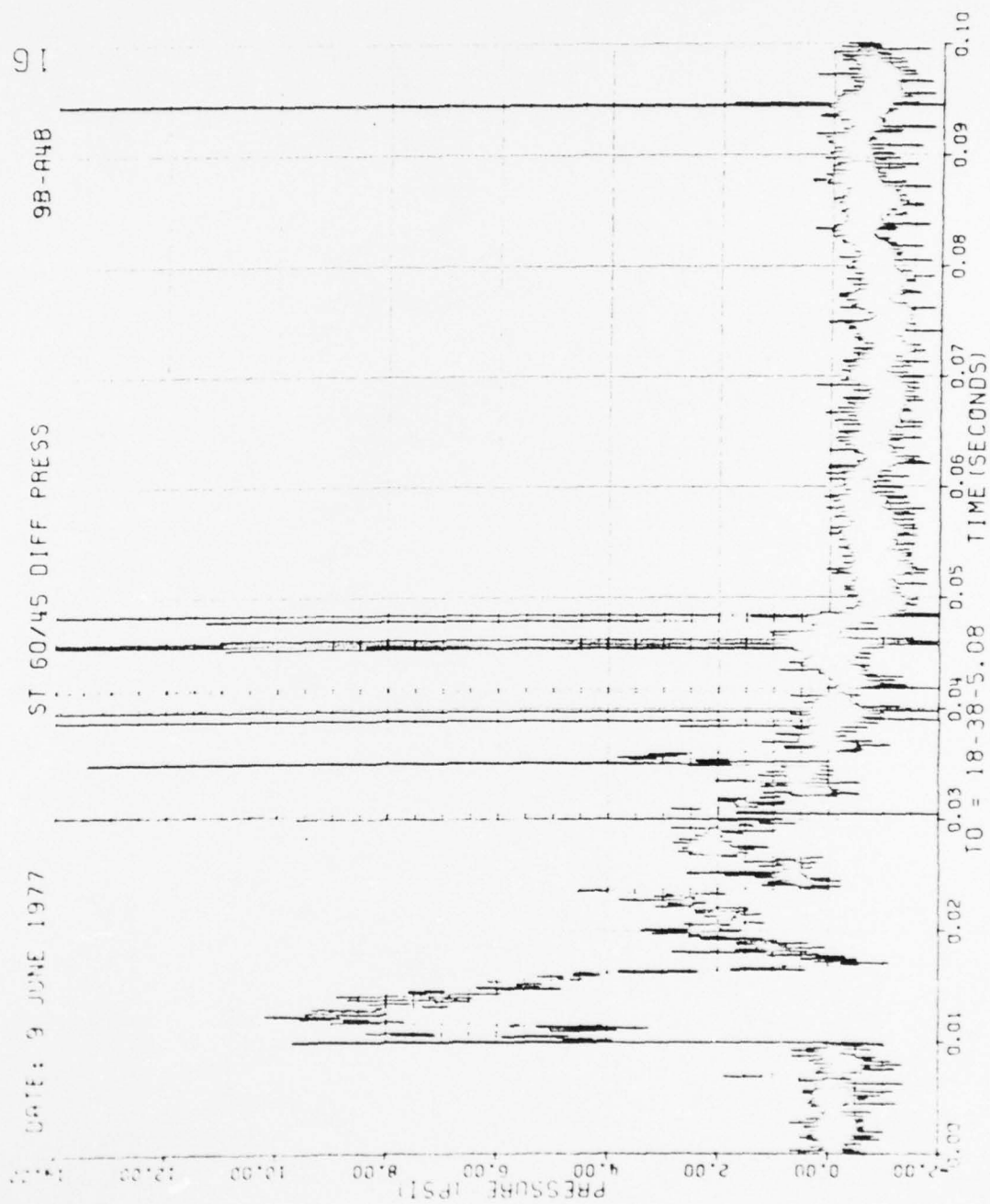


Figure 26. Continued

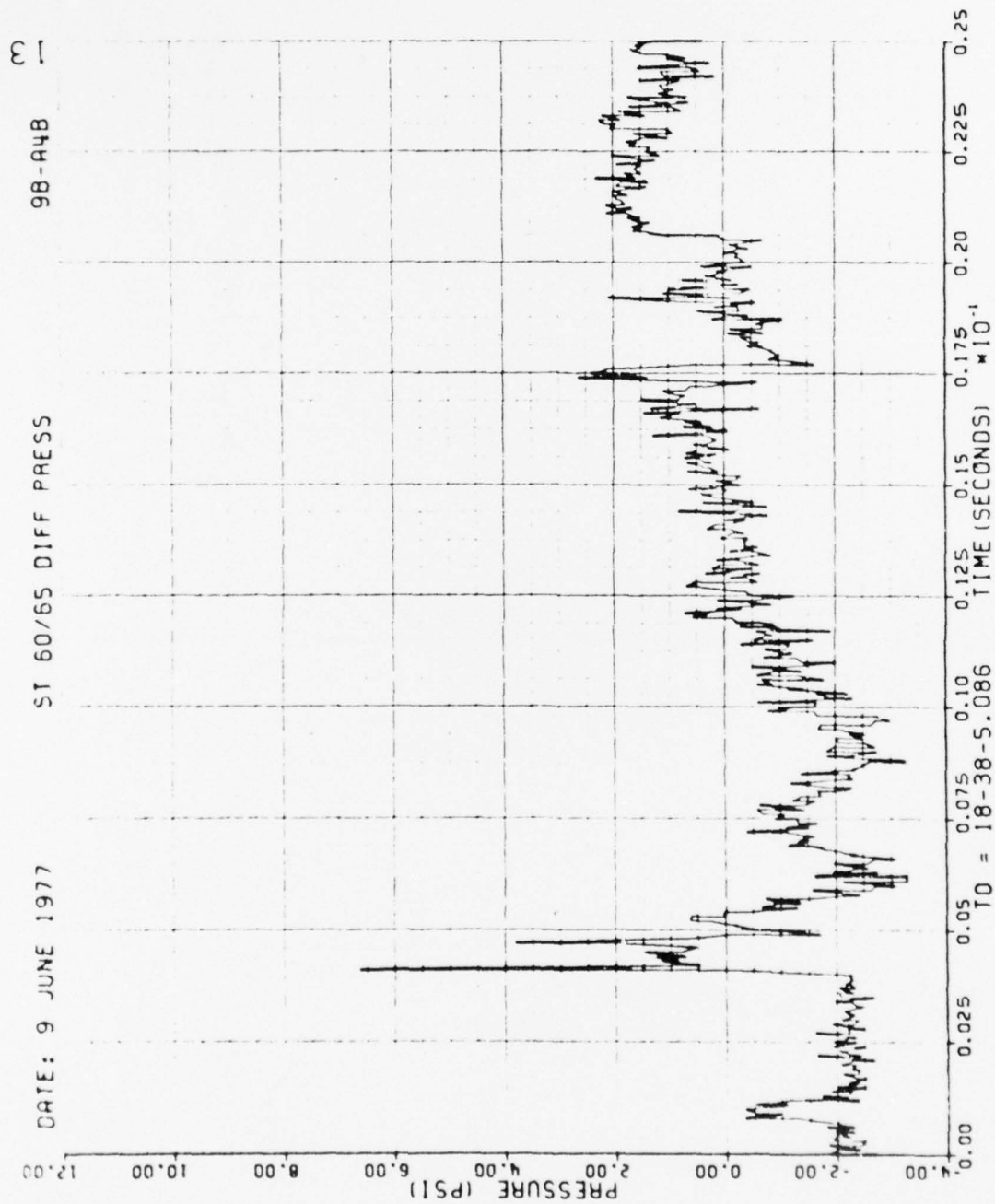


Figure 26. Continued

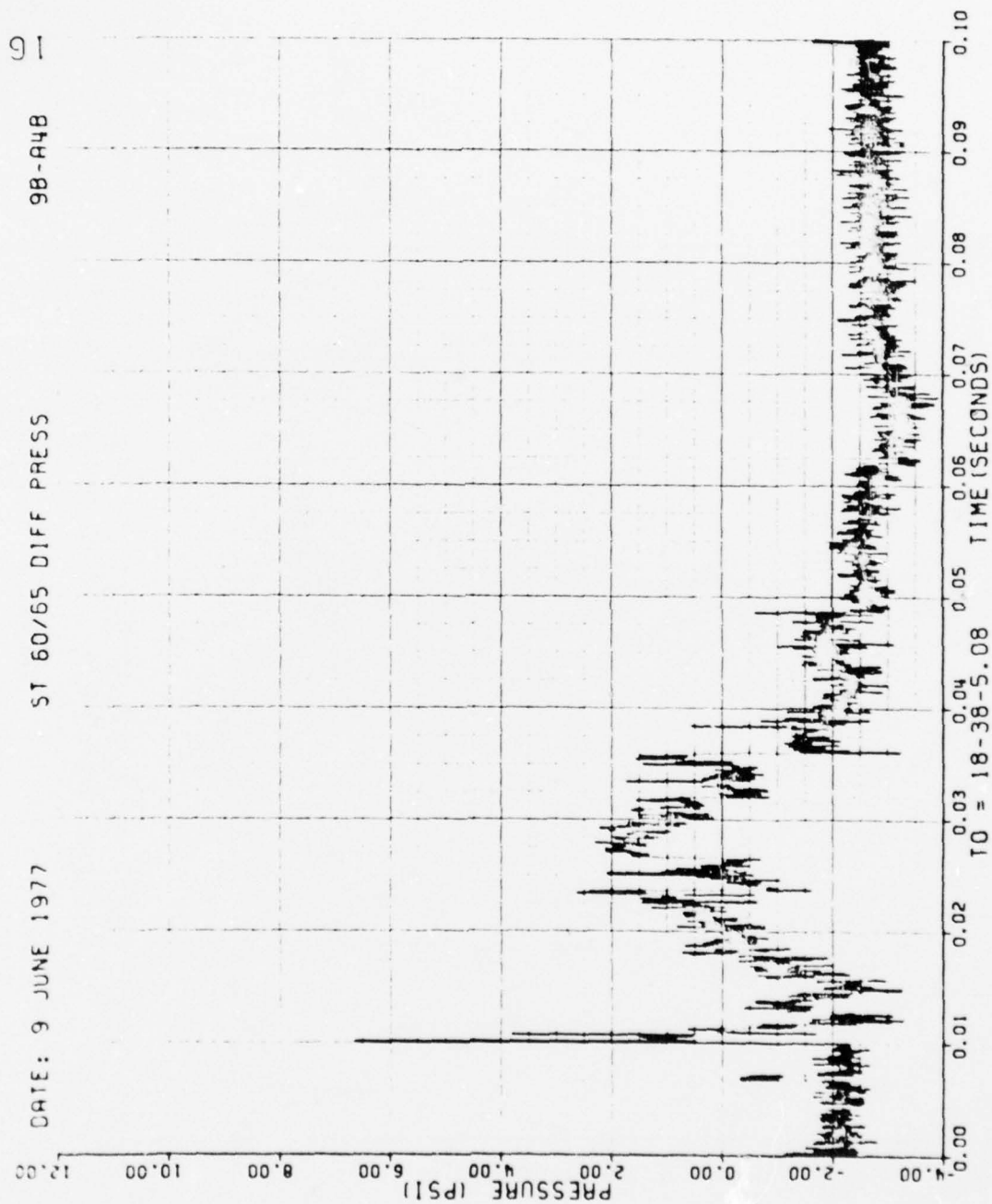


Figure 26. Continued

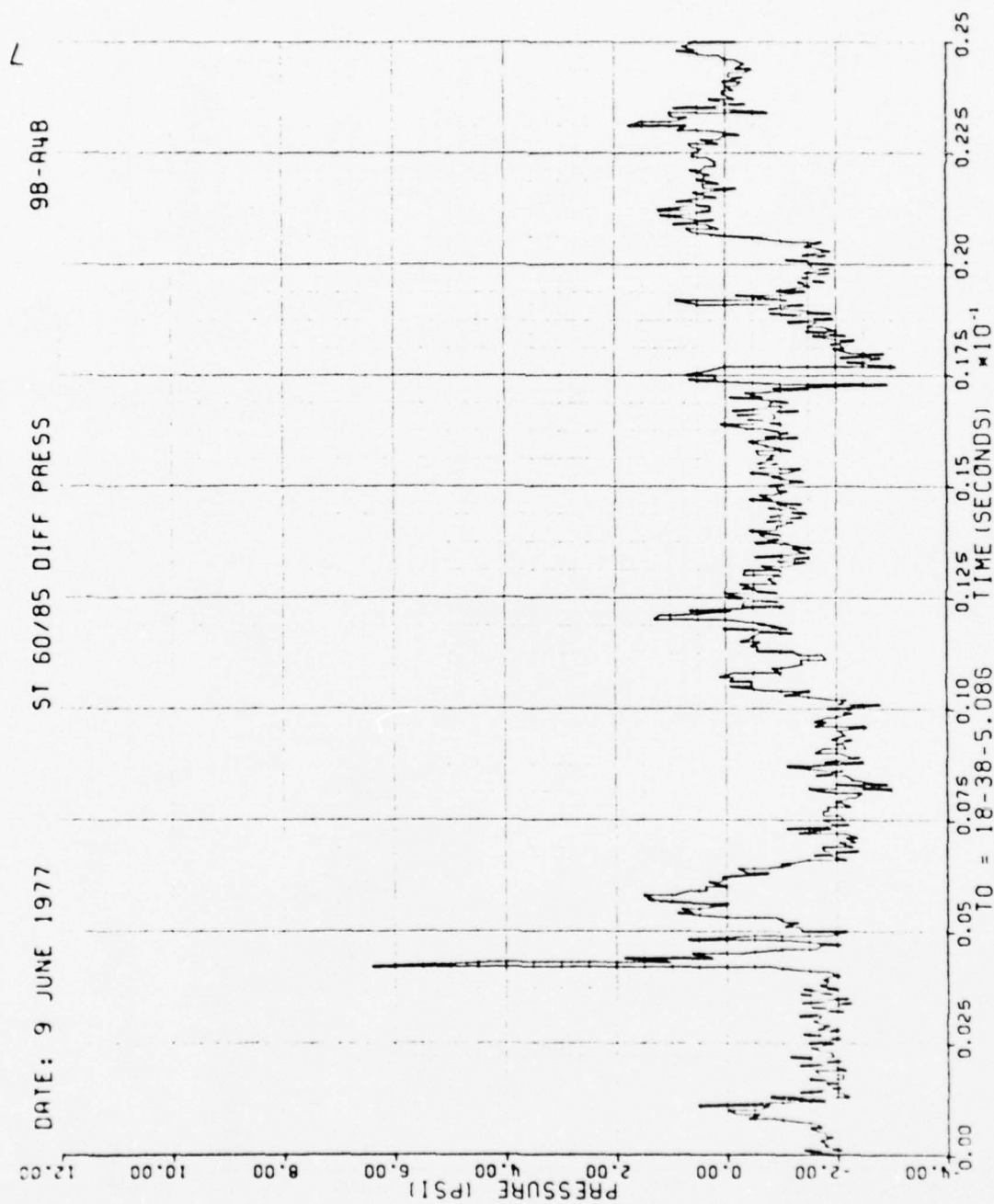


Figure 26. Continued

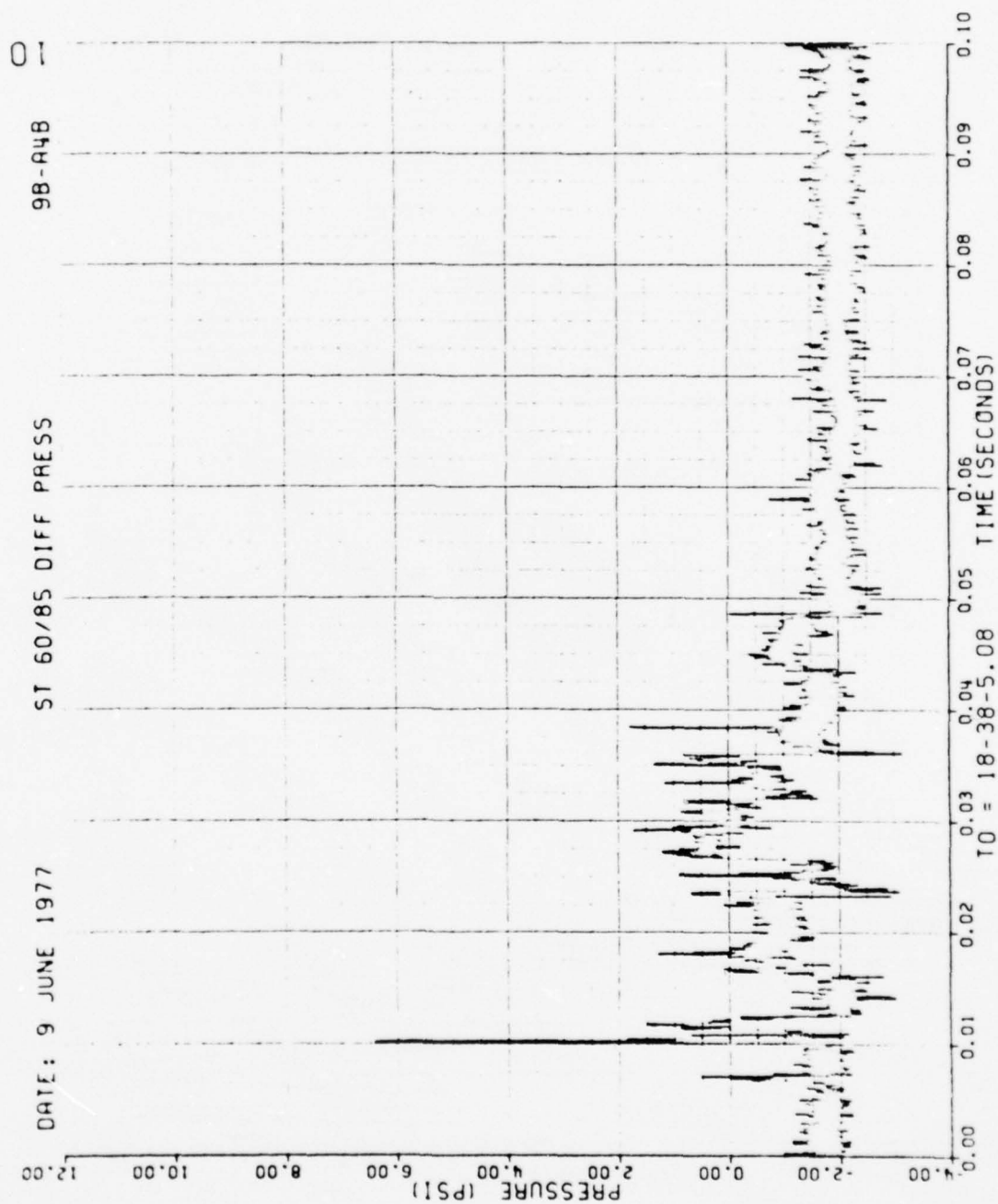


Figure 26. Continued

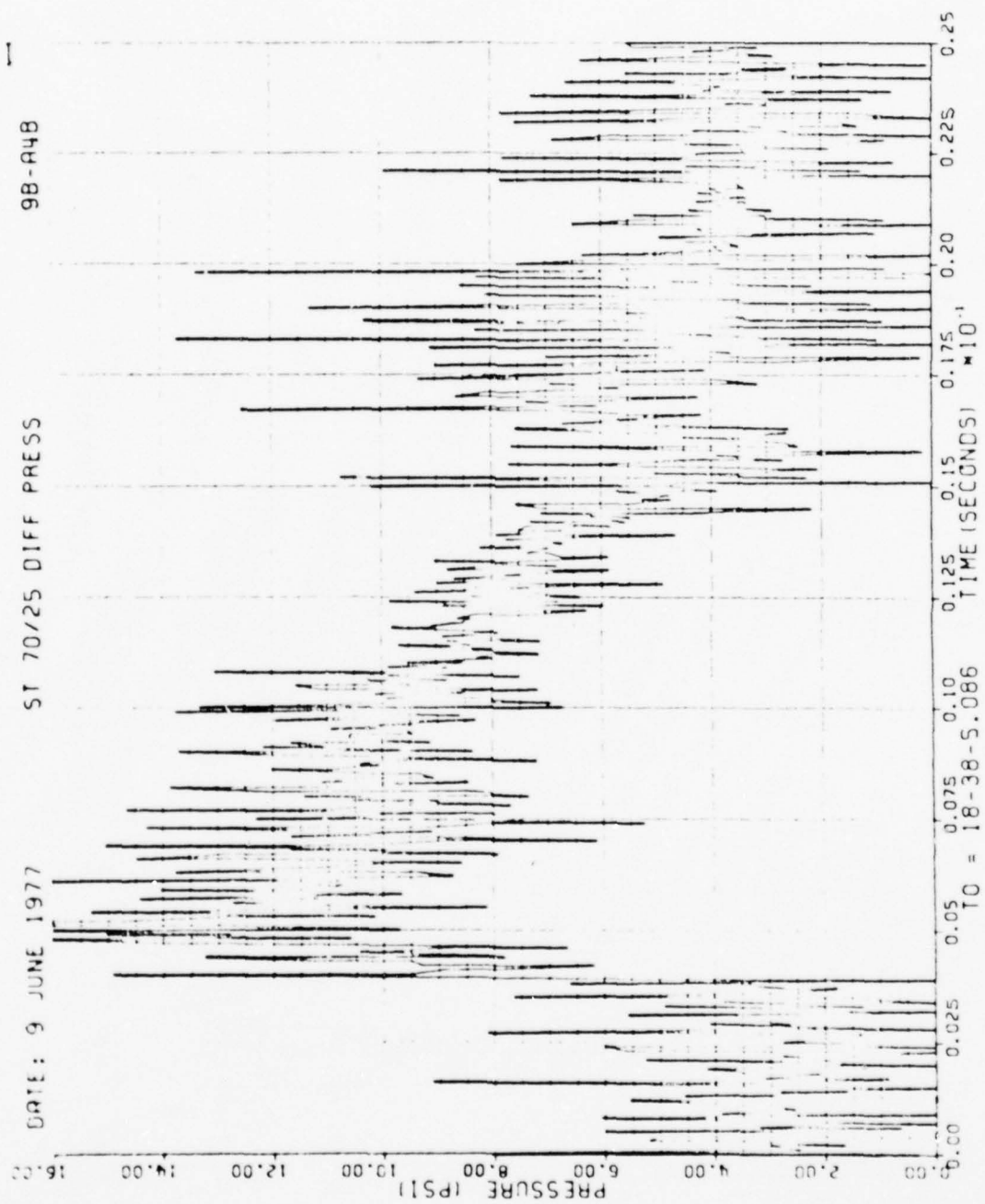


Figure 26. Continued

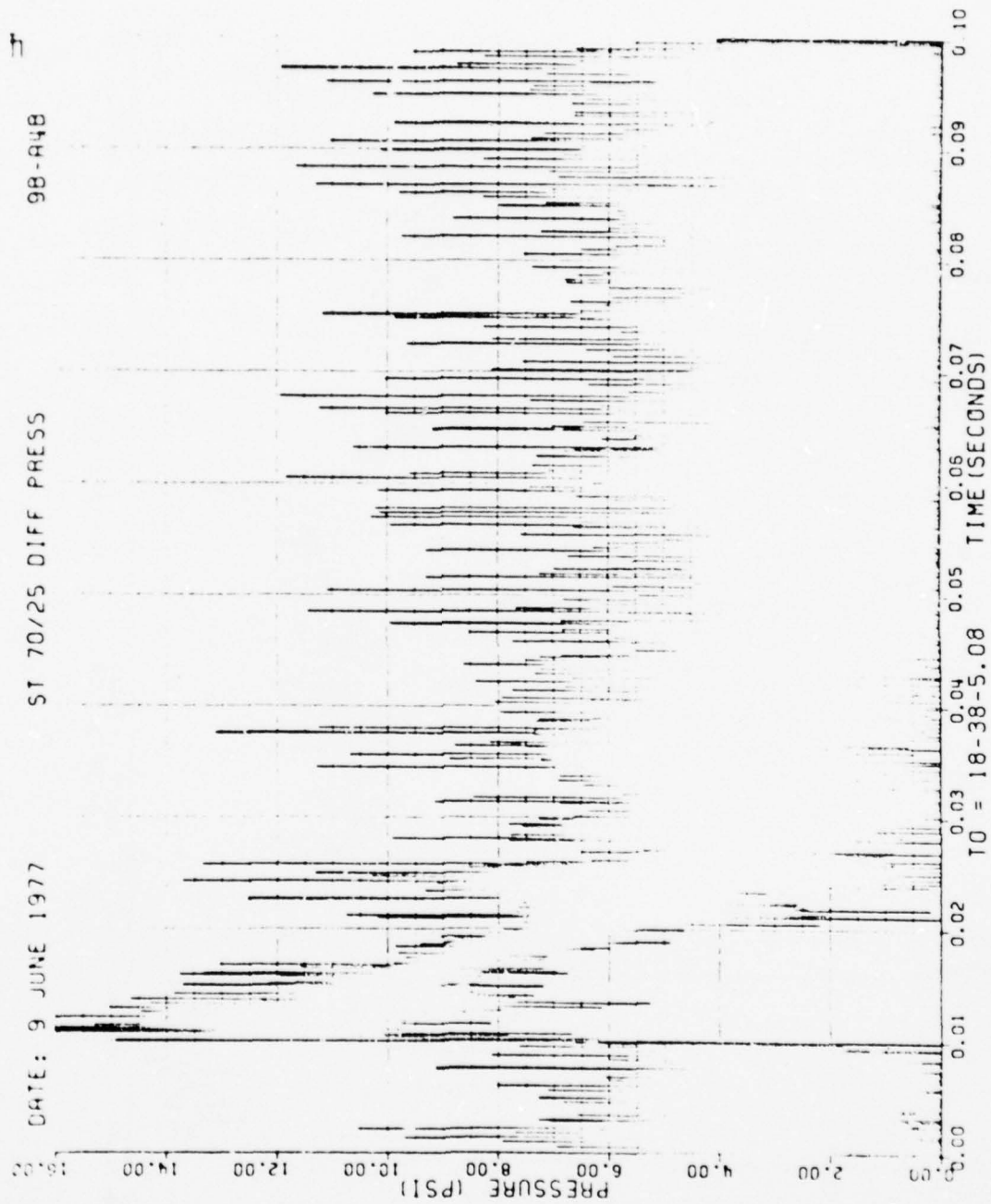


Figure 26. Continued

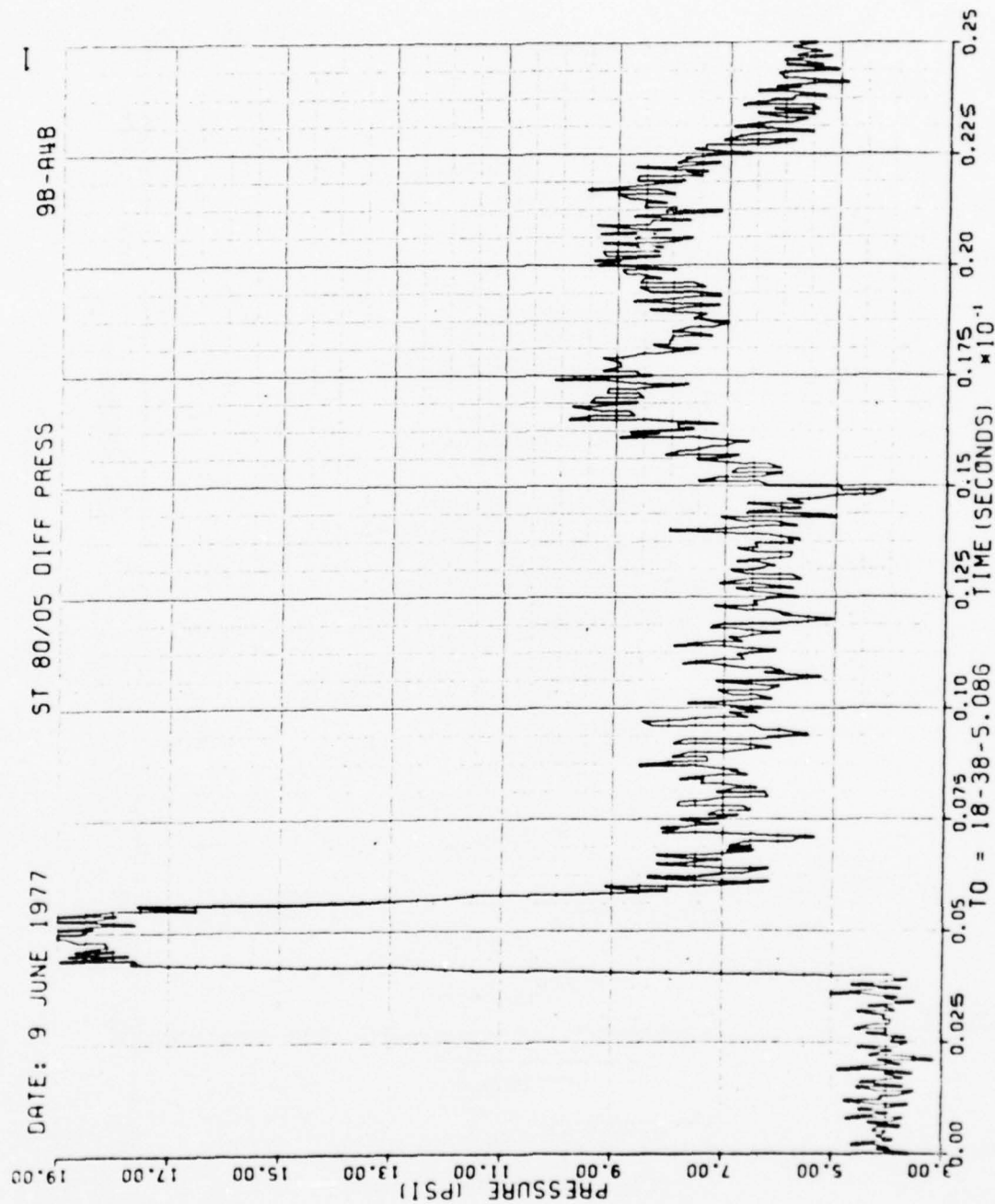


Figure 26. Continued

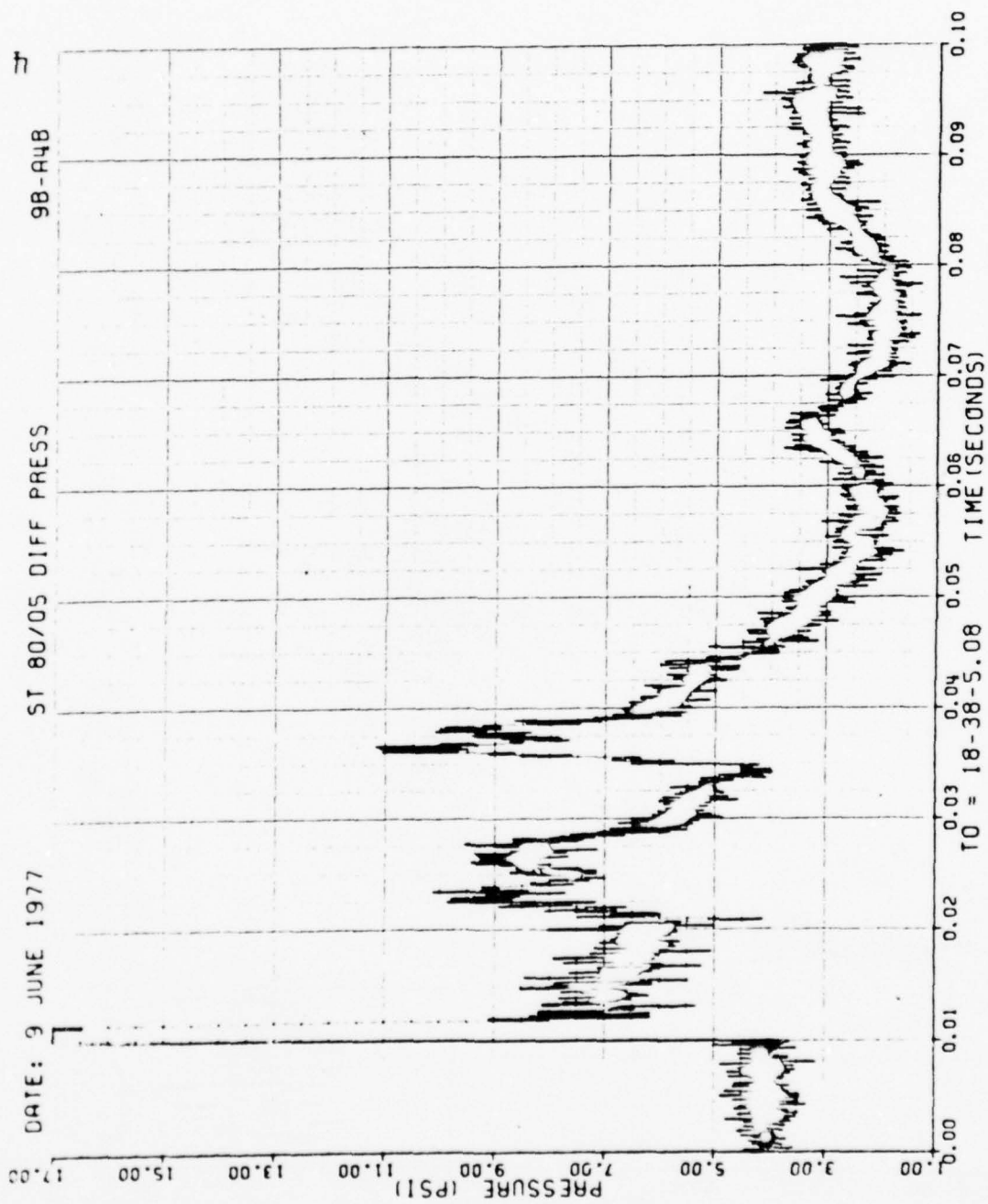


Figure 26. Continued

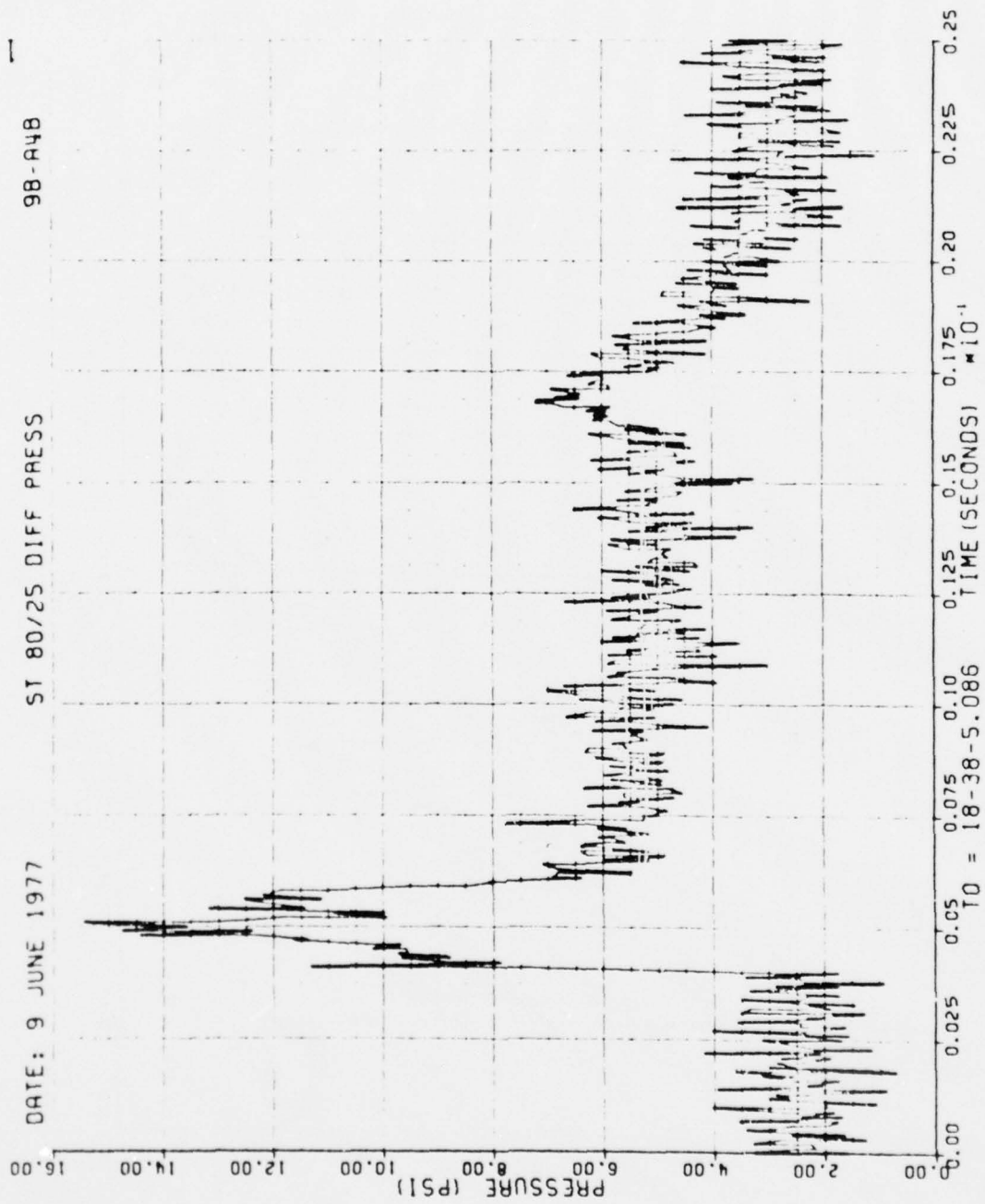


Figure 26. Continued

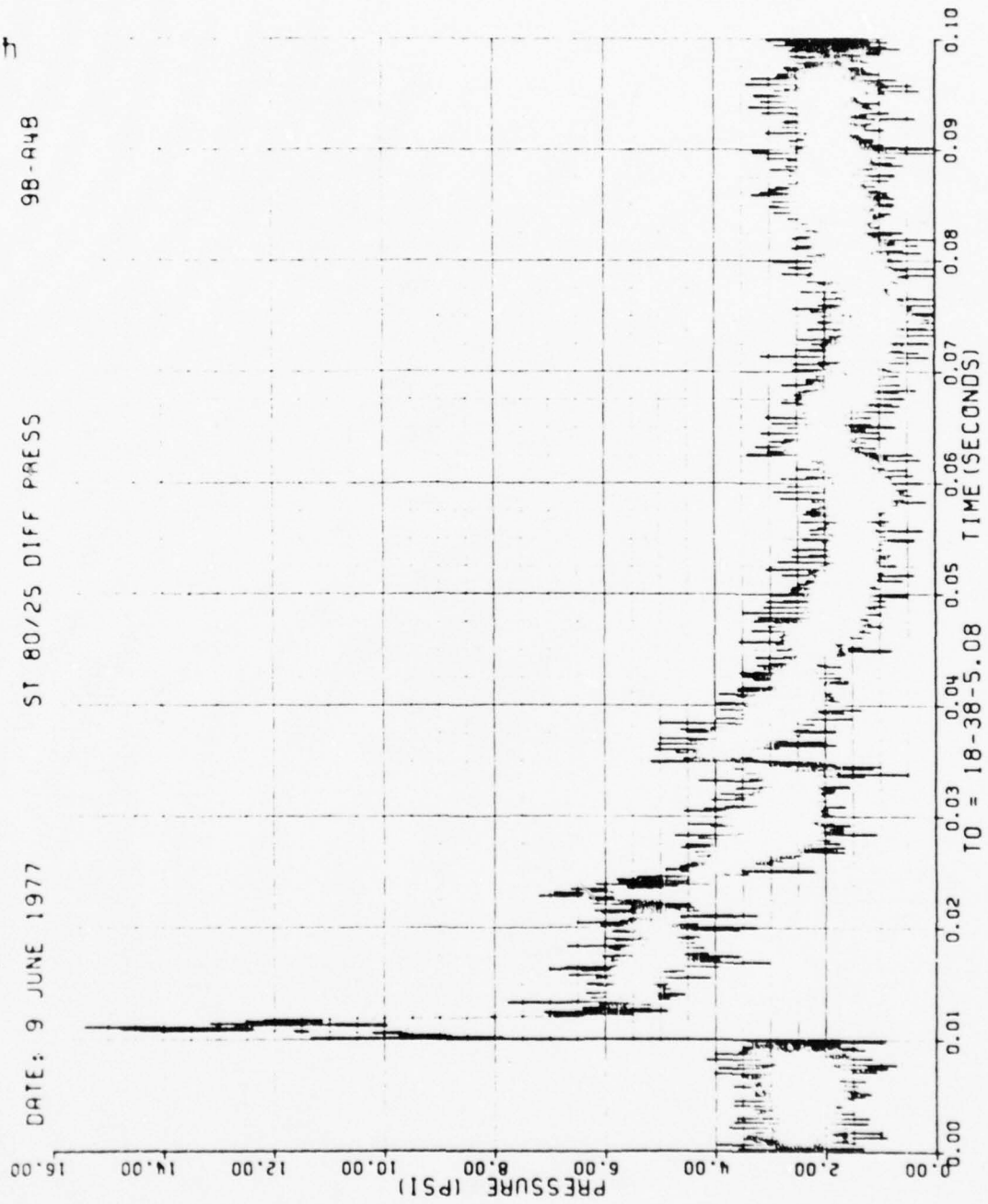


Figure 26. Continued

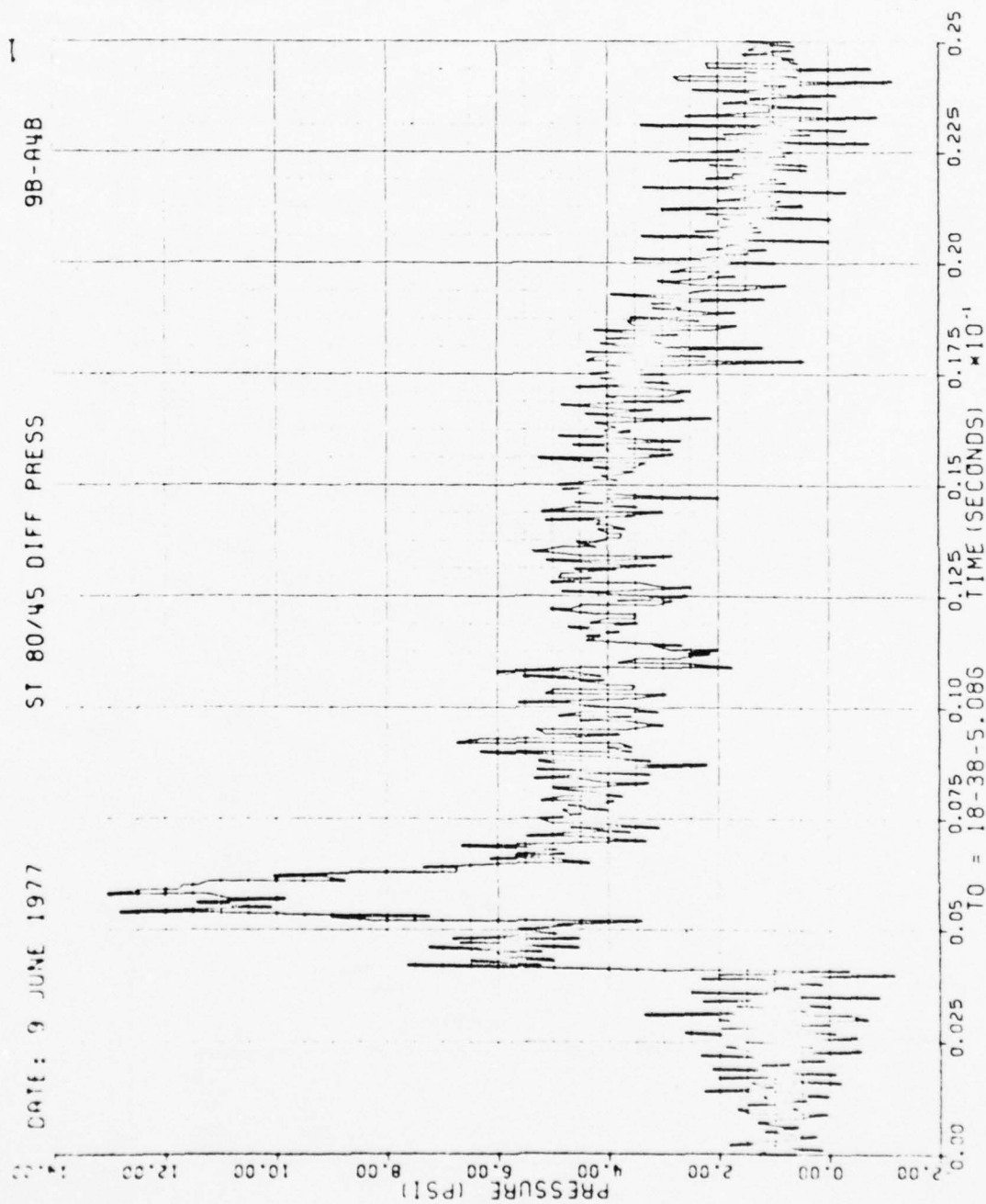


Figure 26. Continued

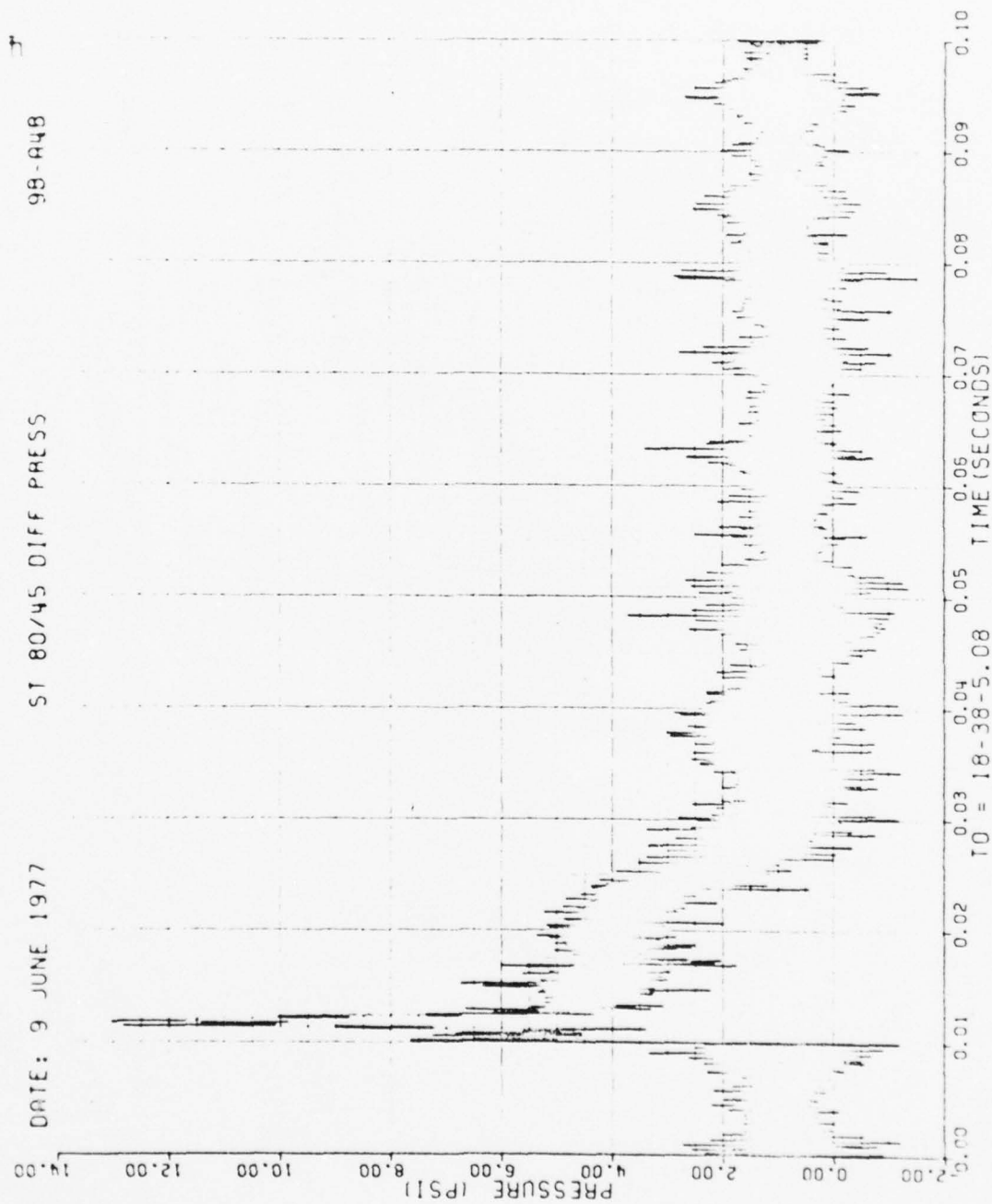


Figure 26. Continued

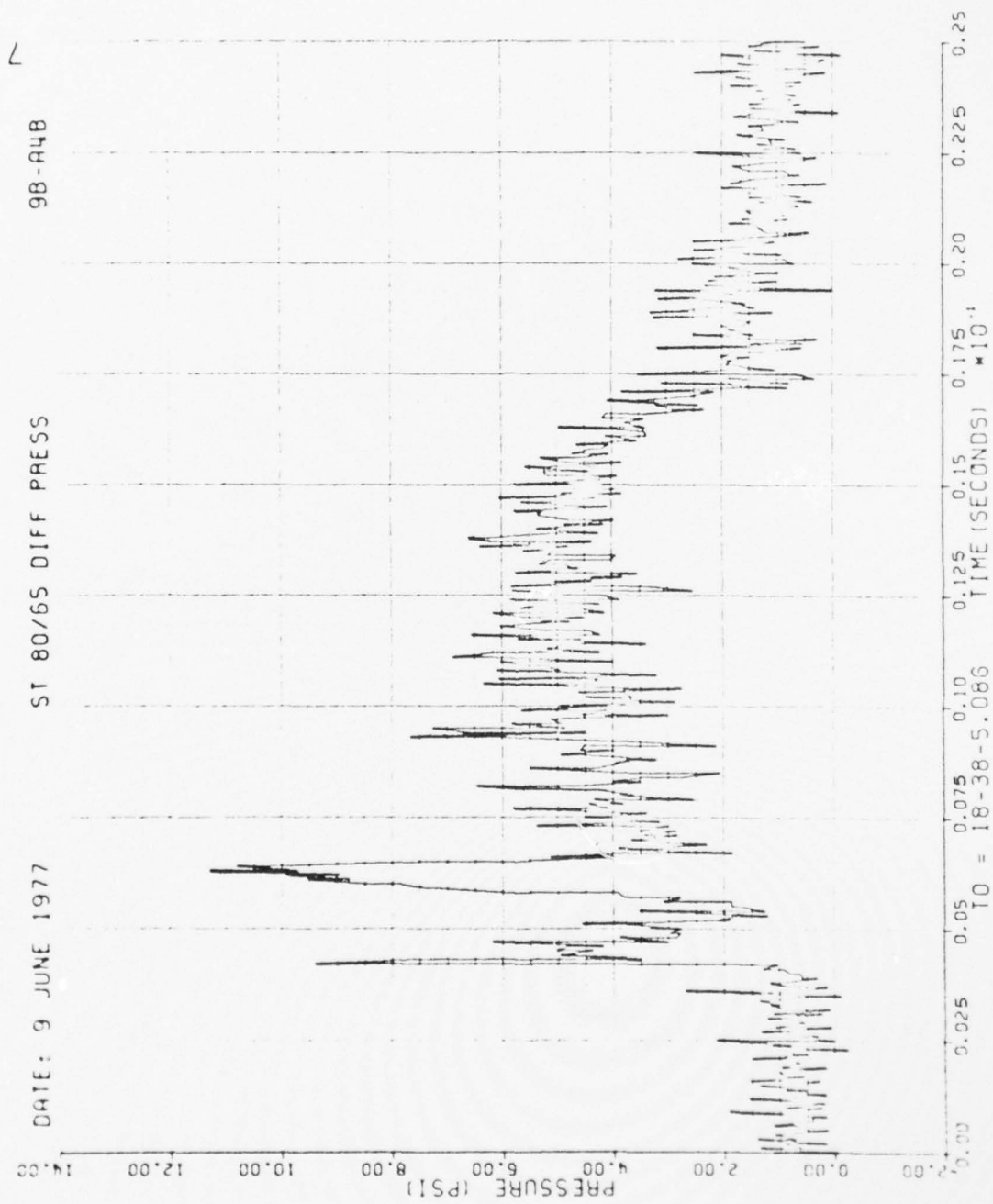


Figure 26. Continued

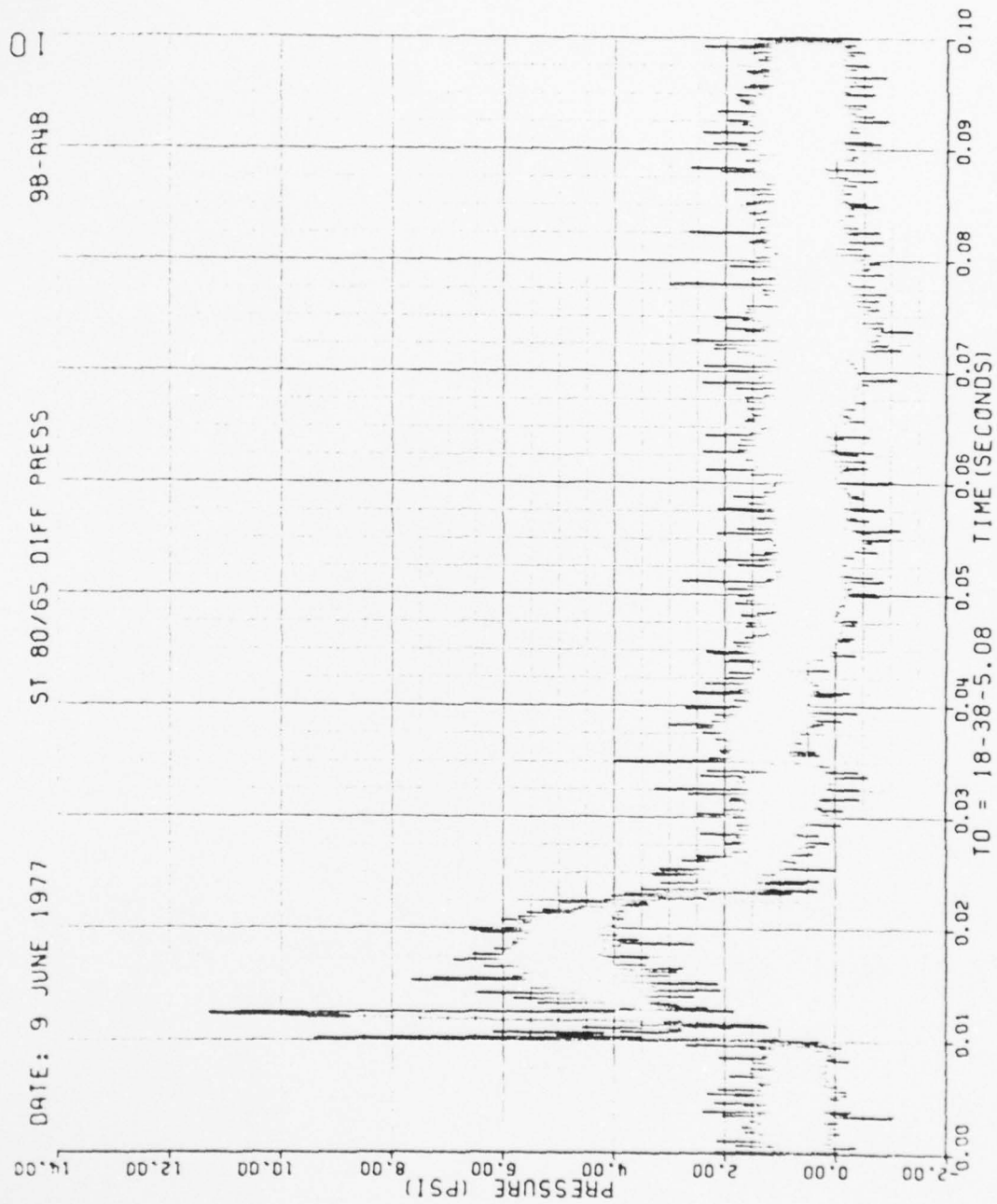


Figure 26. Continued

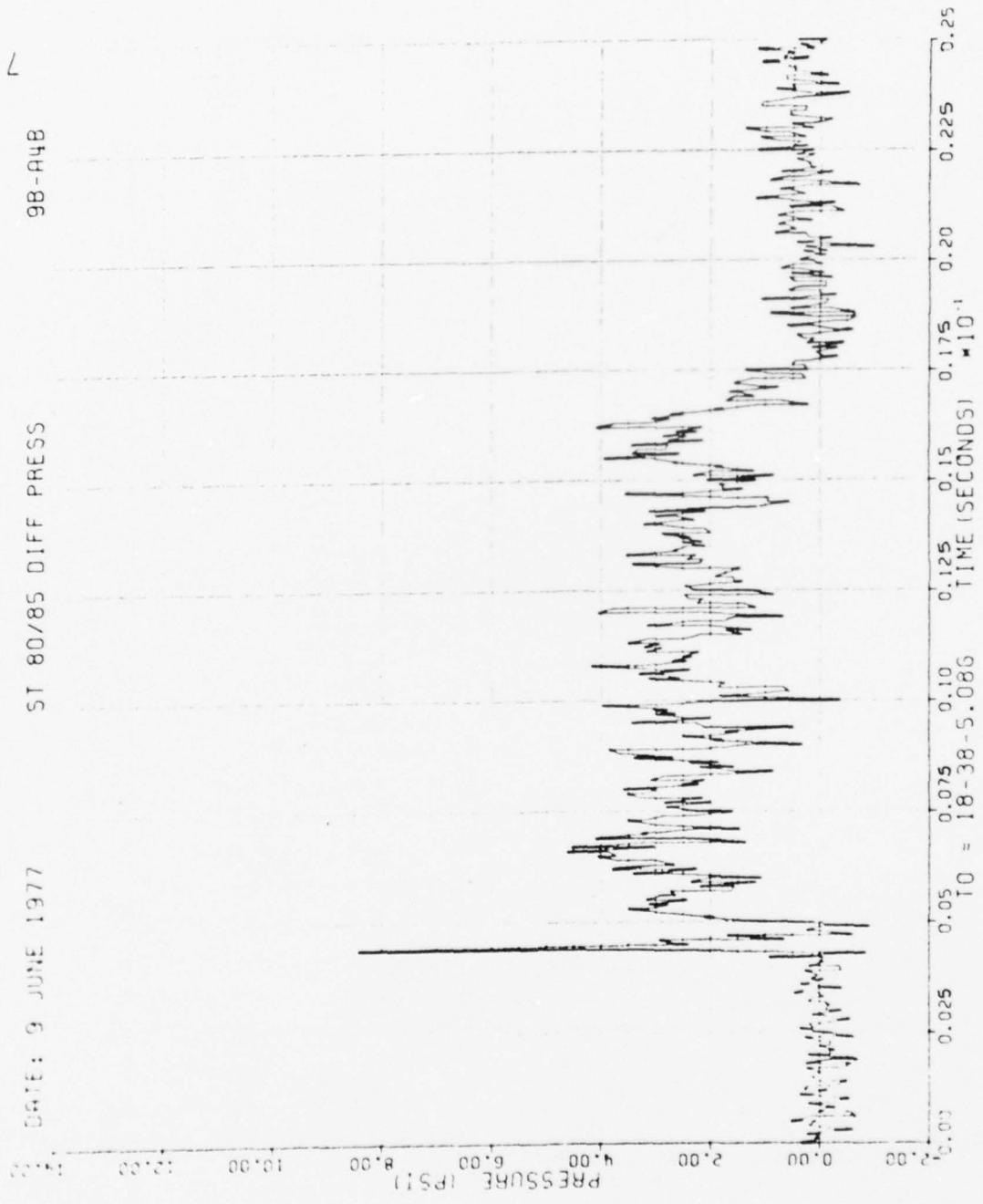


Figure 26. Continued

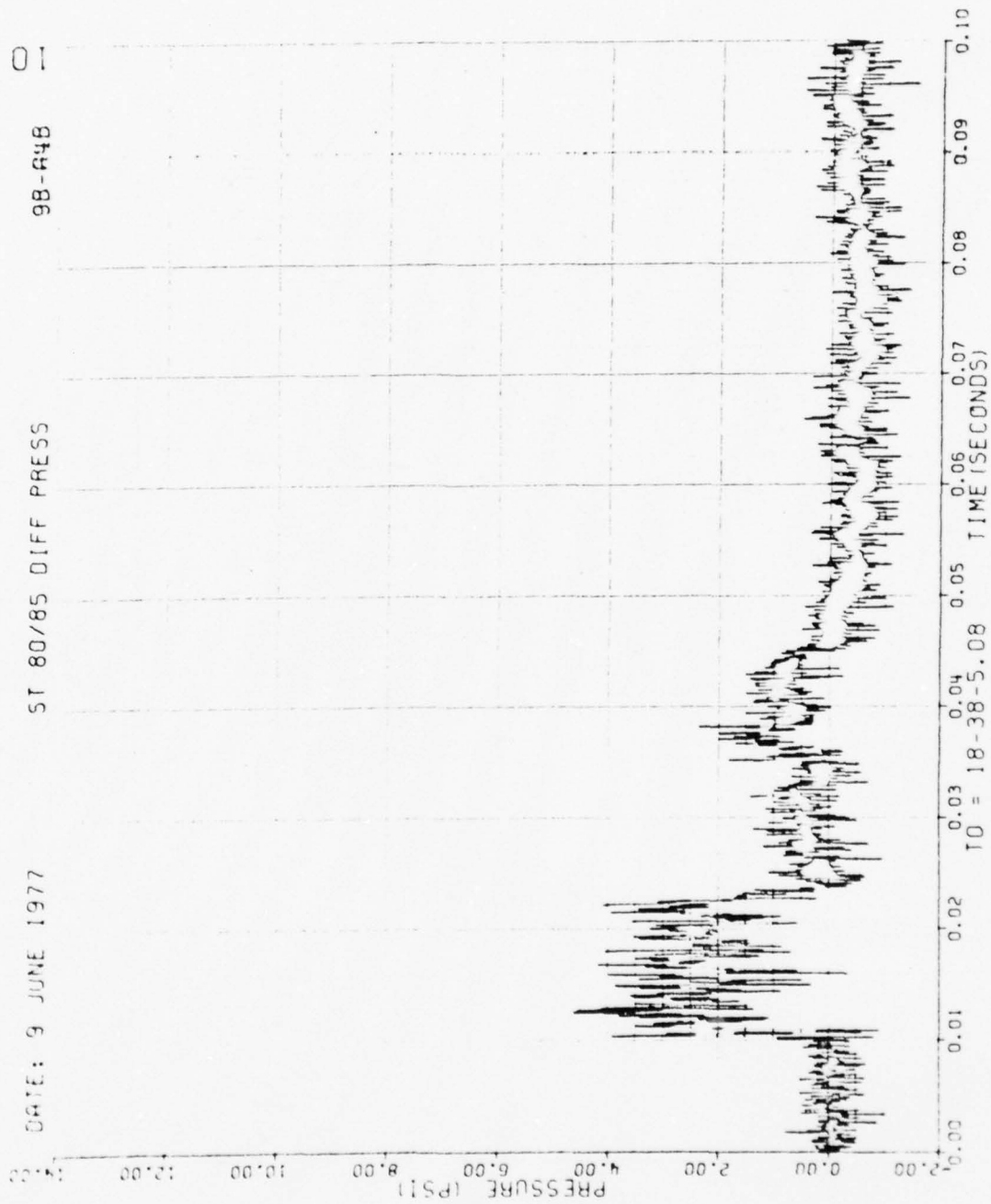


Figure 26. Continued

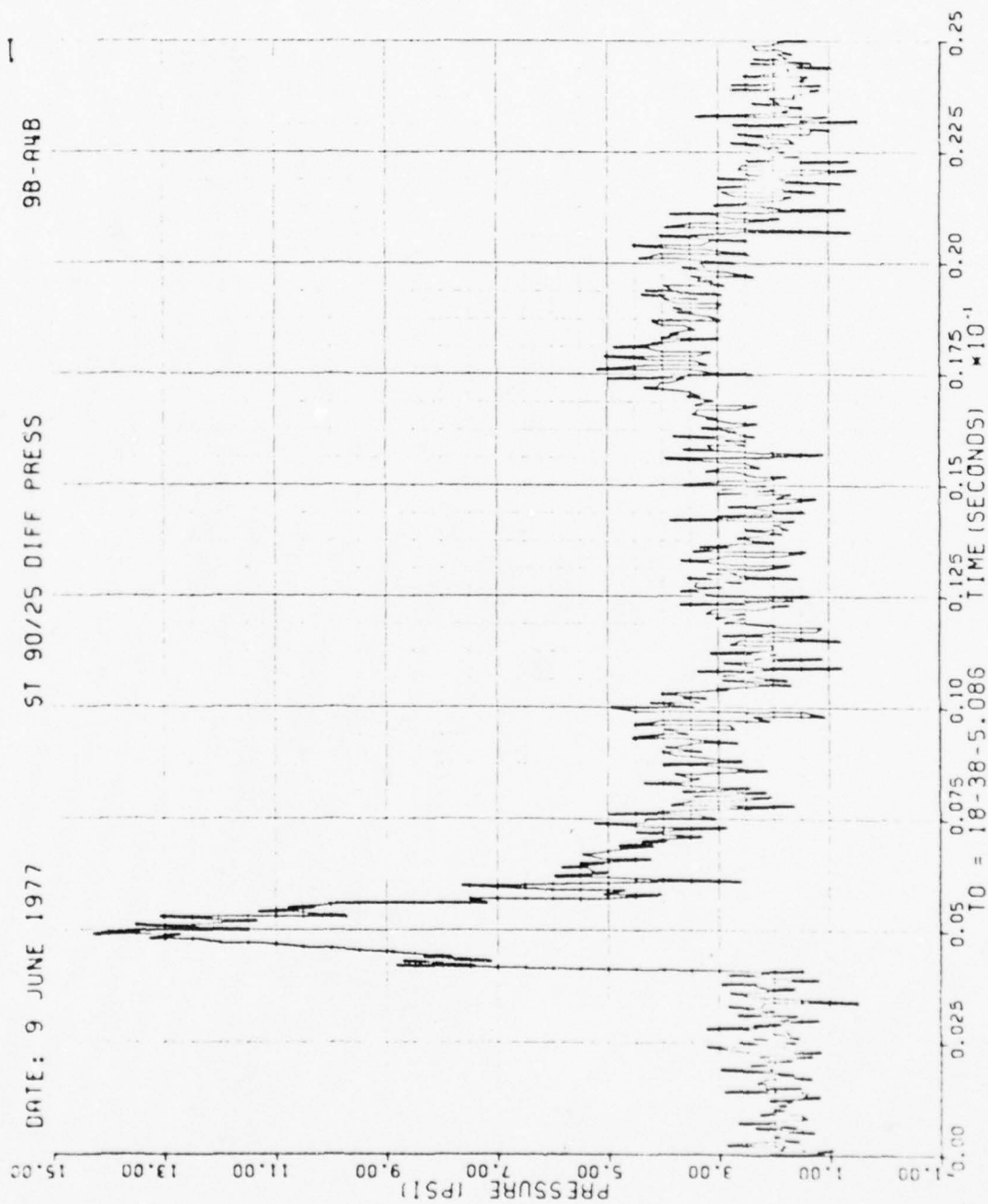


Figure 26. Continued

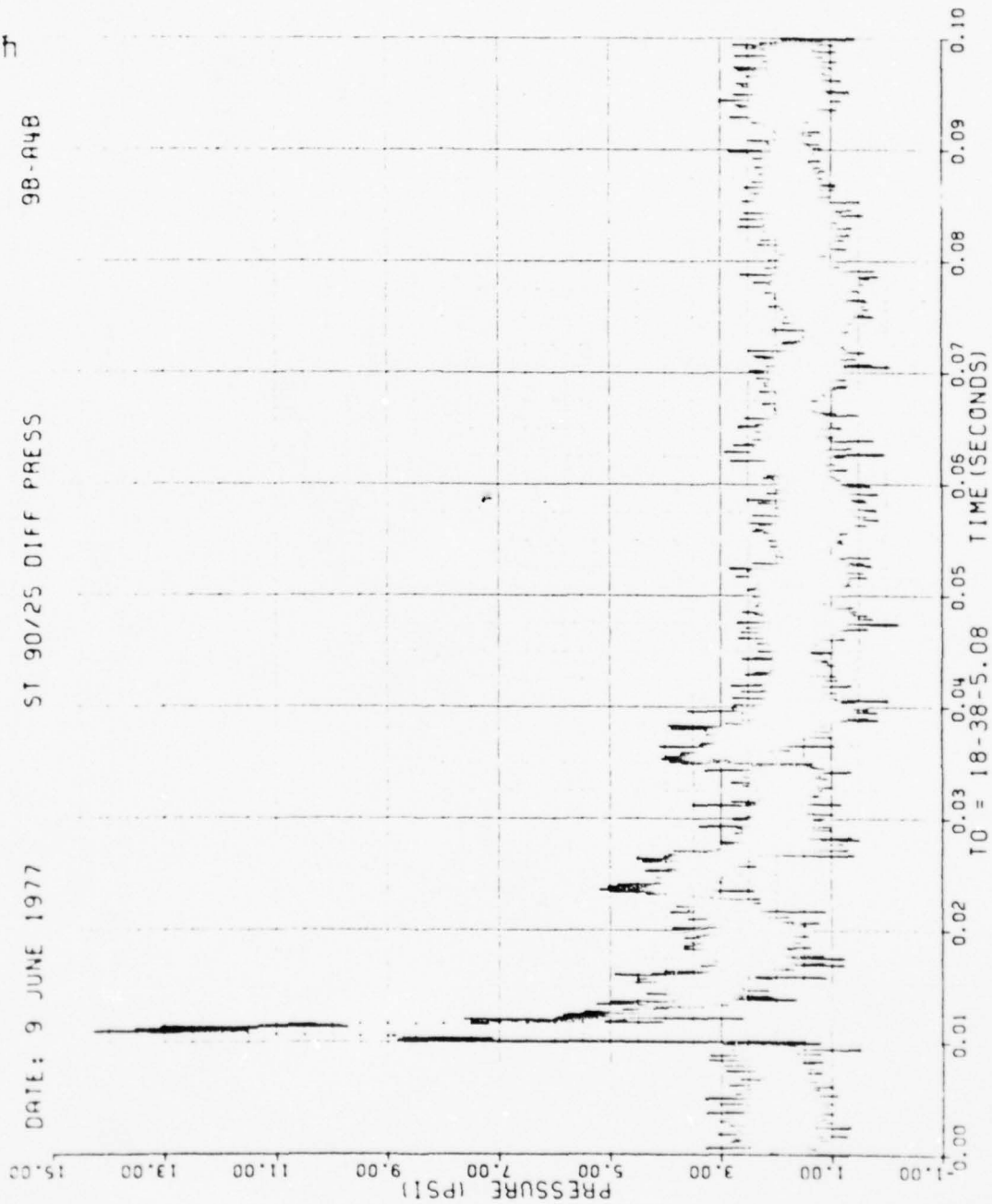


Figure 26. Concluded

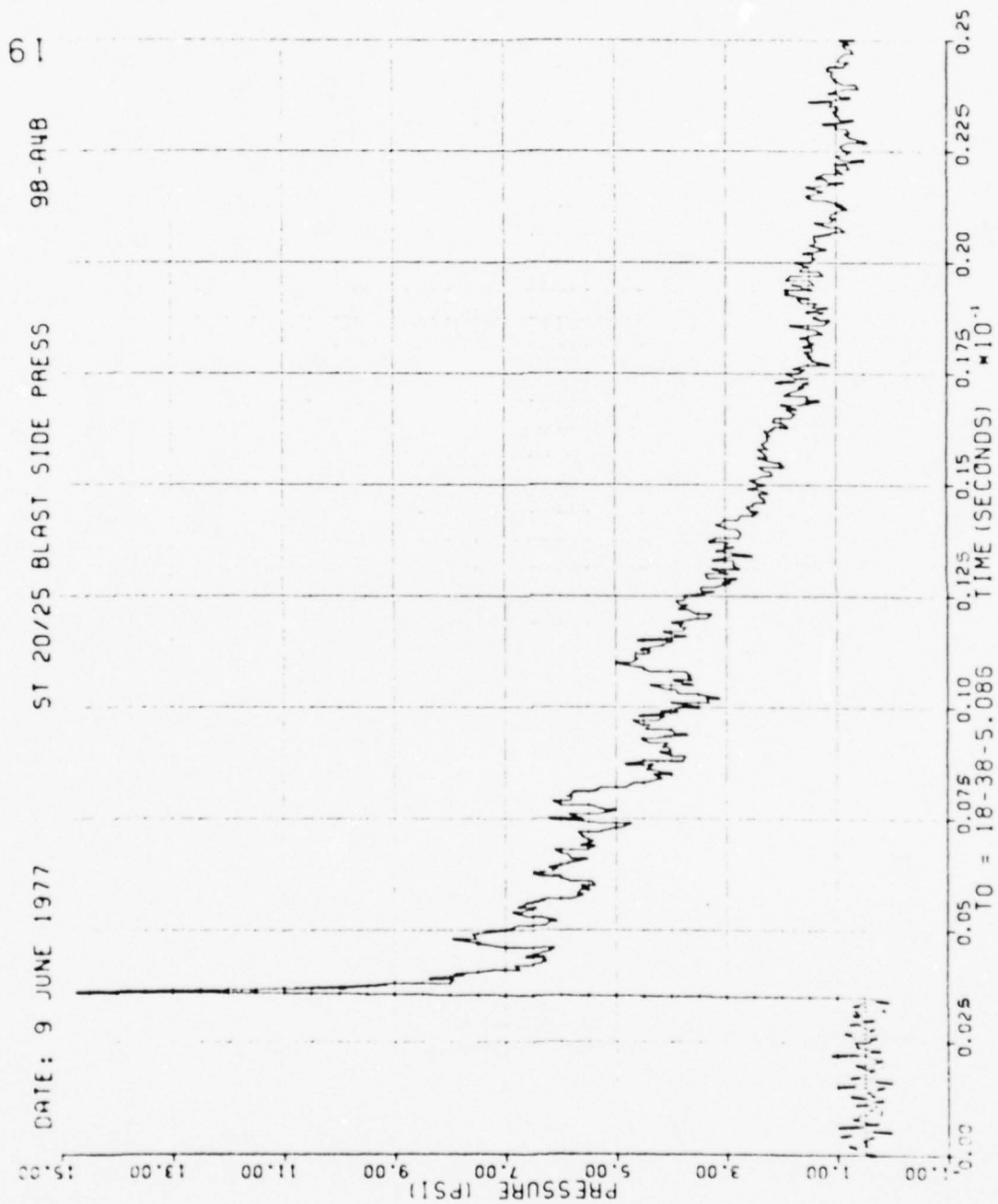


Figure 27. Blastward and Leeward Wing Pressures, Run 9B-A4, Intercept 1.

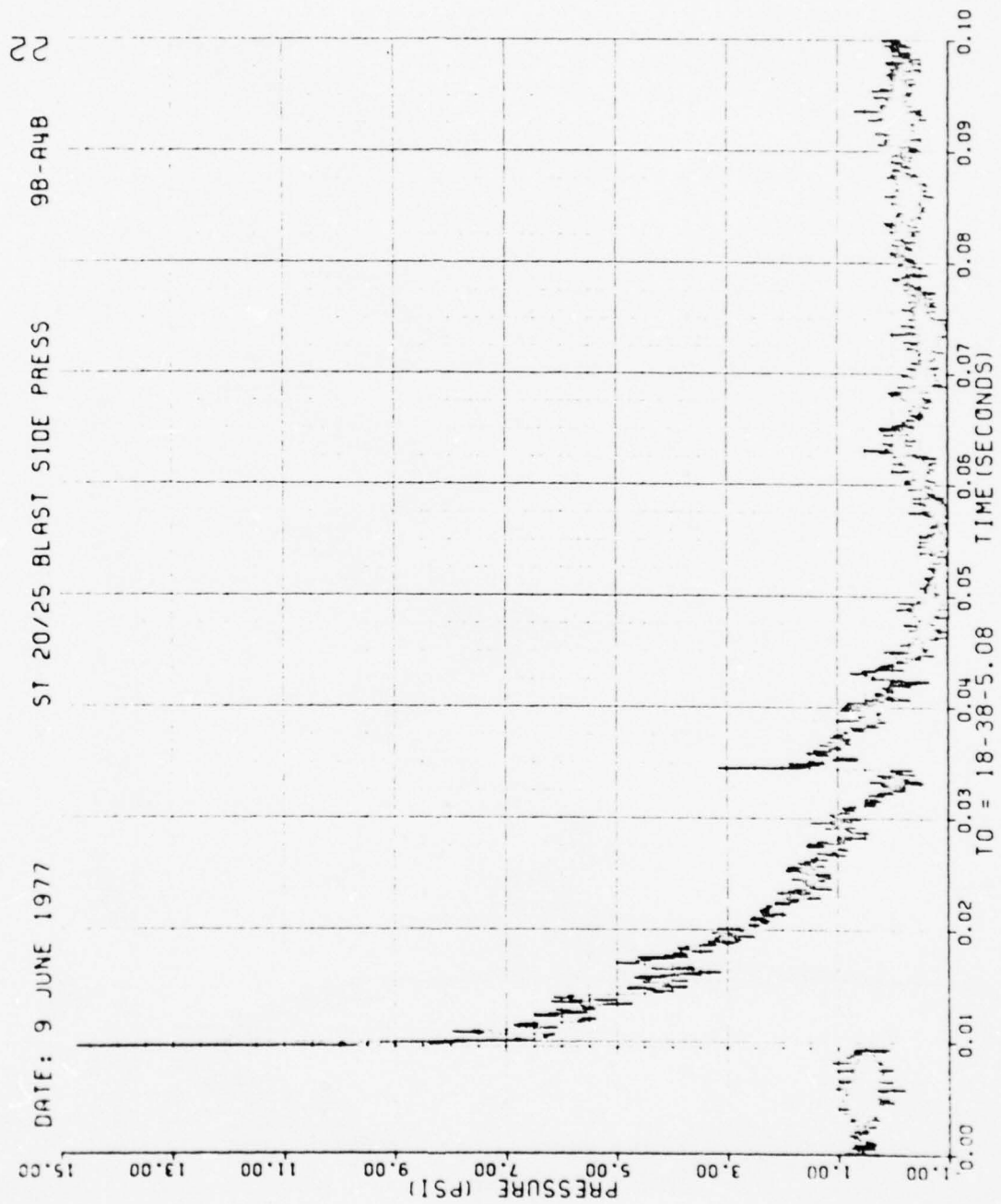


Figure 27. Continued

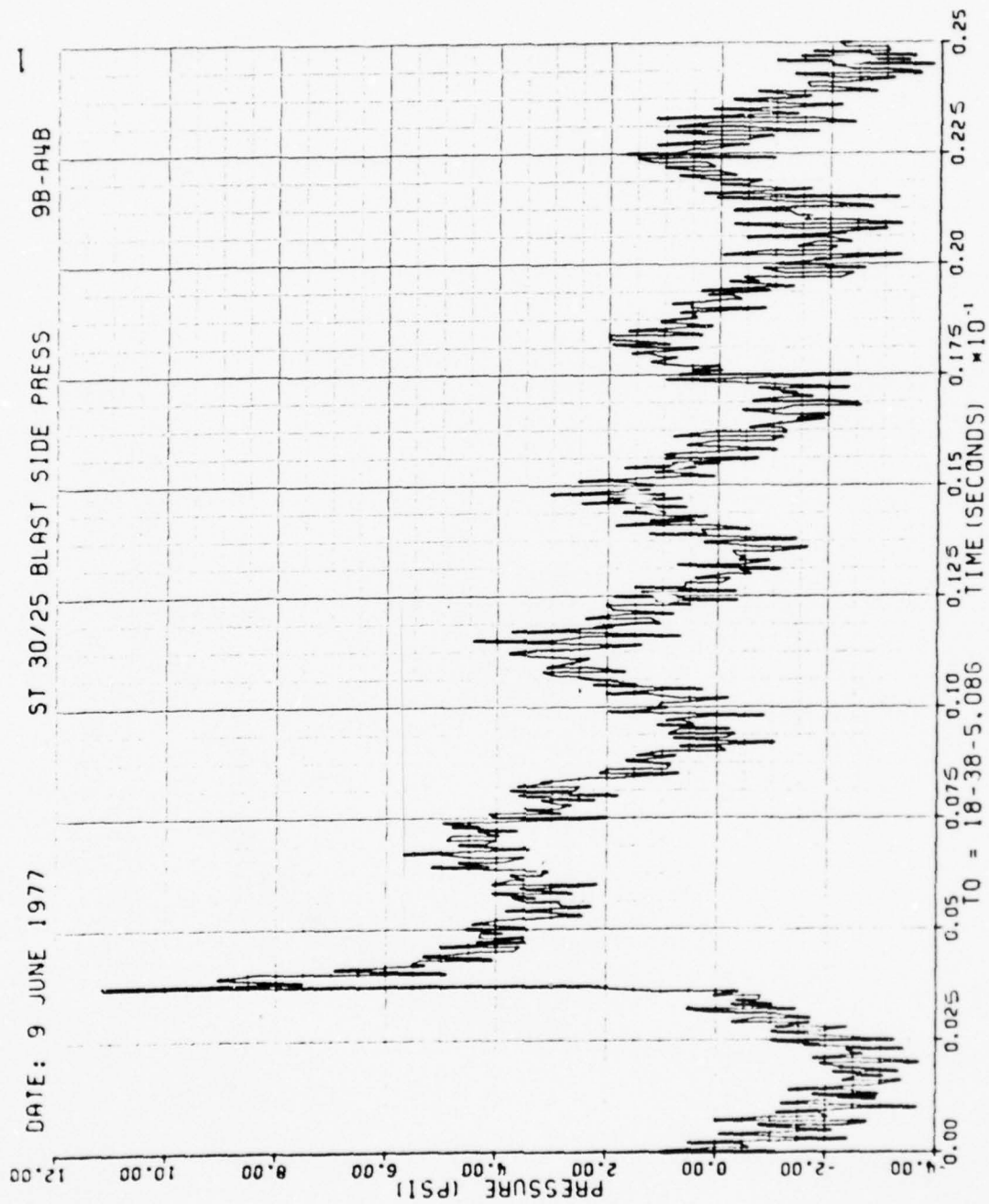


Figure 27. Continued

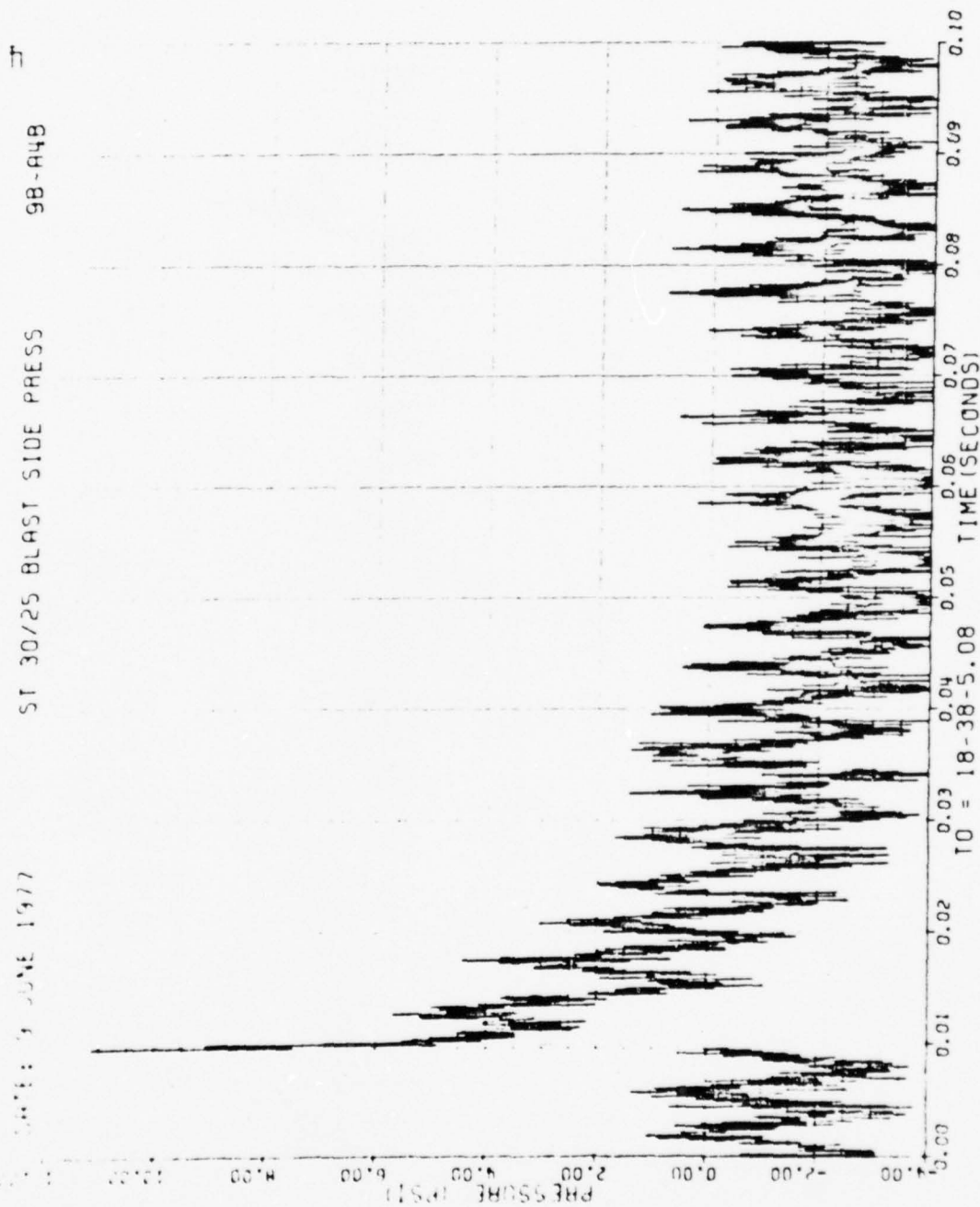


Figure 27. Continued

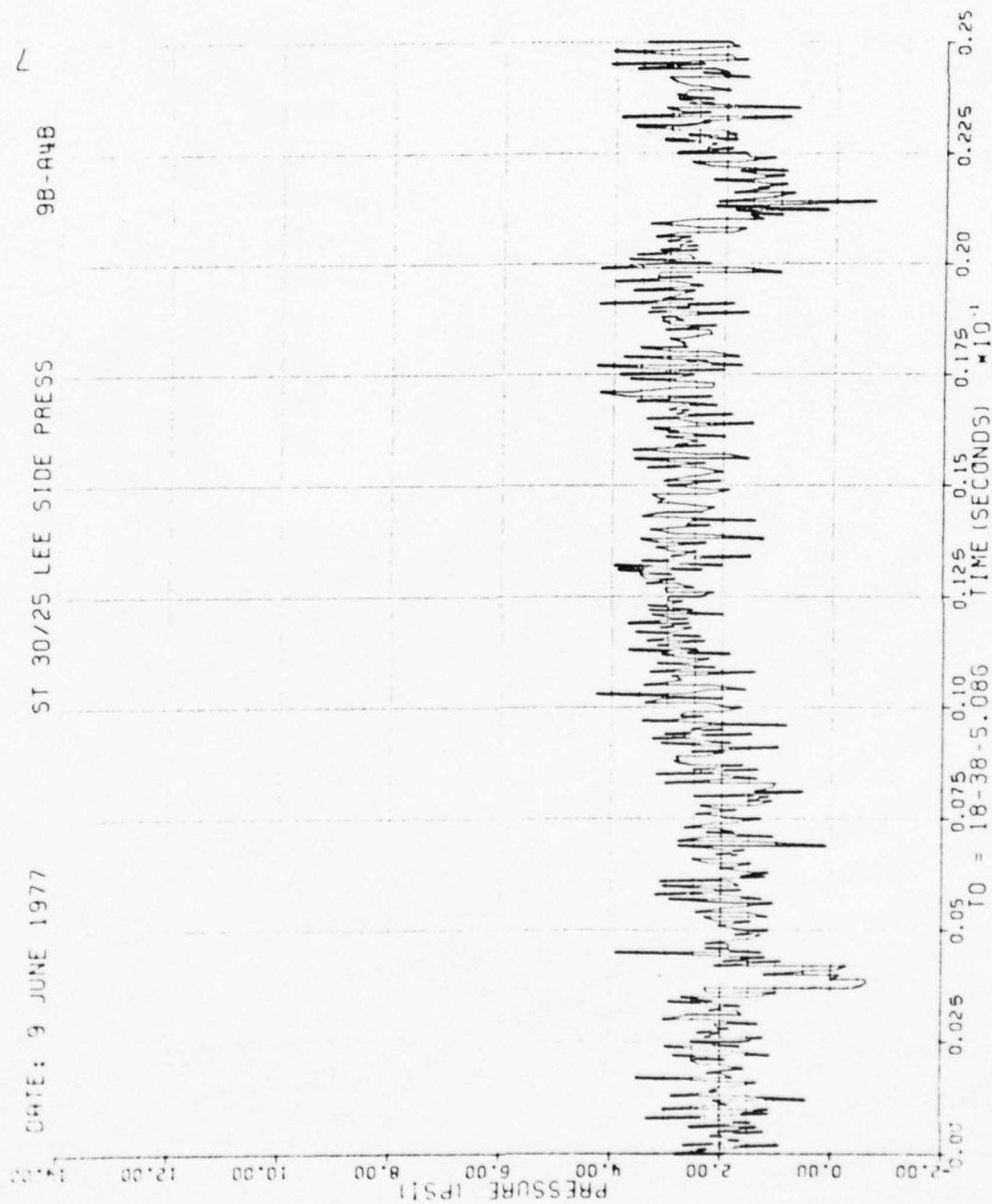


Figure 27. Continued

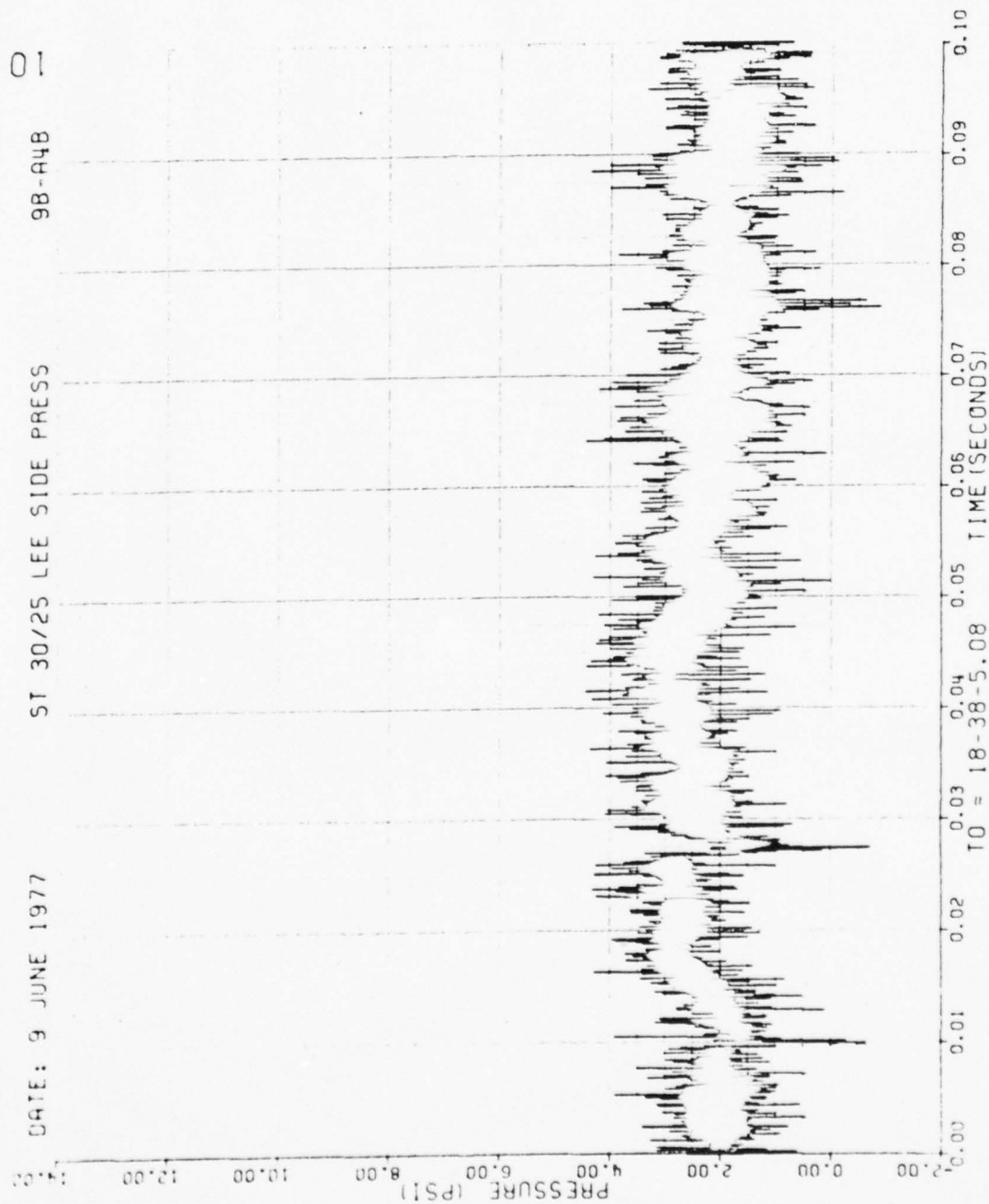


Figure 27. Concluded

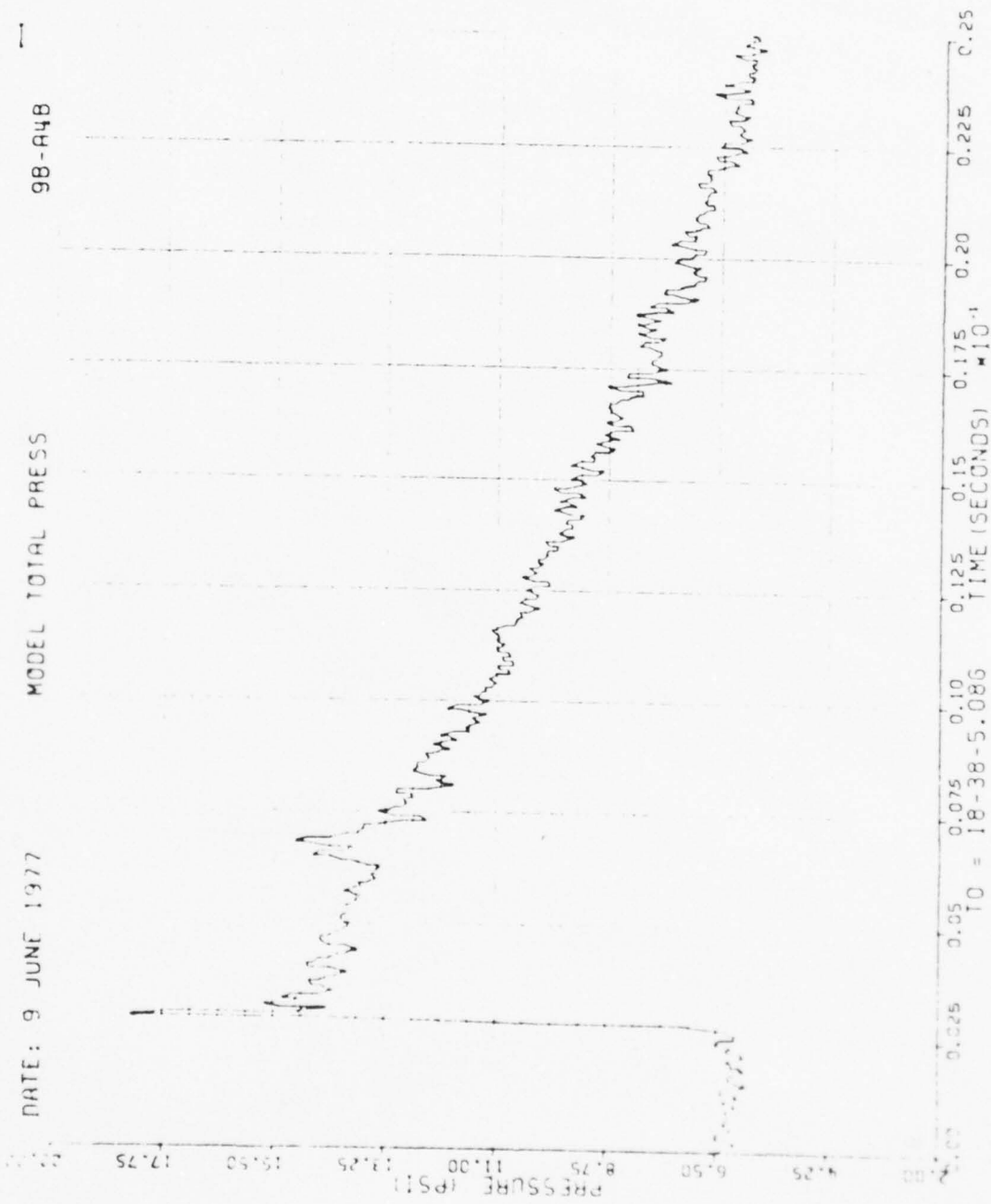


Figure 28. Total Pressure at Model, Run 9B-A4, Intercept 1.

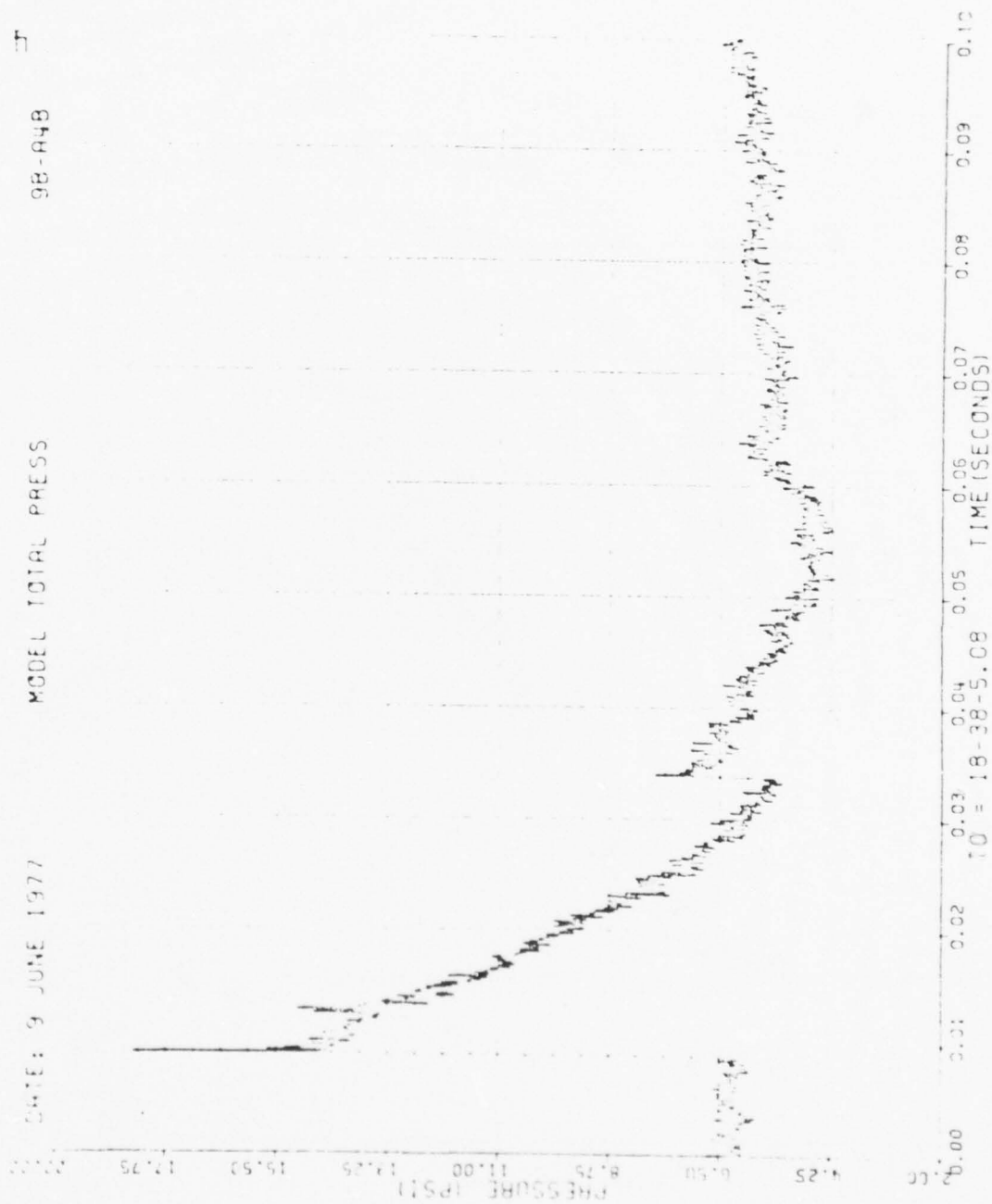


Figure 28. Concluded

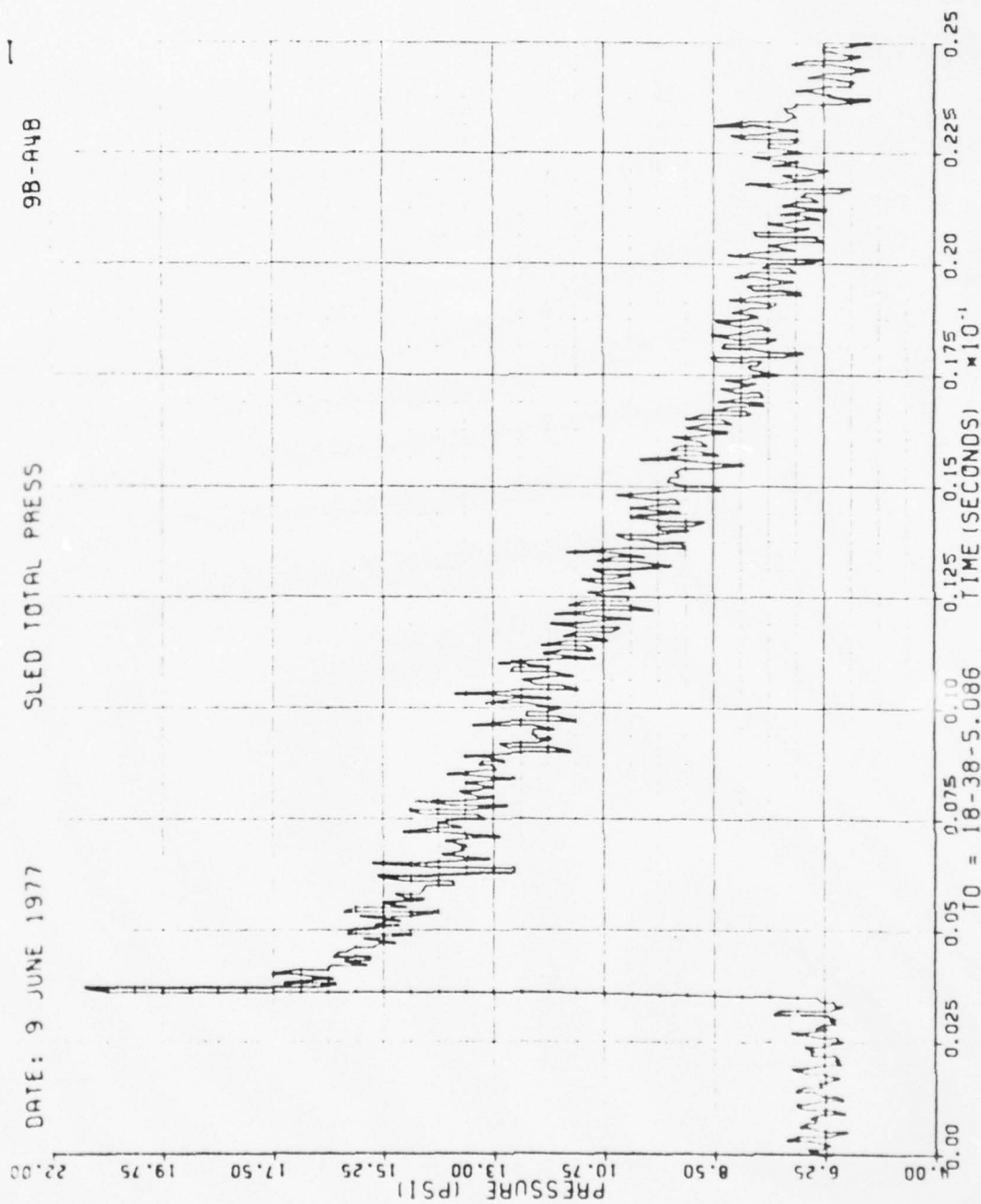


Figure 29. Total Pressure at Sled, Run 9B-A4, Intercept 1.

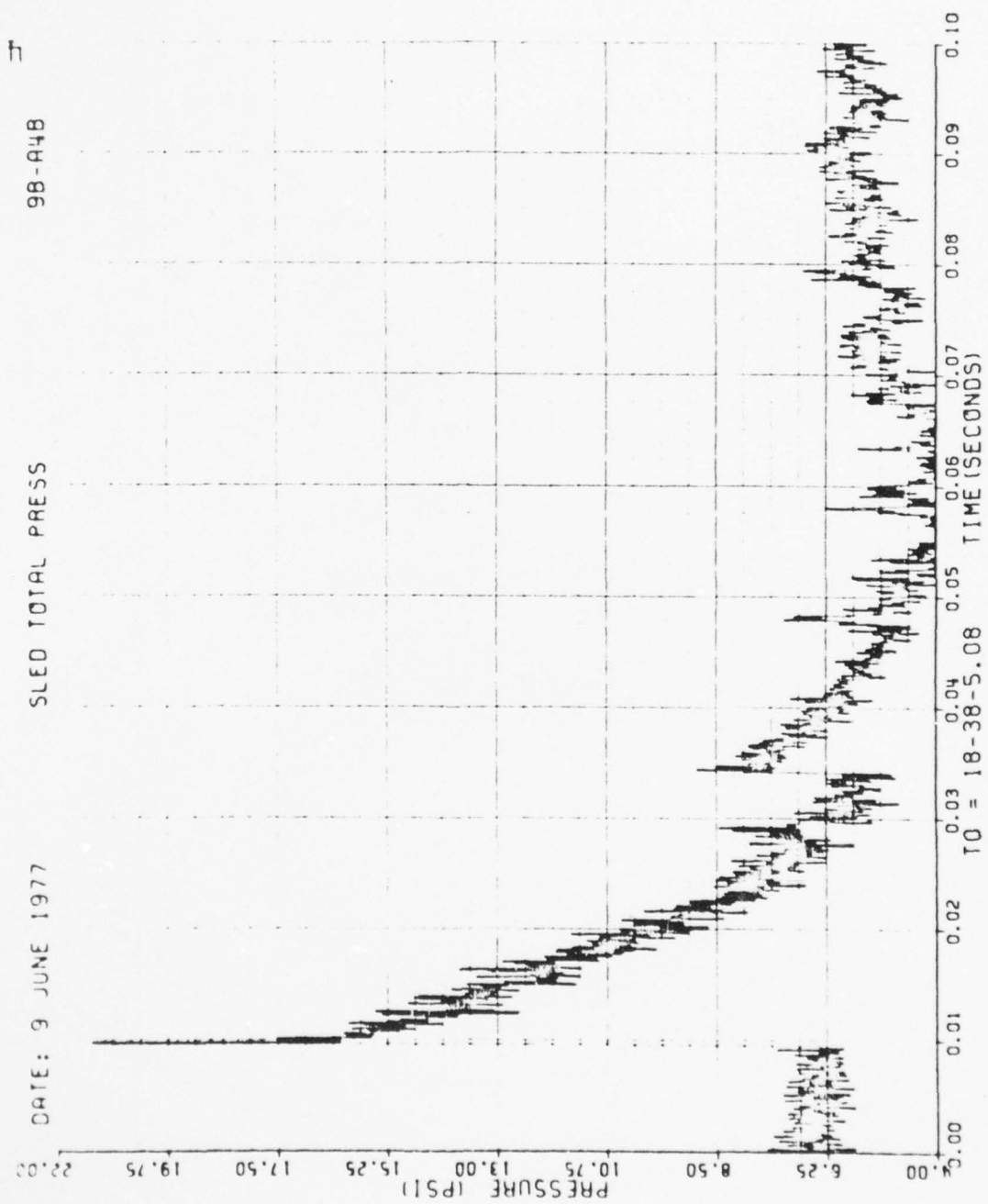


Figure 29. Concluded

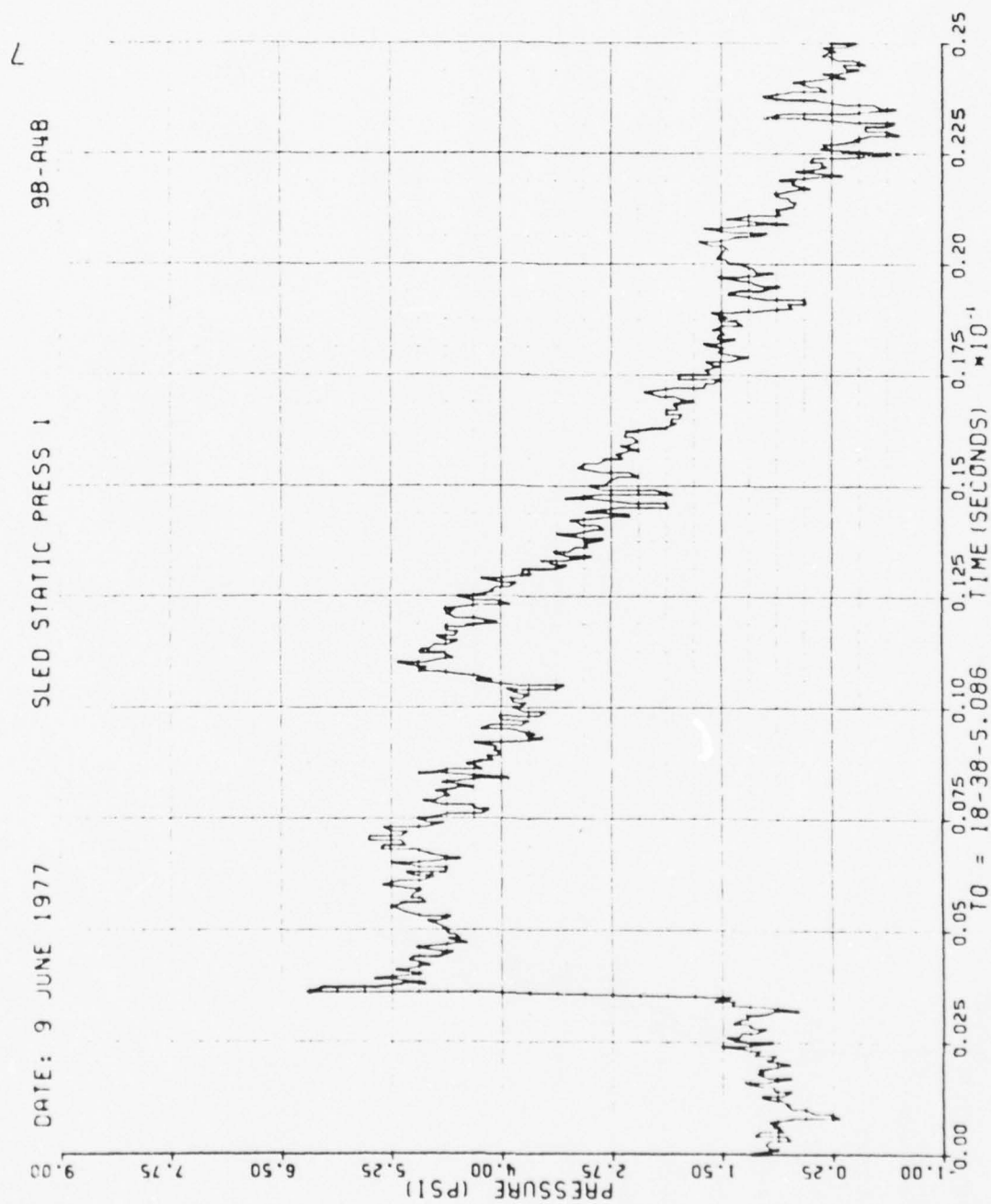


Figure 30. Static Pressure 1 at Sled, Run 9B-A4, Intercept 1.

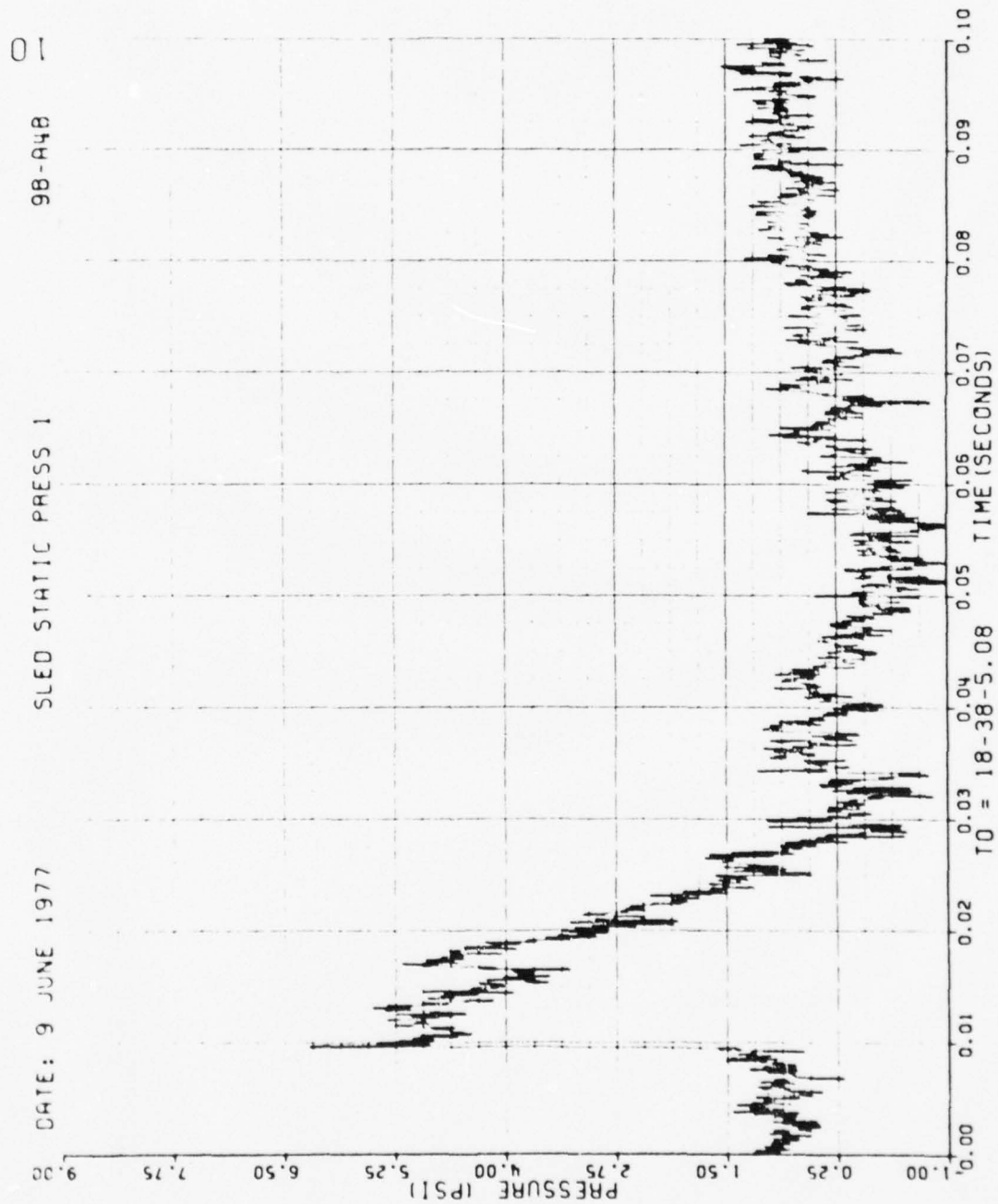


Figure 30. Concluded

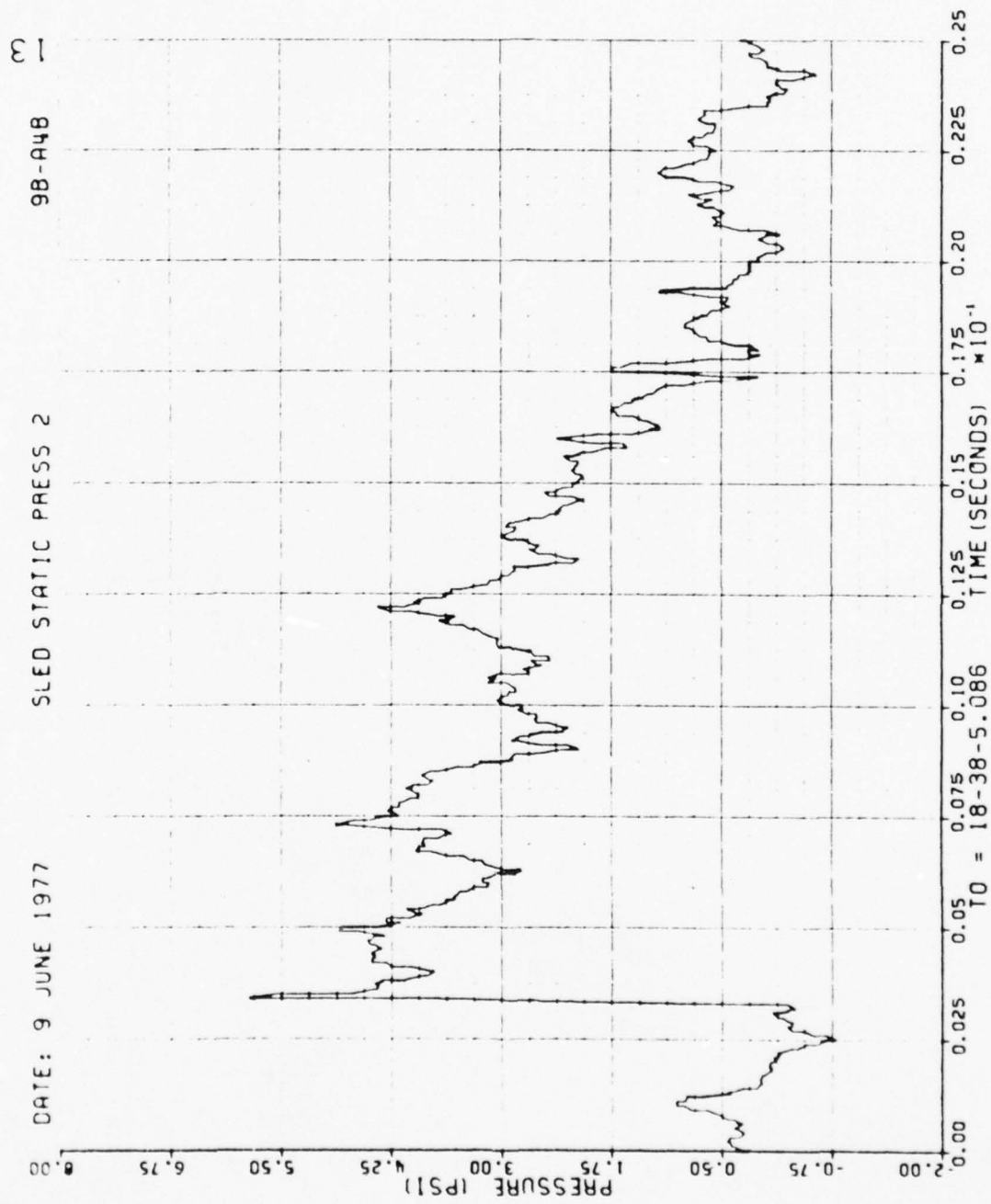


Figure 31. Static Pressure 2 at Sled, Run 9B-A4, Intercept 1.

91

98-A4B

SLED STATIC PRESS 2

DATE: 9 JUNE 1977

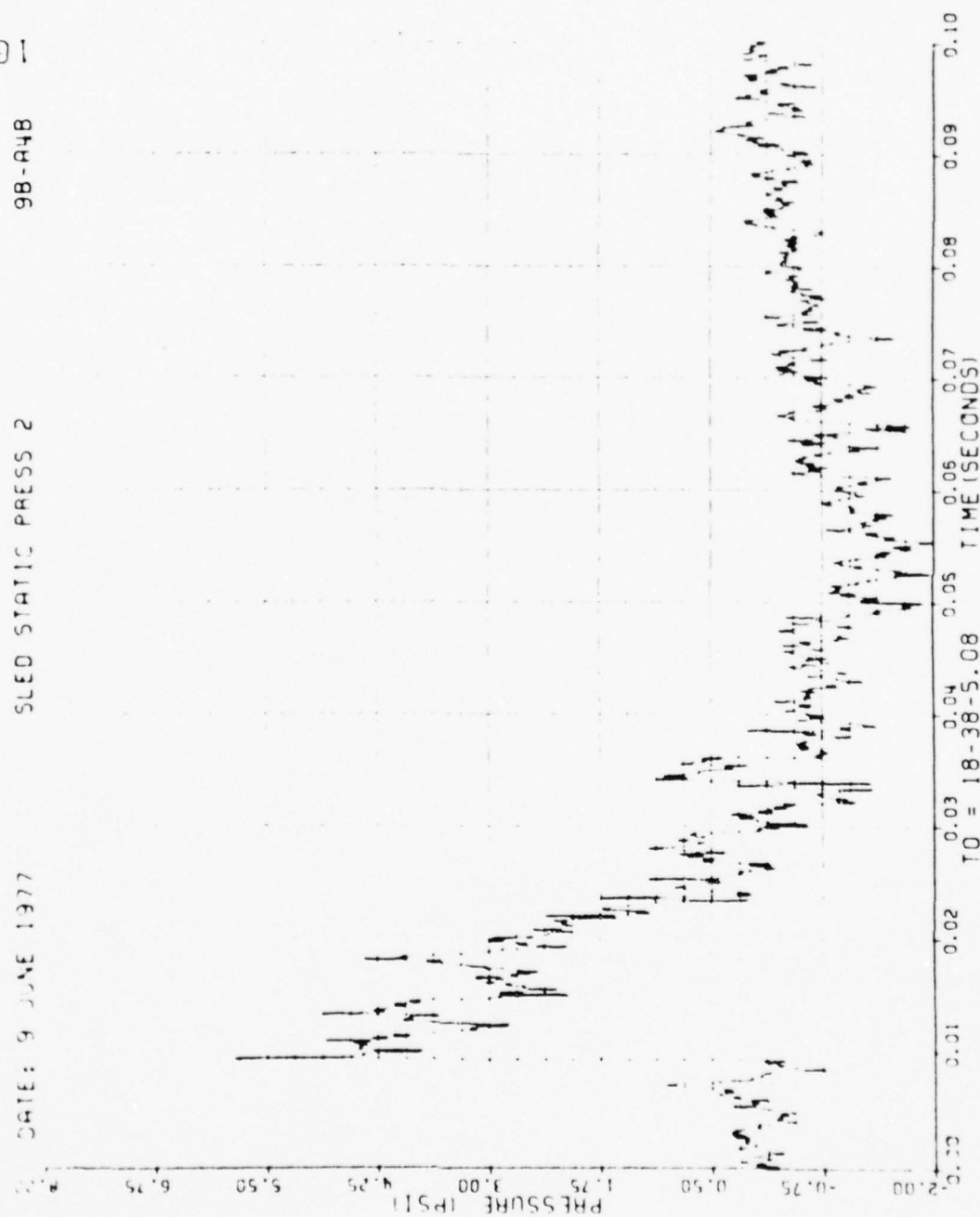


Figure 31. Concluded

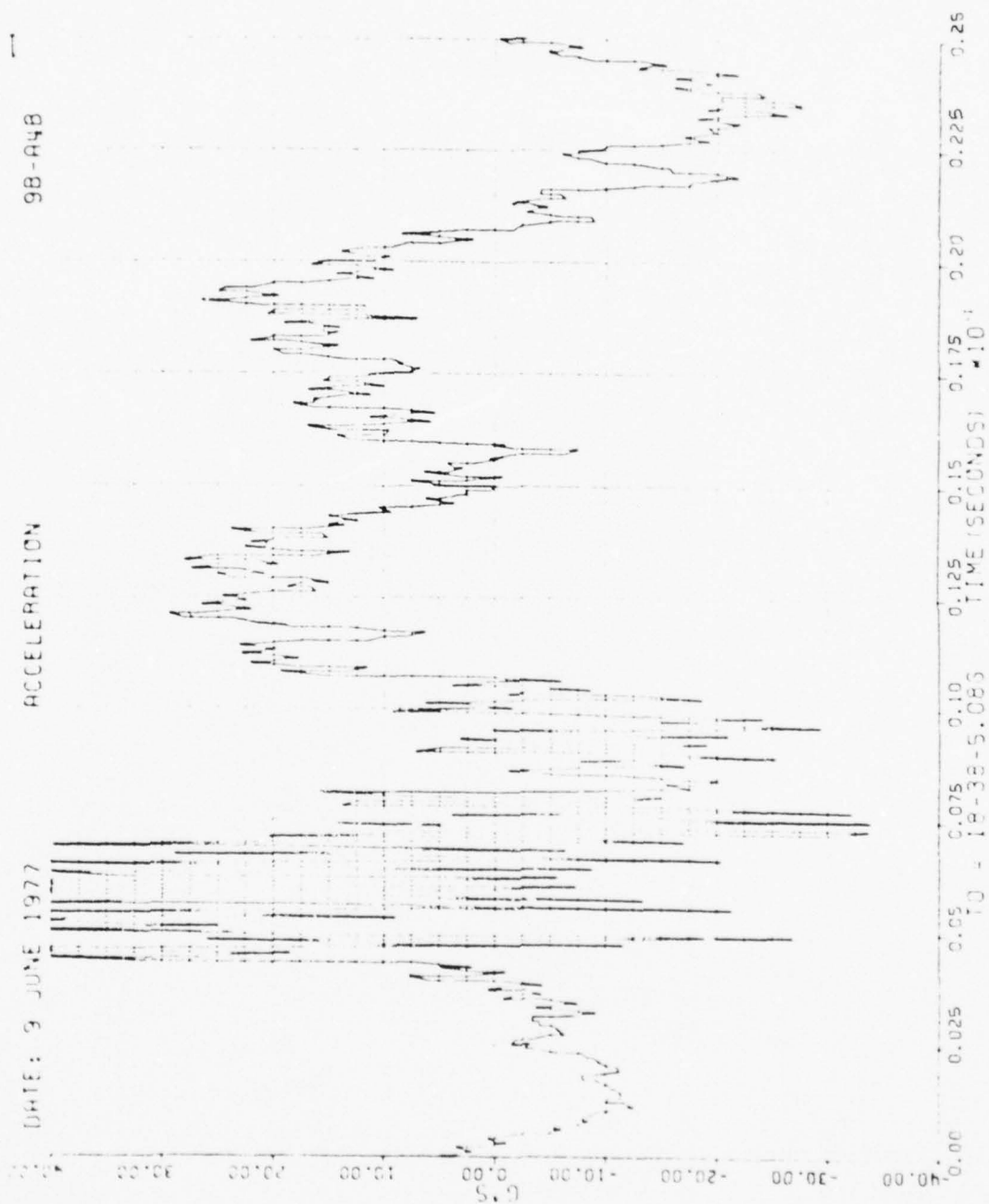


Figure 32. Wing Acceleration, Run 9B-A4, Intercept 1.

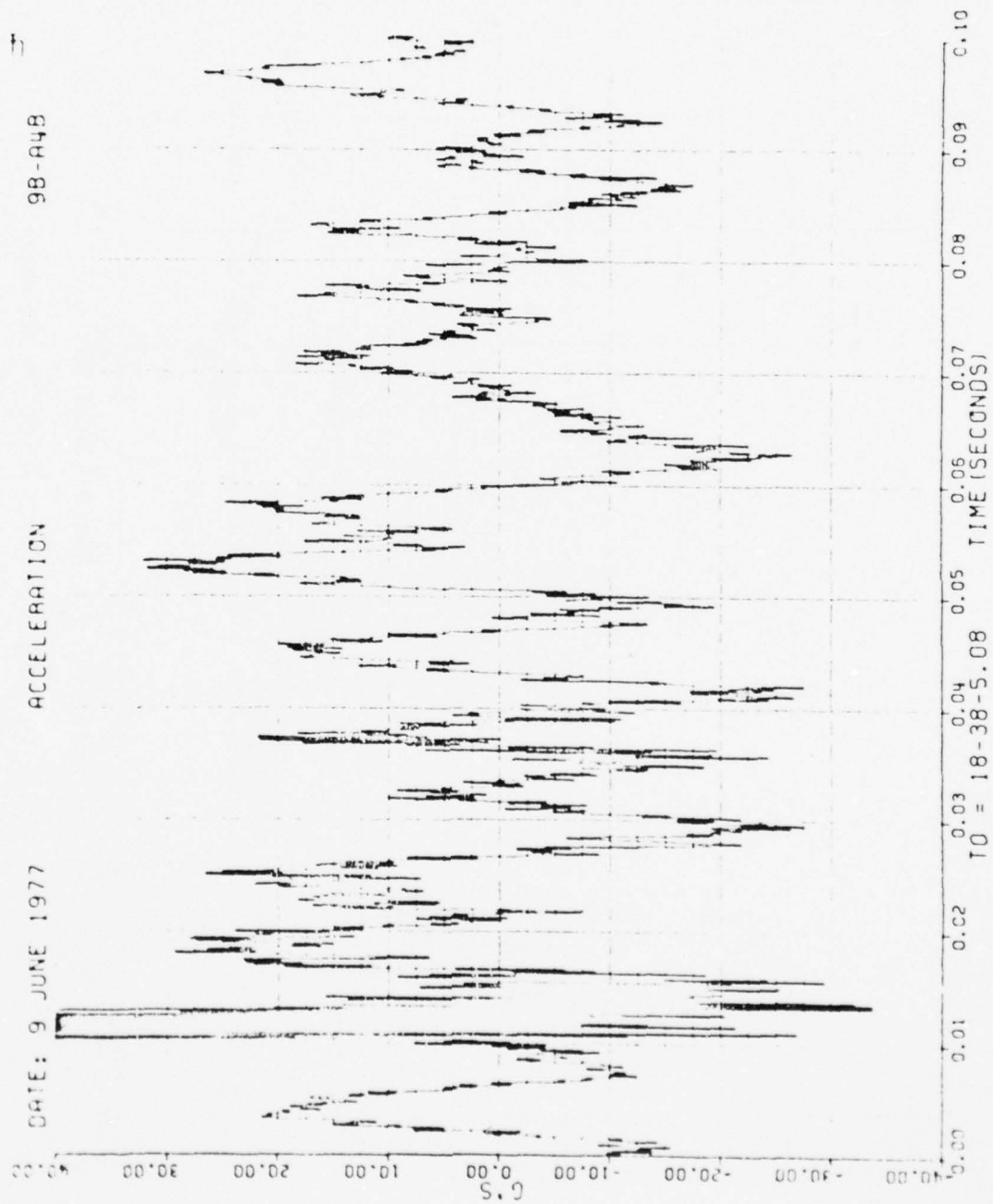


Figure 32. Concluded

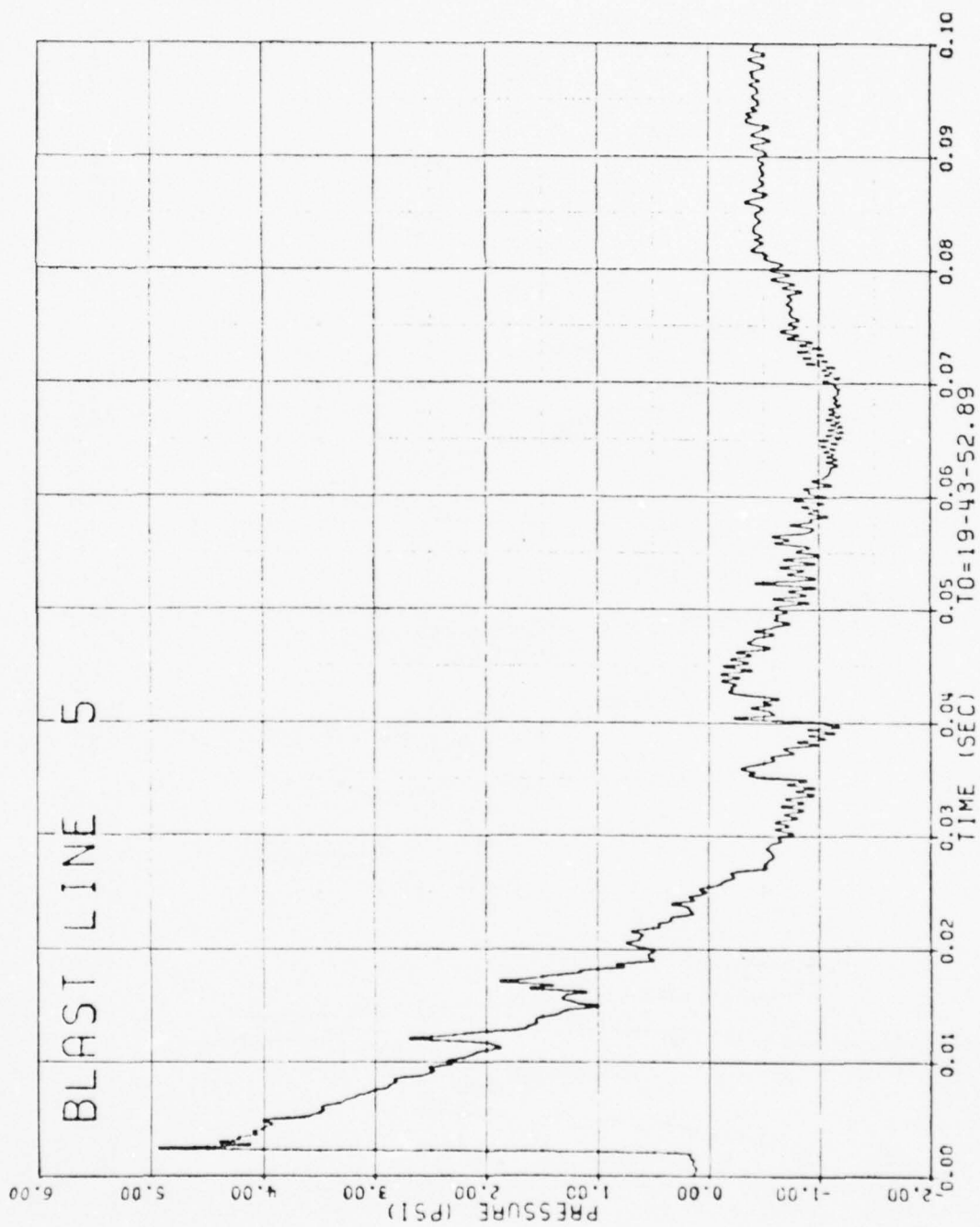


Figure 33. Blast-line Overpressures, Run 9B-A4, Intercept 2.

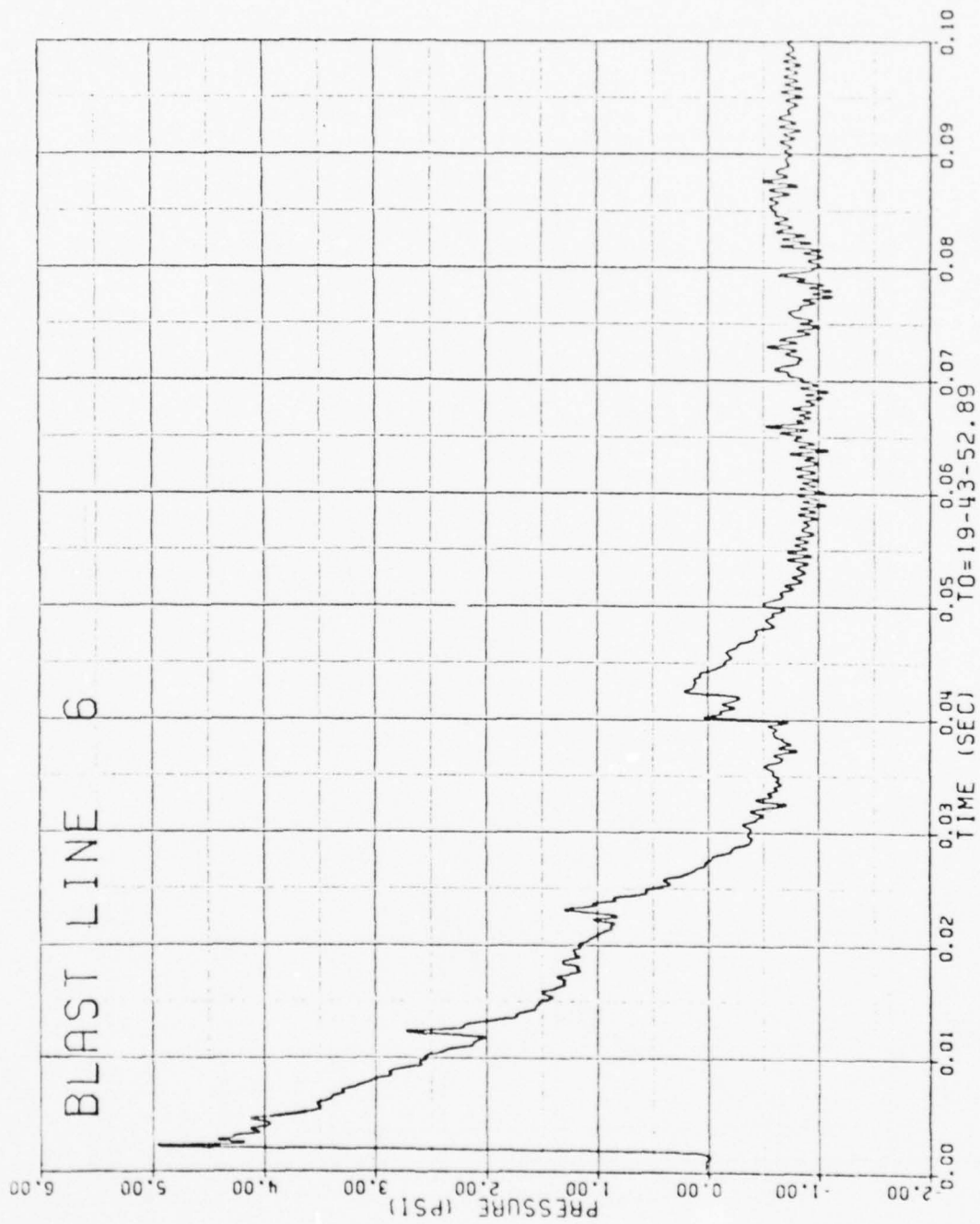


Figure 33. Continued

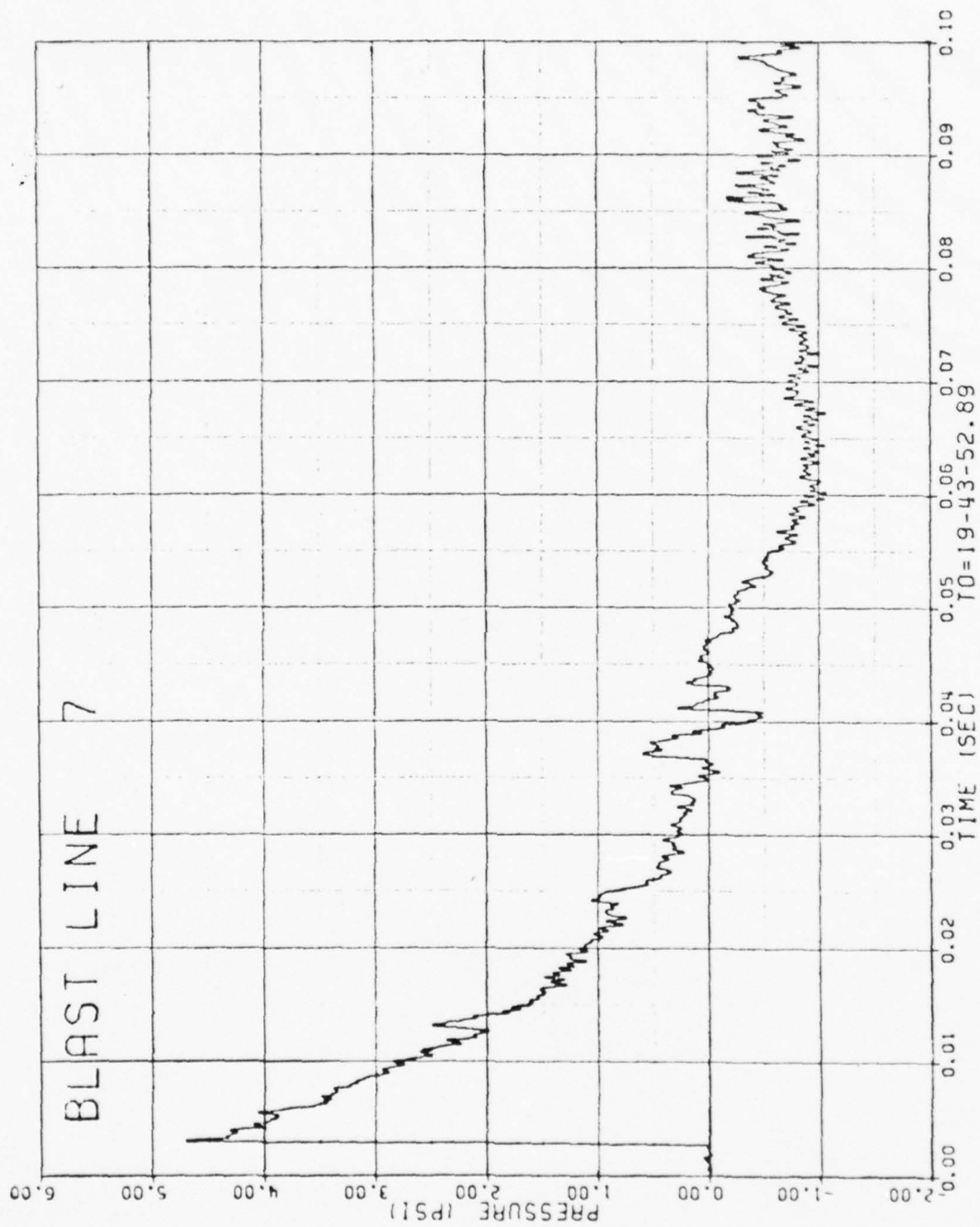


Figure 33. Continued

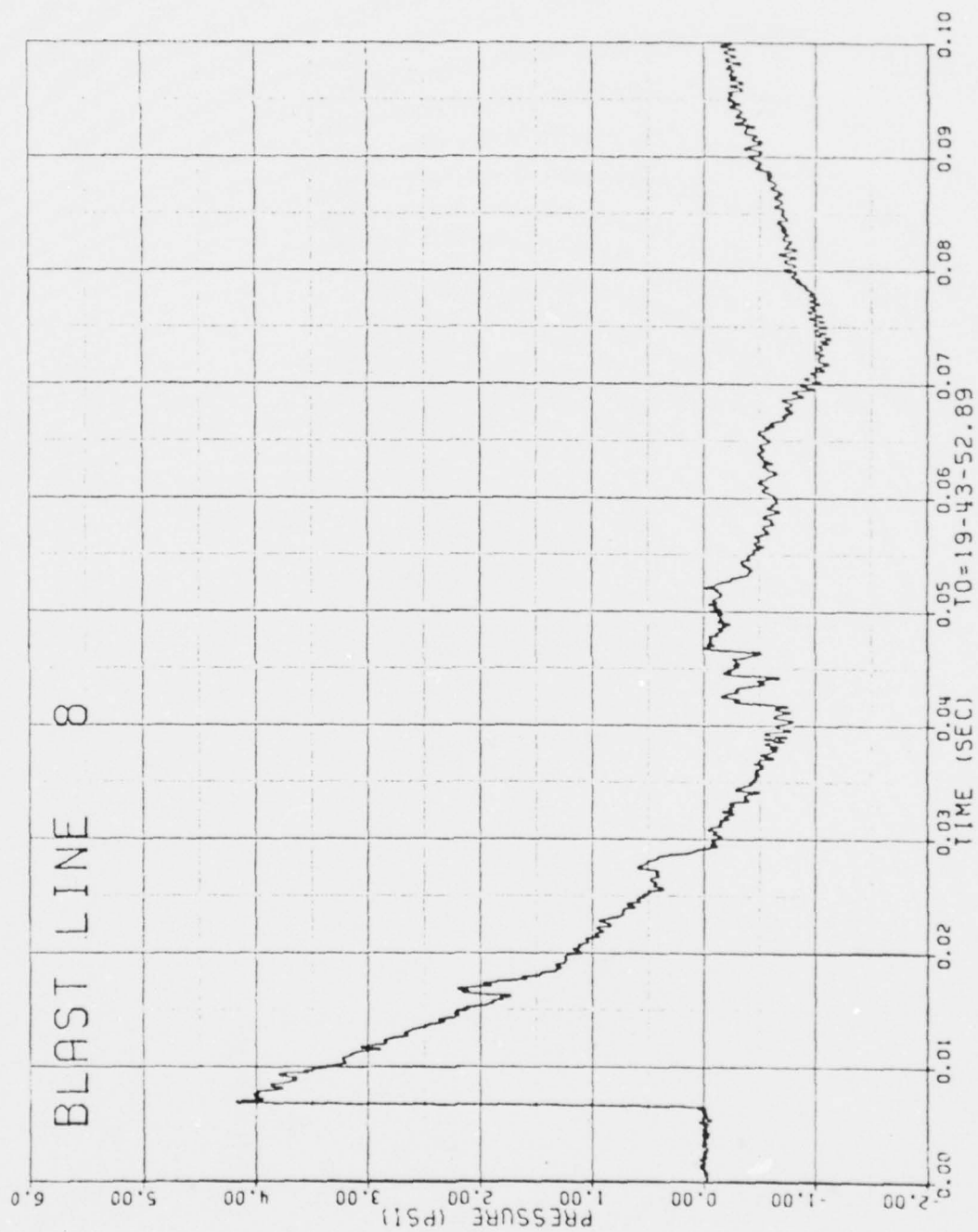


Figure 33. Concluded

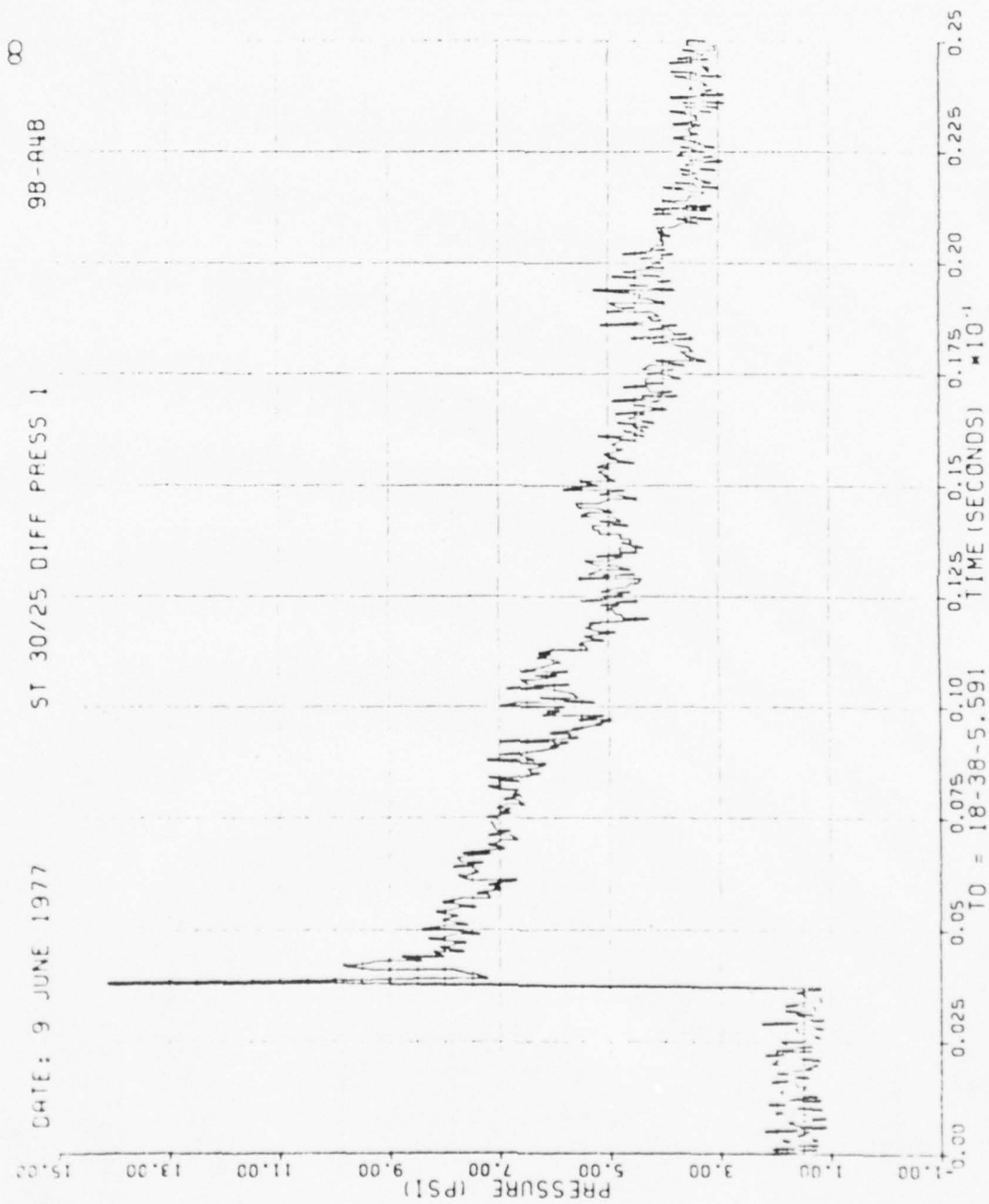


Figure 34. Differential Wing Pressures, Run 9B-A4, Intercept 2.

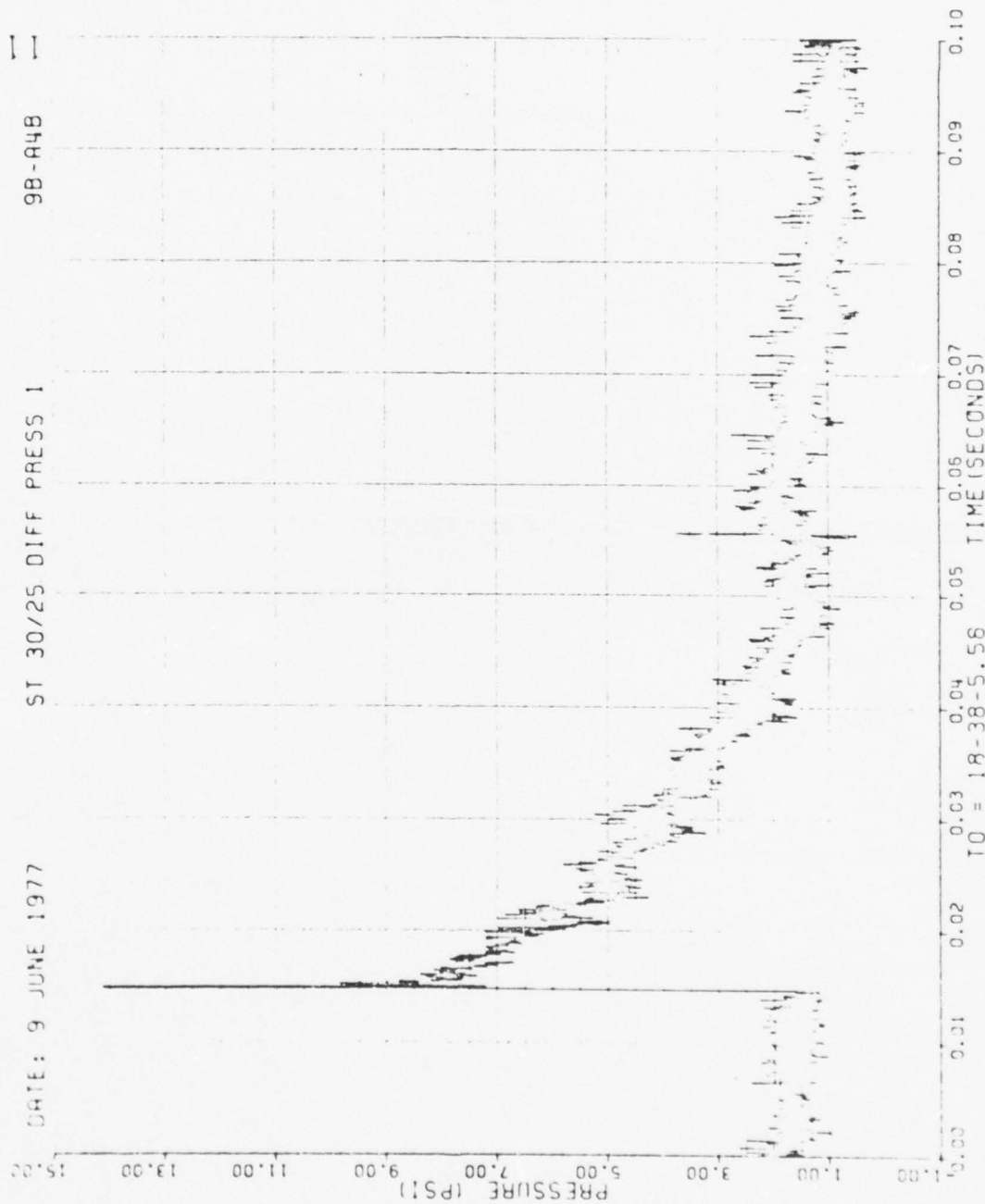


Figure 34. Continued

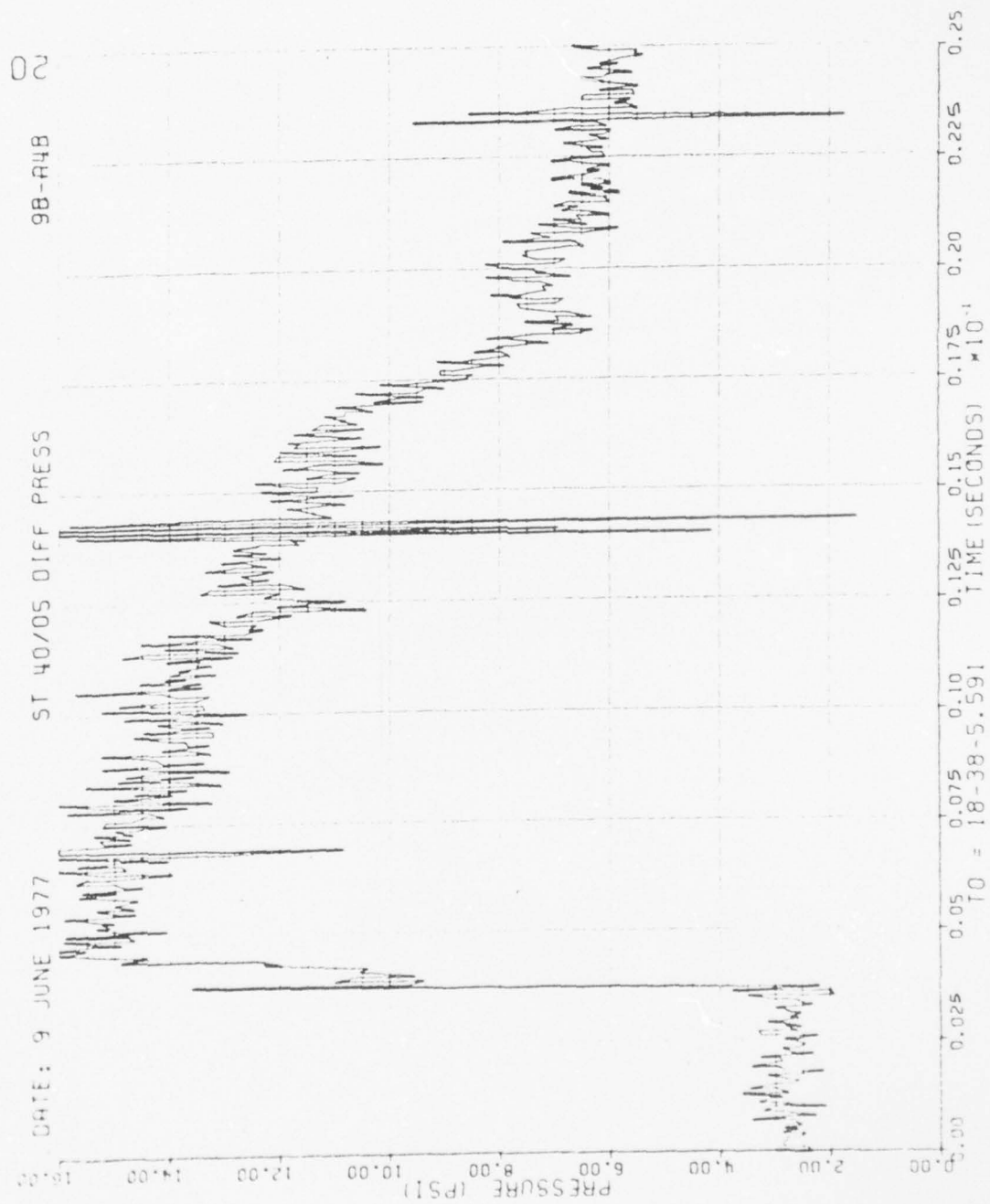


Figure 34. Continued

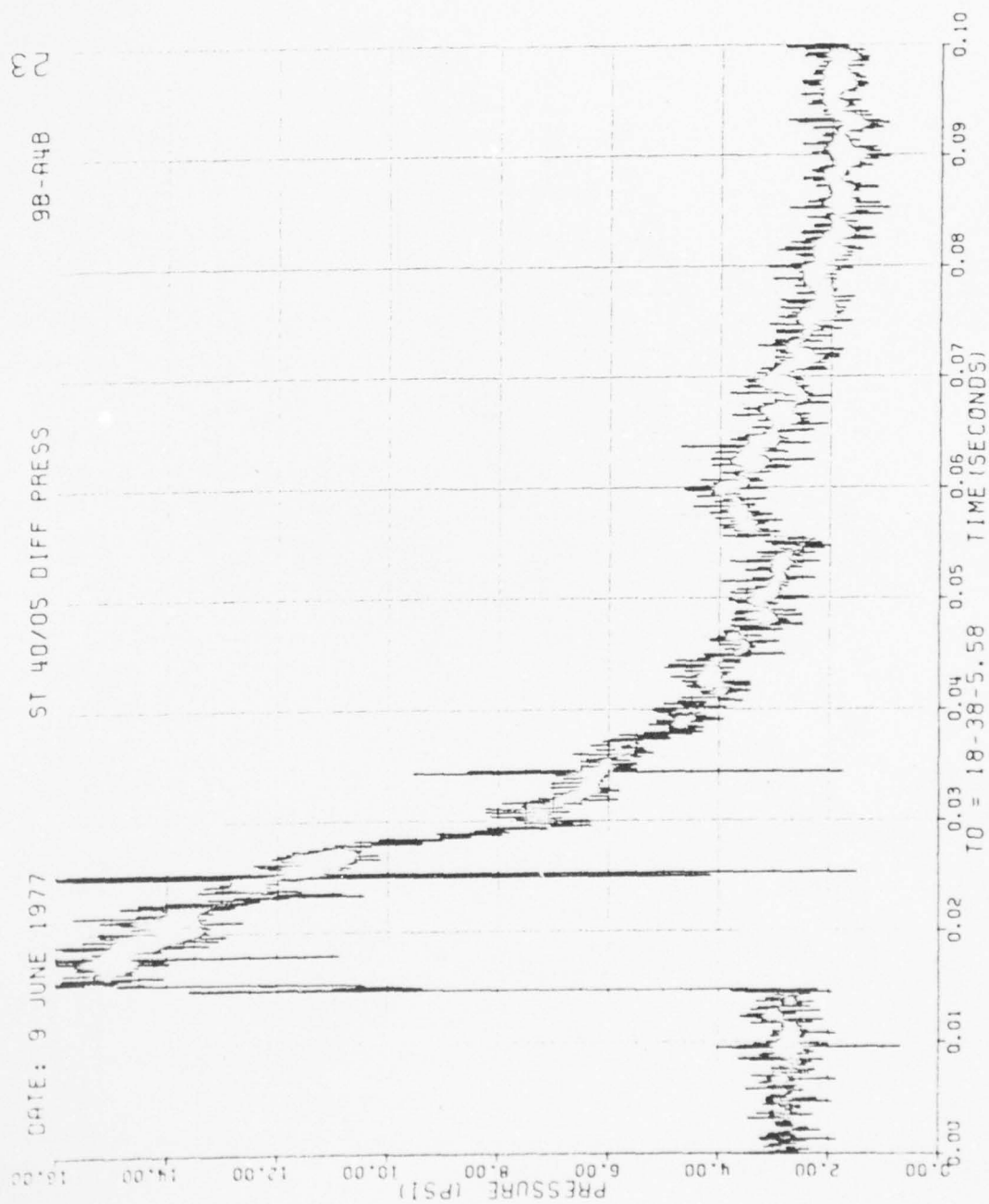


Figure 34. Continued

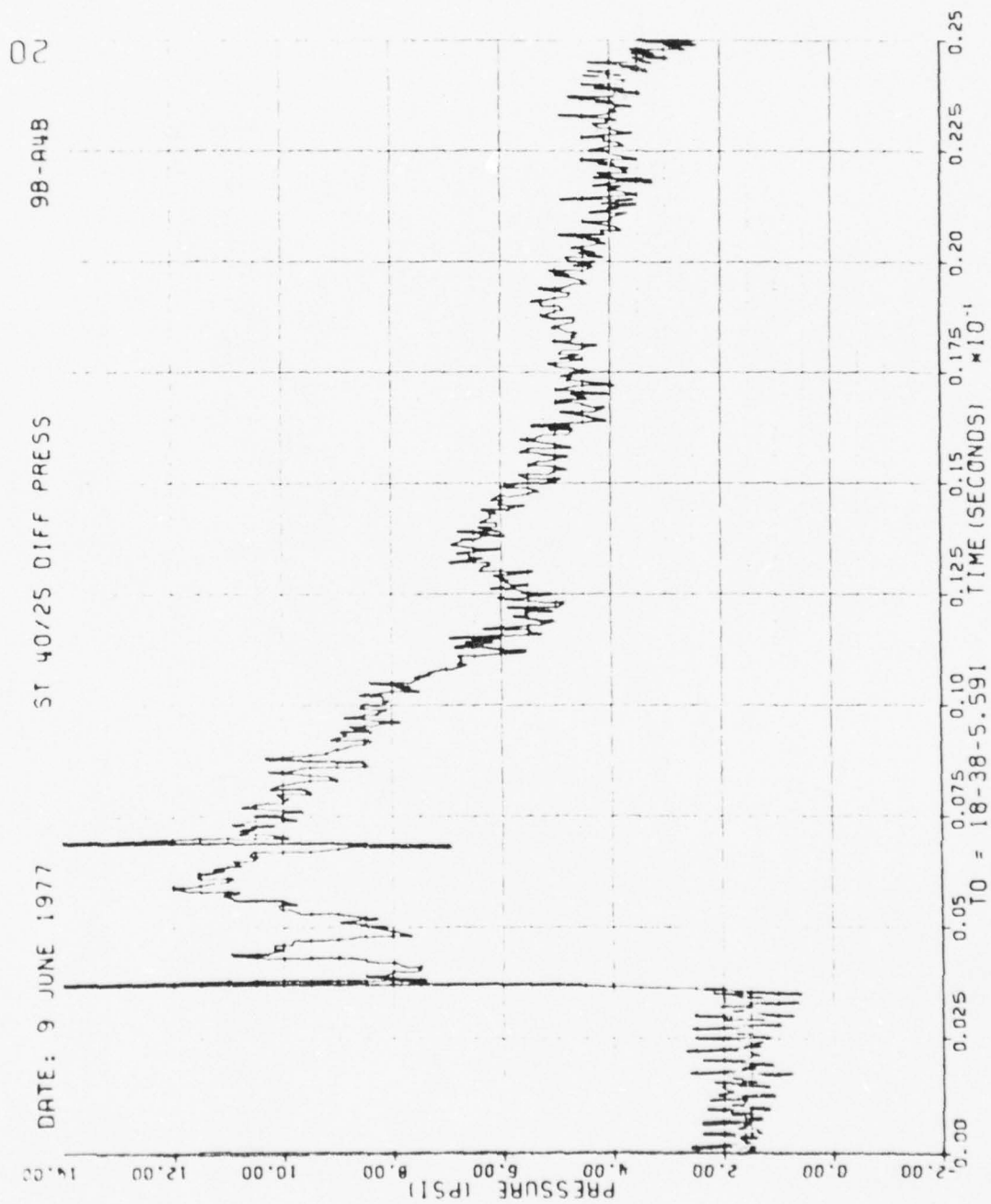


Figure 34. Continued

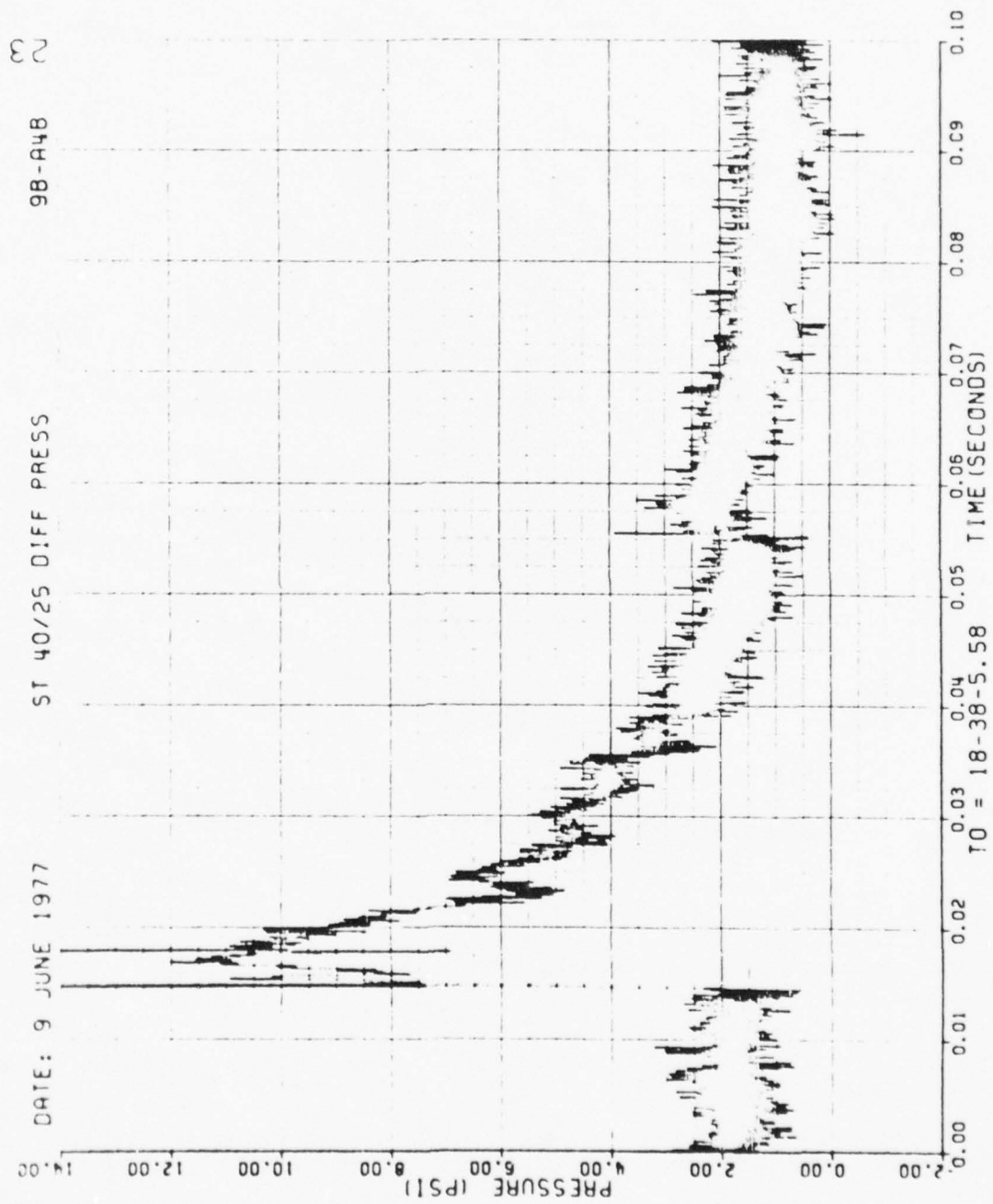


Figure 34. Continued

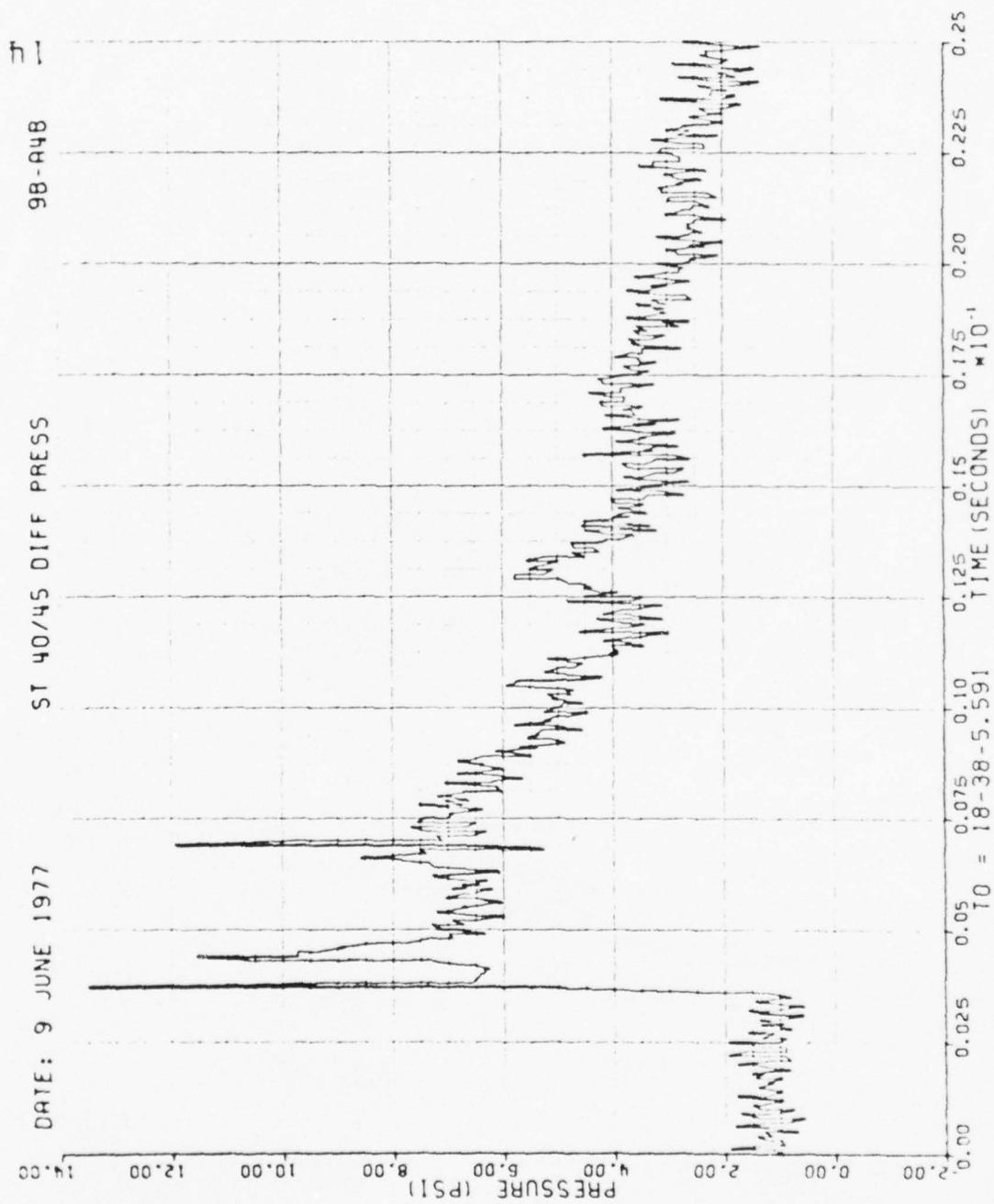


Figure 34. Continued

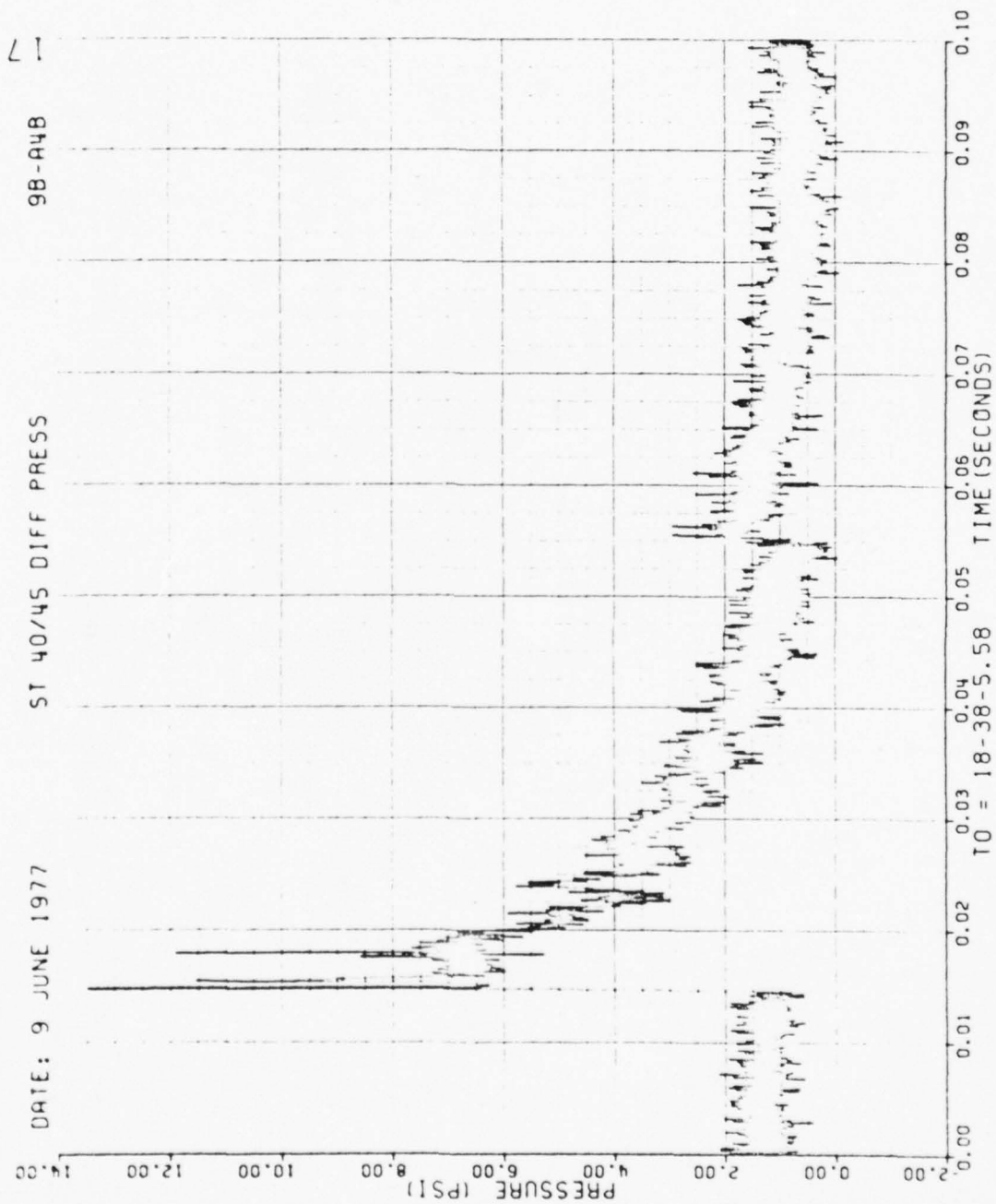


Figure 34. Continued

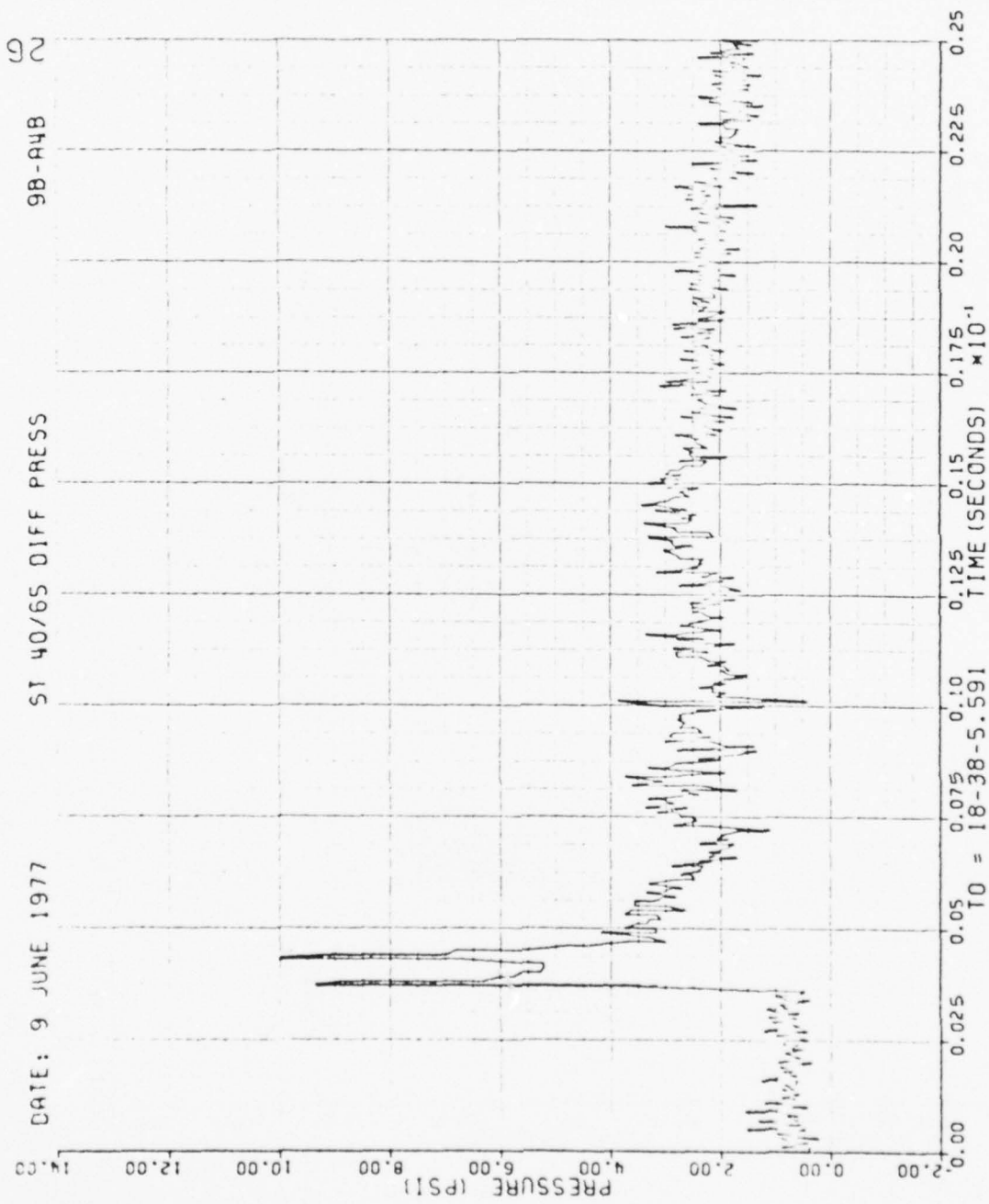


Figure 34. Continued

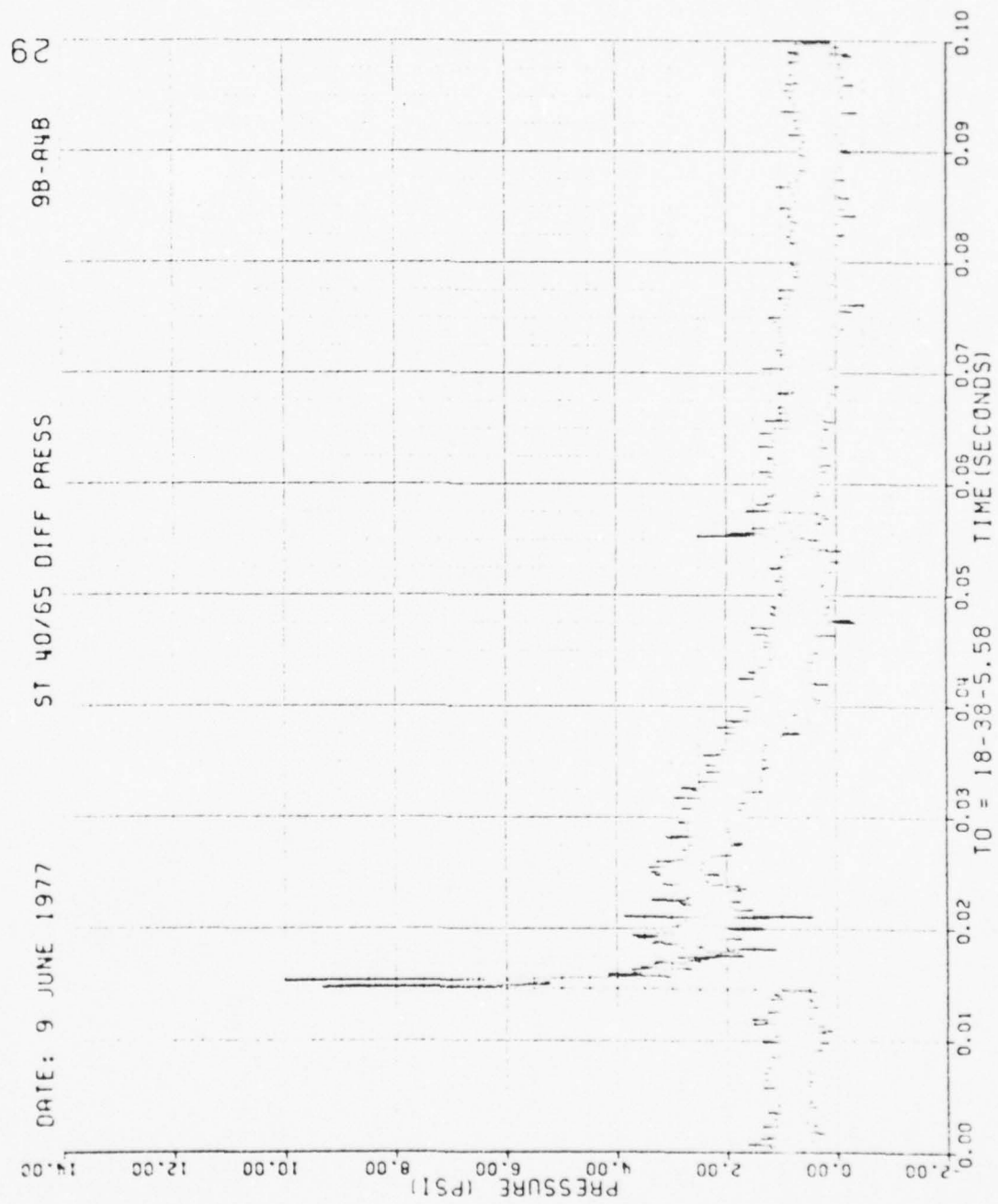


Figure 34. Continued

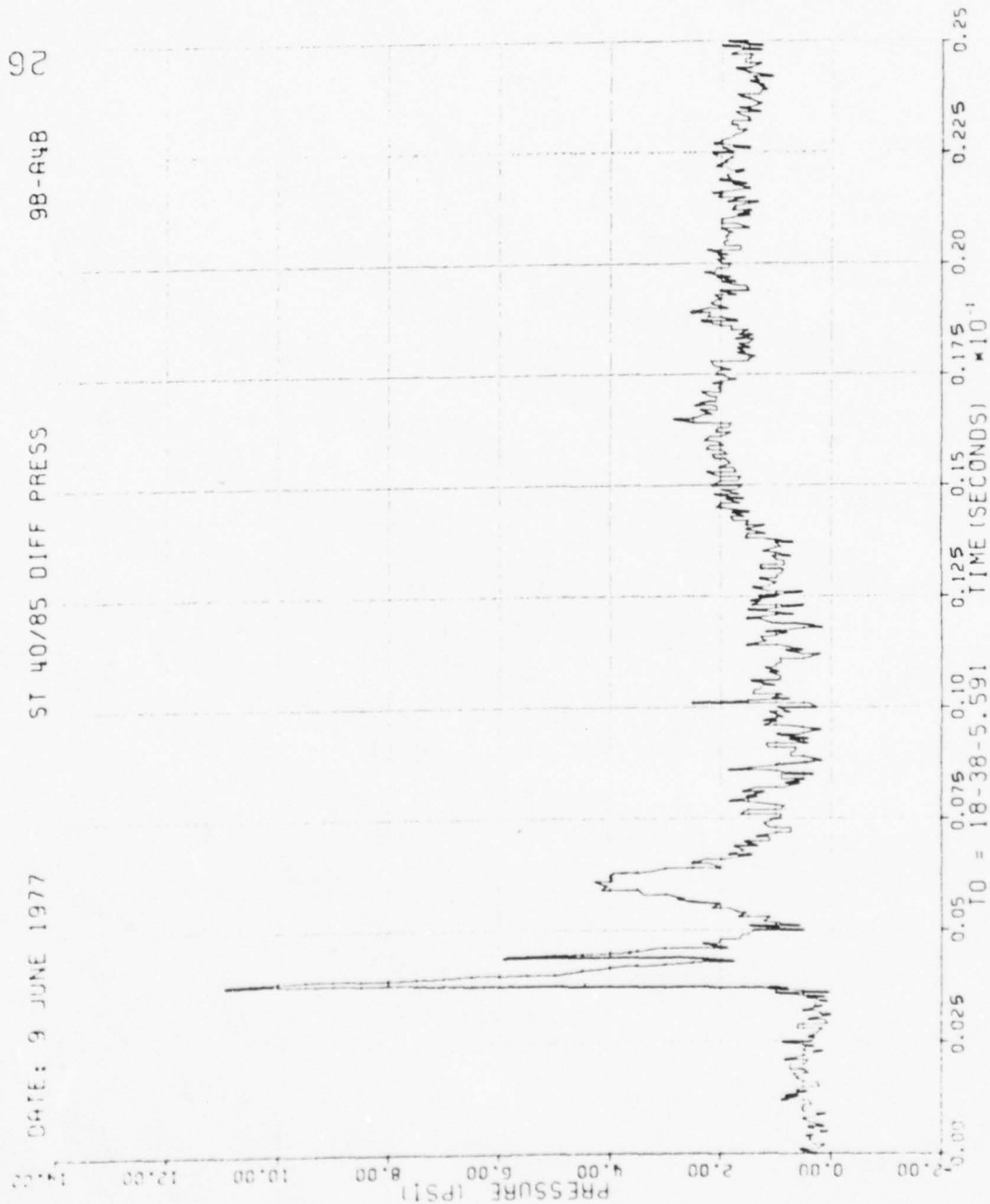


Figure 34. Continued

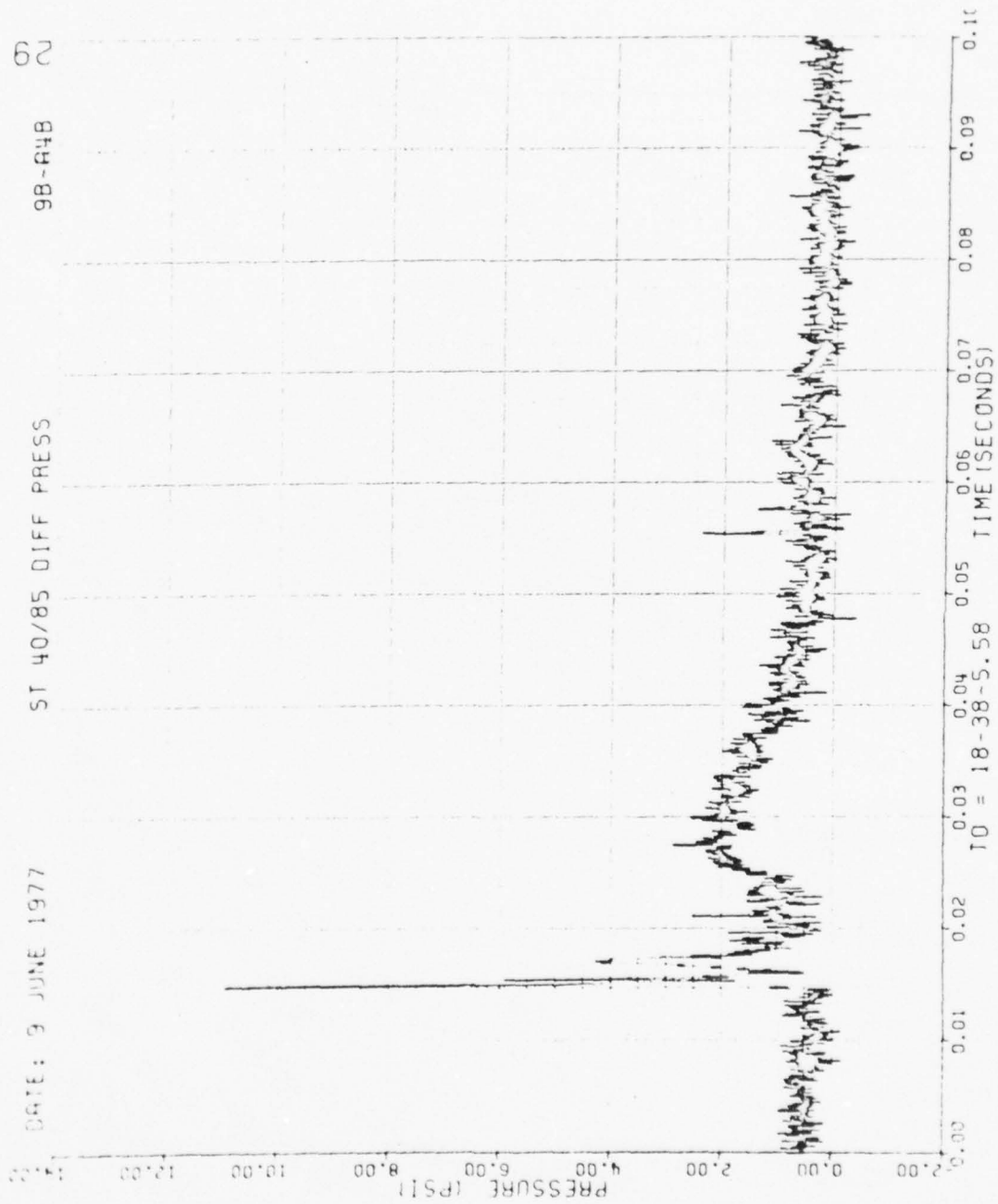


Figure 34. Continued

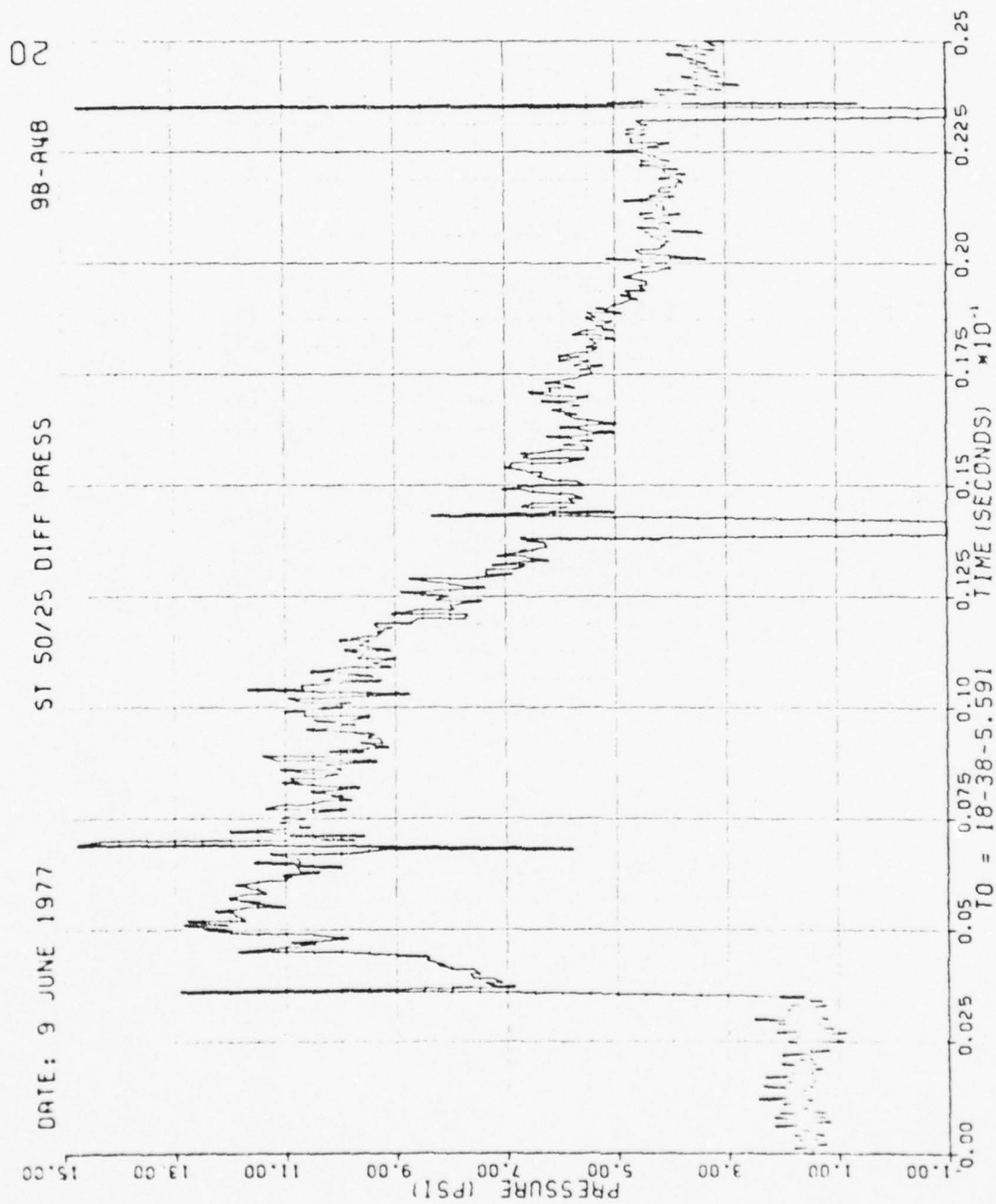


Figure 34. Continued

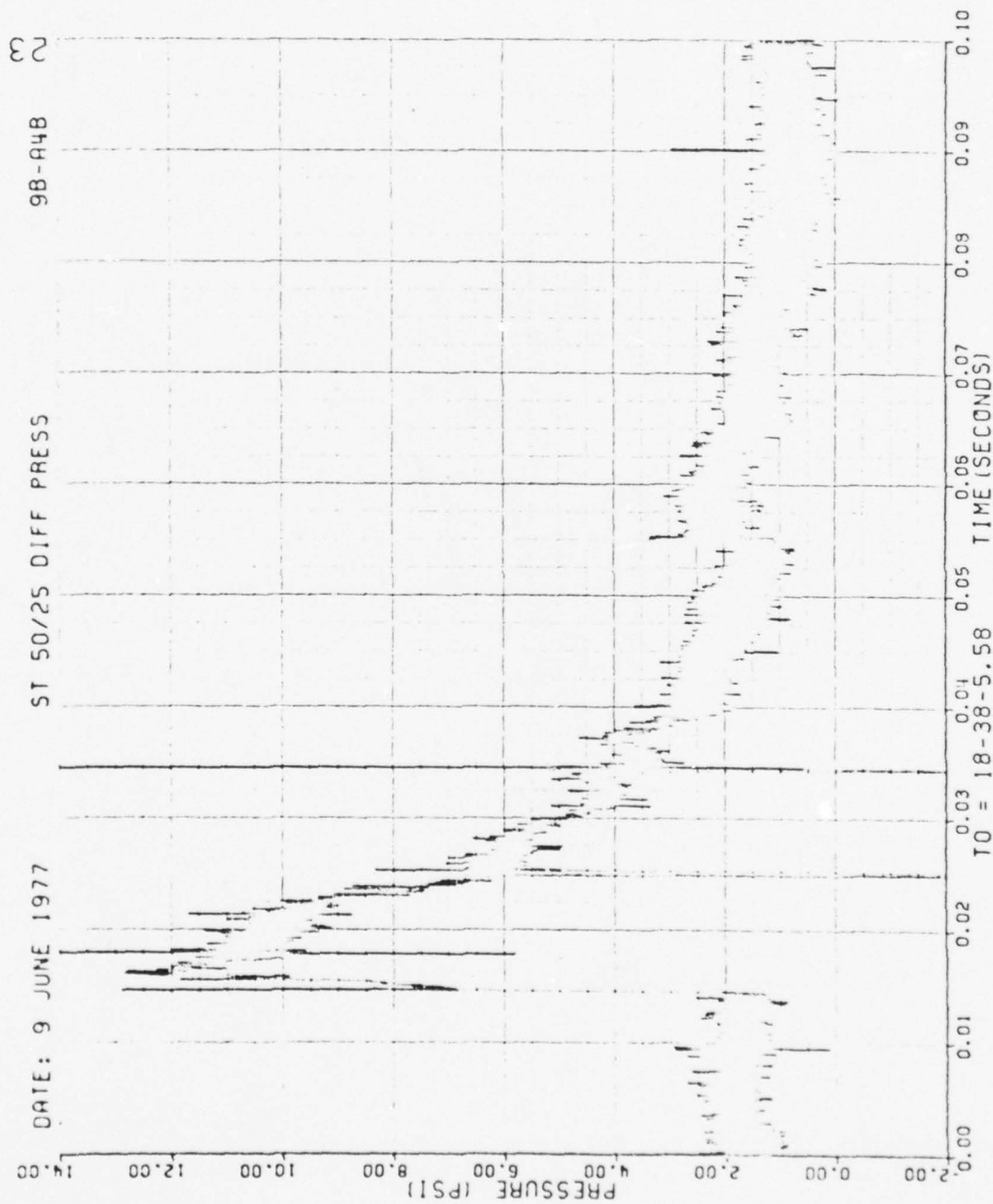


Figure 34. Continued

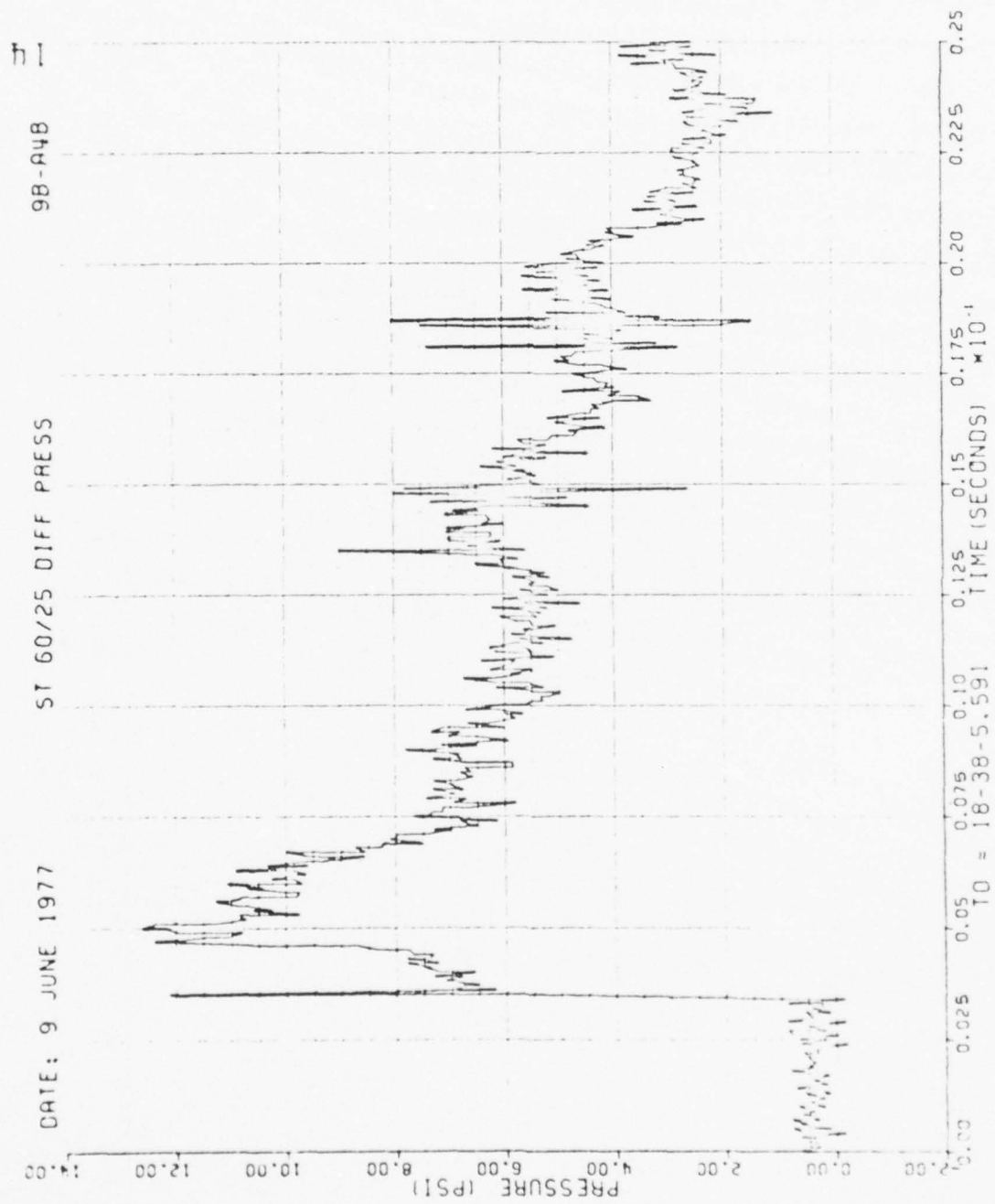


Figure 34. Continued

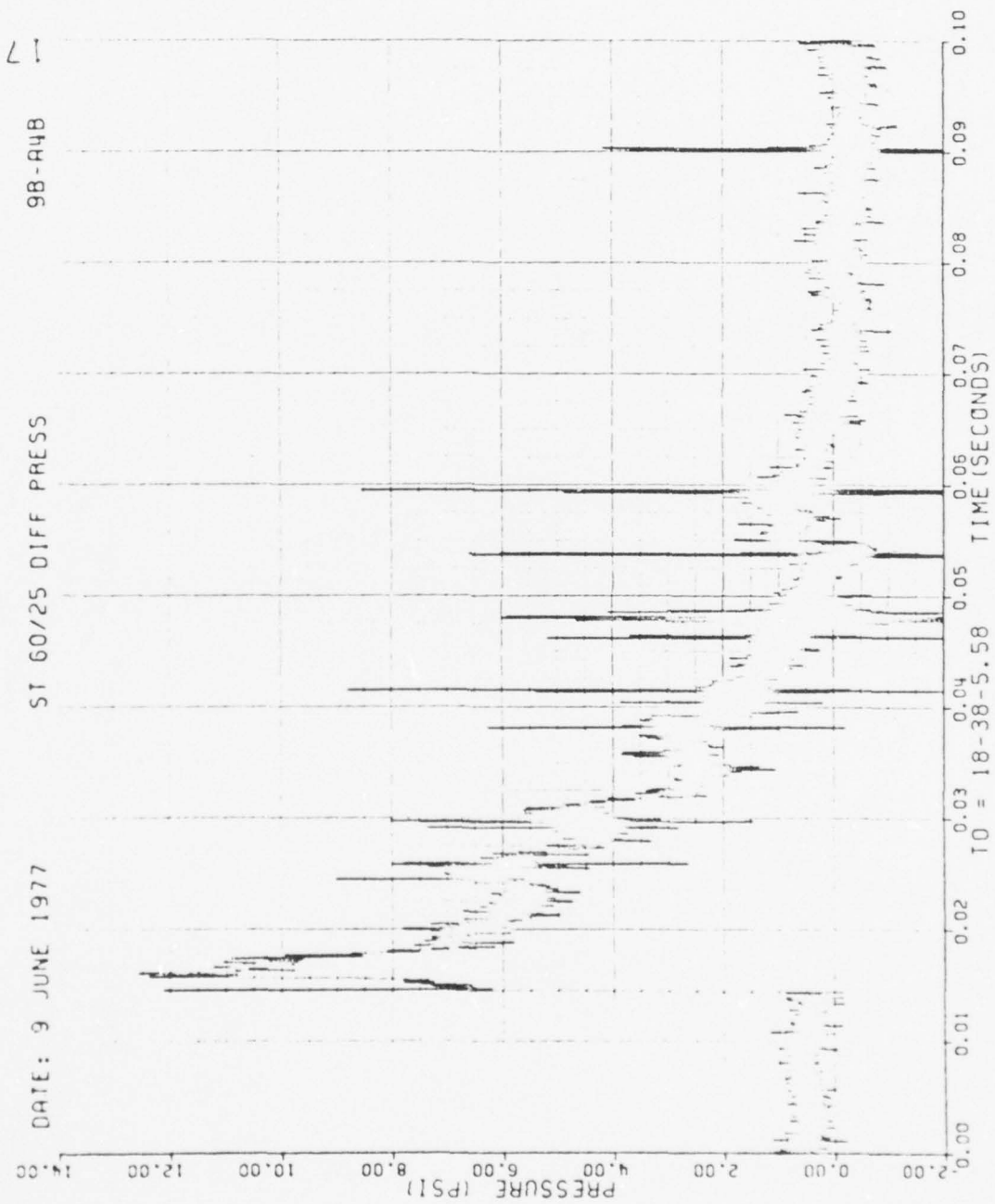


Figure 34. Continued

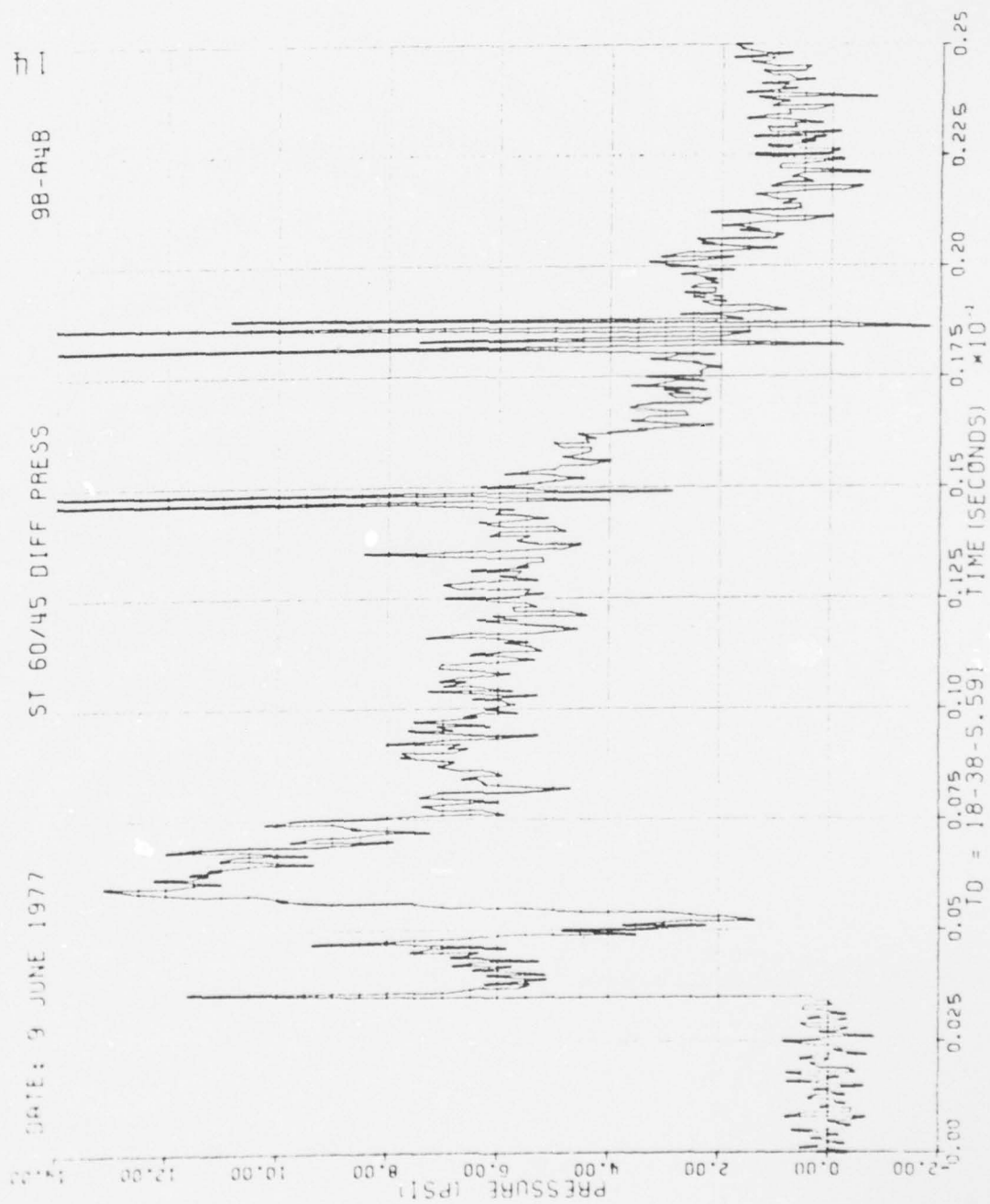


Figure 34. Continued

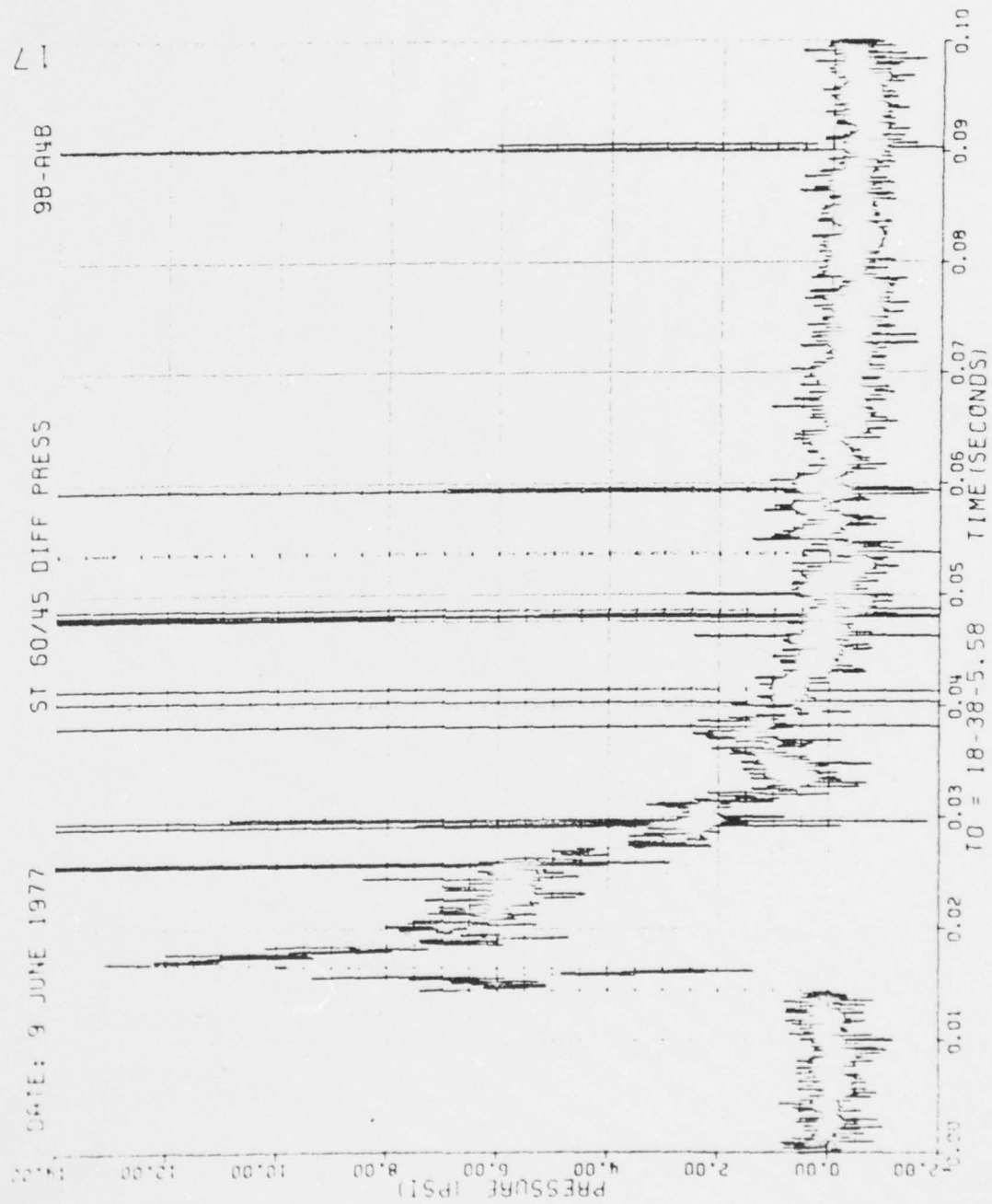


Figure 34. Continued

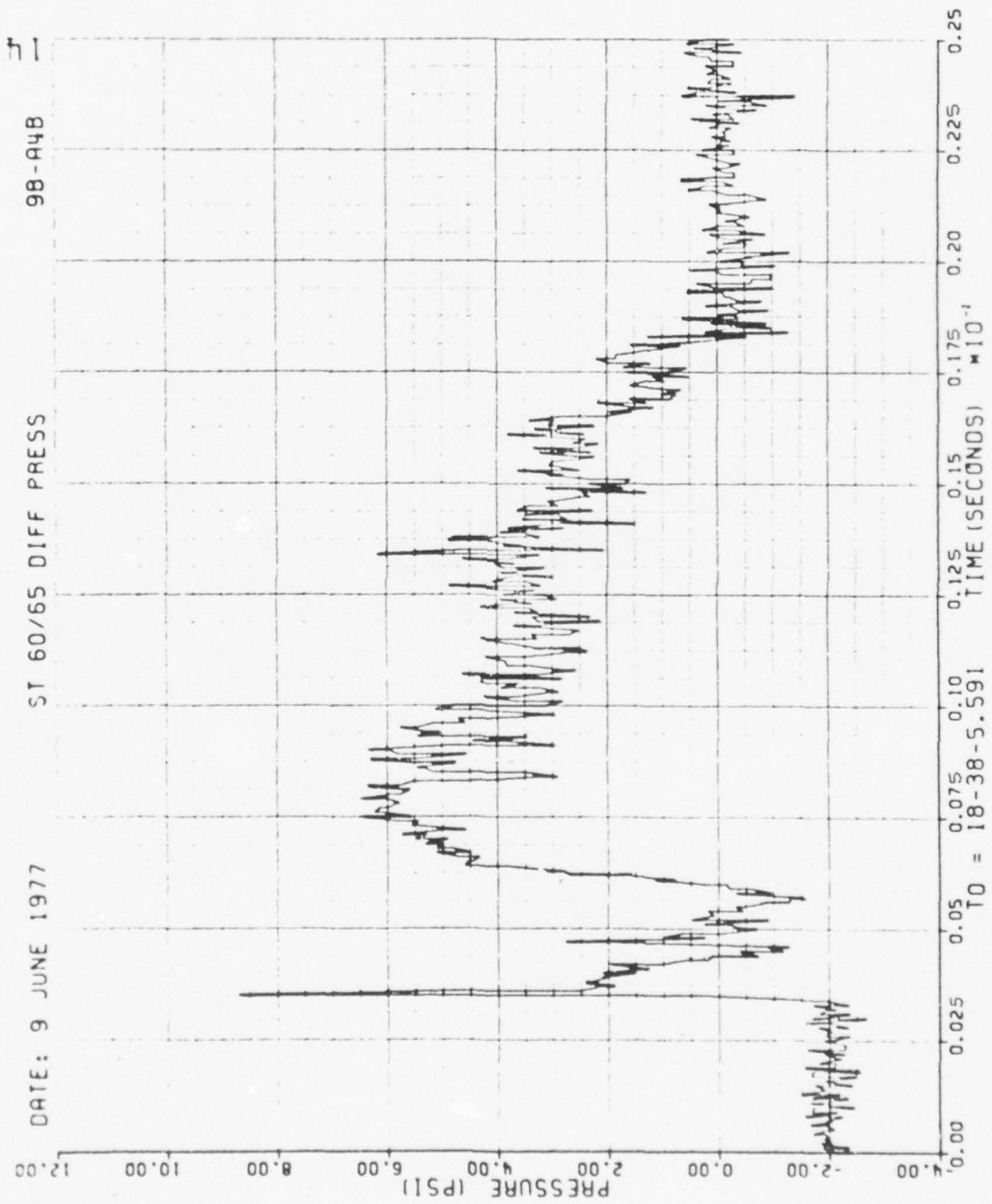


Figure 34. Continued

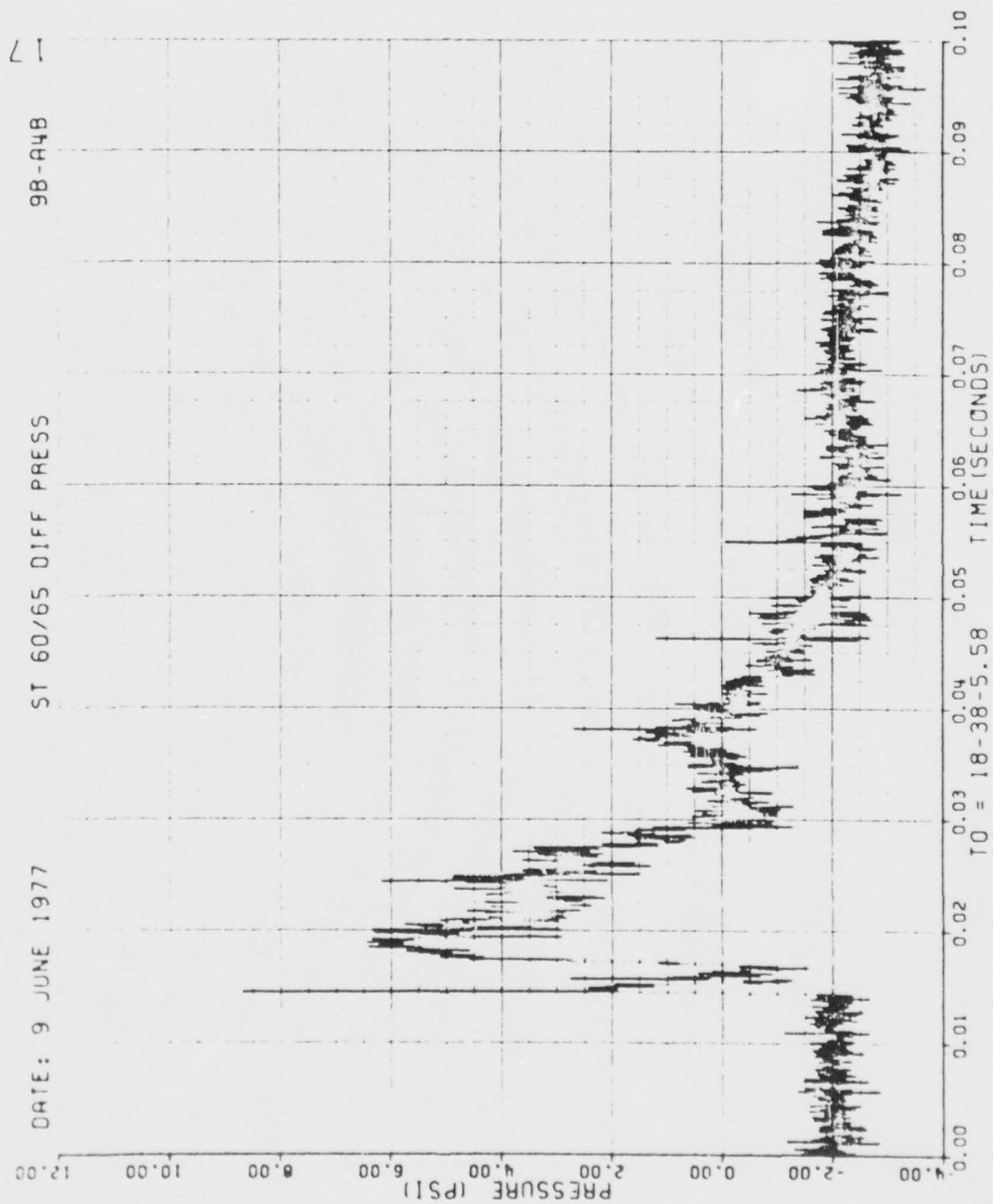


Figure 34. Continued

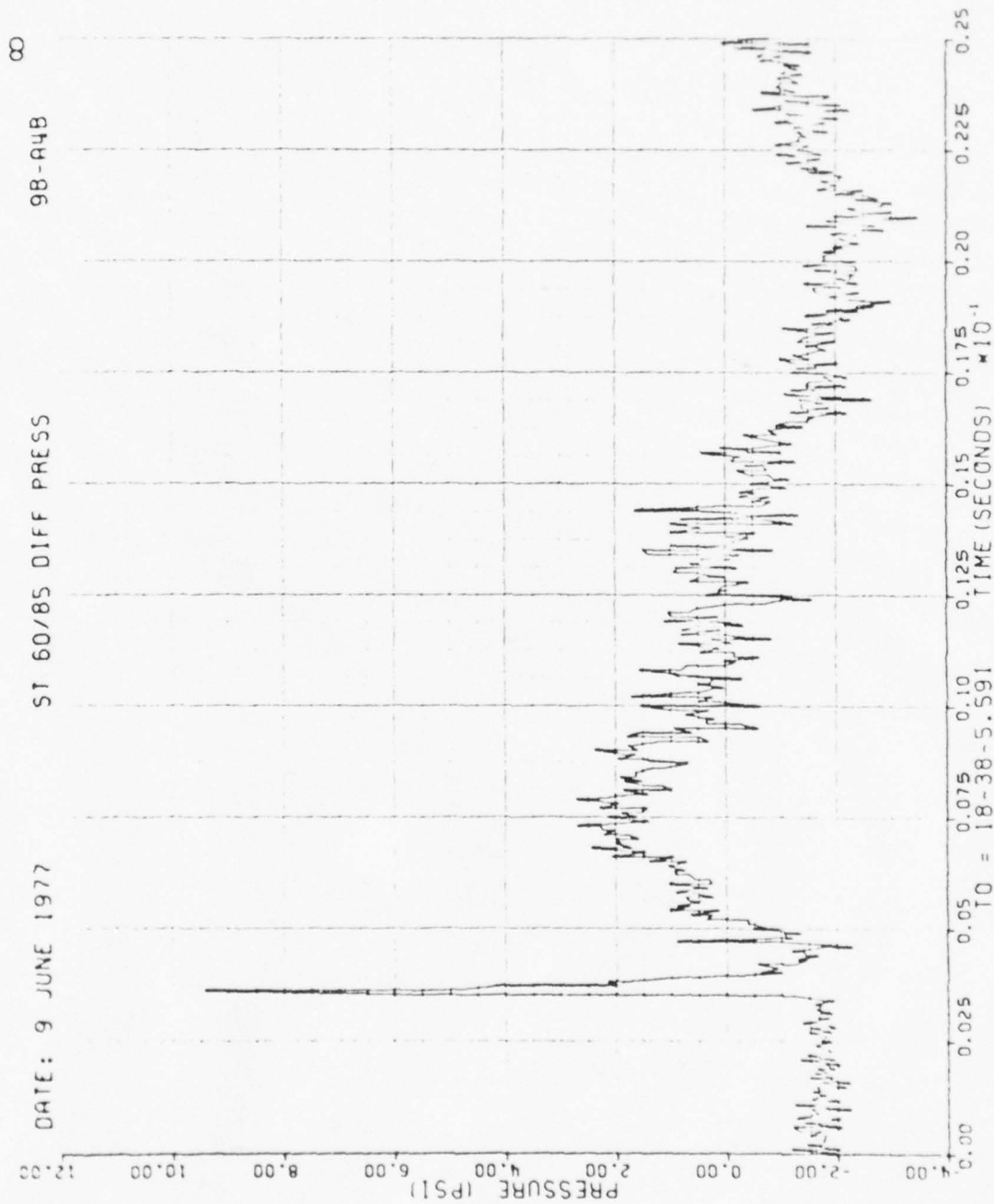


Figure 34. Continued

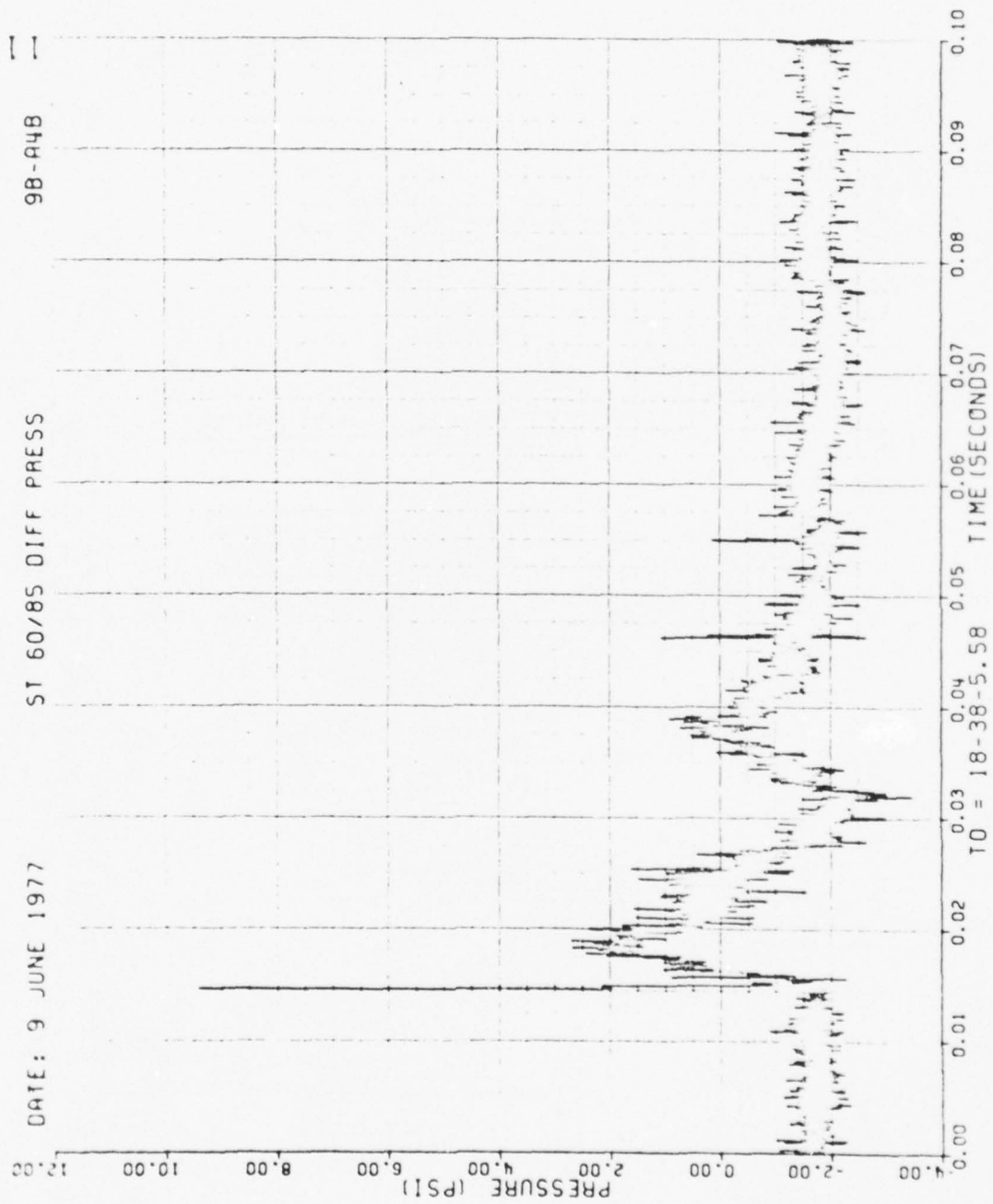


Figure 34. Continued

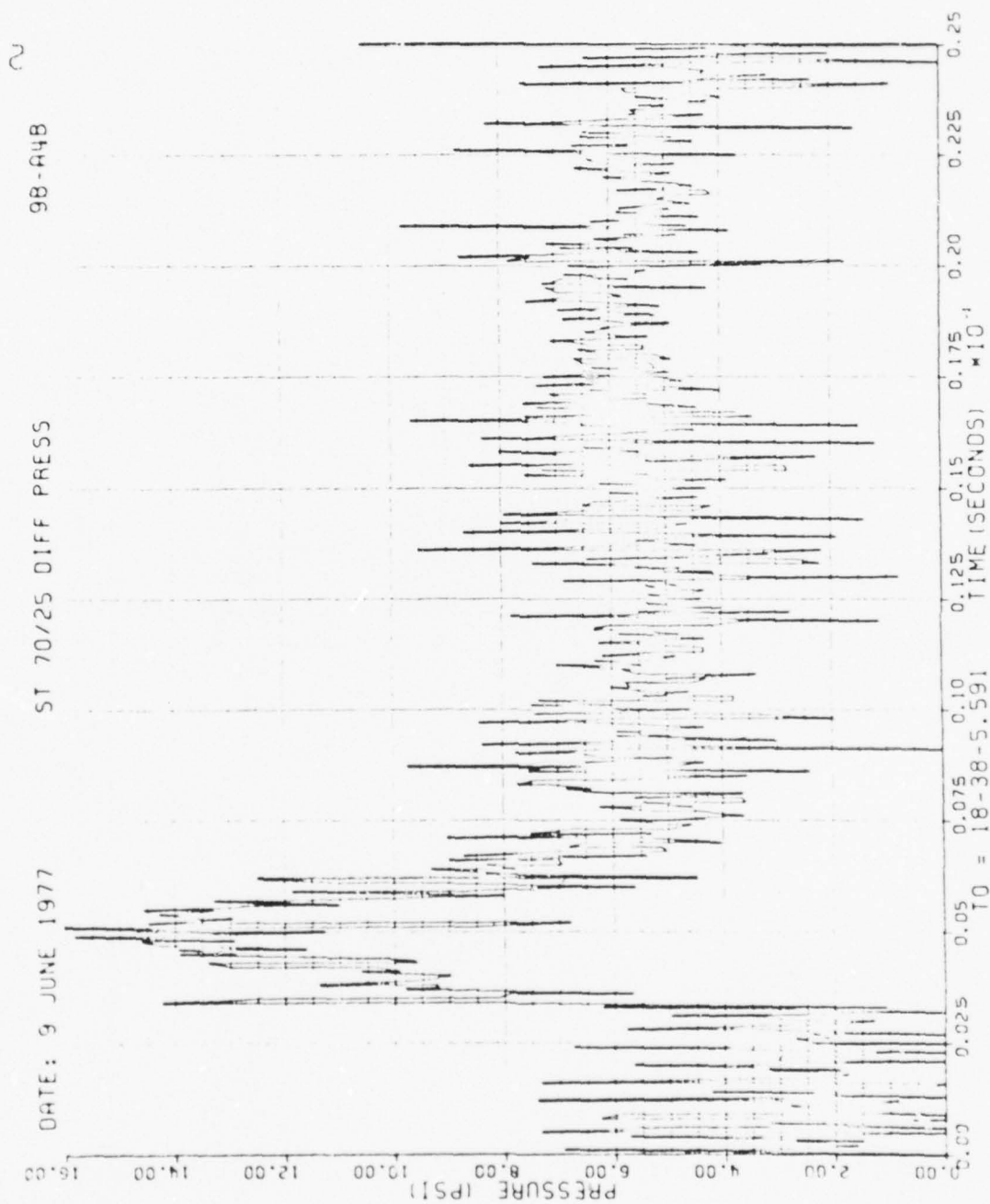


Figure 34. Continued

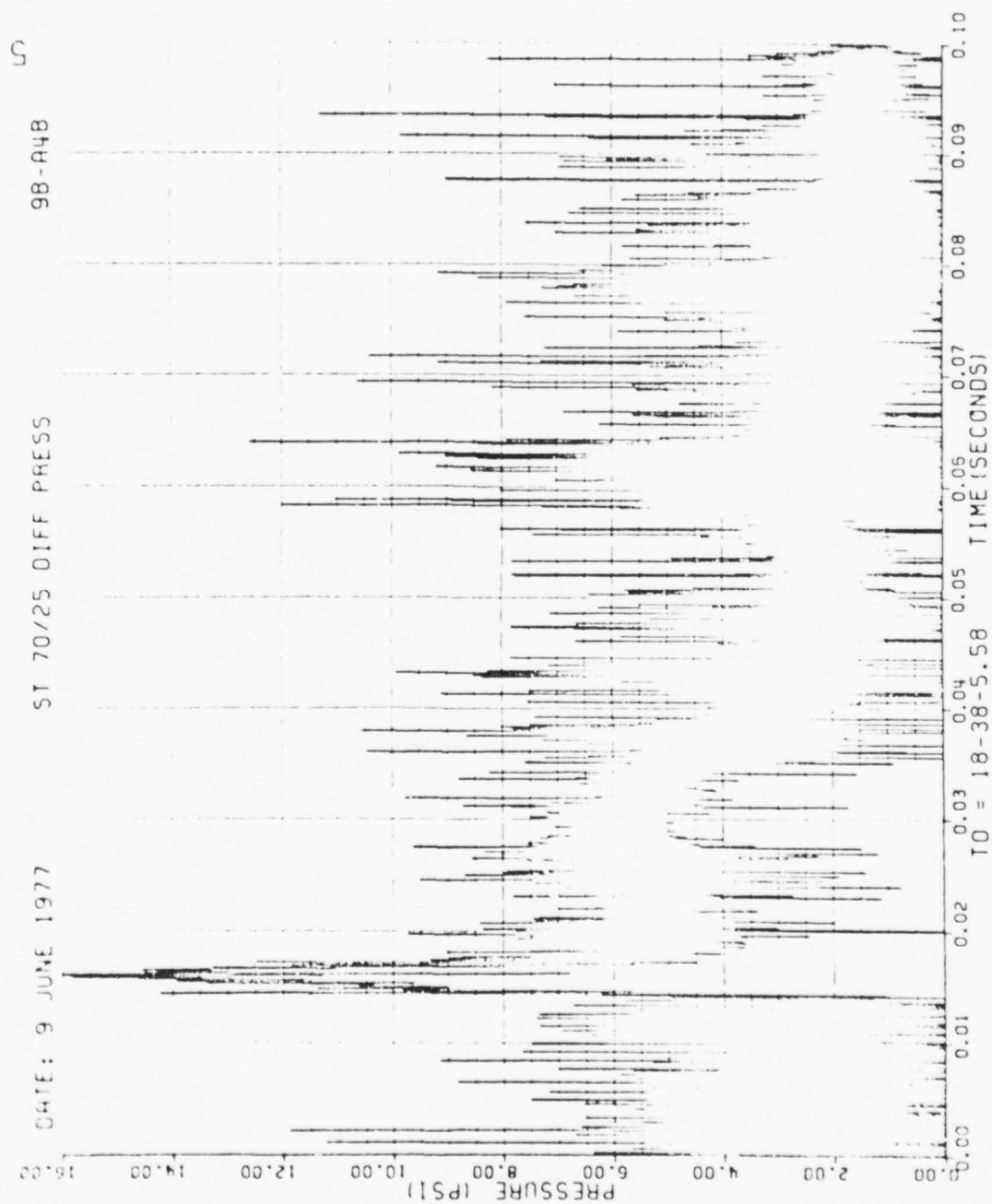


Figure 34. Continued

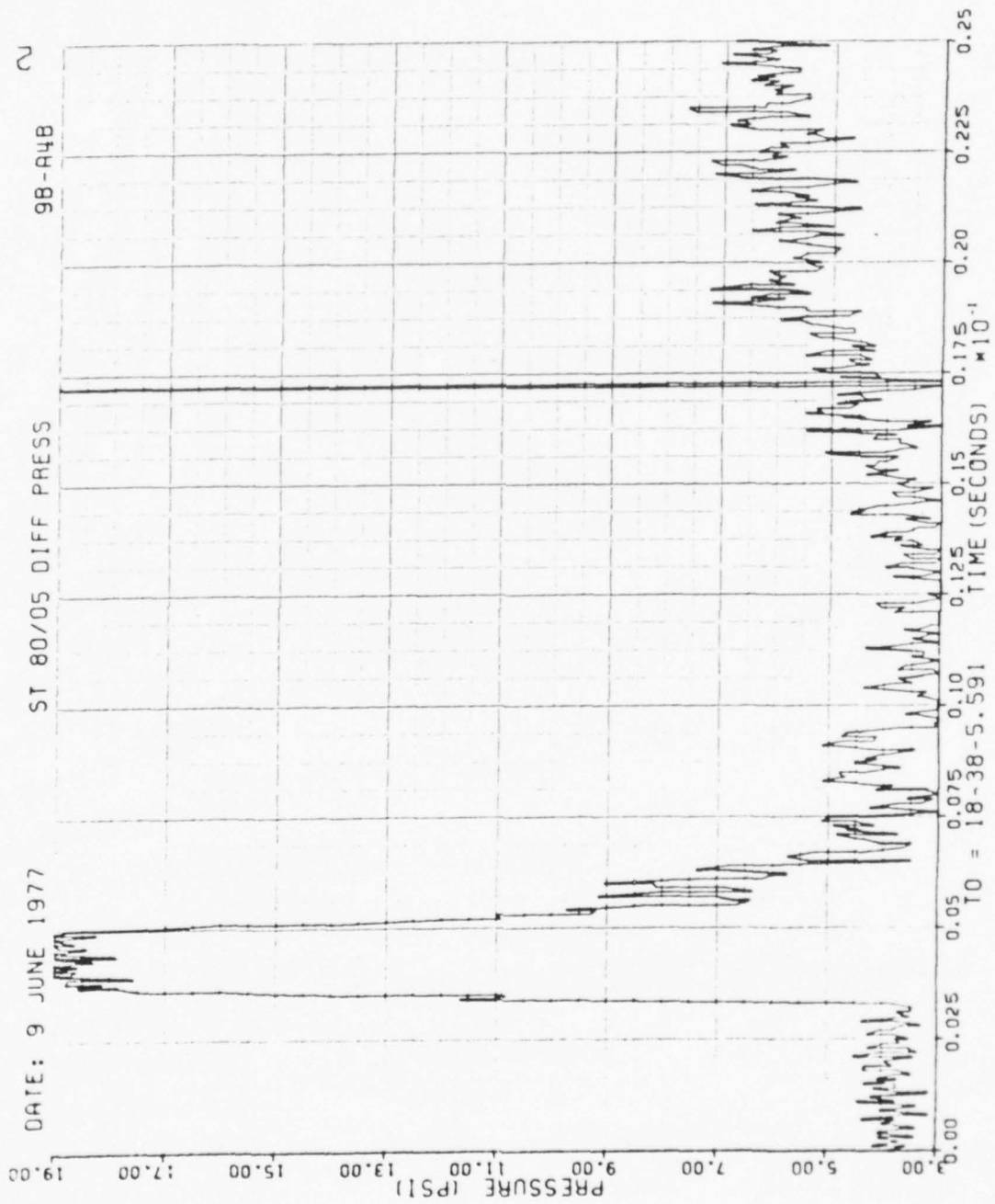


Figure 34. Continued

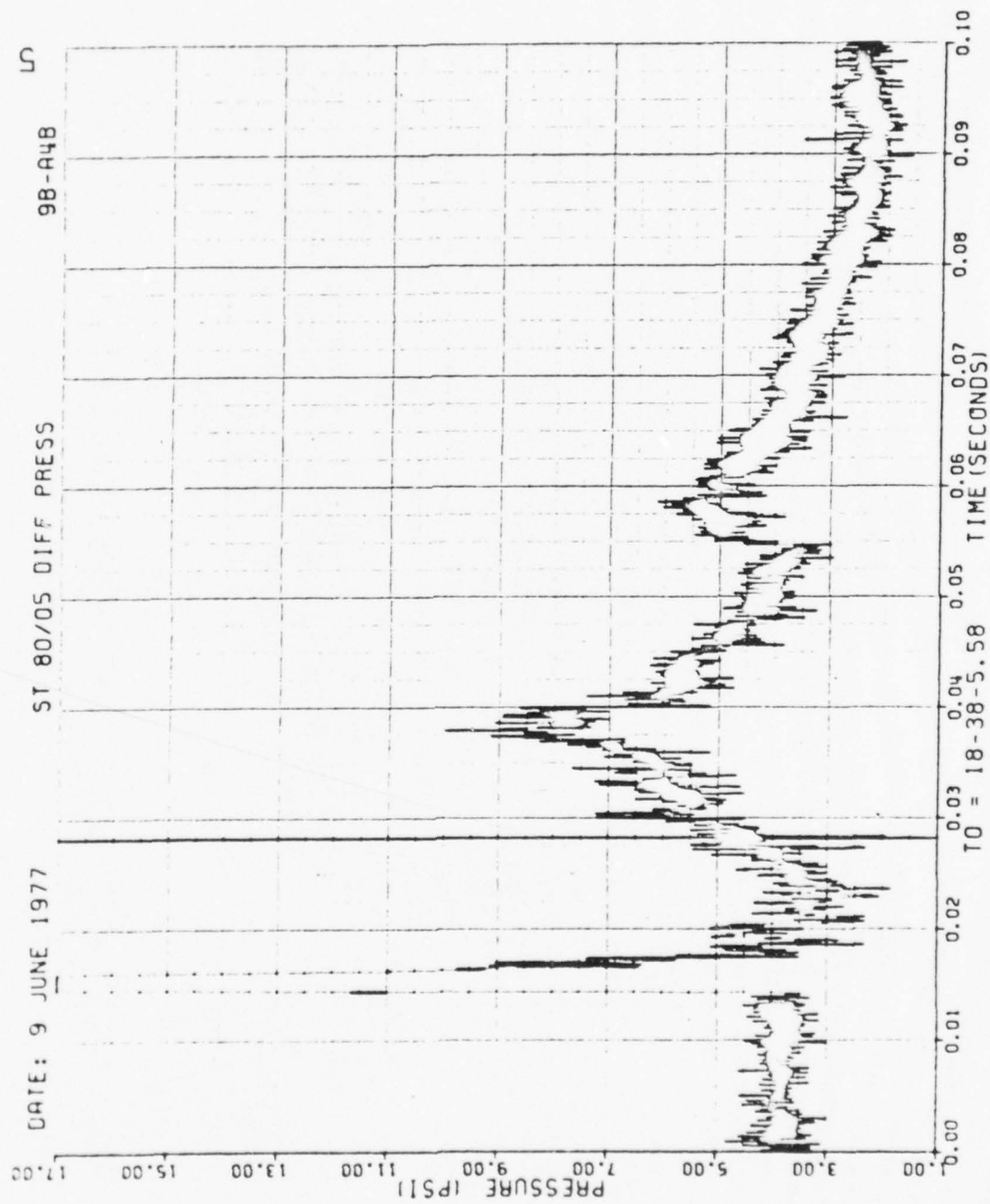


Figure 34. Continued

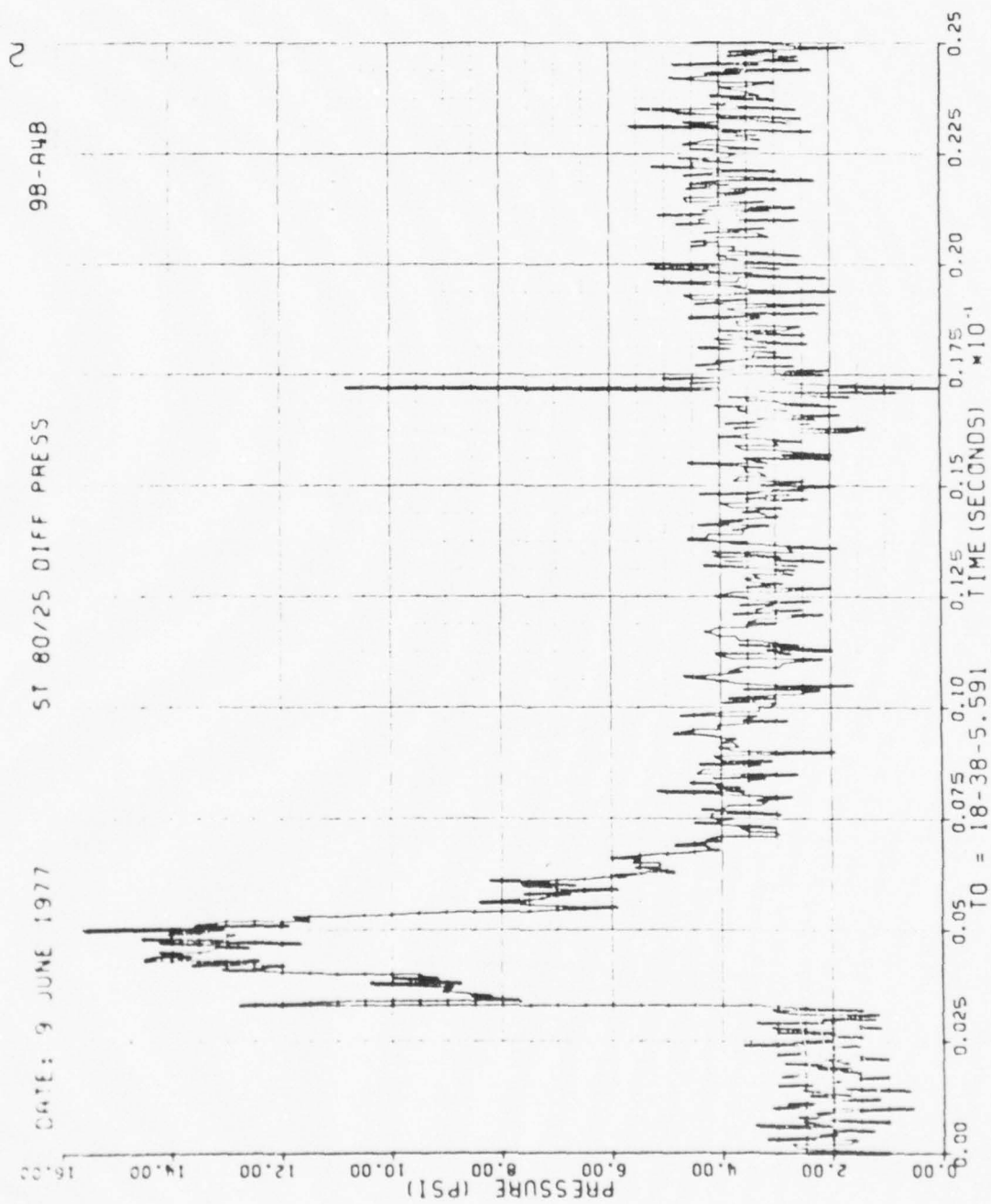


Figure 34. Continued

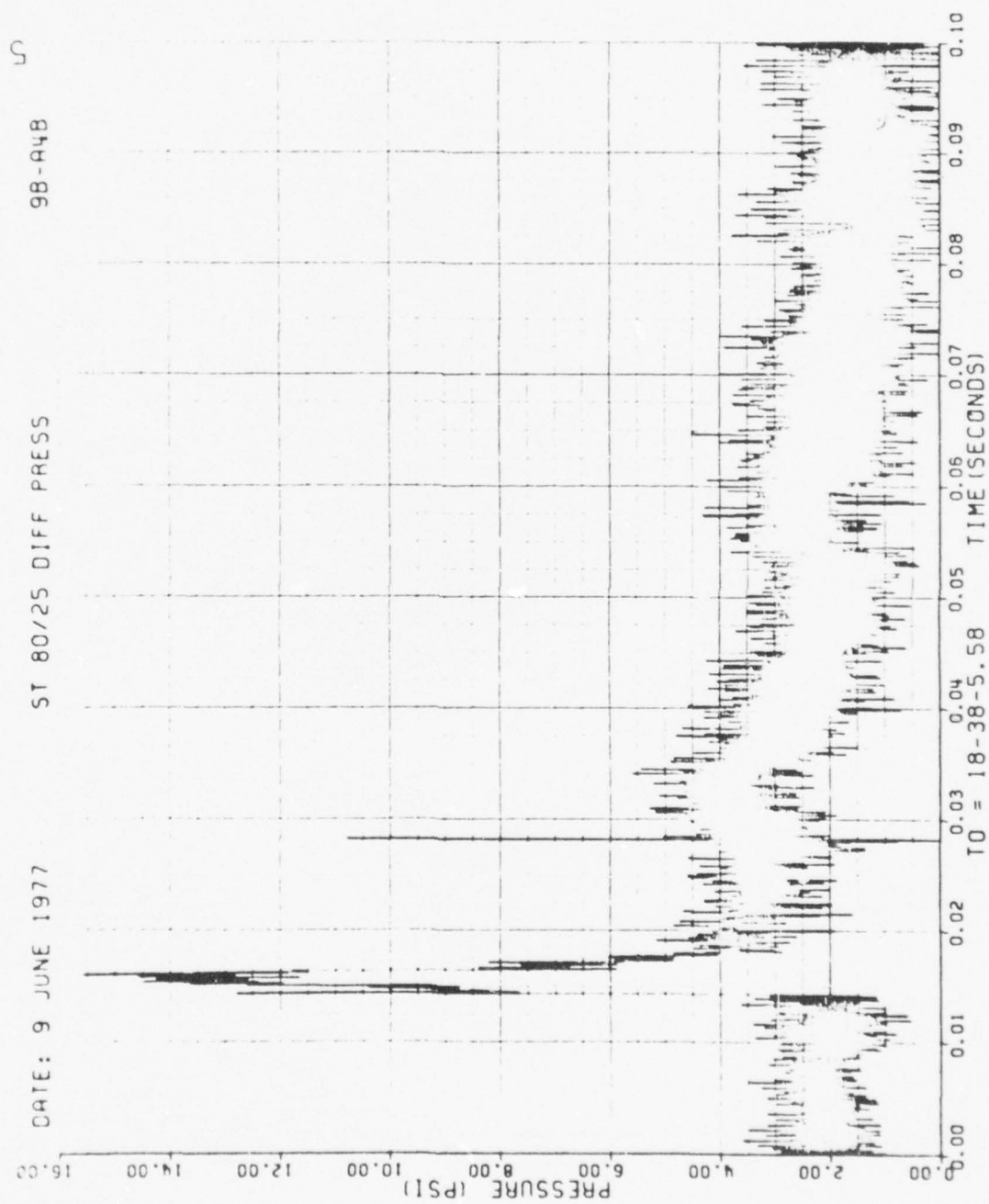


Figure 34. Continued

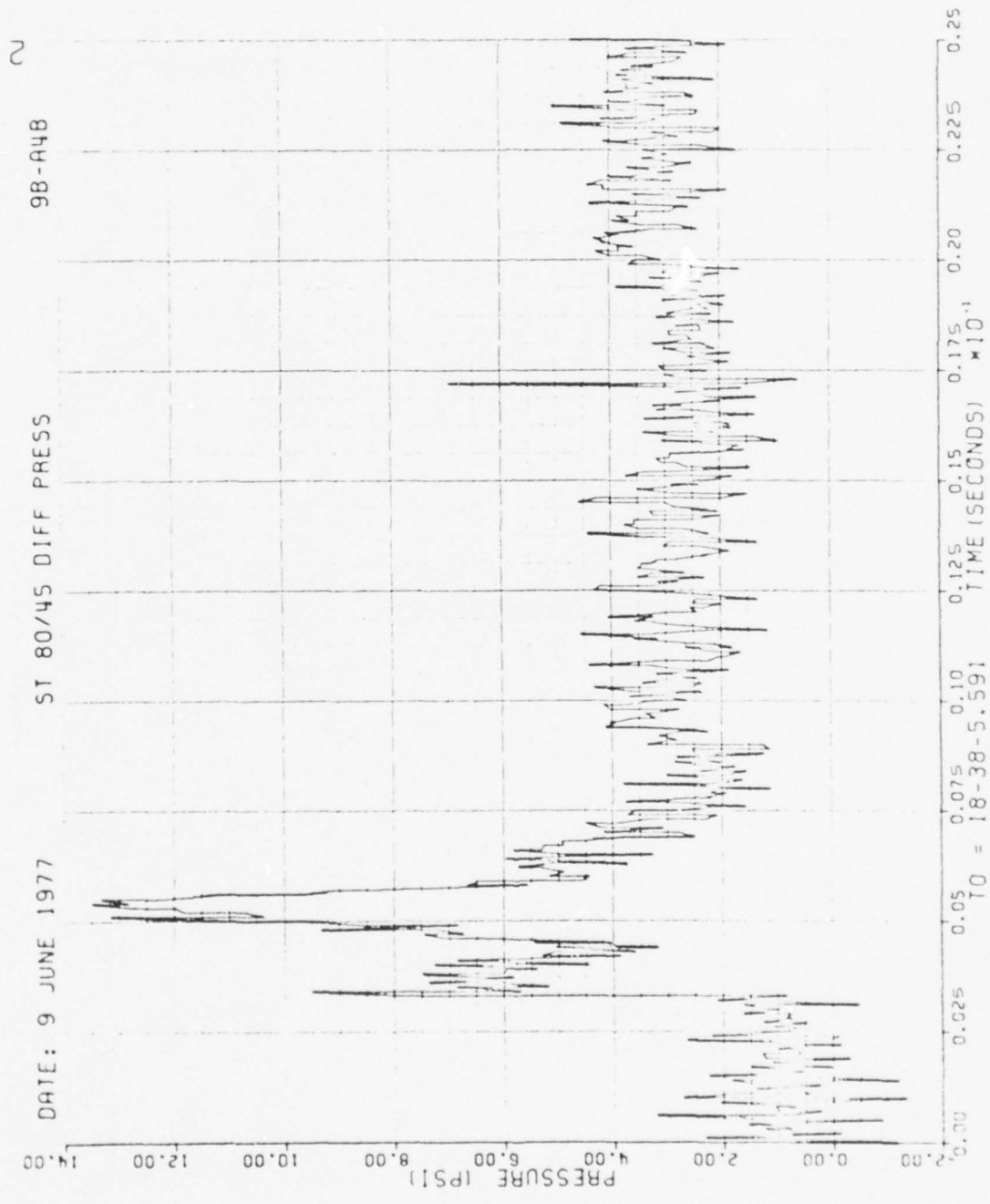


Figure 34. Continued

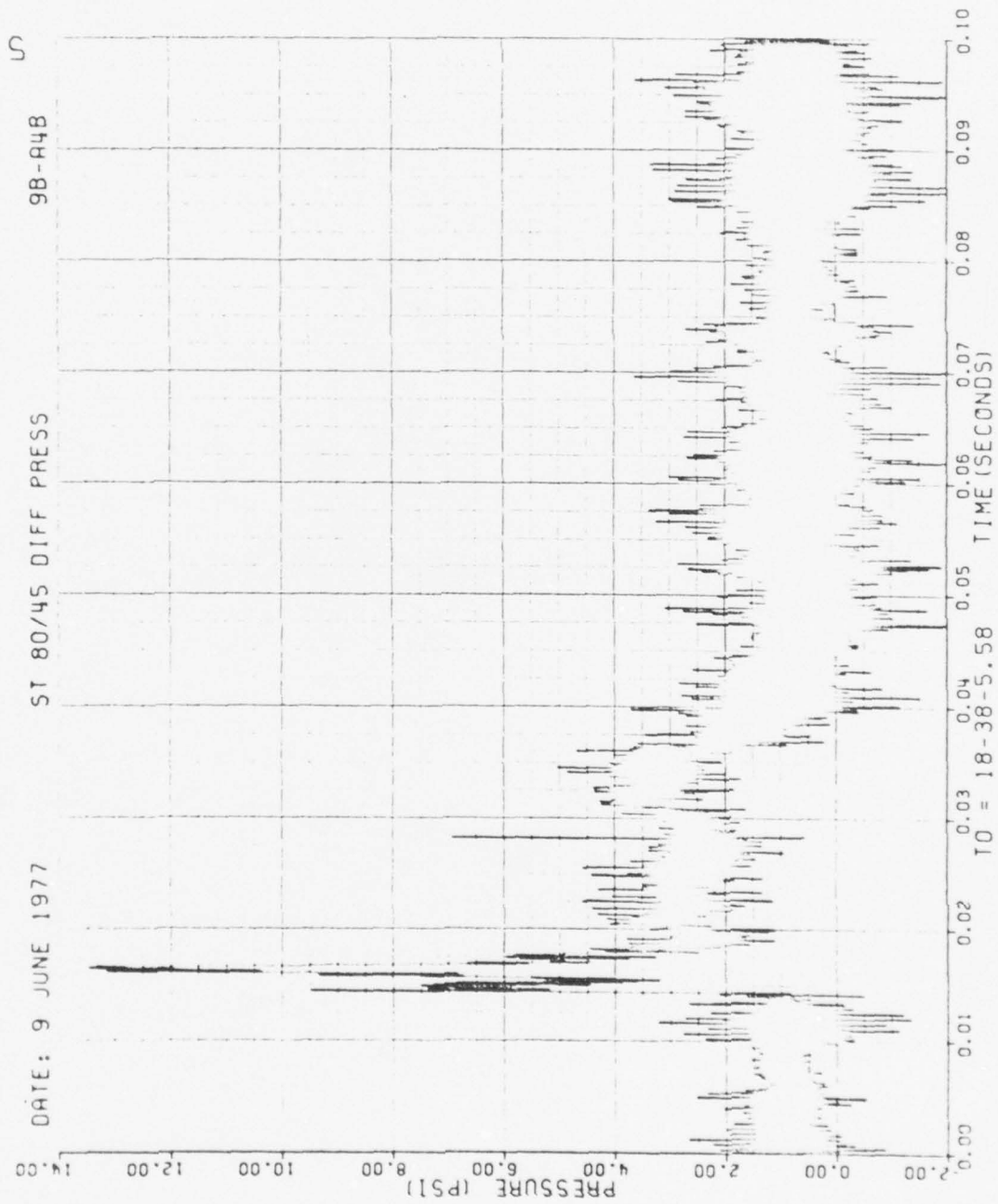


Figure 34. Continued

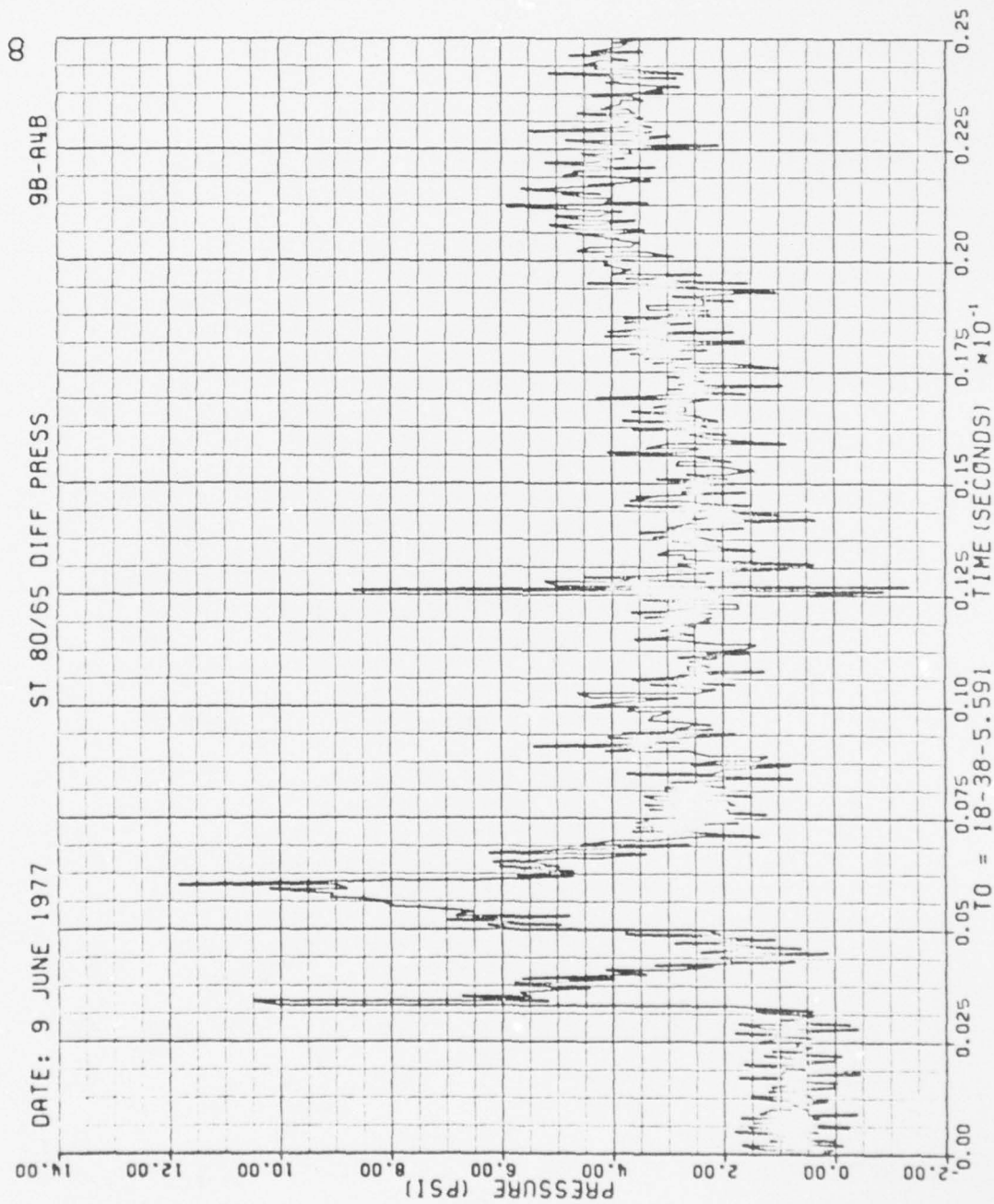


Figure 34. Continued

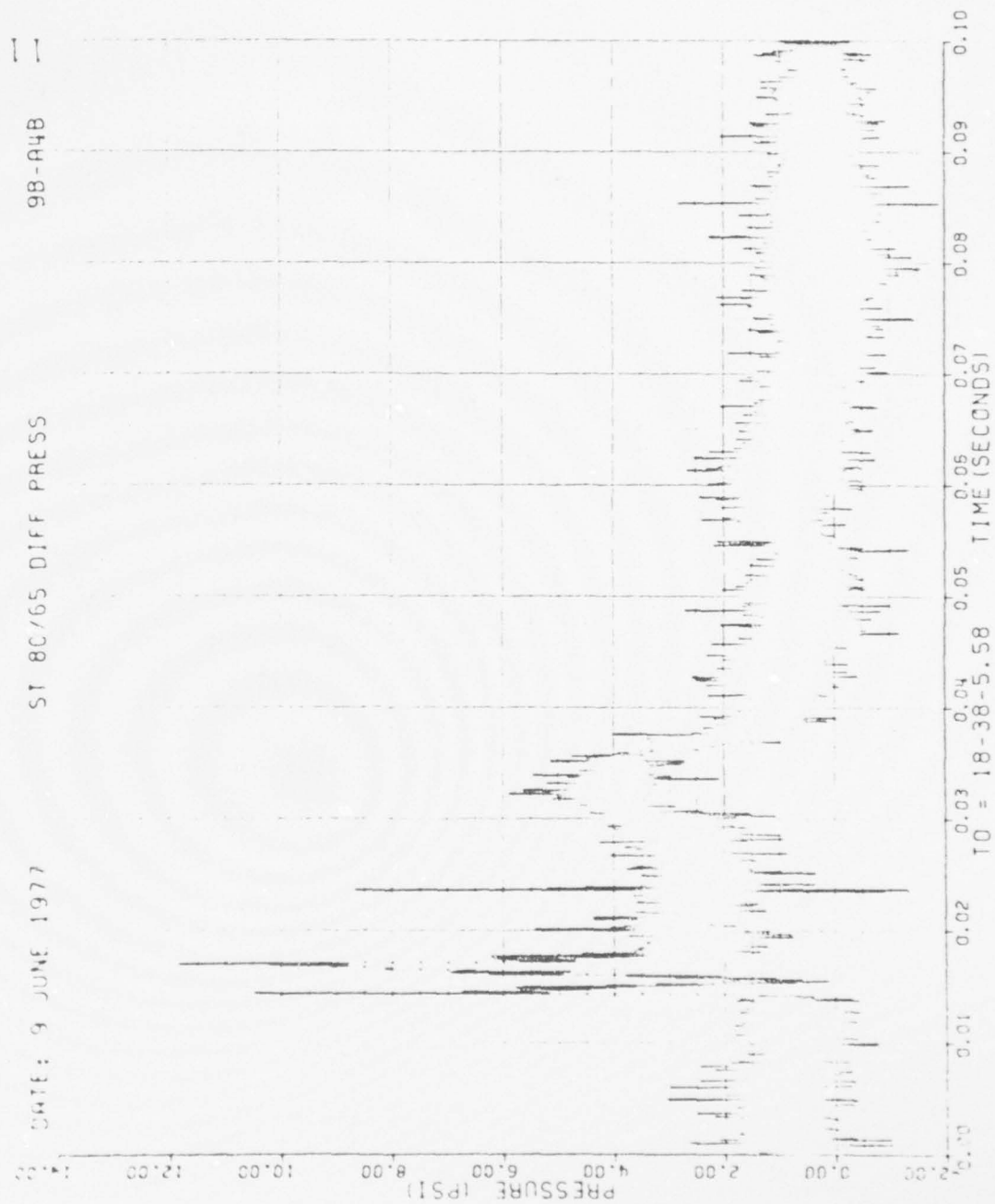


Figure 34. Continued

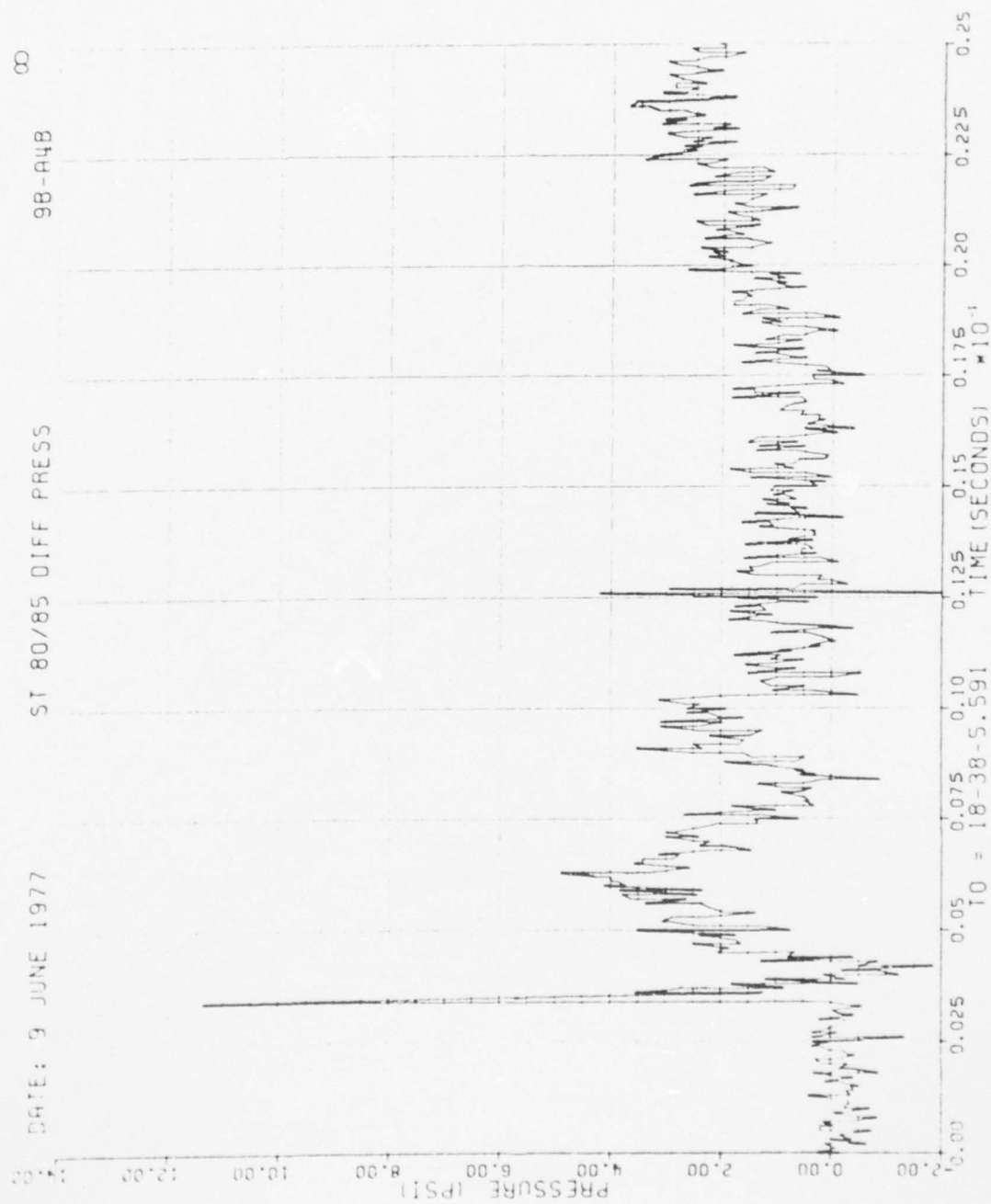


Figure 34. Continued

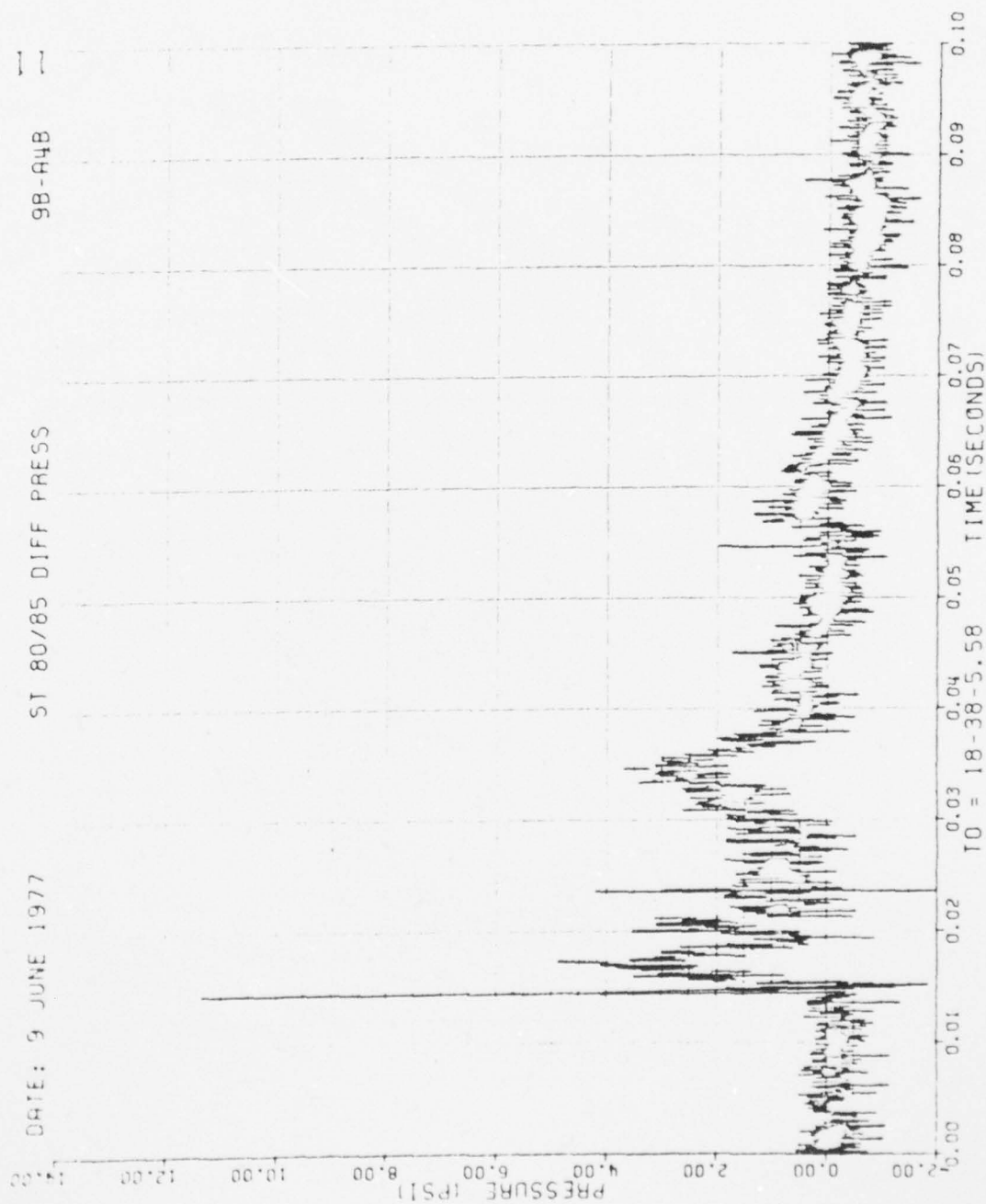


Figure 34. Continued

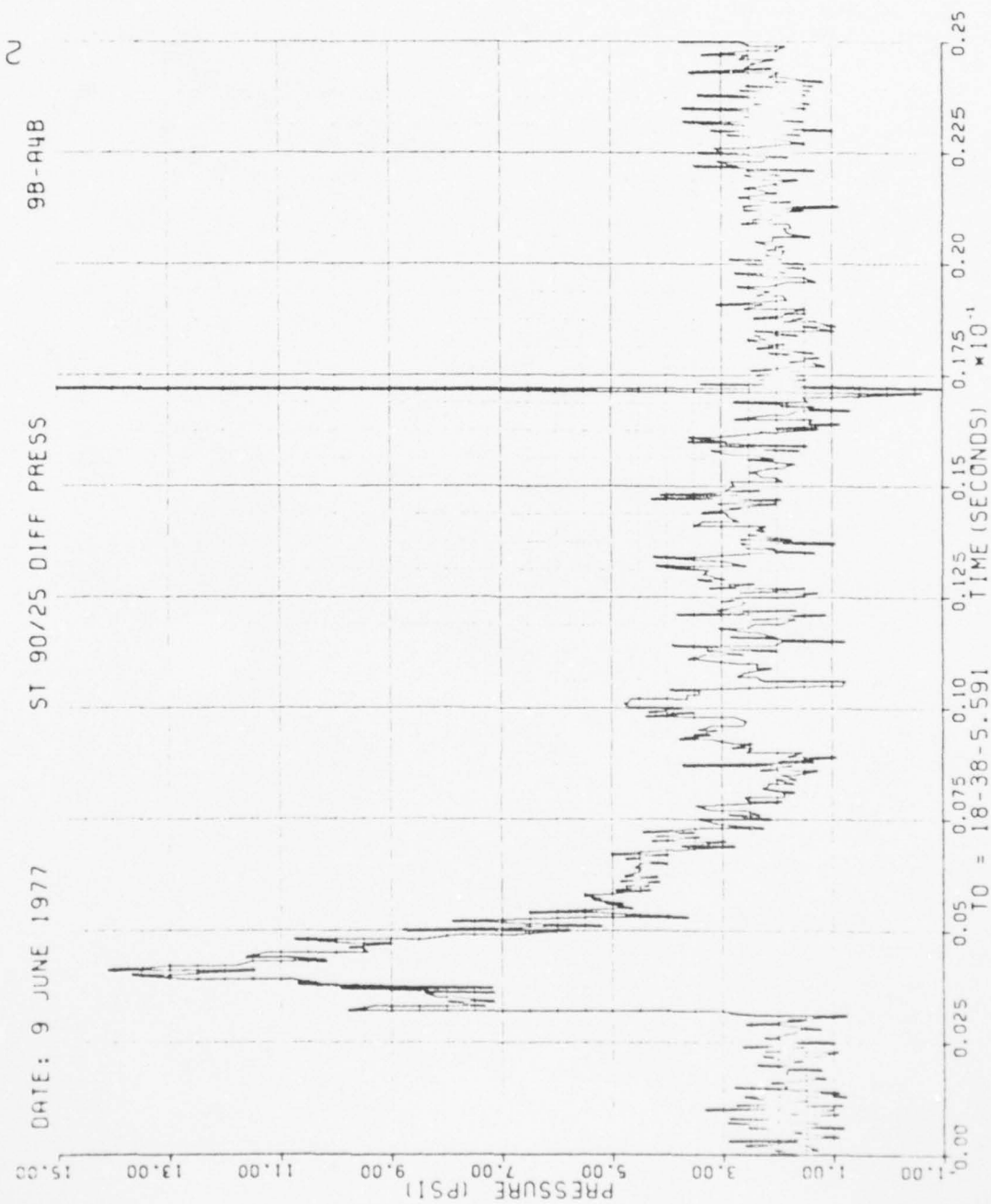


Figure 34. Continued

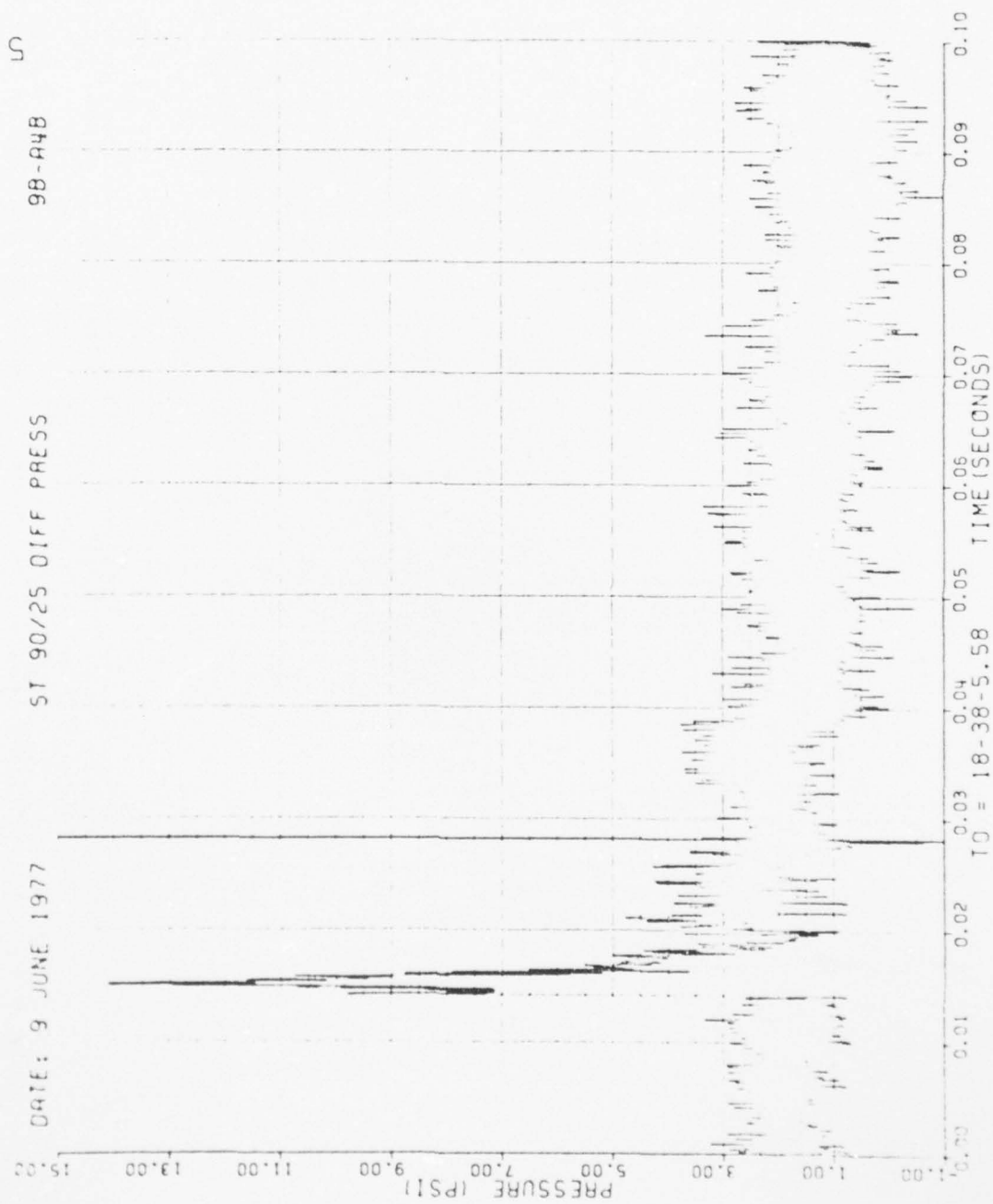


Figure 34. Concluded

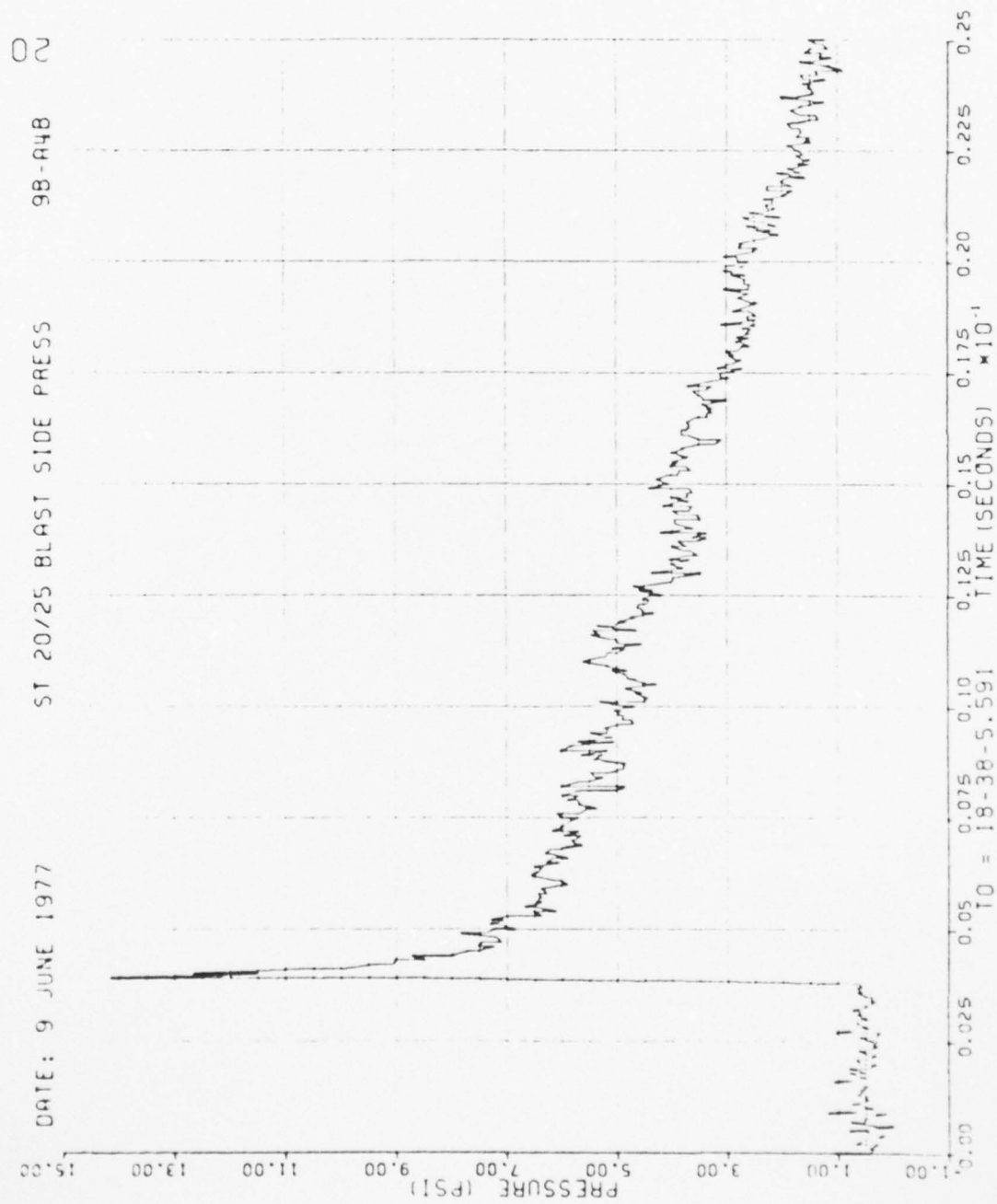


Figure 35. Blastward and Leeward Wing Pressures, Run 9B-A4, Intercept 2.

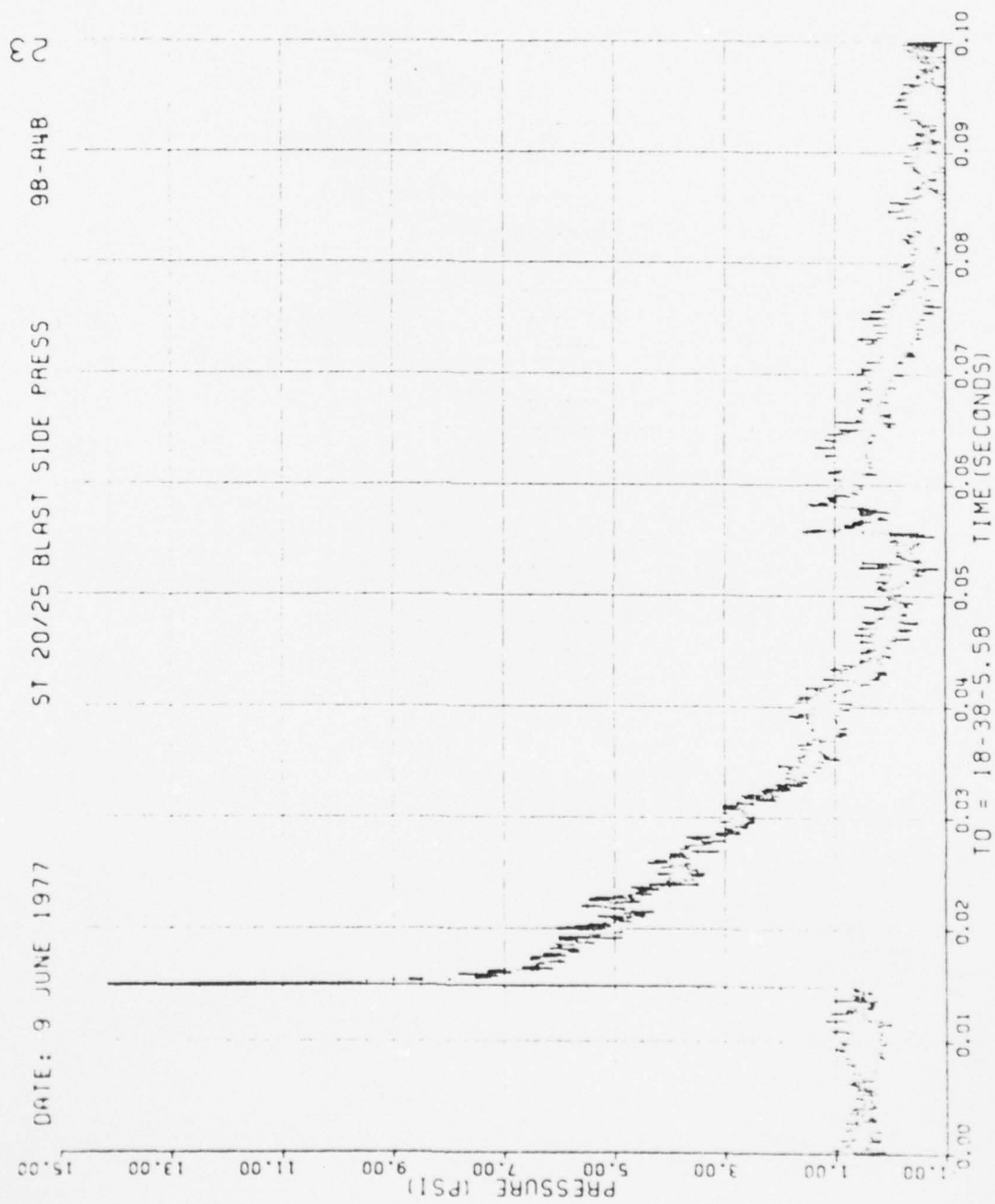


Figure 35. Continued

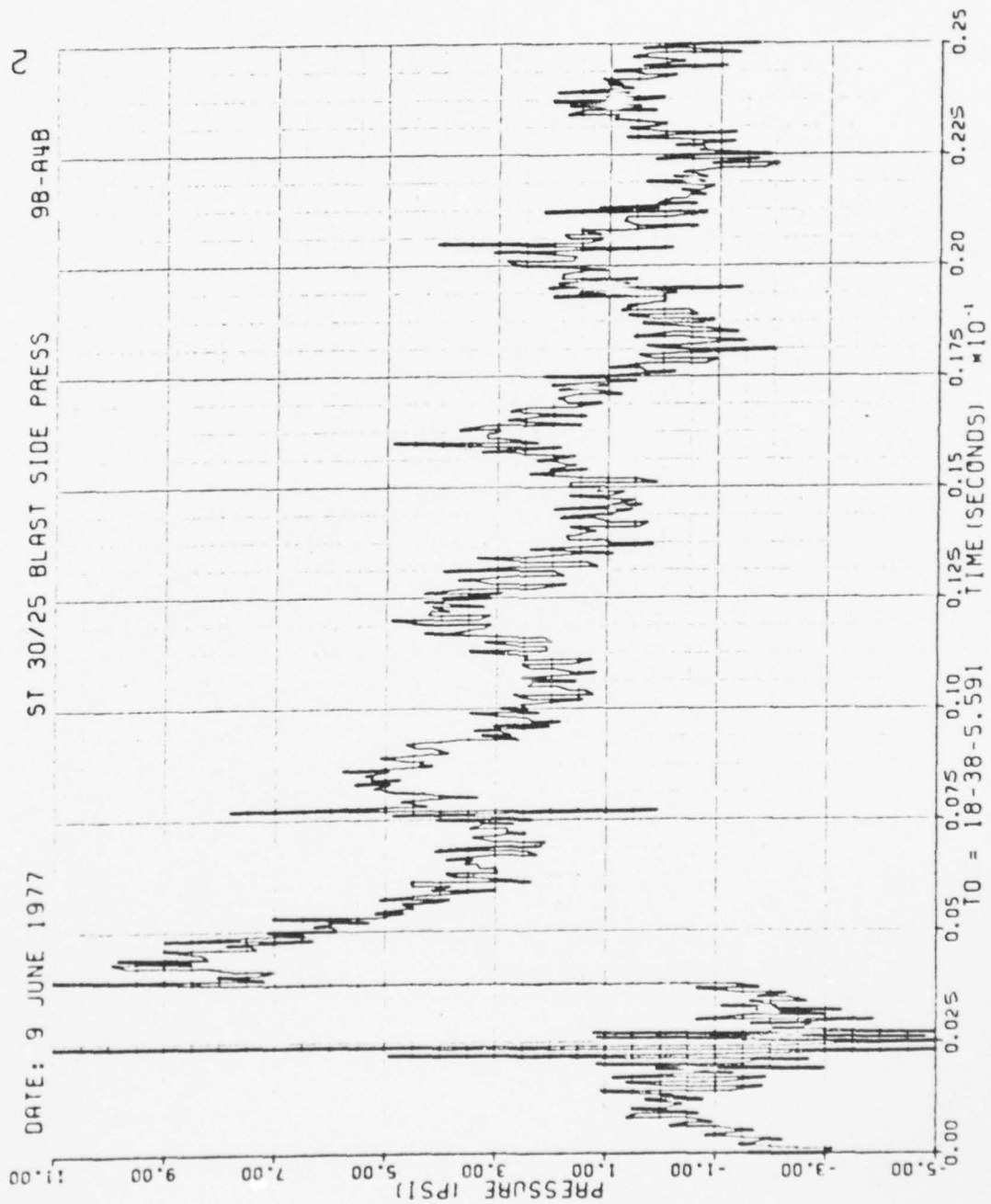


Figure 35. Continued

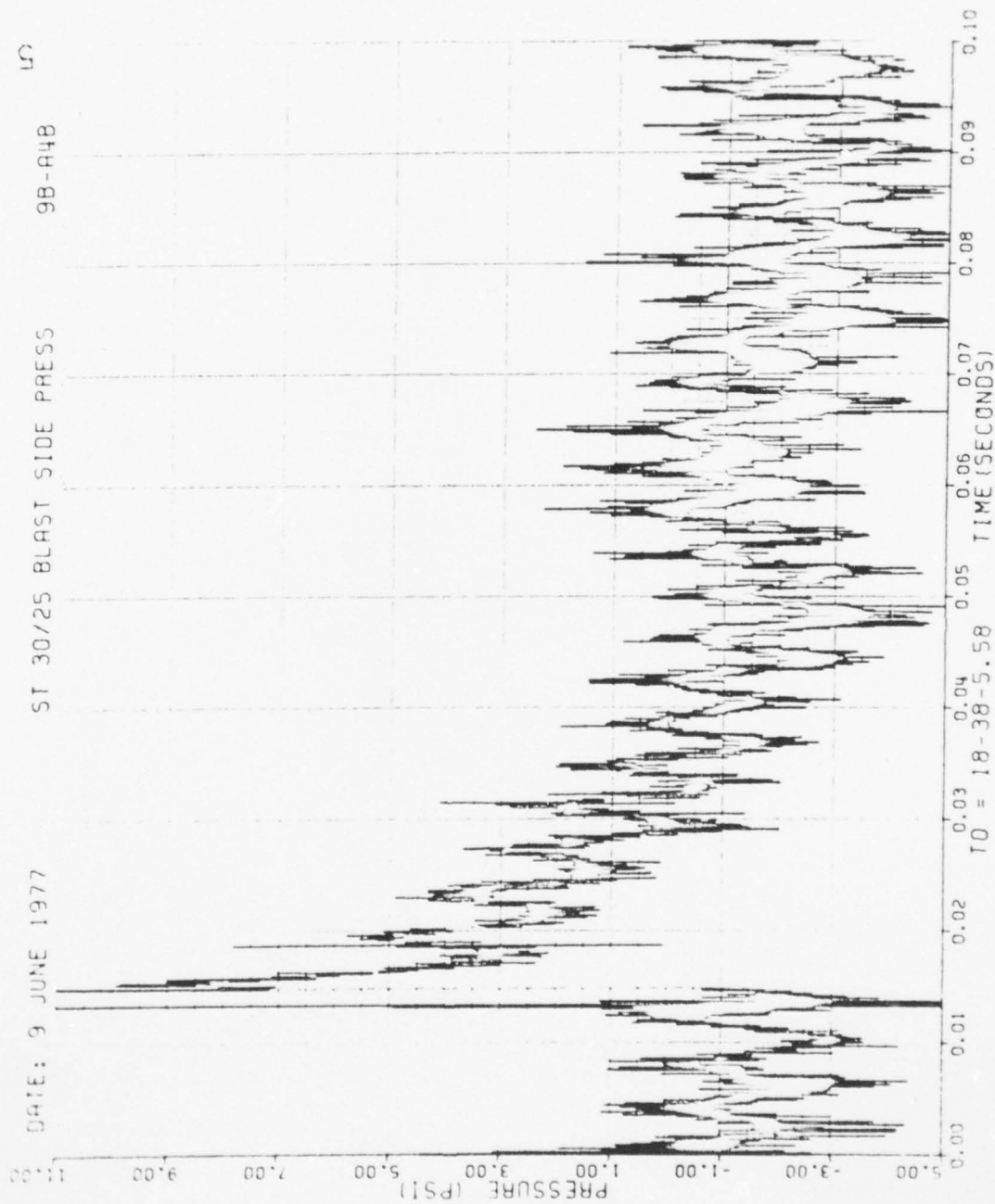


Figure 35. Continued

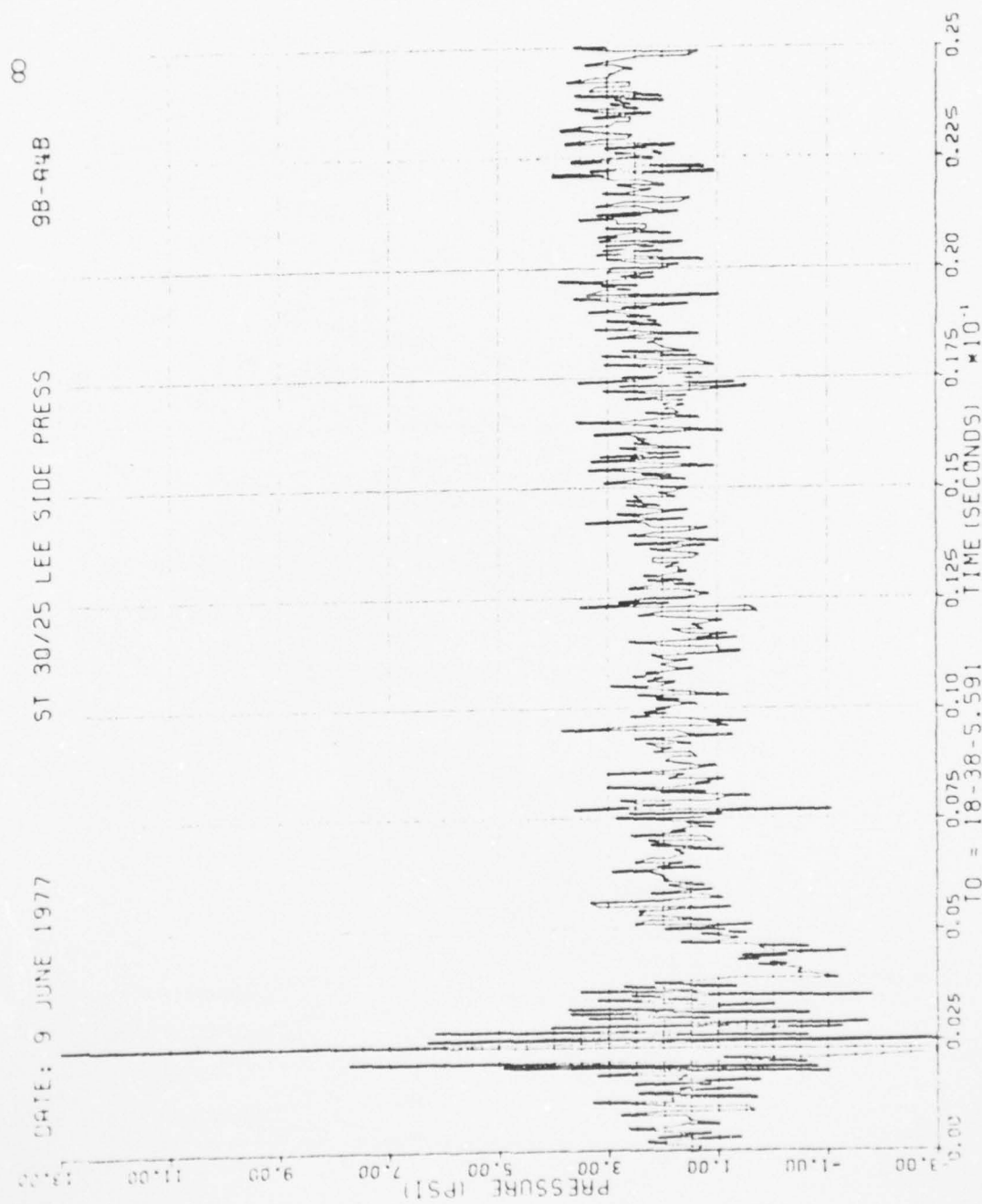


Figure 35. Continued

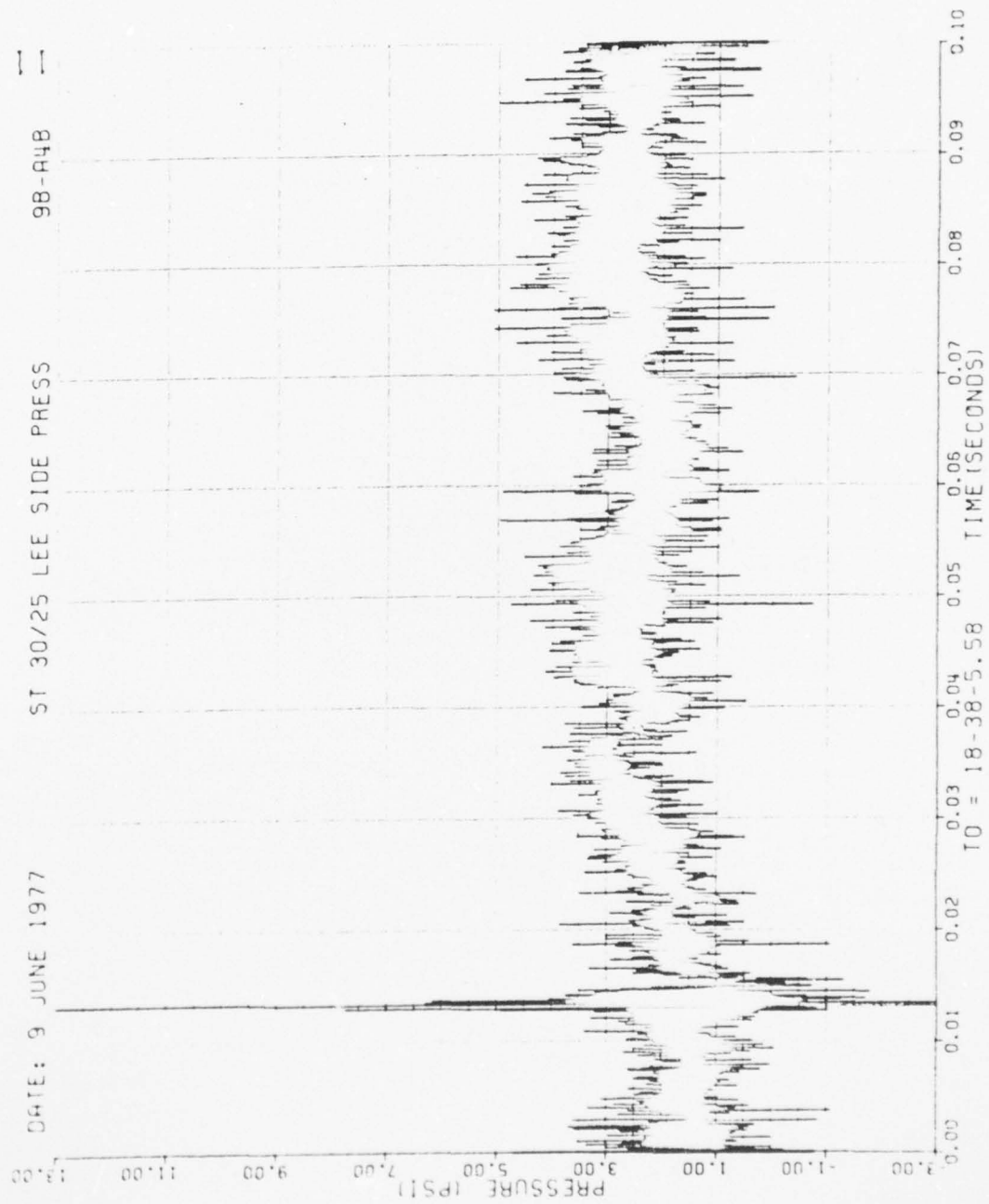


Figure 35. Concluded

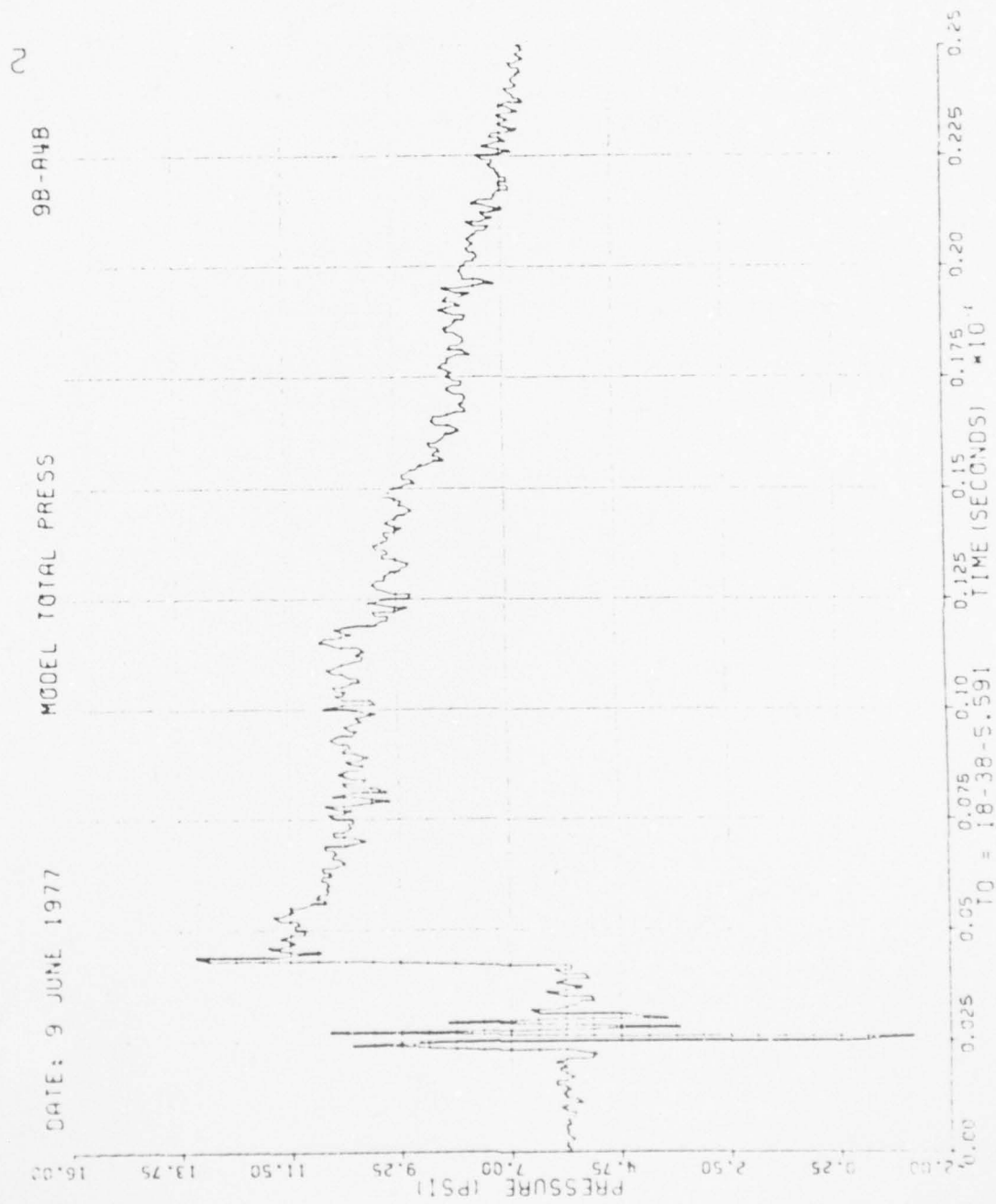


Figure 36. Total Pressure at Model, Run 9B-A4, Intercept 2.

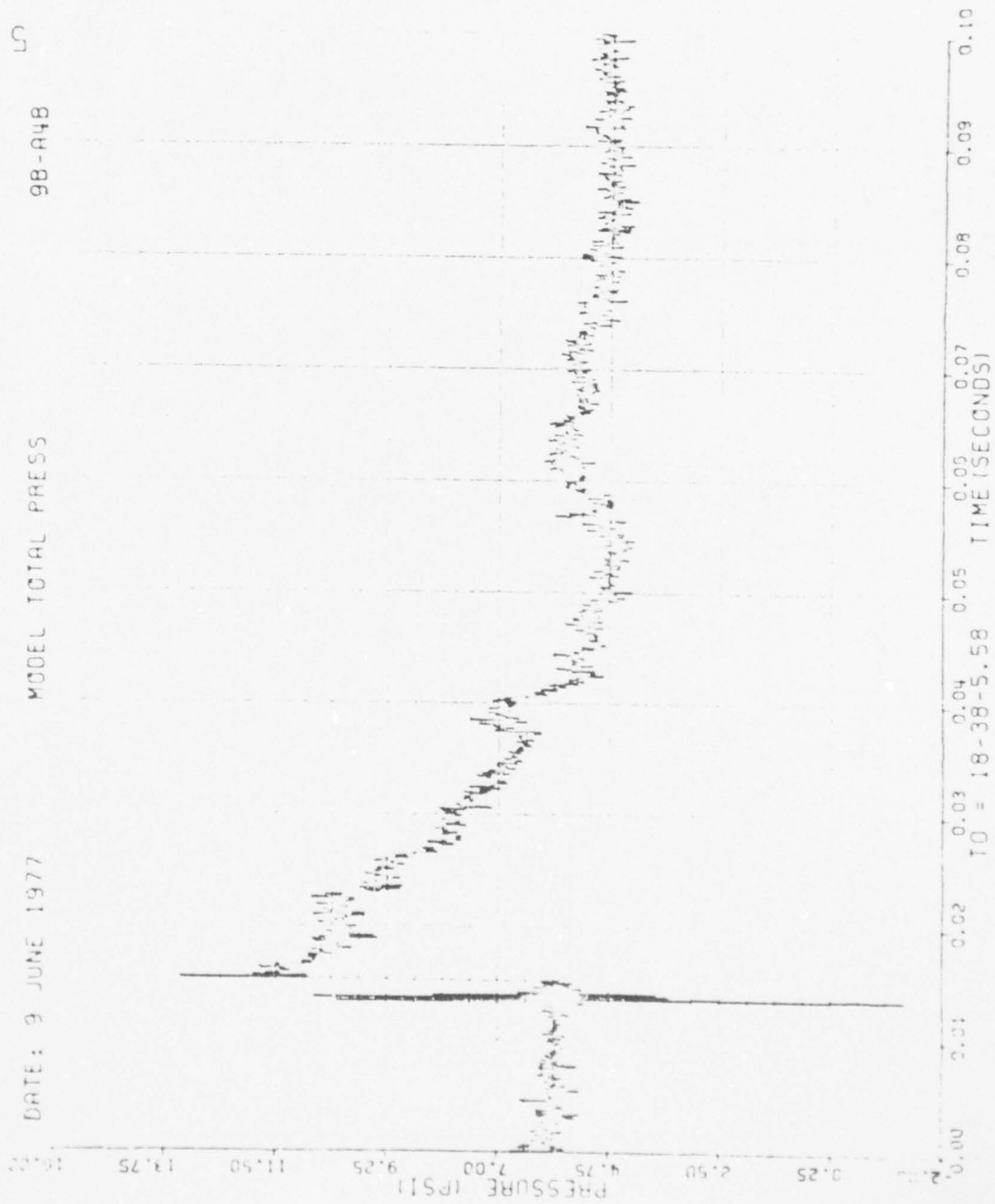


Figure 36. Concluded

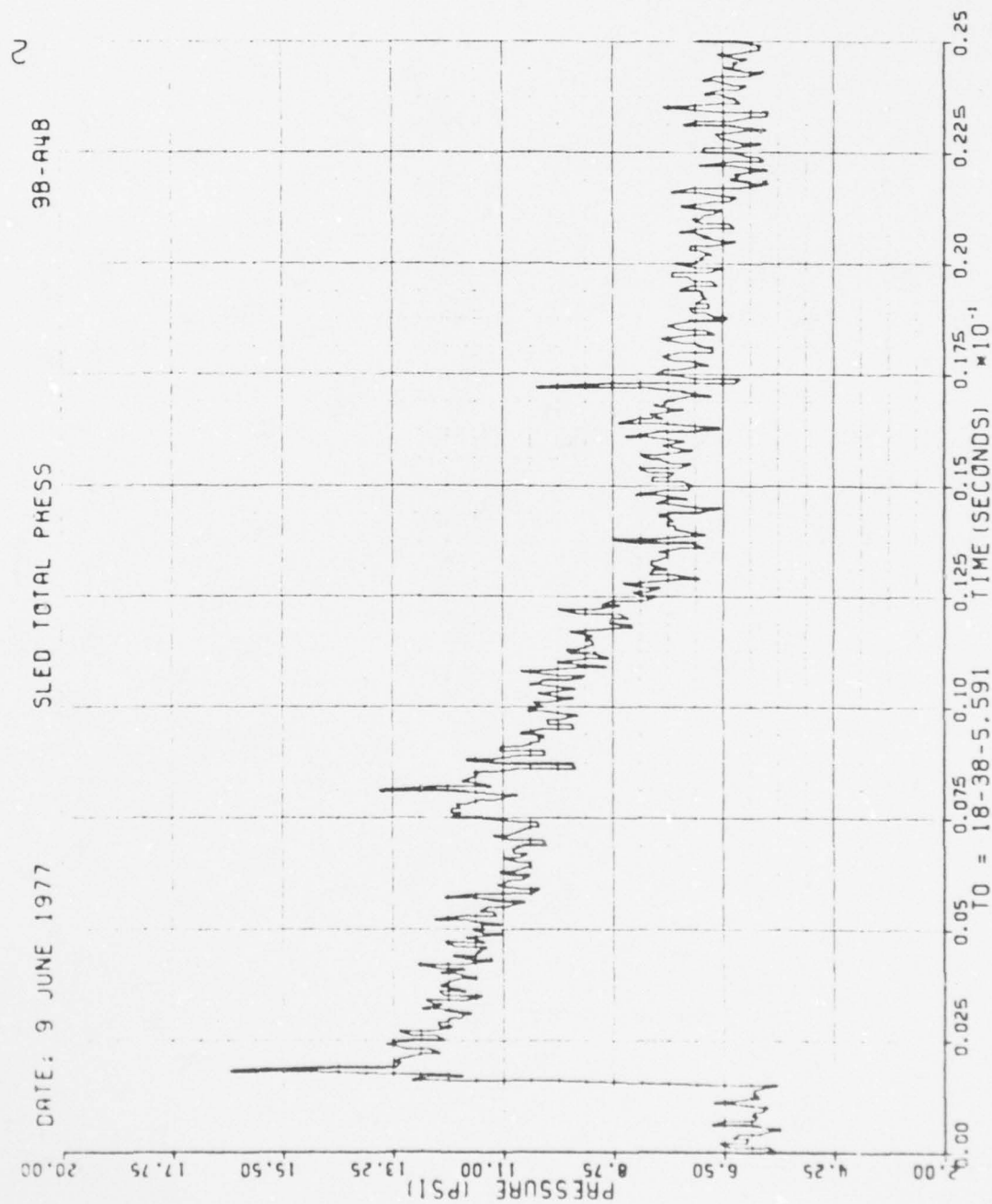


Figure 37. Total Pressure at Sled, Run 9B-A4, Intercept 2.

AD-A062 408

KAMAN AVIDYNE BURLINGTON MASS
MEASUREMENTS OF BLAST PRESSURES ON A RIGID 65 DEG SWEEPBACK WIN--ETC(U)
JAN 78 J R RUETENIK, R F SMILEY

F/G 1/3

DNA001-76-C-0106

UNCLASSIFIED

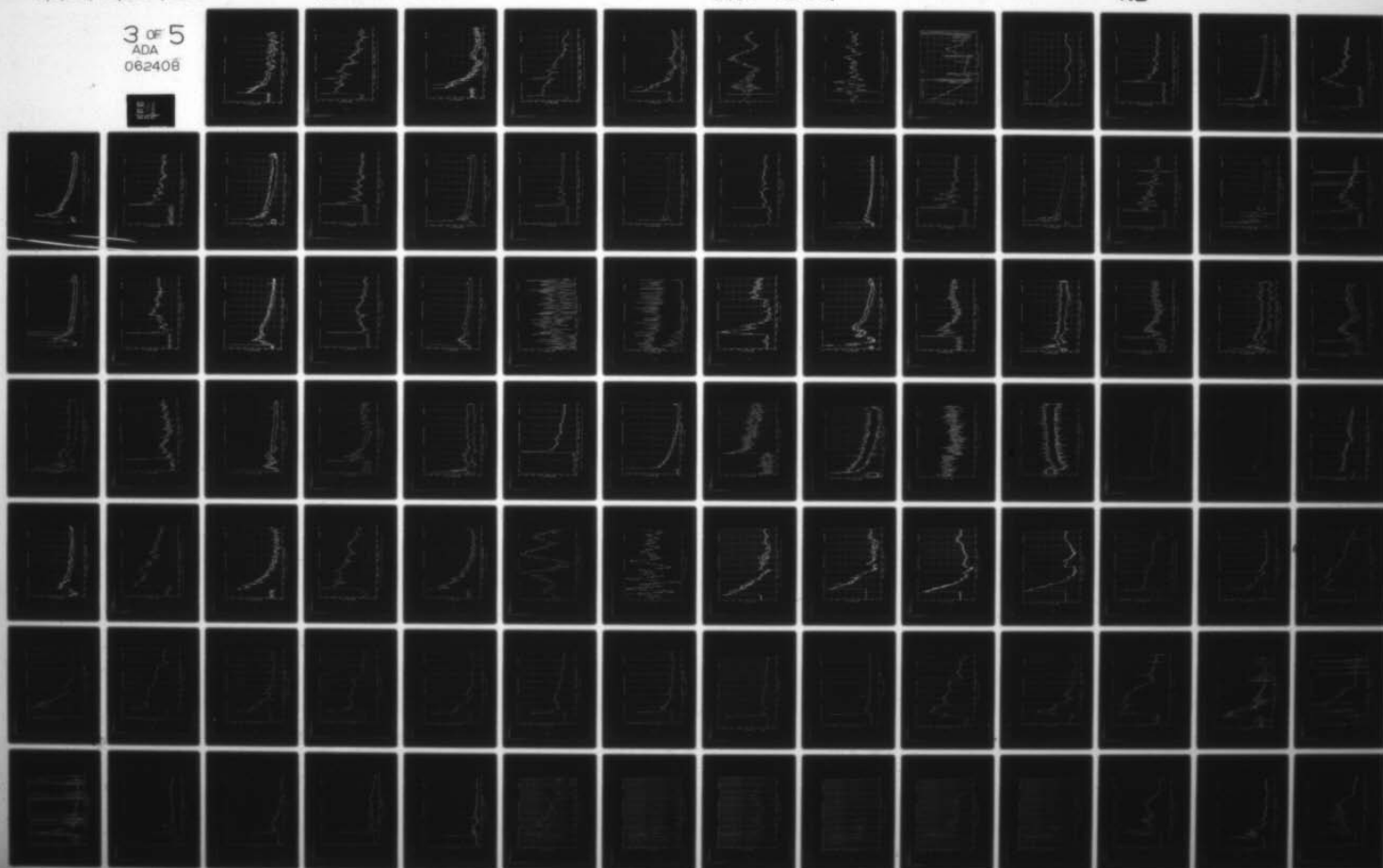
KA-TR-145

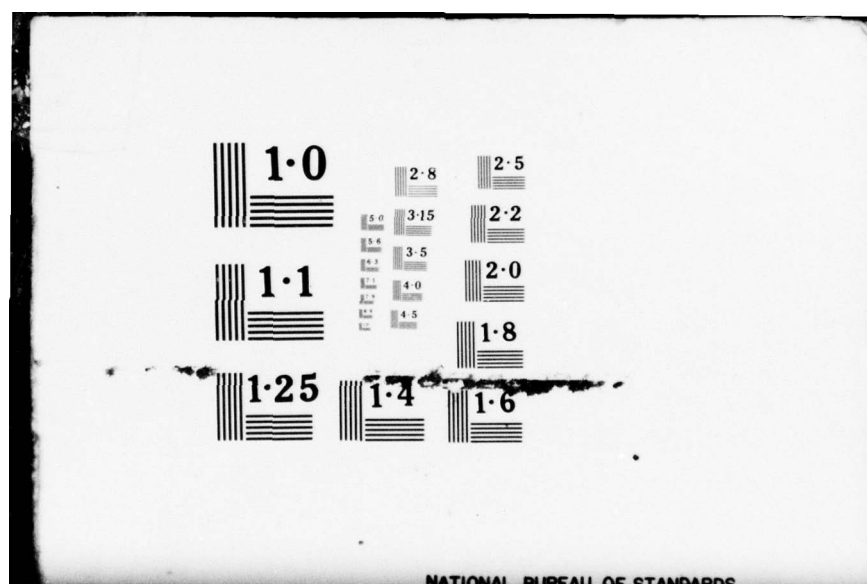
DNA-4504F

NL

3 OF 5
ADA
062408

EL





1.0

2.8

2.5

5.0

3.15

2.2

5.6

3.5

2.0

1.1

6.3

4.0

7.1

4.5

1.8

1.25

1.4

1.6

NATIONAL BUREAU OF STANDARDS

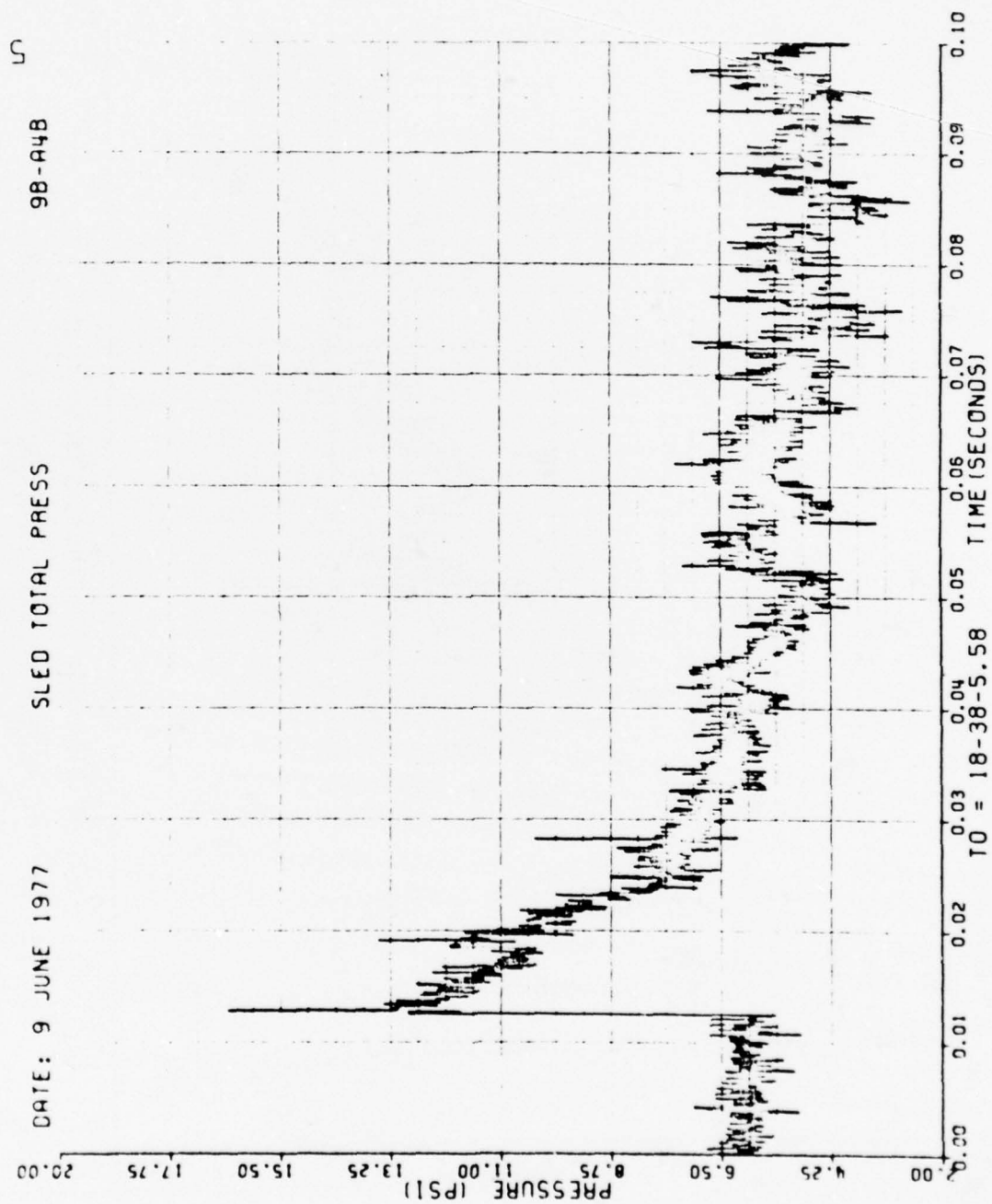


Figure 37. Concluded

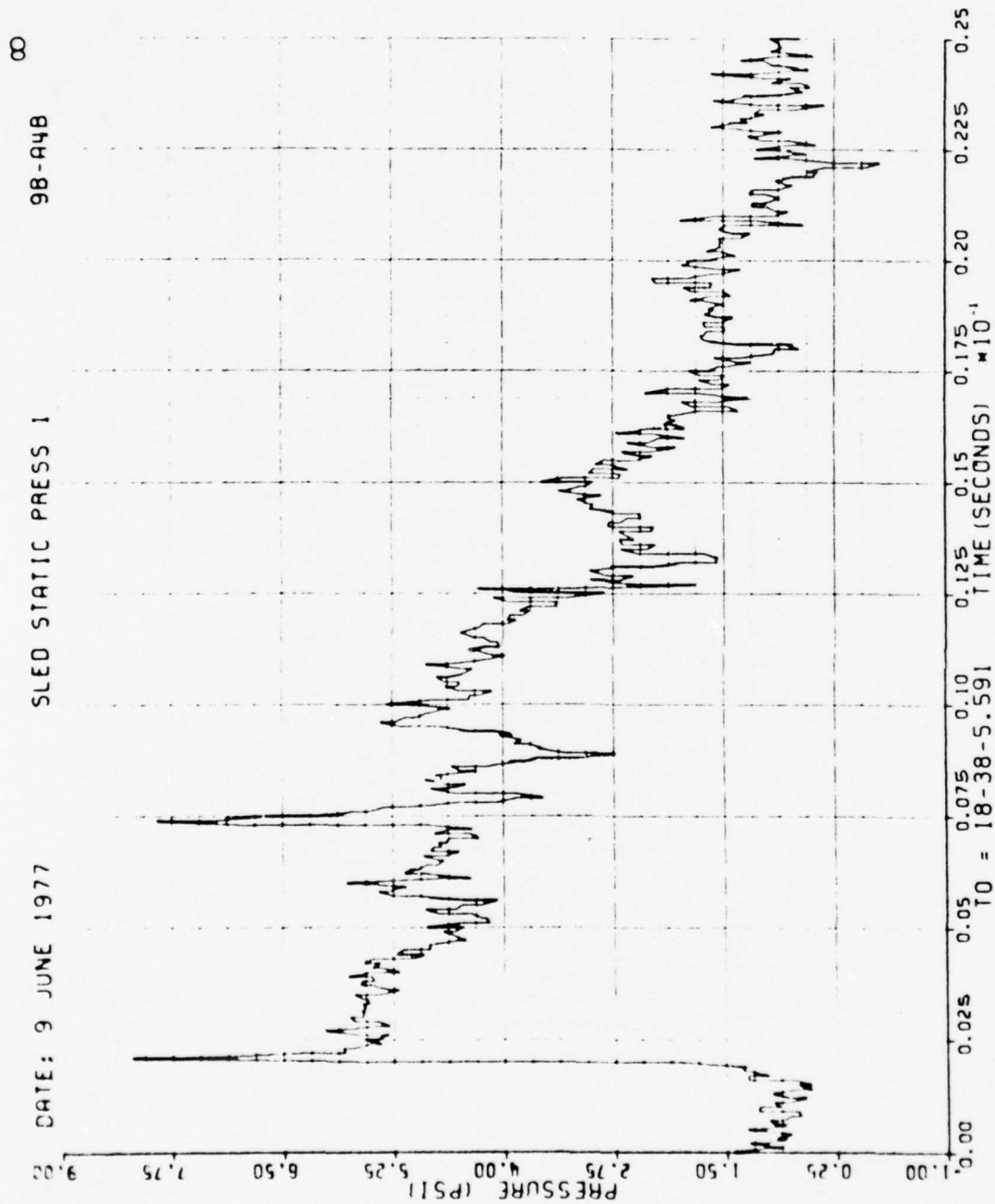


Figure 38. Static Pressure 1 at Sled, Run 9B-A4, Intercept 2.

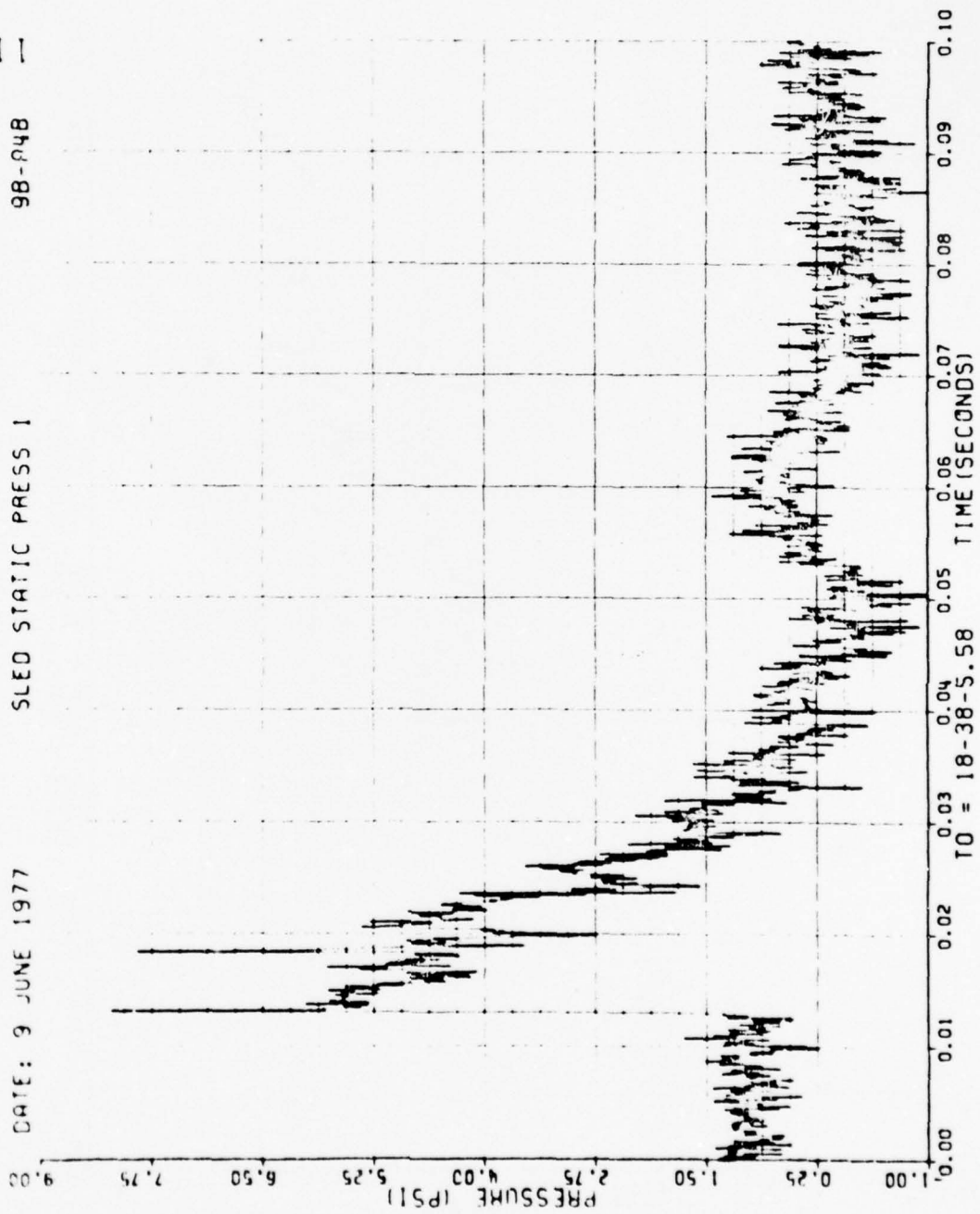


Figure 38. Concluded

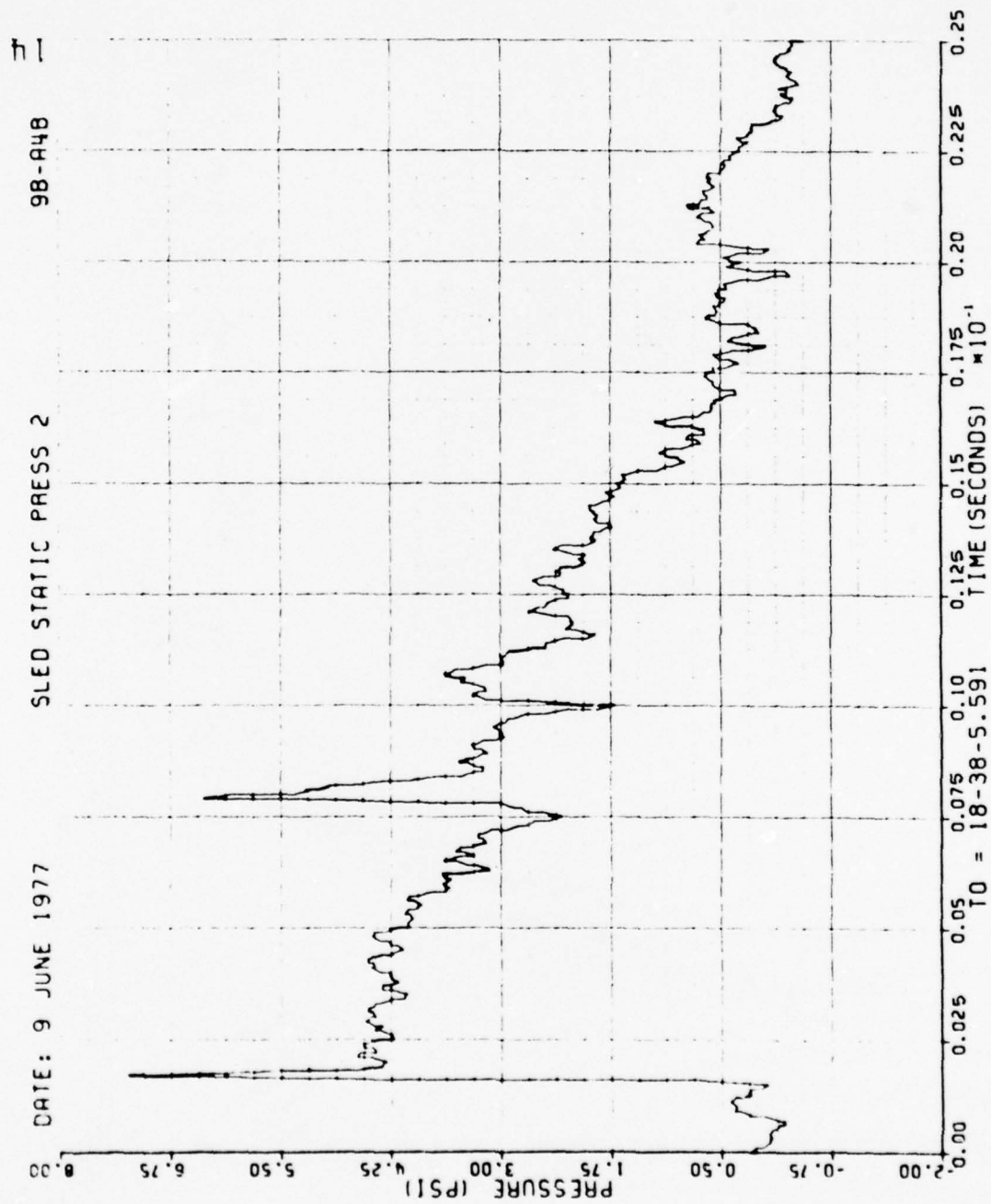


Figure 39. Static Pressure 2 at Sled, Run 98-A4, Intercept 2.

17

9B-A4B

SLED STATIC PRESS 2

DATE: 9 JUNE 1977

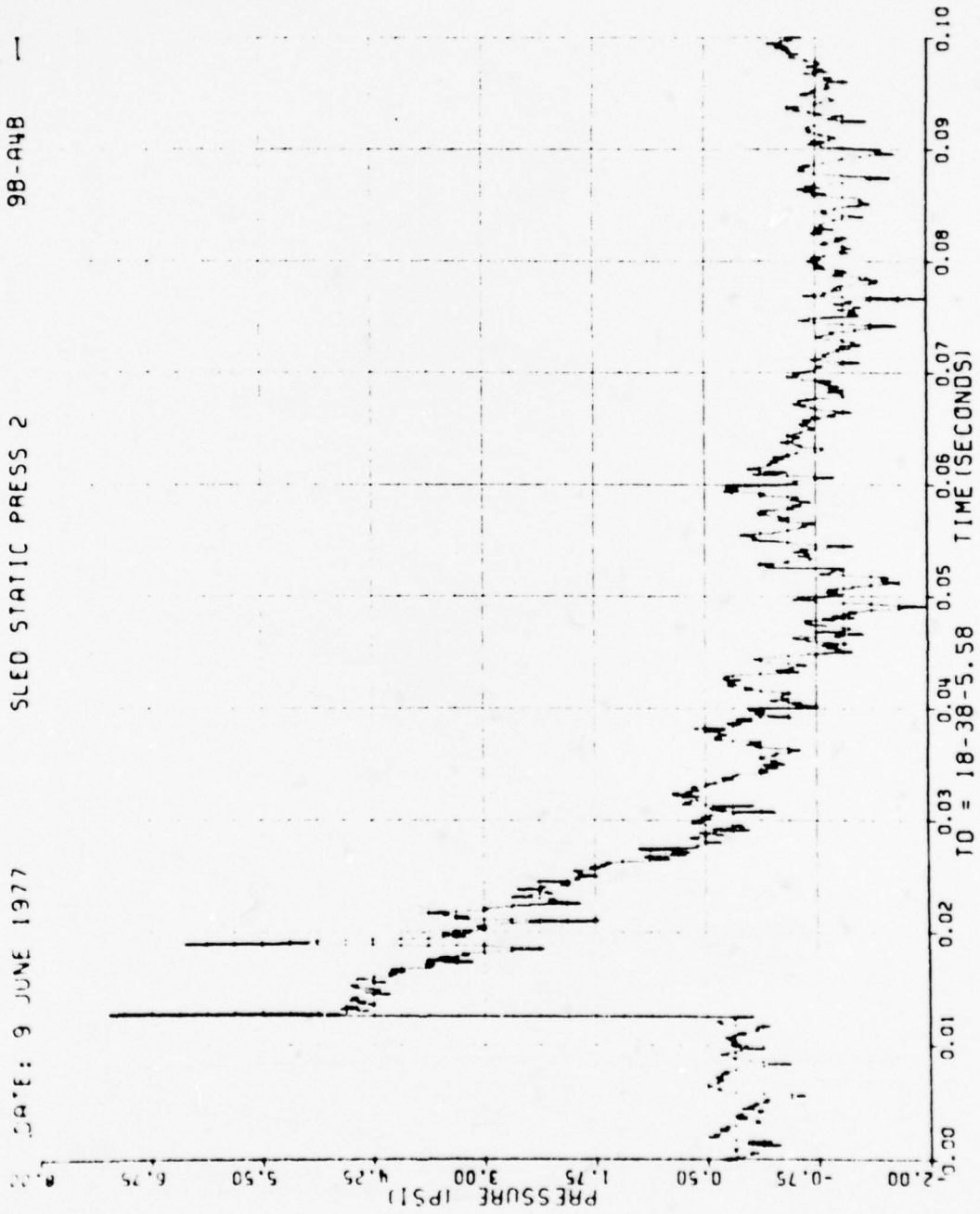


Figure 39. Concluded

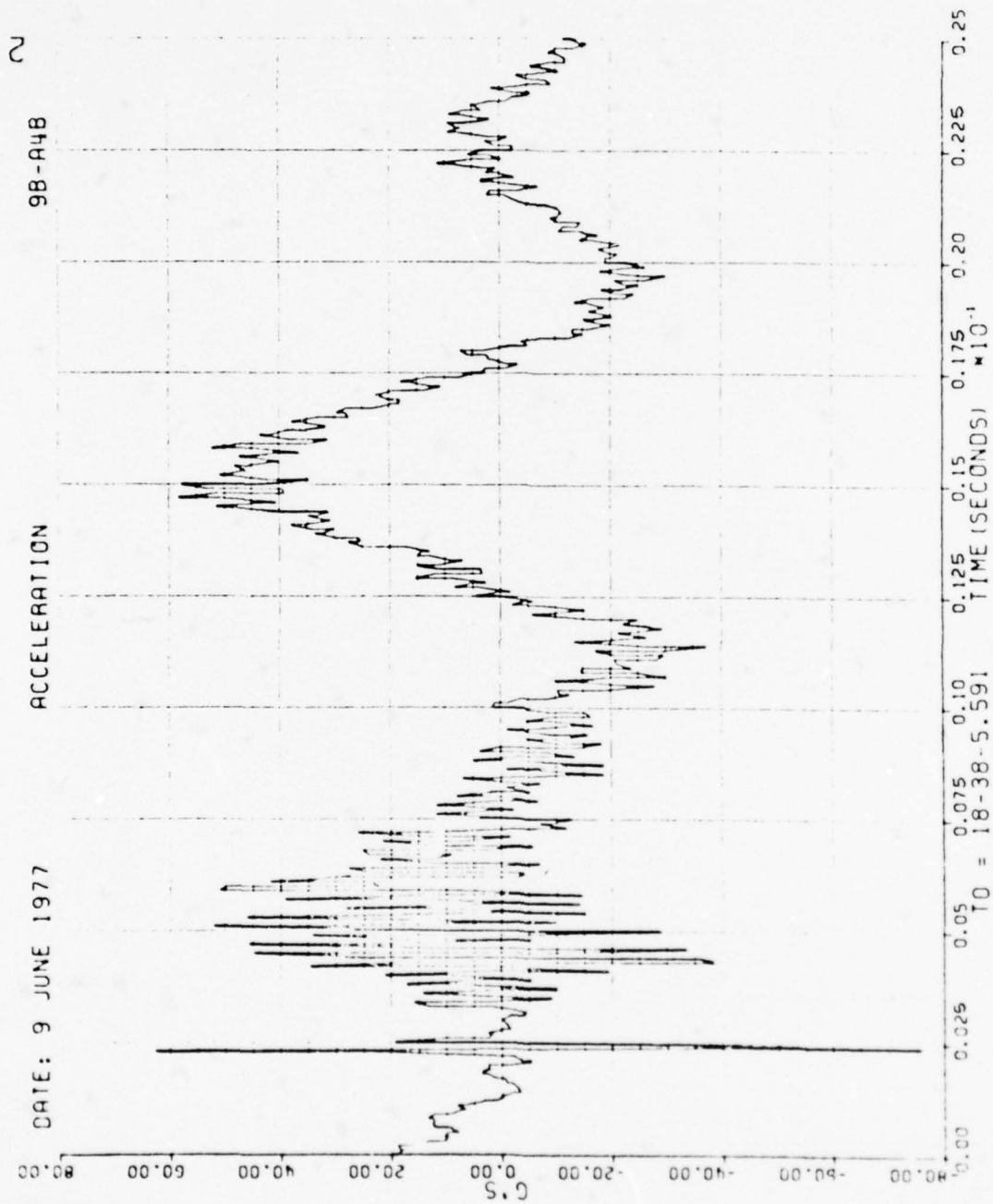


Figure 40. Wing Acceleration, Run 9B-A4, Intercept 2.

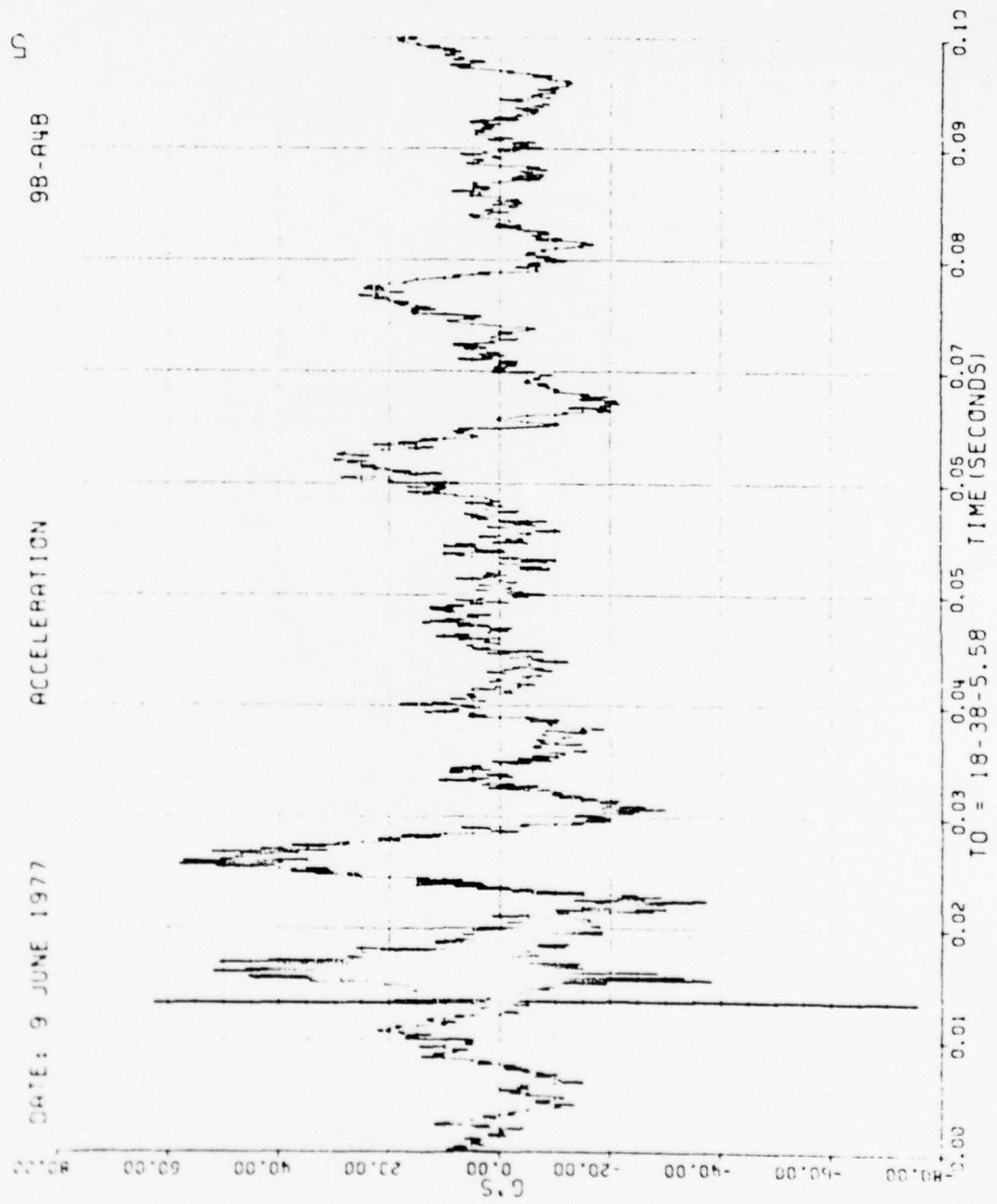


Figure 40. Concluded

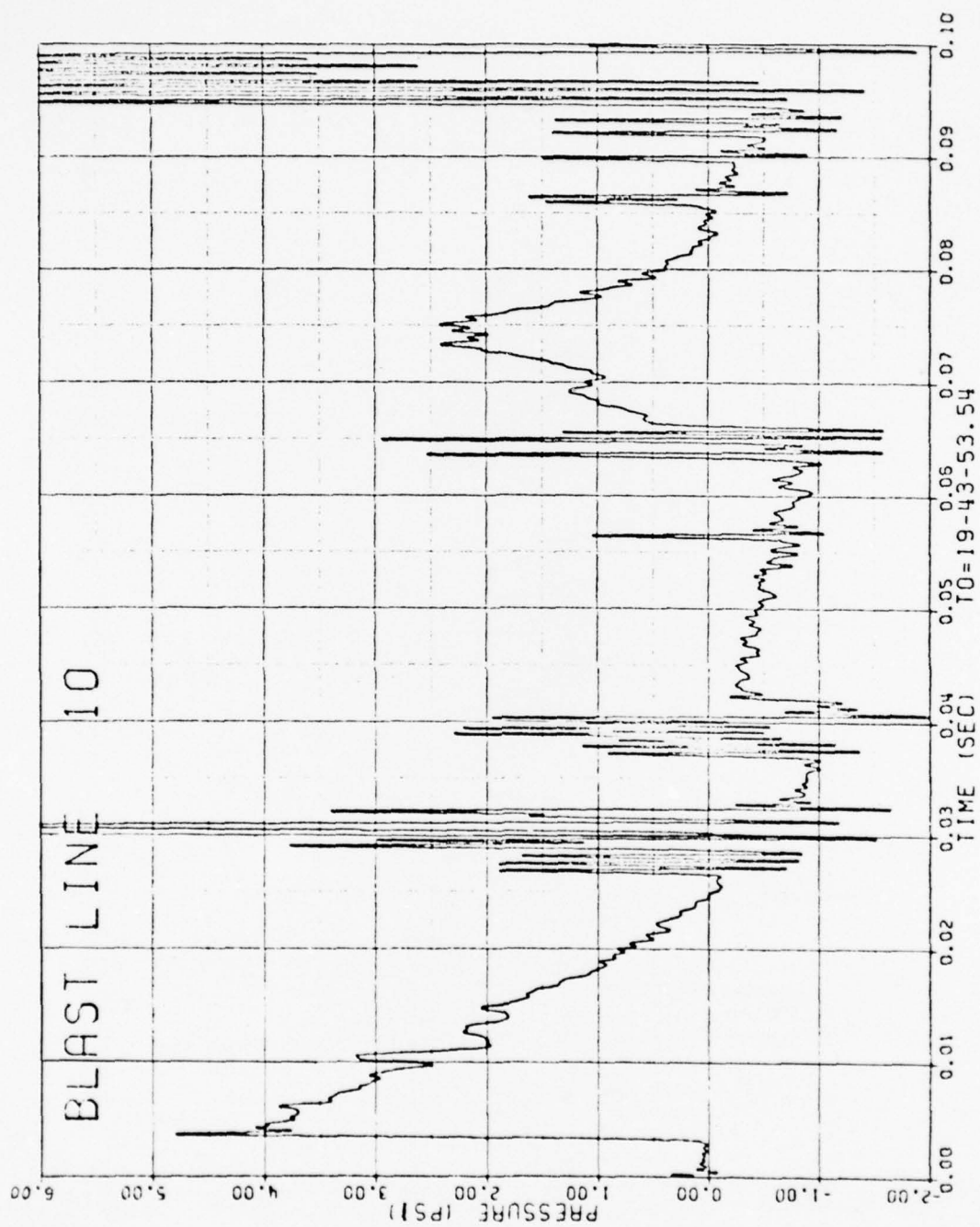


Figure 41. Blast-Line Overpressures, Run 9B-A4, Intercept 3.

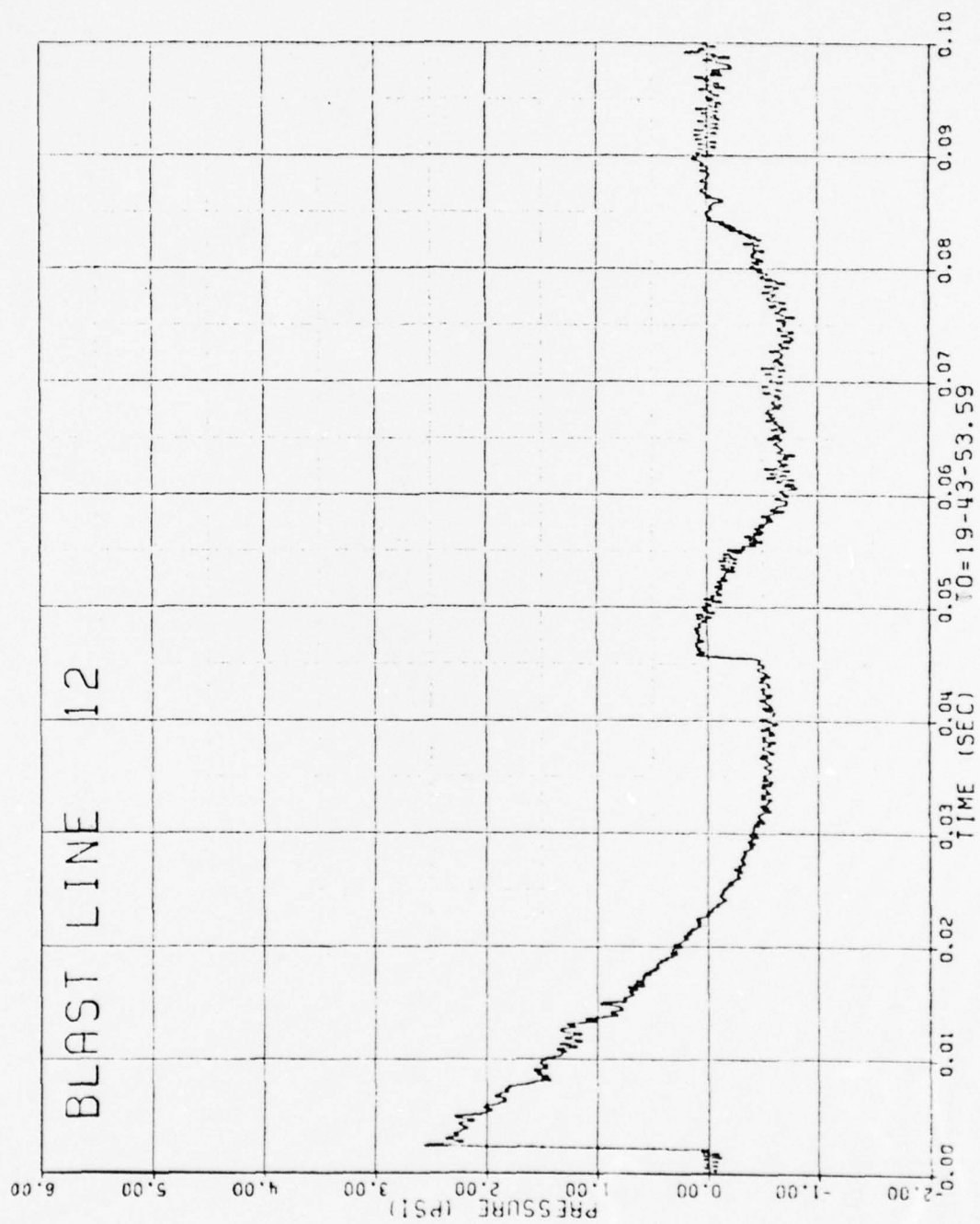


Figure 41. Concluded

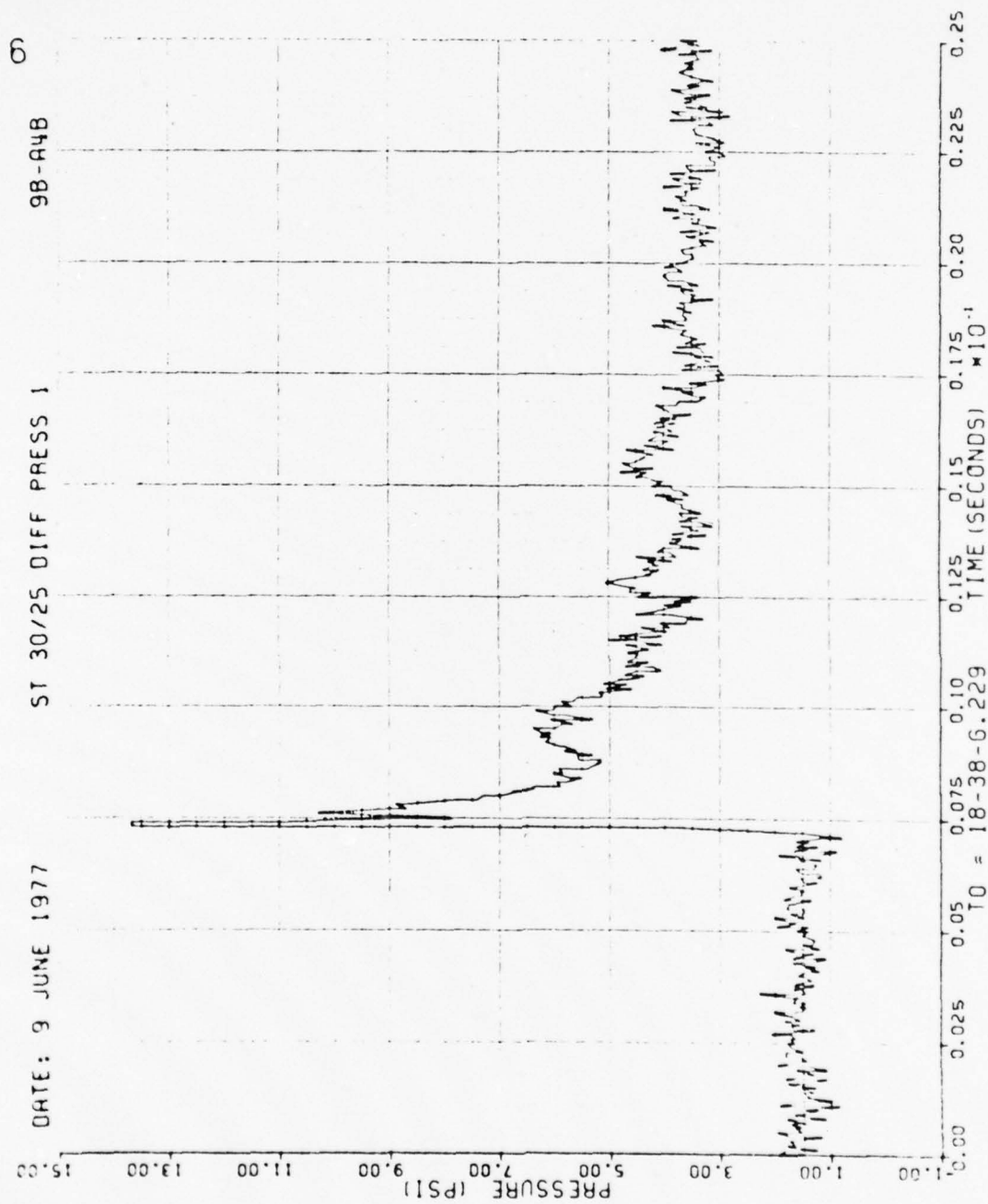


Figure 42. Differential Wing Pressures, Run 9B-A4, Intercept 3.

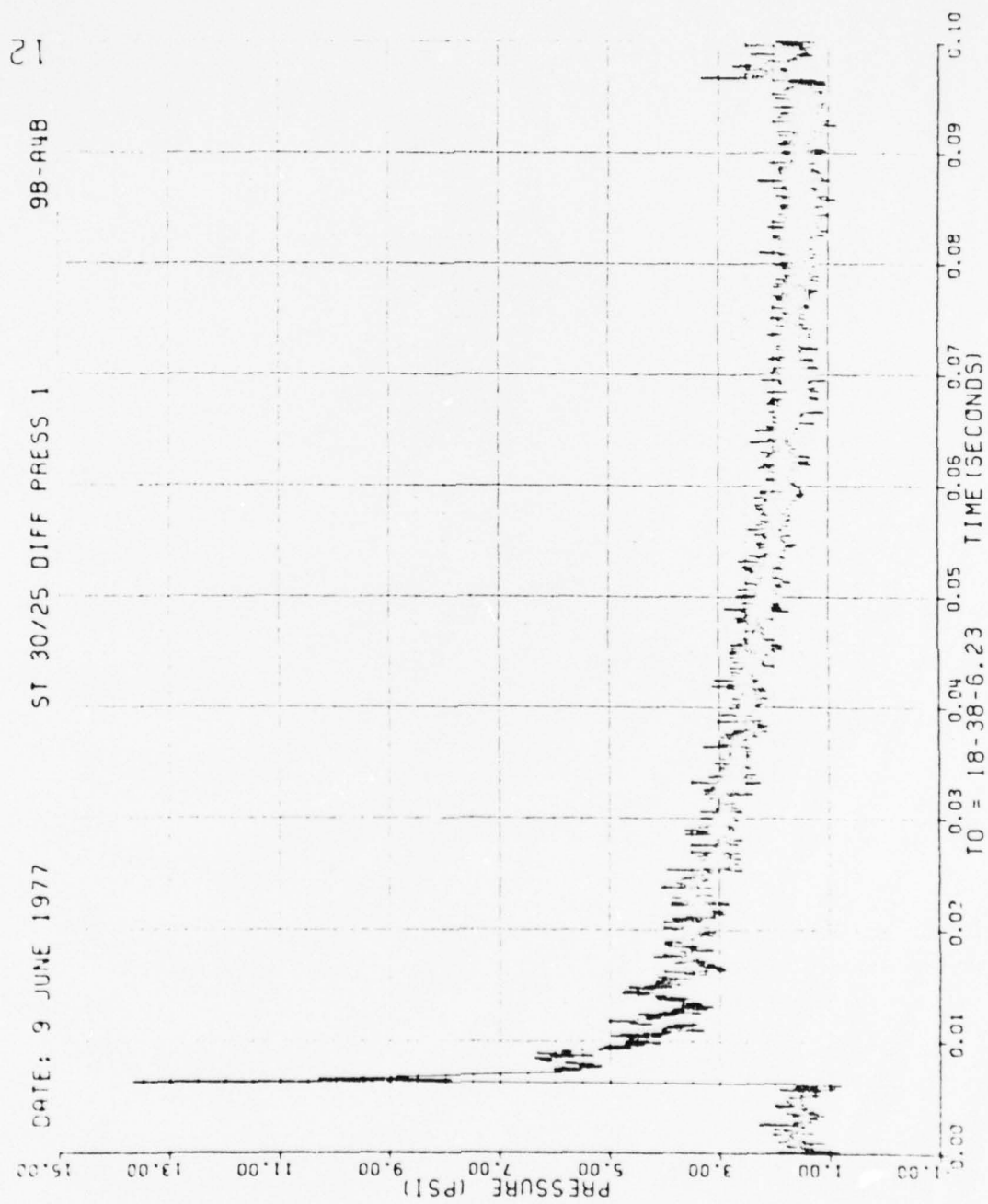


Figure 42. Continued

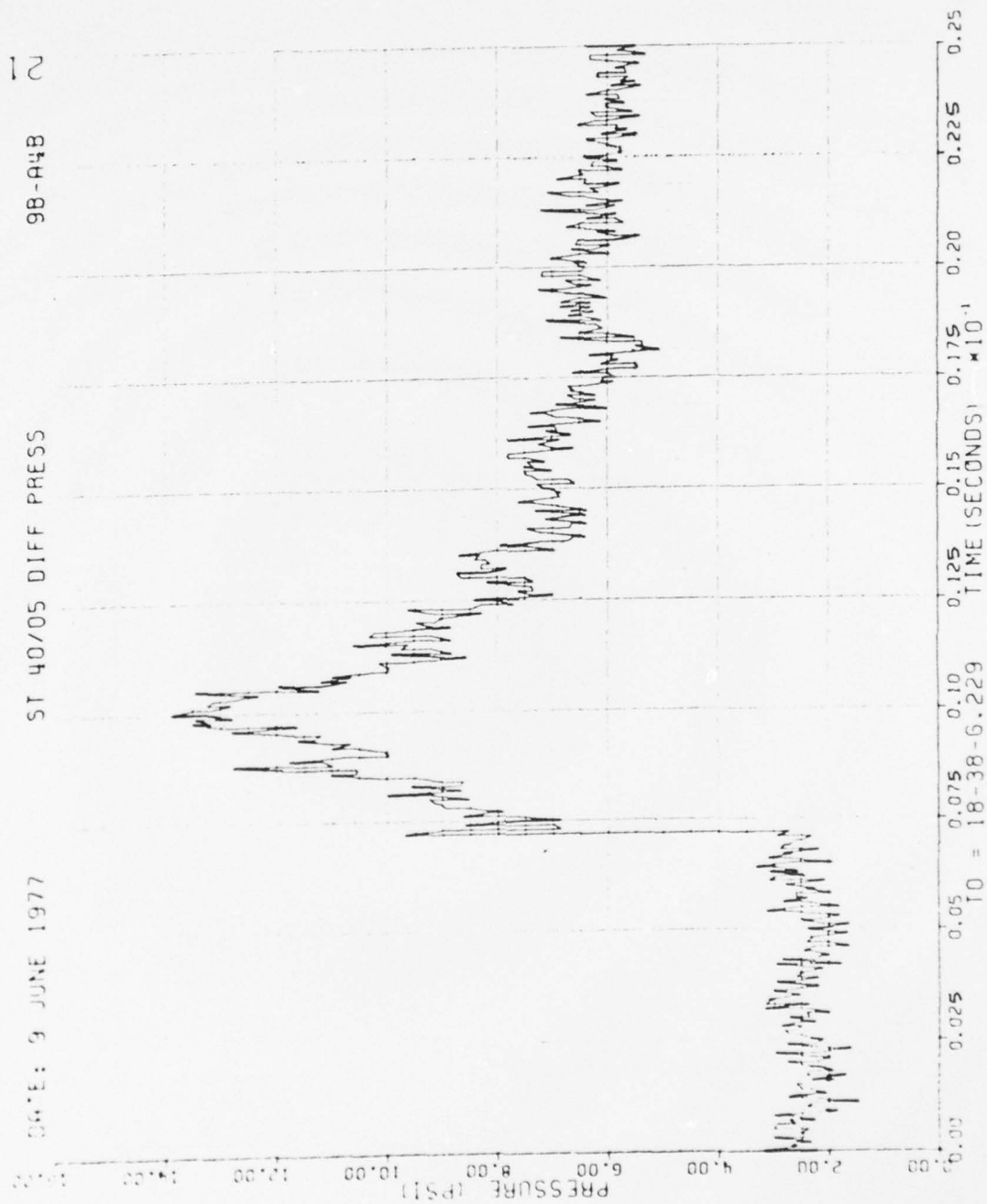


Figure 42. Continued

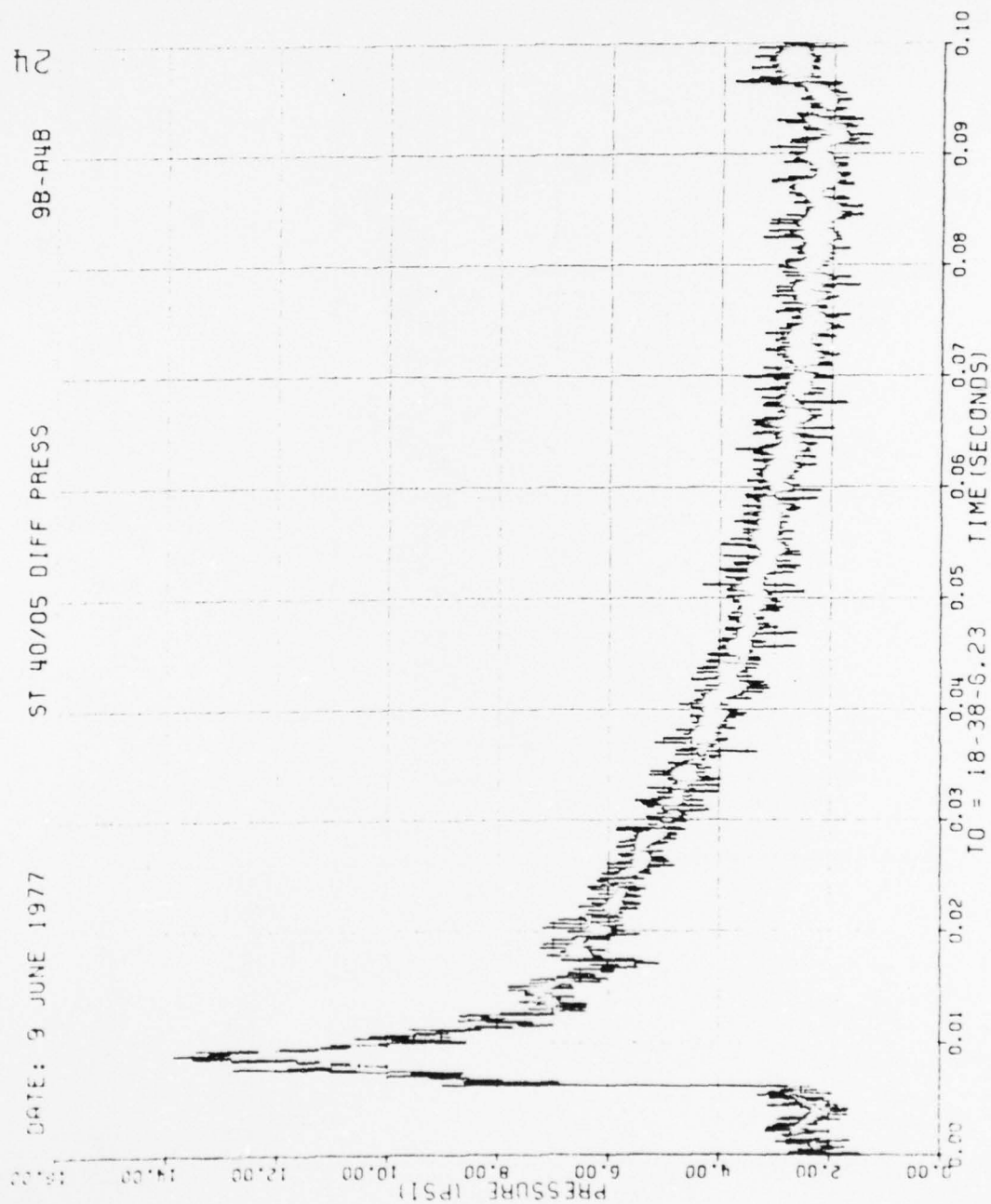


Figure 42. Continued

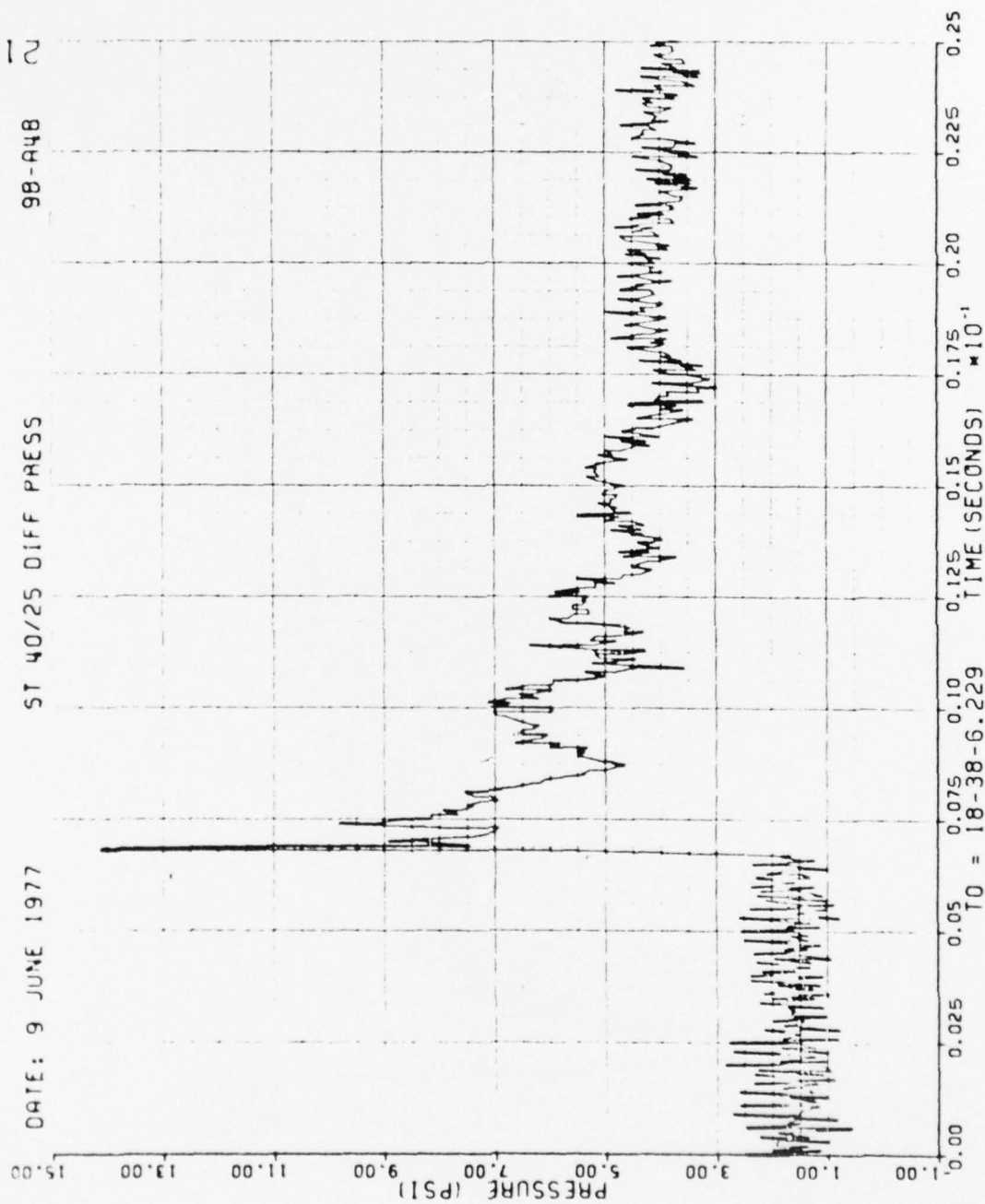


Figure 42. Continued

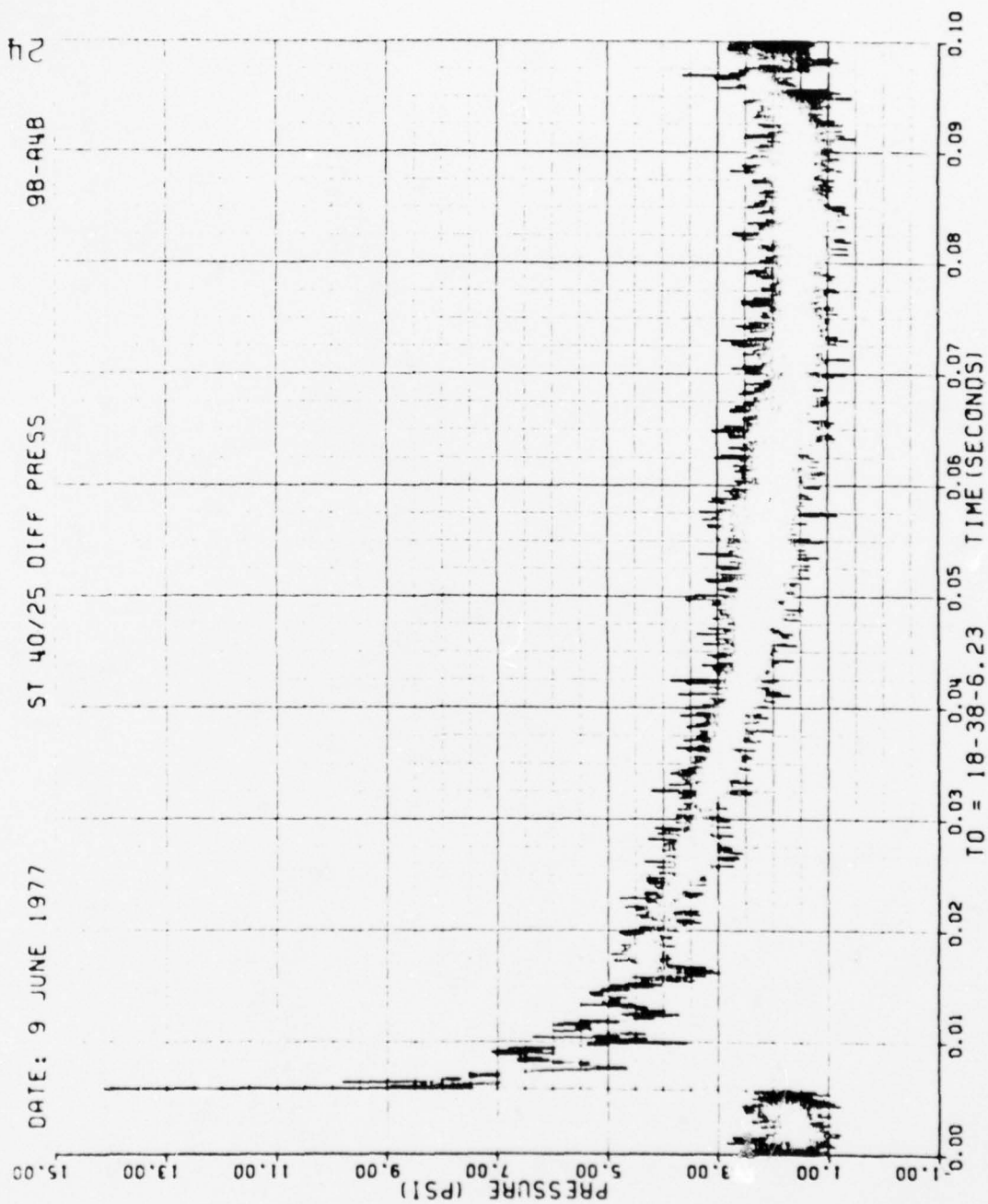


Figure 42. Continued

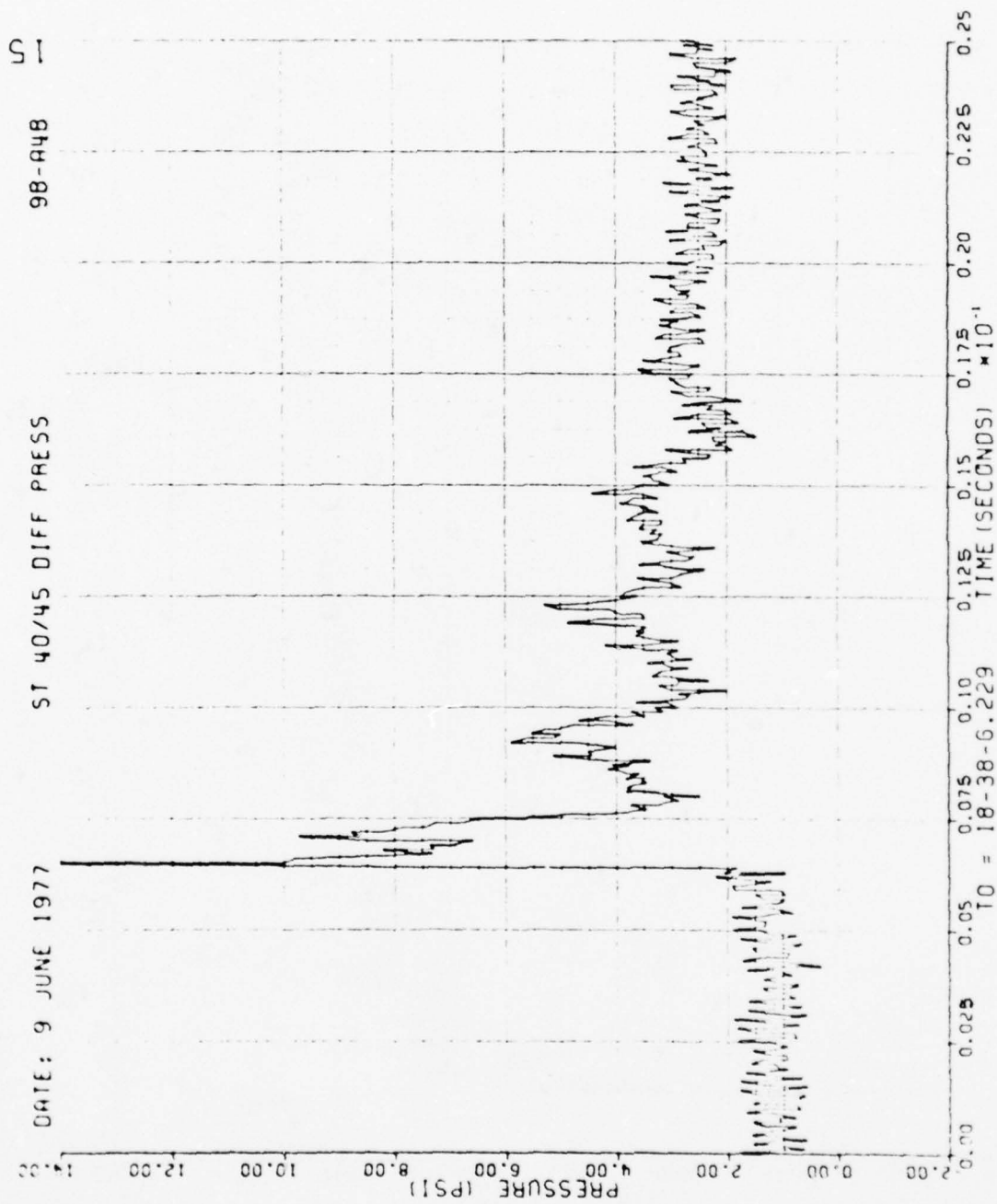


Figure 42. Continued

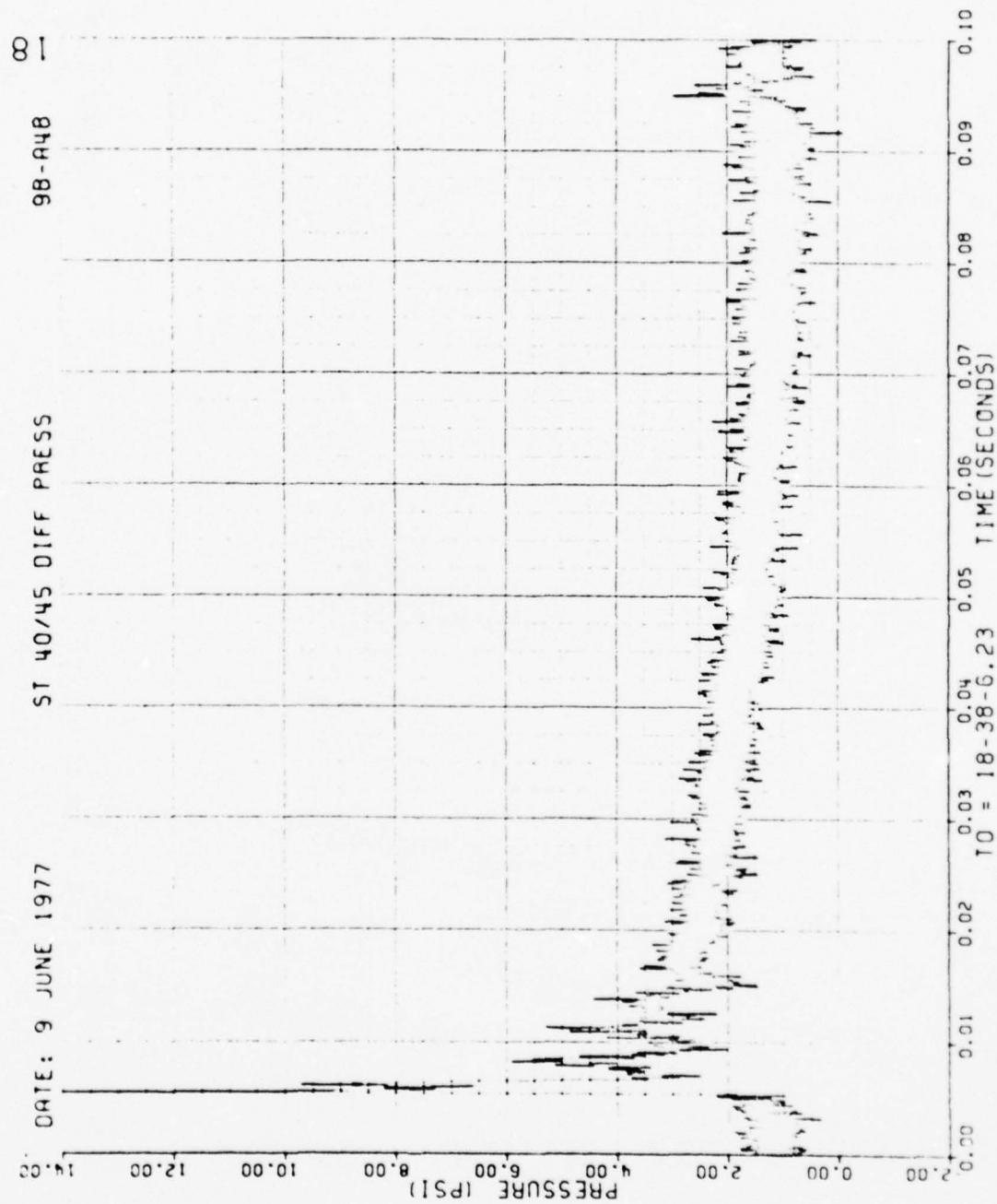


Figure 42. Continued

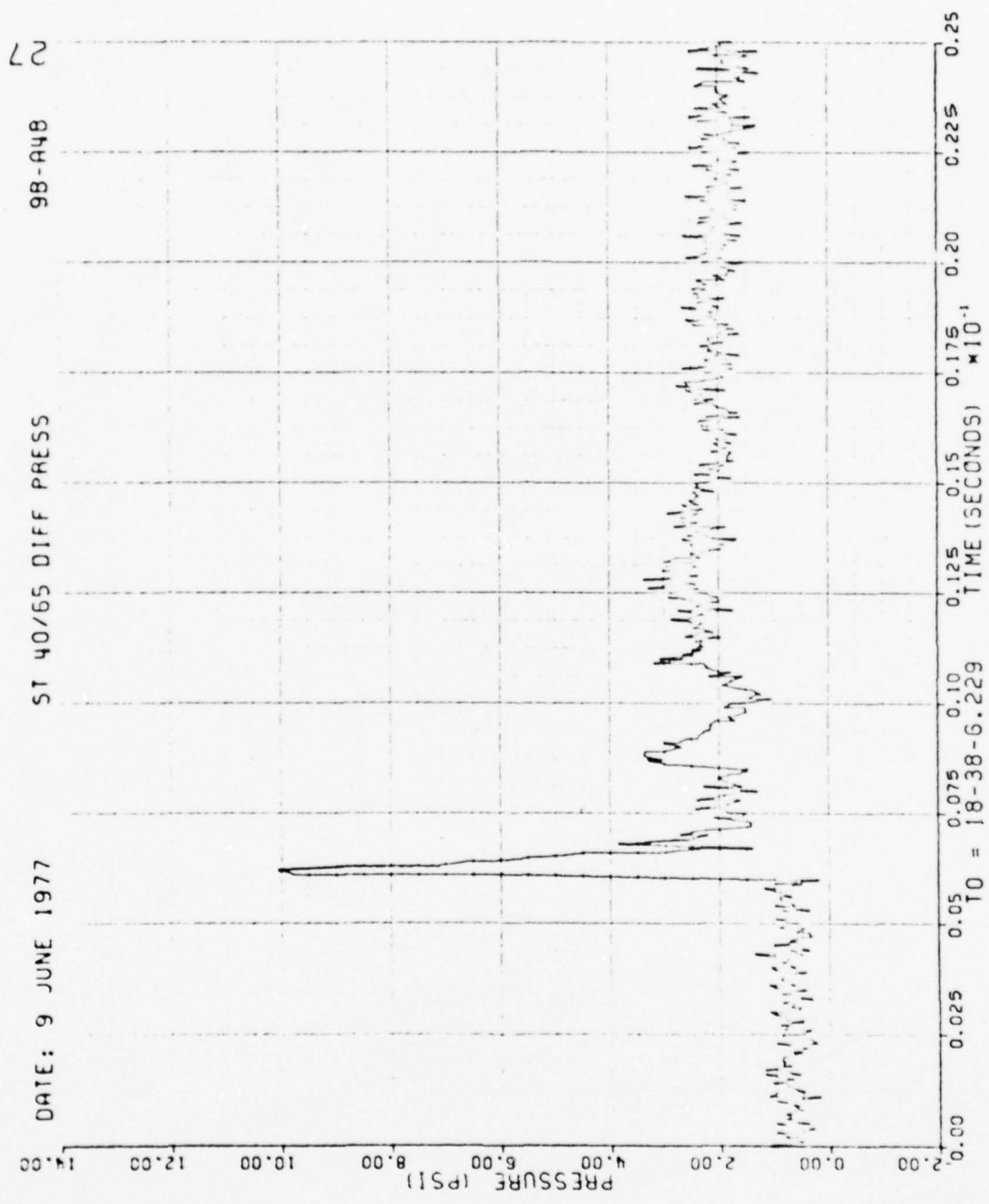


Figure 42. Continued

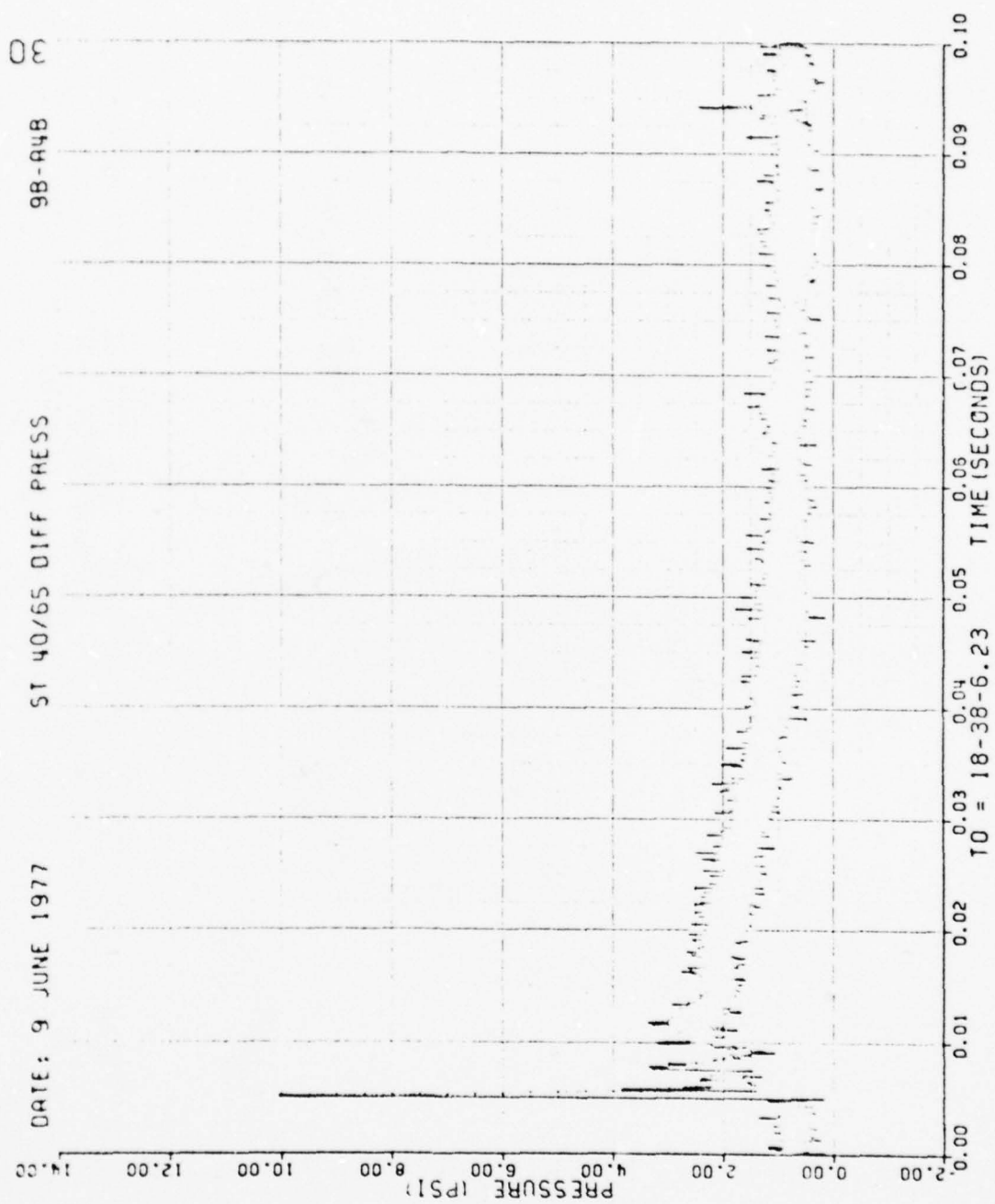


Figure 42. Continued

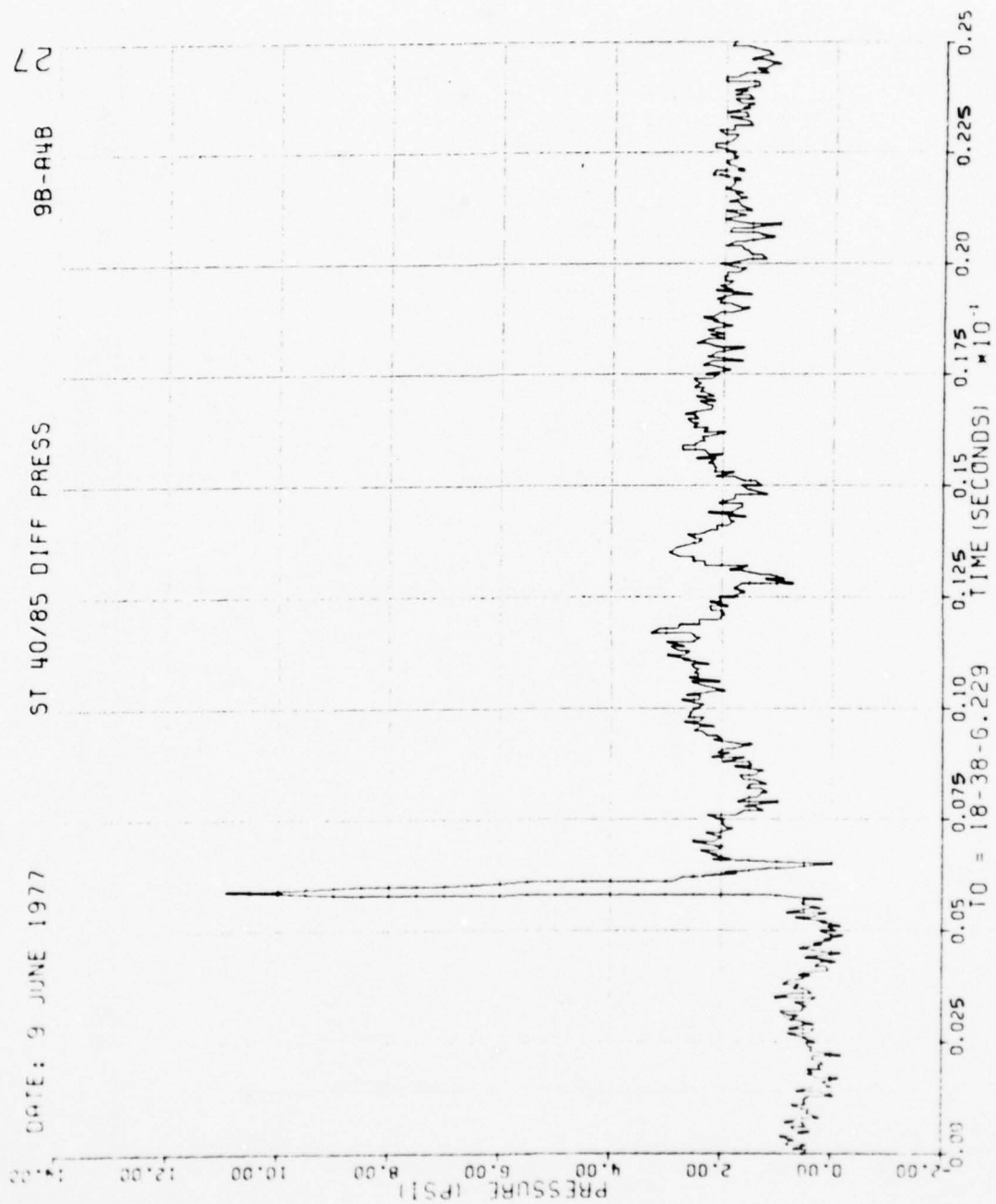


Figure 42. Continued

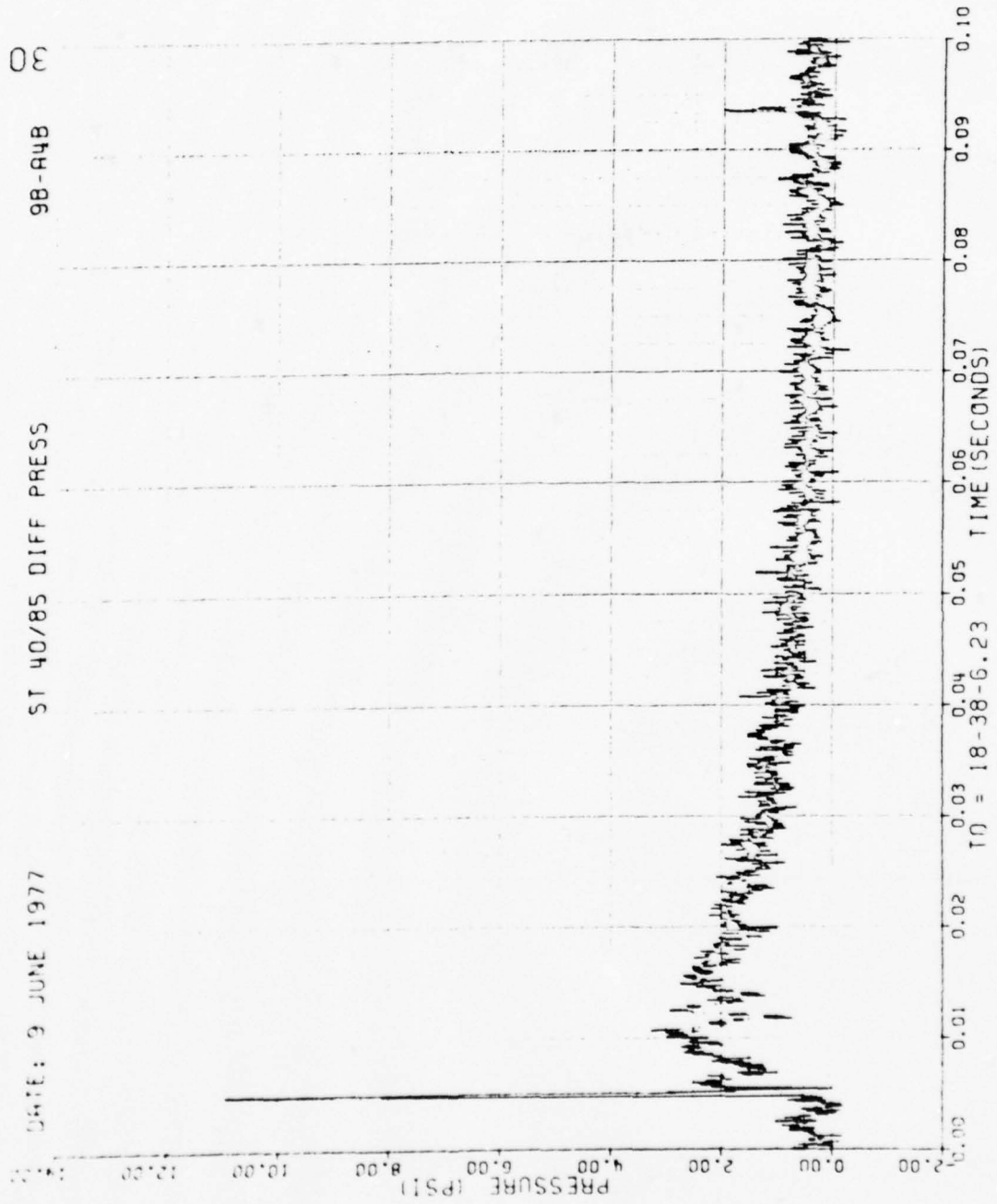


Figure 42. Continued

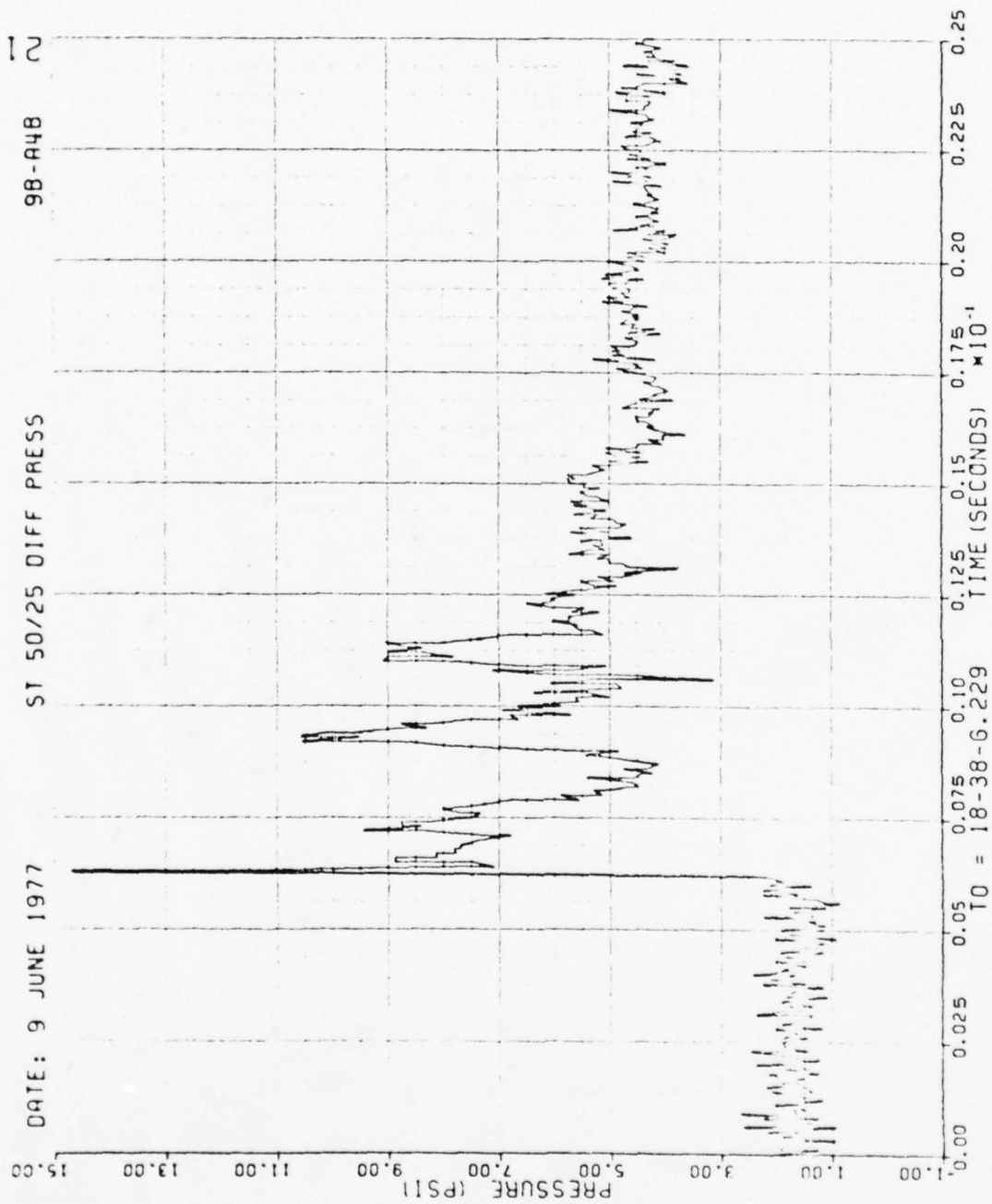


Figure 42. Continued

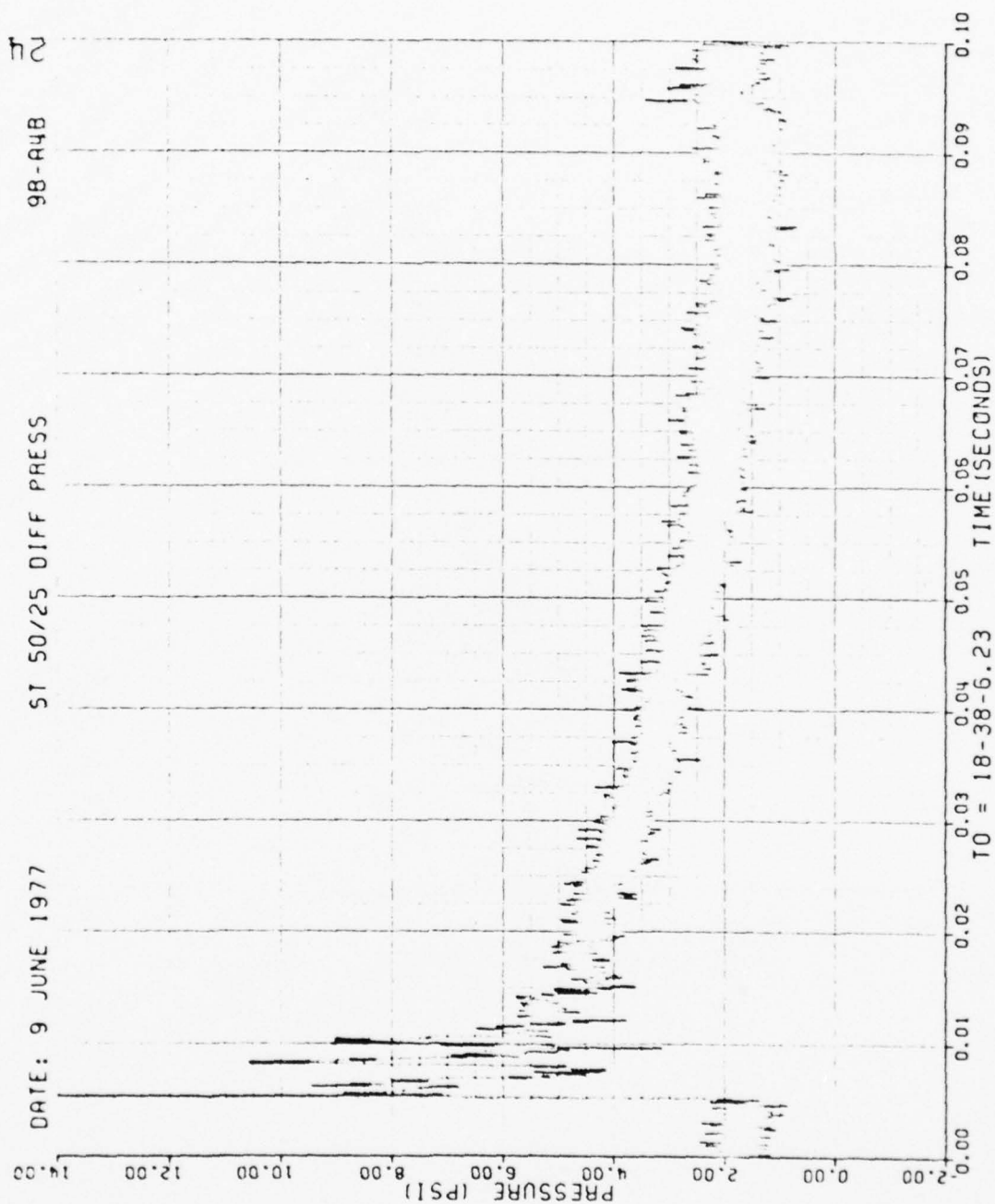


Figure 42. Continued

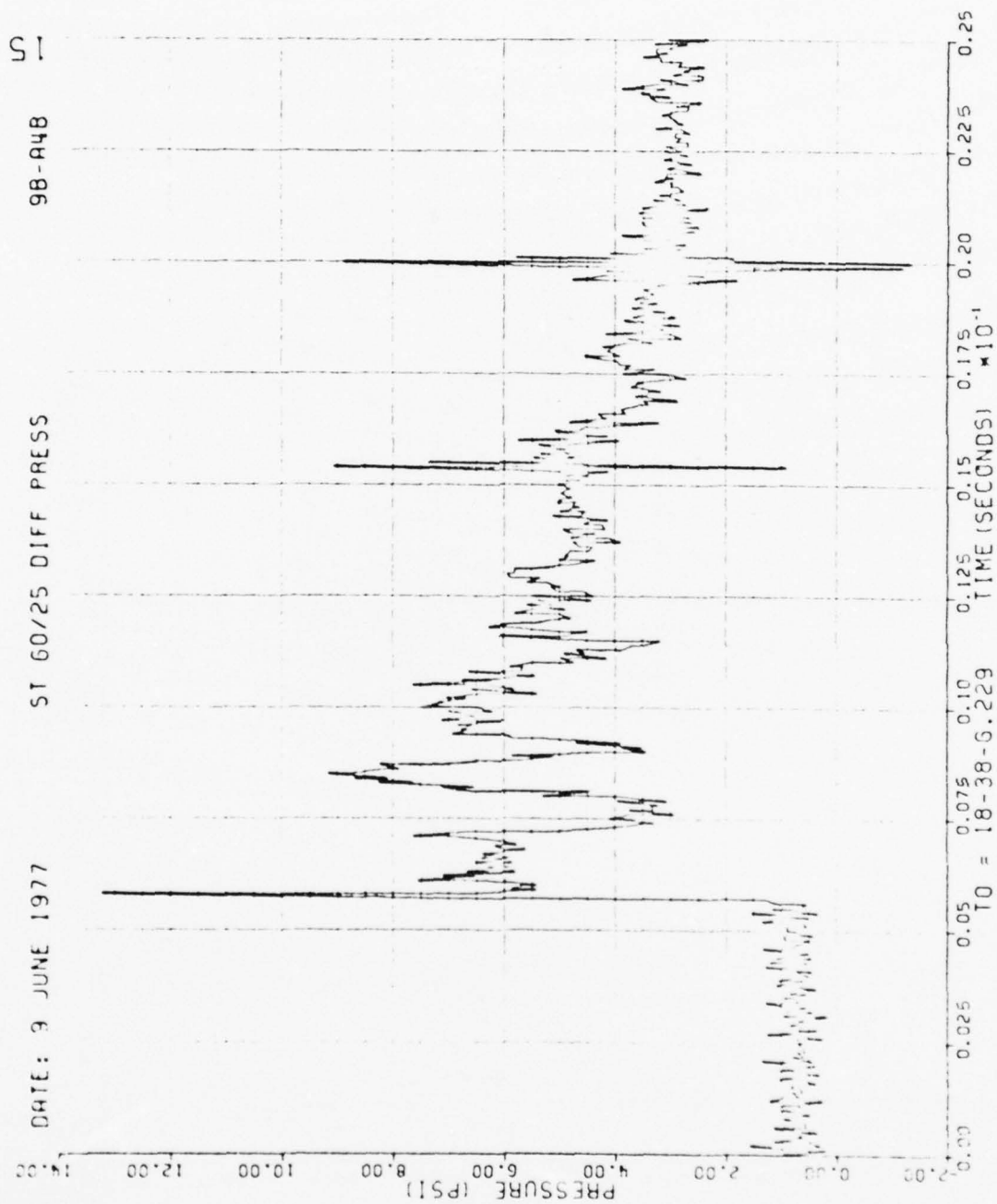


Figure 42. Continued

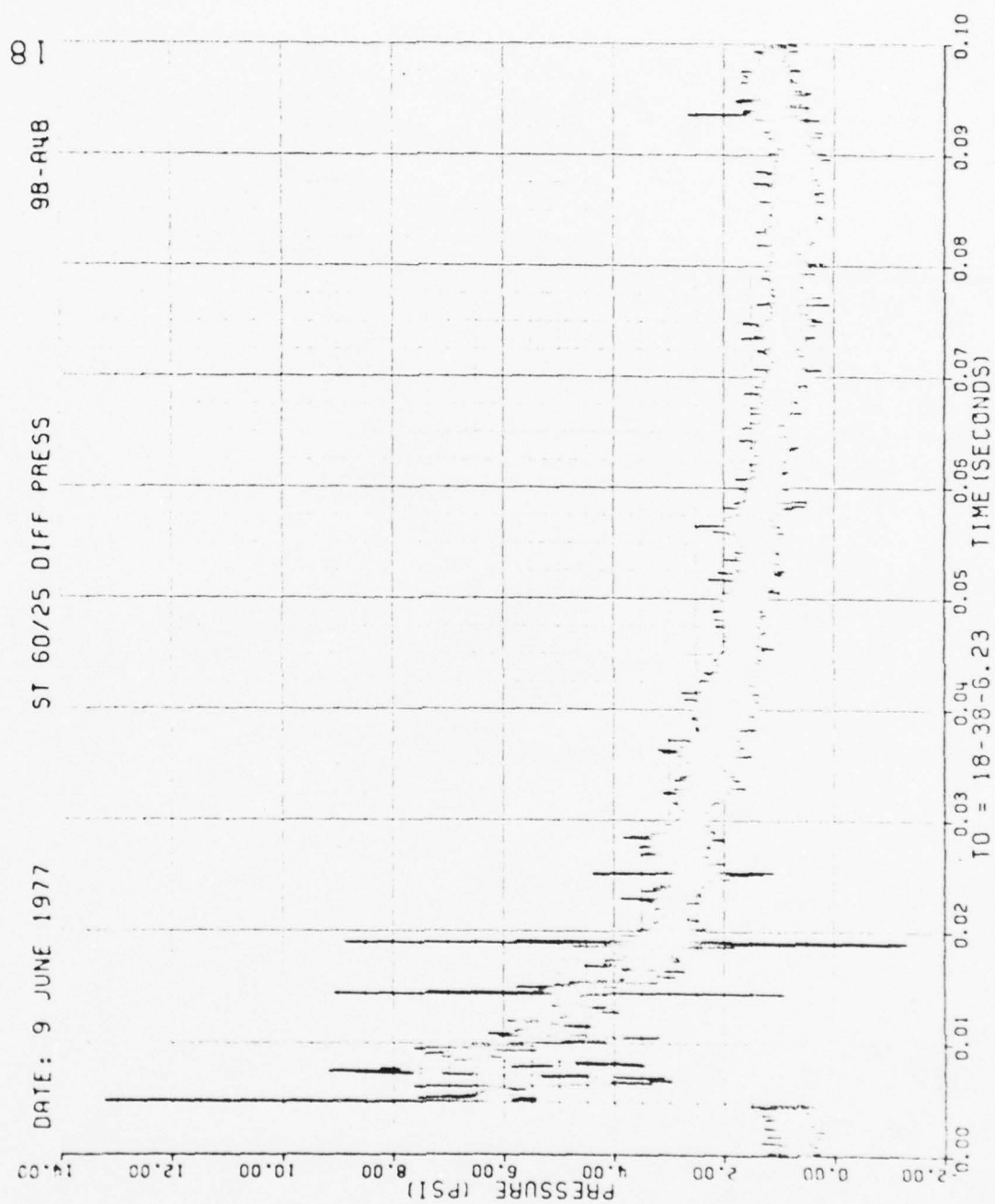


Figure 42. Continued

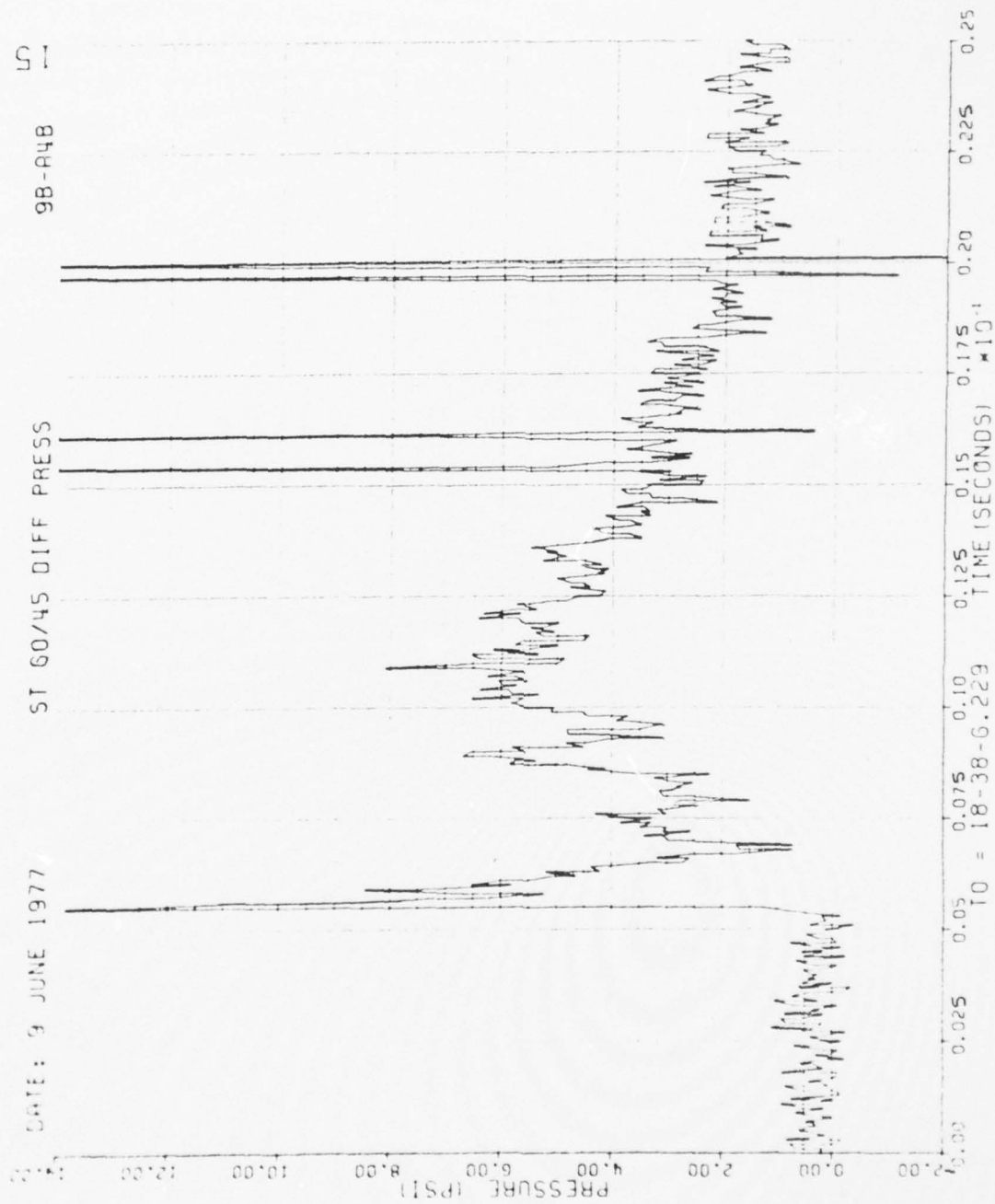


Figure 42. Continued

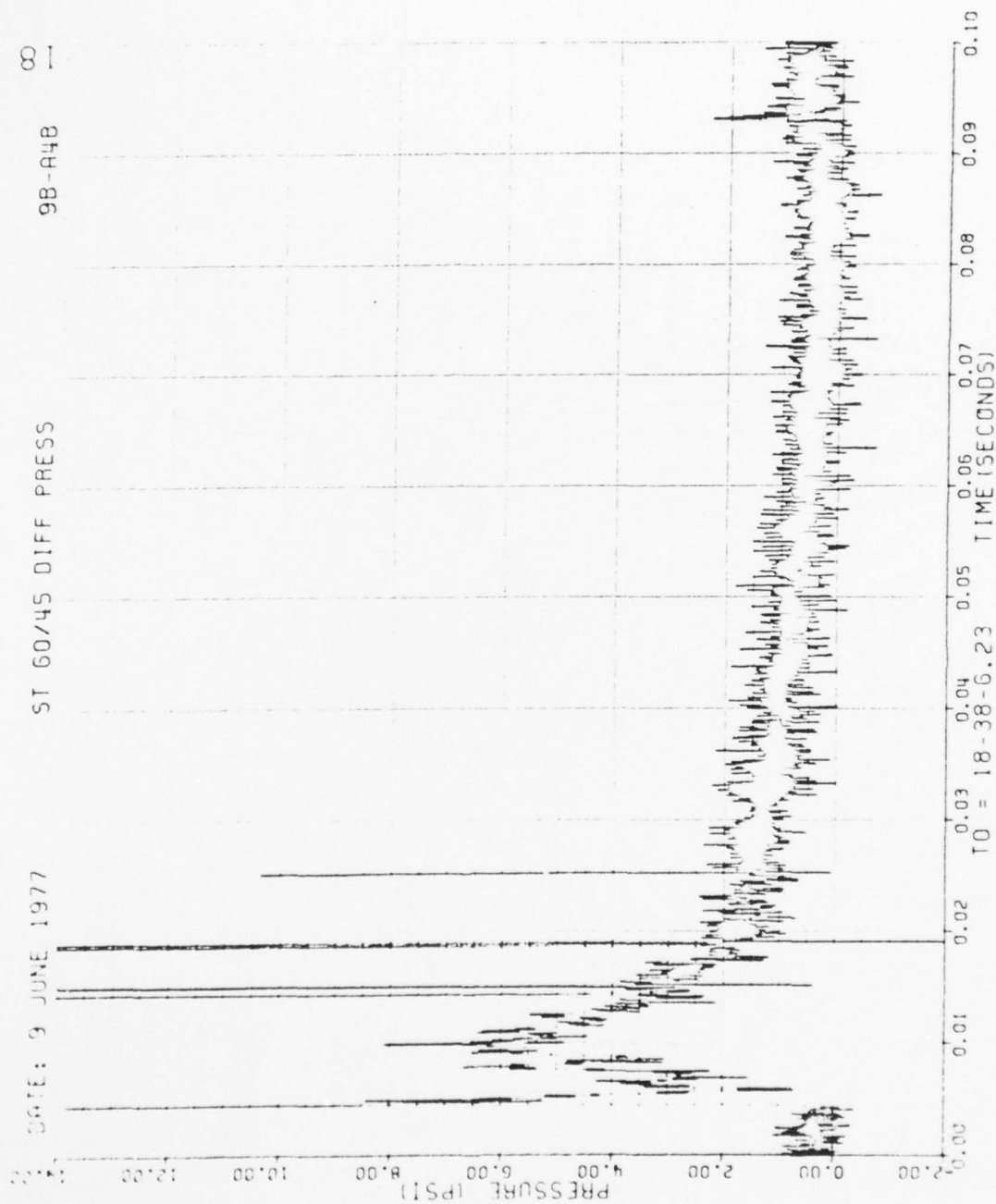


Figure 42. Continued

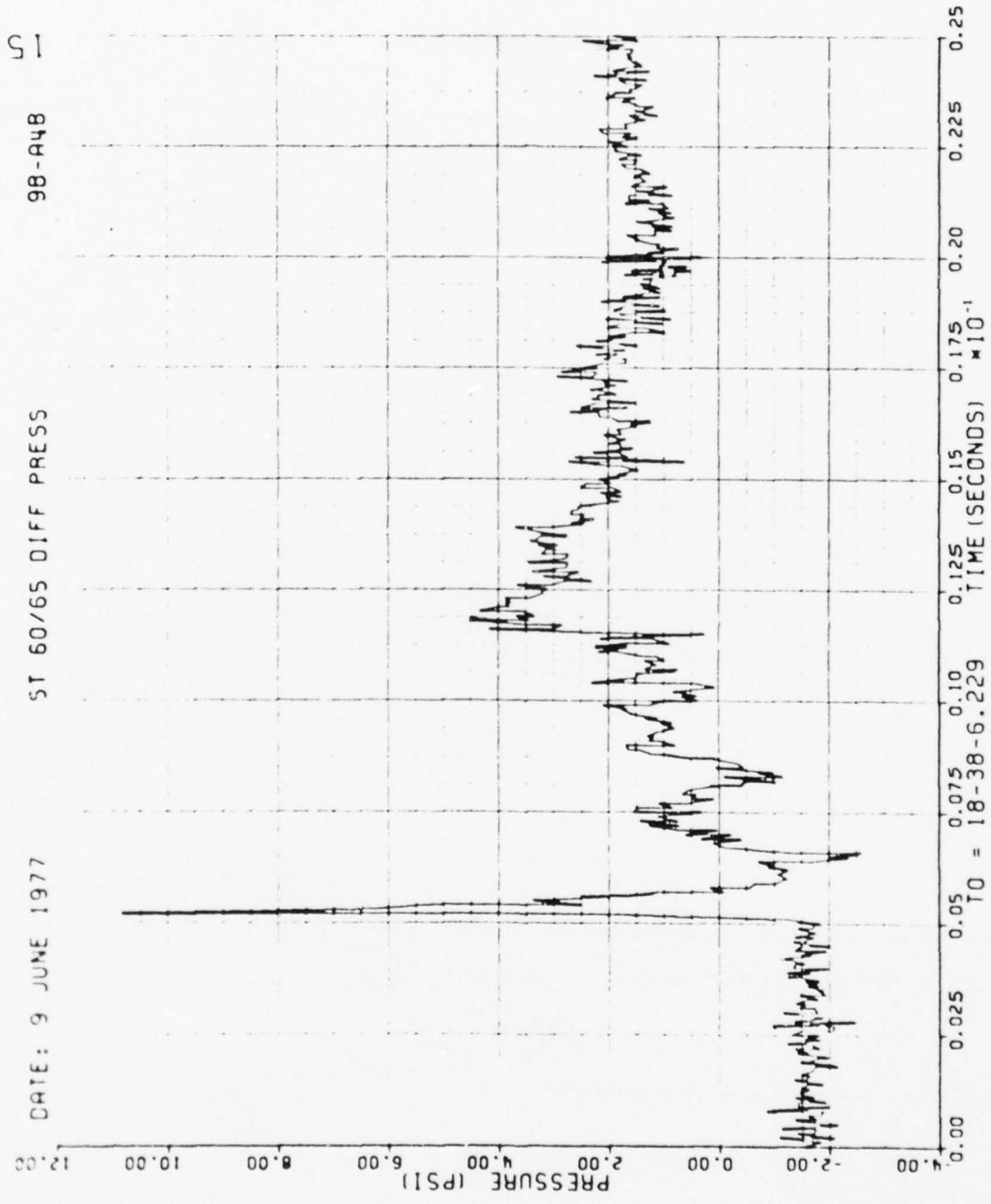


Figure 42. Continued

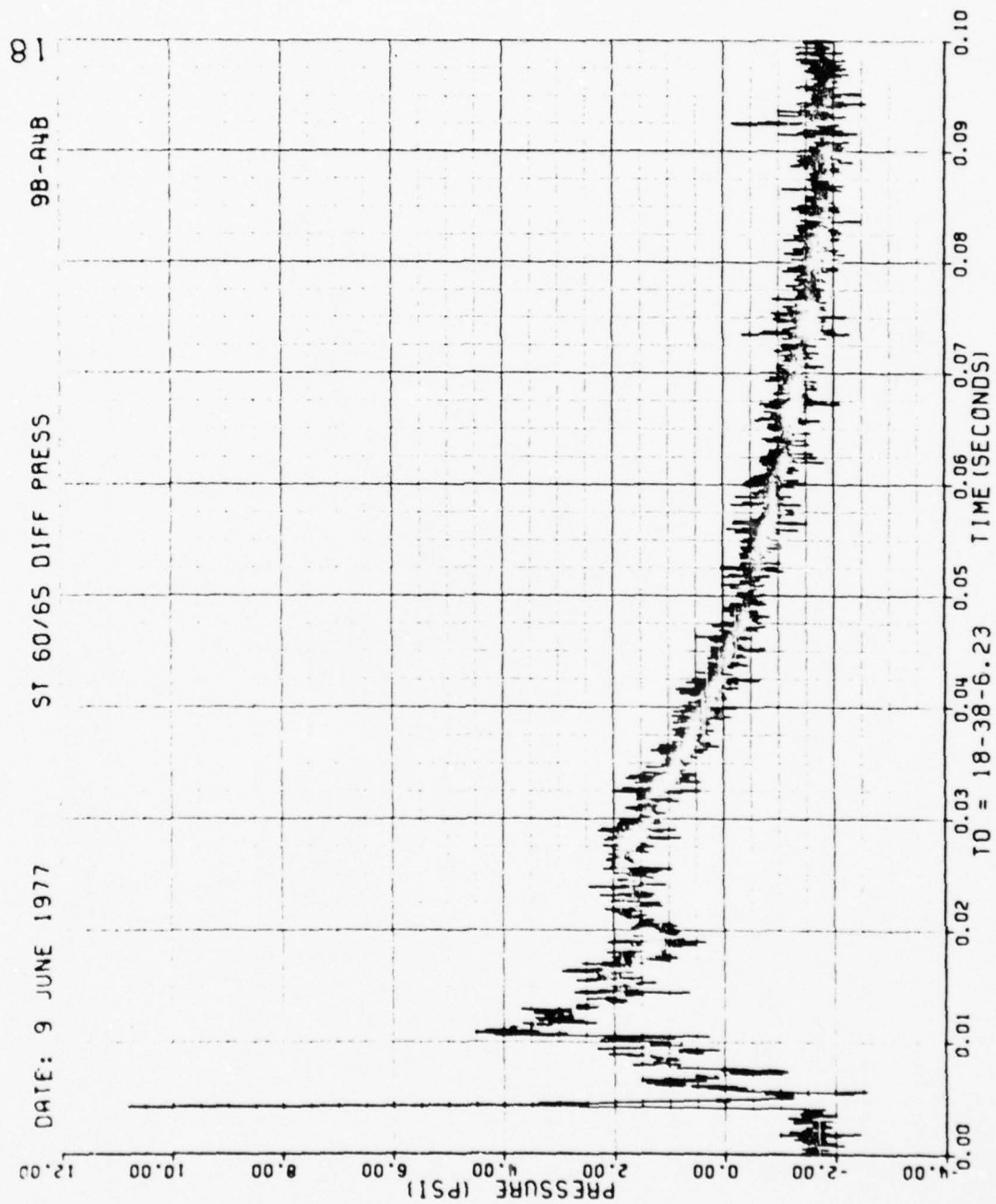


Figure 42. Continued

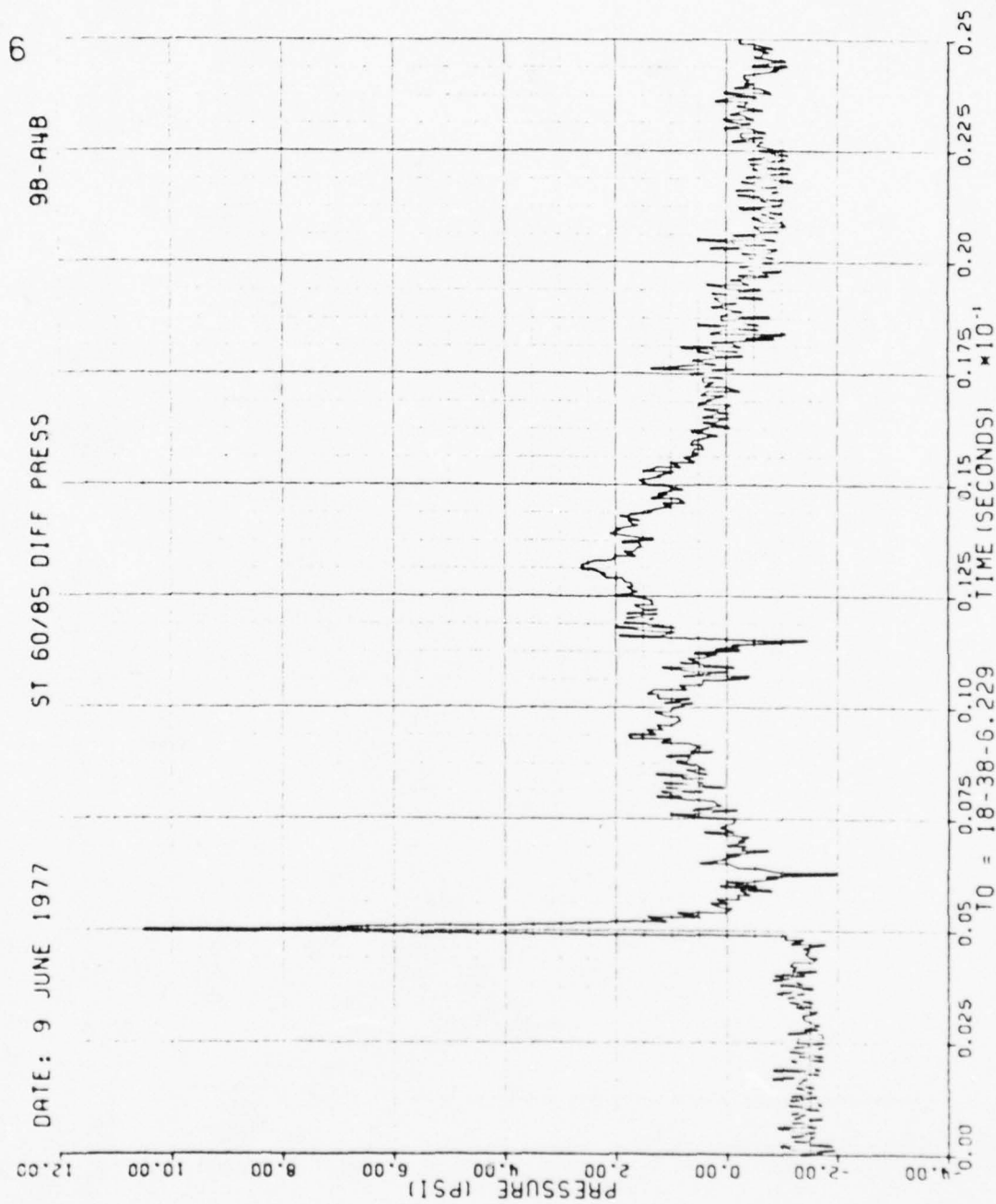


Figure 42. Continued

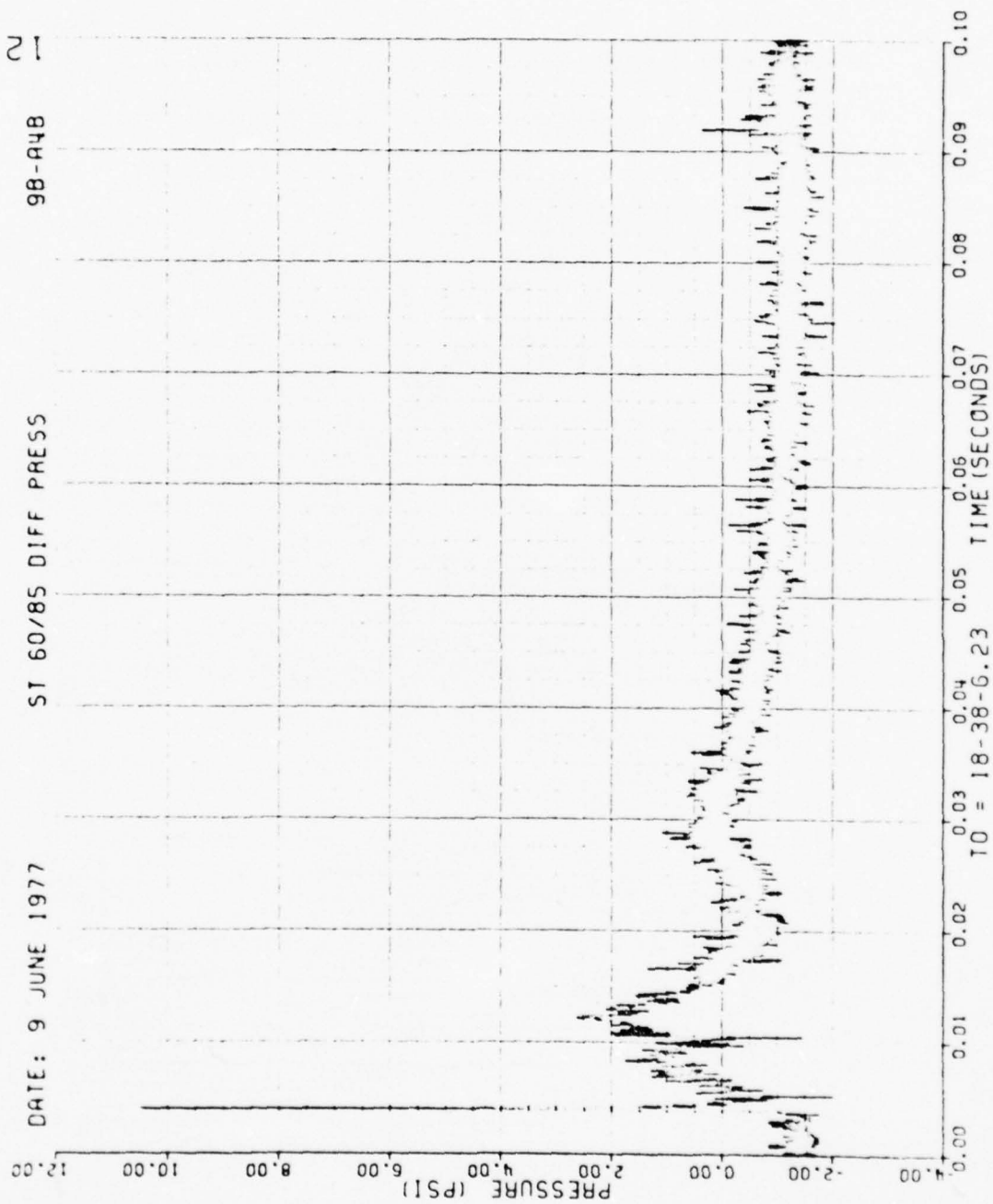


Figure 42. Continued

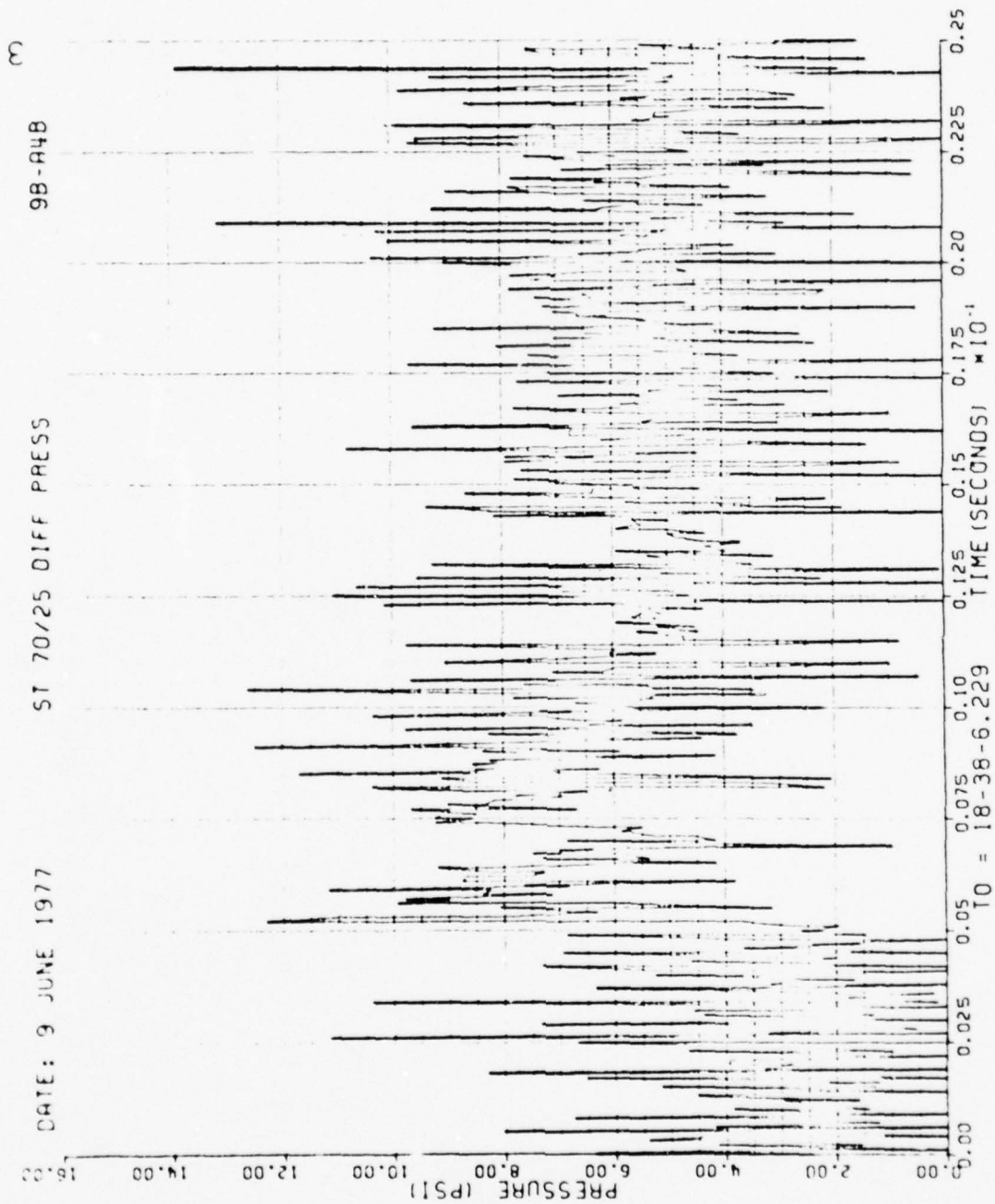


Figure 42. Continued

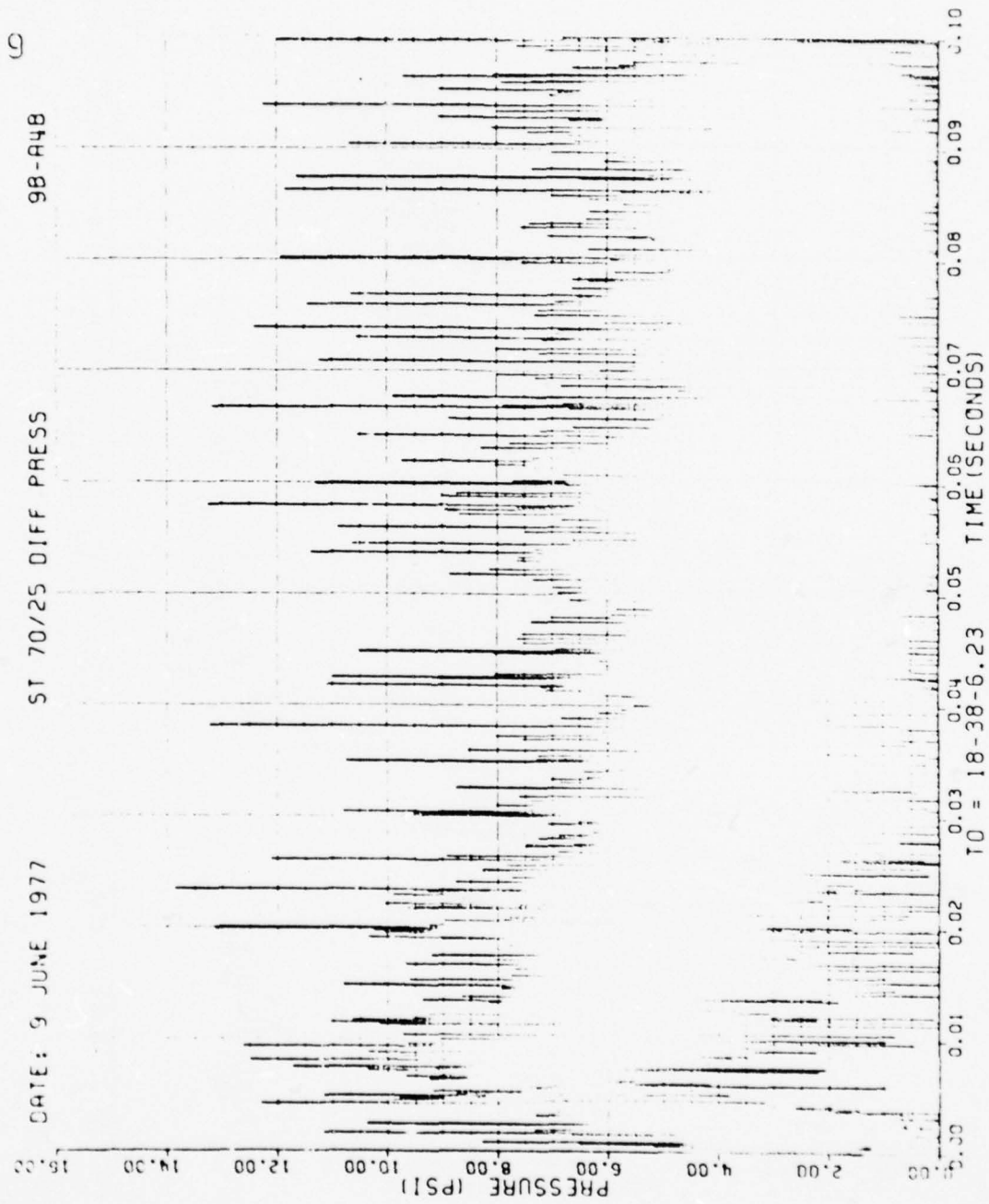


Figure 42. Continued

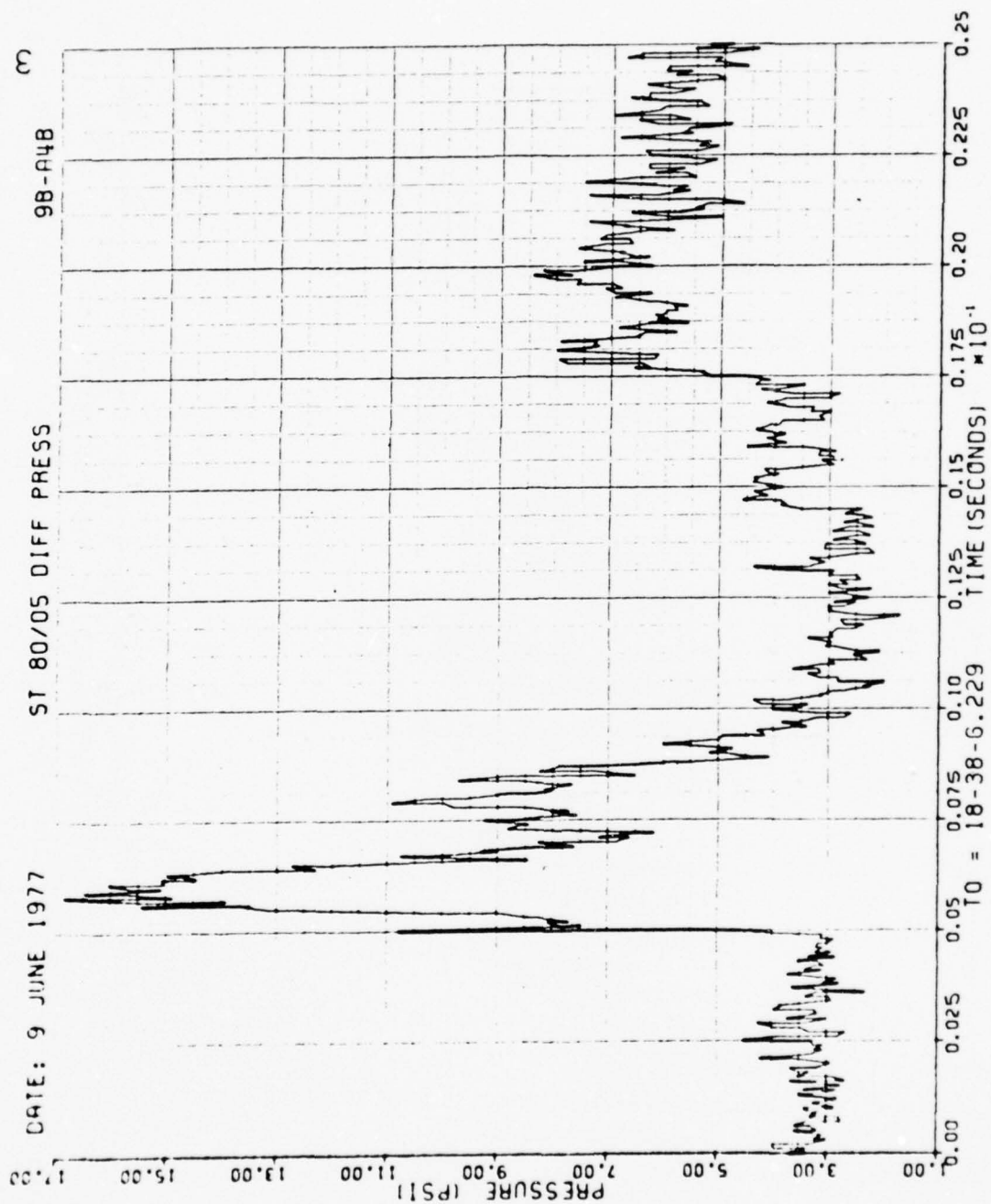


Figure 42. Continued

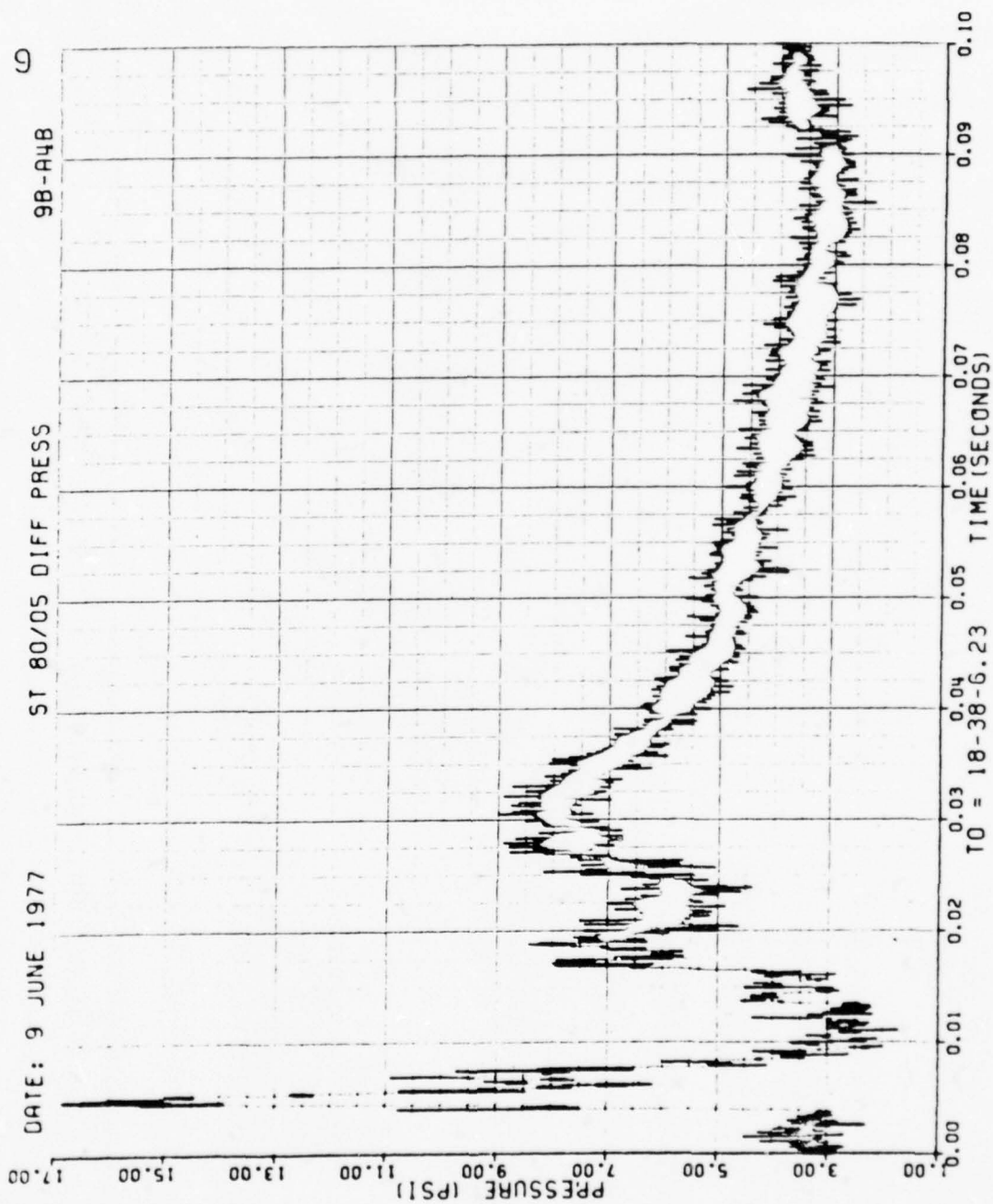


Figure 42. Continued

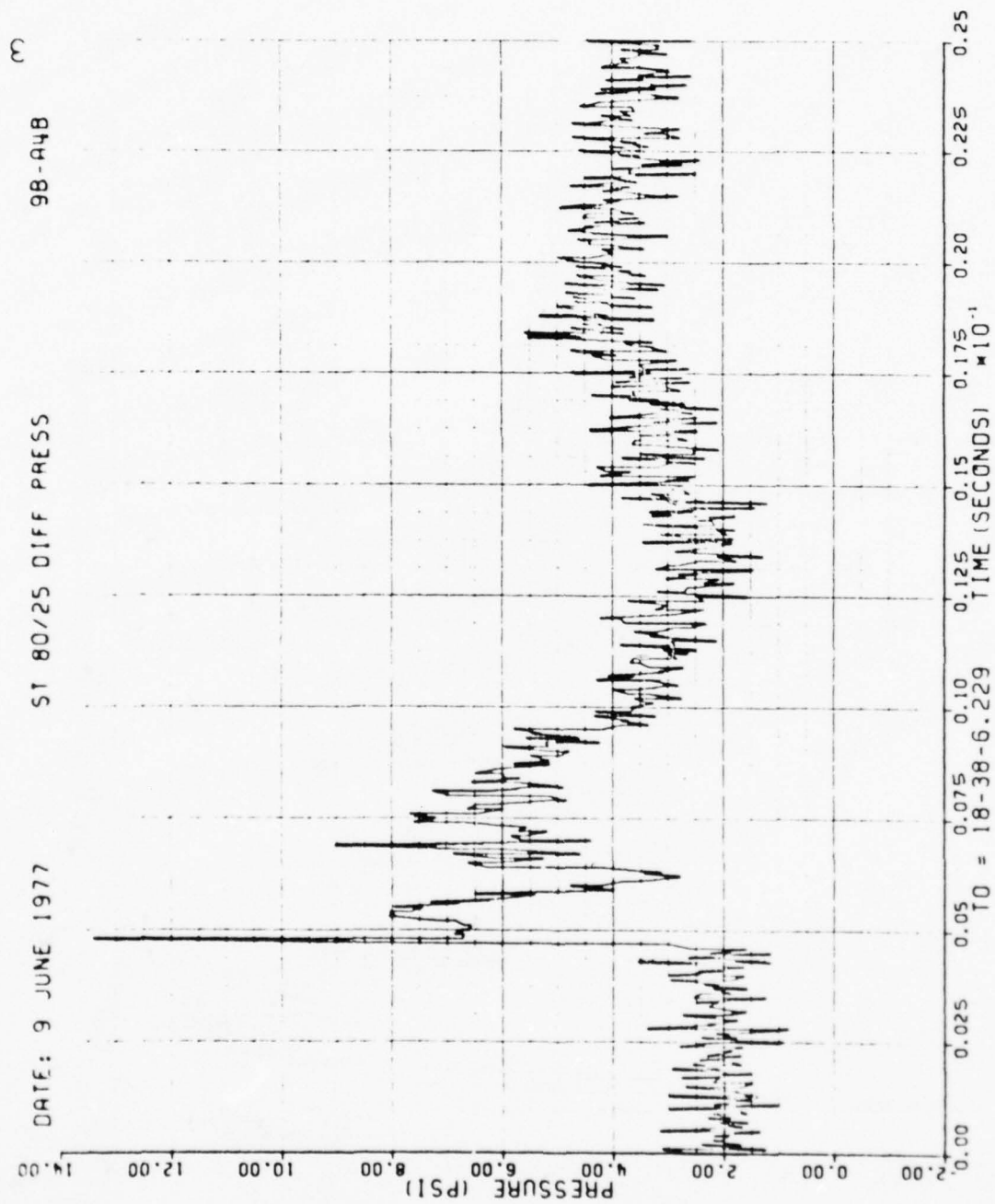


Figure 42. Continued

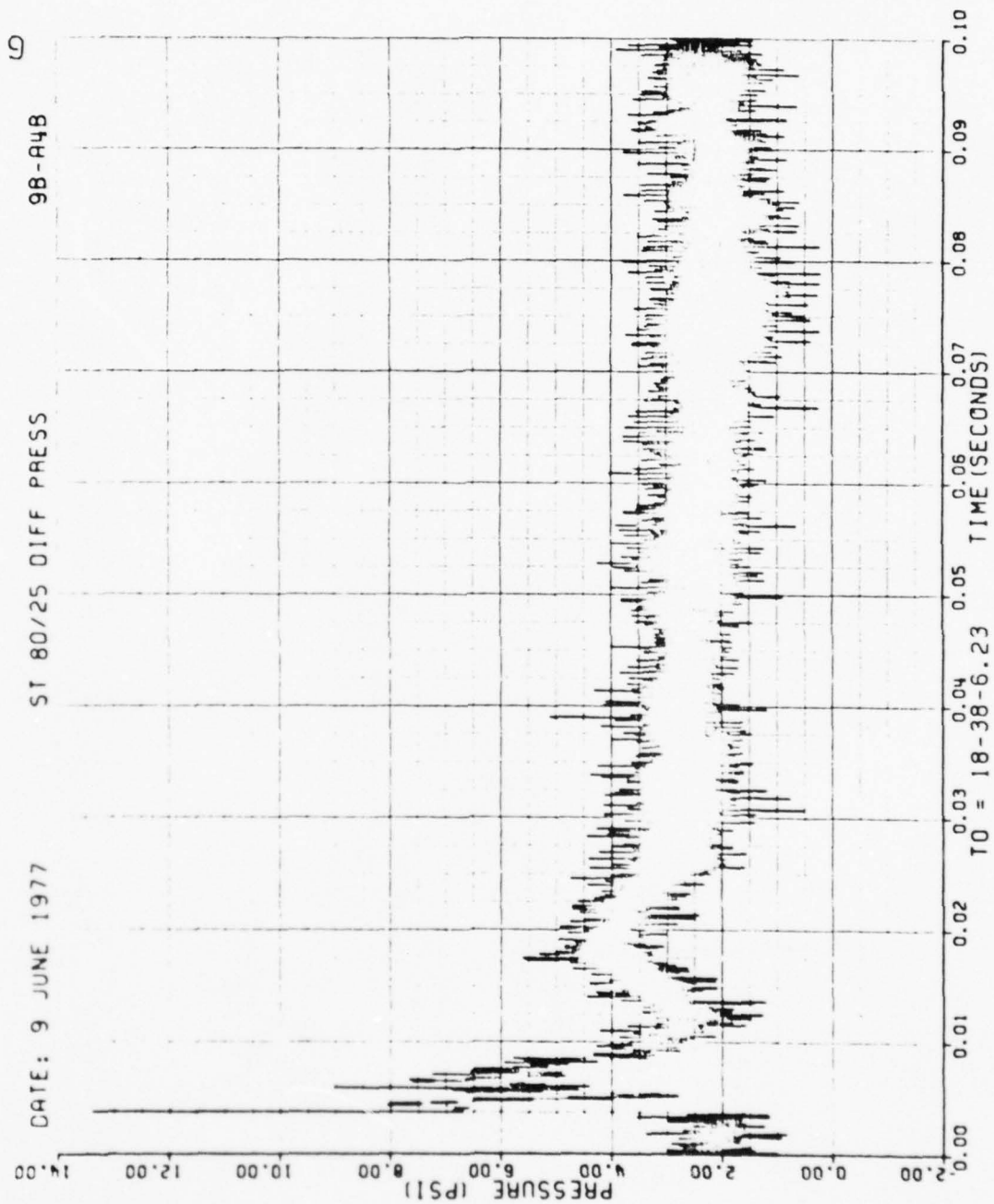


Figure 42. Continued

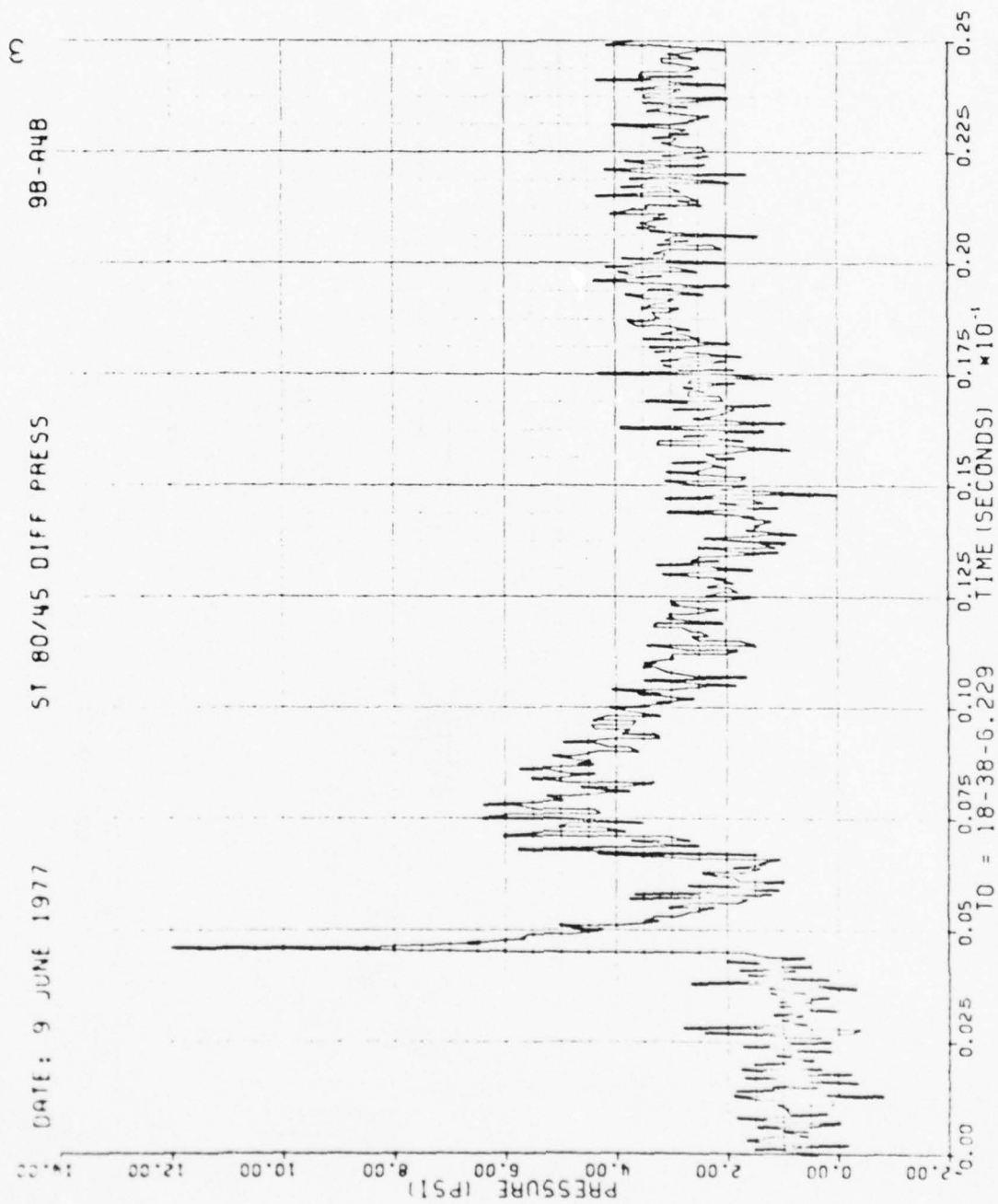


Figure 42. Continued

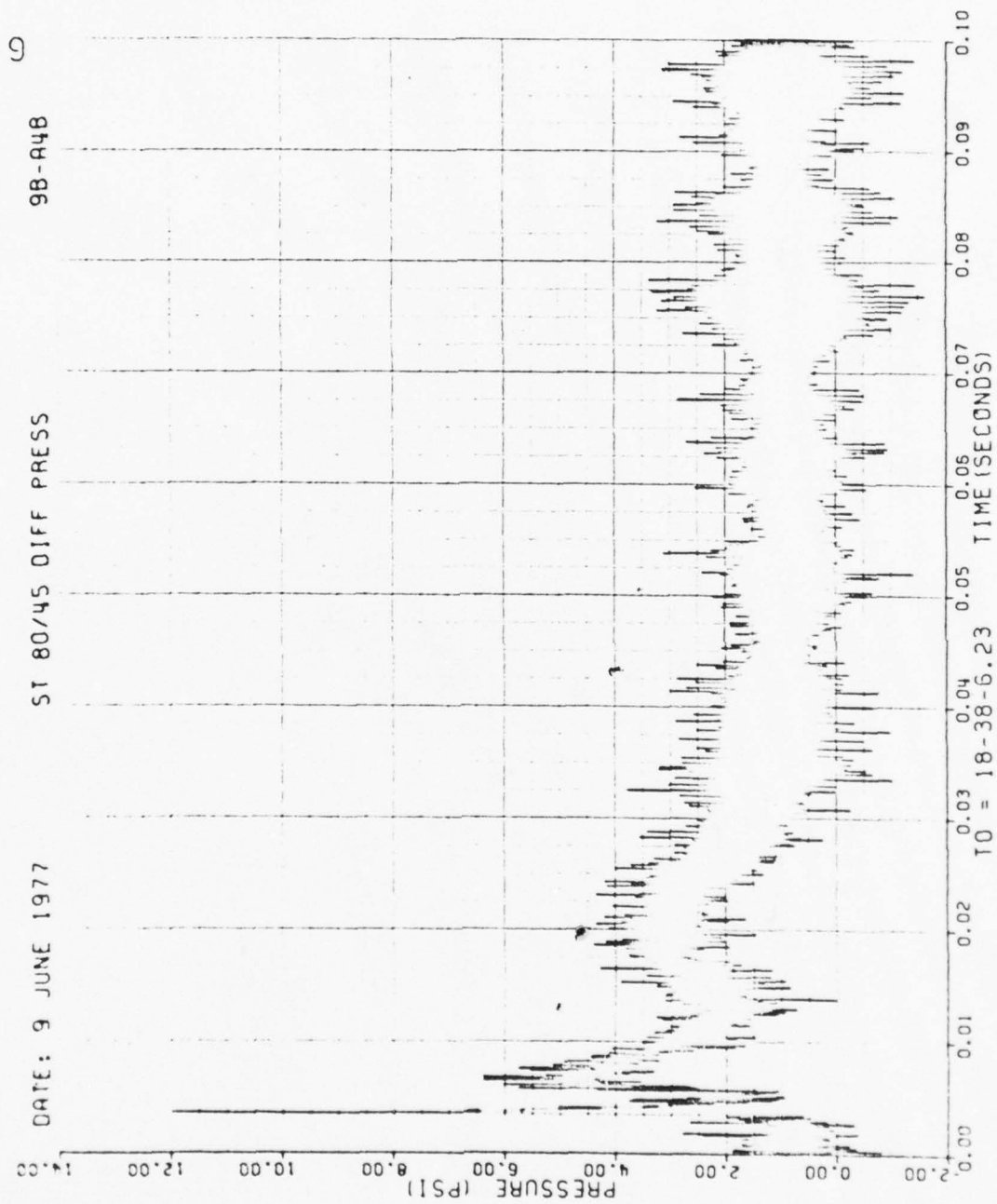


Figure 42. Continued

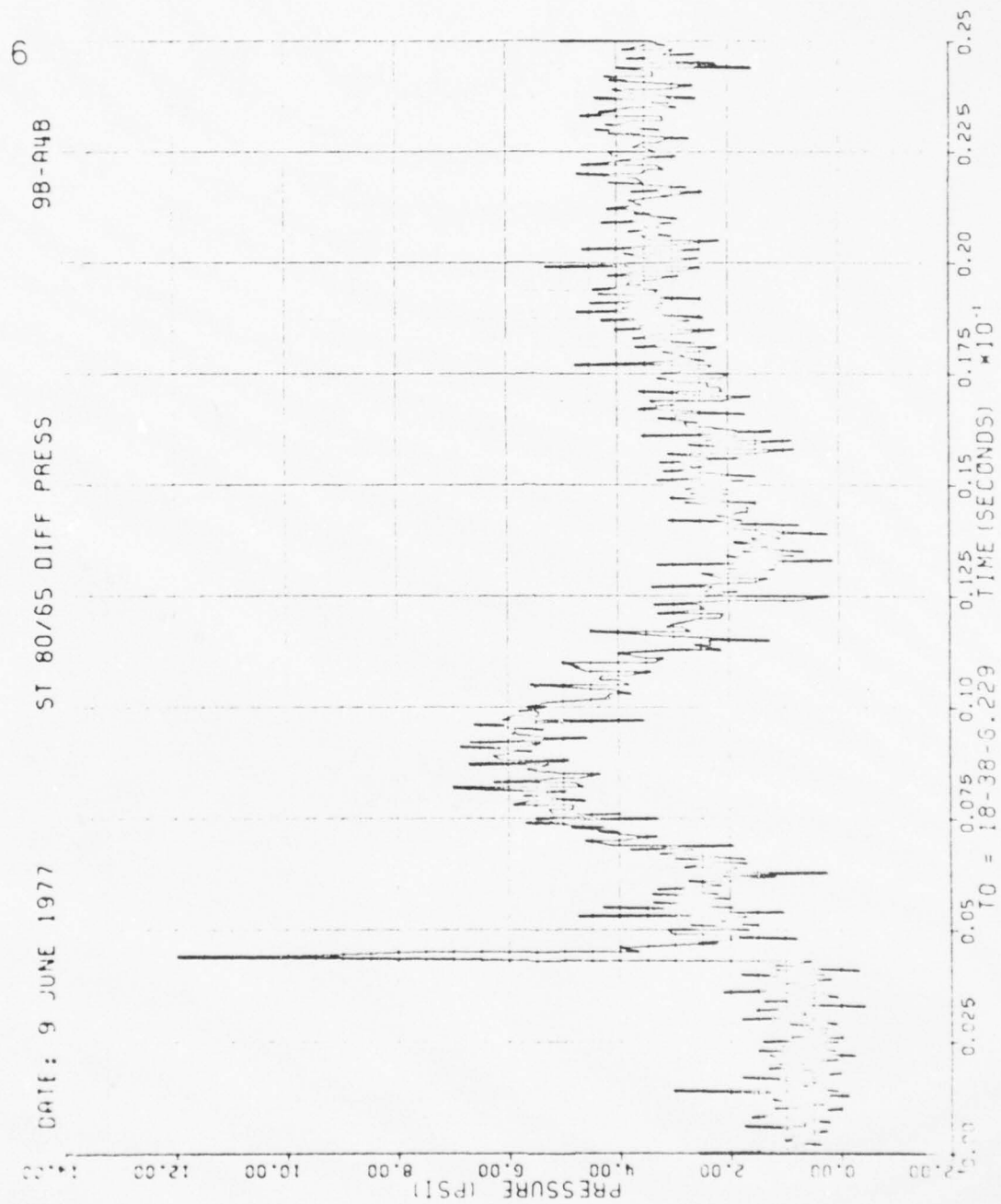


Figure 42. Continued

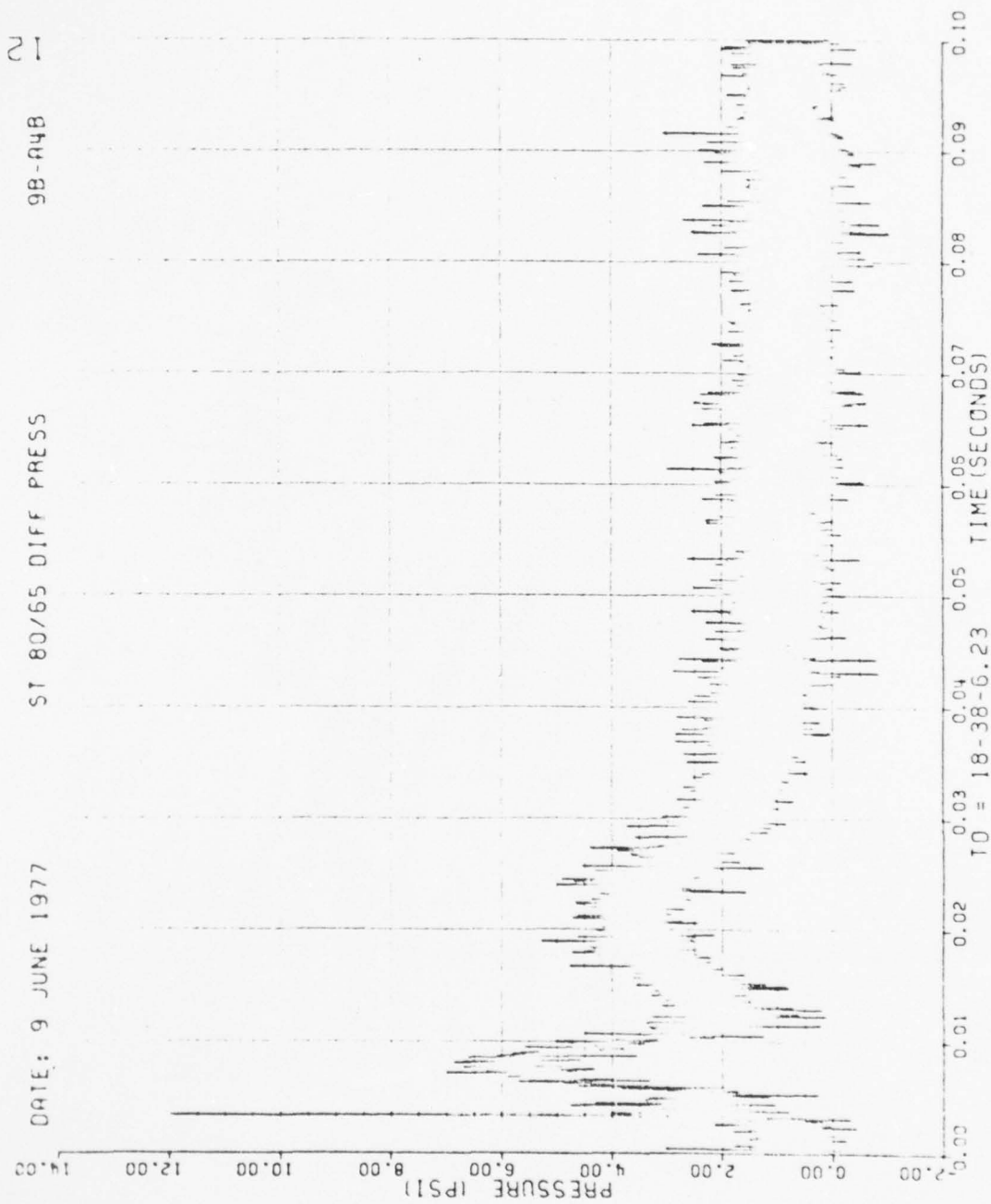


Figure 42. Continued

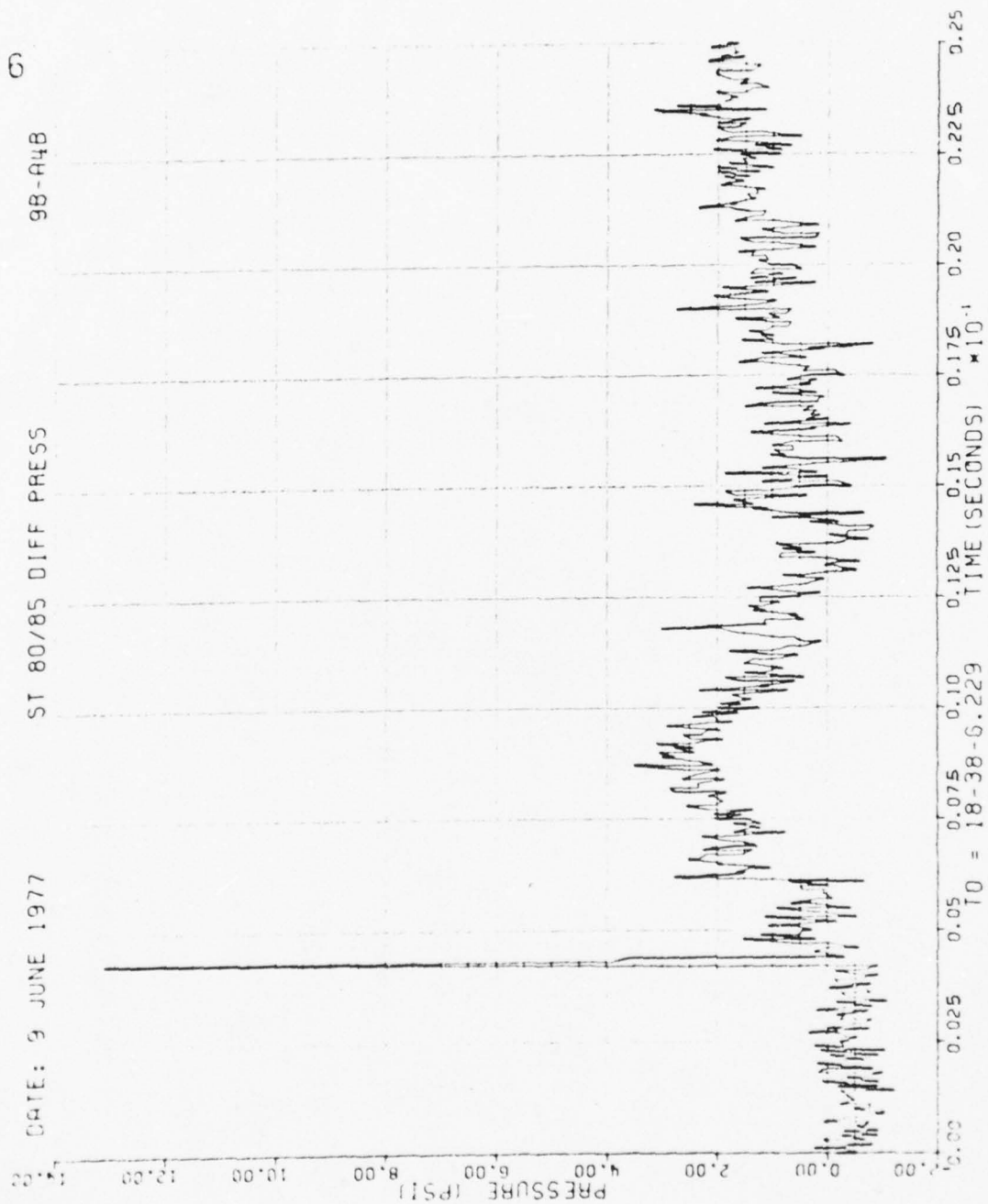


Figure 42. Continued

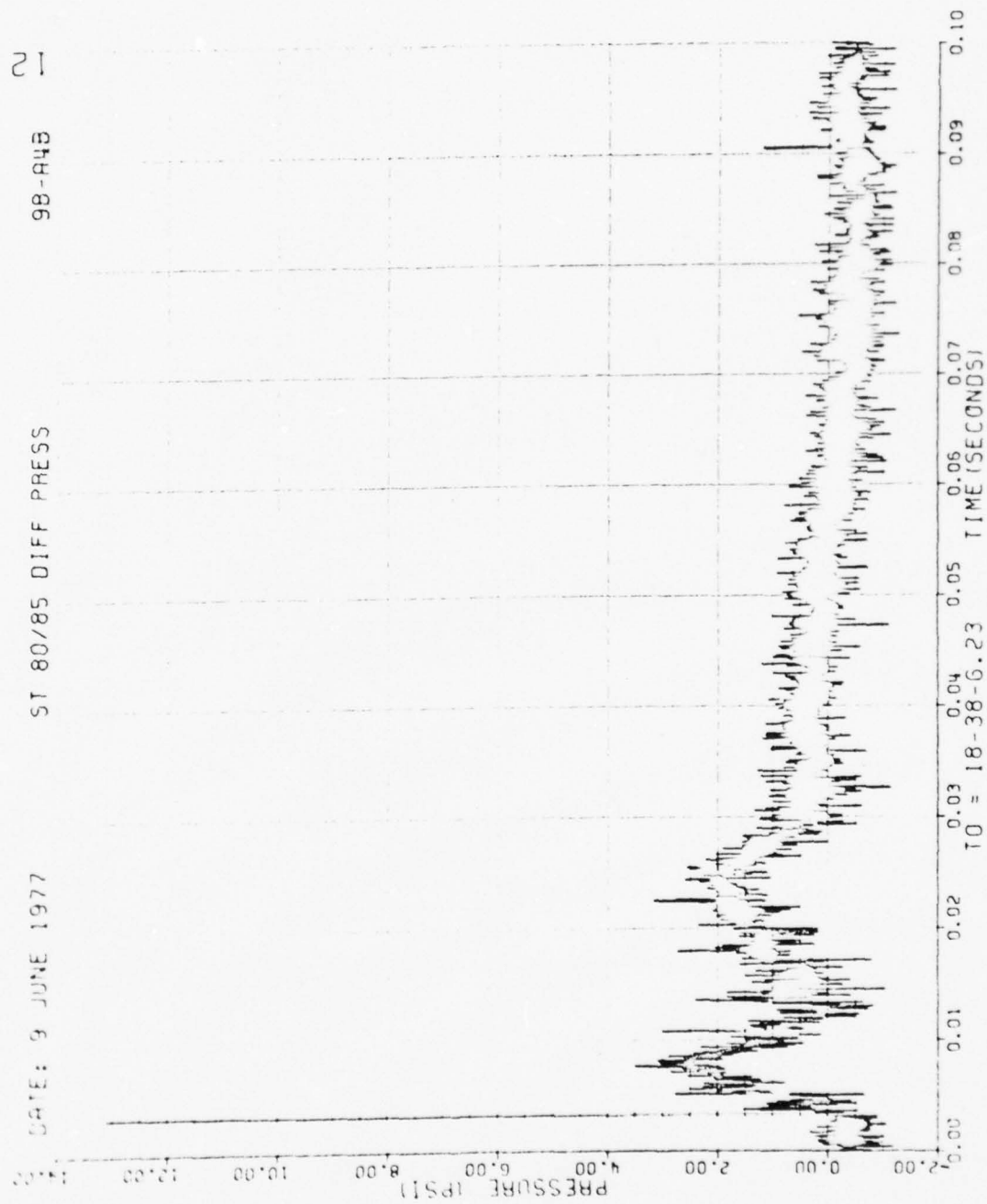


Figure 42. Continued

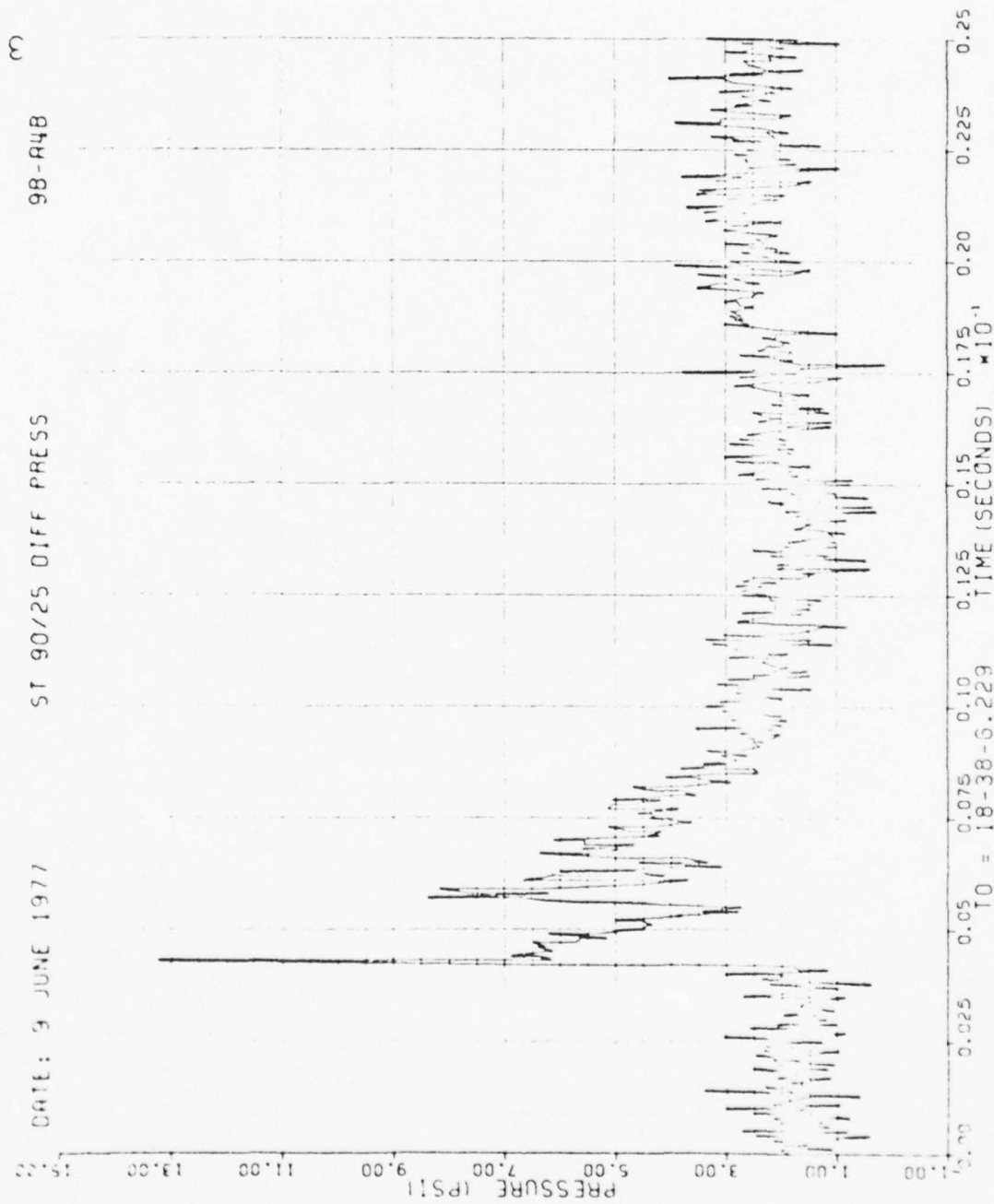


Figure 42. Continued

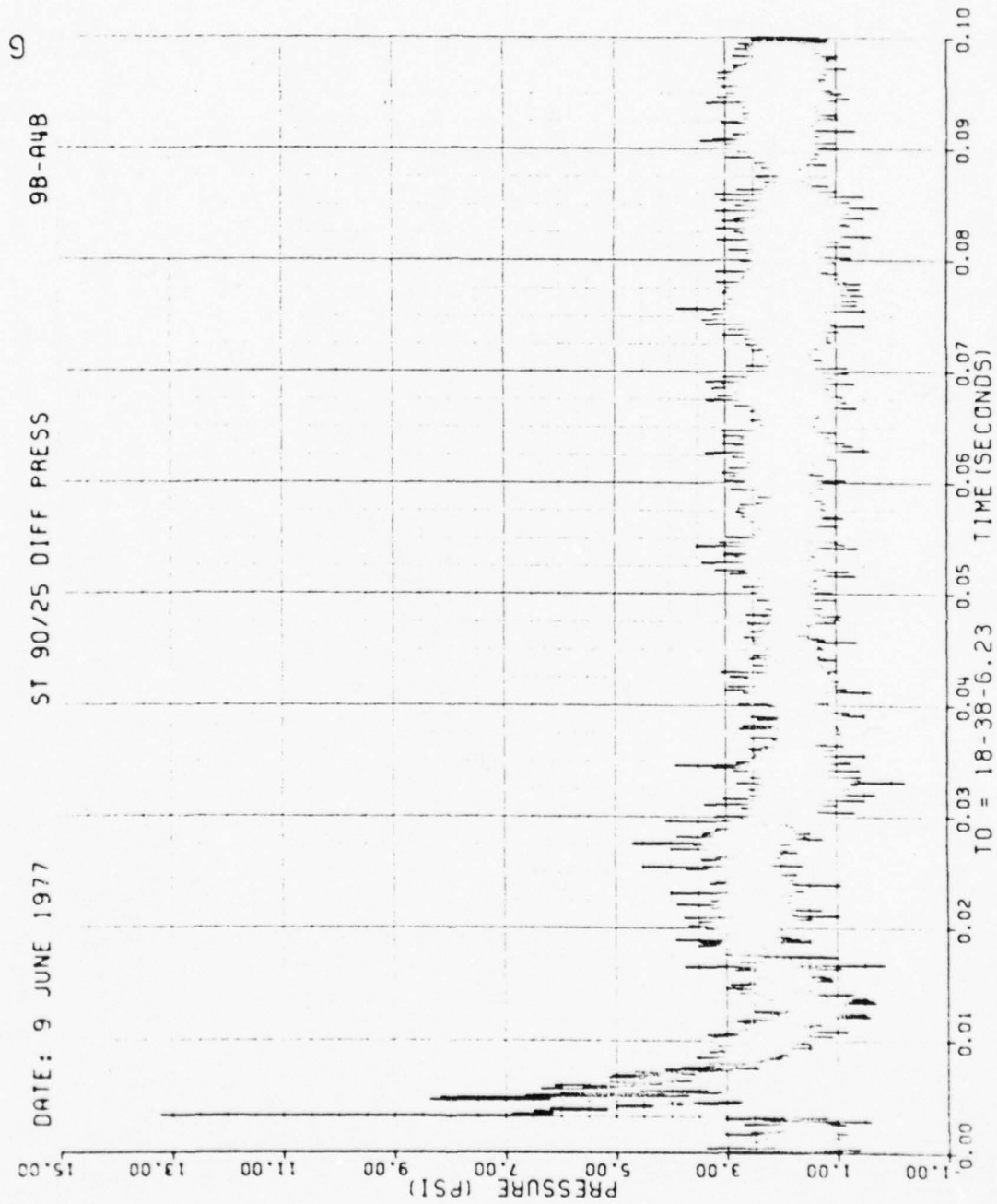


Figure 42. Concluded

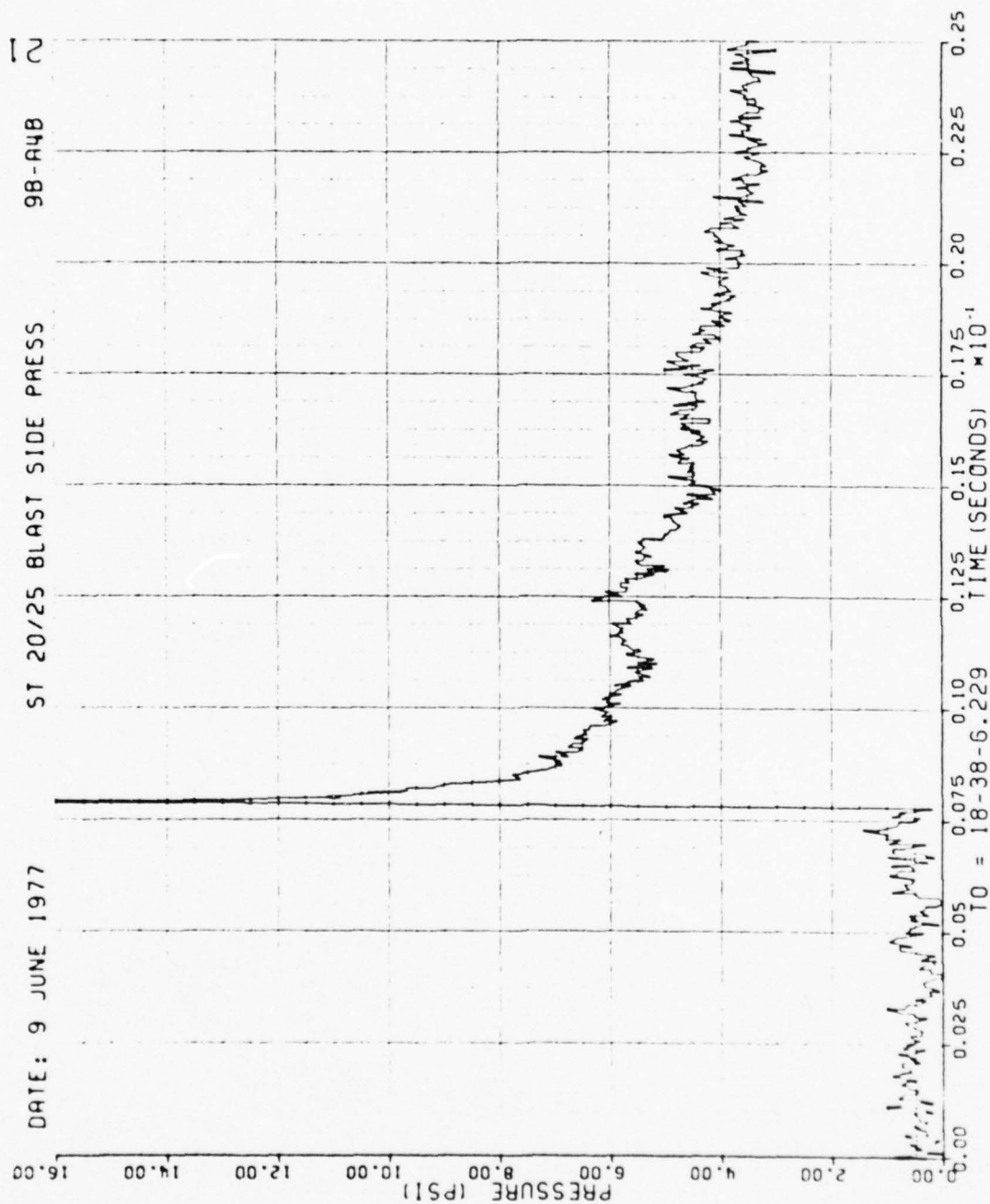


Figure 43. Blastward and Leeward Wing Pressures, Run 9B-A4, Intercept 3.

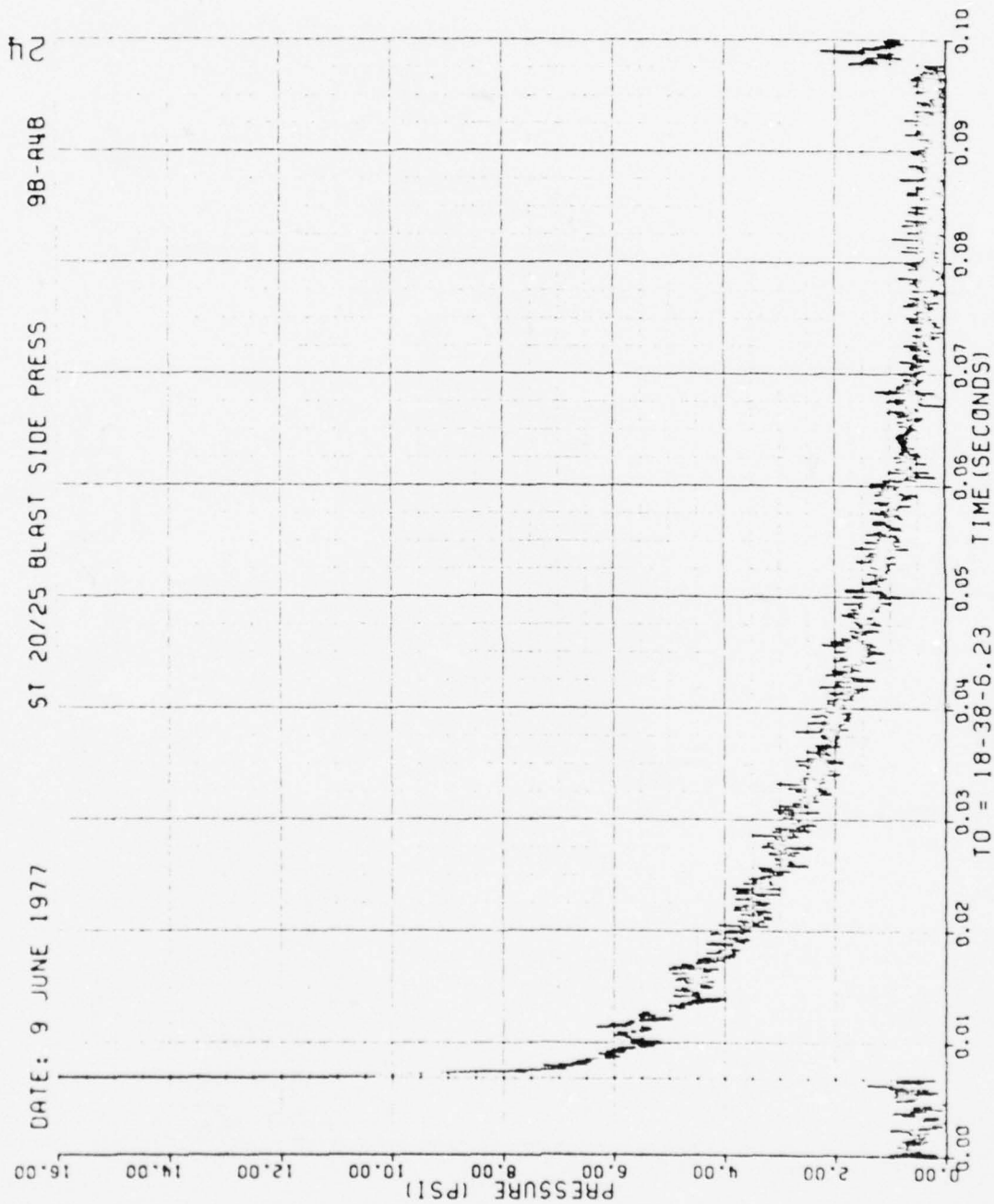


Figure 43. Continued

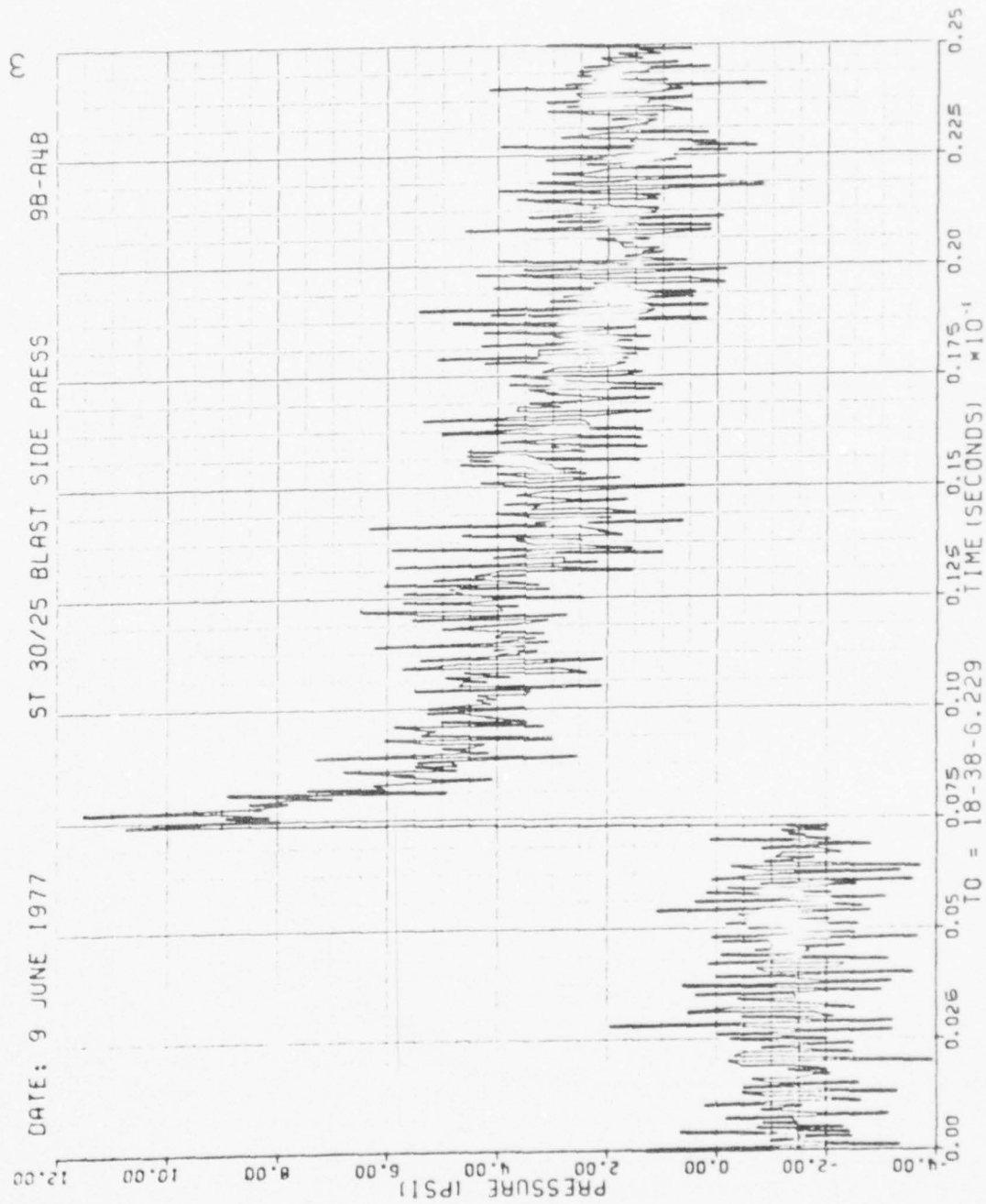


Figure 43. Continued

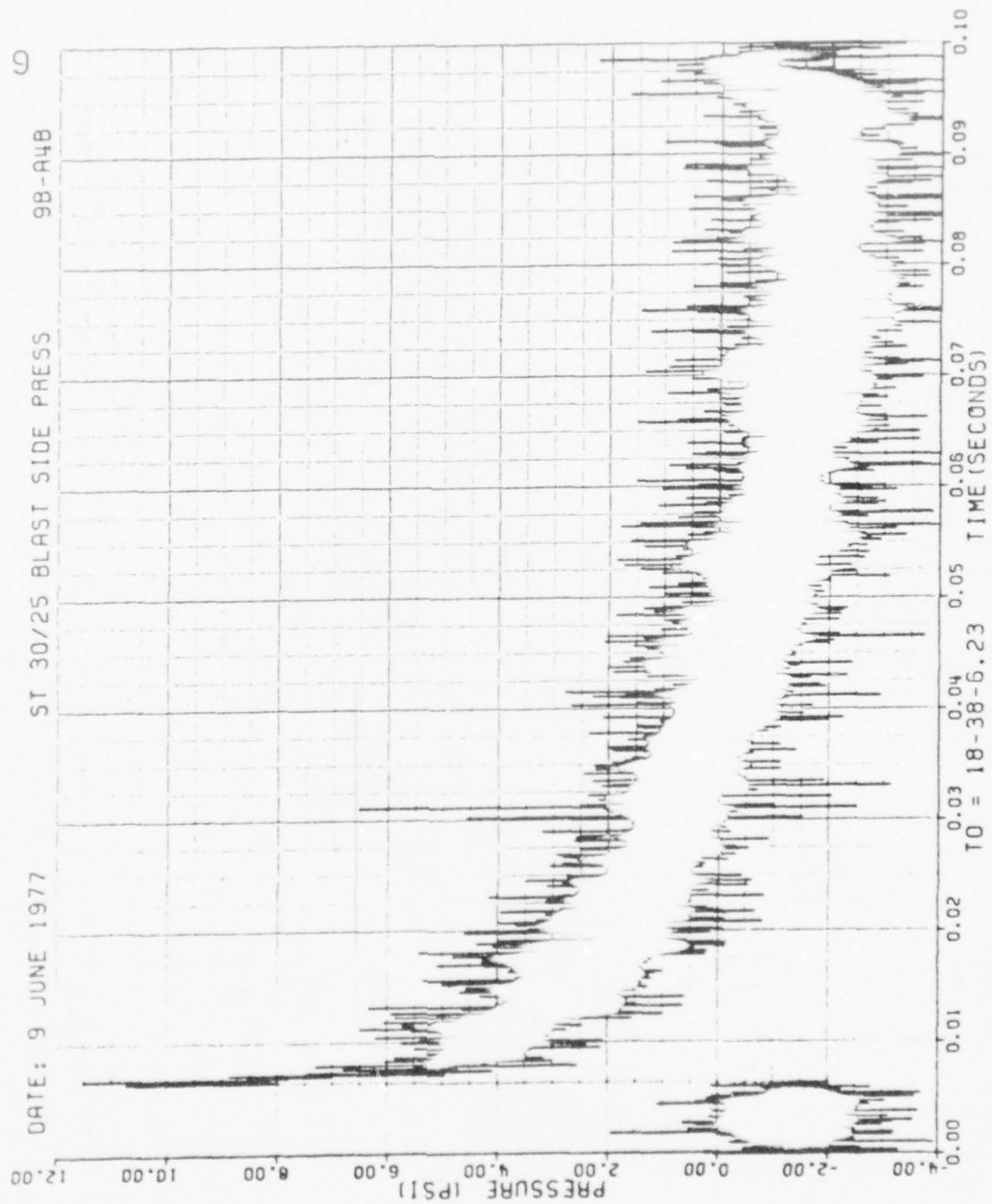


Figure 43. Continued

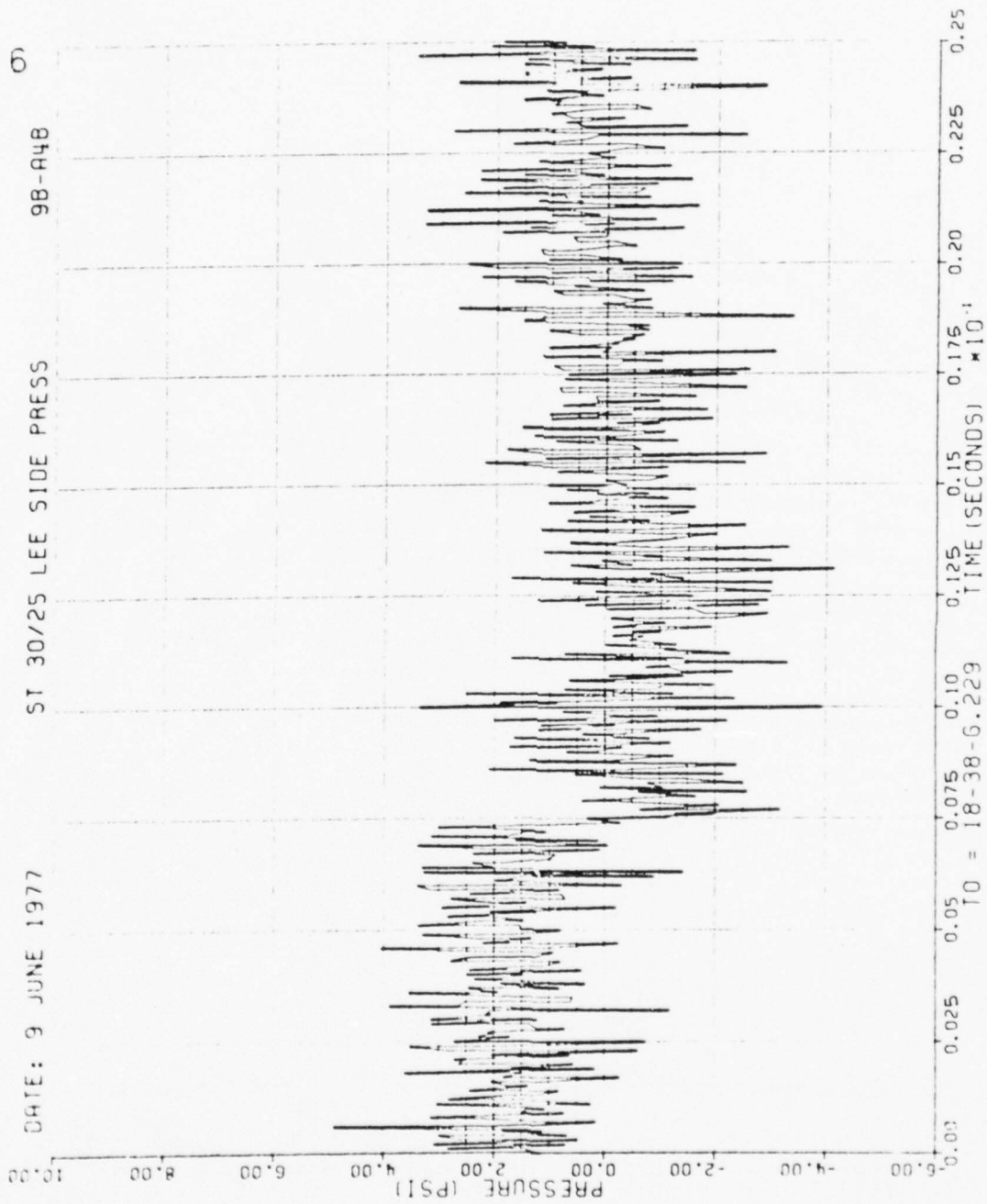


Figure 43. Continued

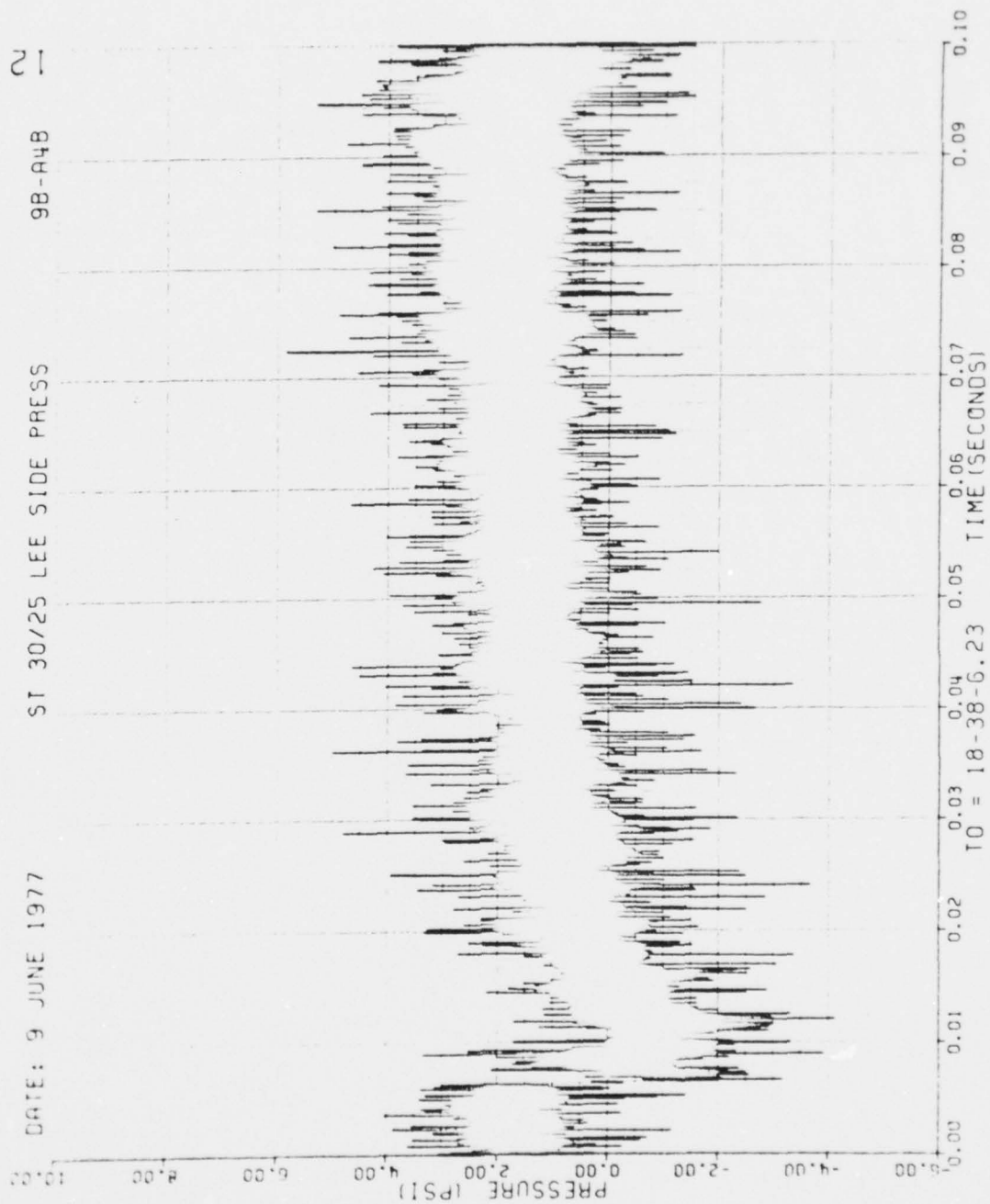


Figure 43. Concluded

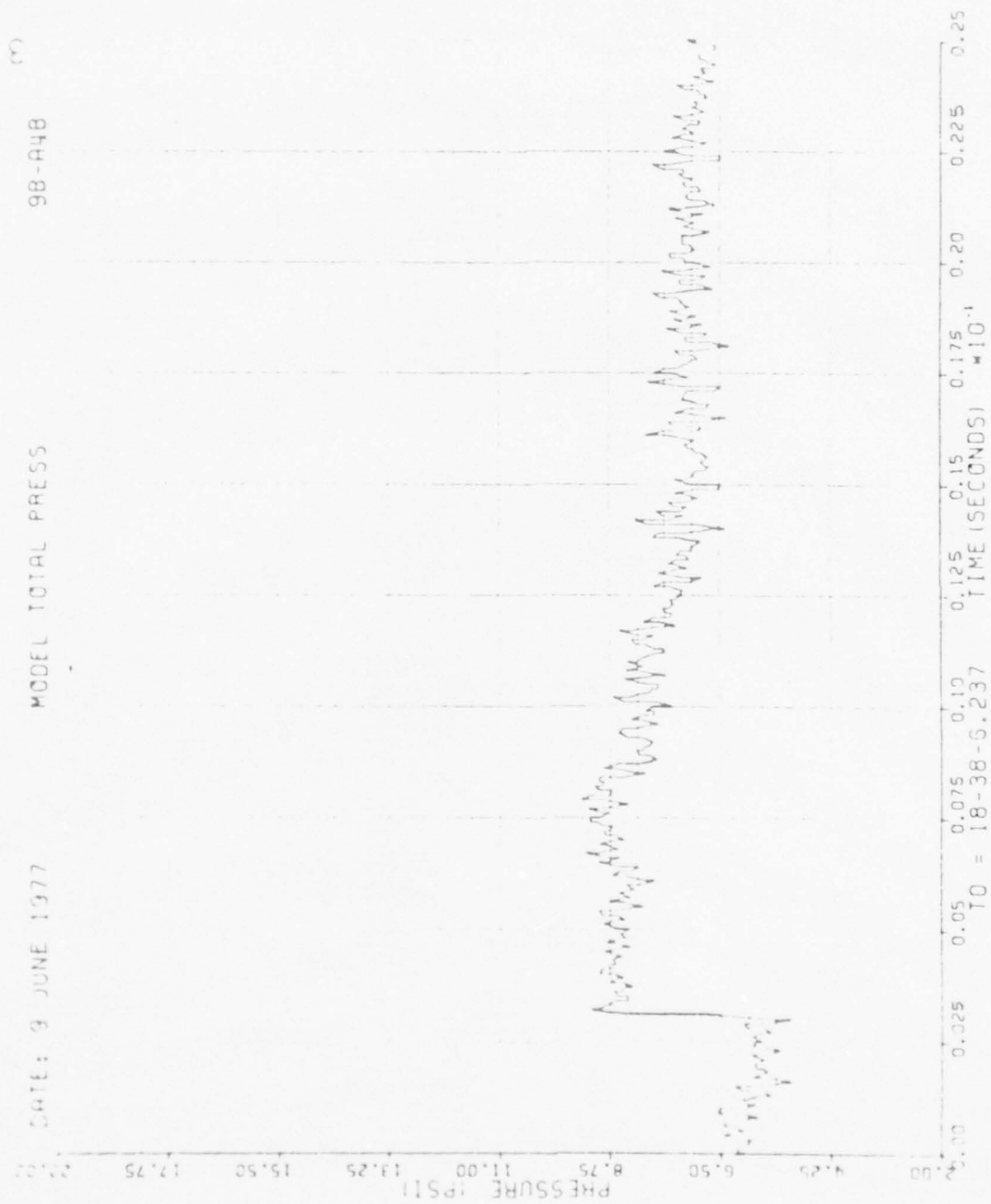


Figure 44. Total Pressure at Model, Run 9B-A4, Intercept 3.

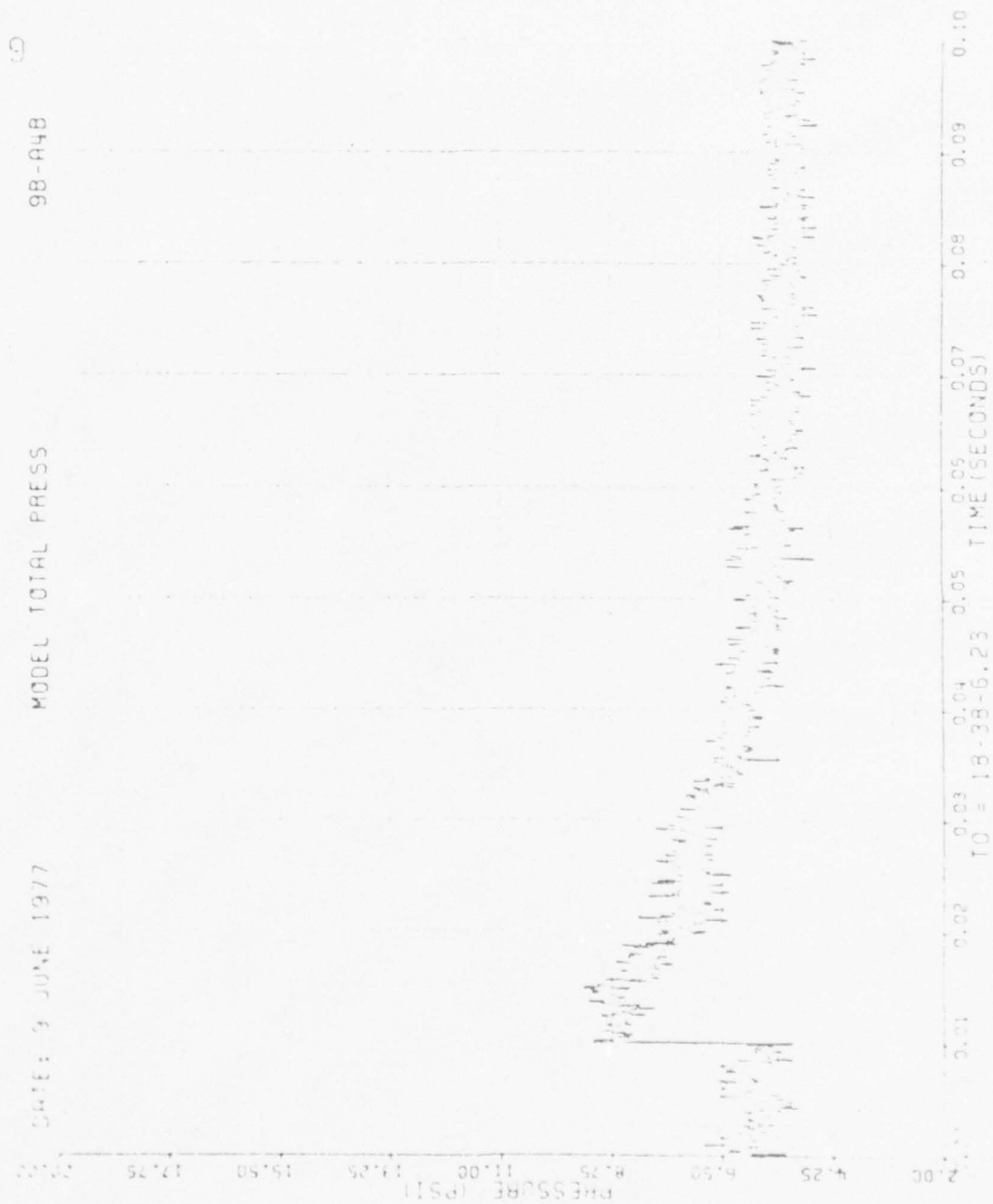


Figure 44. Concluded

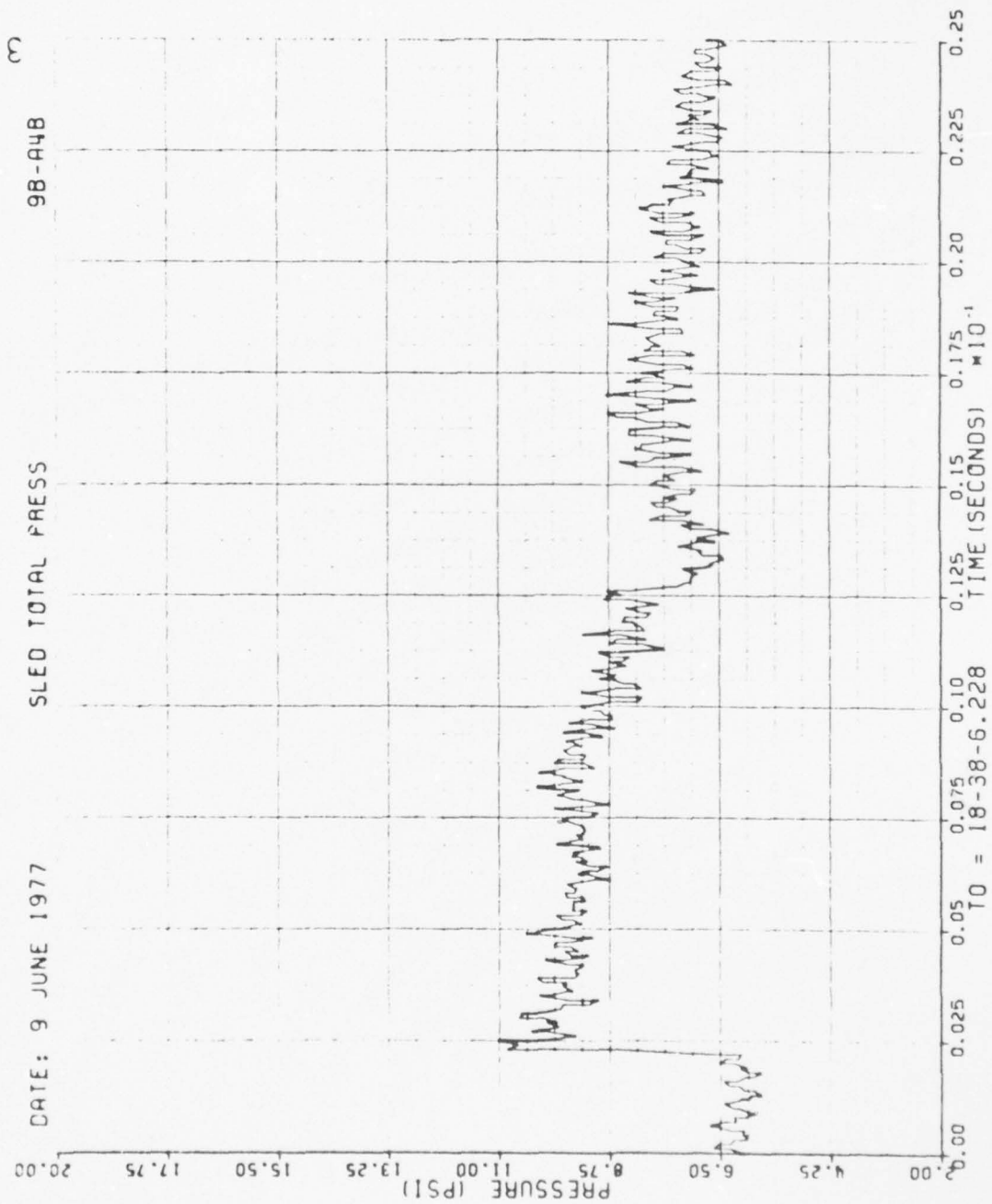


Figure 45. Total Pressure at Sled, Run 9B-A4, Intercept 3.

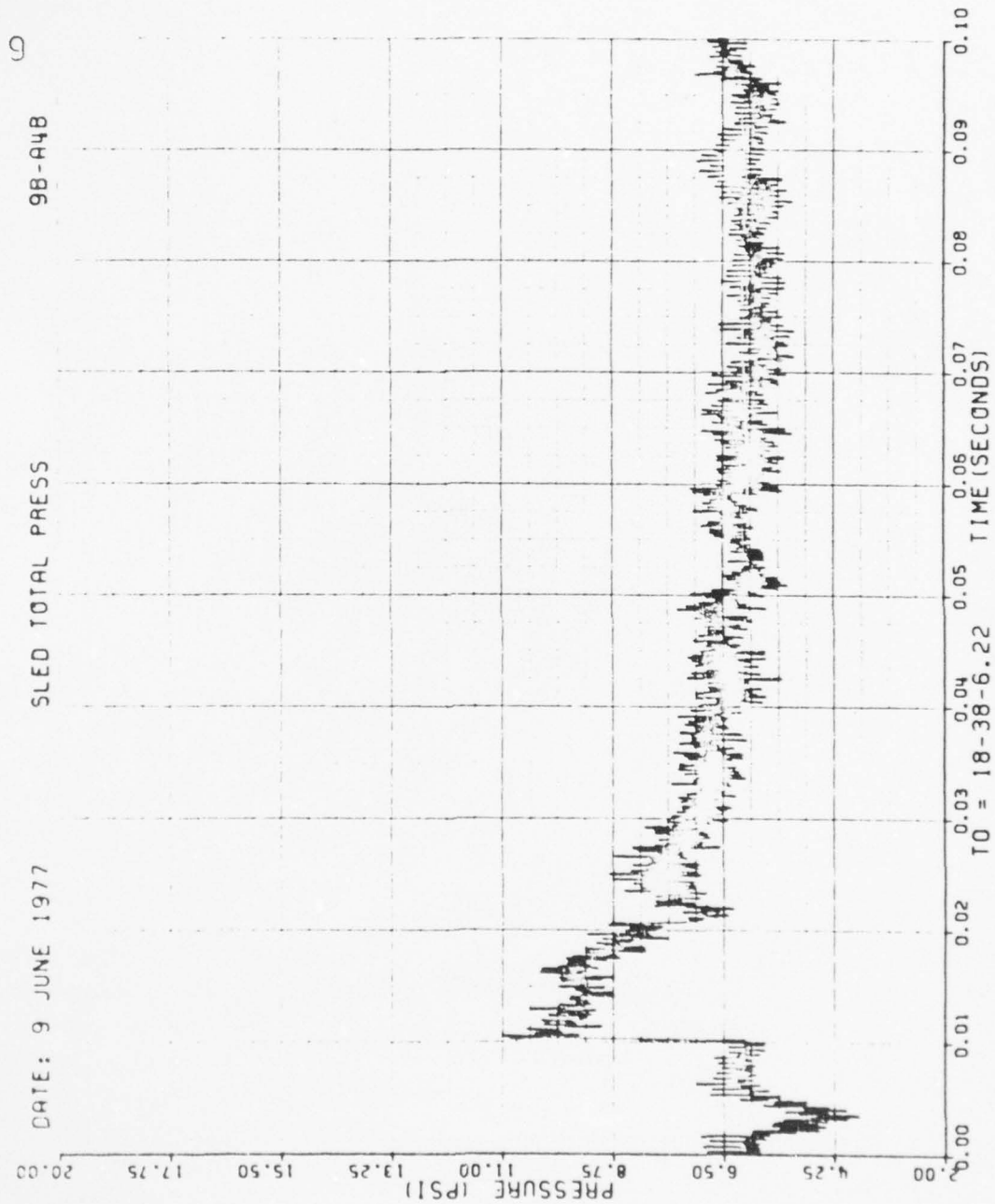


Figure 45. Concluded

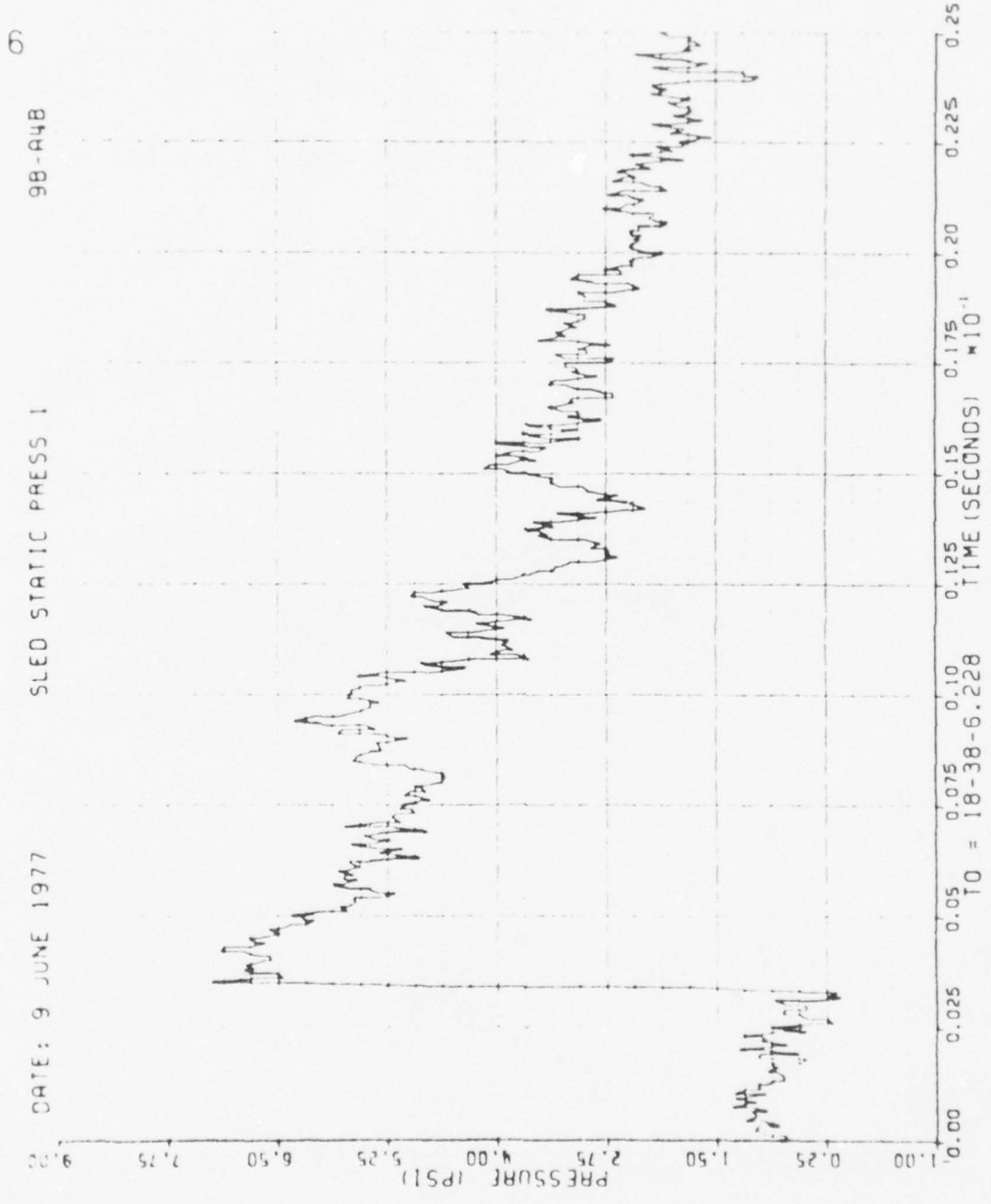


Figure 46. Static Pressure 1 at Sled, Run 9B-A4, Intercept 3.

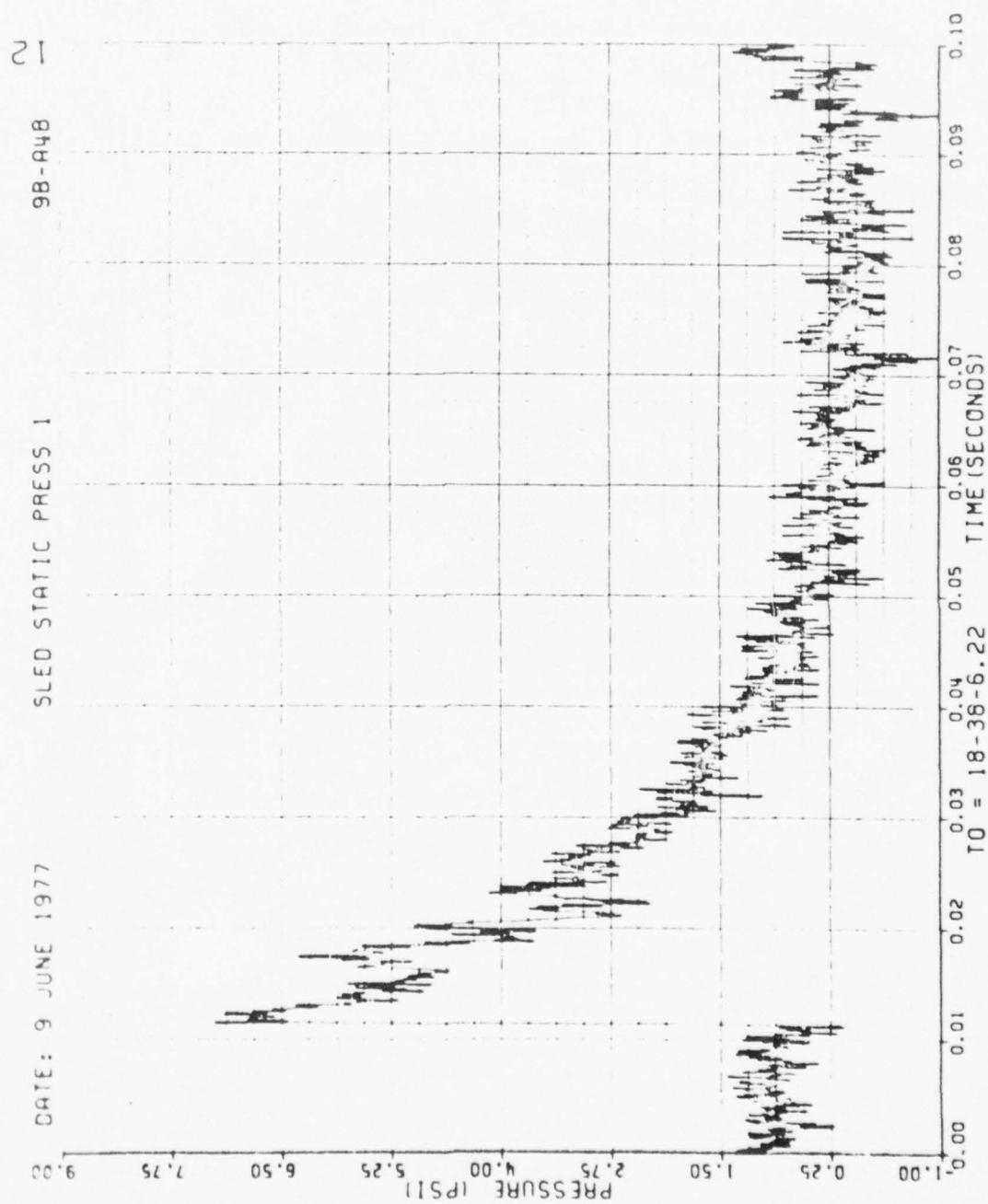


Figure 46. Concluded

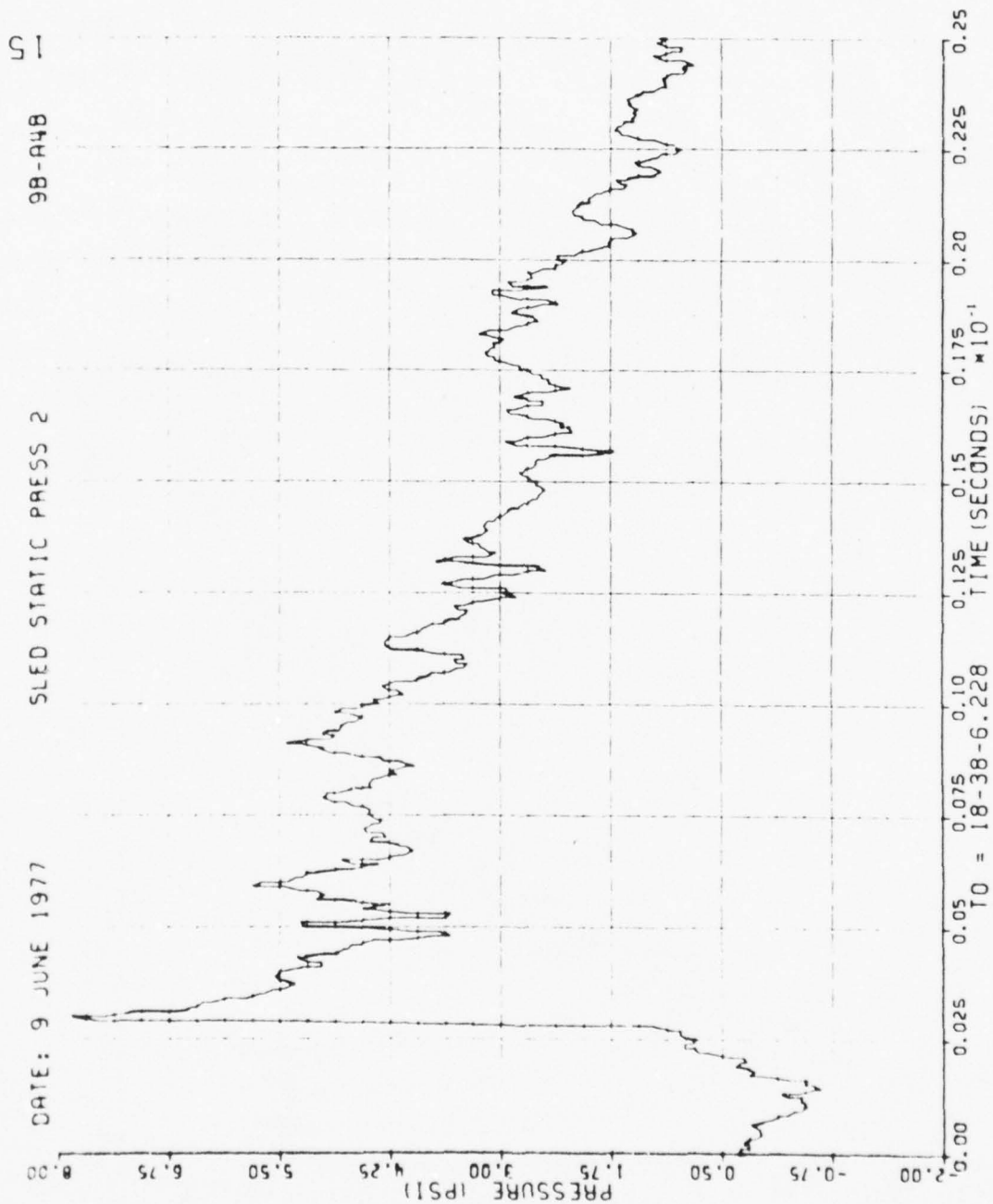


Figure 47. Static Pressure 2 at Sled, Run 9B-A4, Intercept 3.

81

98-A4B

SLED STATIC PRESS 2

DATE: 9 JUNE 1977

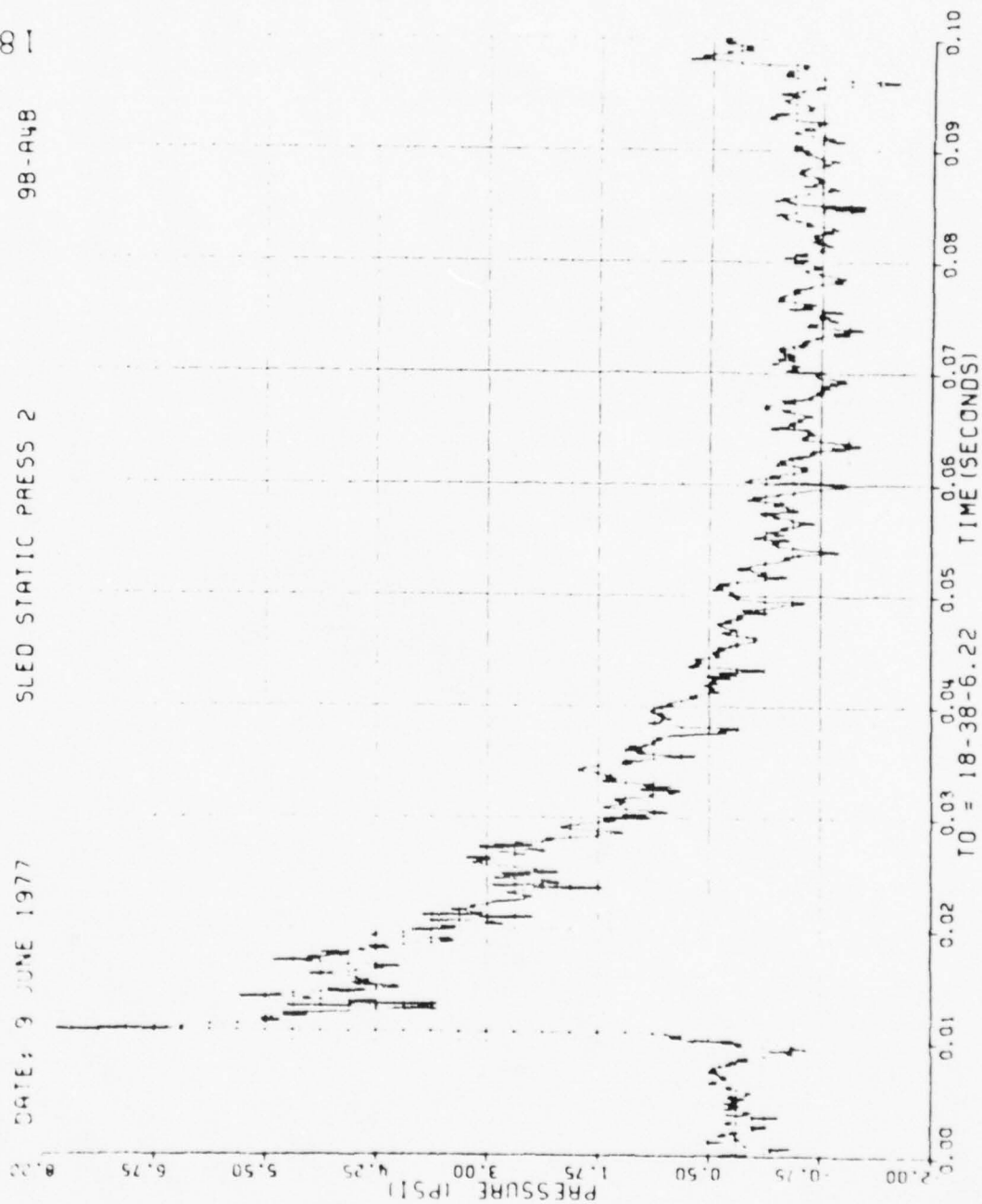


Figure 47. Concluded

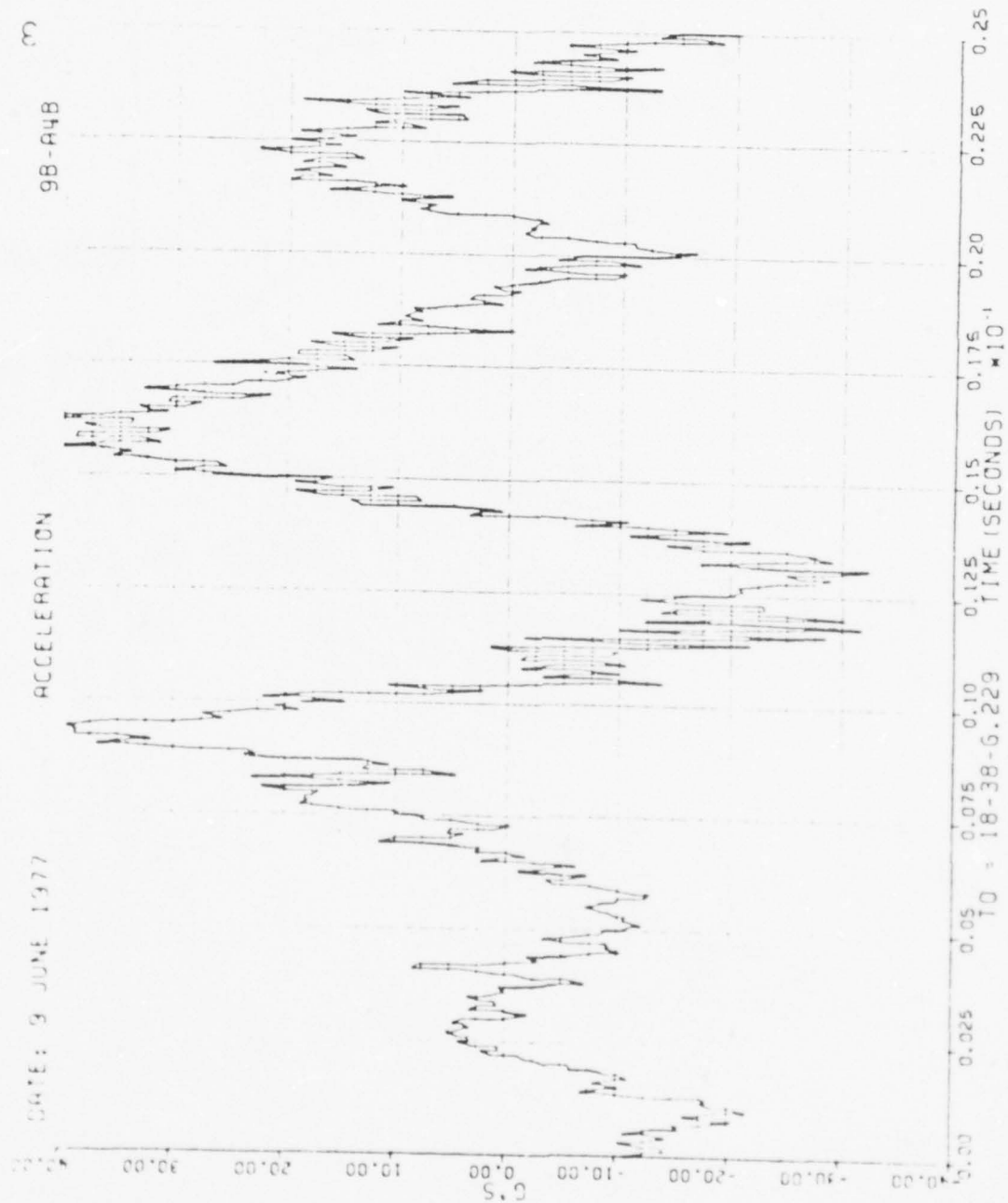


Figure 48. Wing Acceleration, Run 9B-A4, Intercept 3.

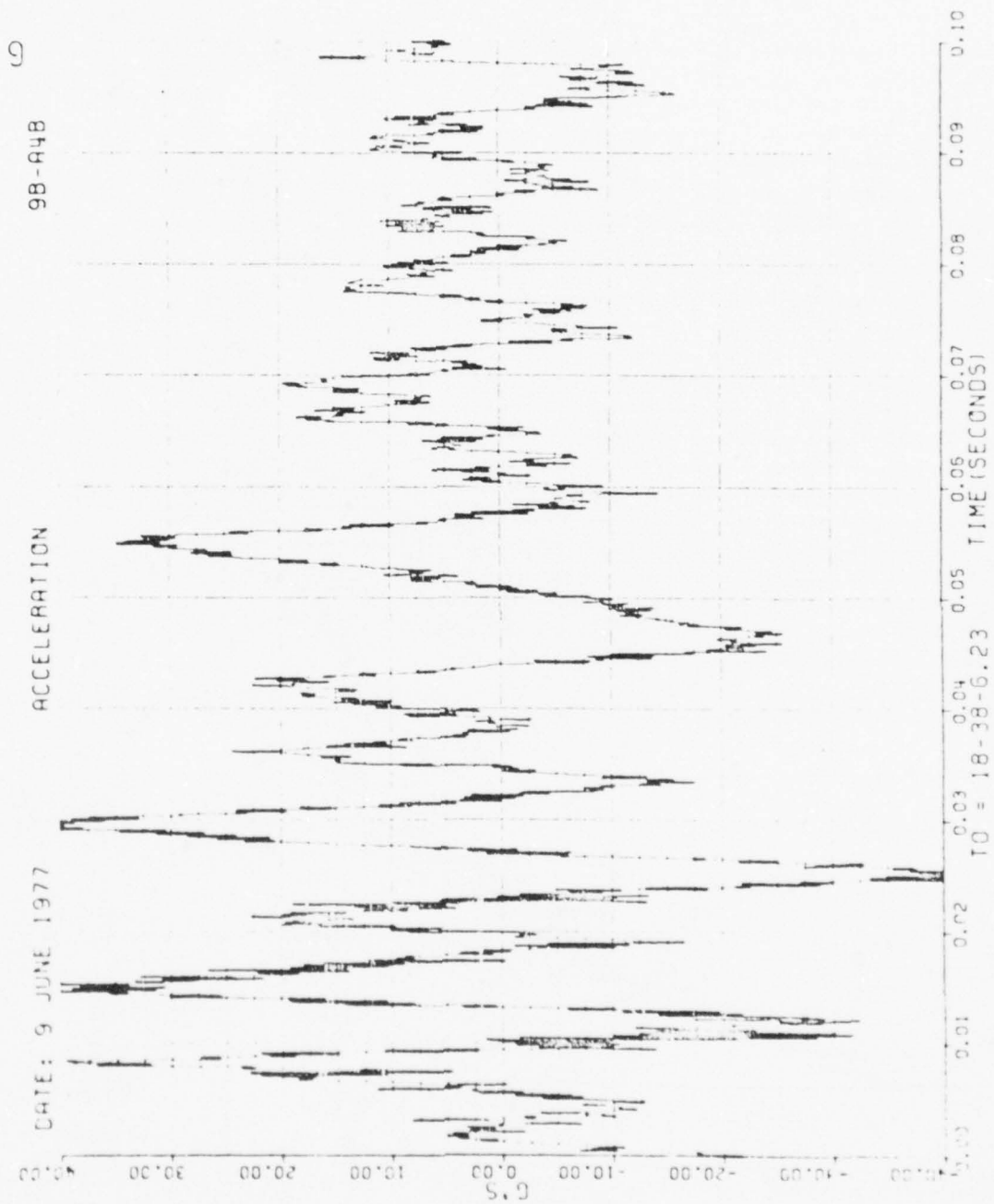


Figure 48. Concluded

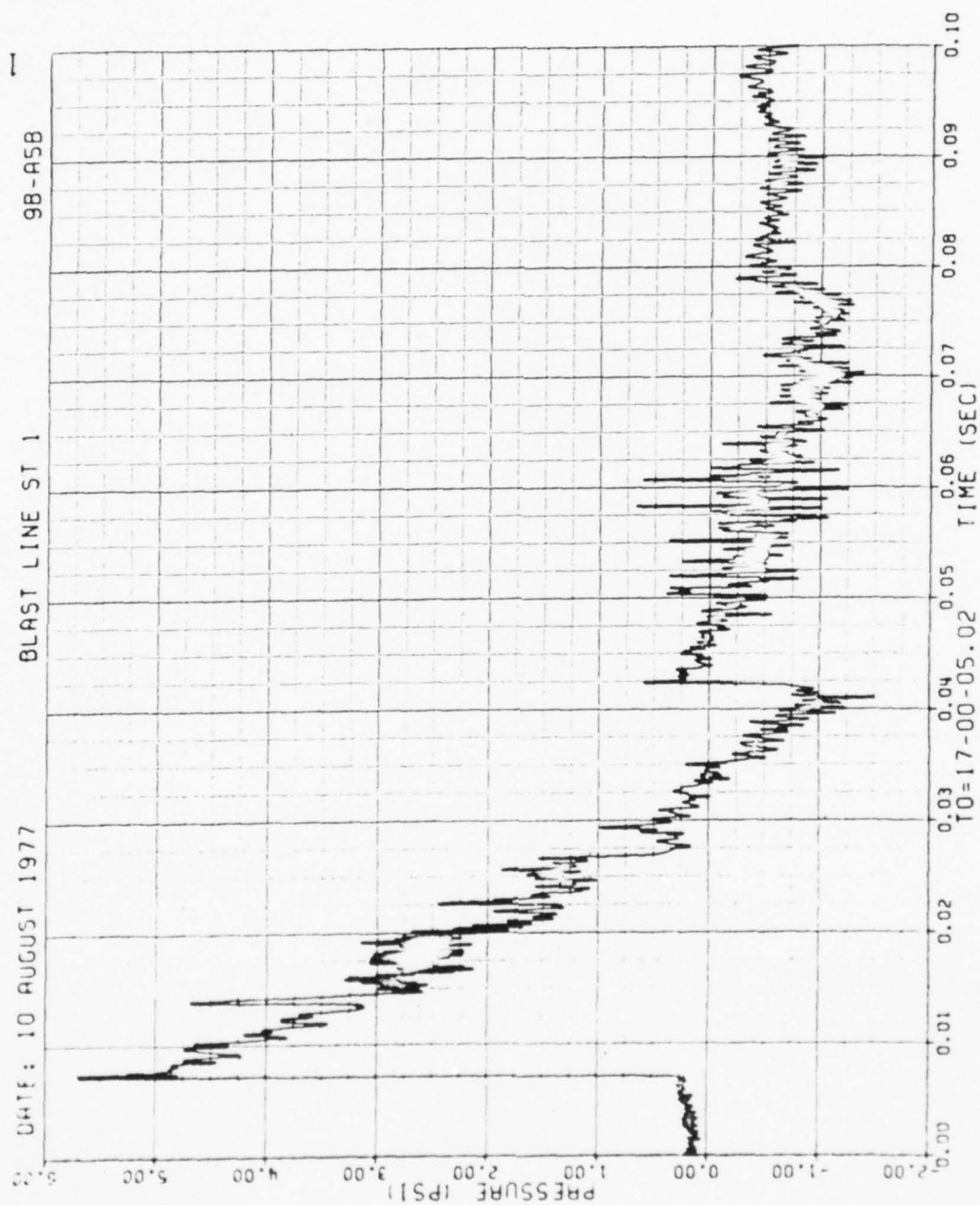


Figure 49. Blast-line Overpressures, Run 9B-A5, Intercept 1.

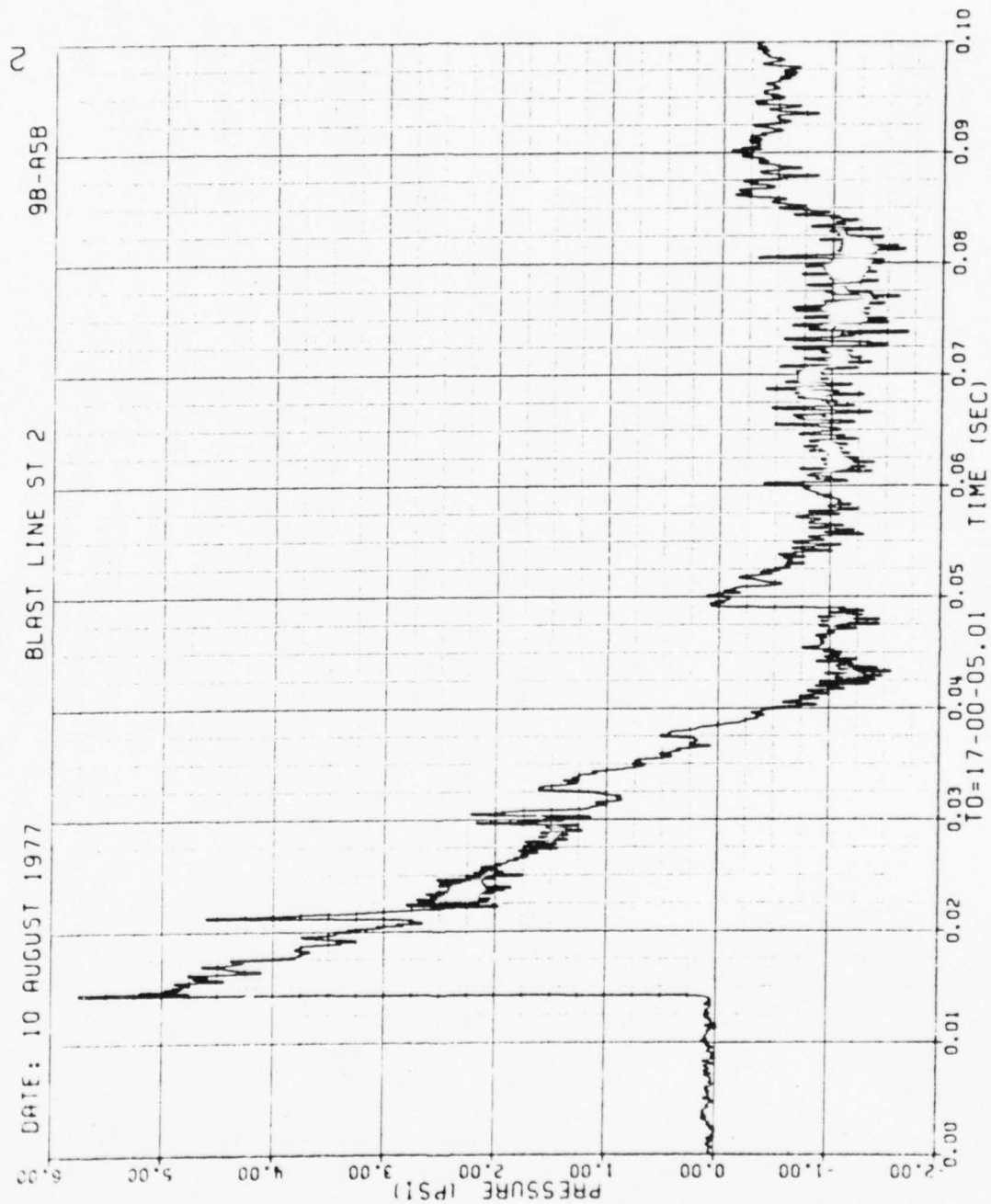


Figure 49. Continued

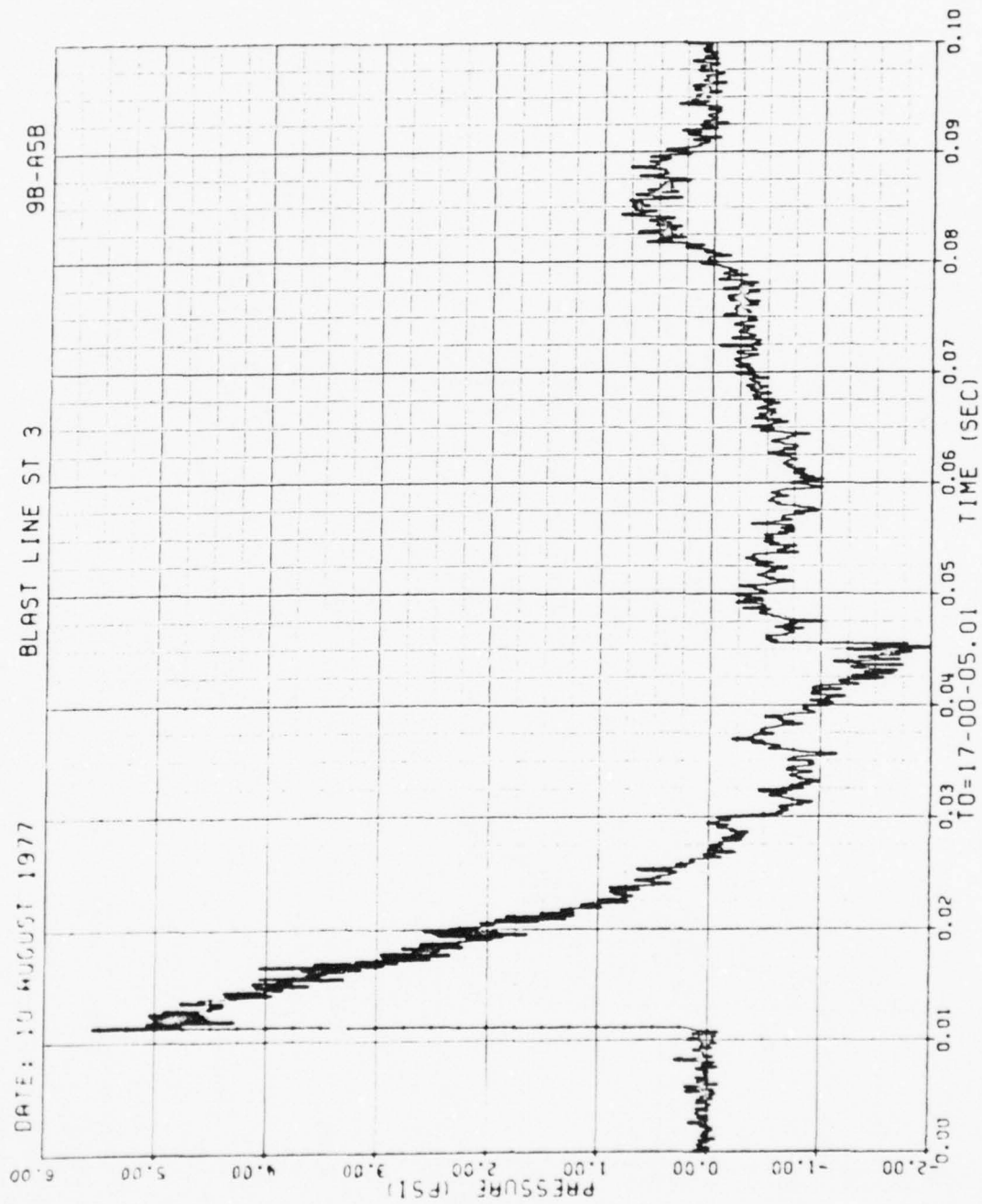


Figure 49. Continued

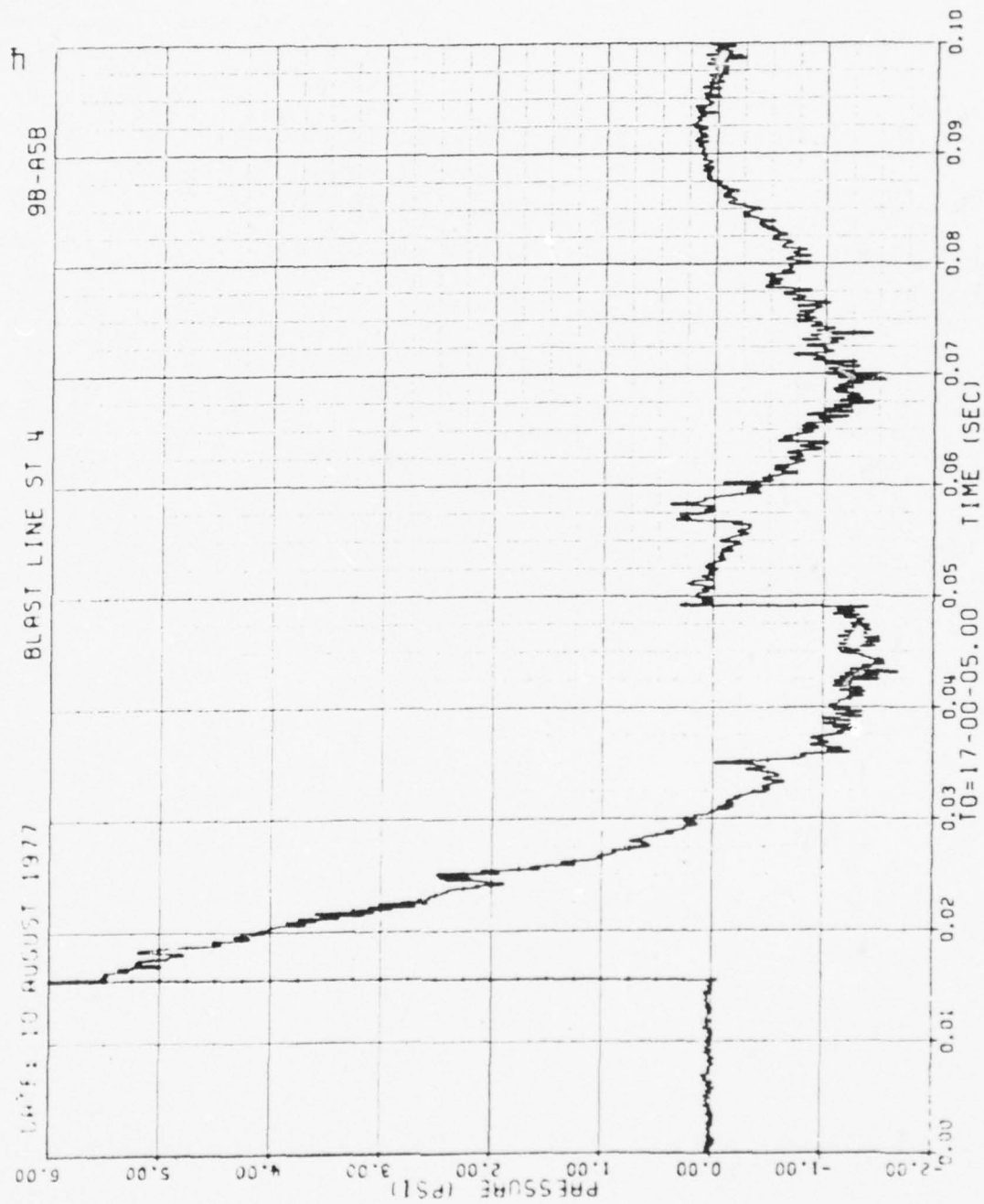


Figure 49. Concluded

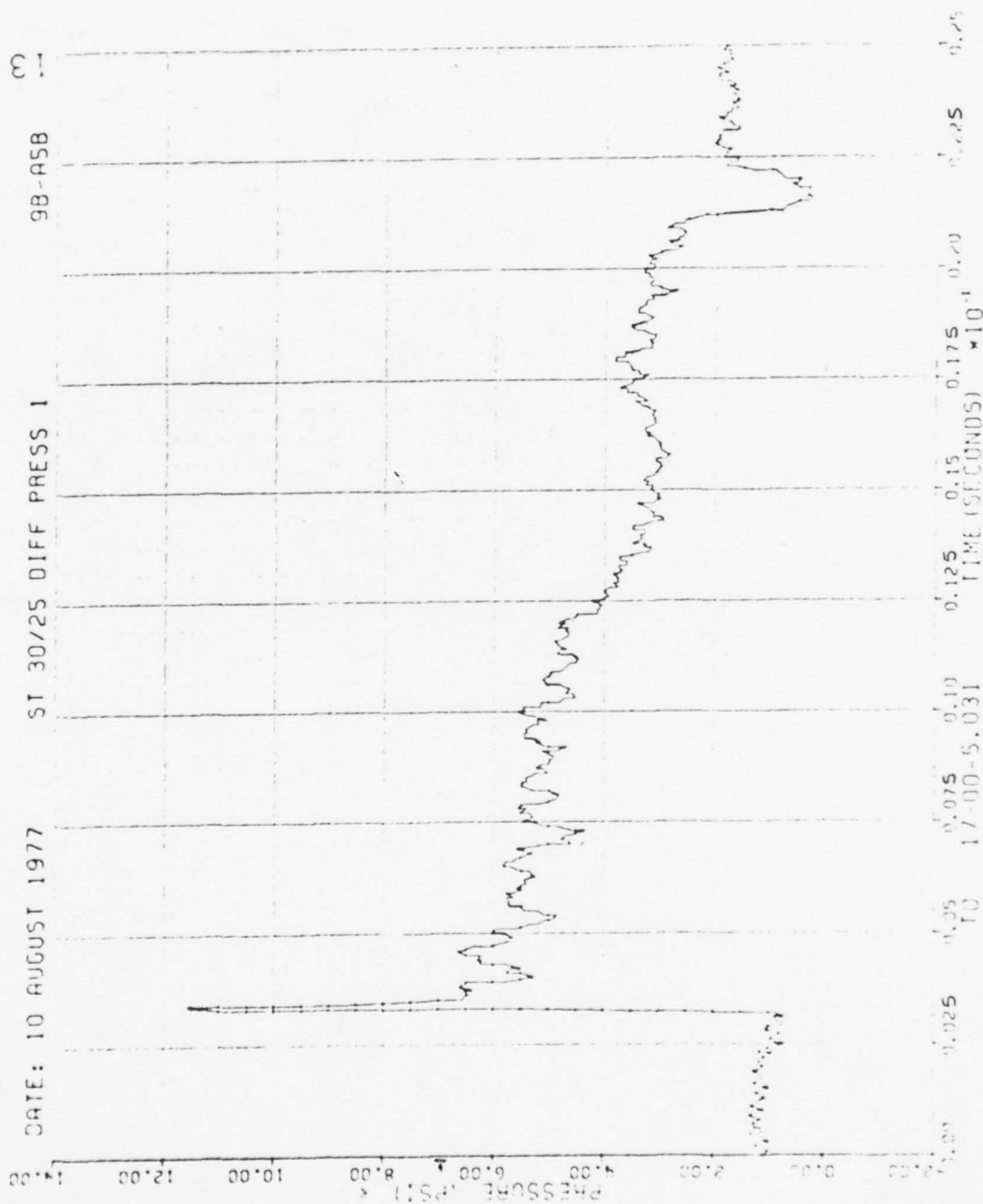


Figure 50. Differential Wing Pressures, Run 9B-A5, Intercept 1.

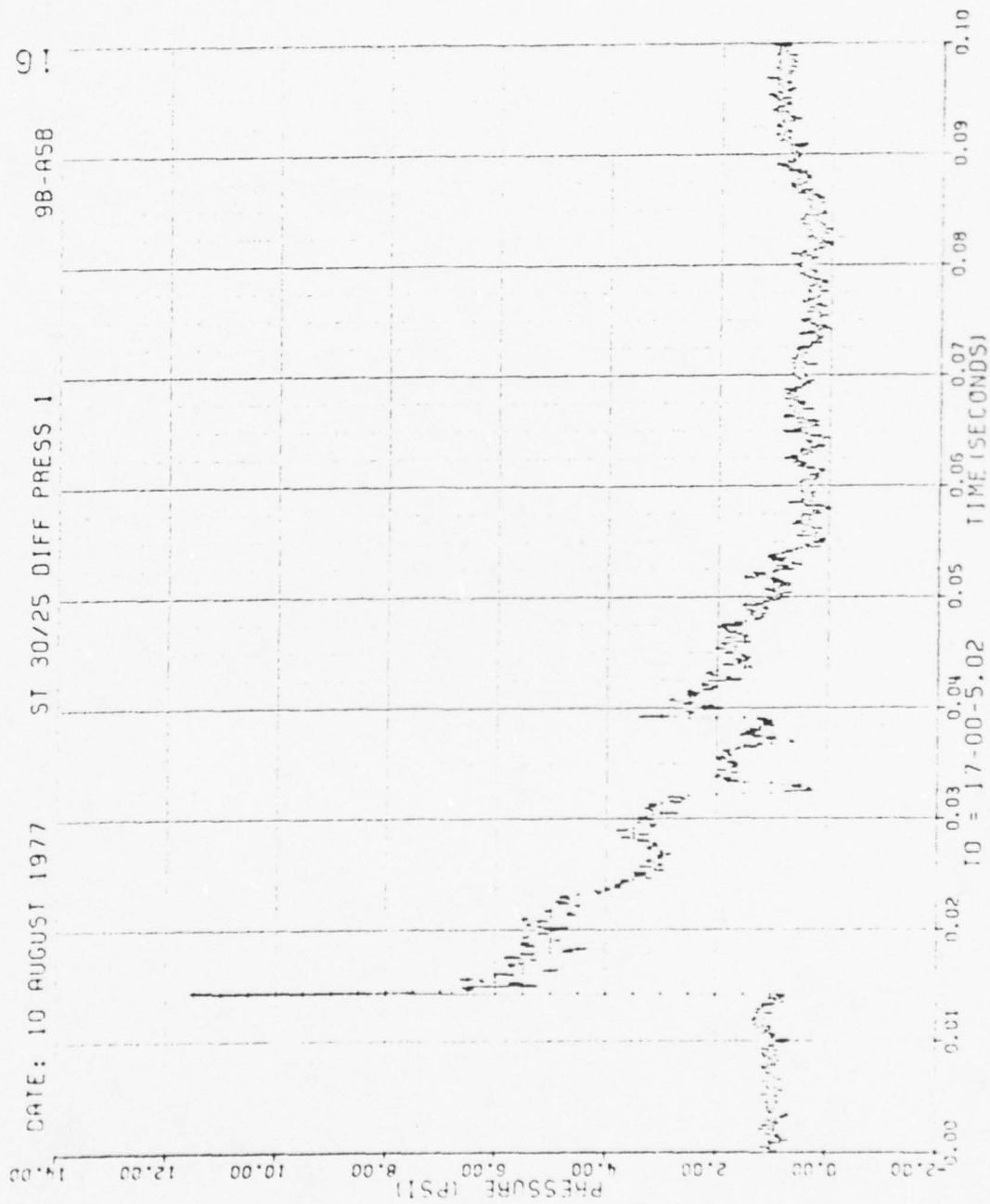


Figure 50. Continued

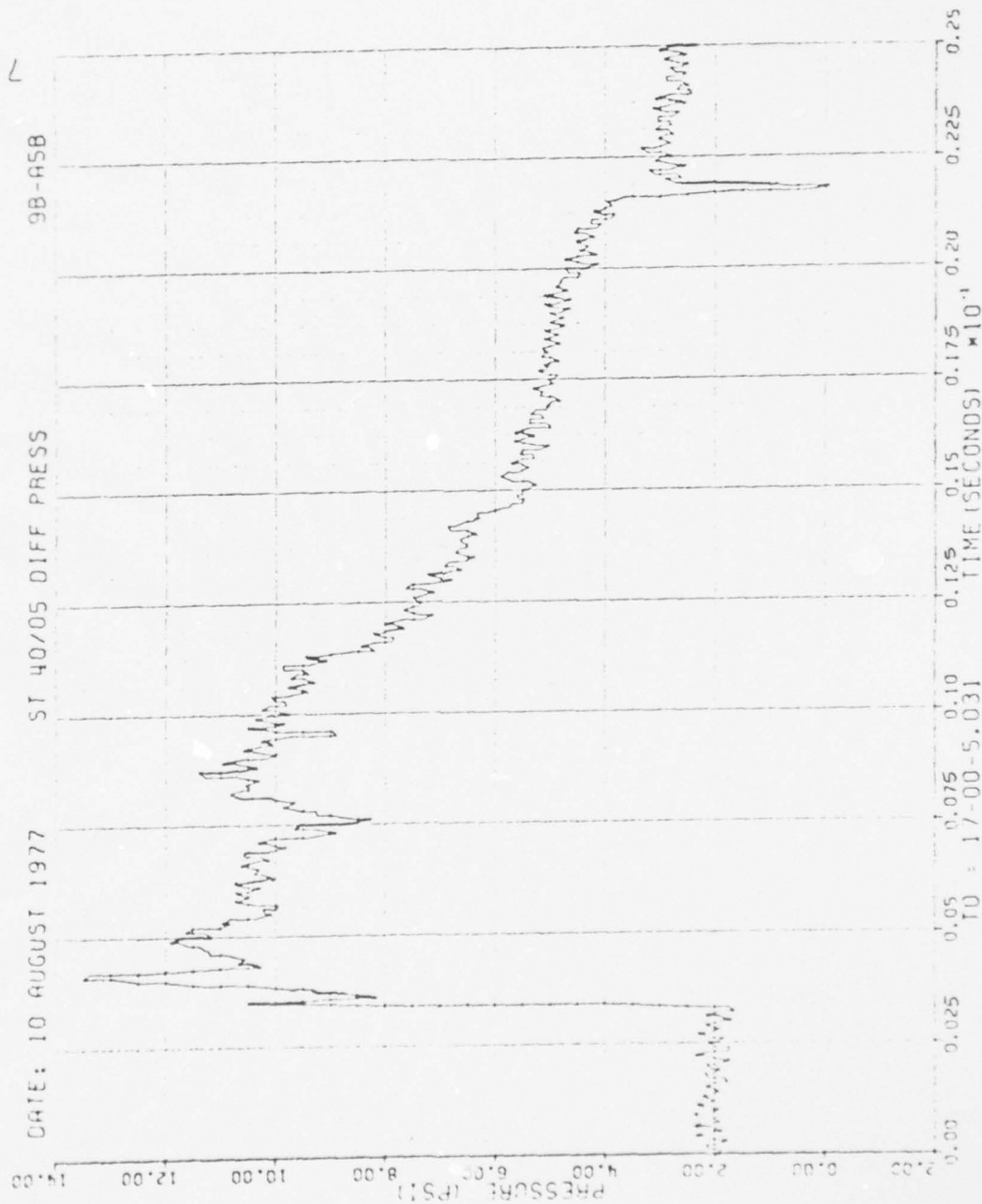


Figure 50. Continued

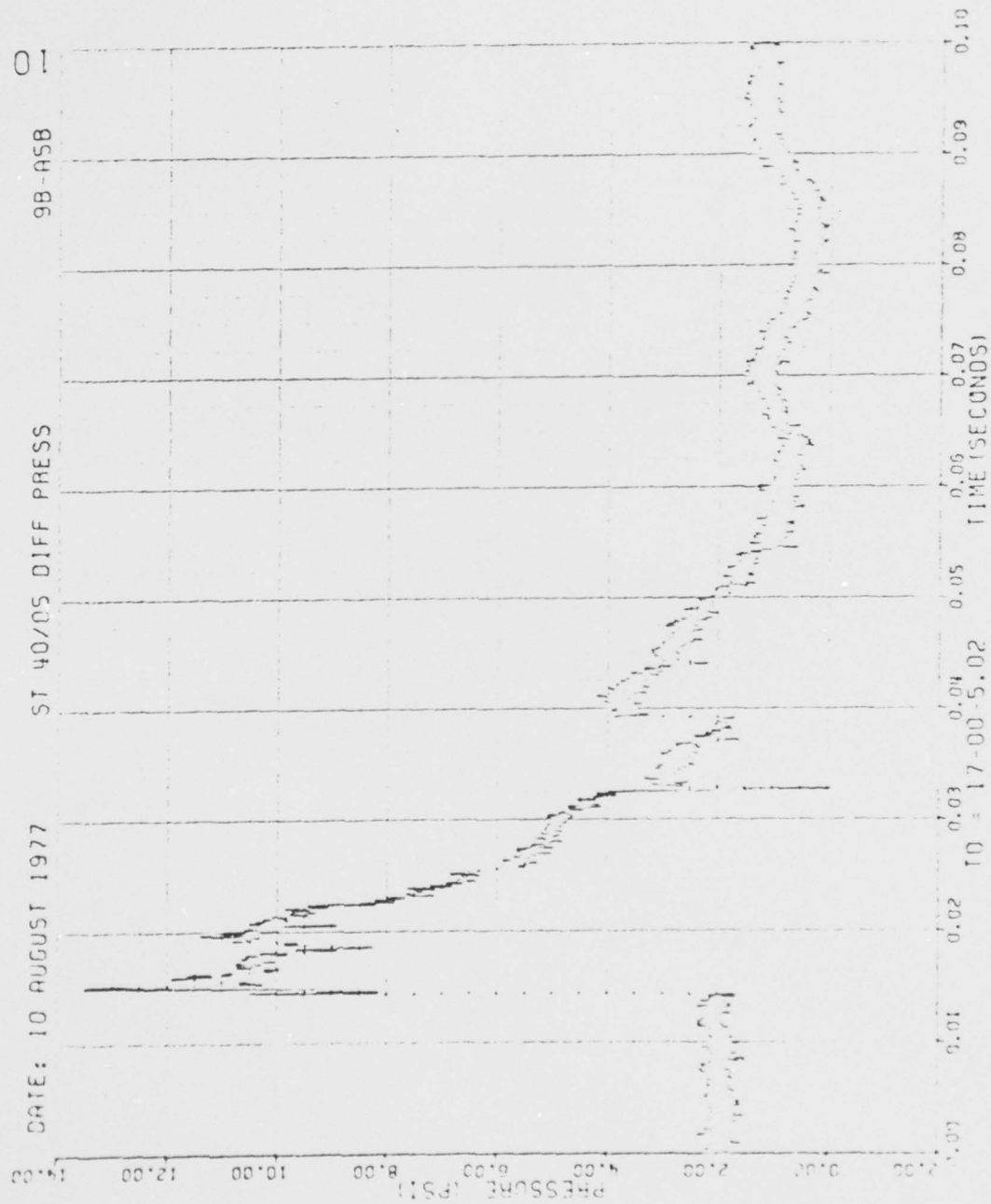


Figure 50. Continued

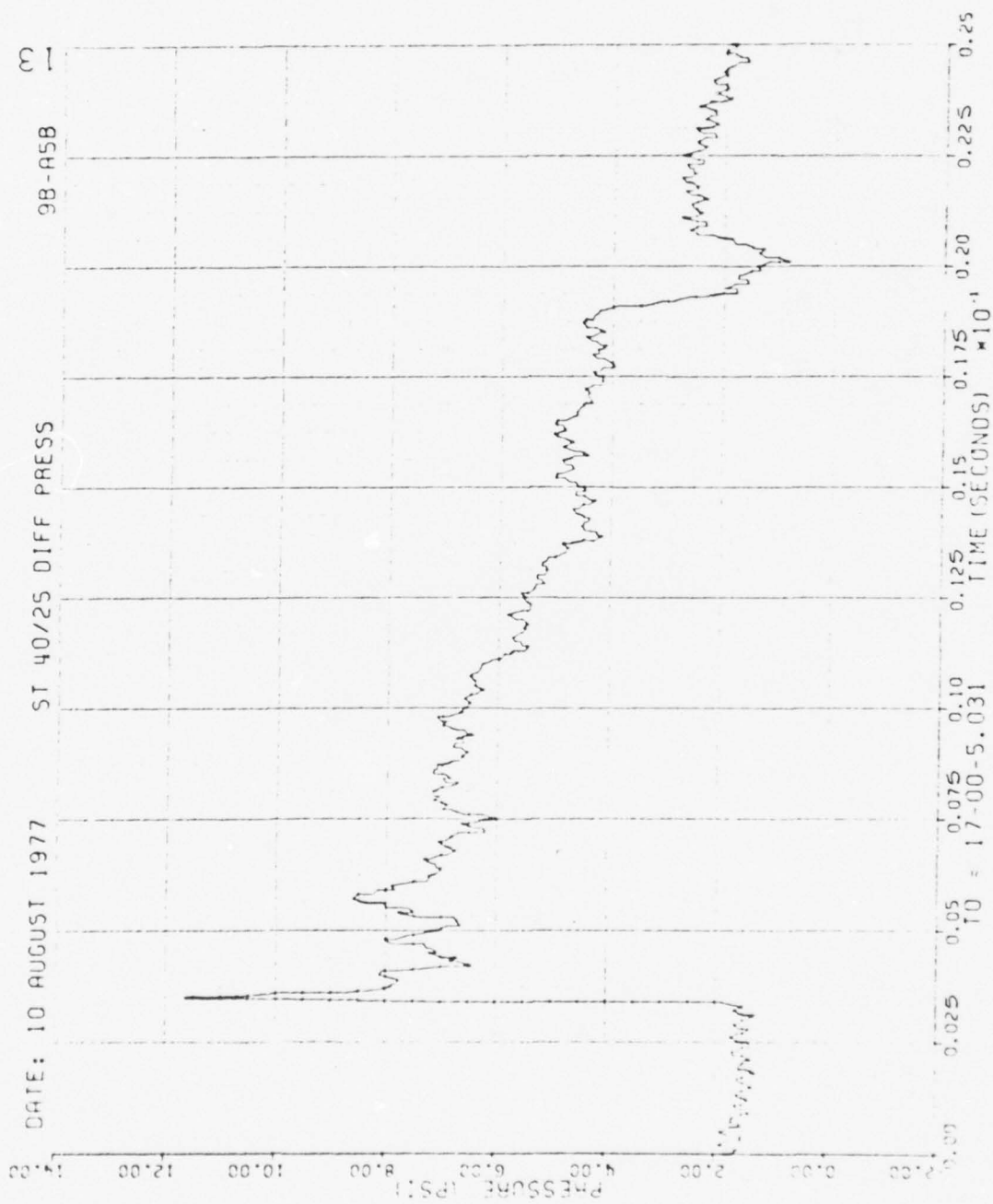


Figure 50. Continued

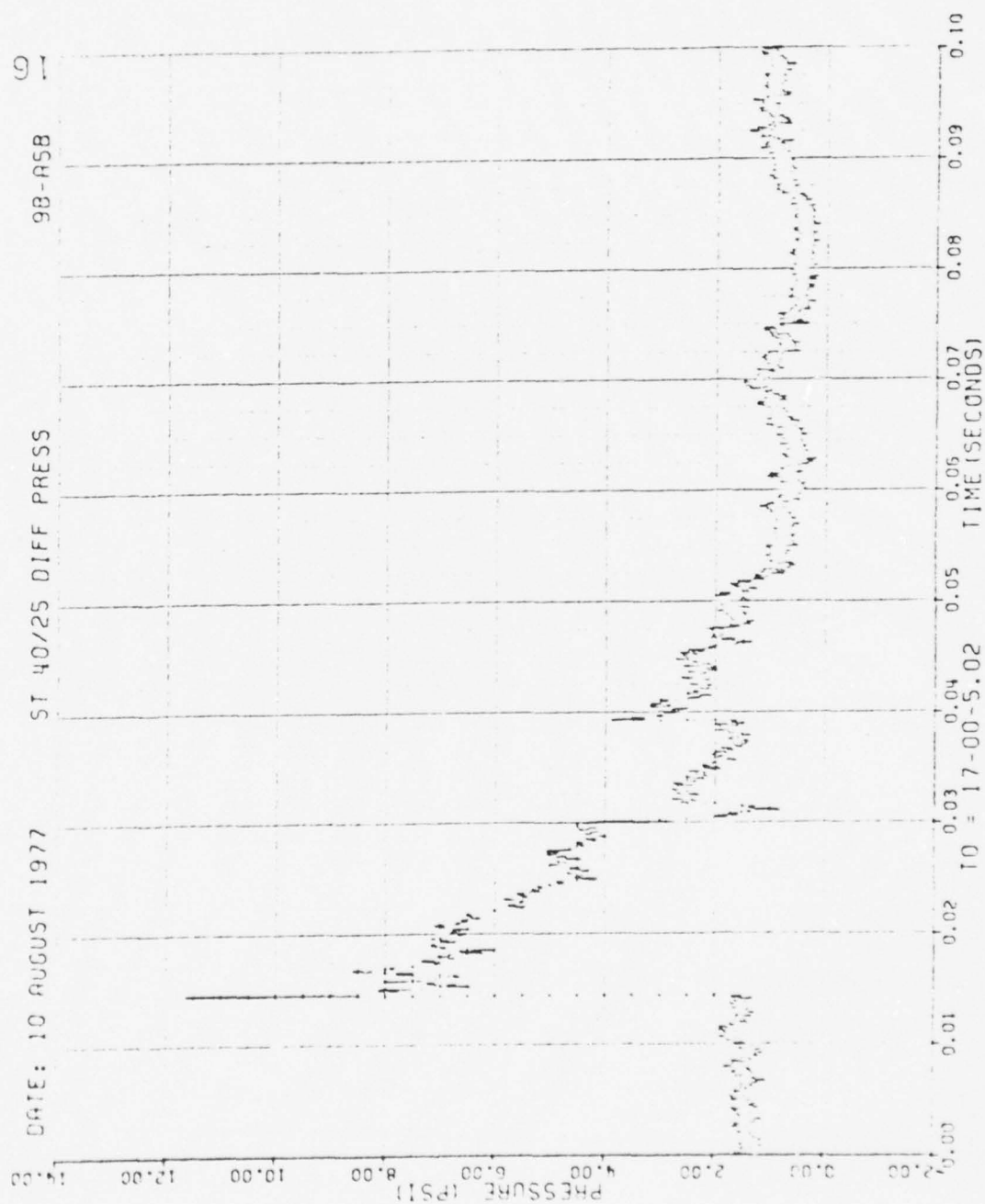


Figure 50. Continued

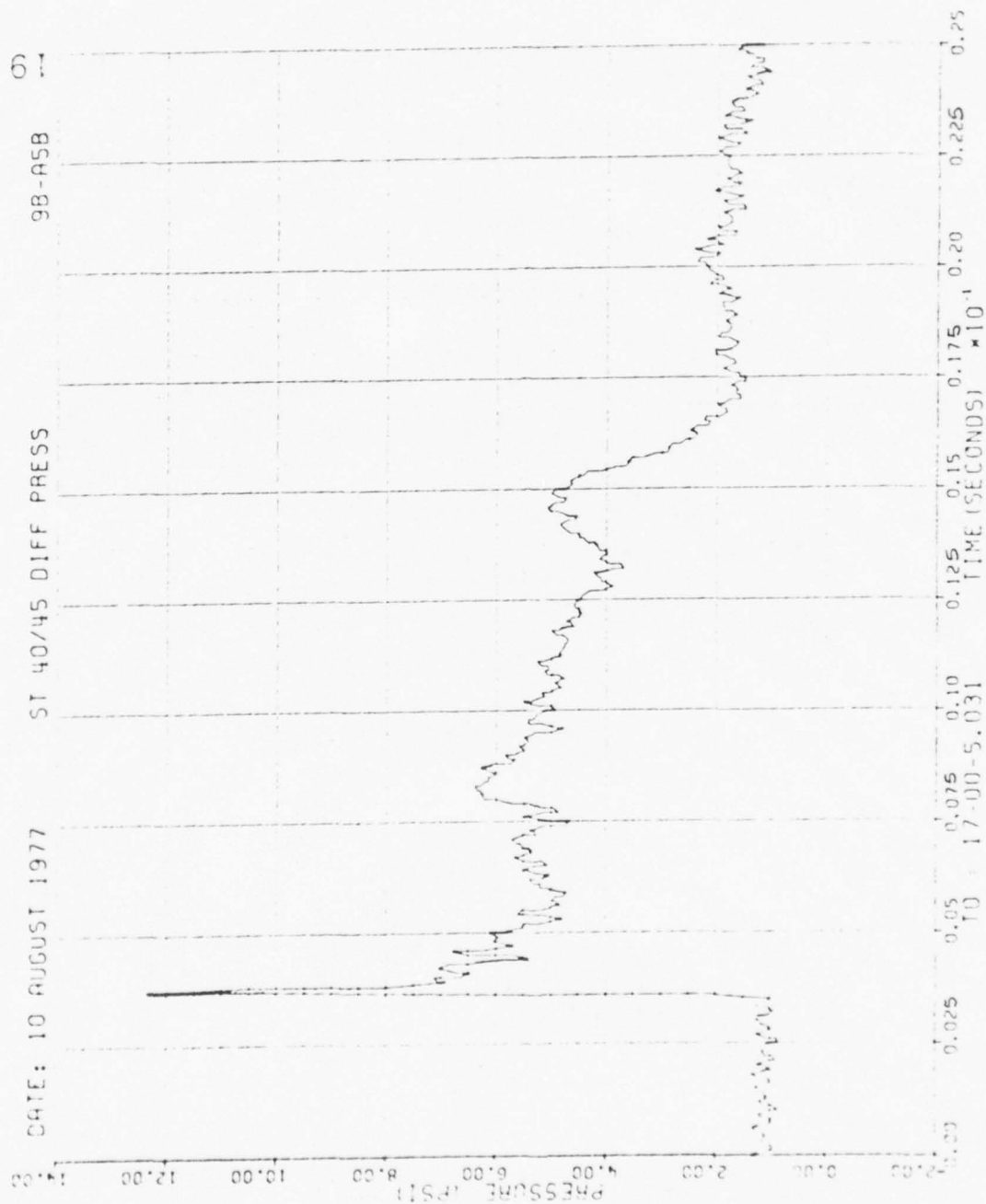


Figure 50. Continued

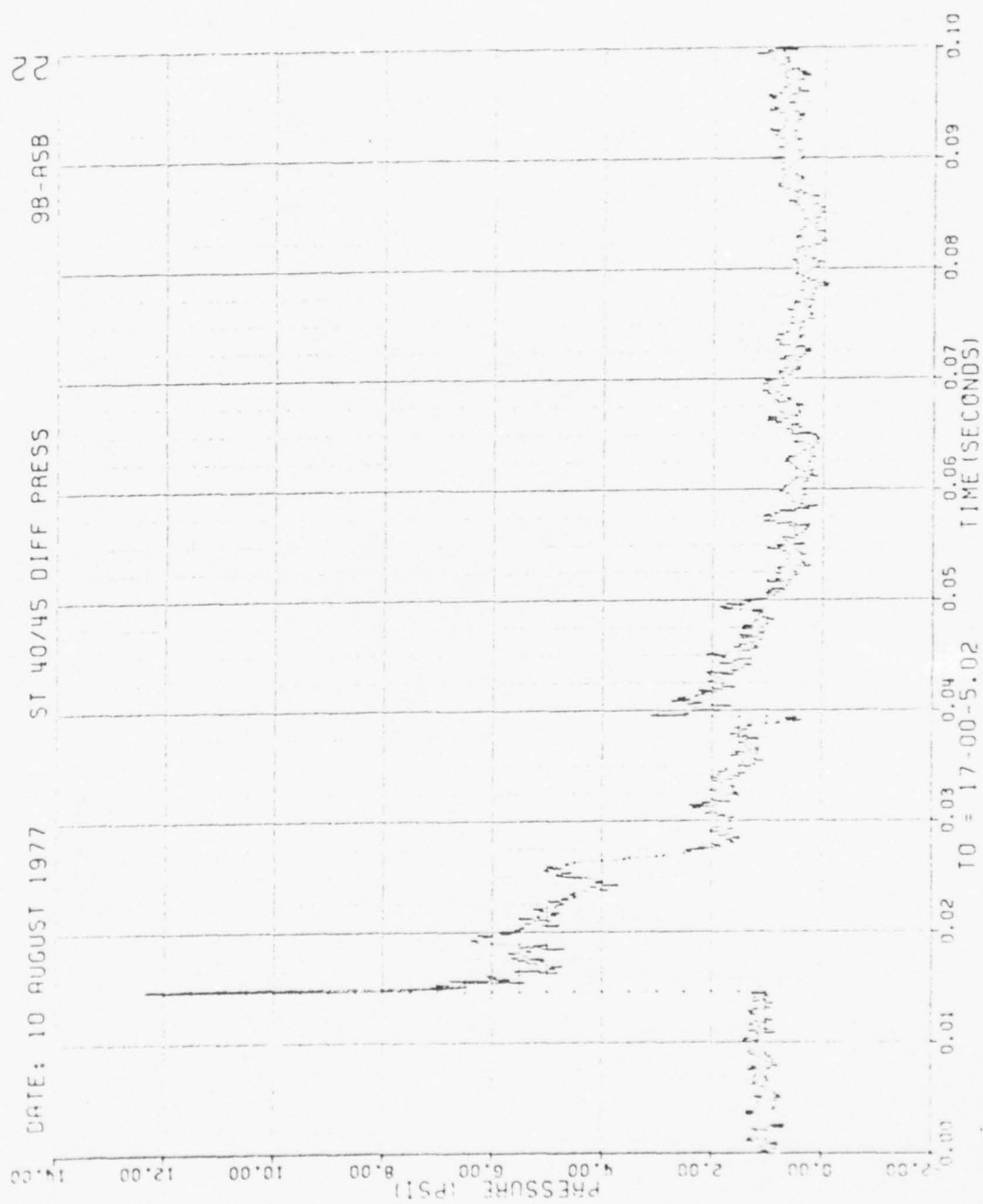


Figure 50. Continued

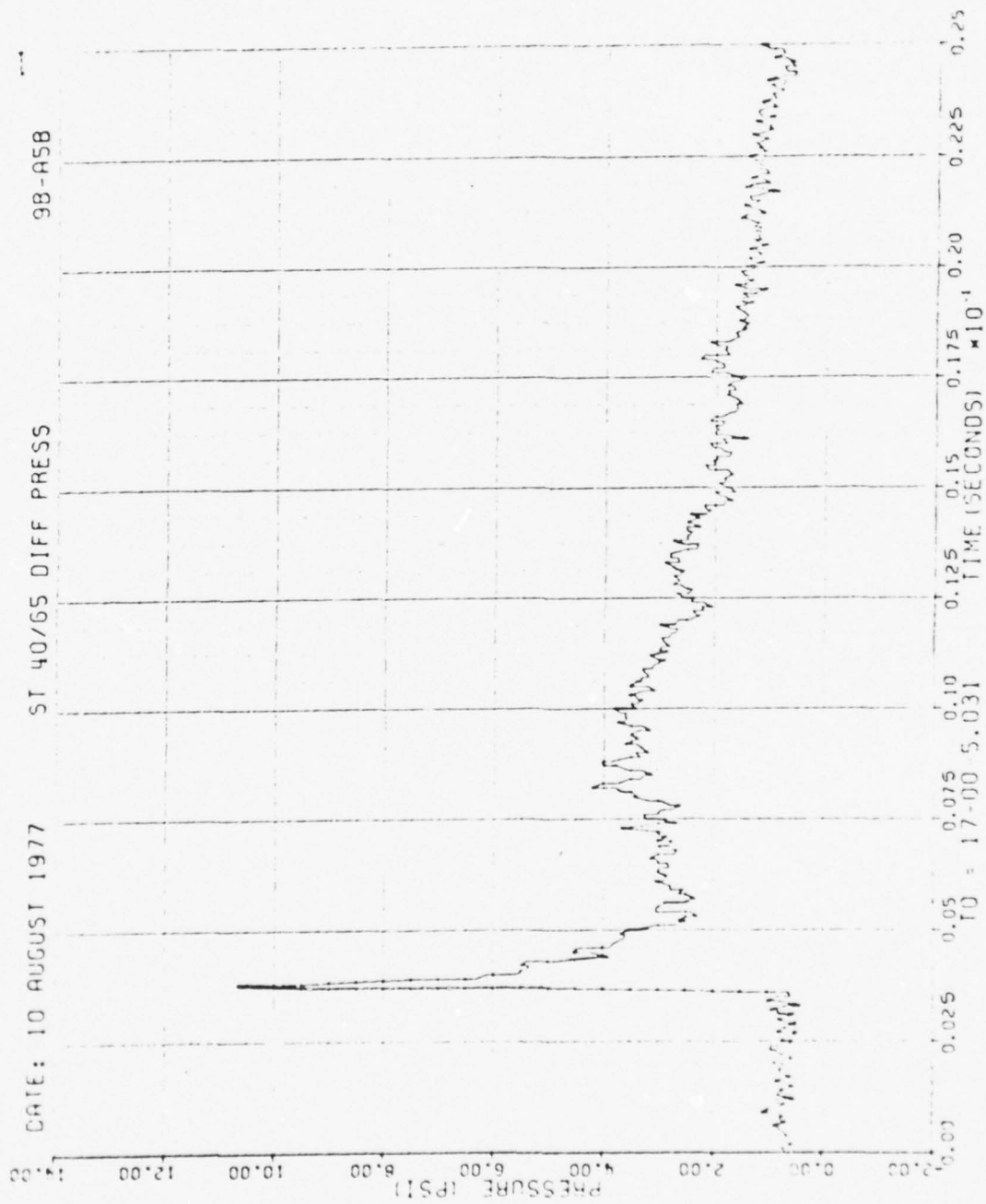


Figure 50. Continued

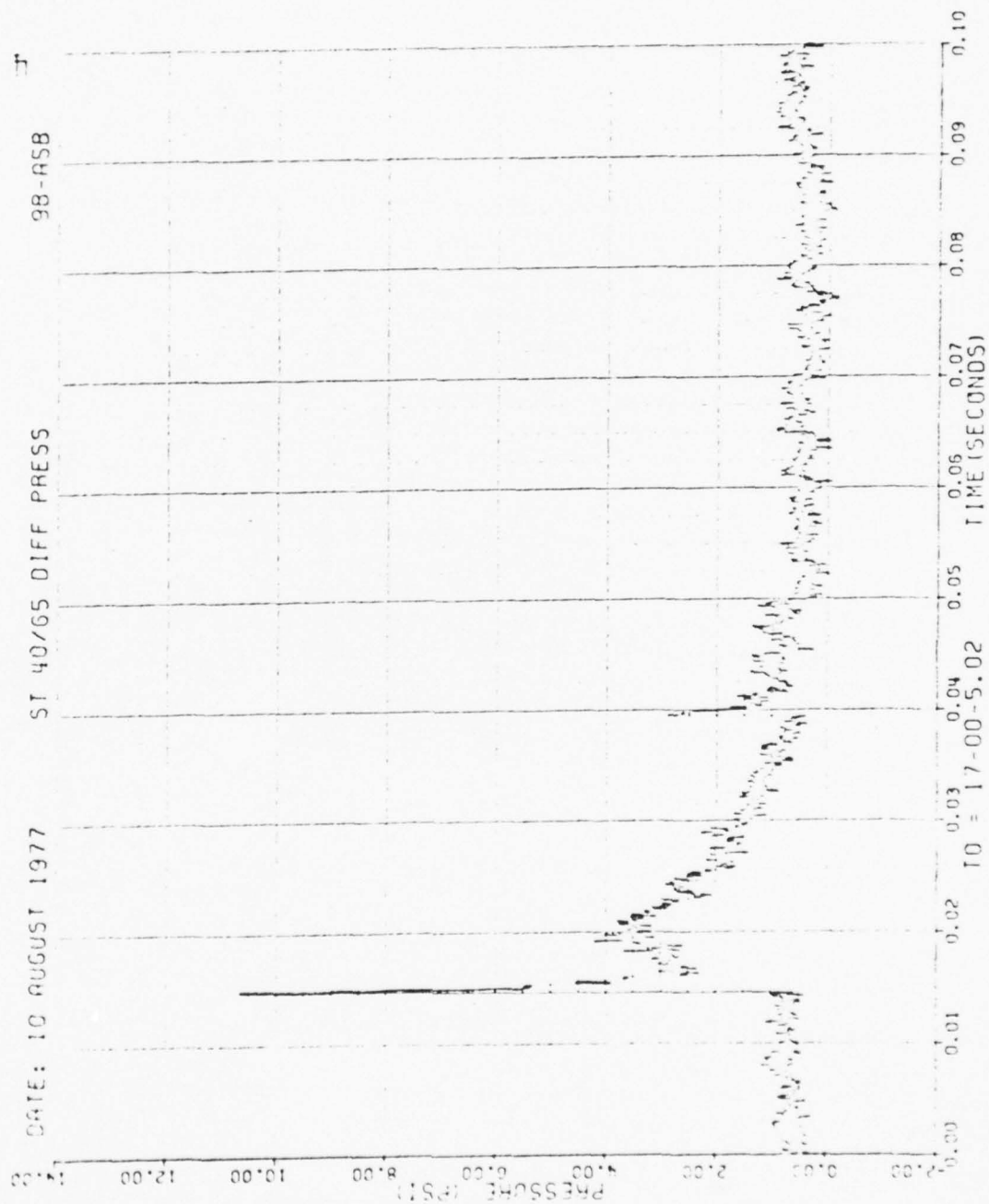


Figure 50. Continued

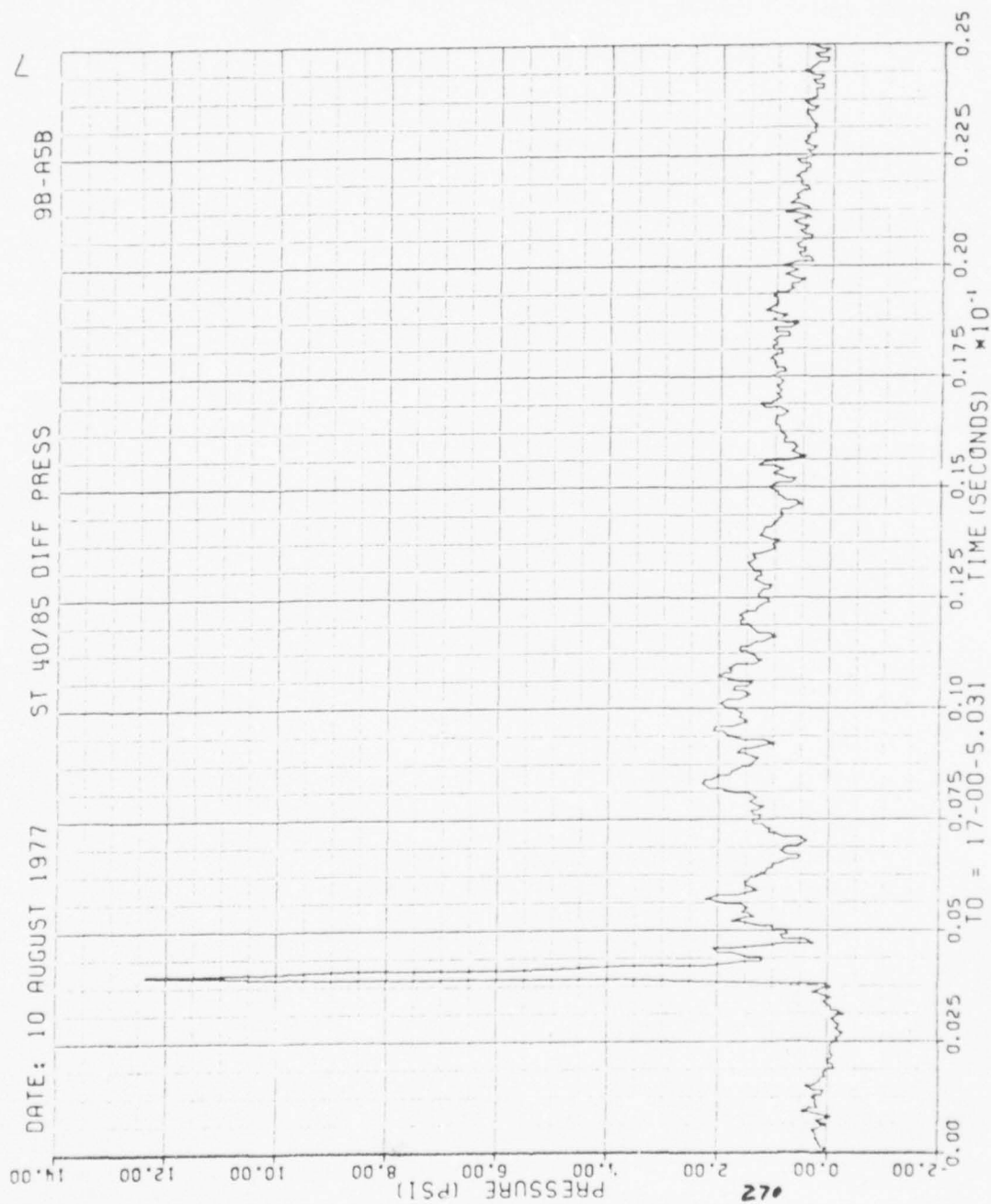


Figure 50. Continued

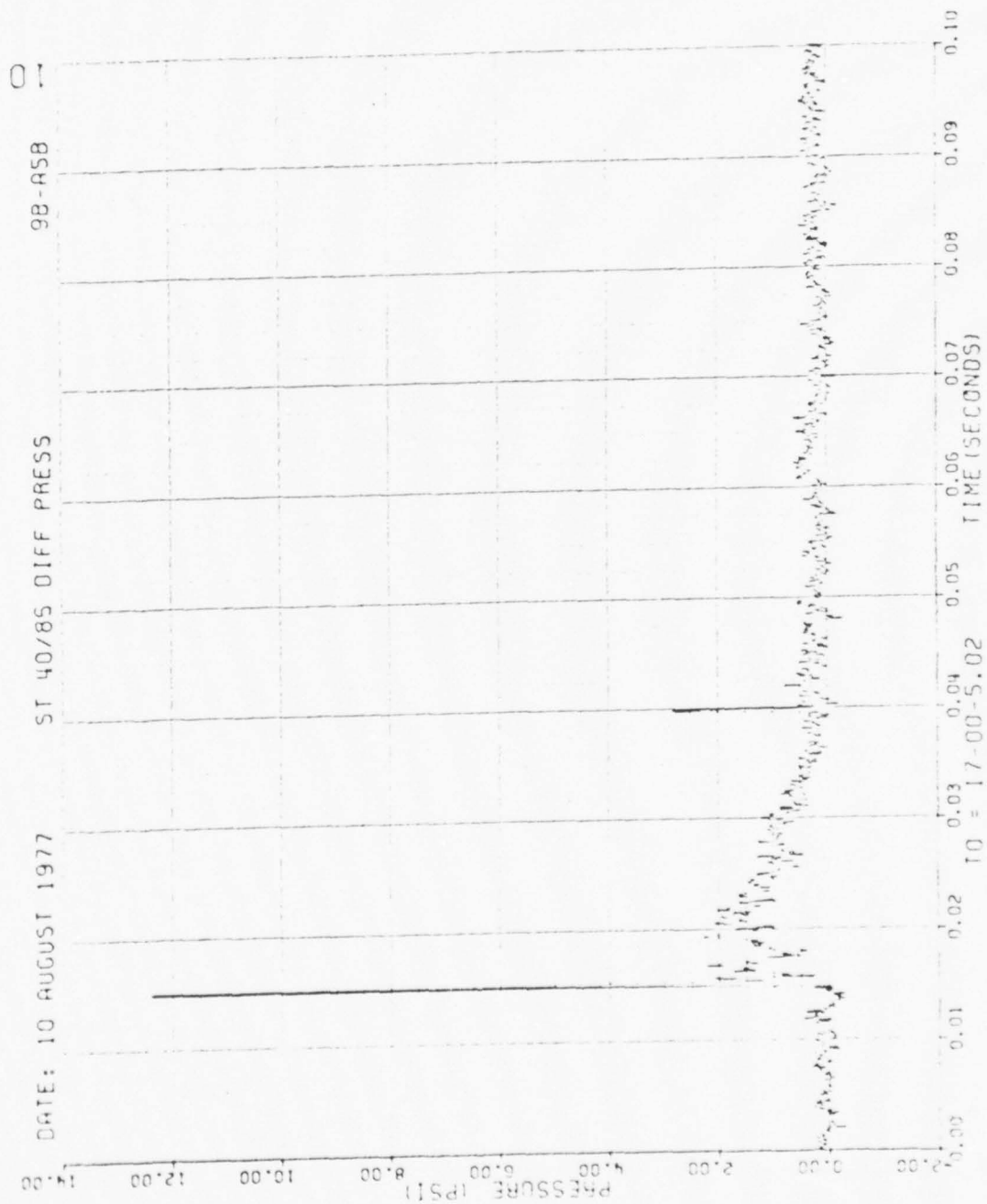


Figure 50. Continued

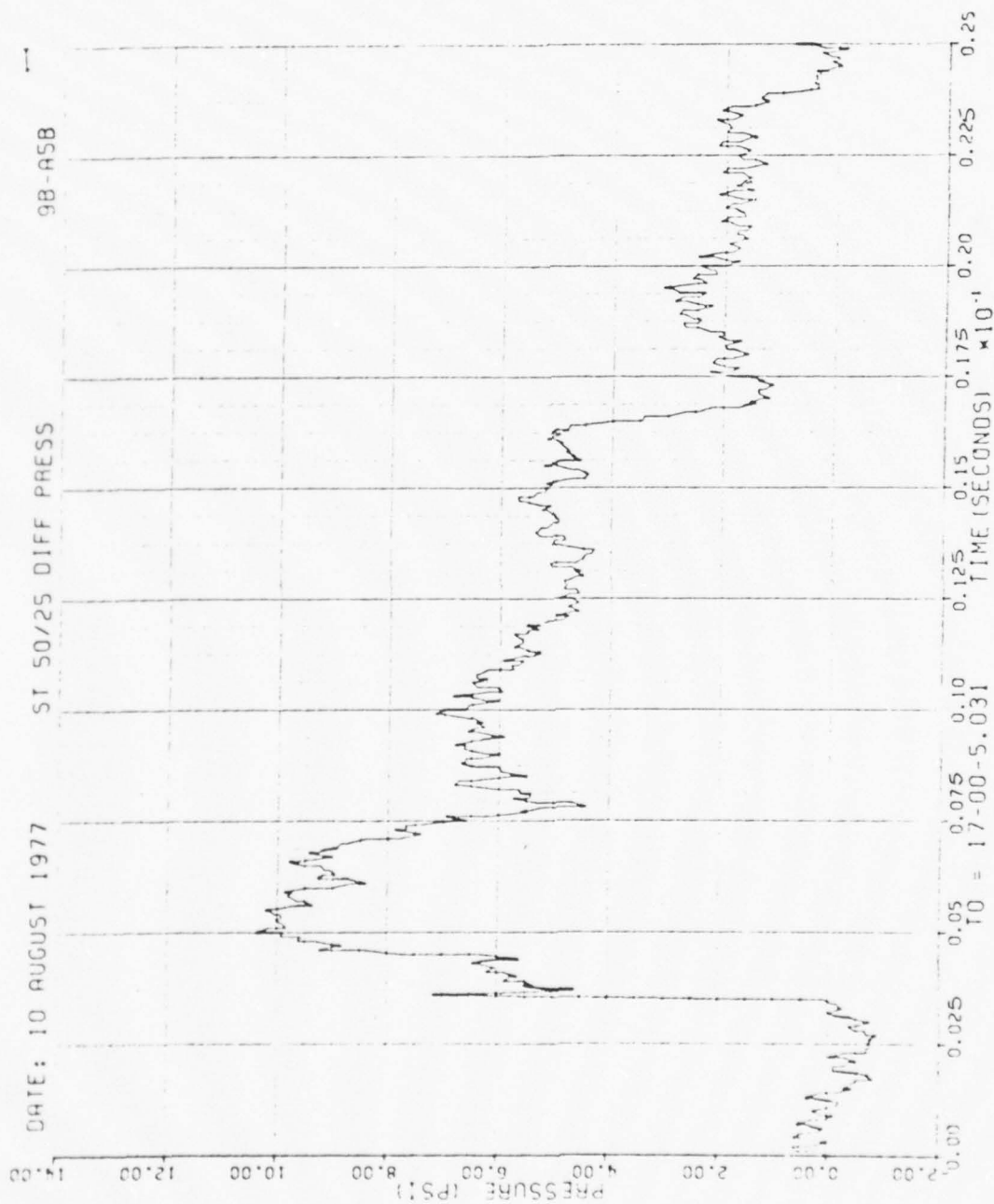


Figure 50. Continued

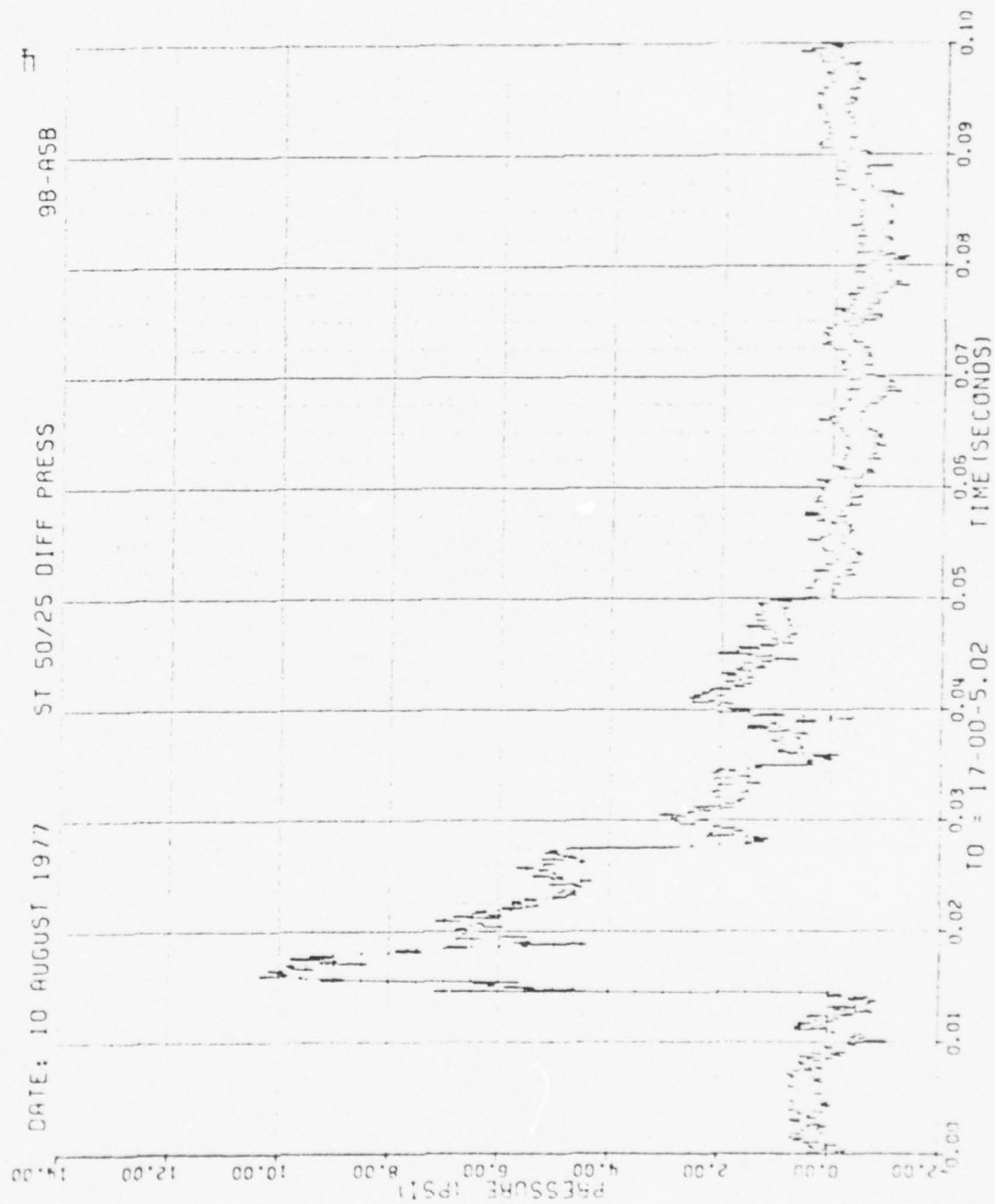


Figure 50. Continued

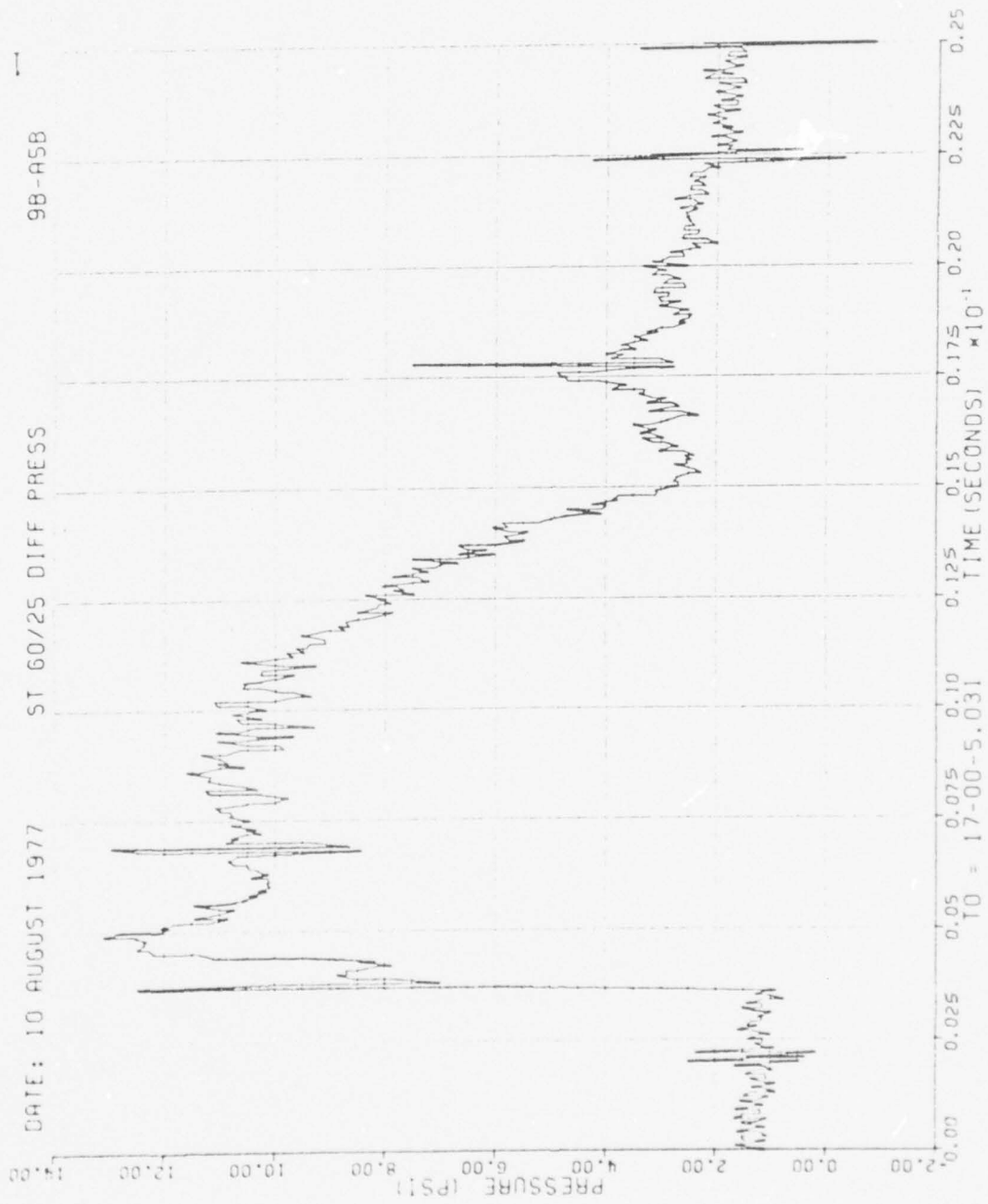


Figure 50. Continued

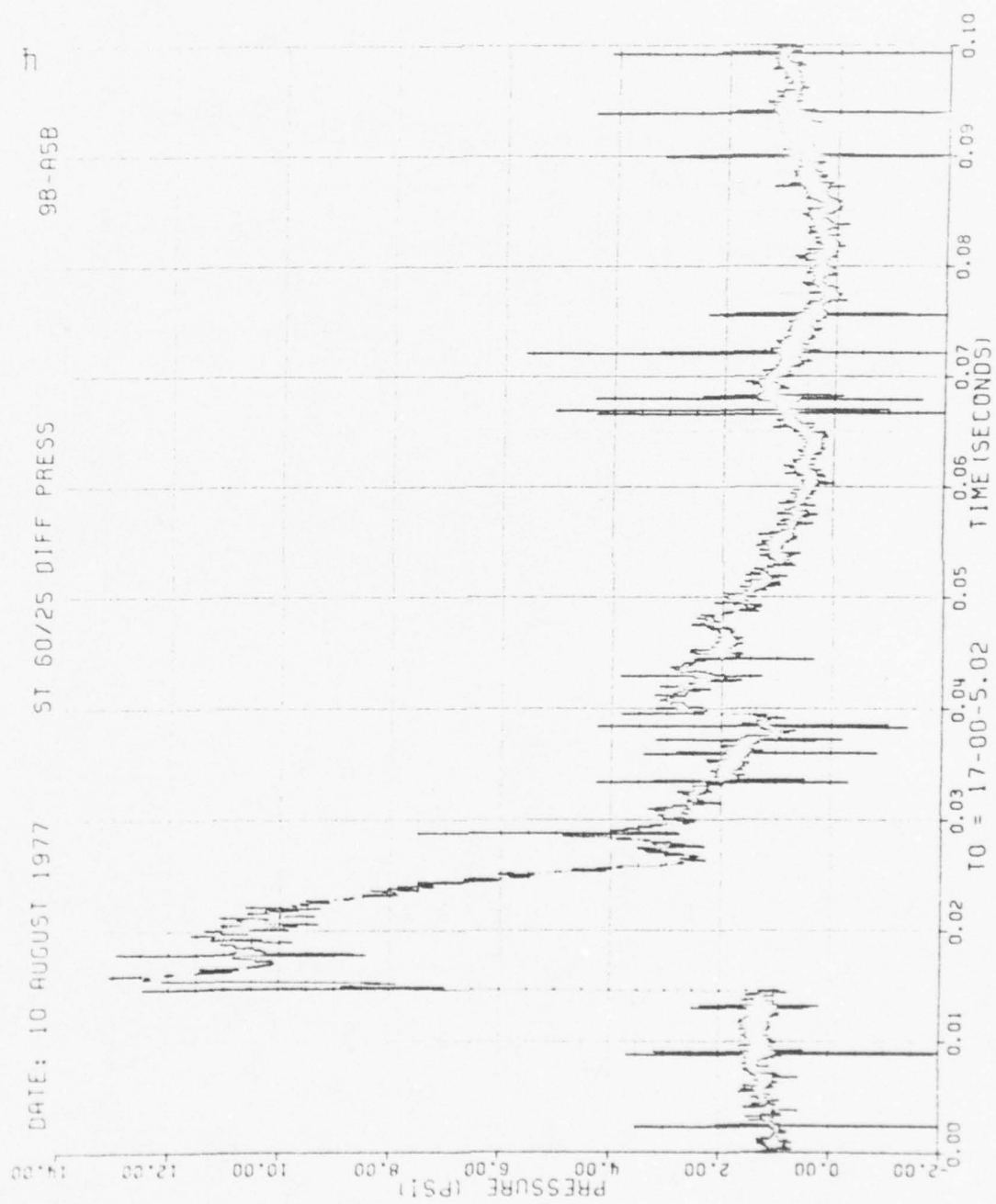


Figure 50. Continued

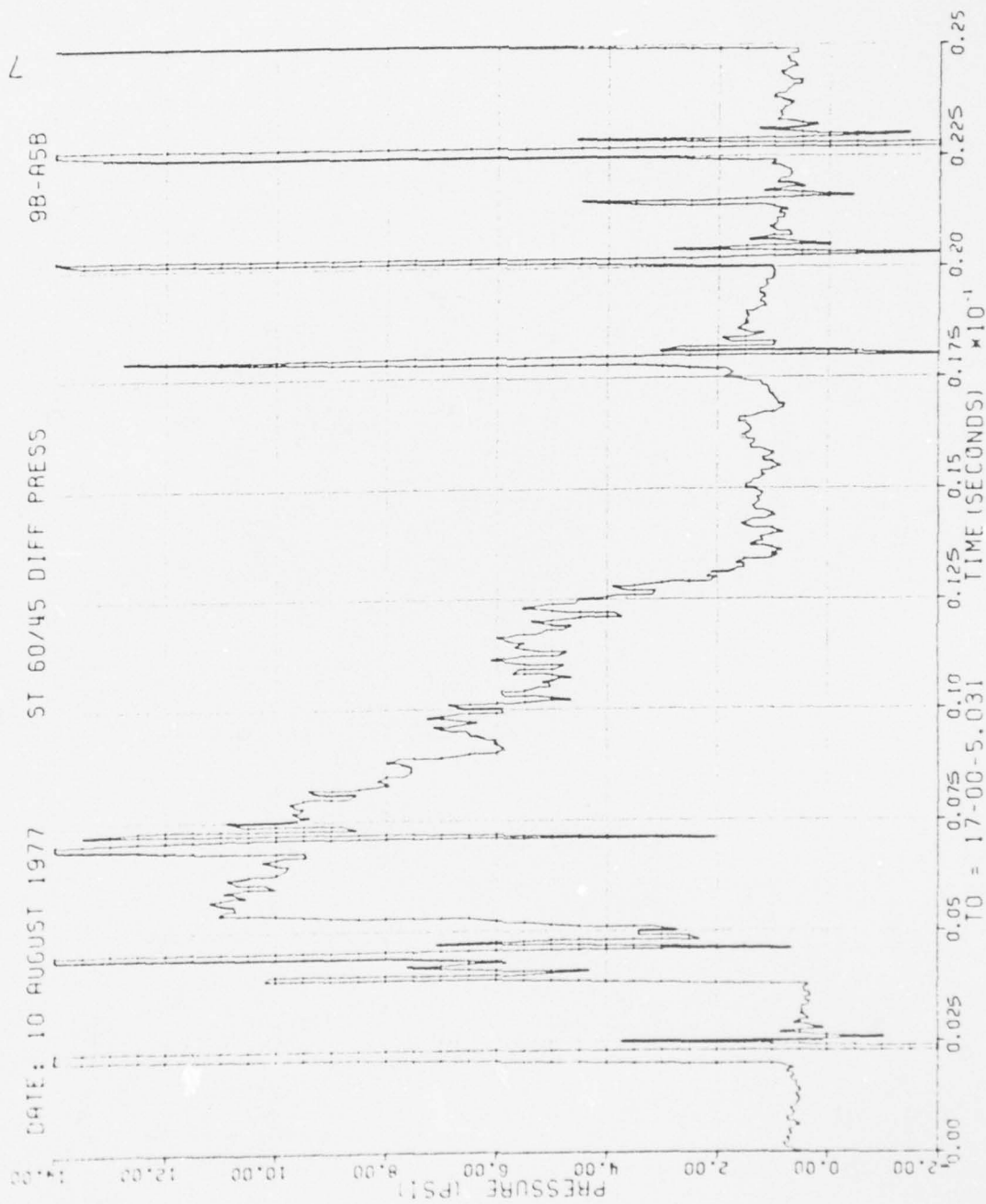


Figure 50. Continued

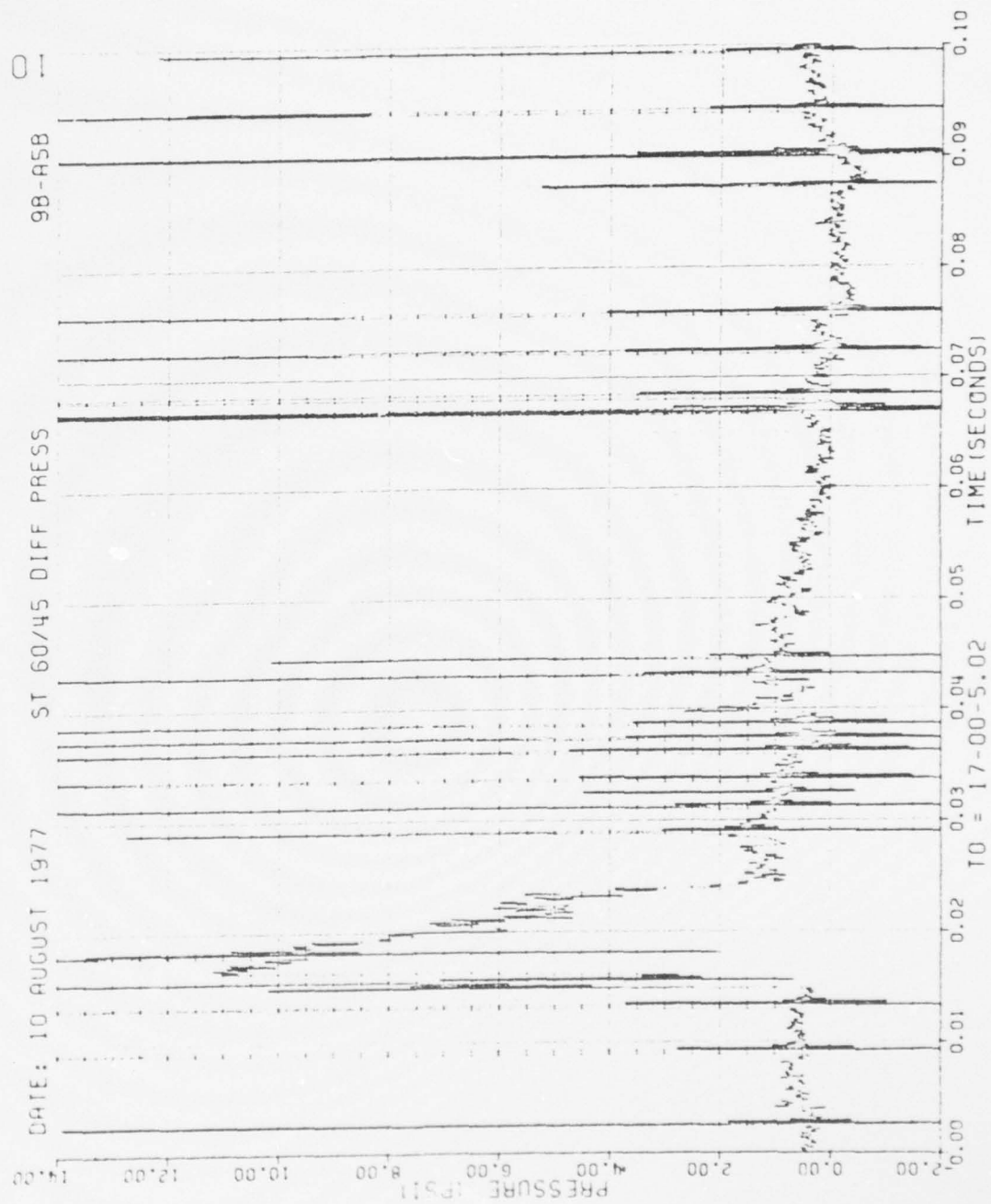


Figure 50. Continued

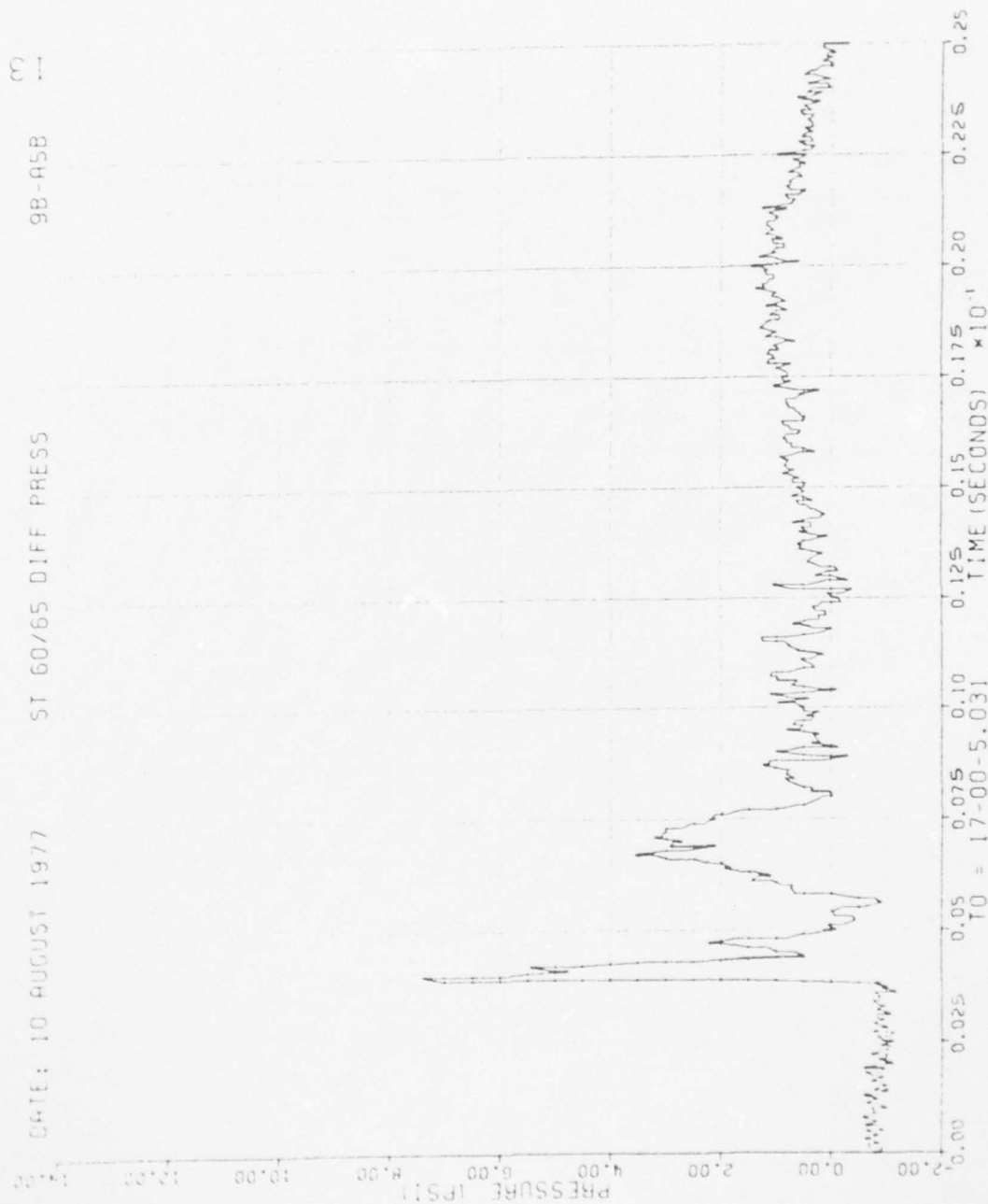


Figure 50. Continued

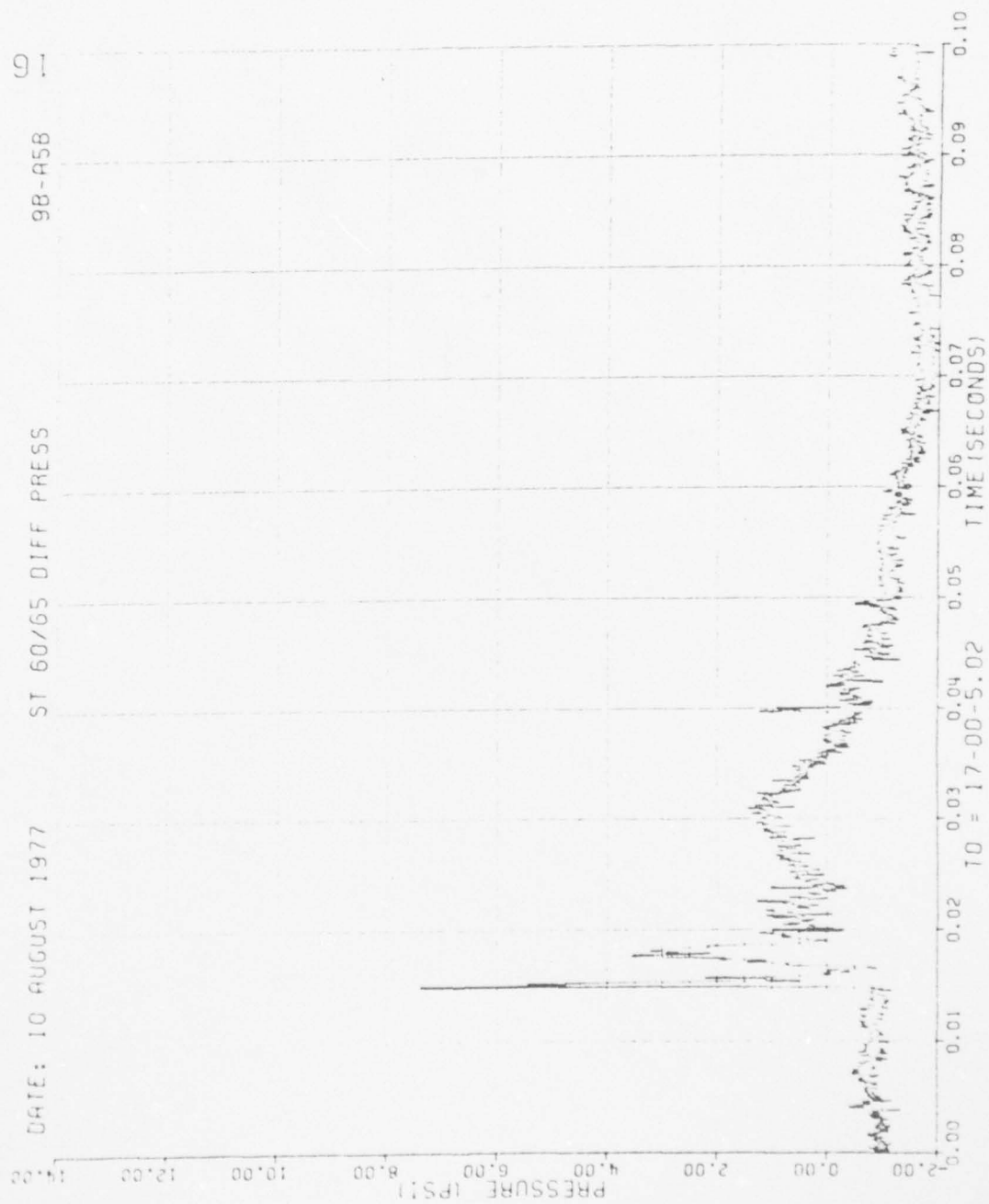


Figure 50. Continued

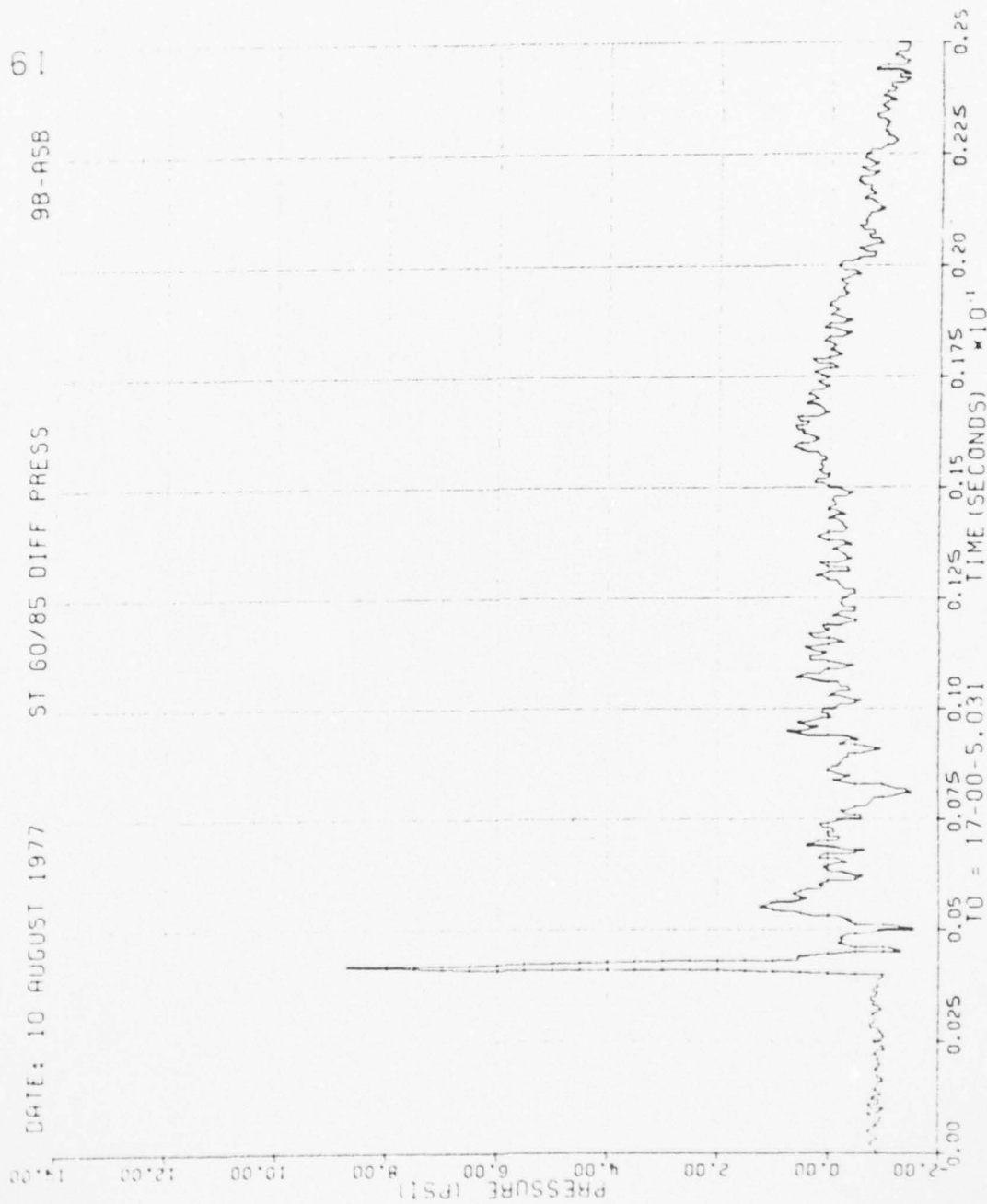


Figure 50. Continued

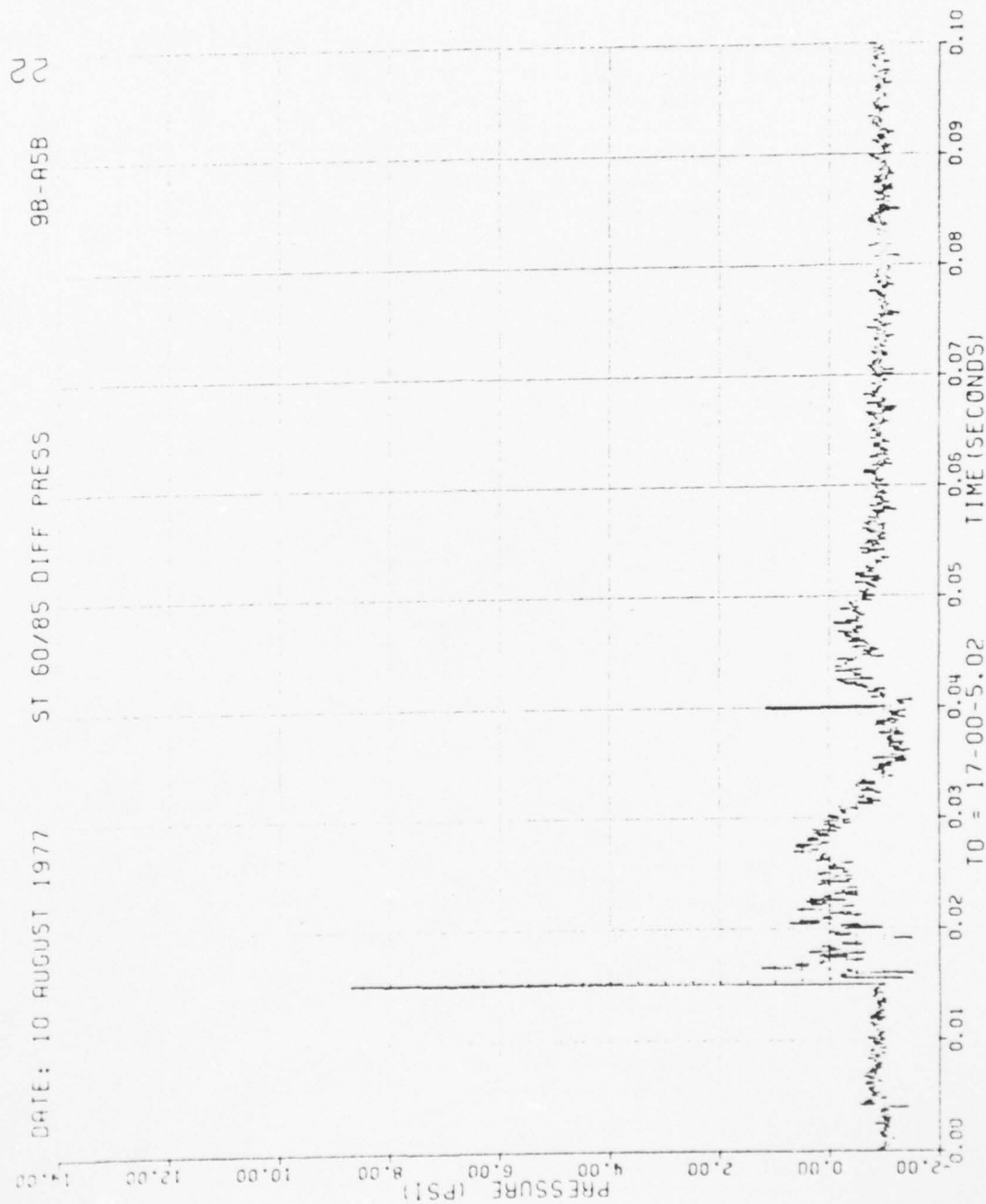


Figure 50. Continued

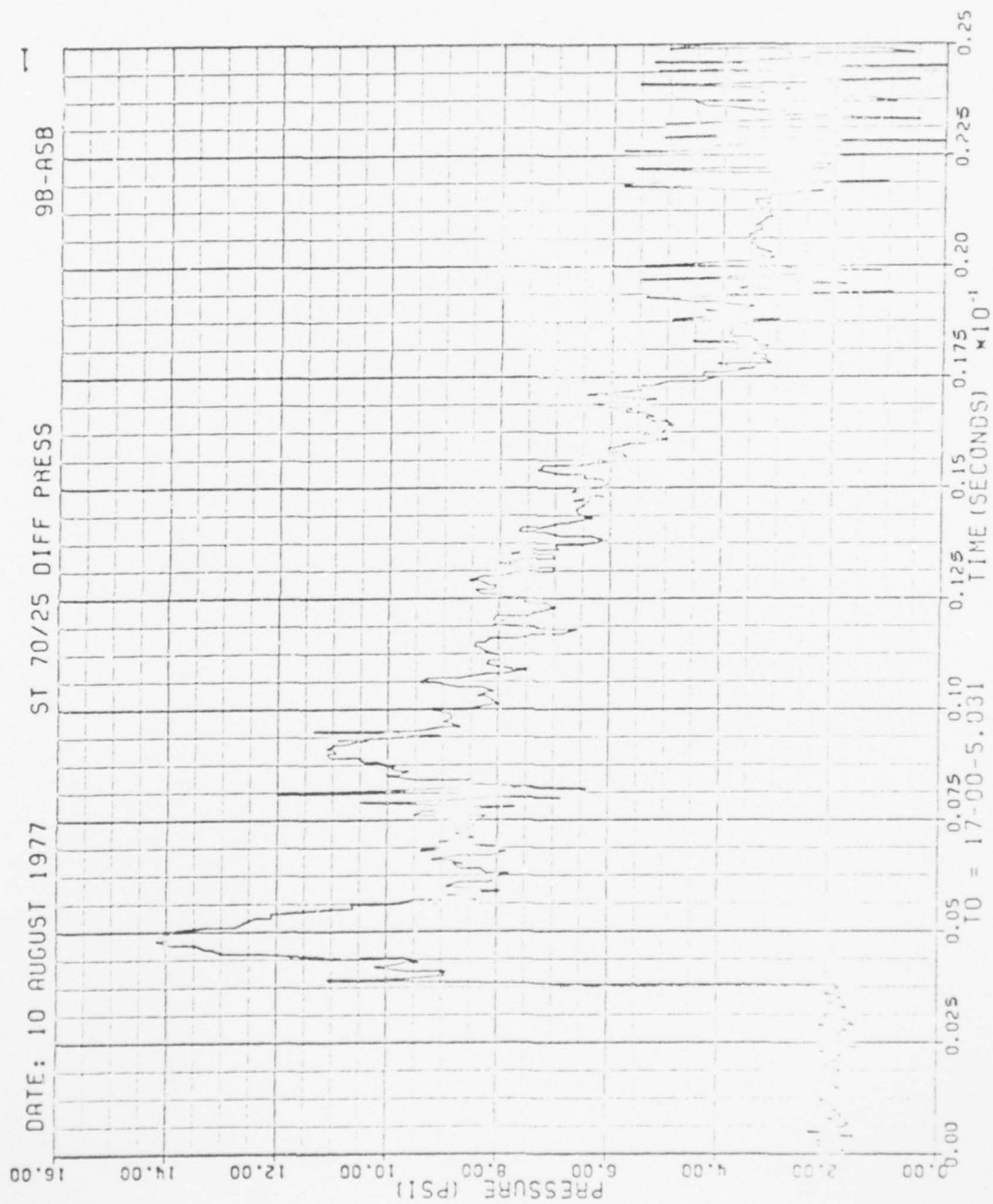


Figure 50. Continued

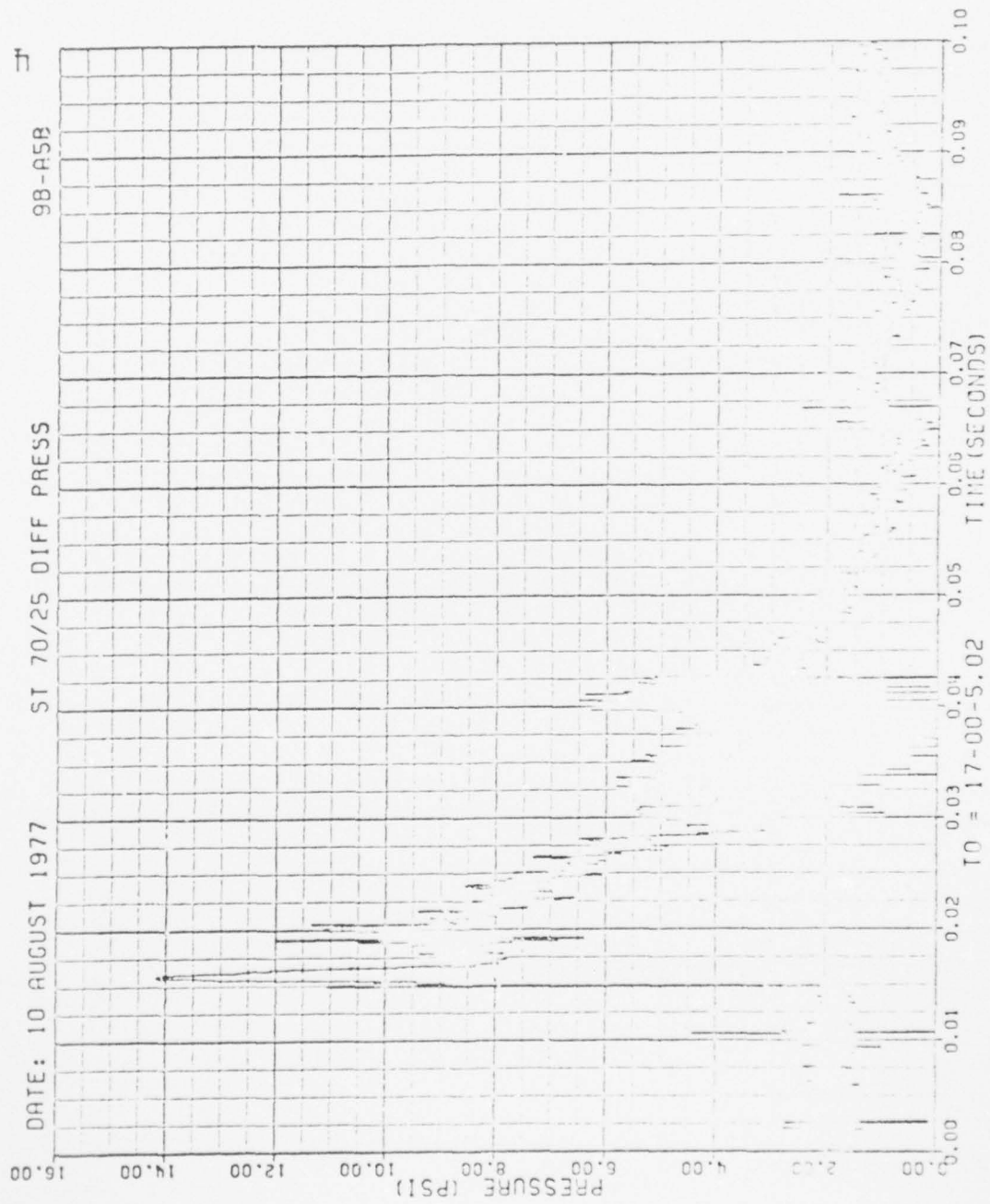


Figure 50. Continued

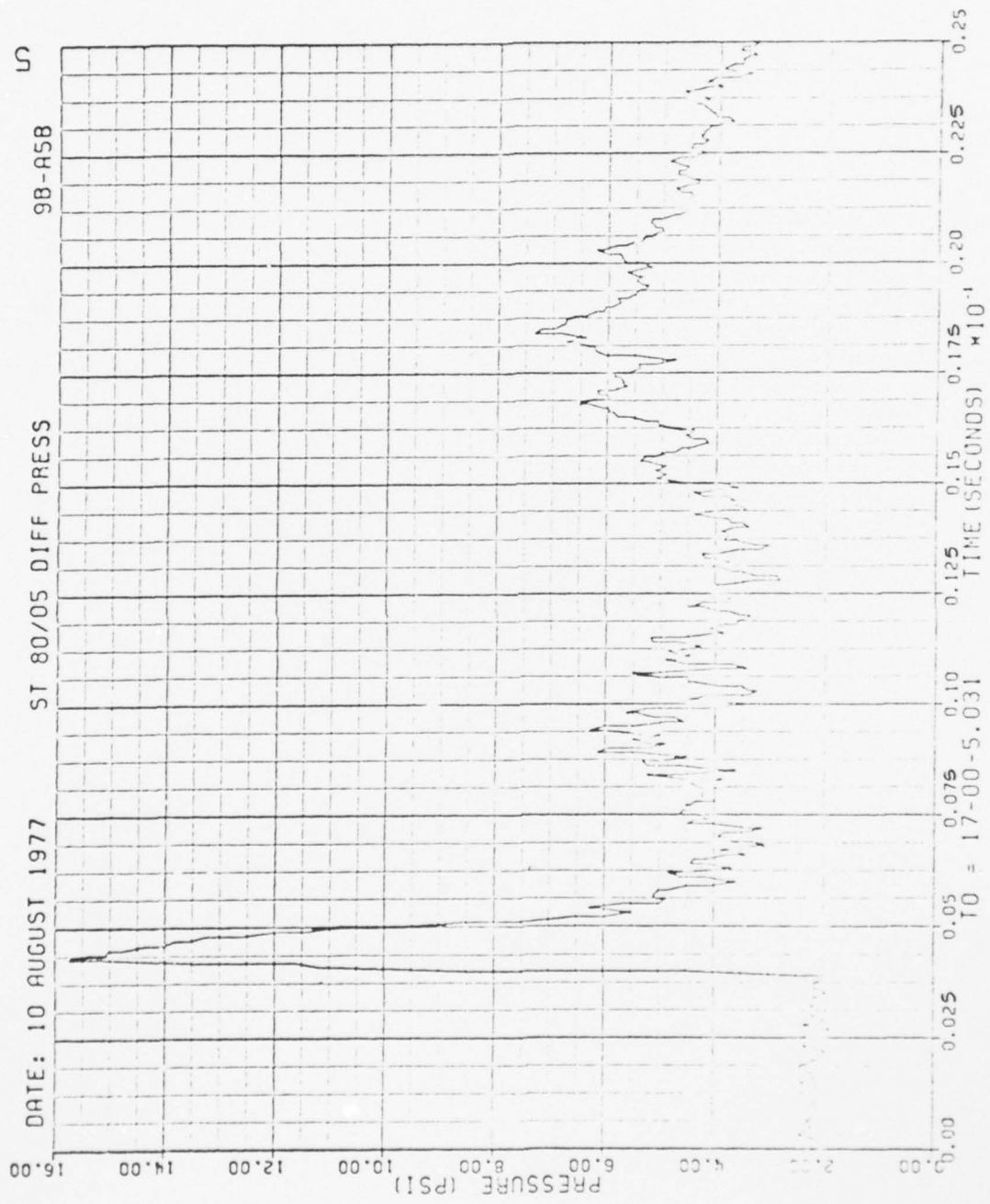


Figure 50. Continued

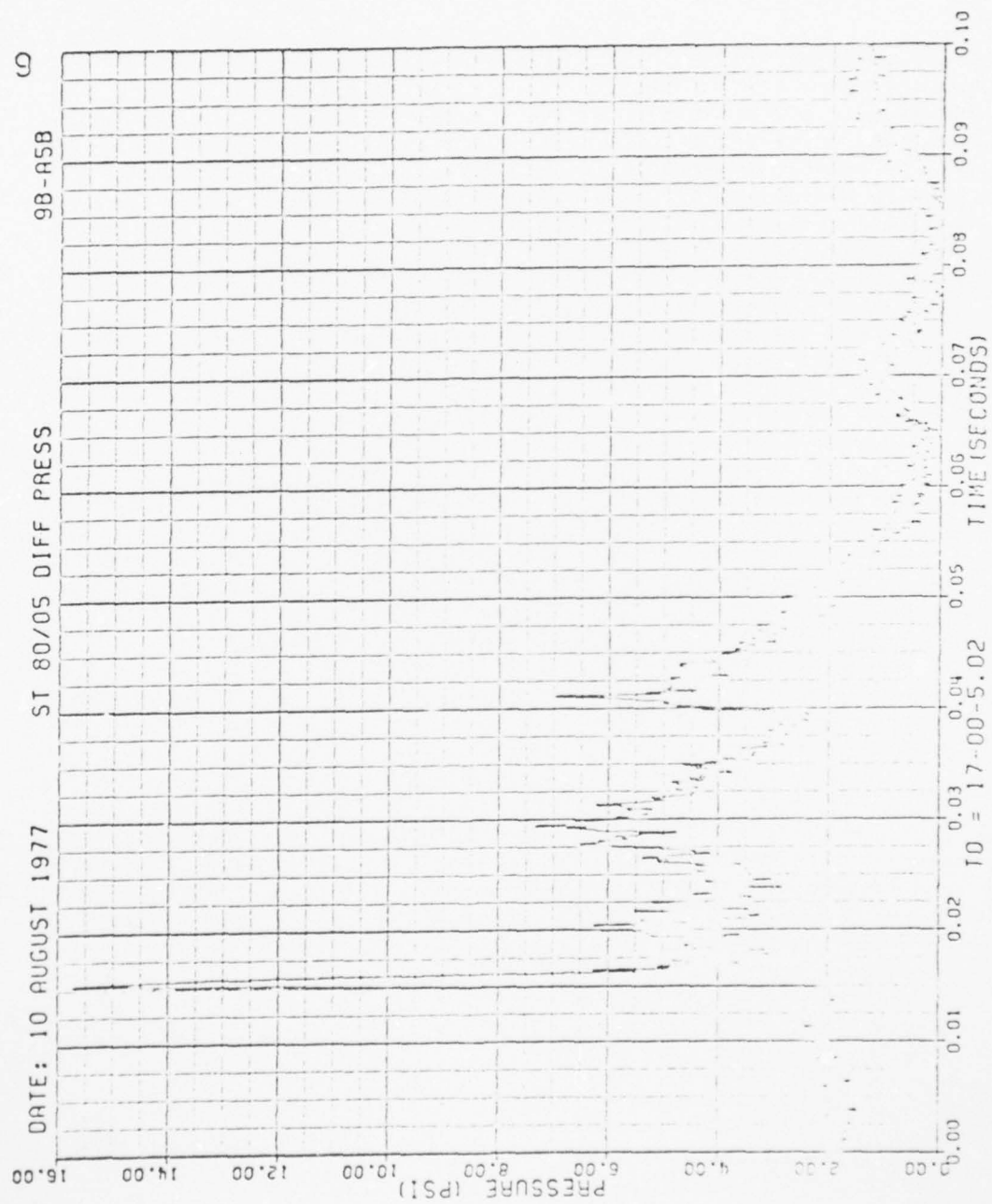


Figure 50. Continued

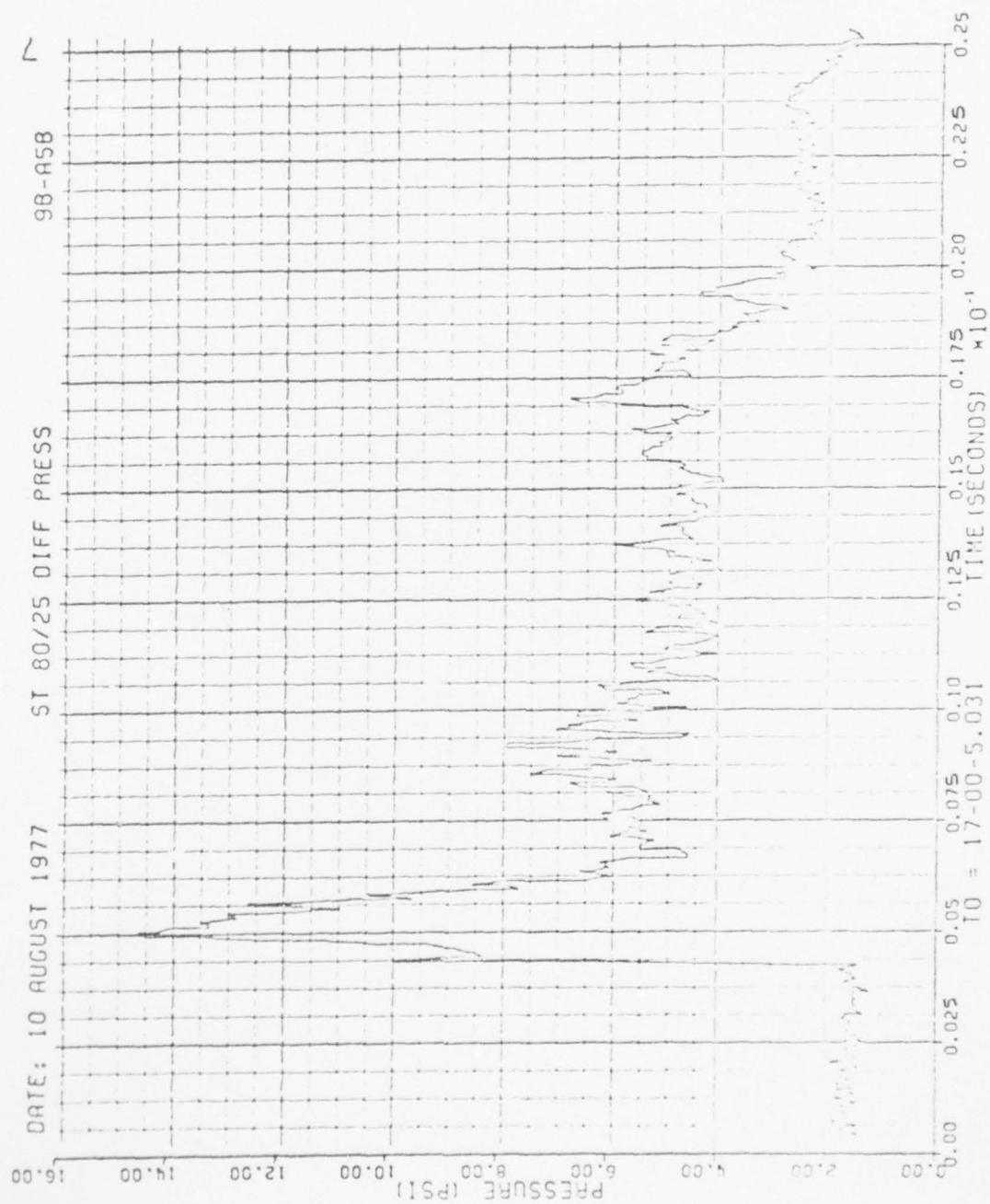


Figure 50. Continued

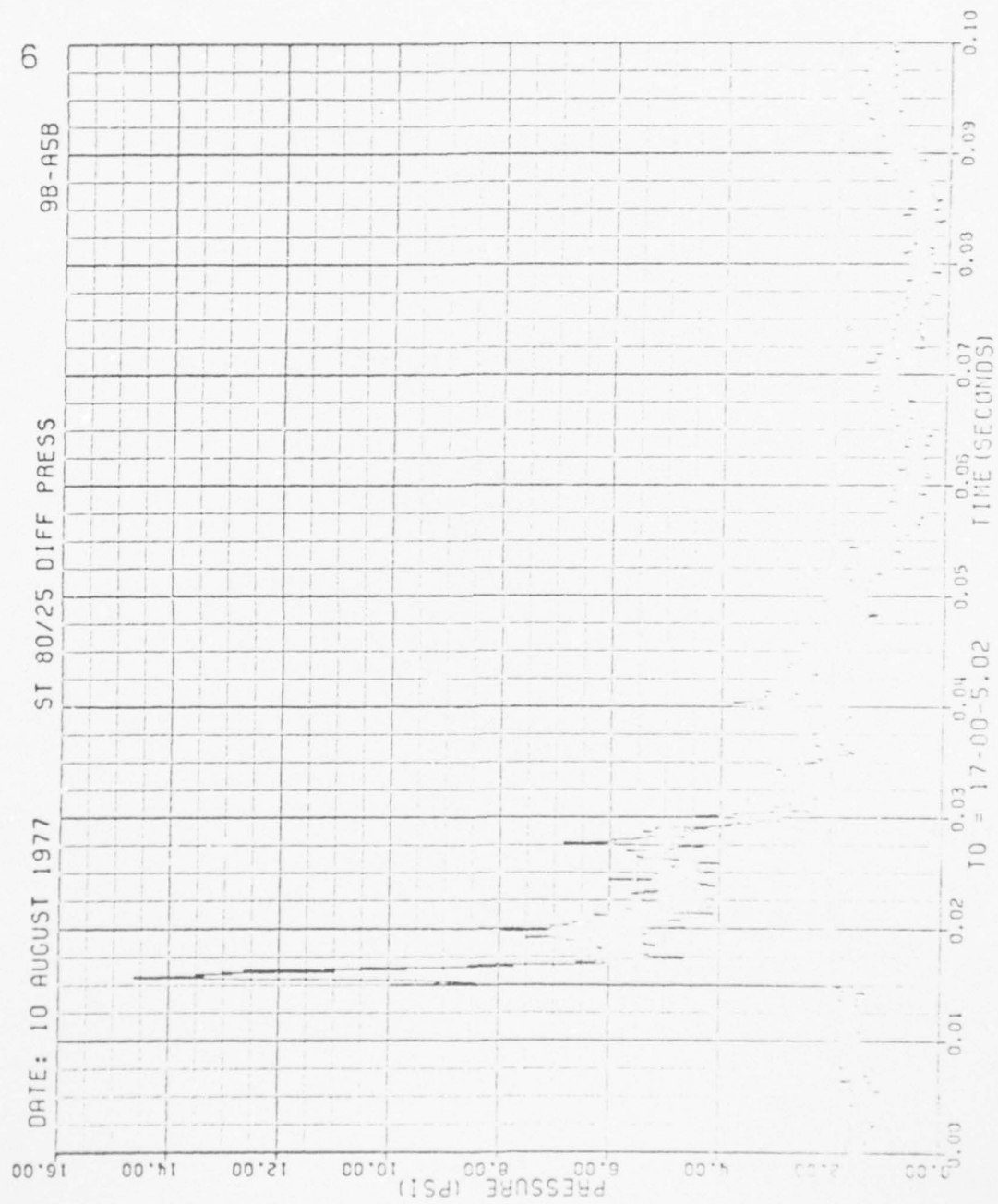


Figure 50. Continued

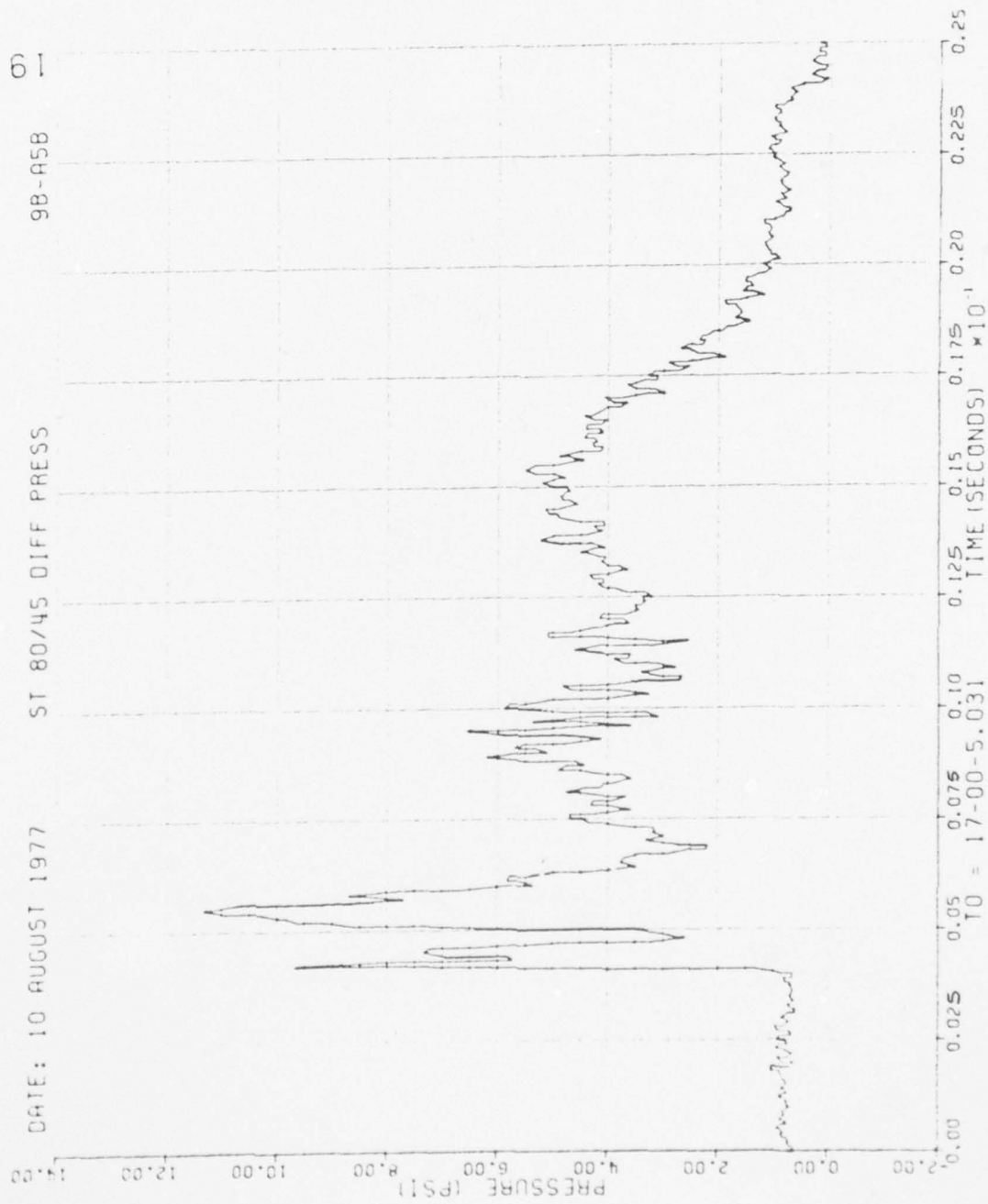


Figure 50. Continued

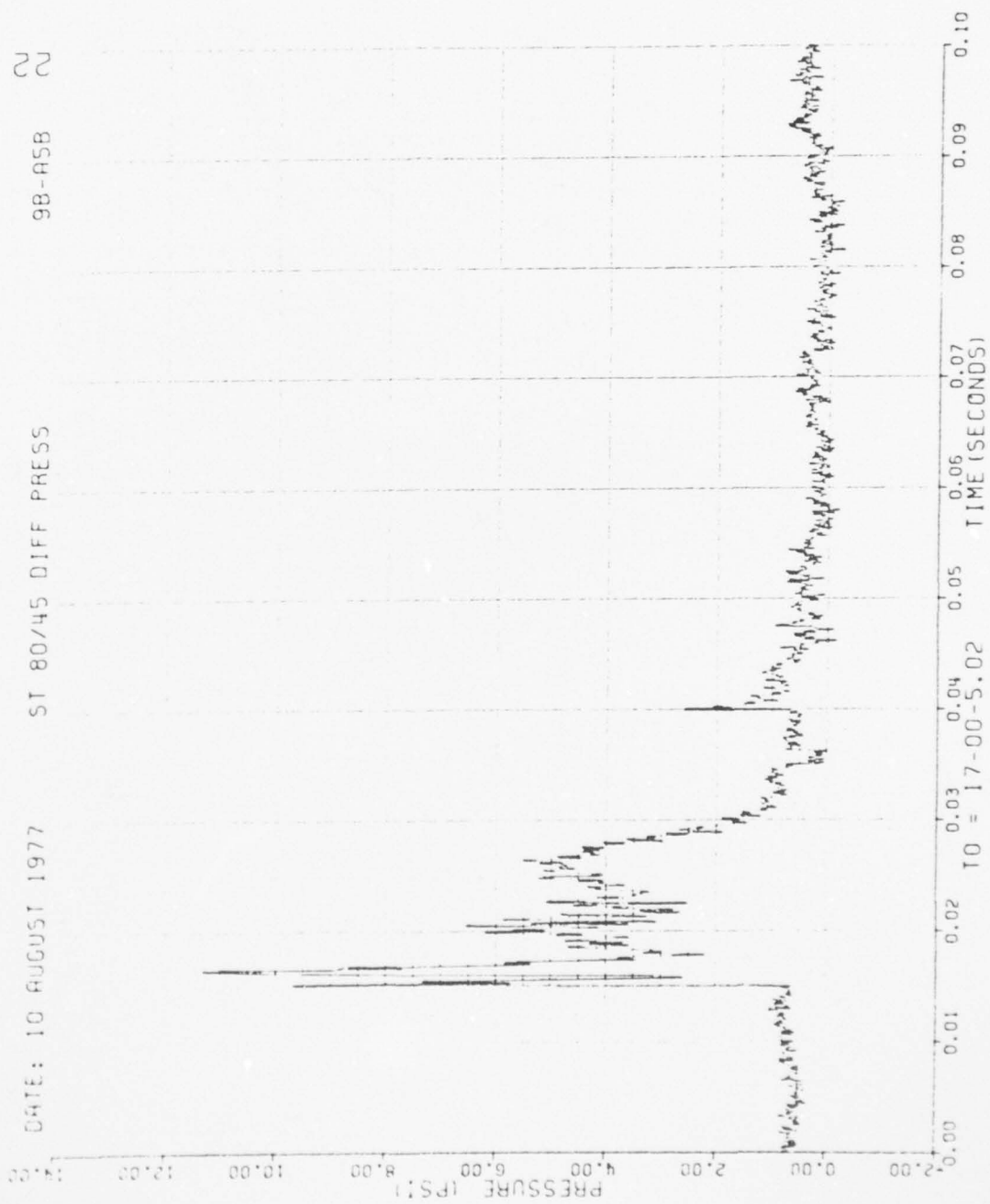


Figure 50. Continued

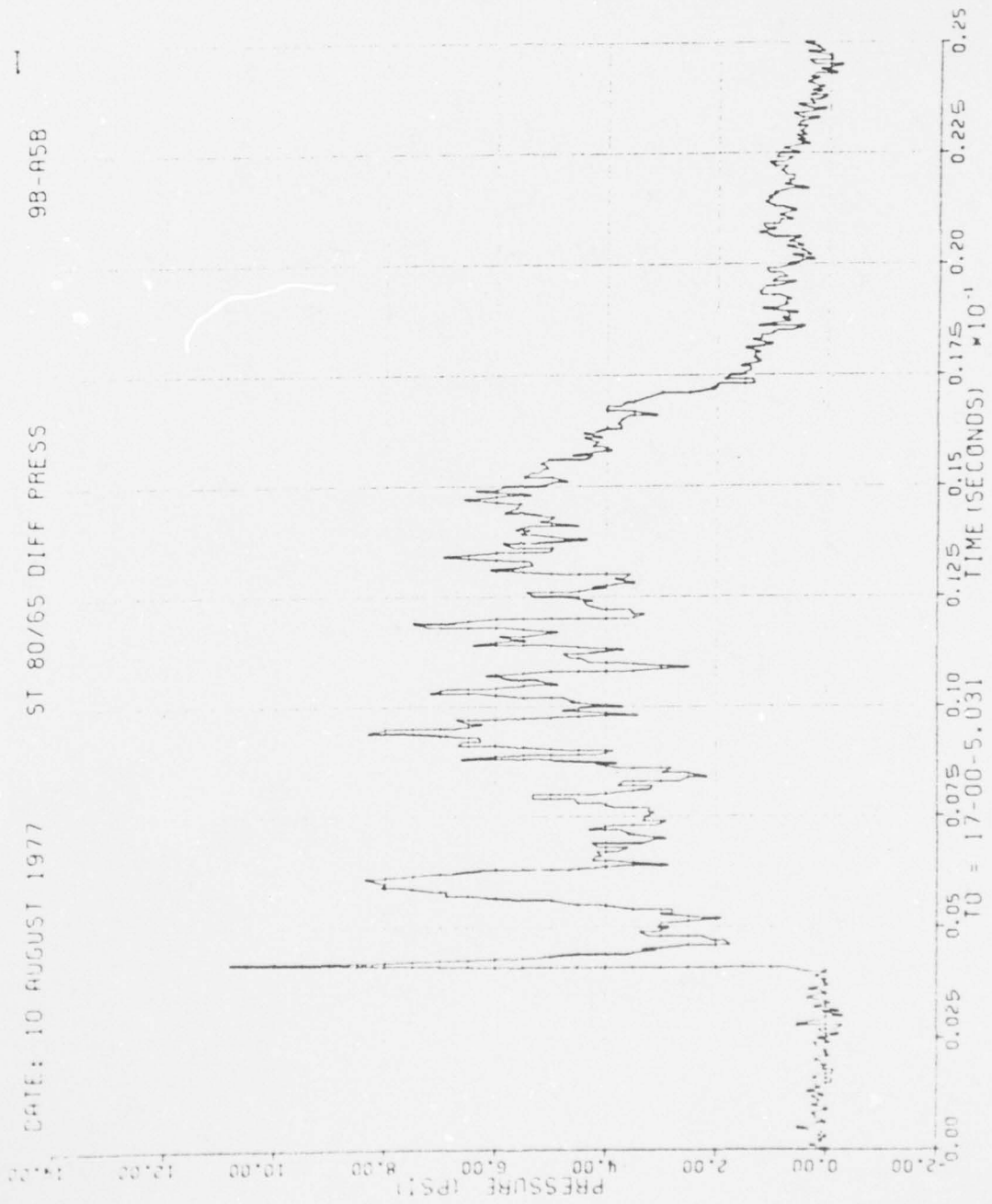


Figure 50. Continued

AD-A062 408

KAMAN AVIDYNE BURLINGTON MASS
MEASUREMENTS OF BLAST PRESSURES ON A RIGID 65 DEG SWEPTBACK WIN--ETC(U)
JAN 78 J R RUETENIK, R F SMILEY

F/G 1/3

DNA001-76-C-0106

UNCLASSIFIED

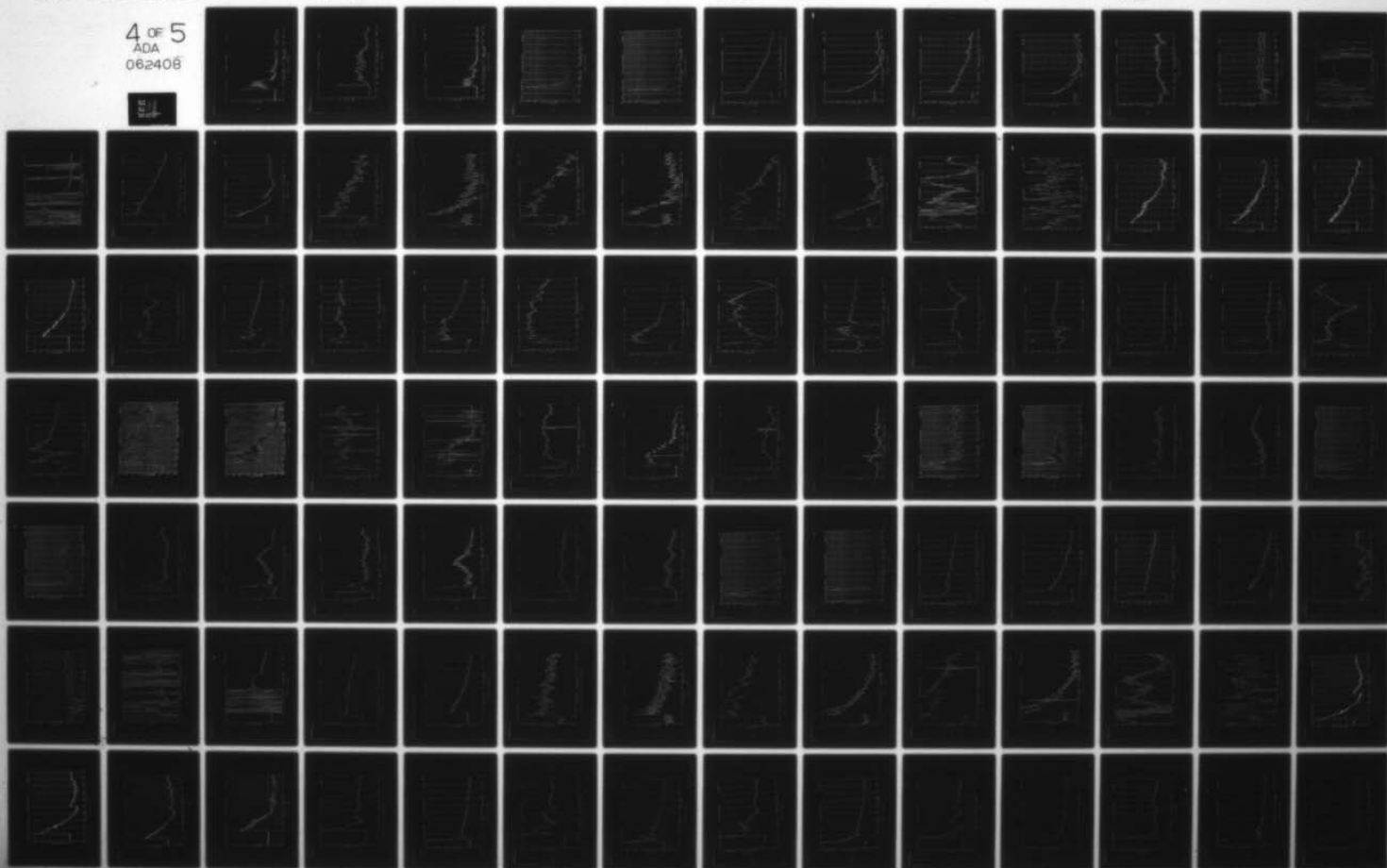
KA-TR-145

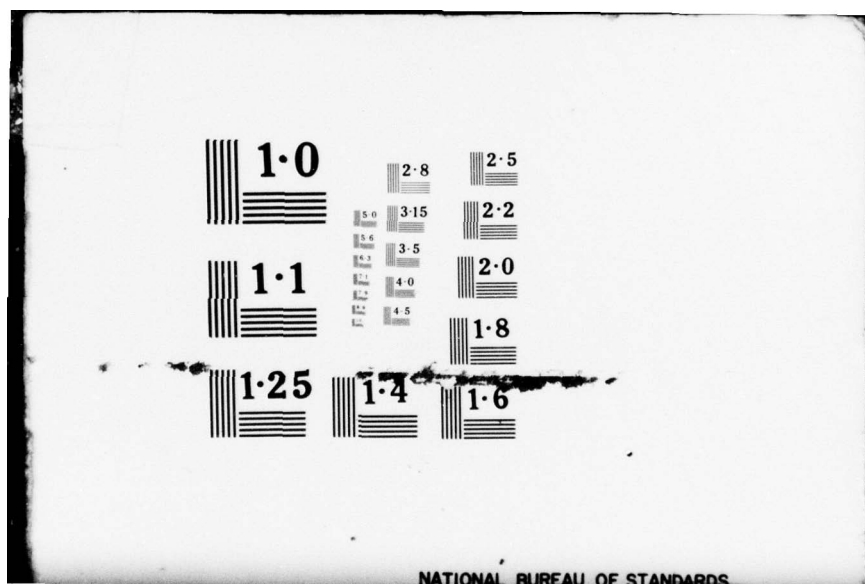
DNA-4504F

NL

4 OF 5
ADA
062408

EL





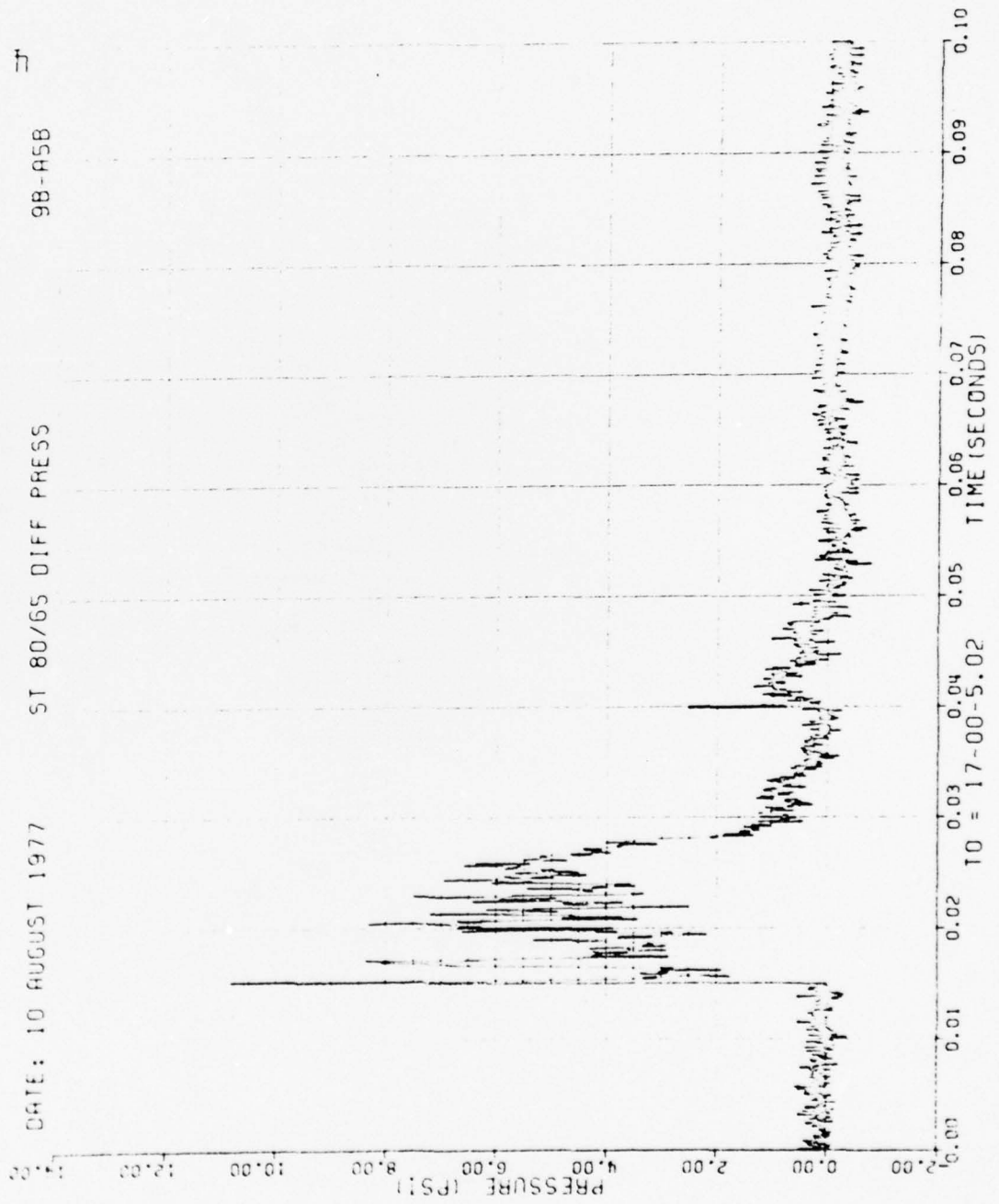


Figure 50. Continued

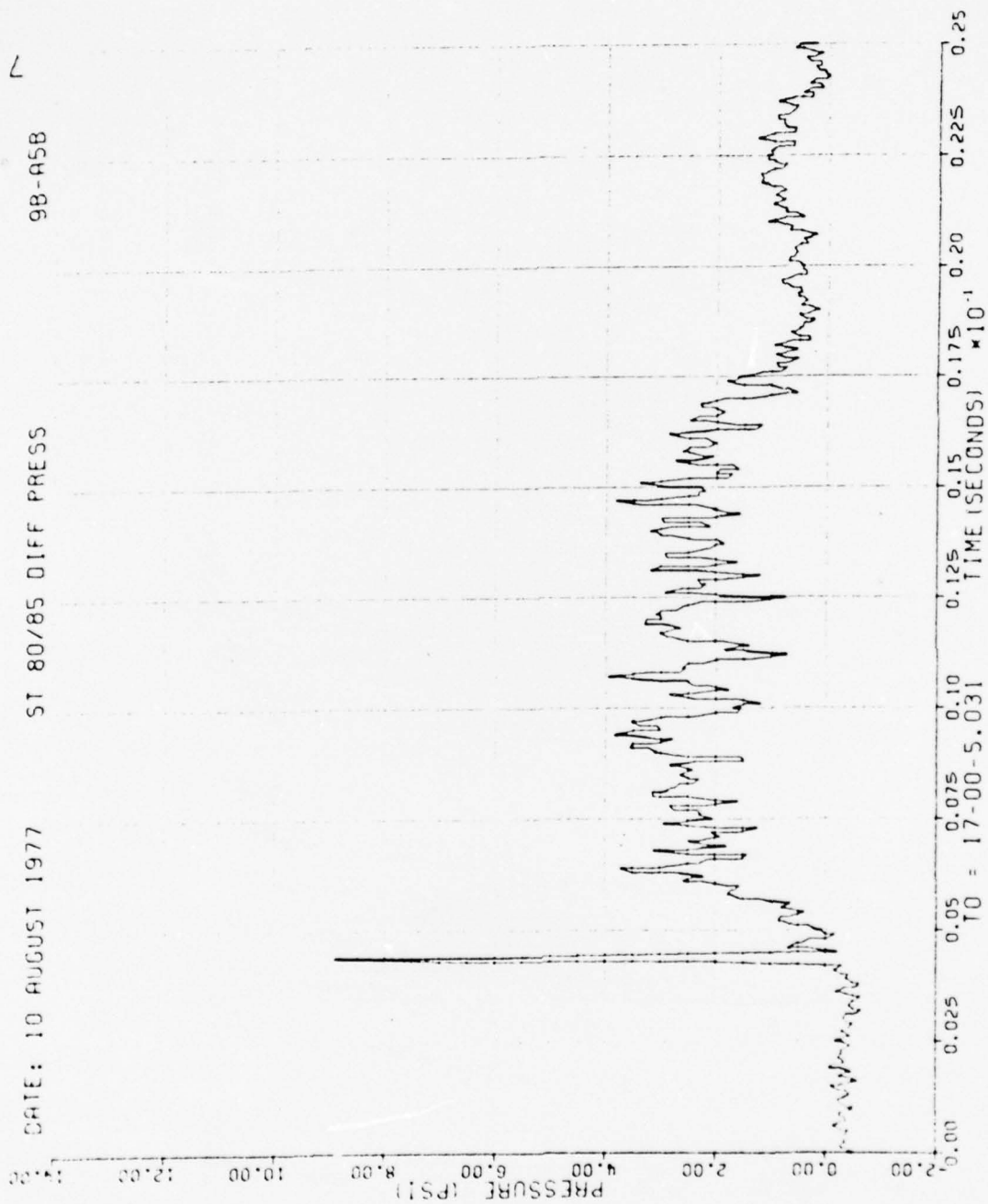


Figure 50. Continued

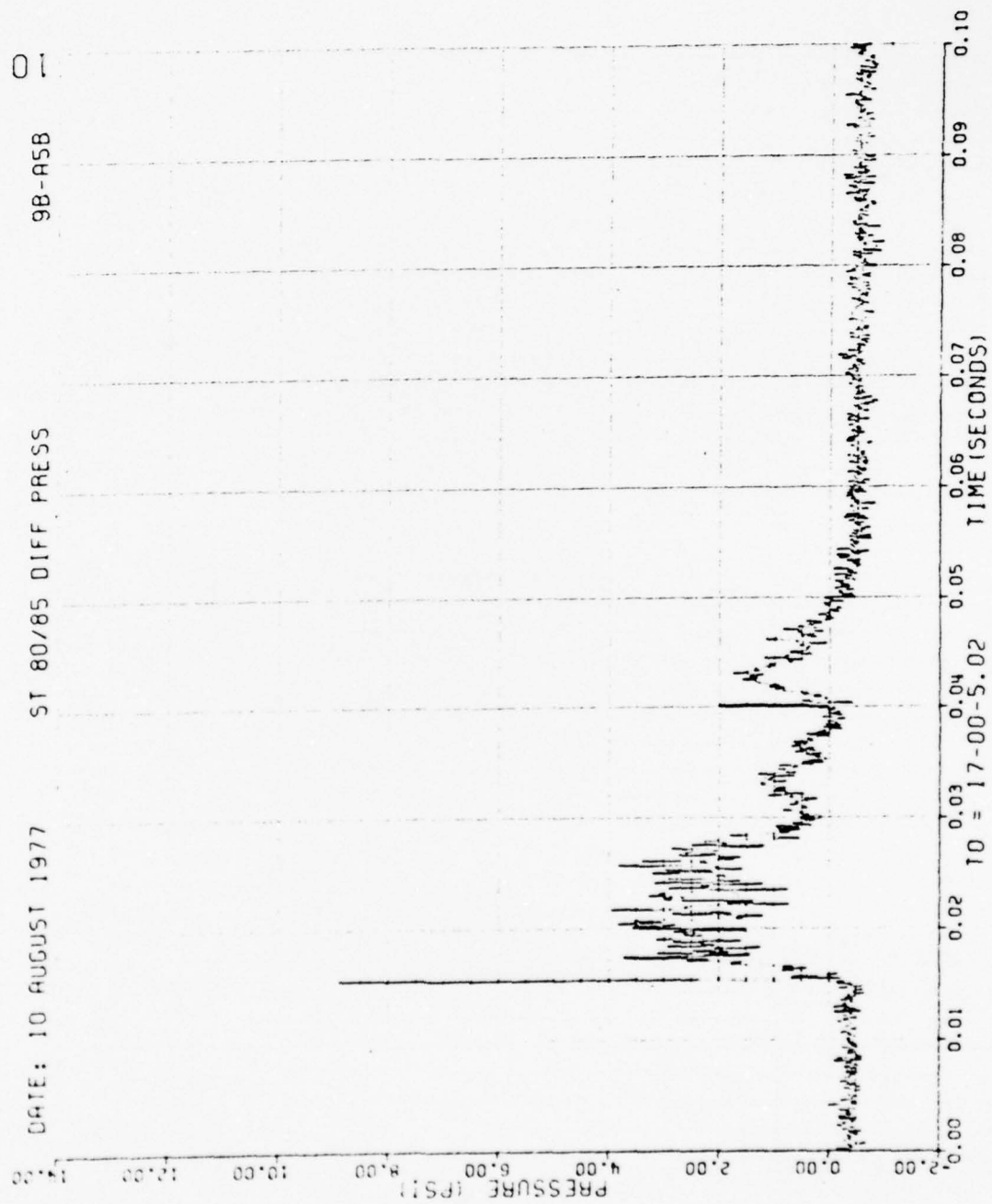


Figure 50. Continued

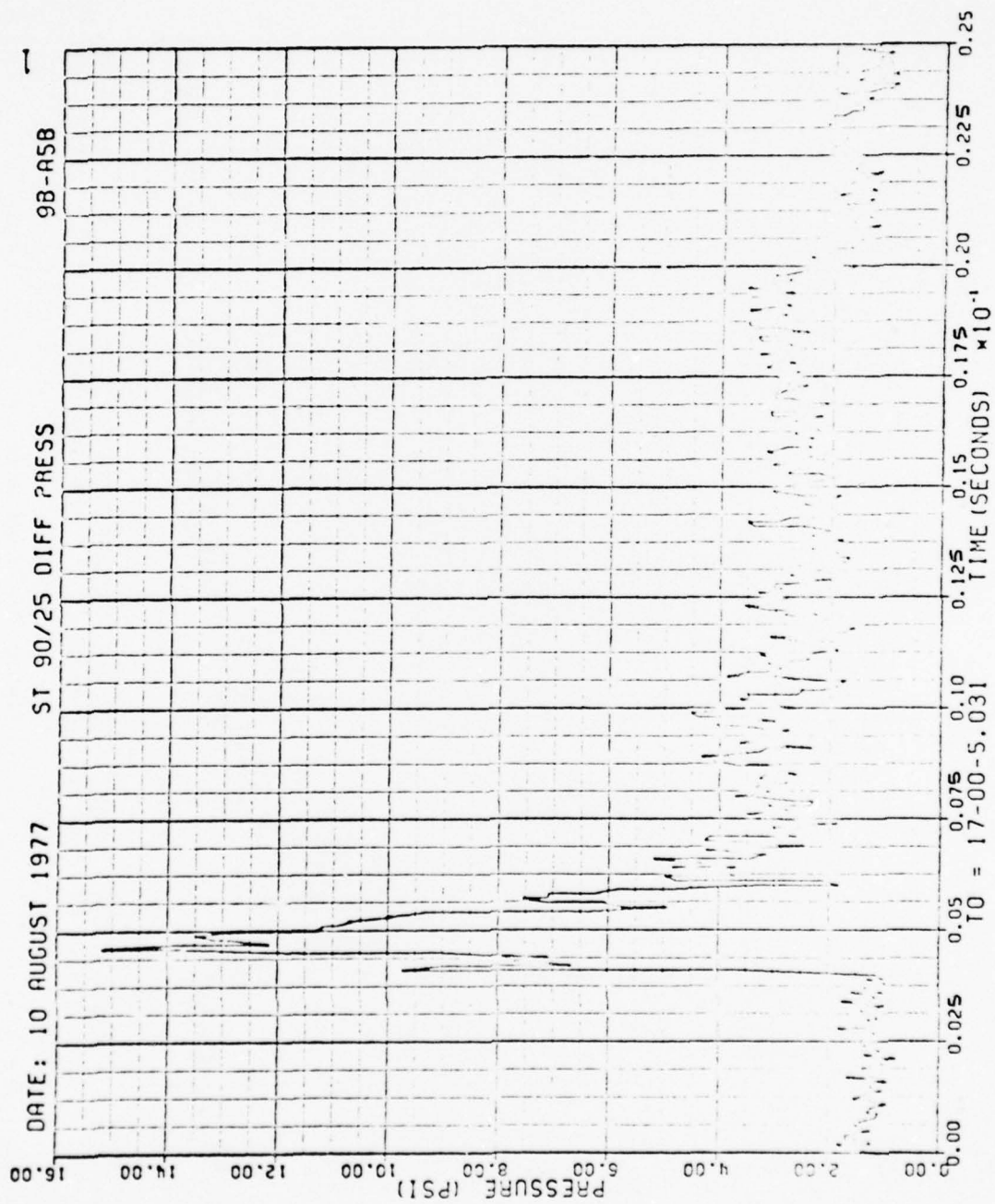


Figure 50. Continued

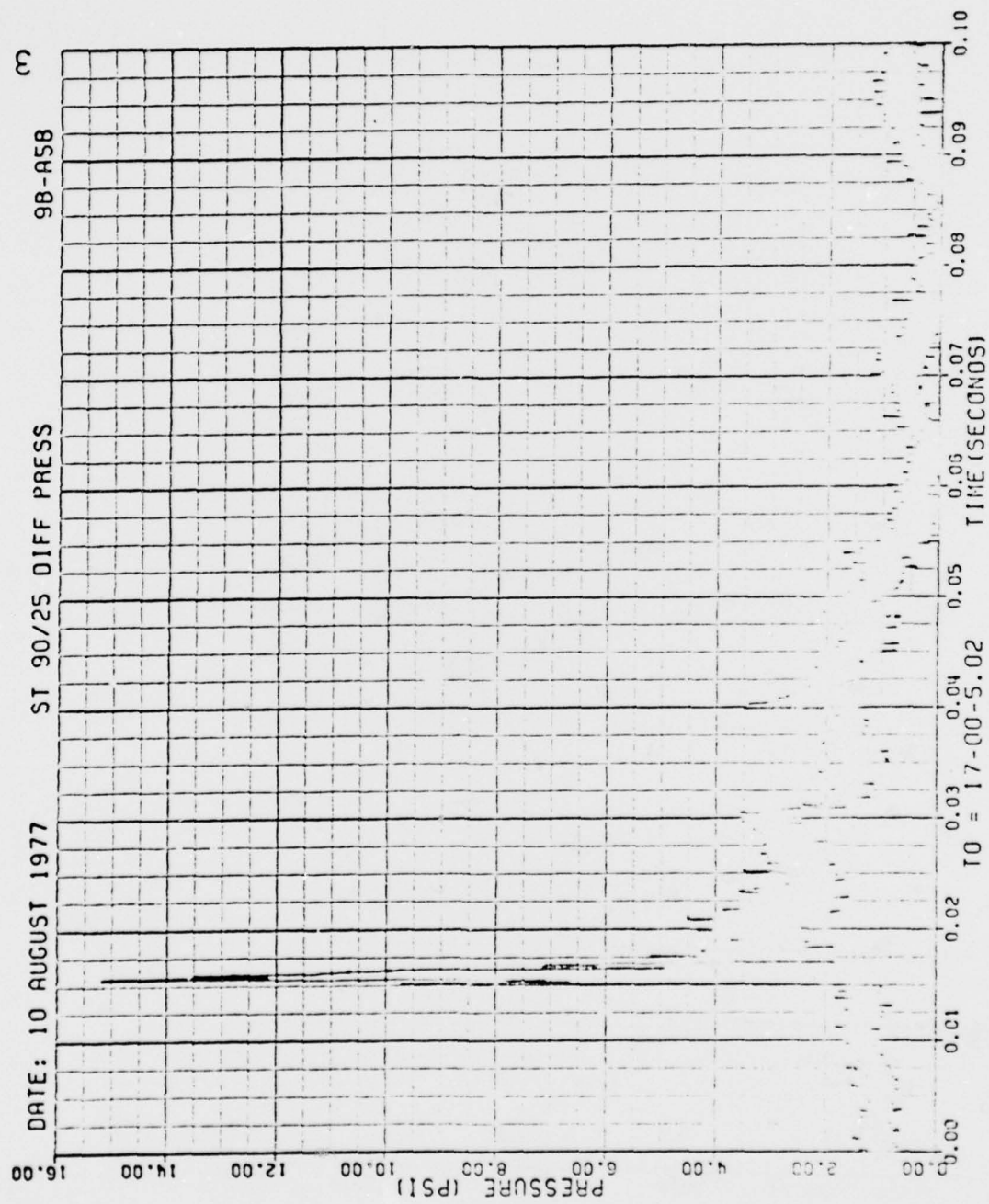


Figure 50. Concluded

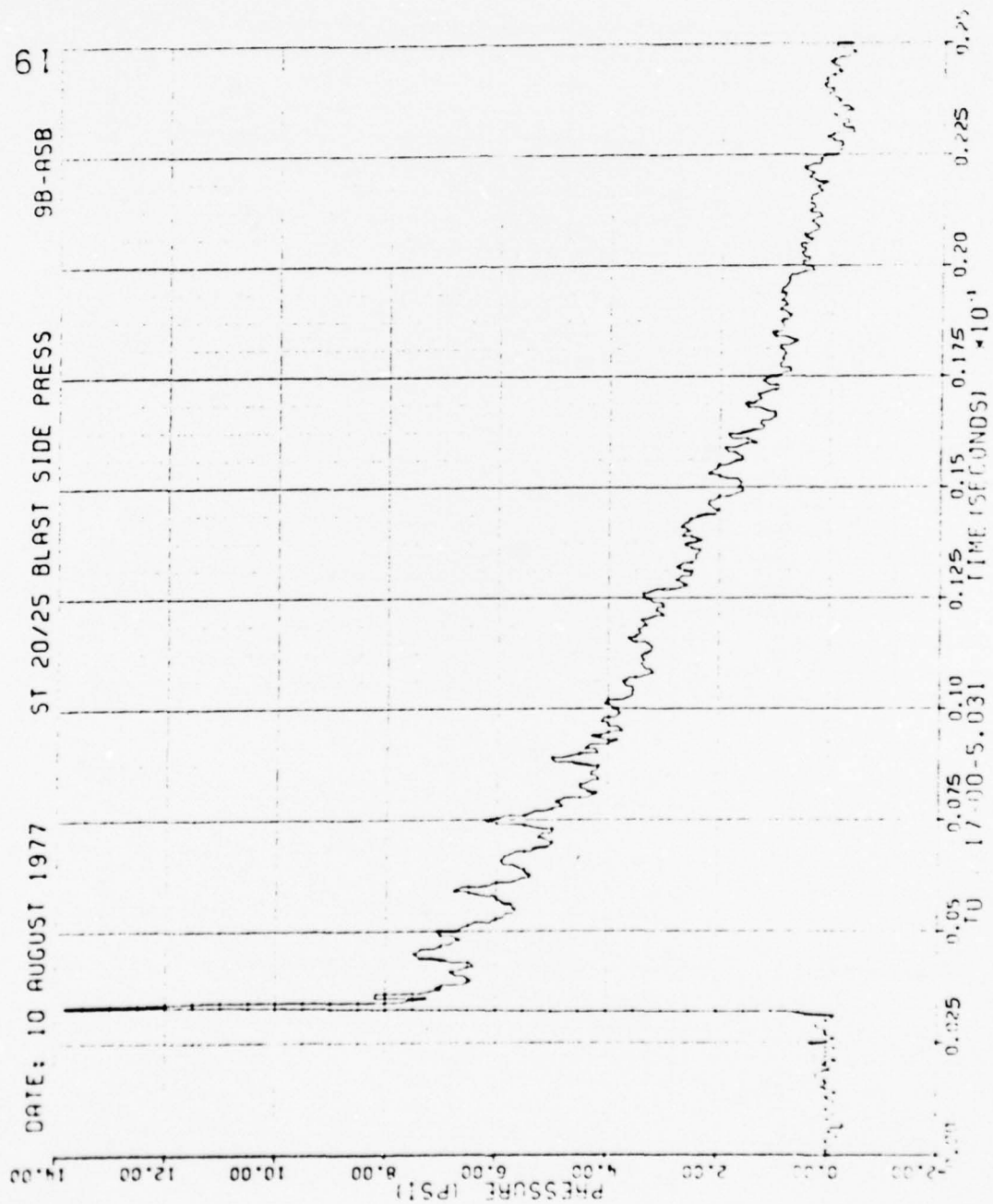


Figure 51. Blastward and Leeward Wing Pressures, Run 9B-A5, Intercept 1.

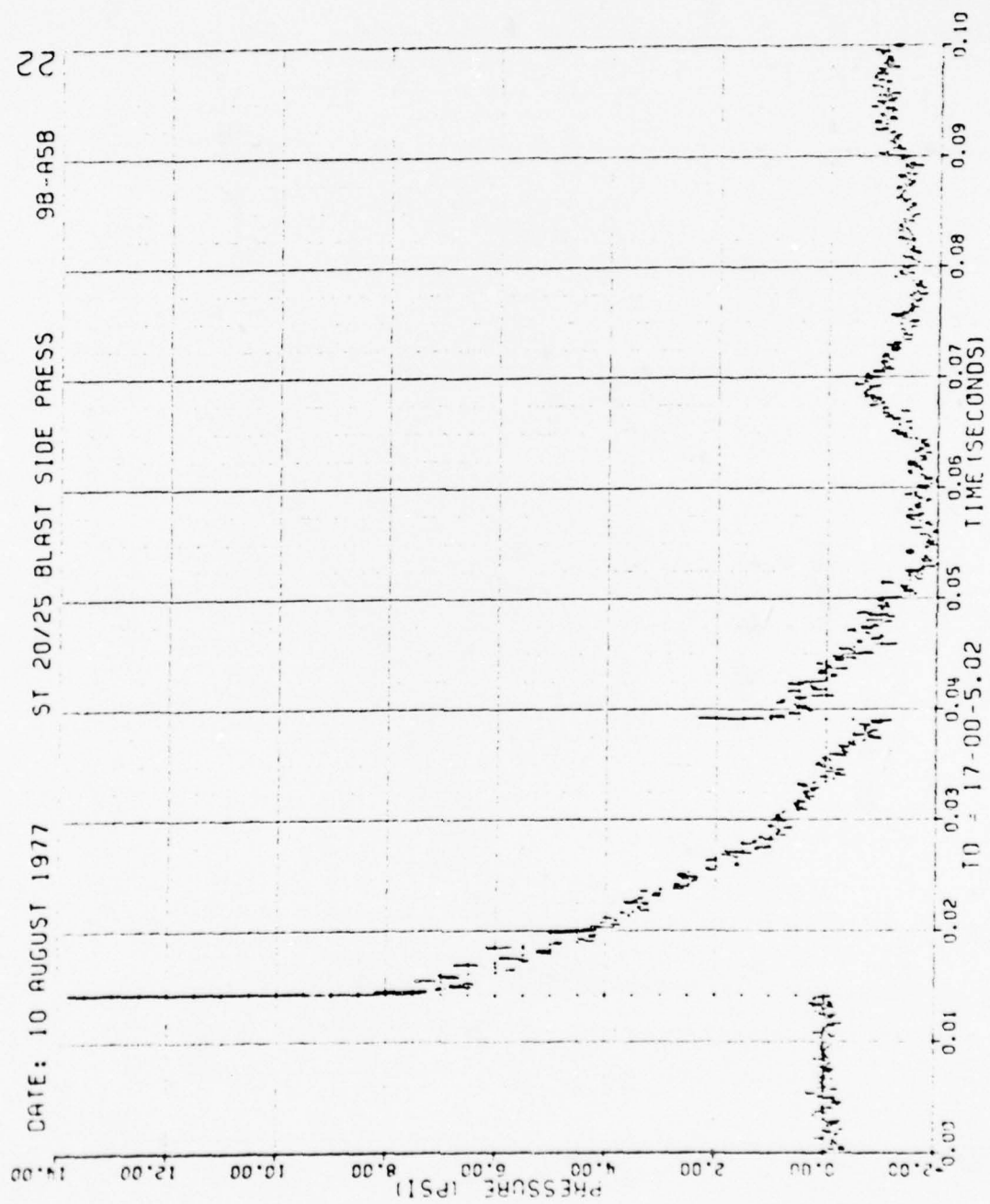


Figure 51. Continued

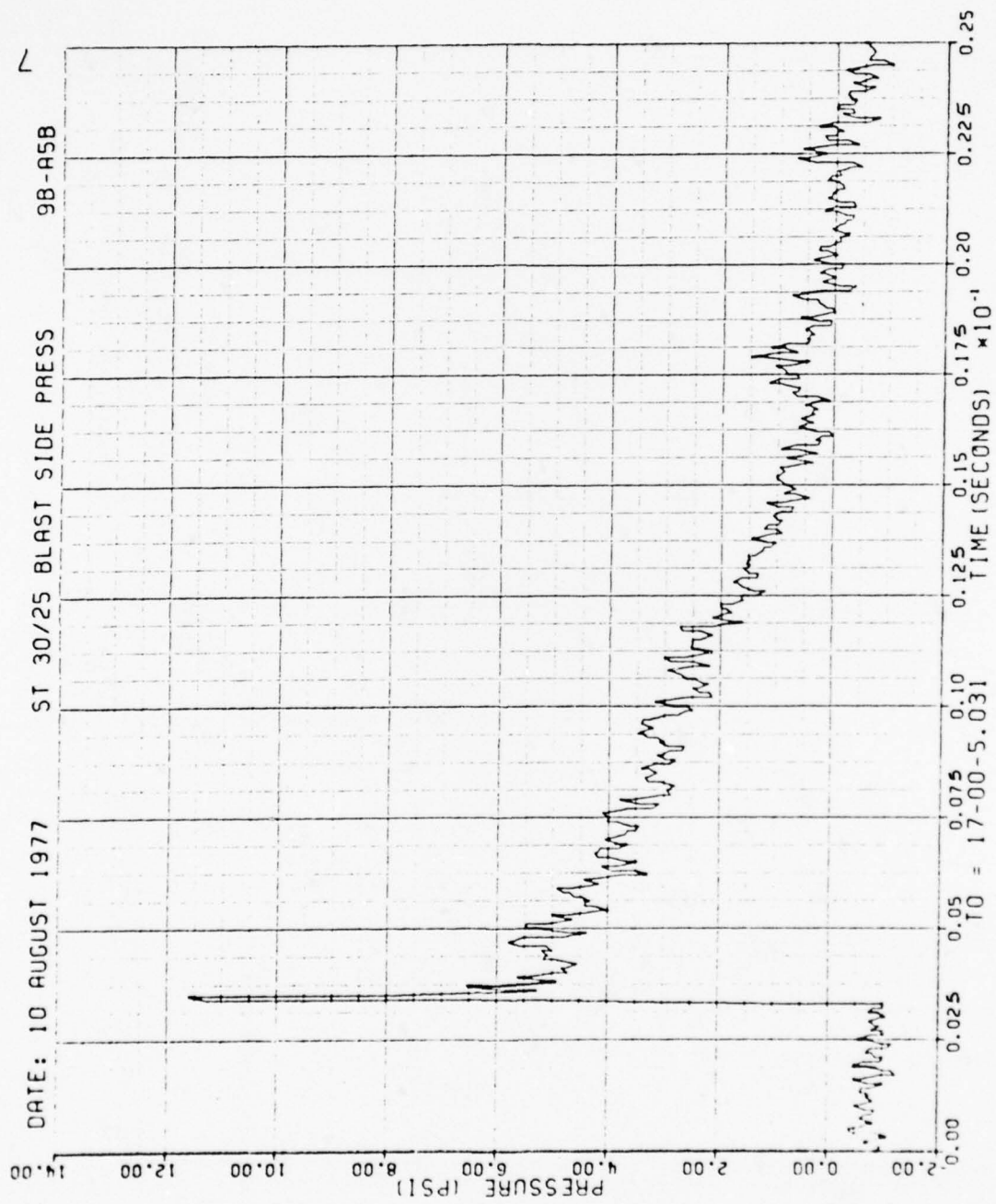


Figure 51. Continued

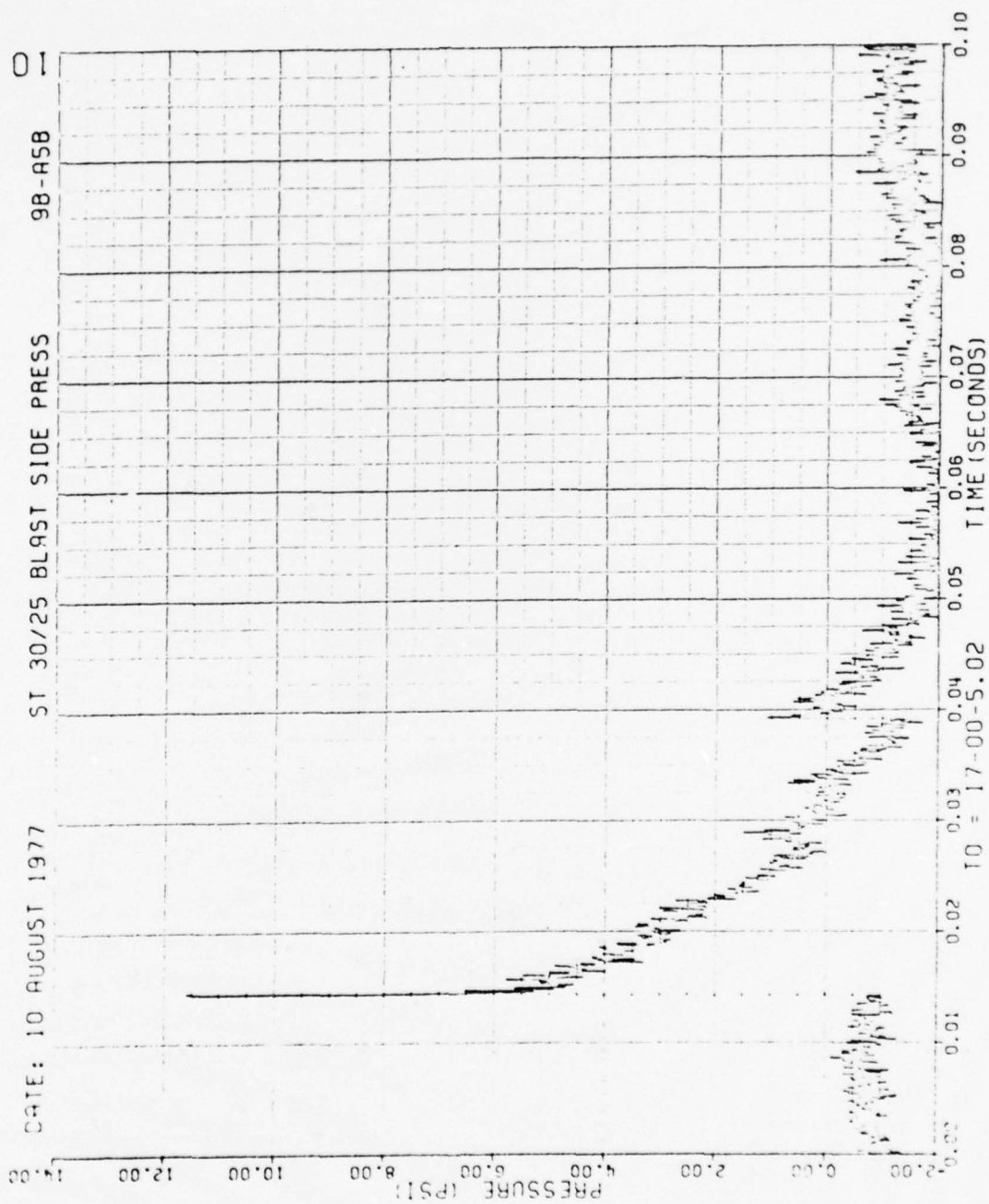


Figure 51. Continued

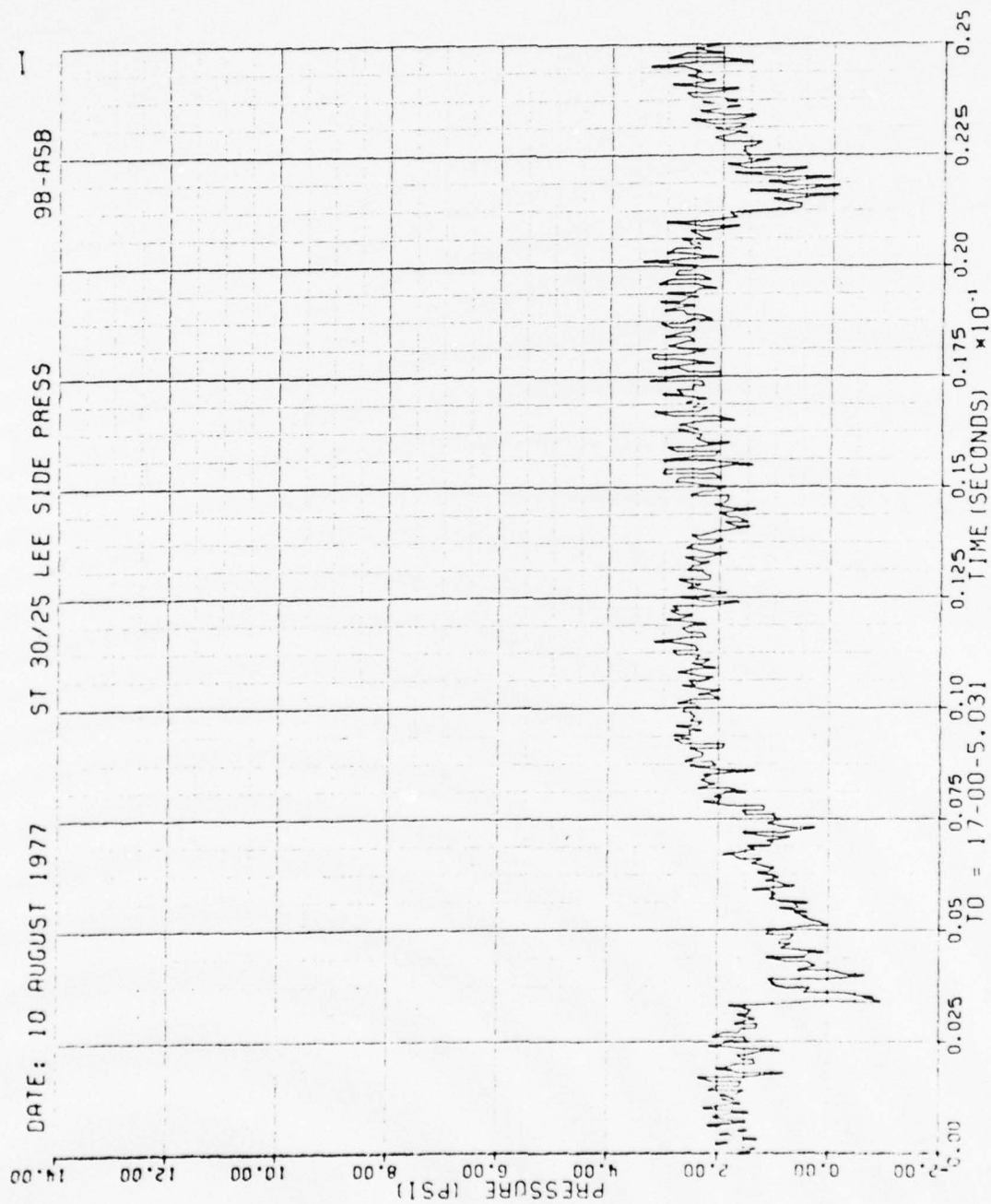


Figure 51. Continued

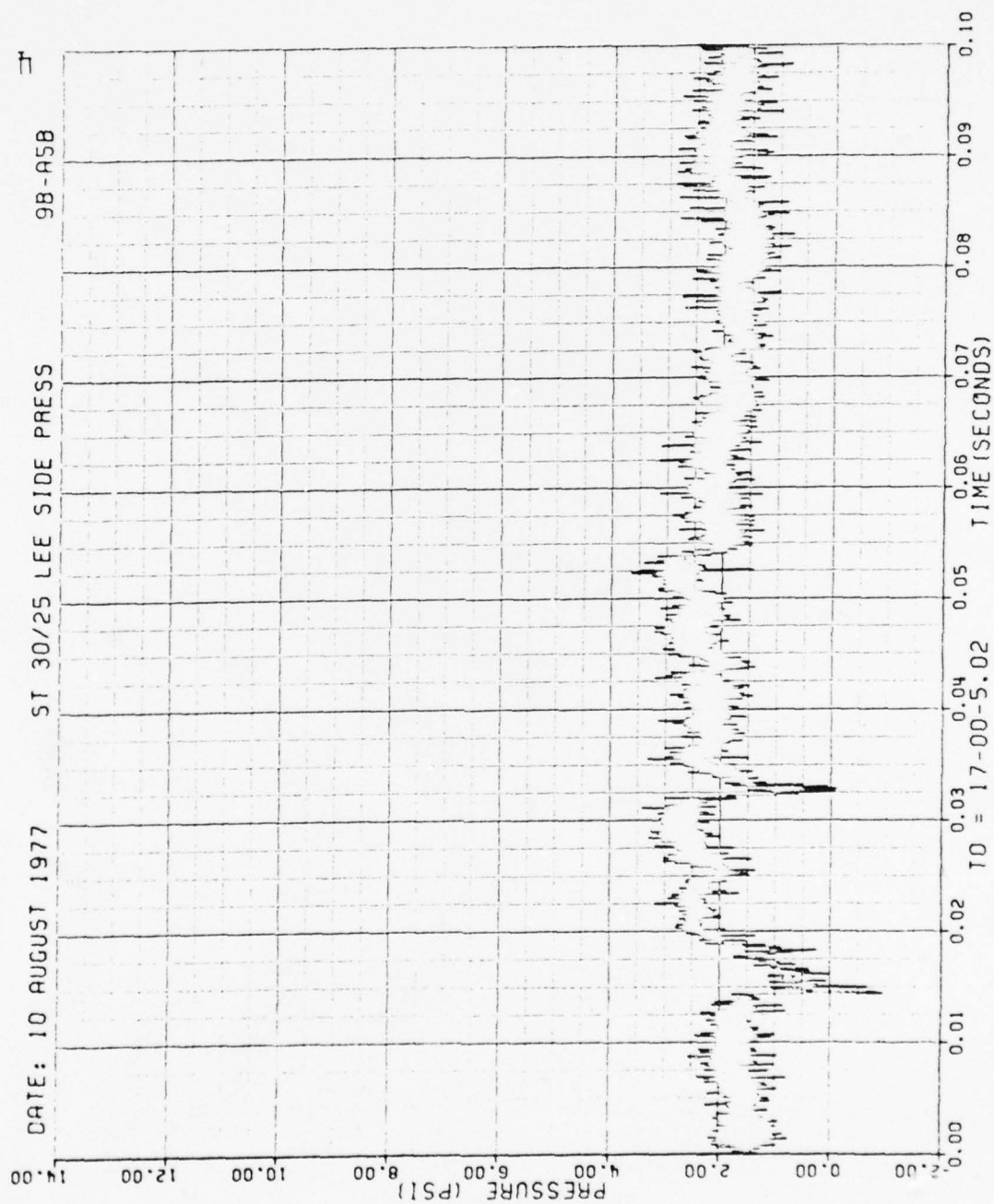


Figure 51. Continued

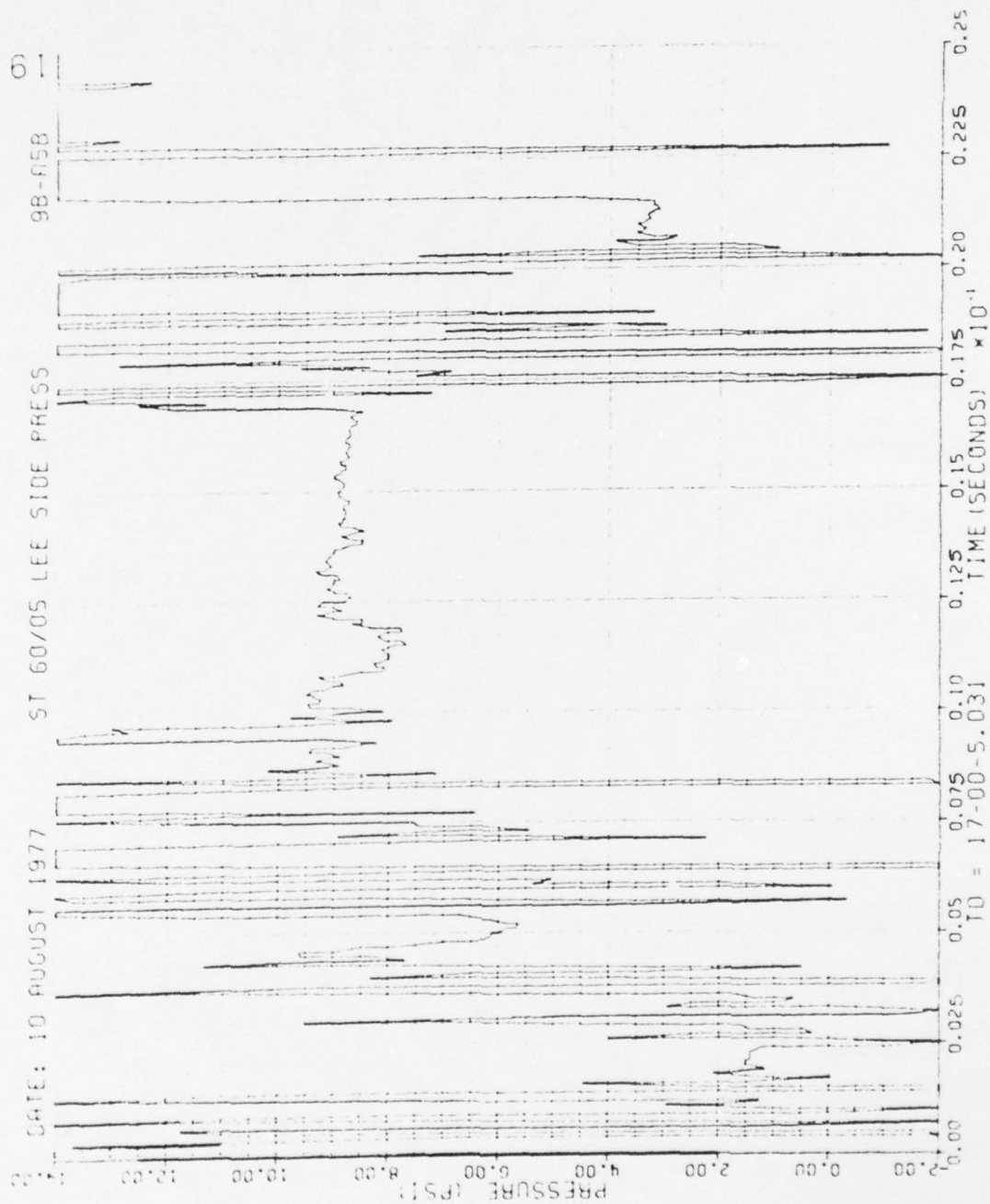


Figure 5L. Continued

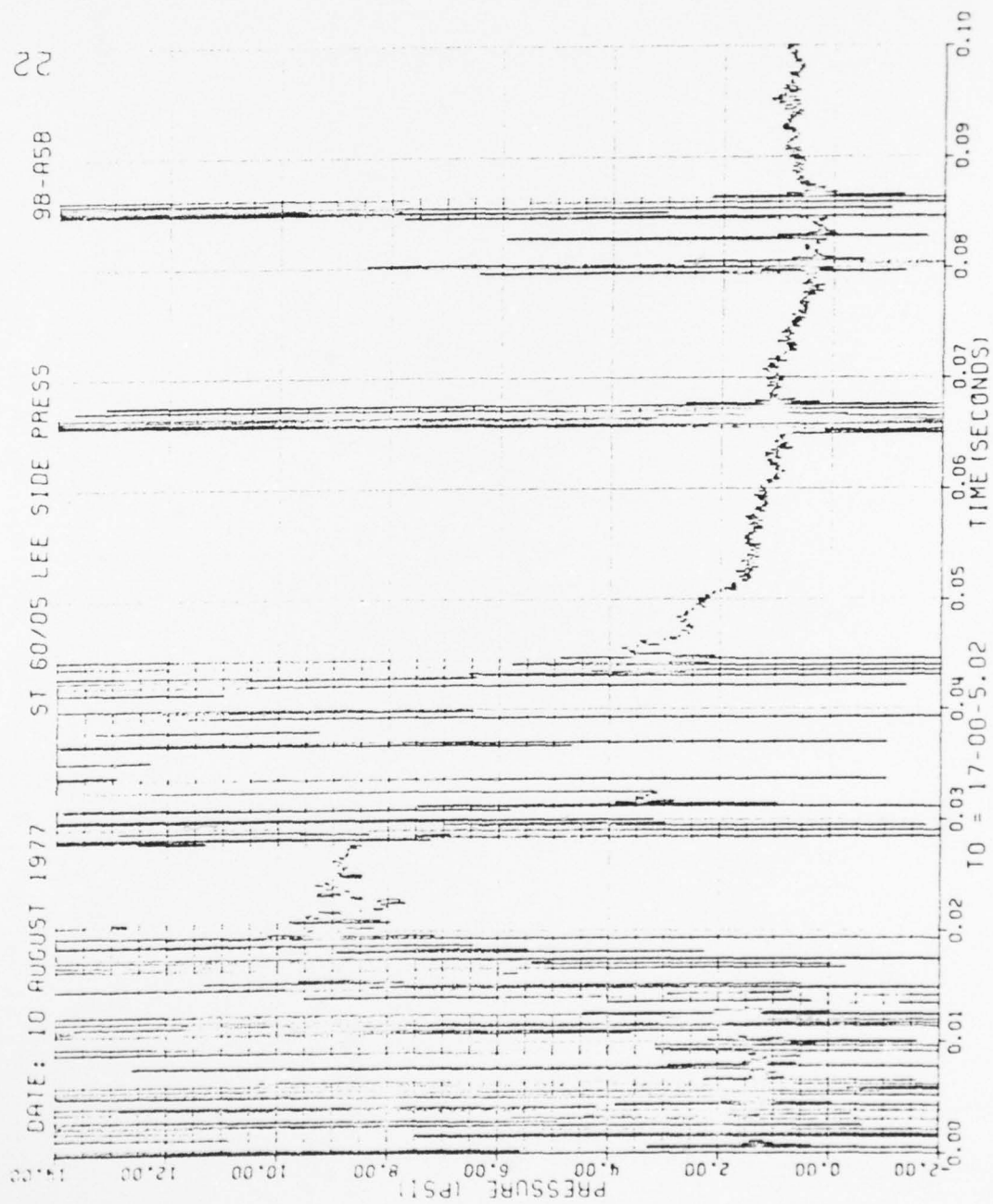


Figure 51. Concluded

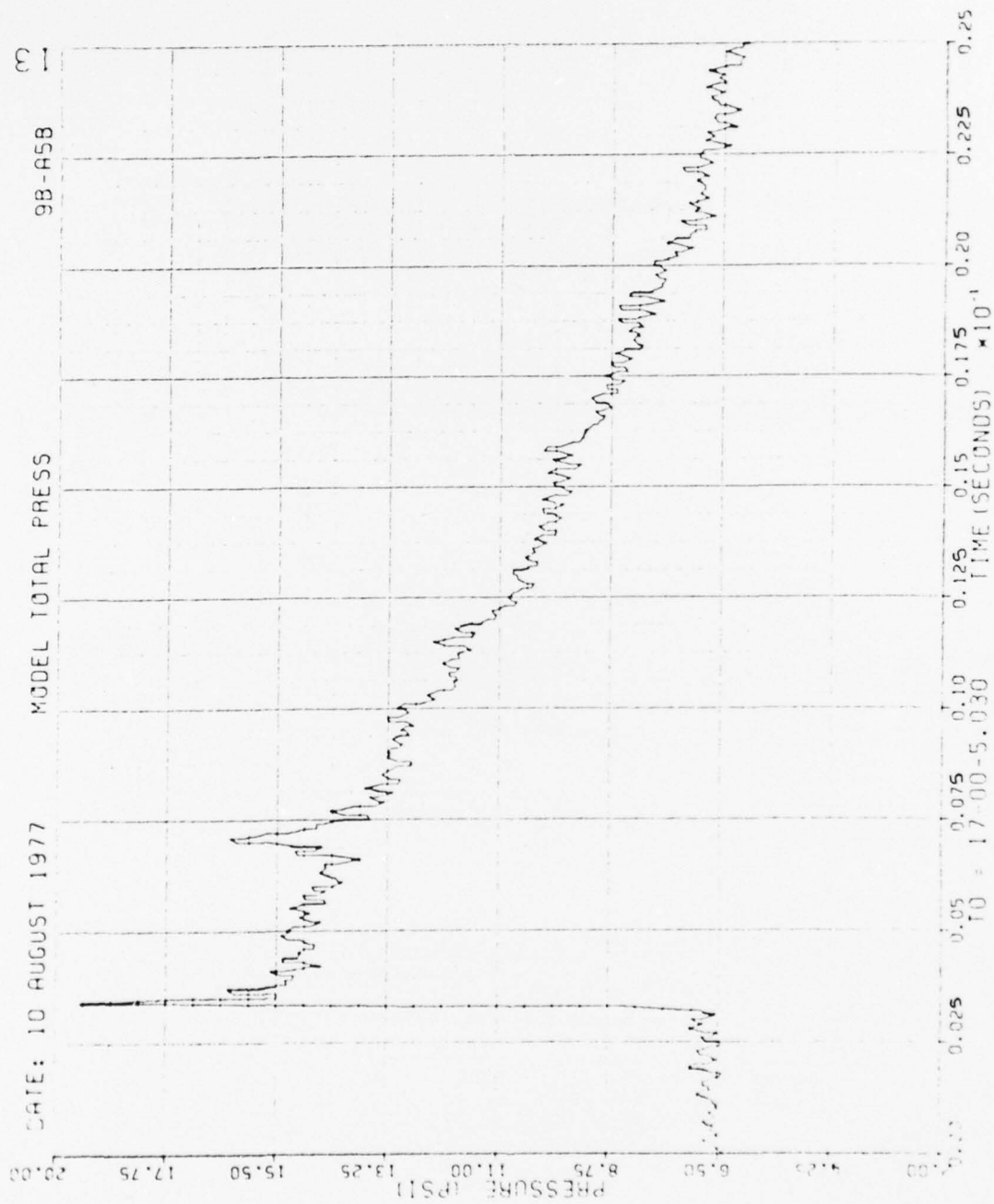


Figure 52. Total Pressure at Model, Run 9B-A5, Intercept 1.

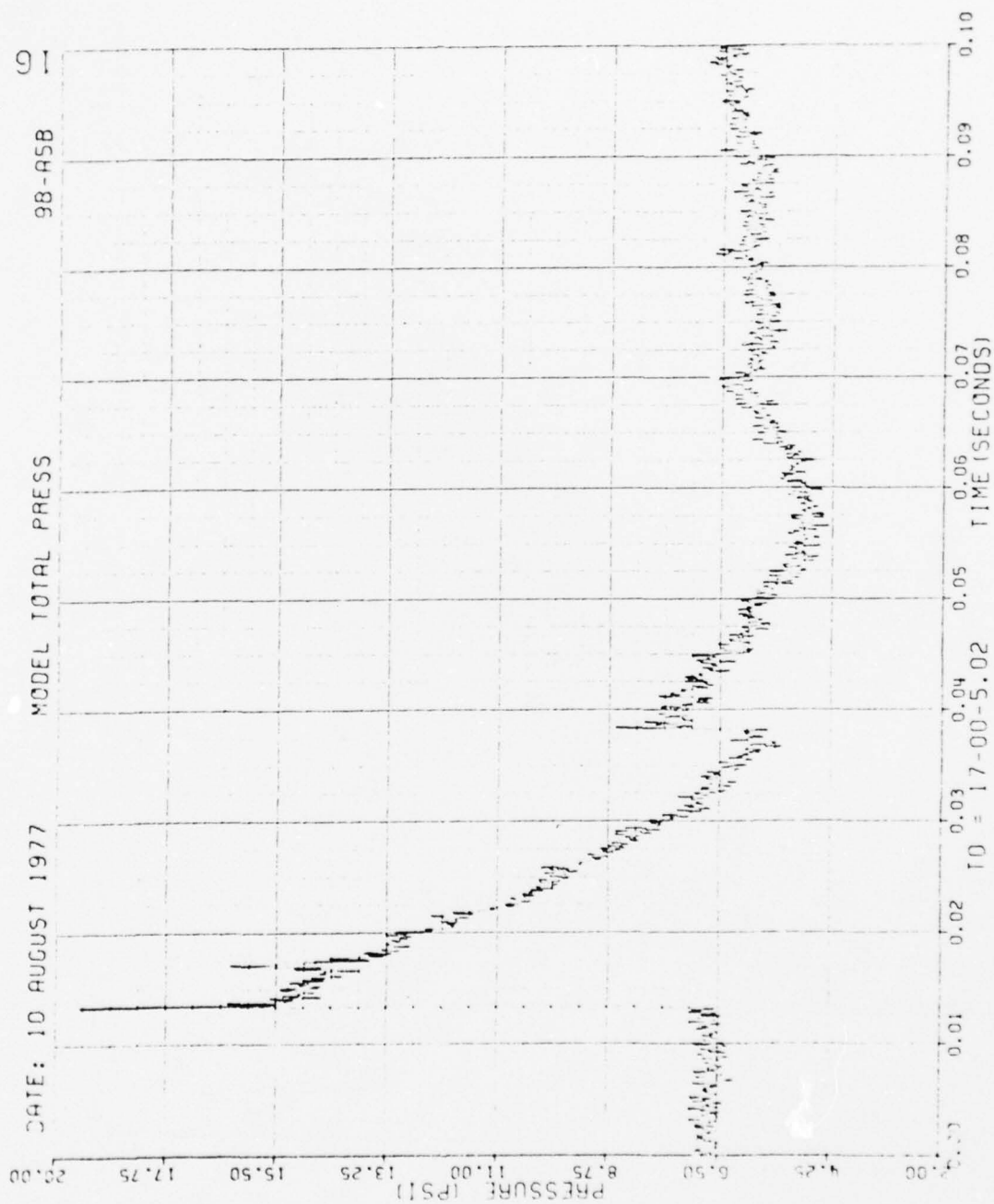


Figure 52. Concluded

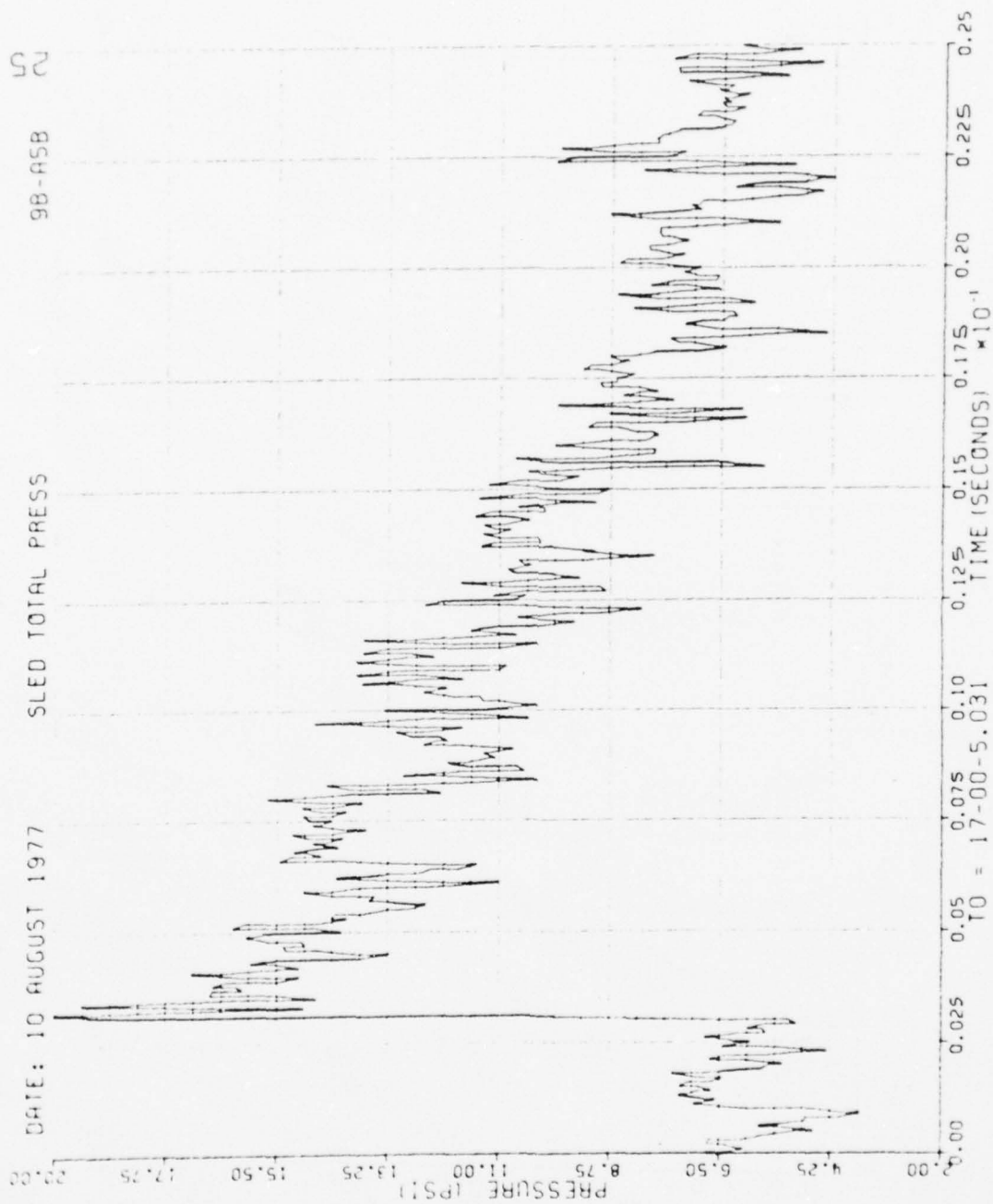


Figure 53. Total Pressure at Sled, Run 9B-A5, Intercept 1.

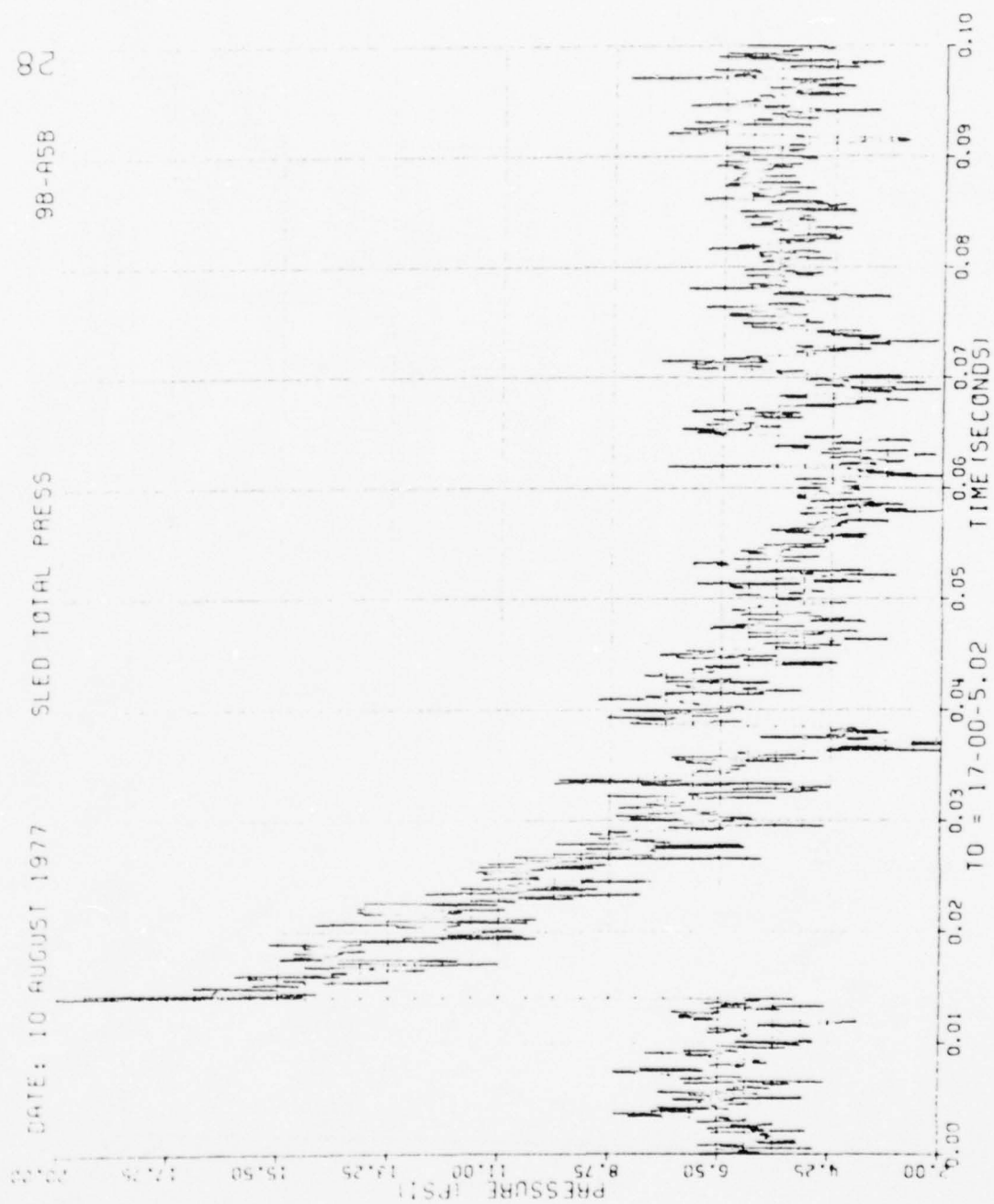


Figure 53. Concluded

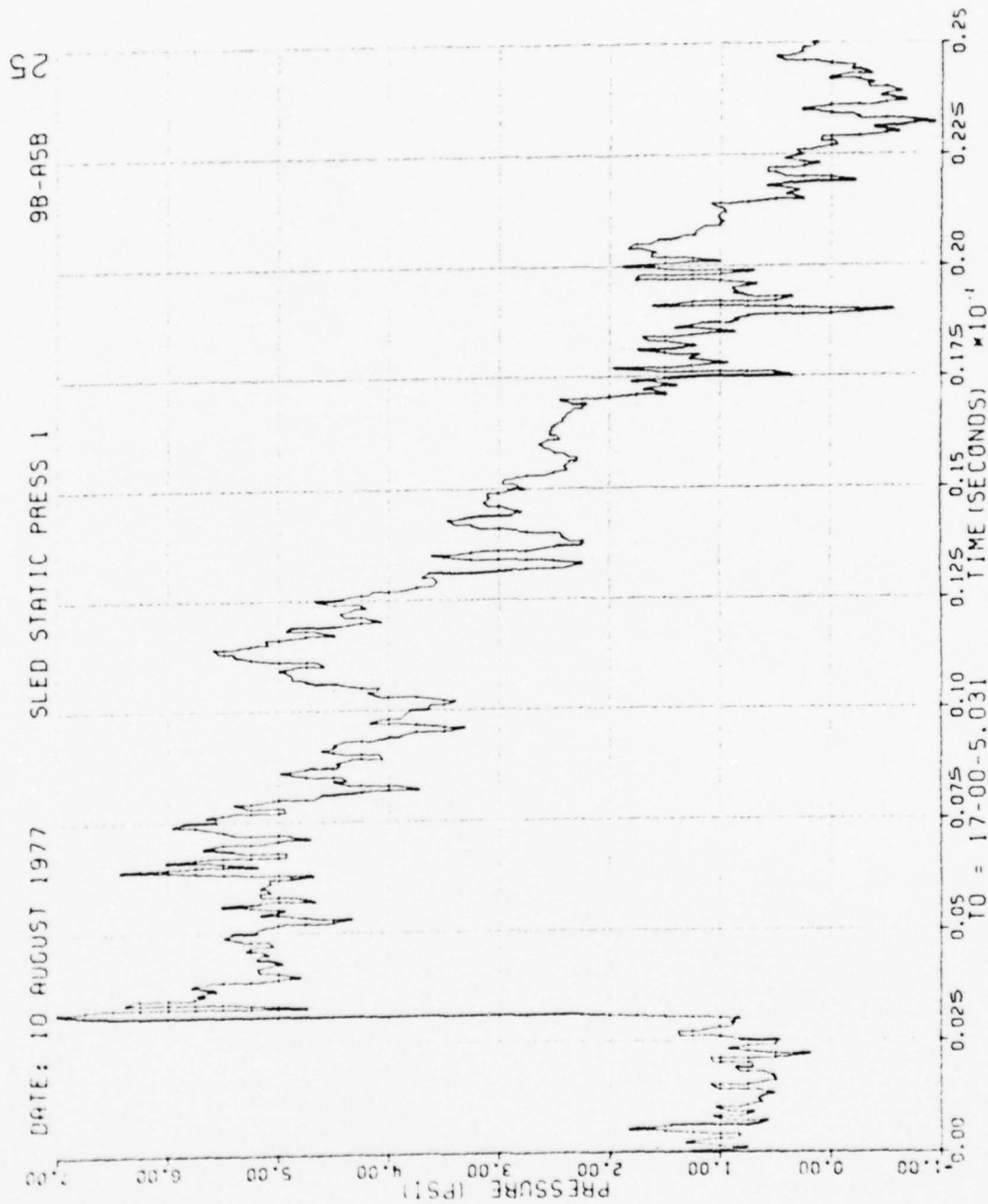


Figure 54. Static Pressure 1 at Sled, Run 9B-A5, Intercept 1.

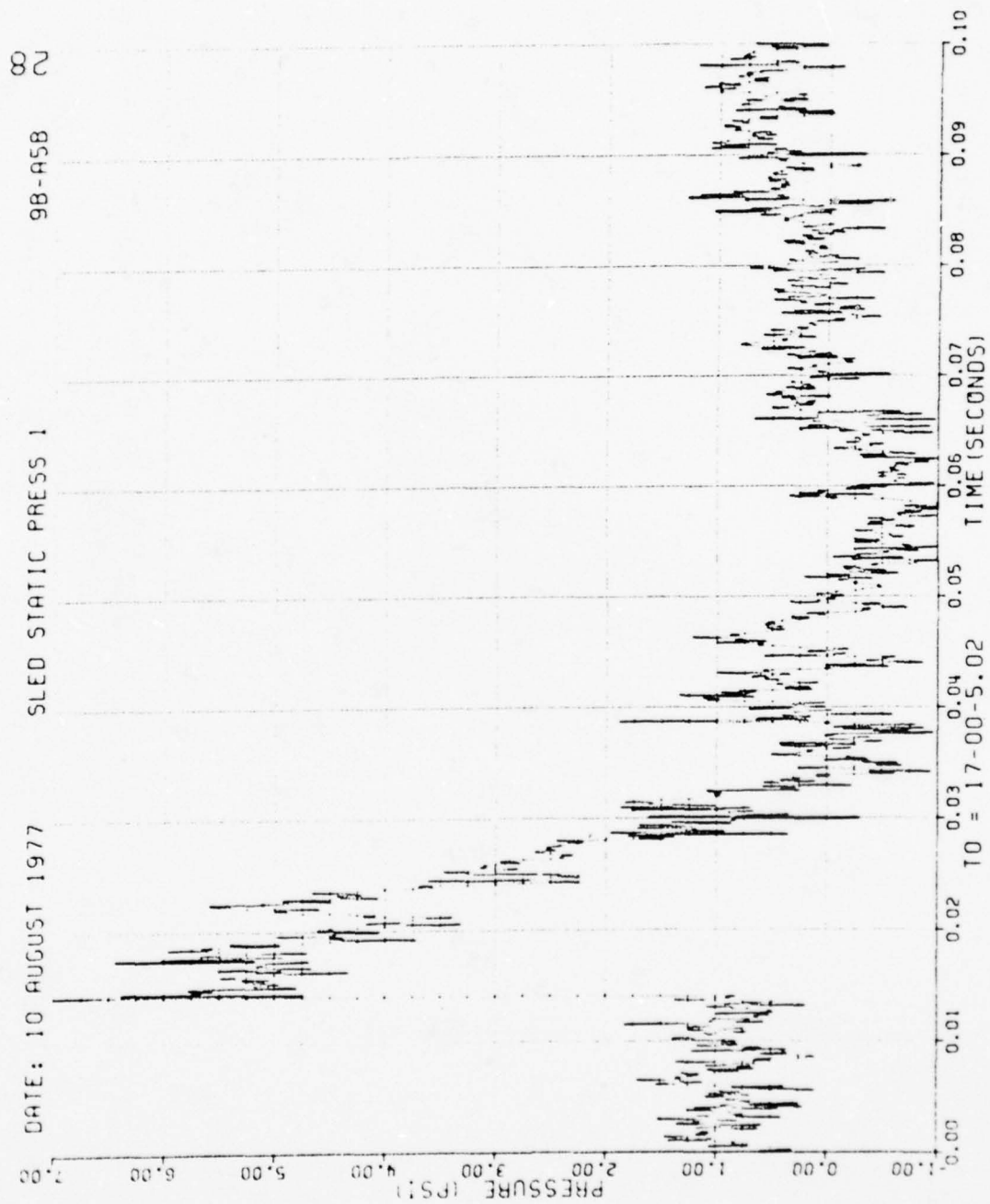


Figure 54. Concluded

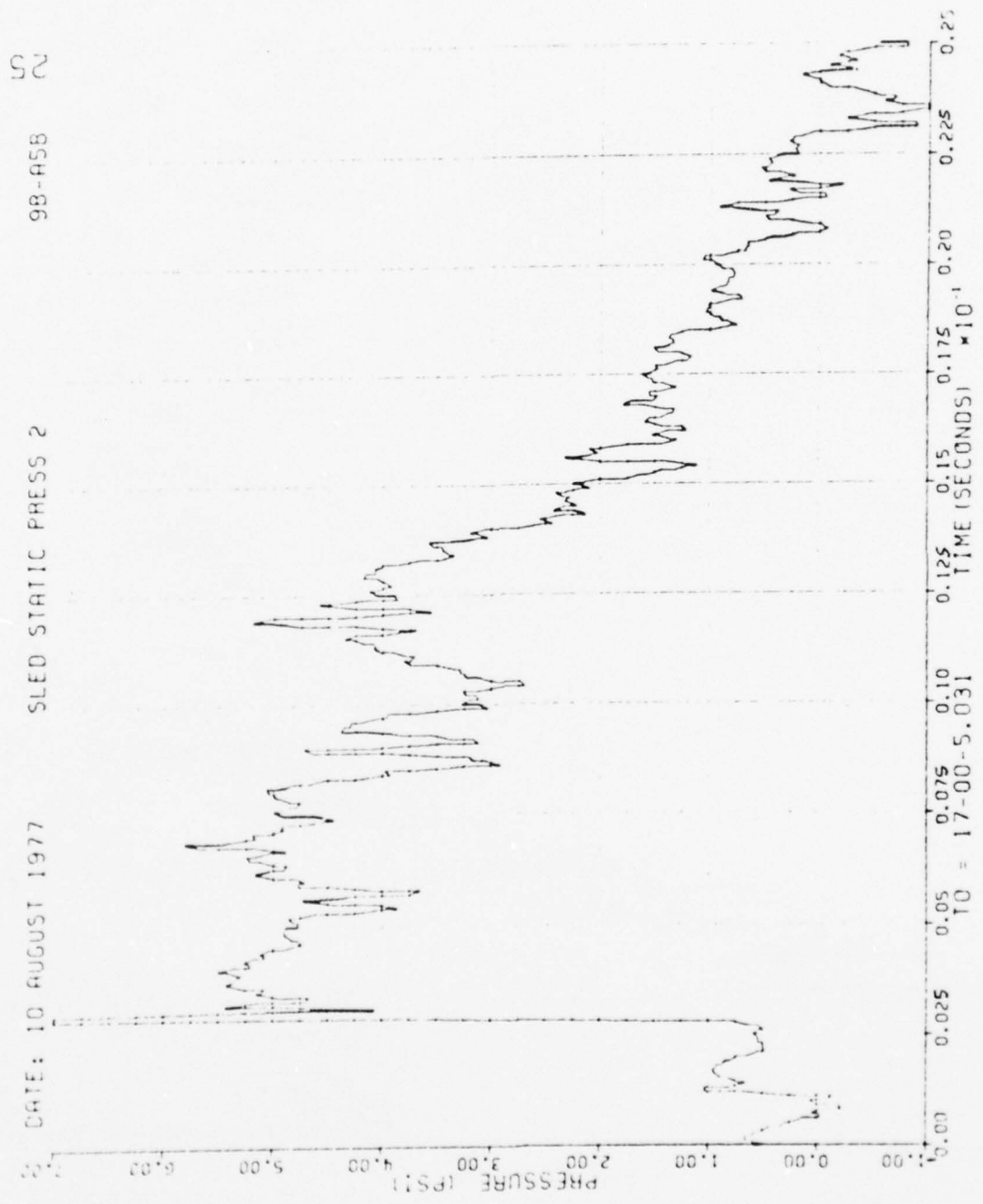


Figure 55. Static Pressure 2 at Sled, Run 9B-A5, Intercept 2.

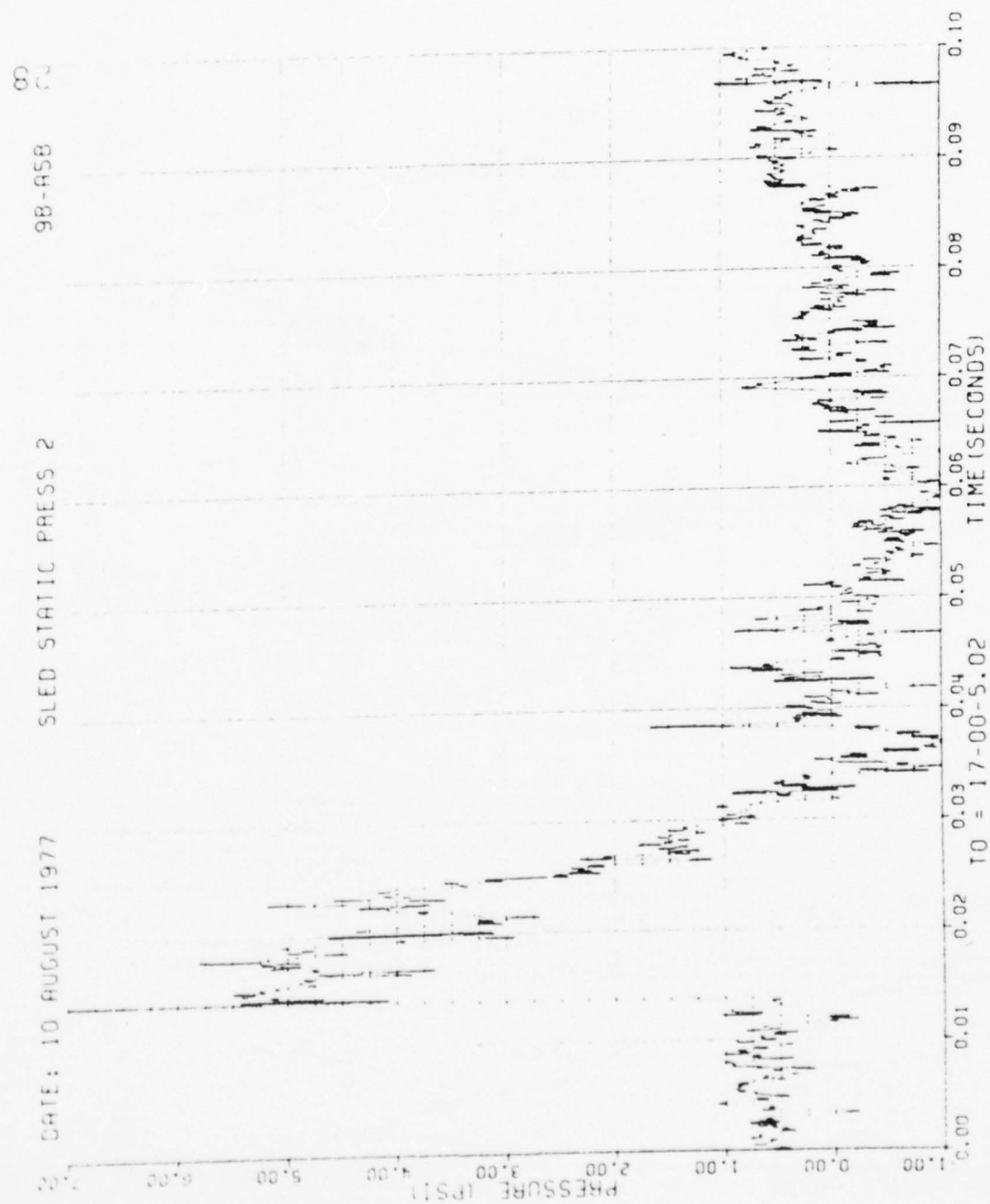


Figure 55. Concluded

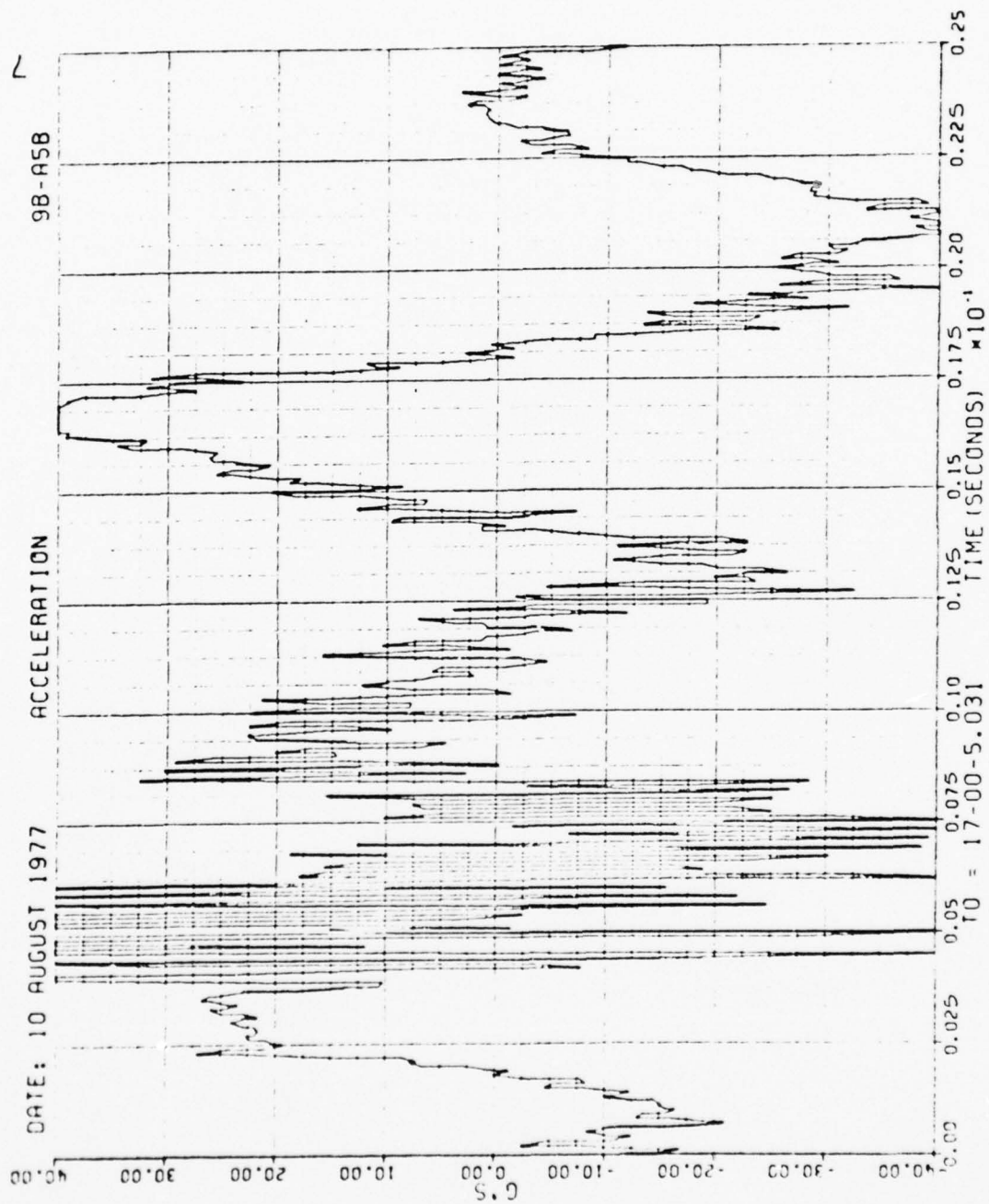


Figure 56. Wing Acceleration, Run 98-A5, Intercept 1.

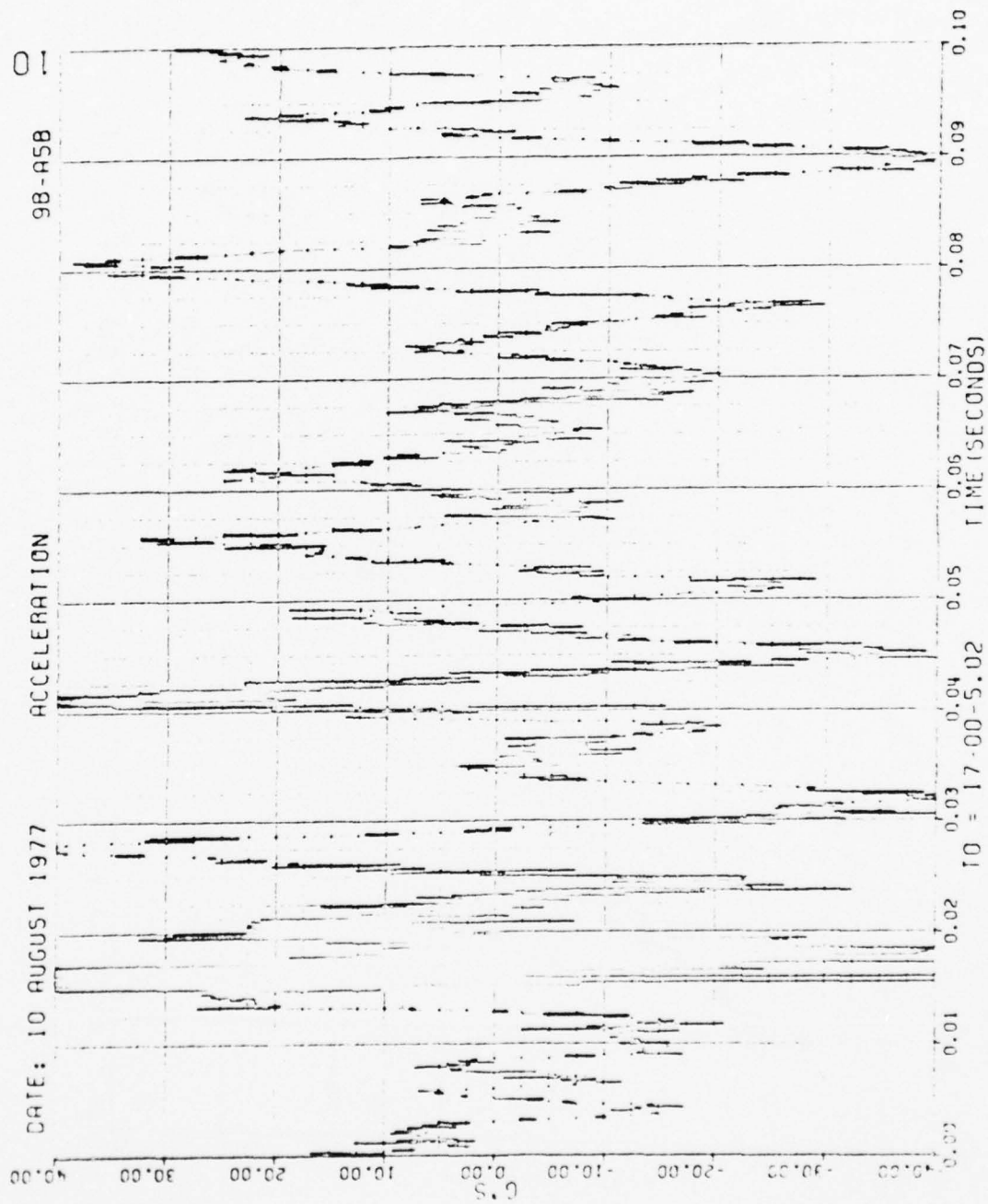


Figure 56. Concluded

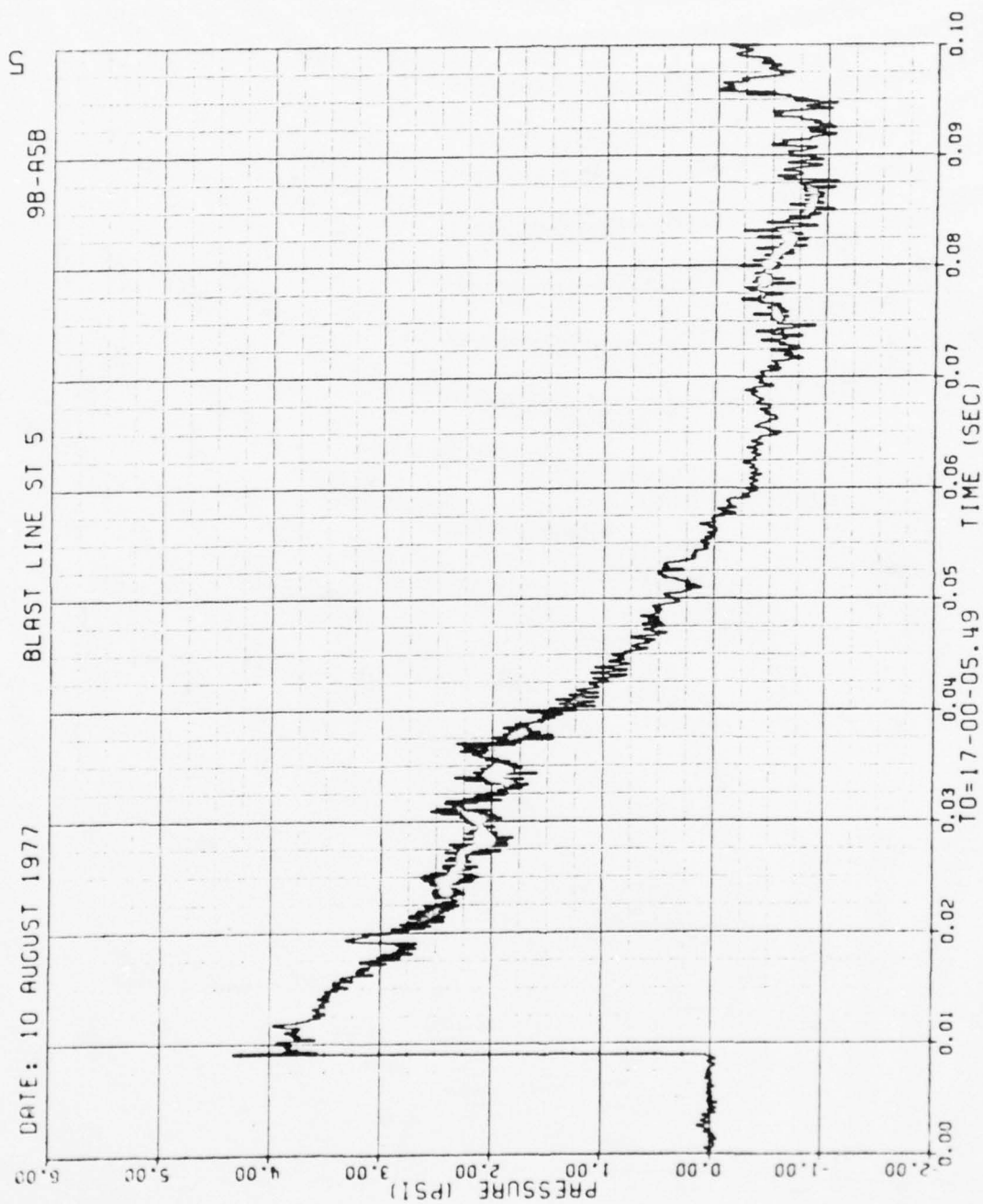


Figure 57. Blast-line Overpressures, Run 9B-A5, Intercept 2.

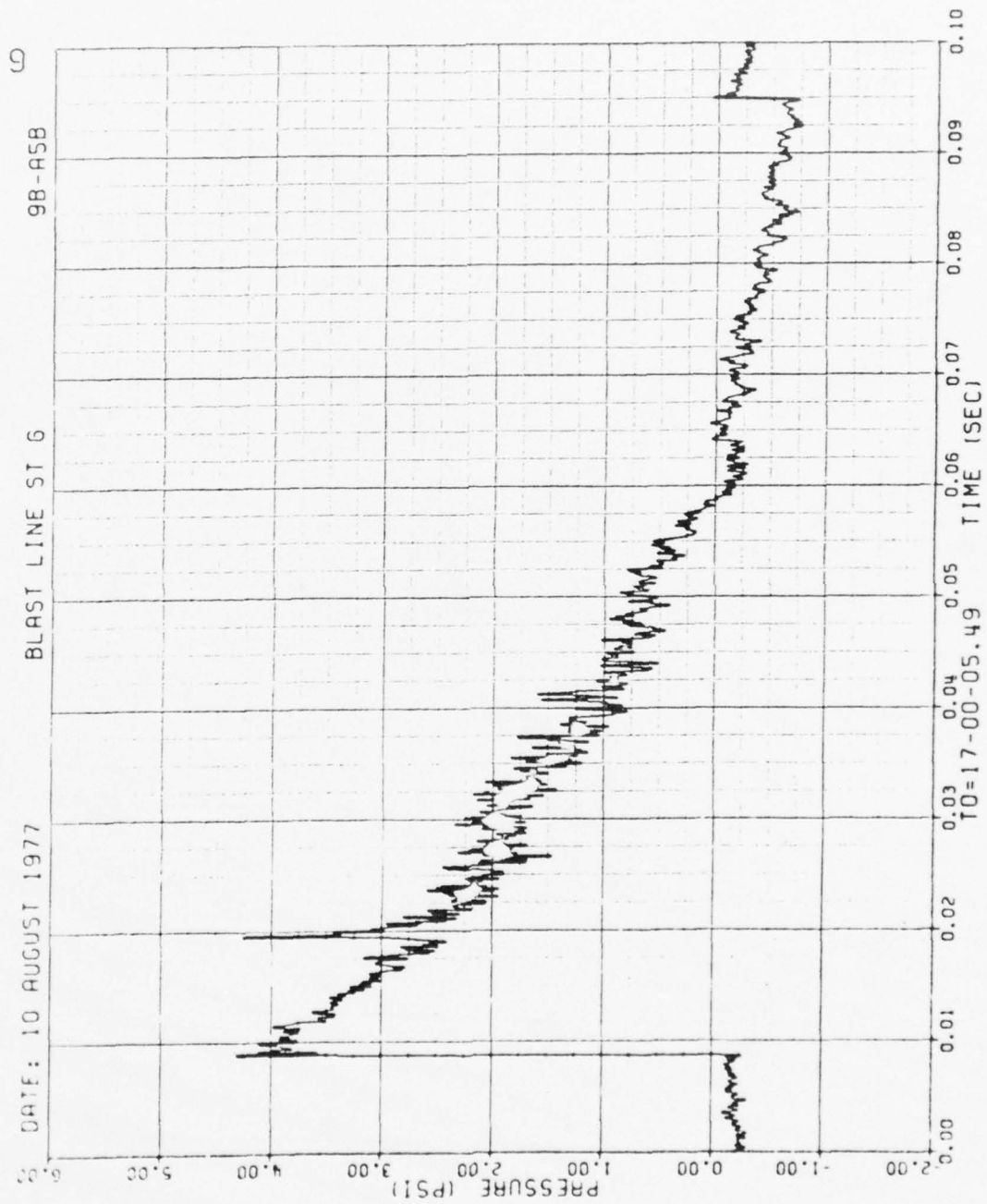


Figure 57. Continued

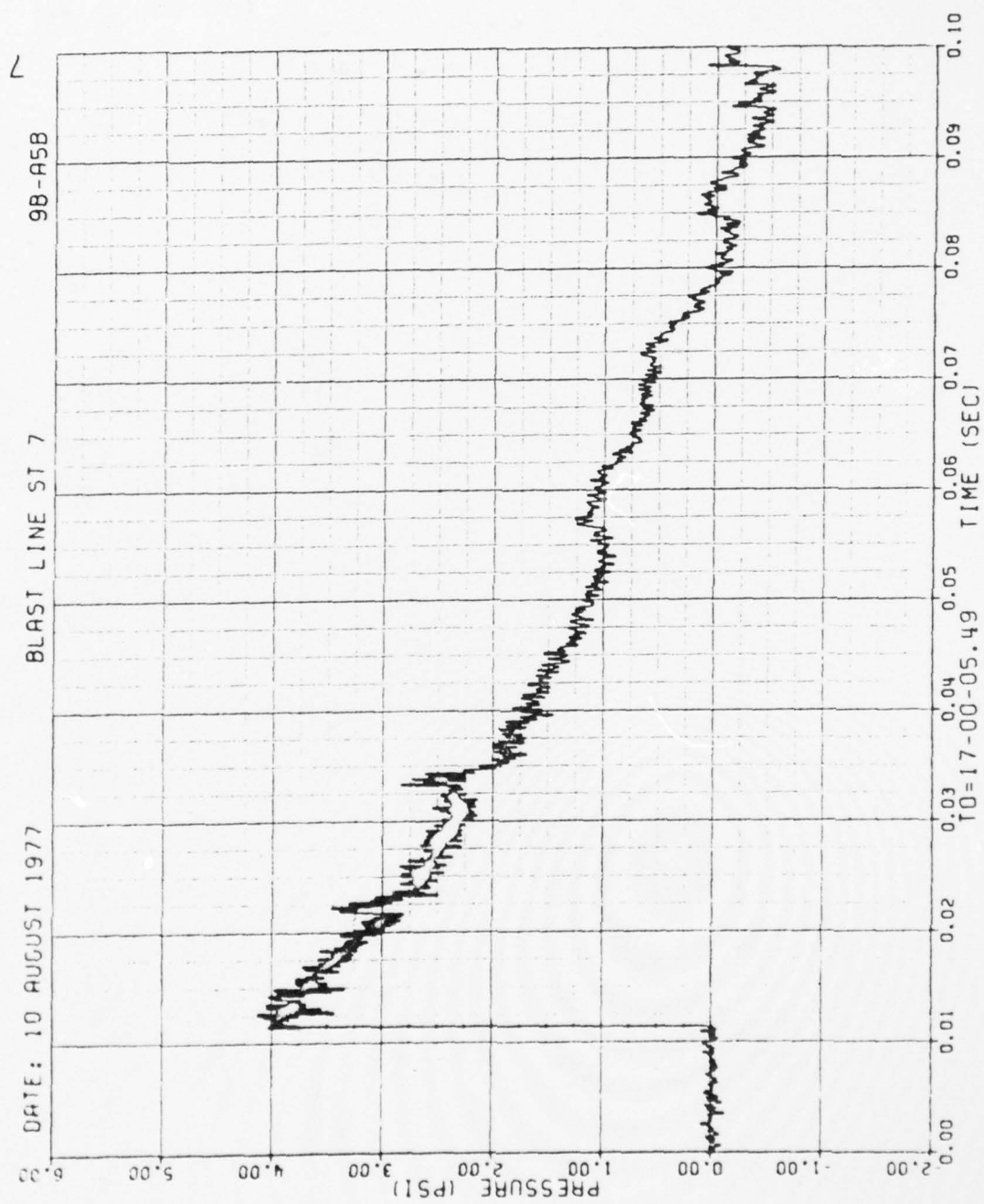


Figure 57. Continued

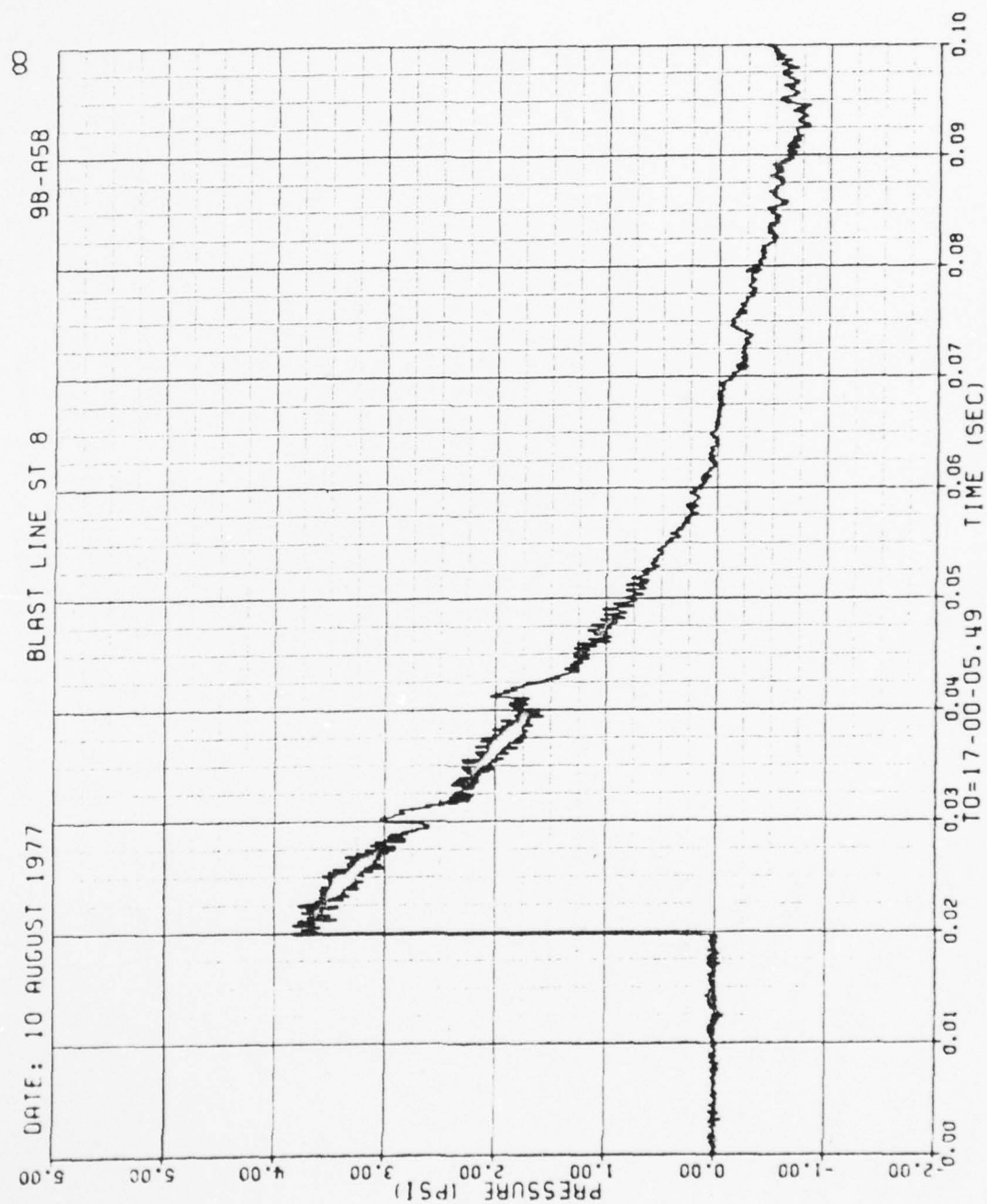


Figure 57. Concluded

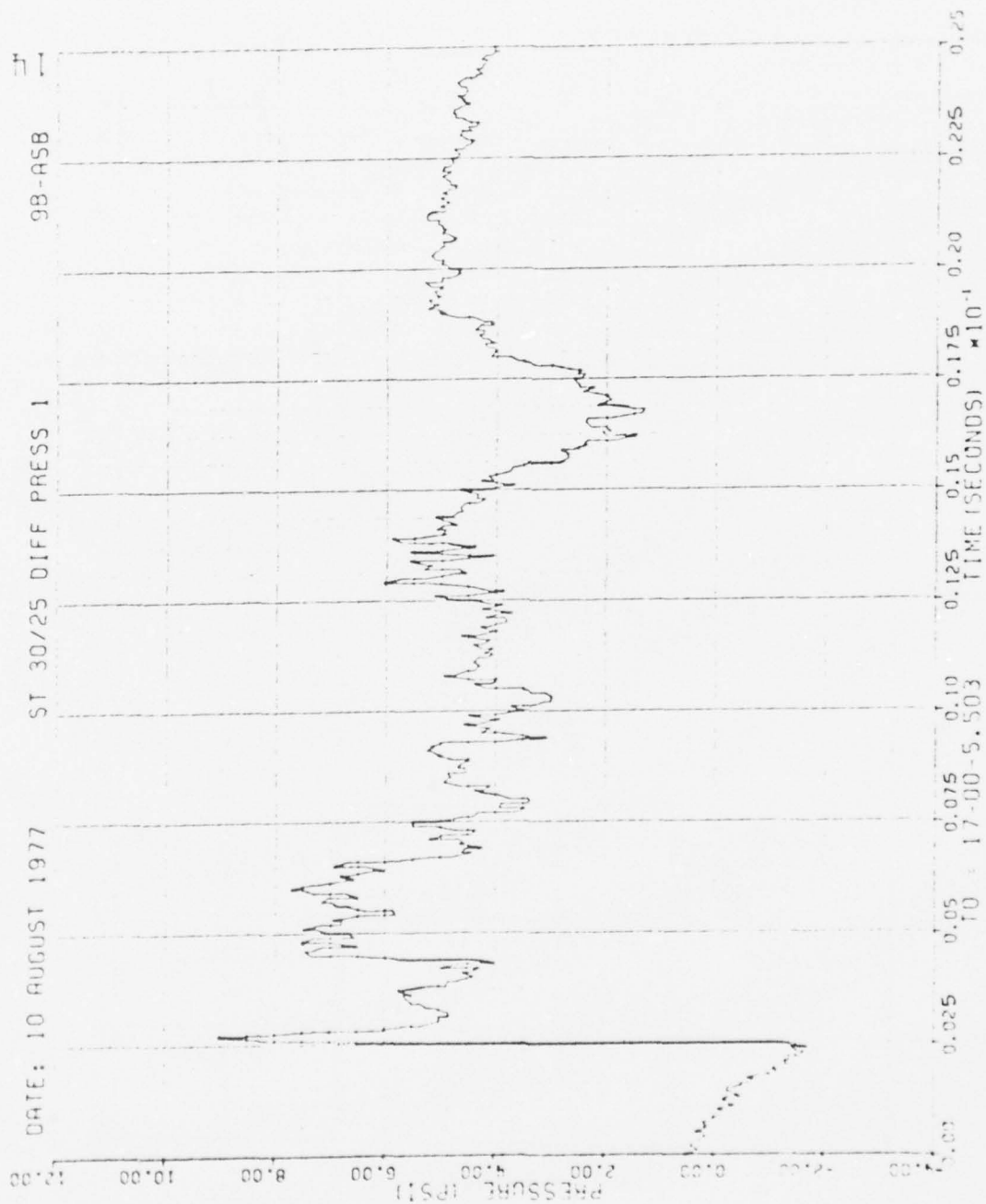


Figure 58. Differential Wing Pressures, Run 9B-A5, Intercept 2.

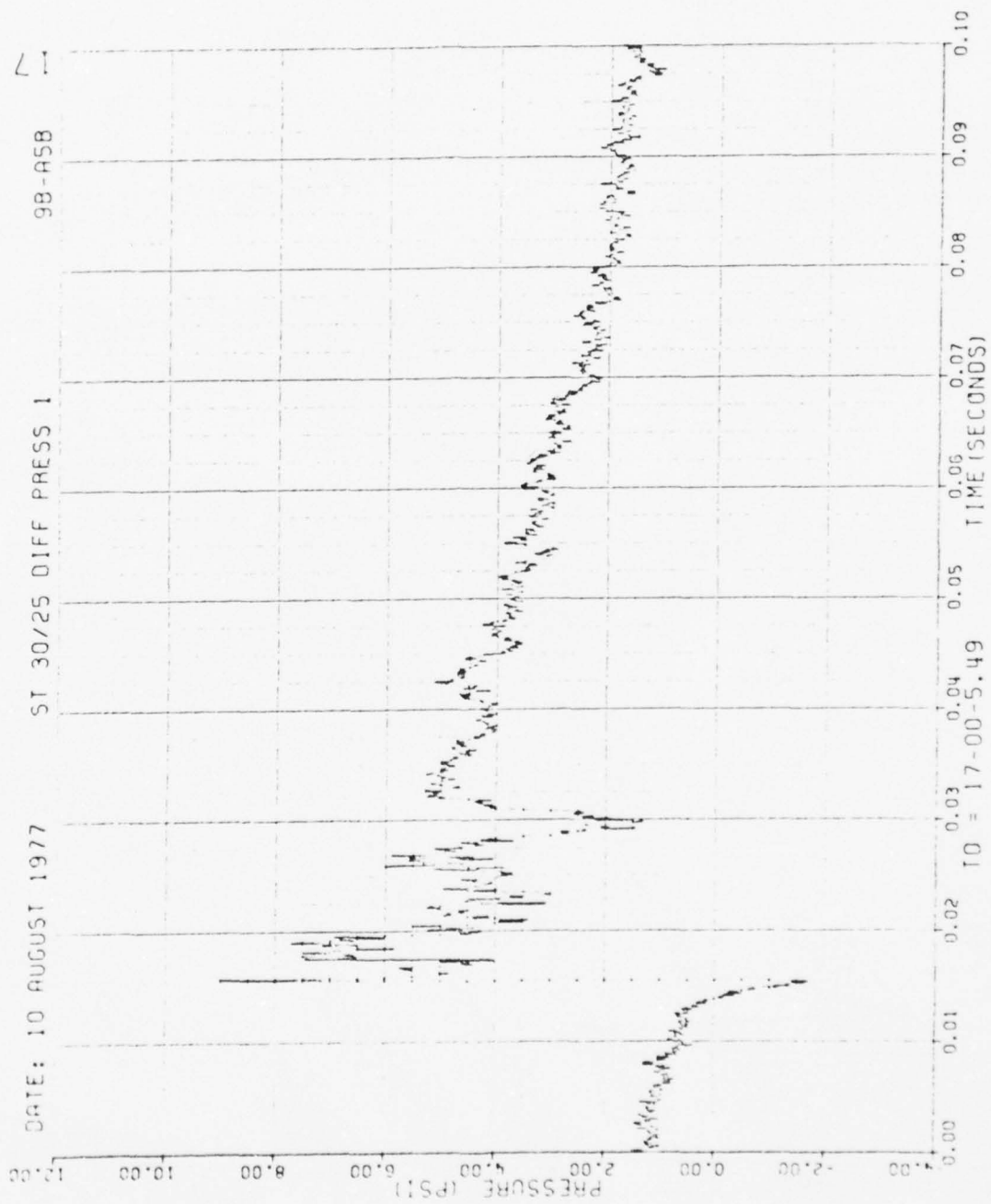


Figure 58. Continued

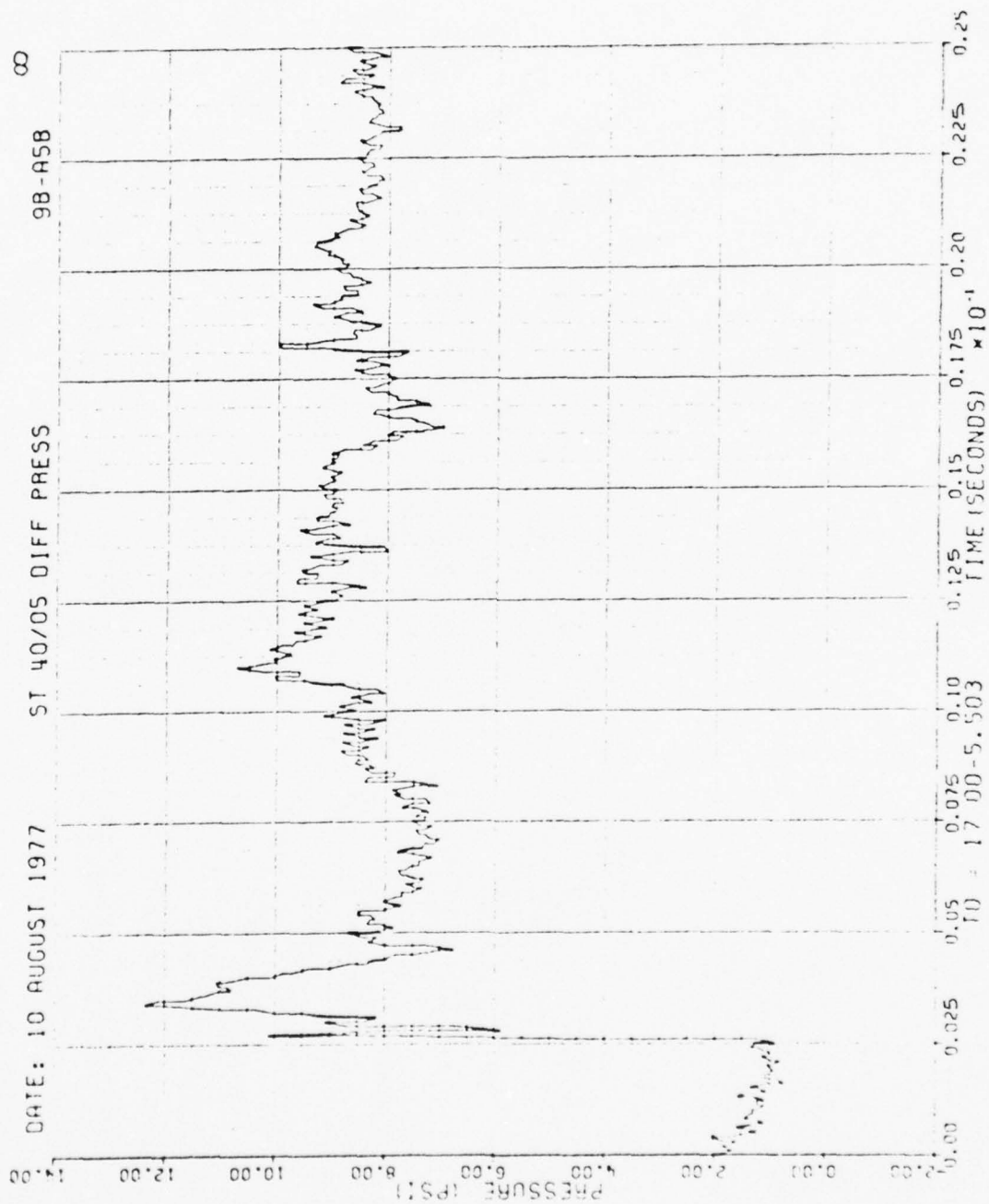


Figure 58. Continued

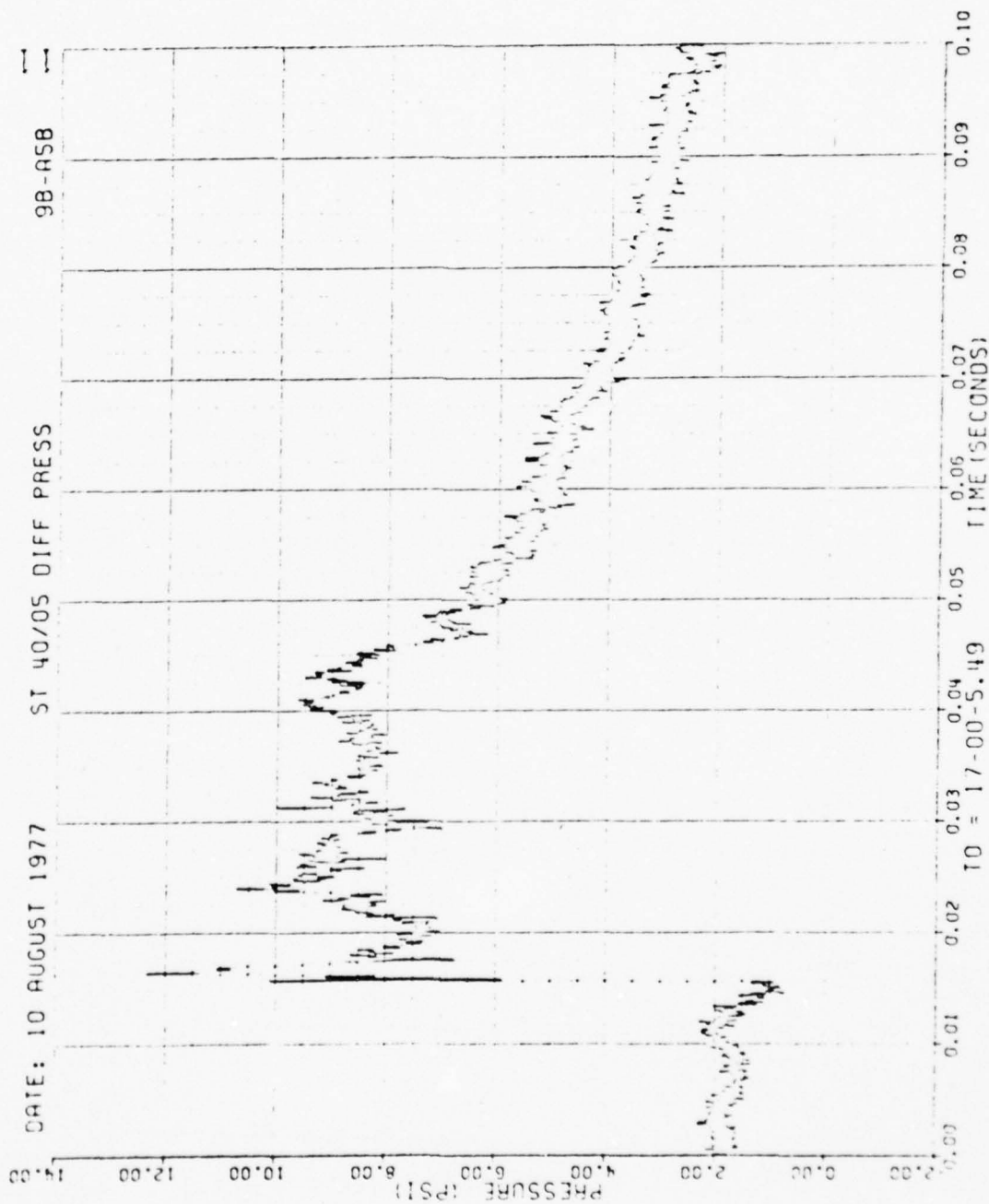


Figure 58. Continued

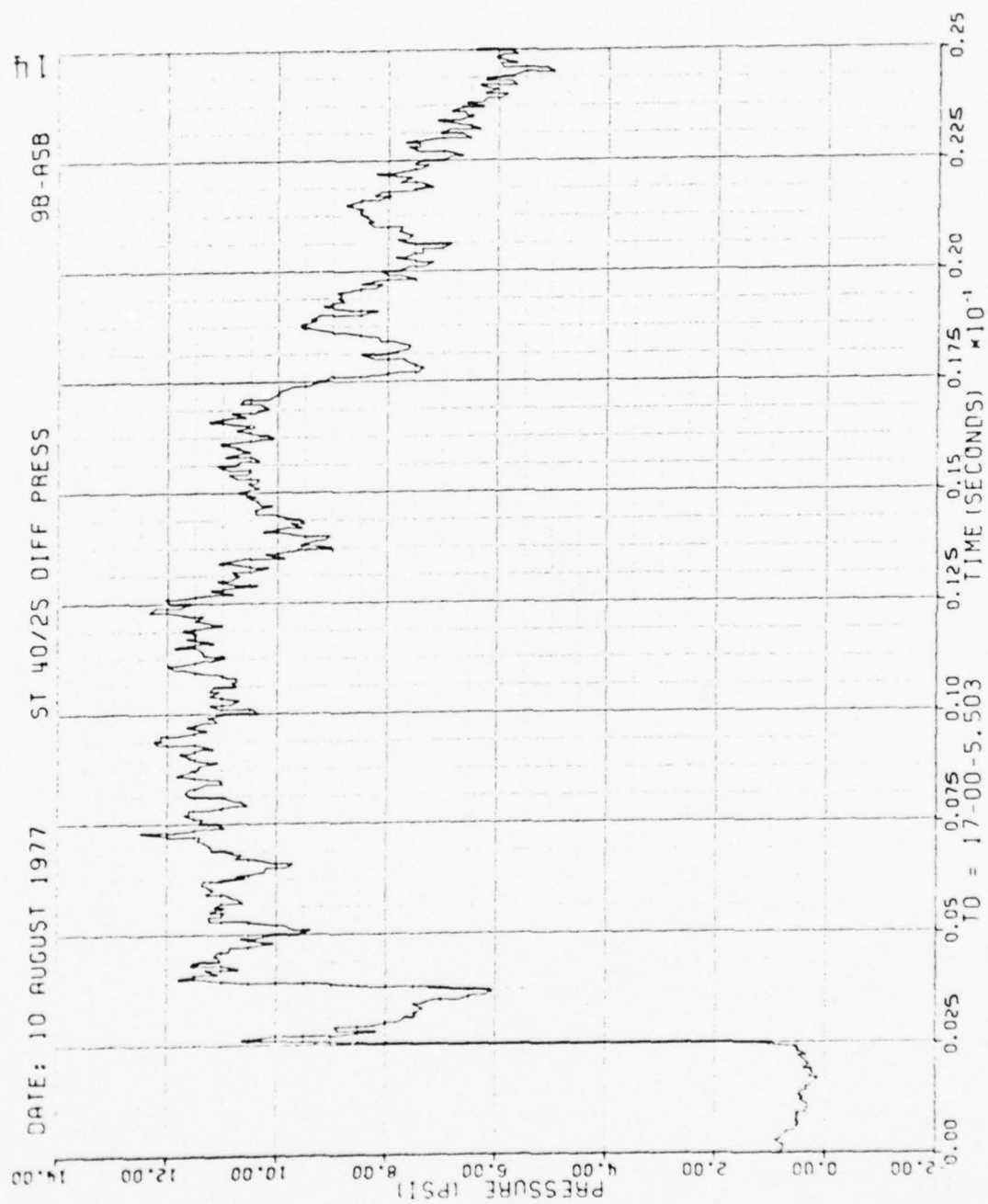


Figure 58. Continued

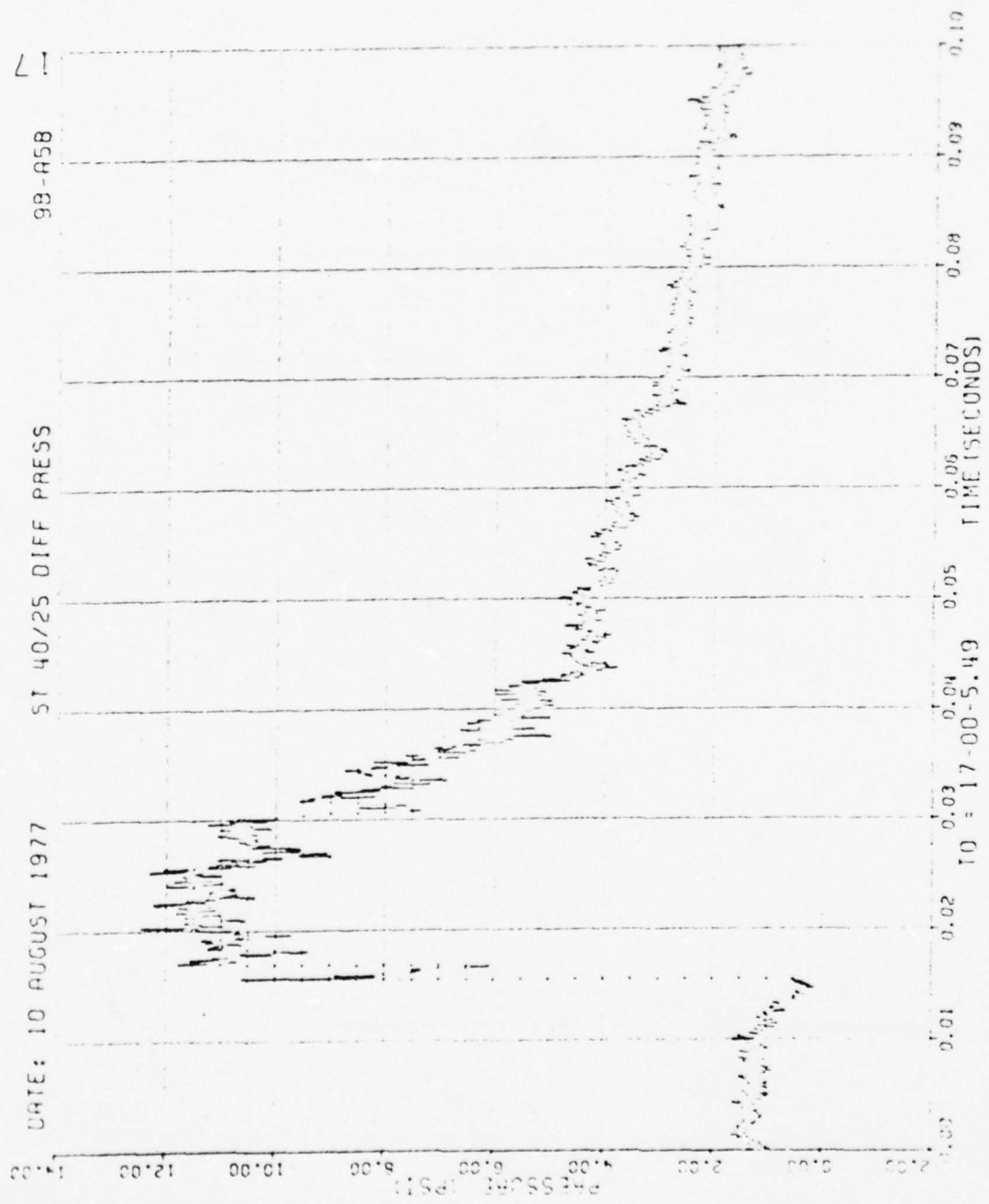


Figure 58. Continued

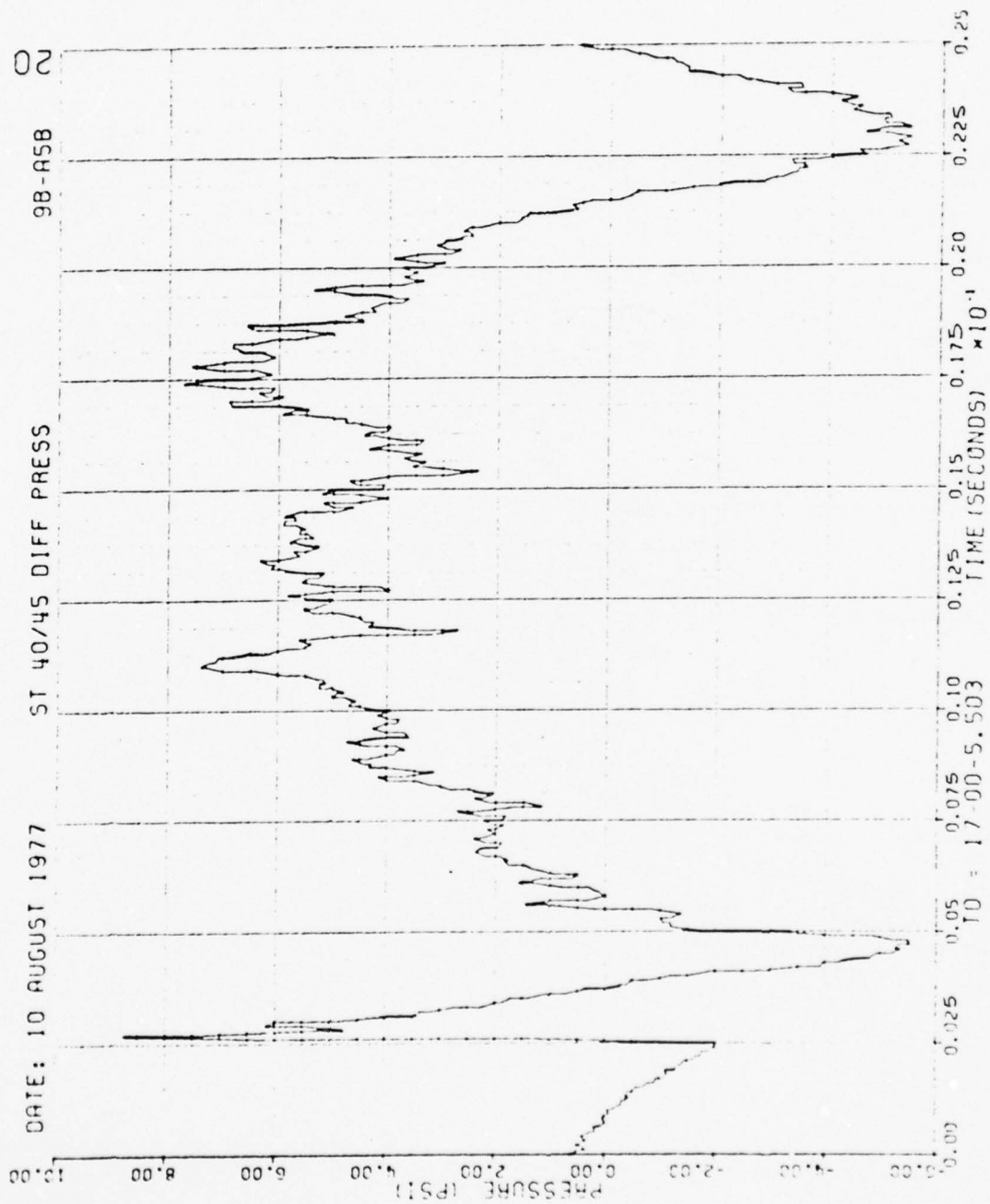


Figure 58. Continued

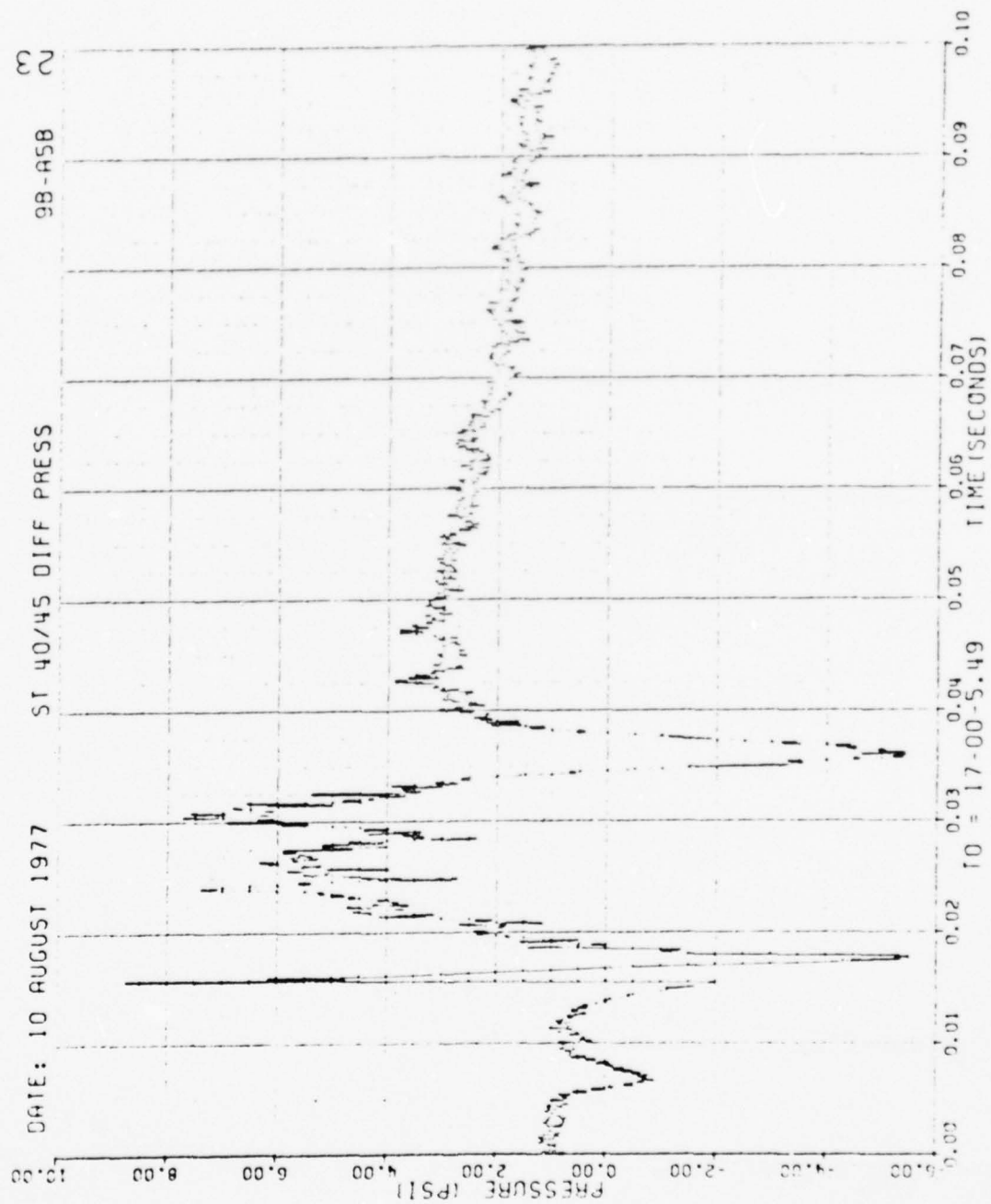


Figure 58. Continued

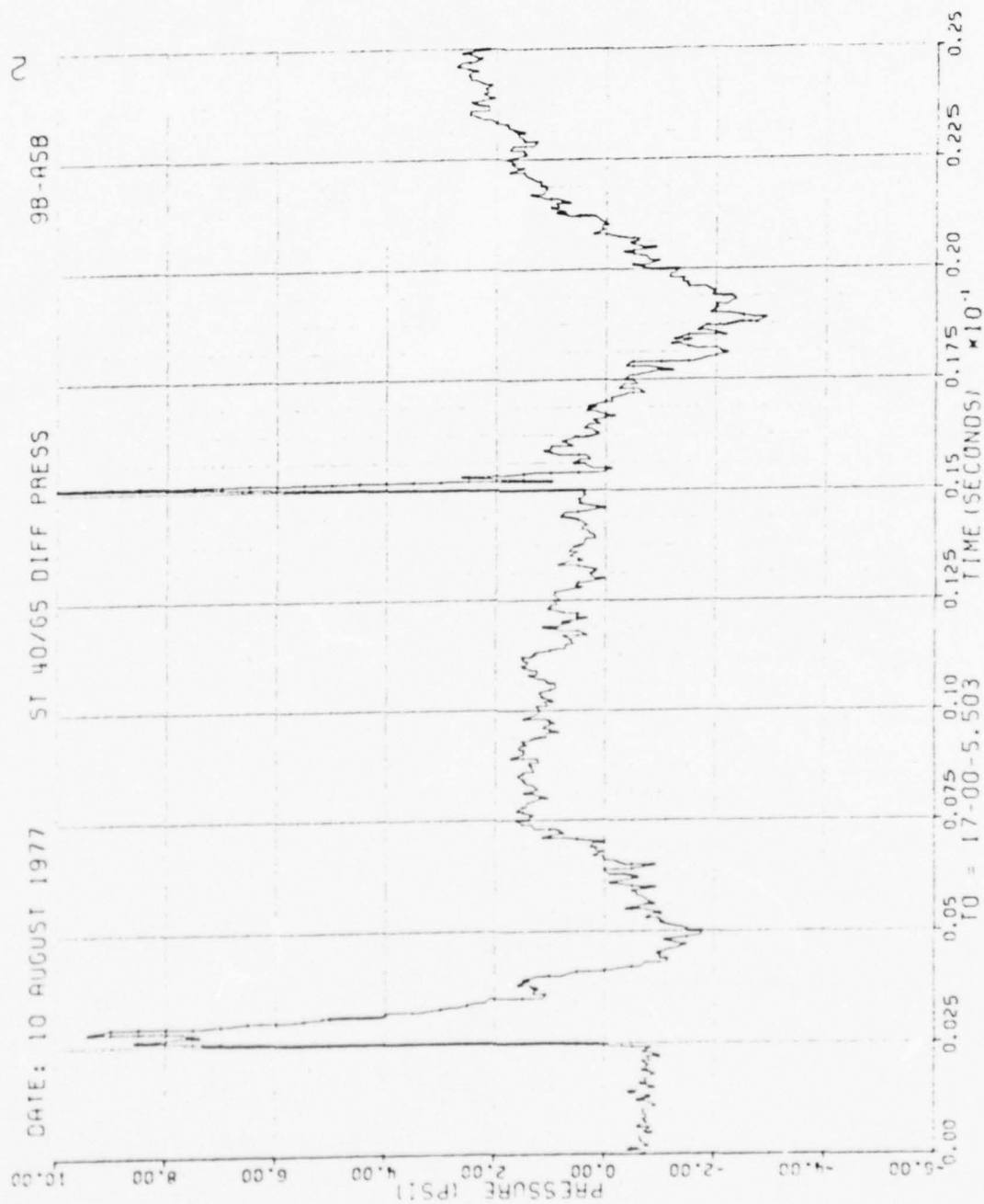


Figure 58. Continued

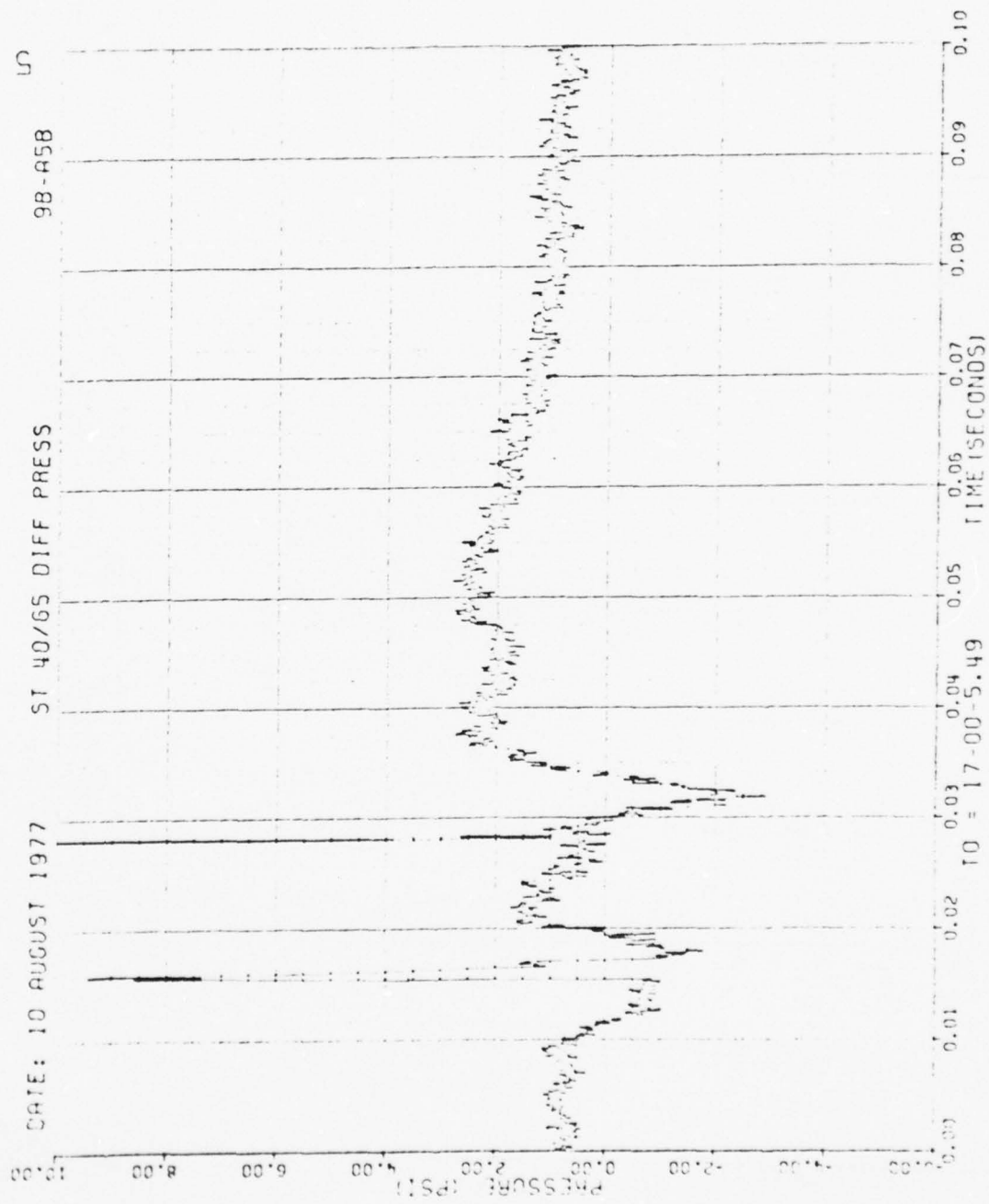


Figure 58. Continued

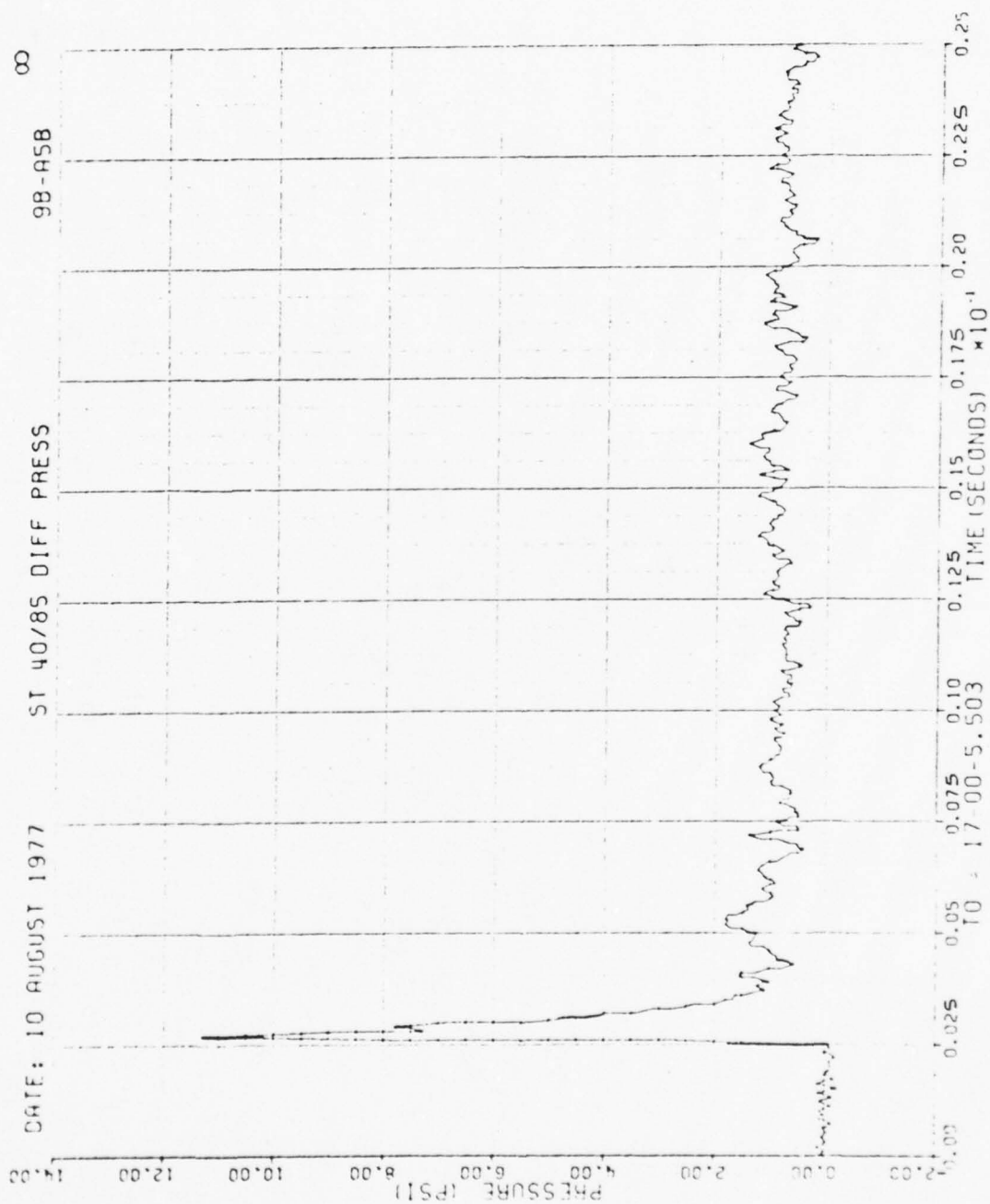


Figure 58. Continued

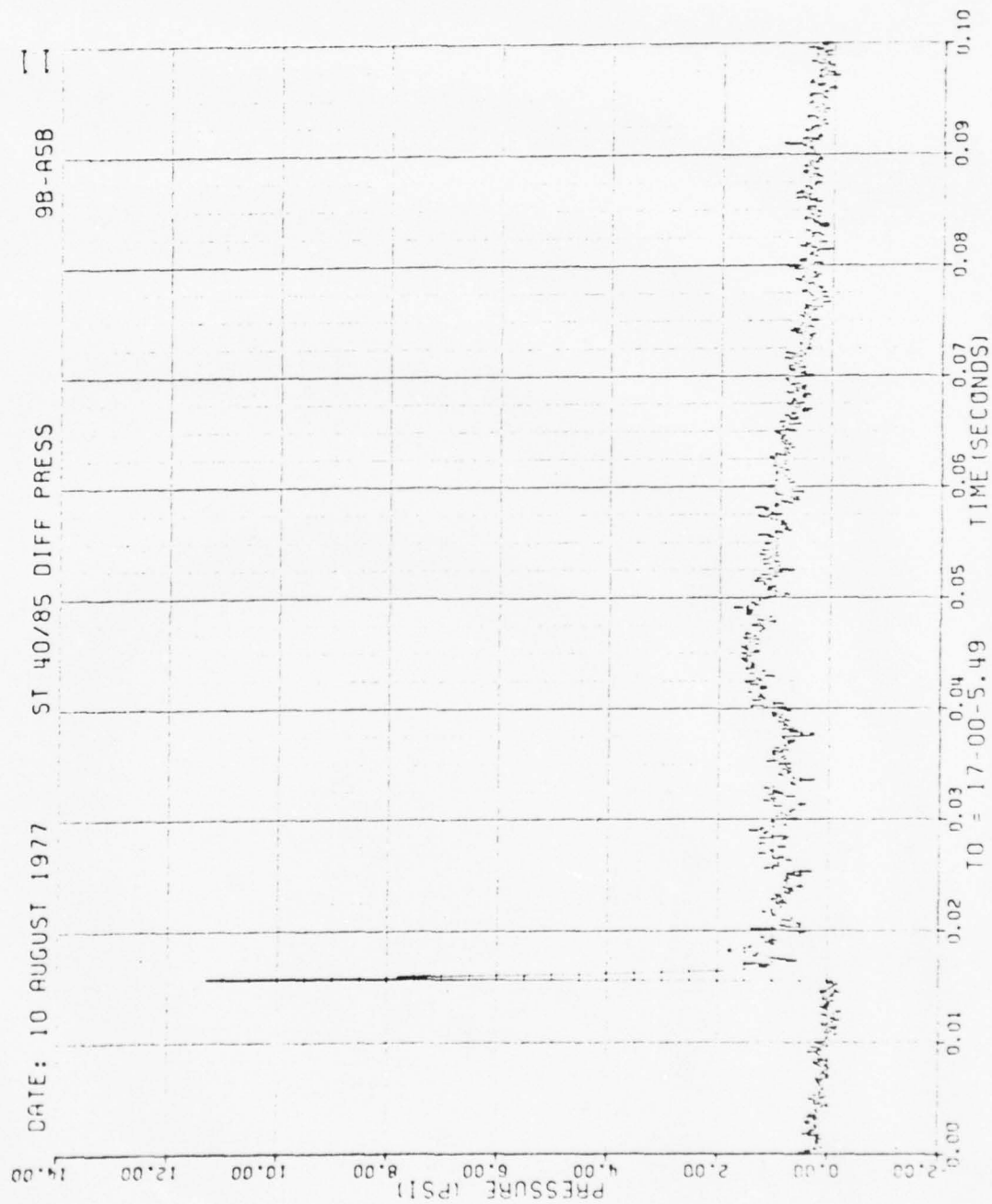


Figure 58. Continued

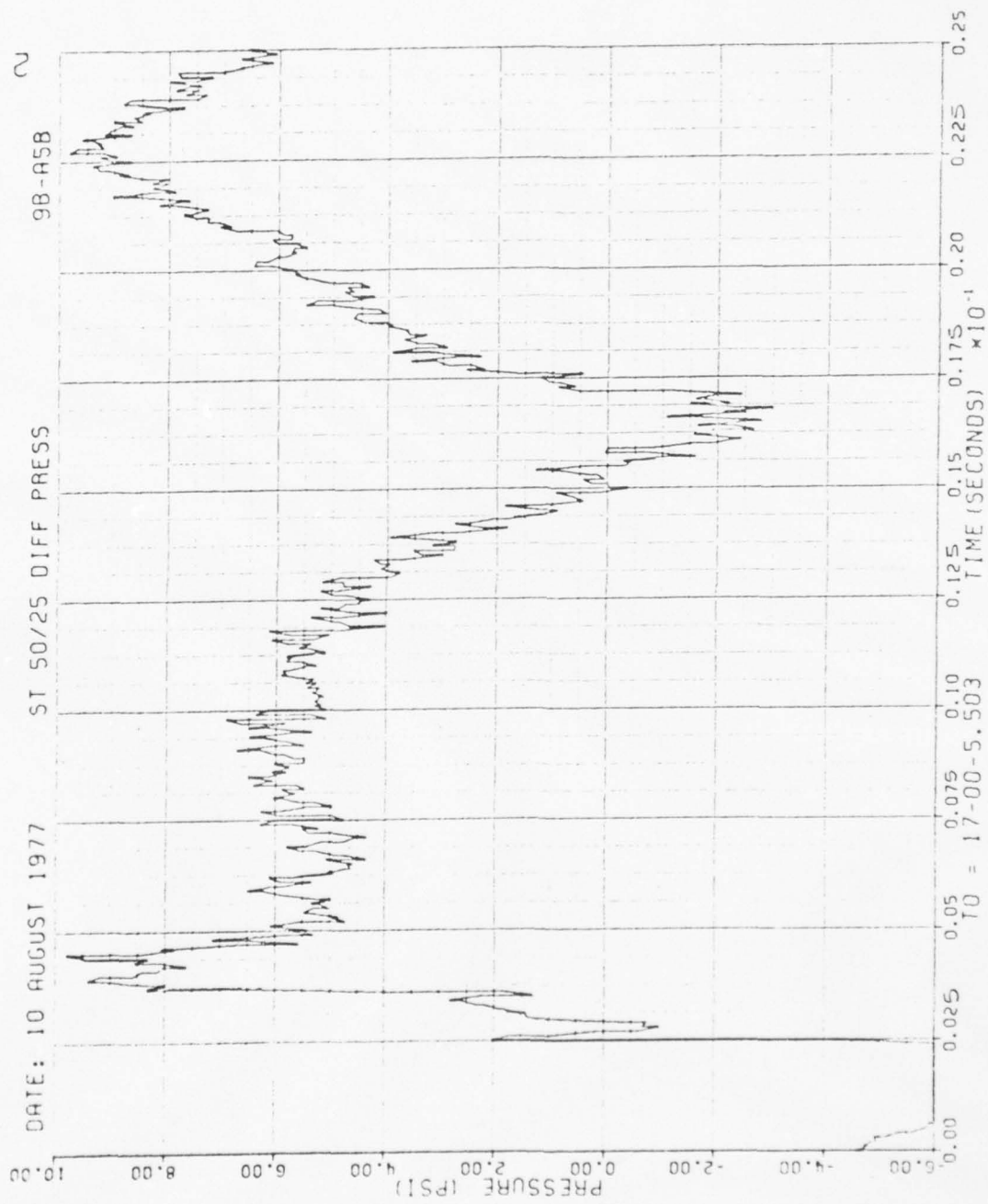


Figure 58. Continued

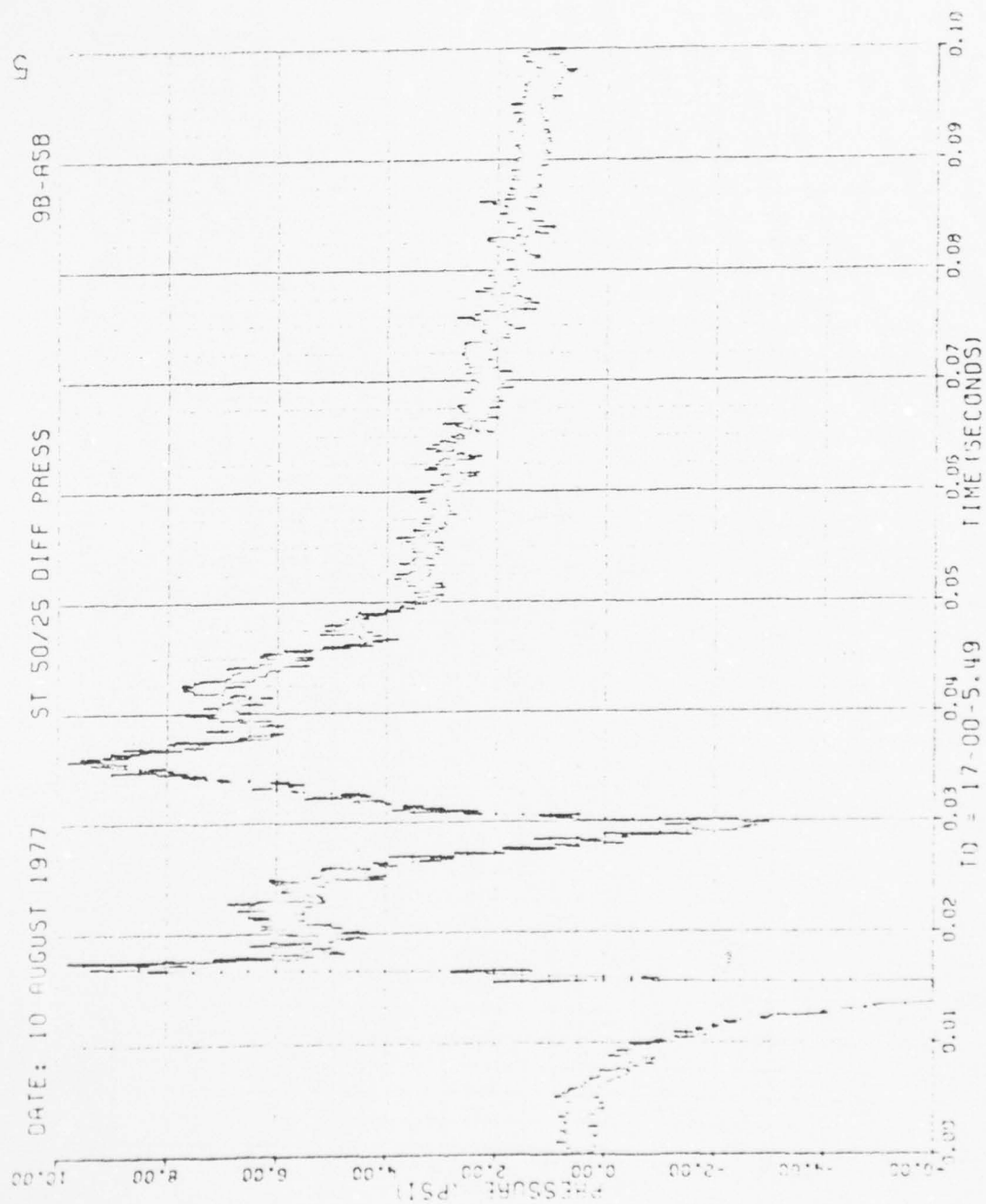


Figure 58. Continued

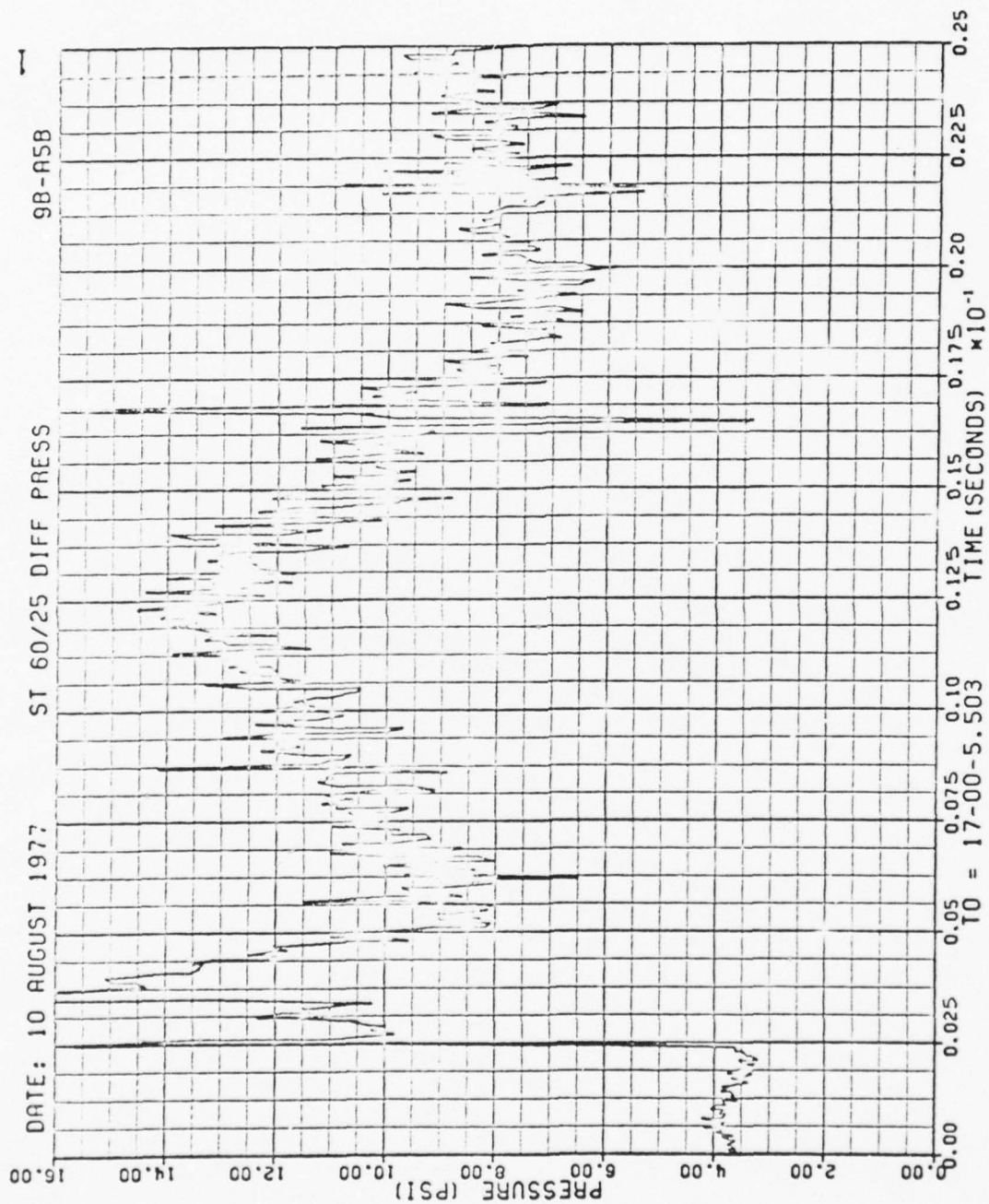


Figure 58. Continued

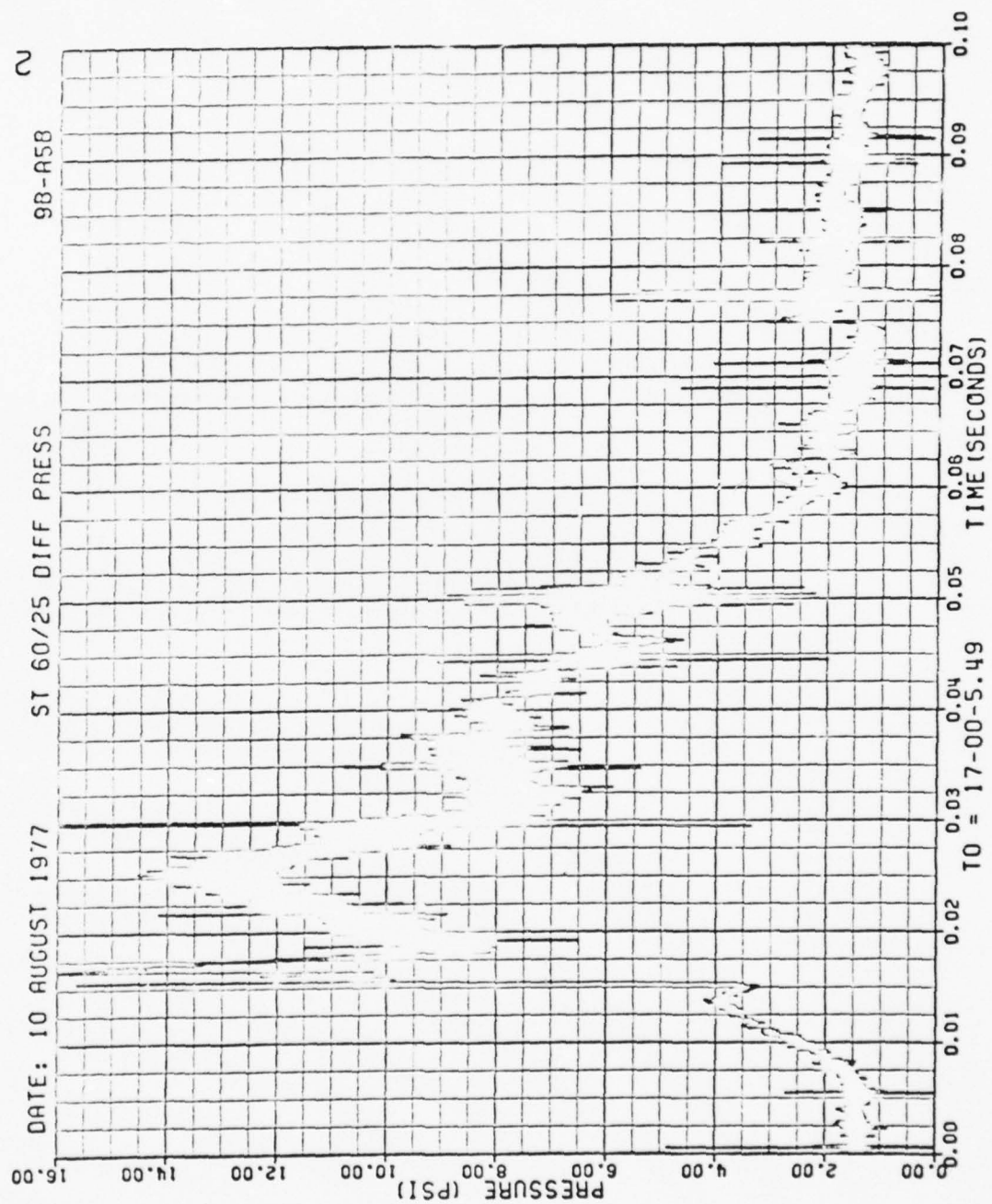


Figure 58. Continued

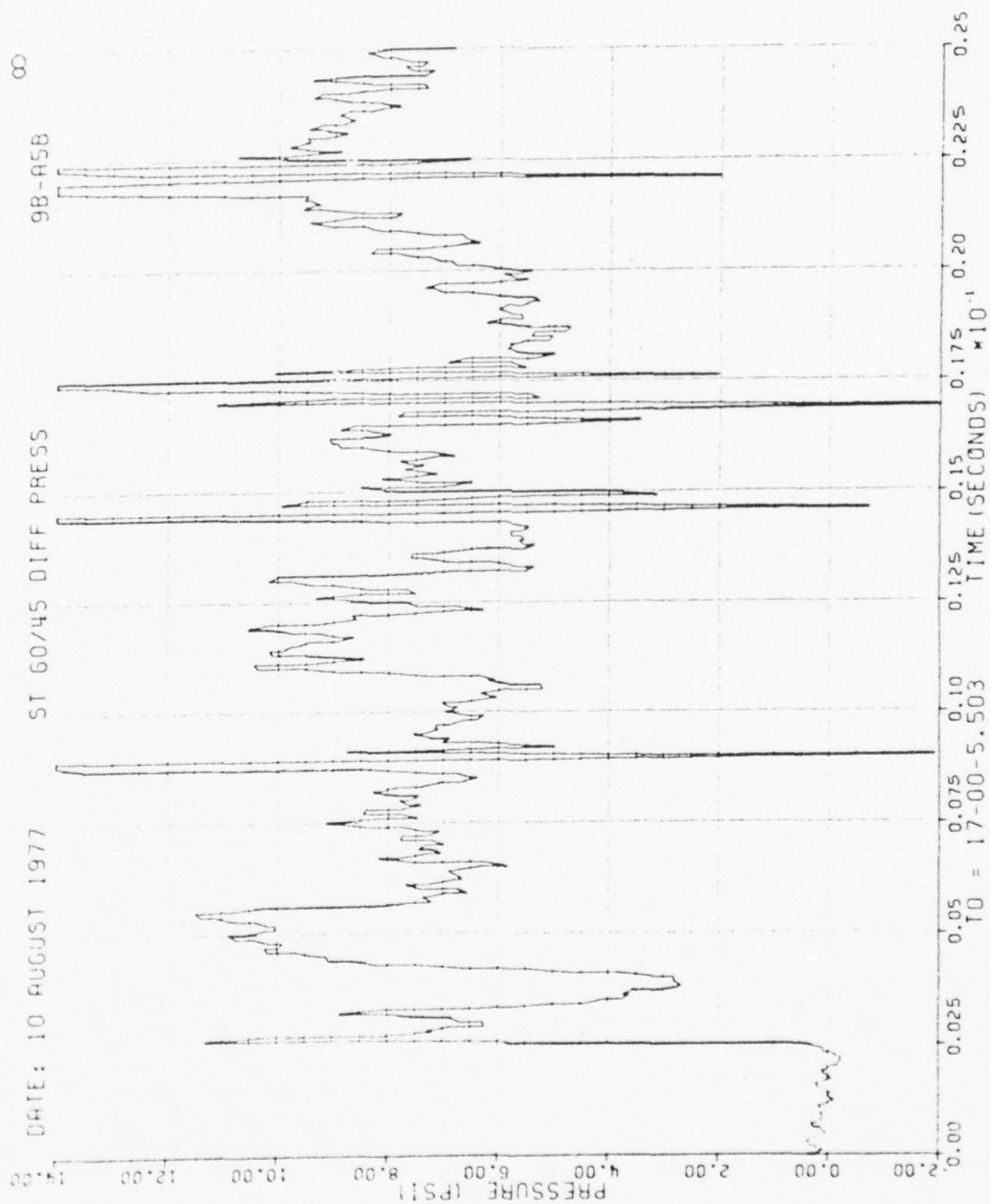


Figure 58. Continued

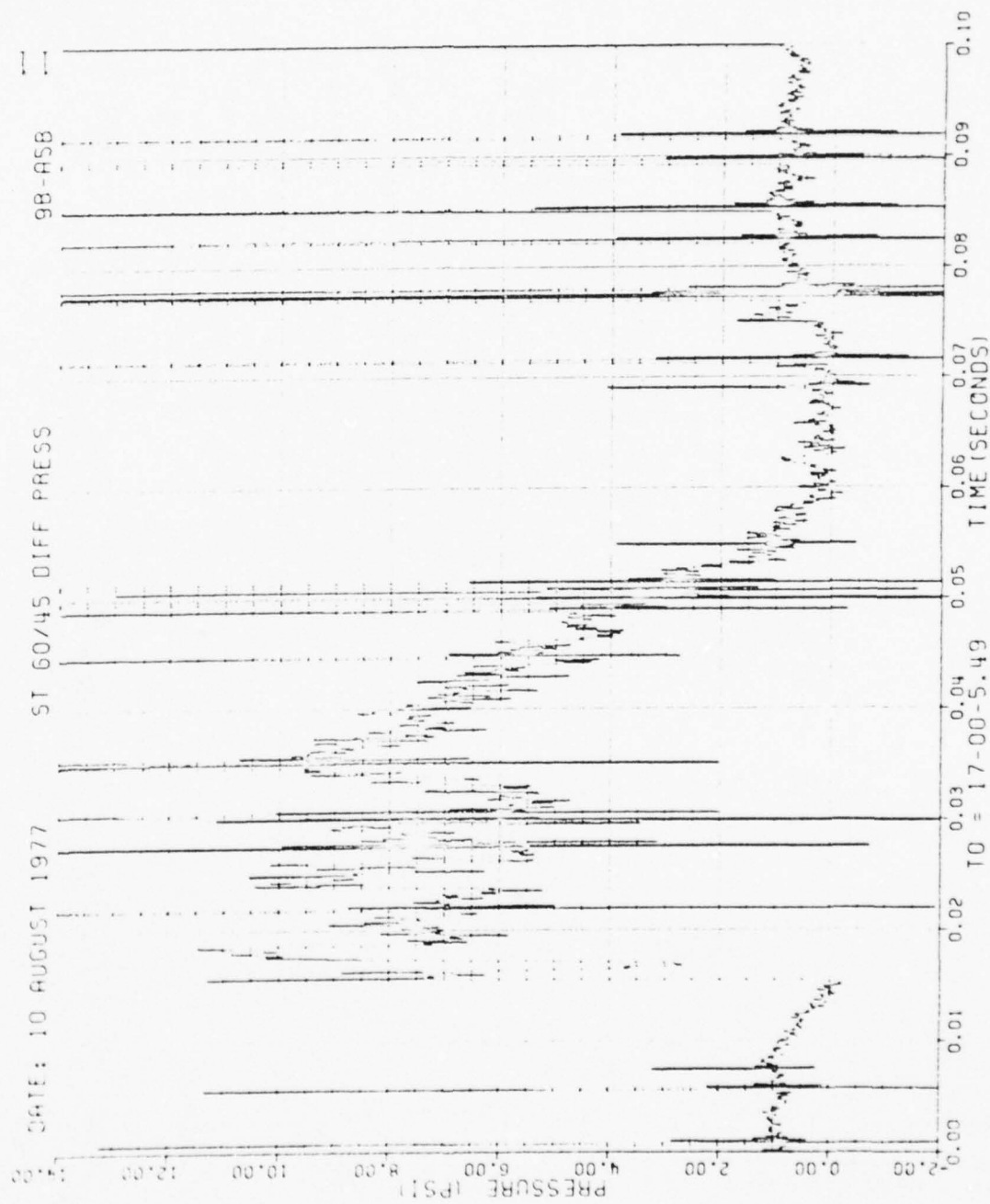


Figure 58. Continued

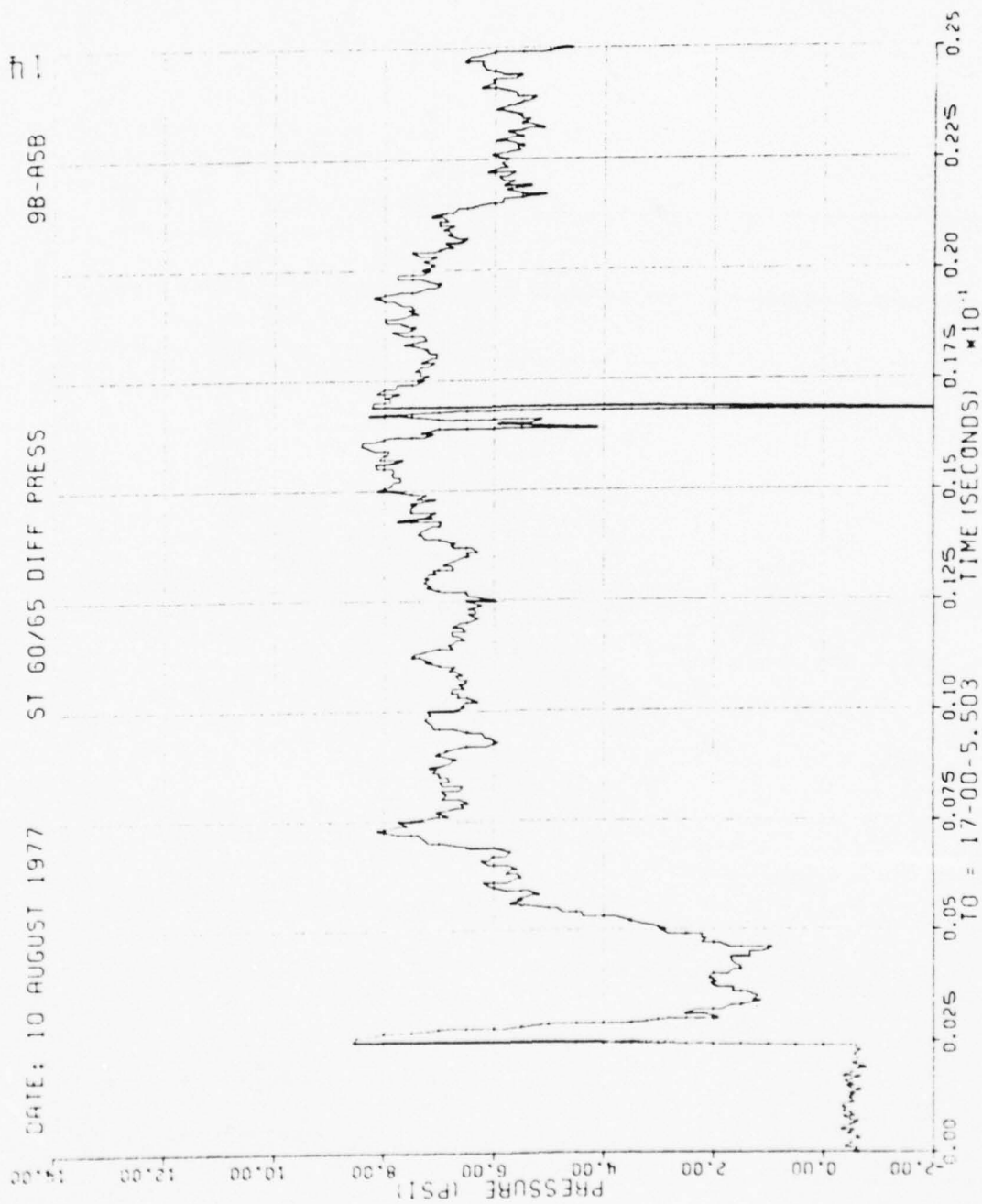


Figure 58. Continued

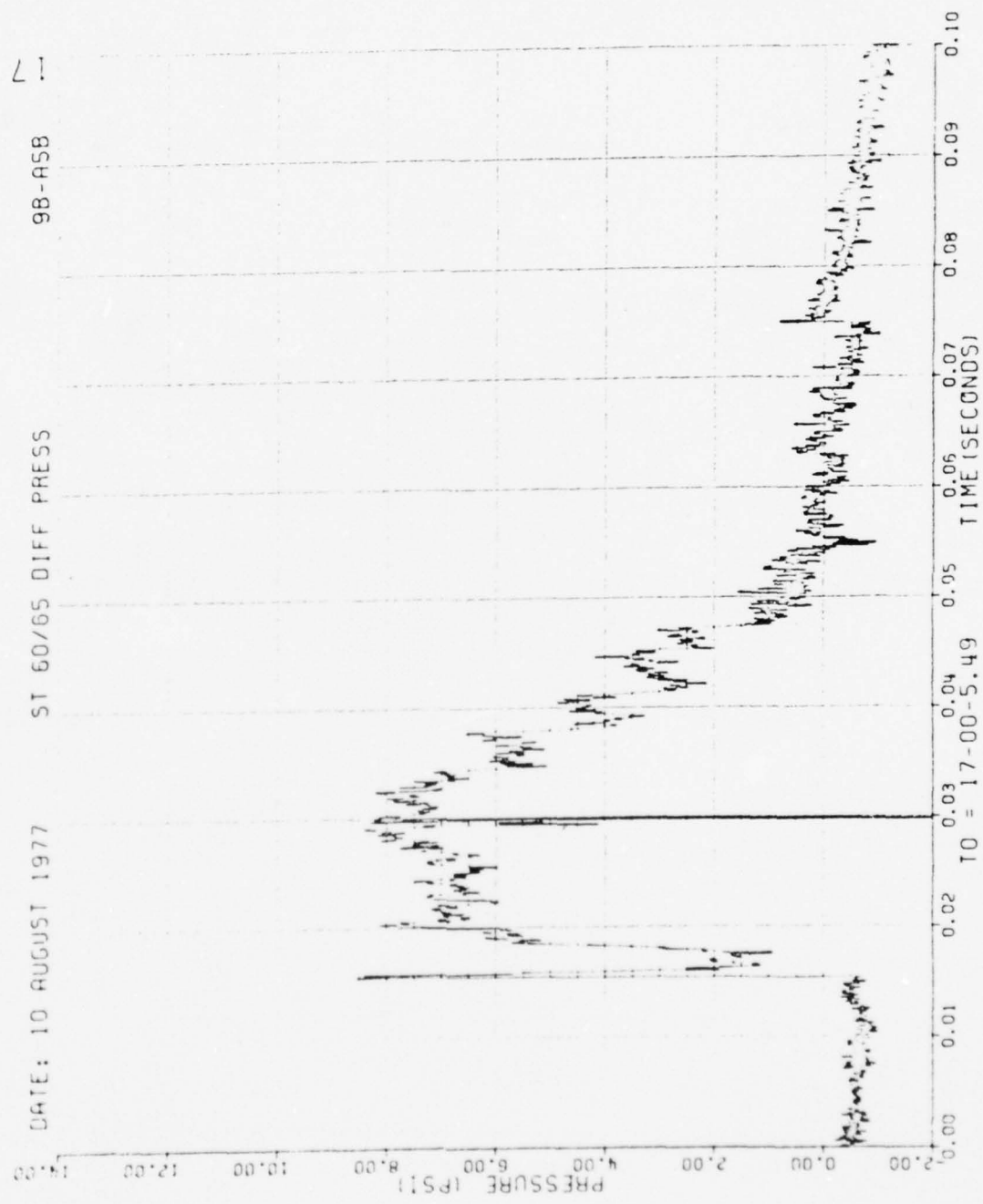


Figure 58. Continued

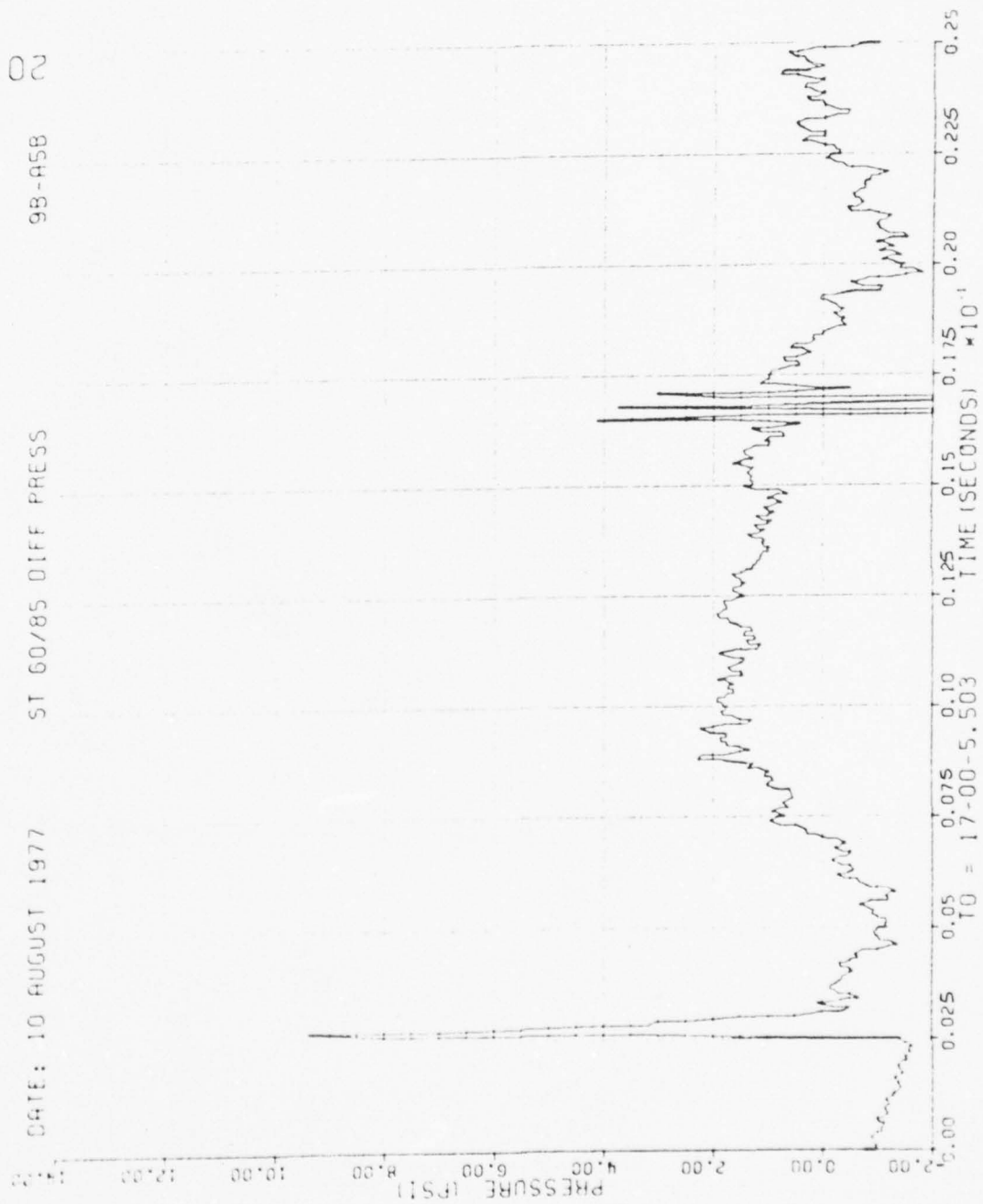


Figure 58. Continued

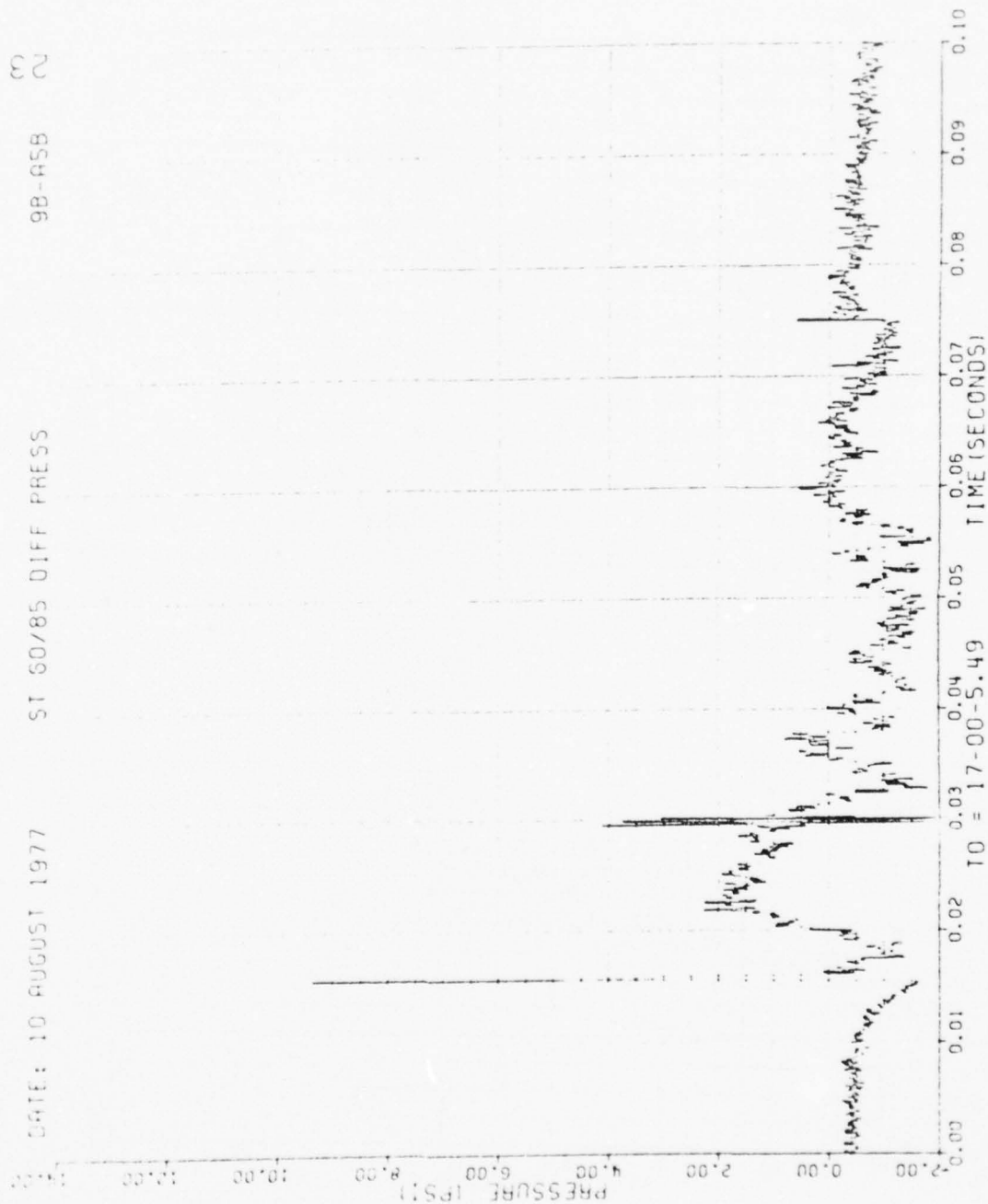


Figure 58. Continued

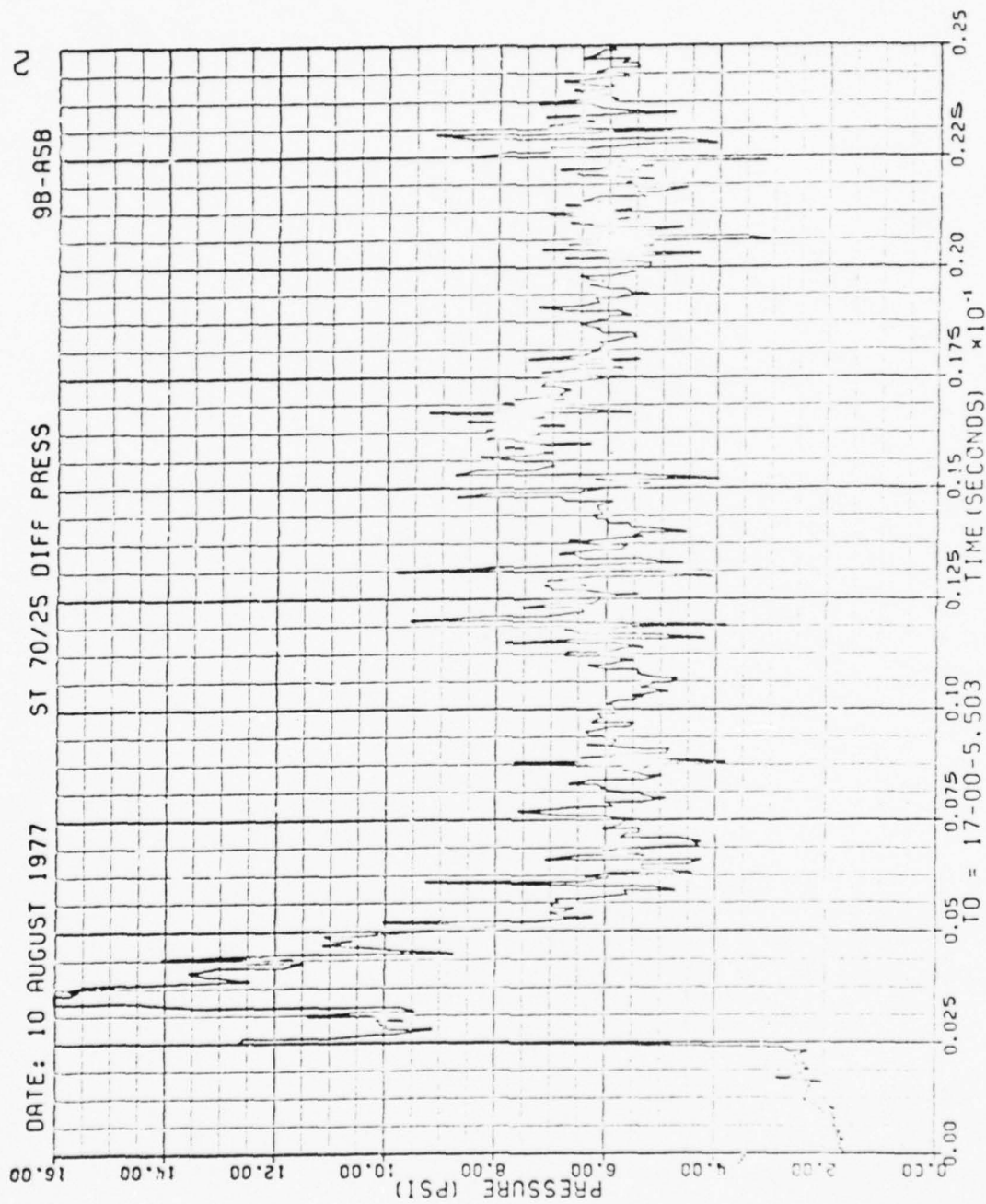


Figure 58. Continued

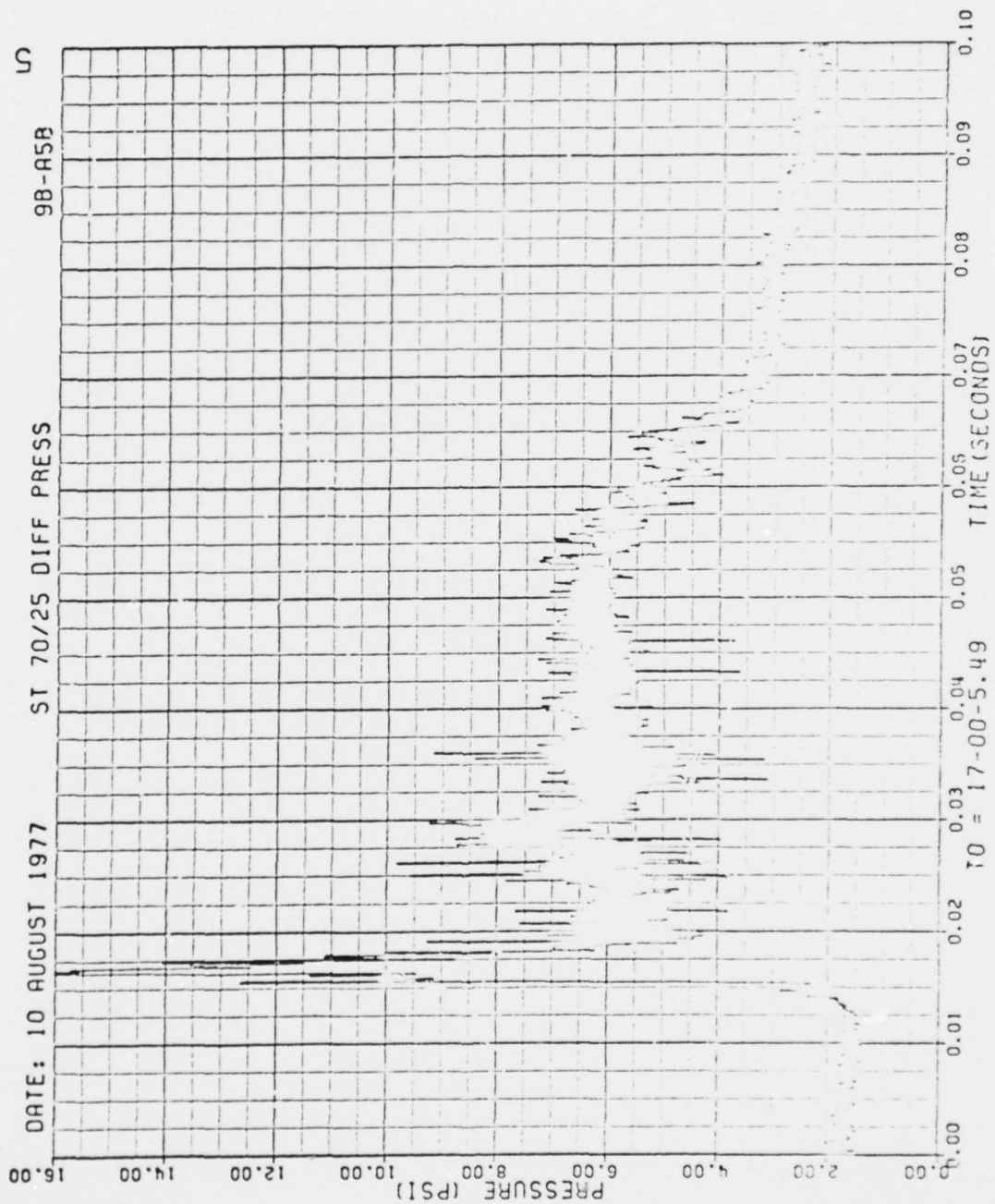


Figure 58. Continued

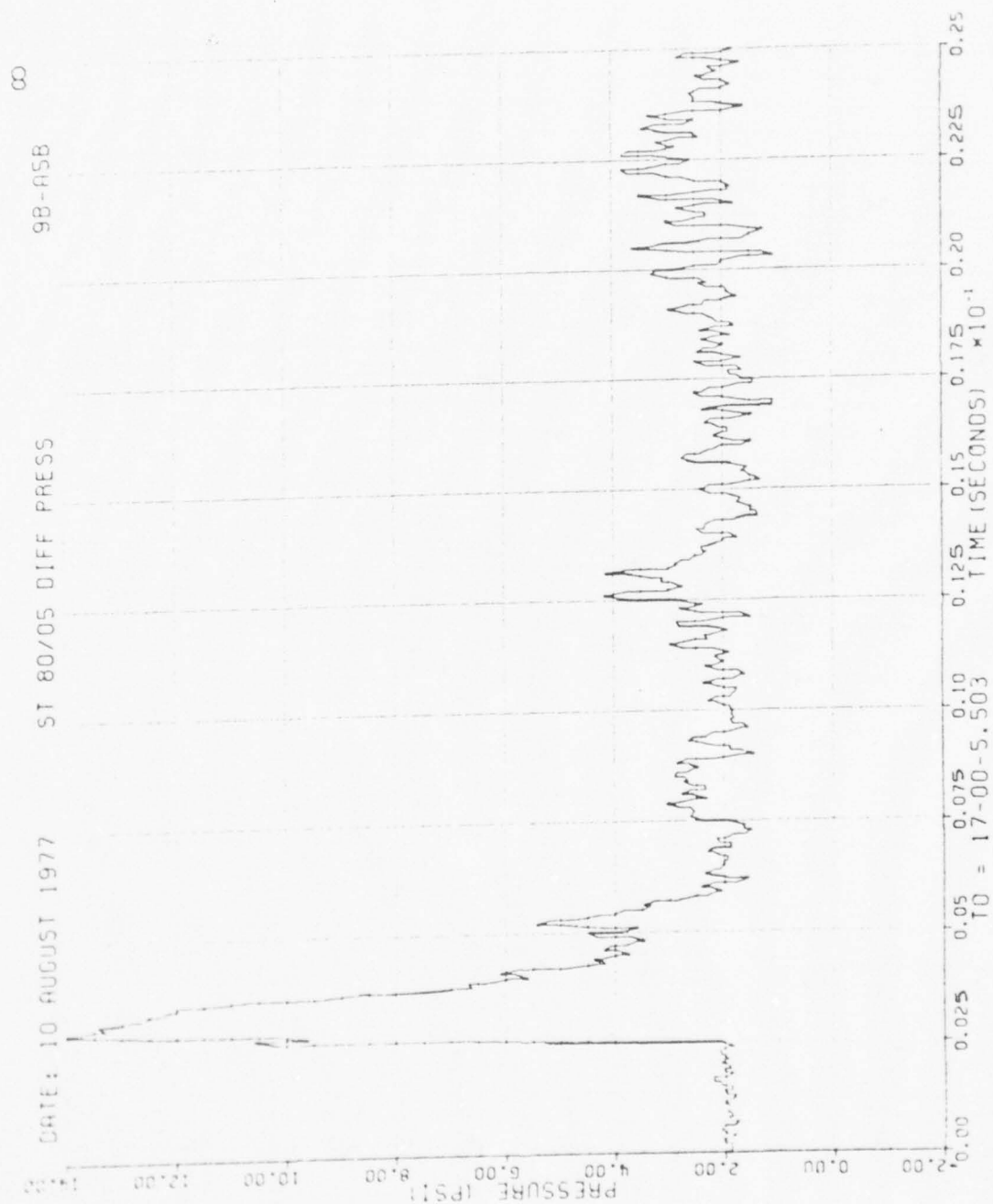


Figure 58. Continued

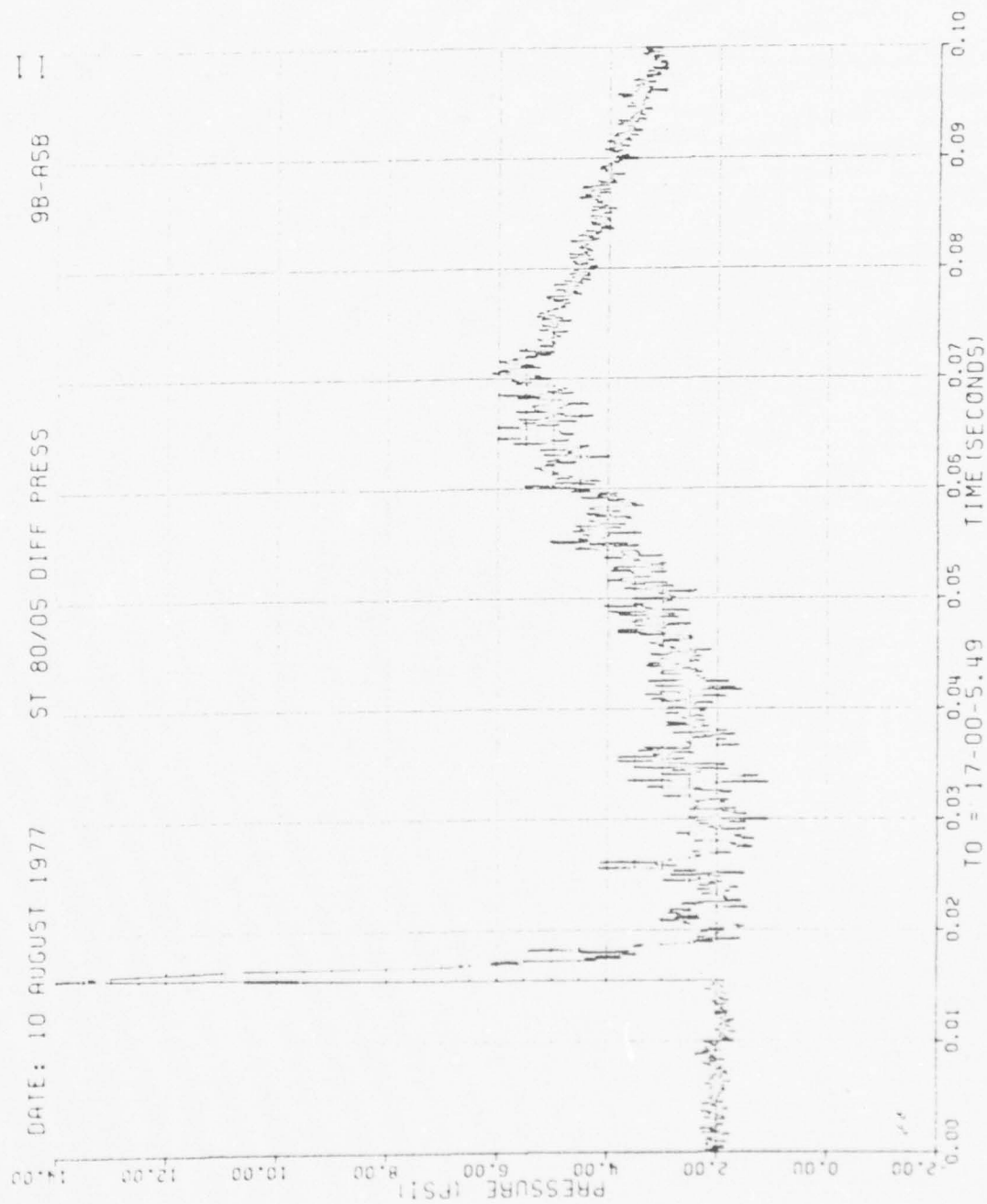


Figure 58. Continued

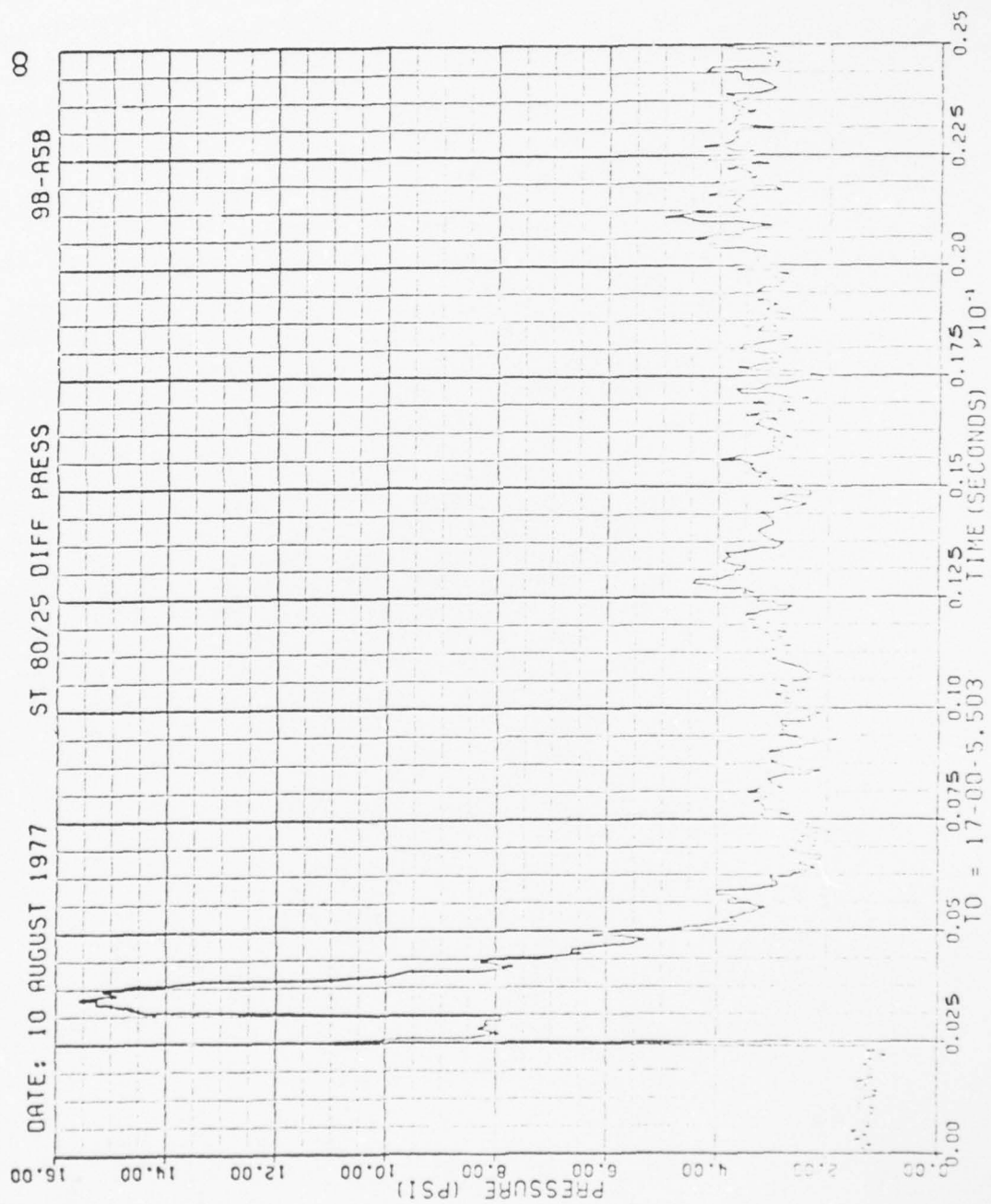


Figure 58. Continued

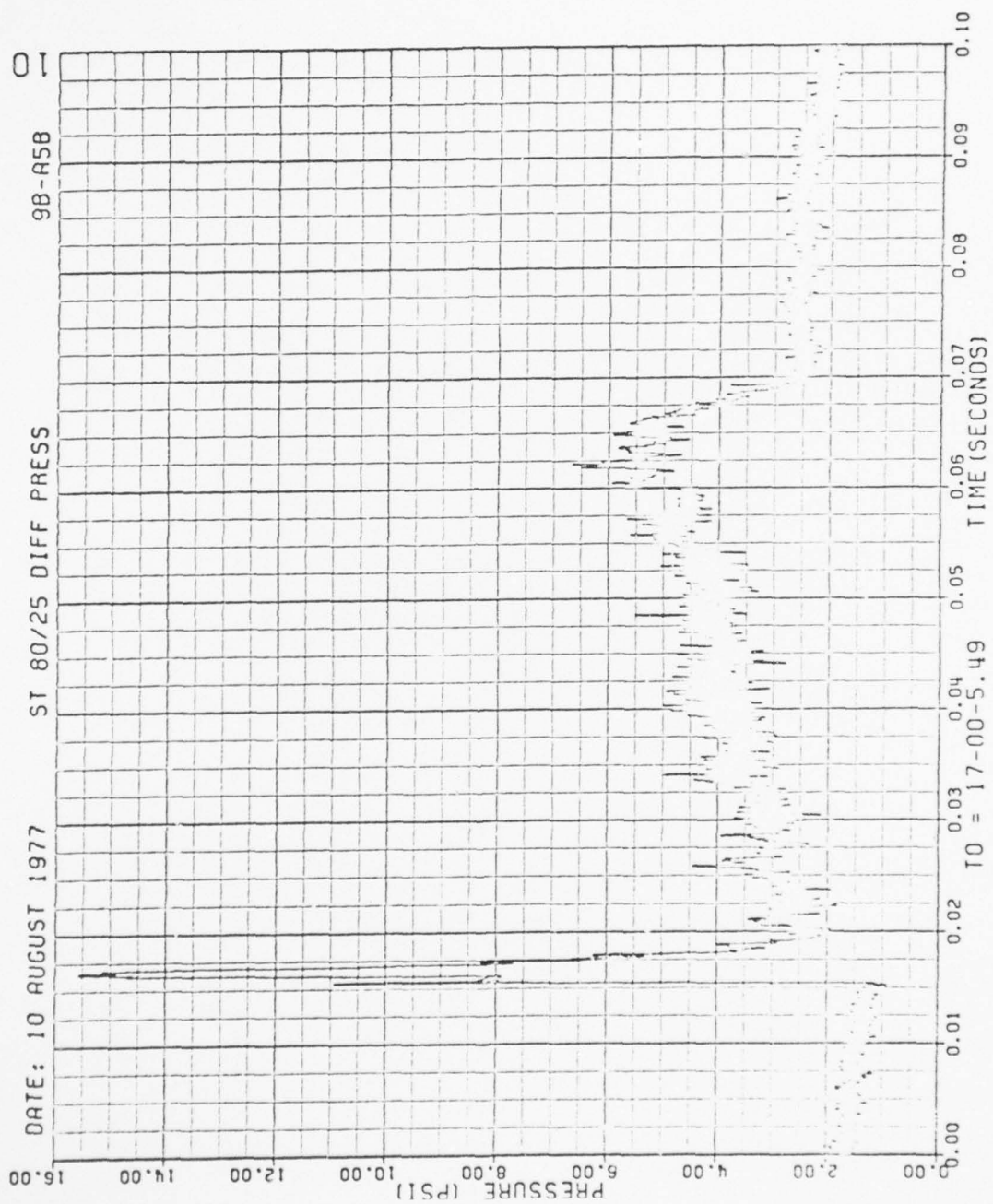


Figure 58. Continued

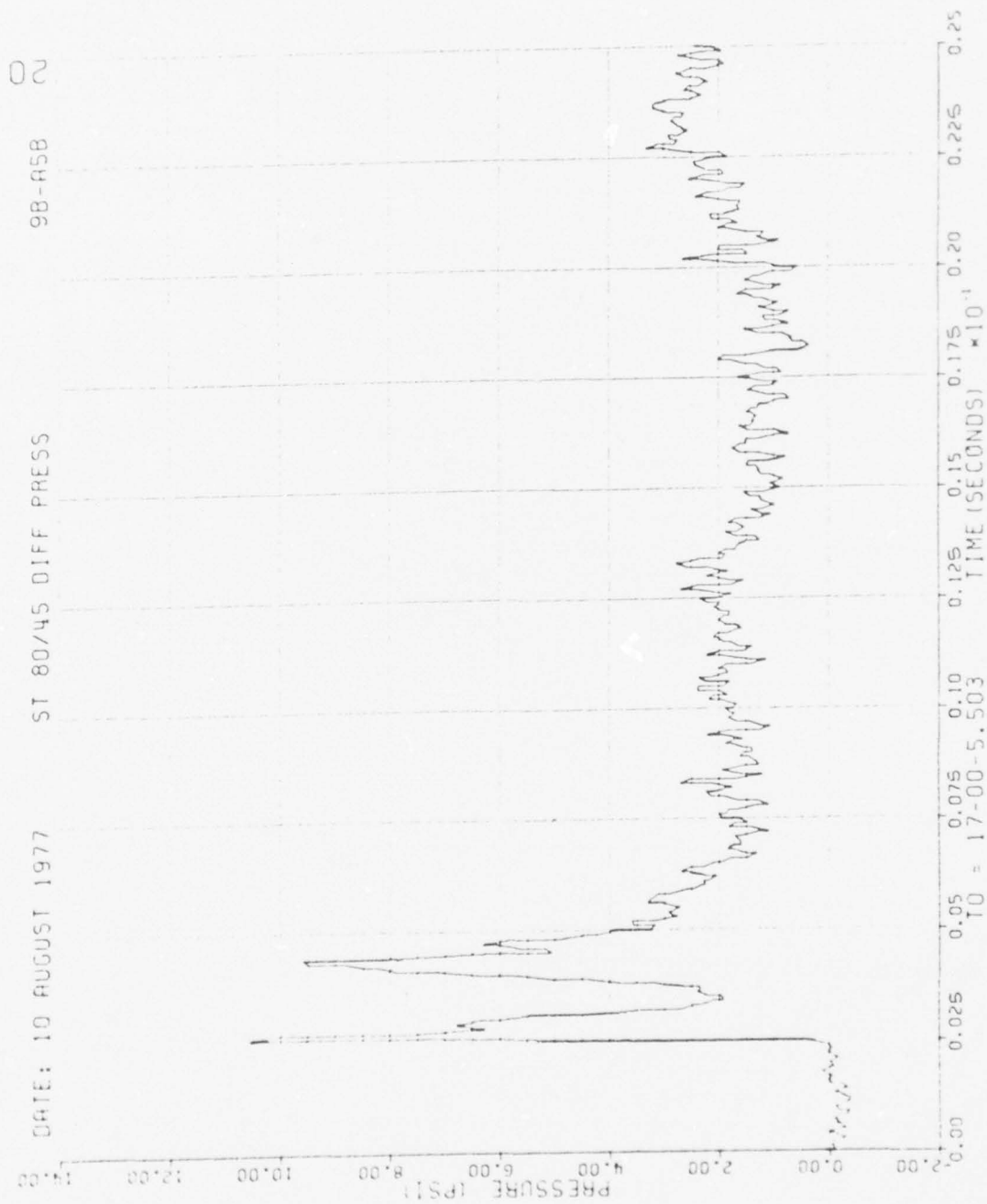


Figure 58. Continued

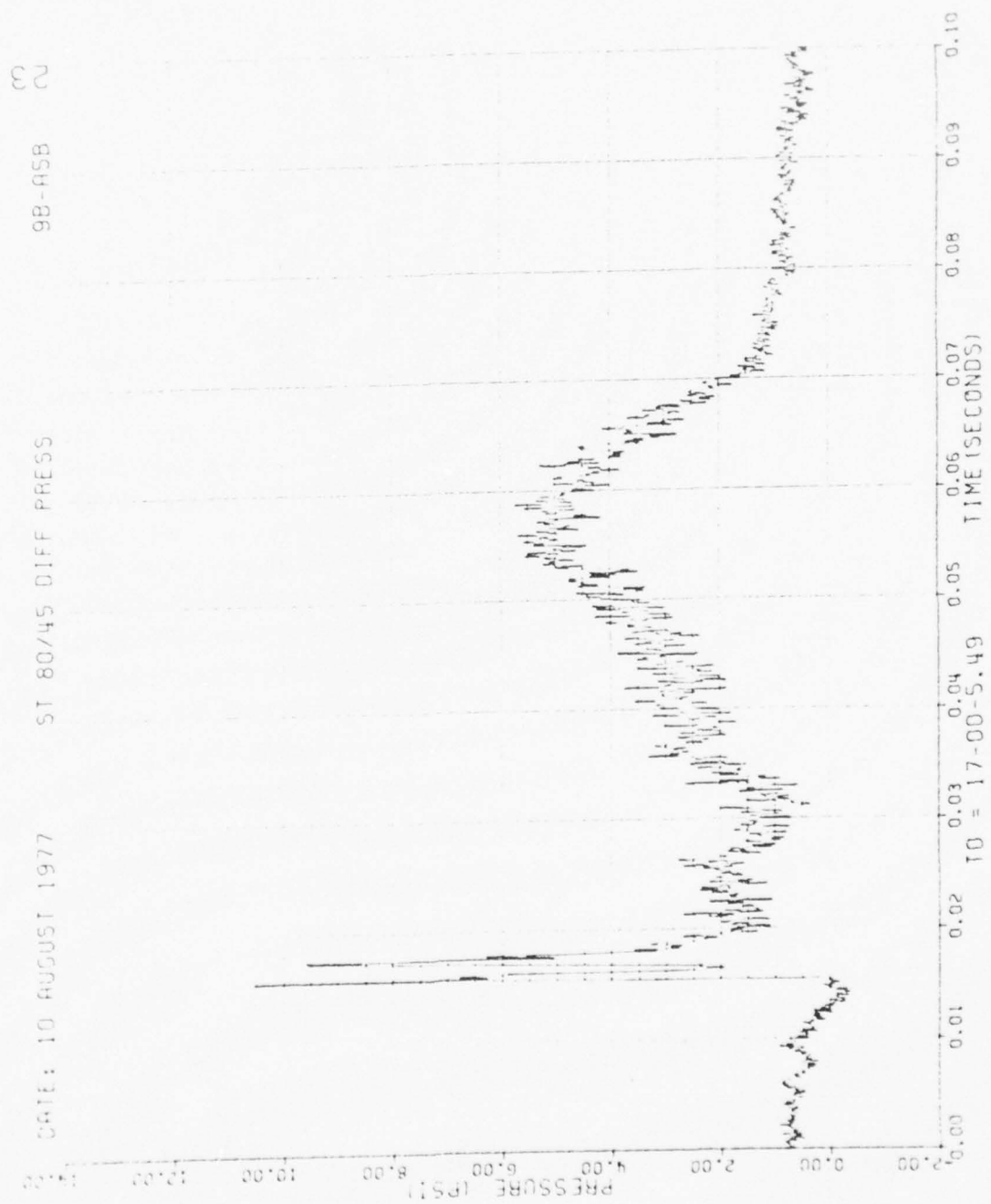


Figure 58. Continued

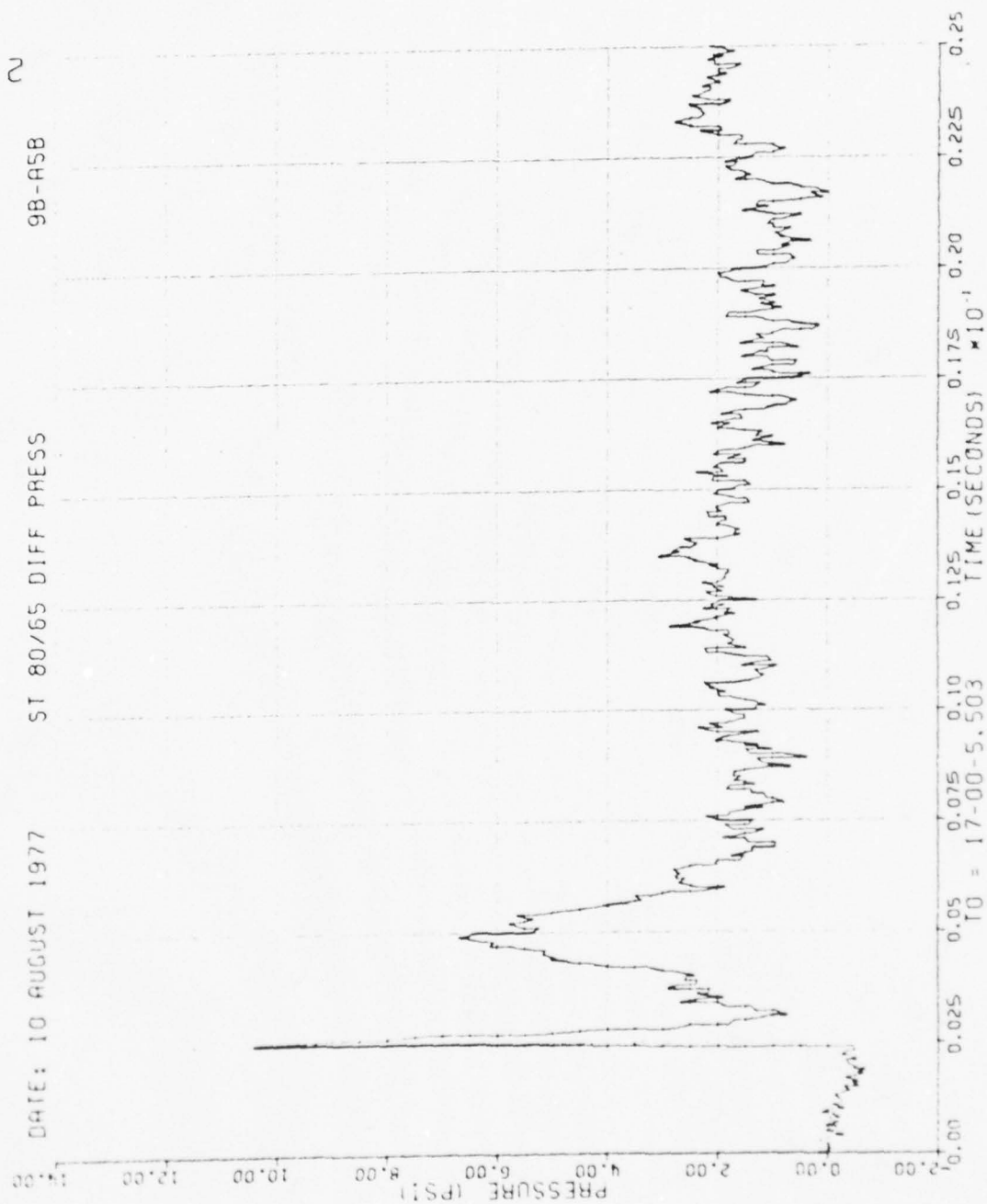


Figure 58. Continued

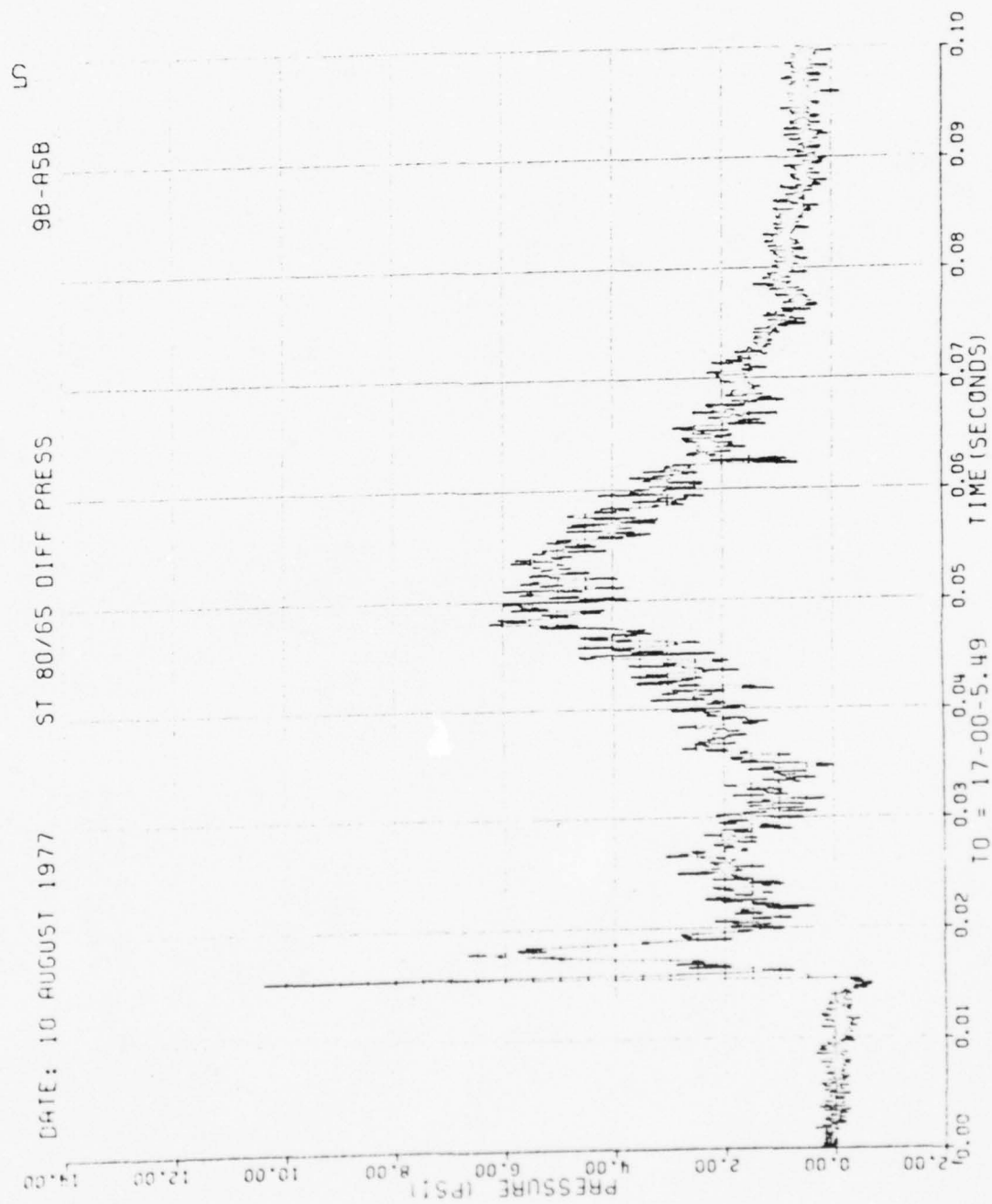


Figure 58. Continued

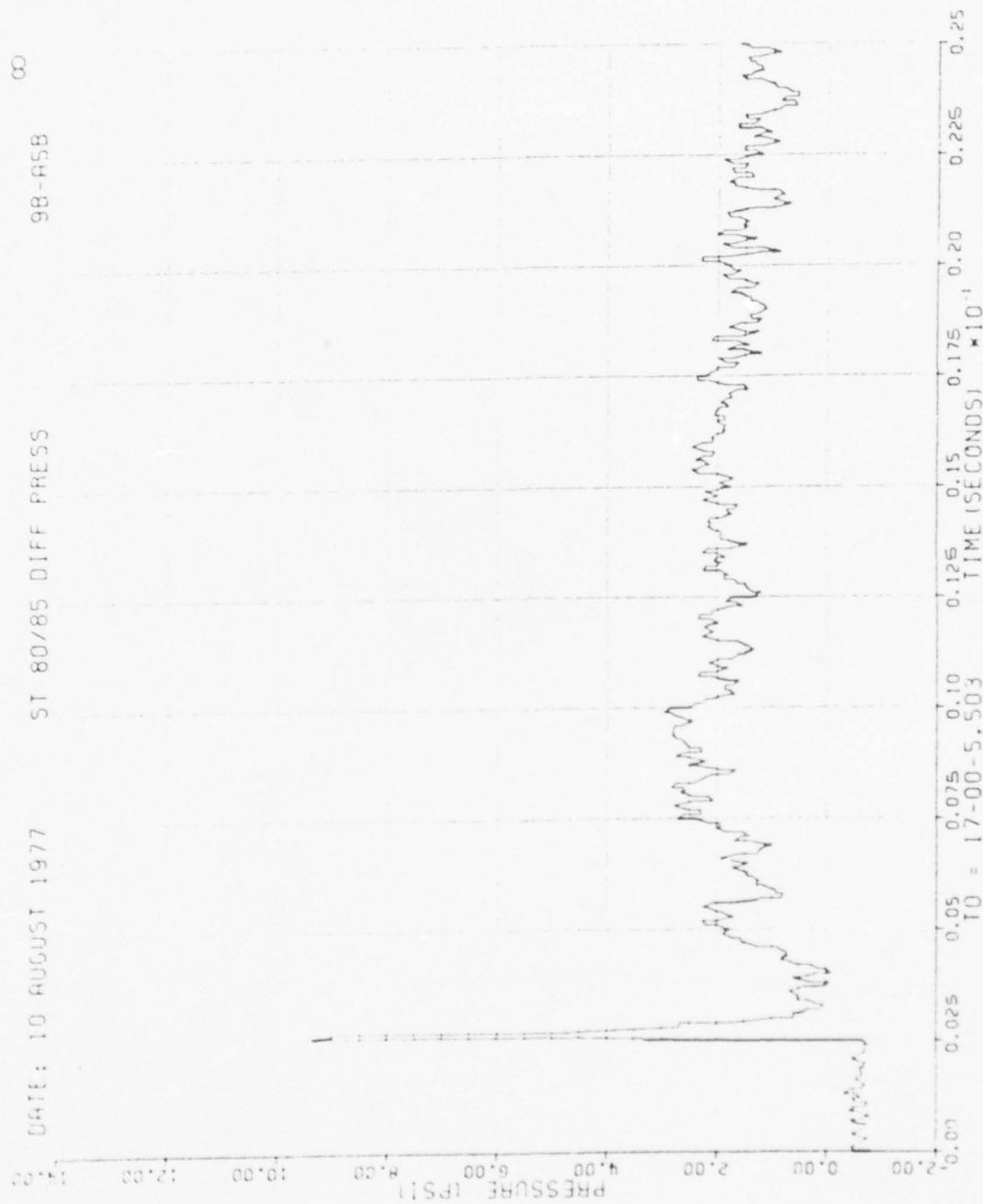


Figure 58. Continued

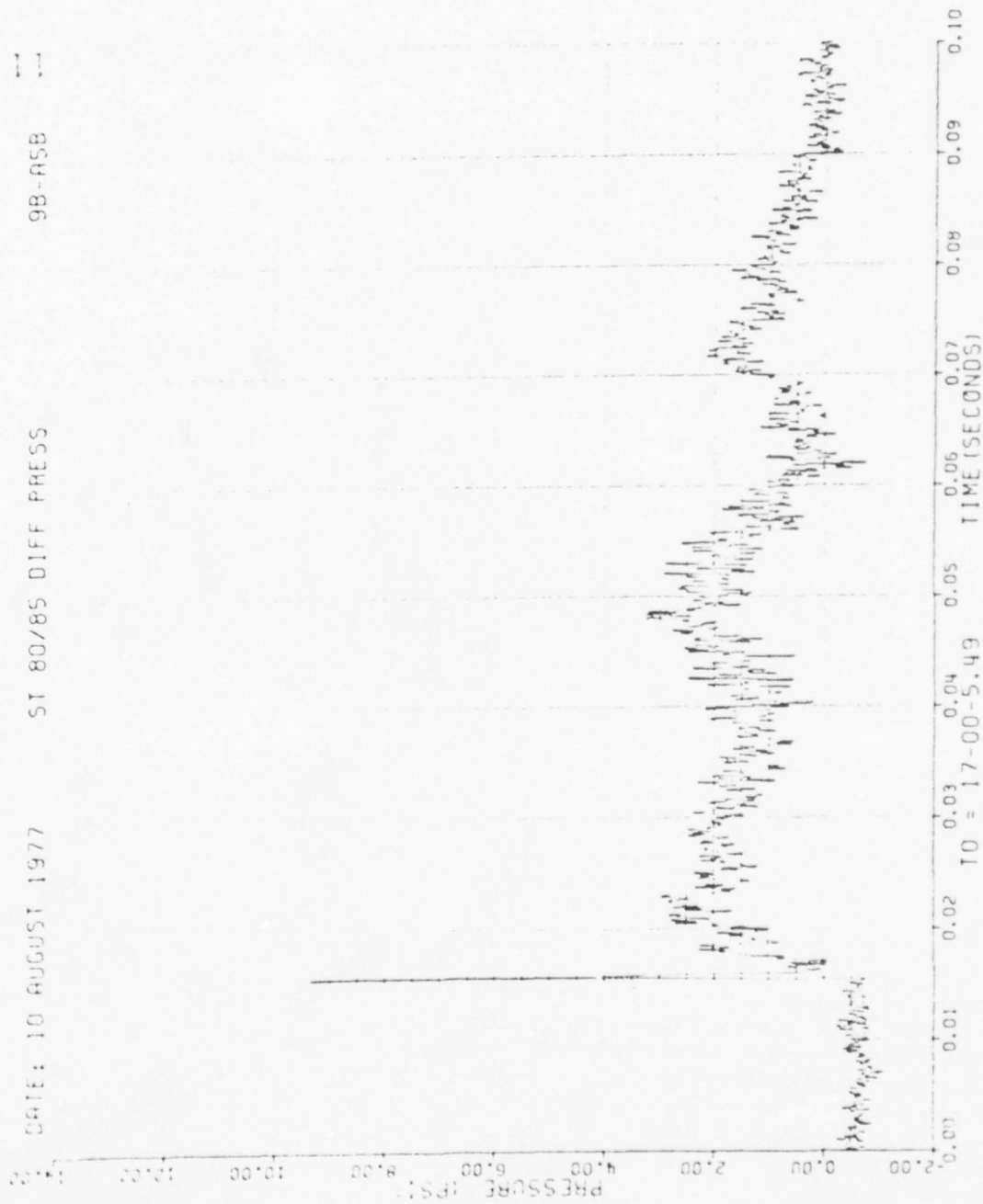


Figure 58. Continued

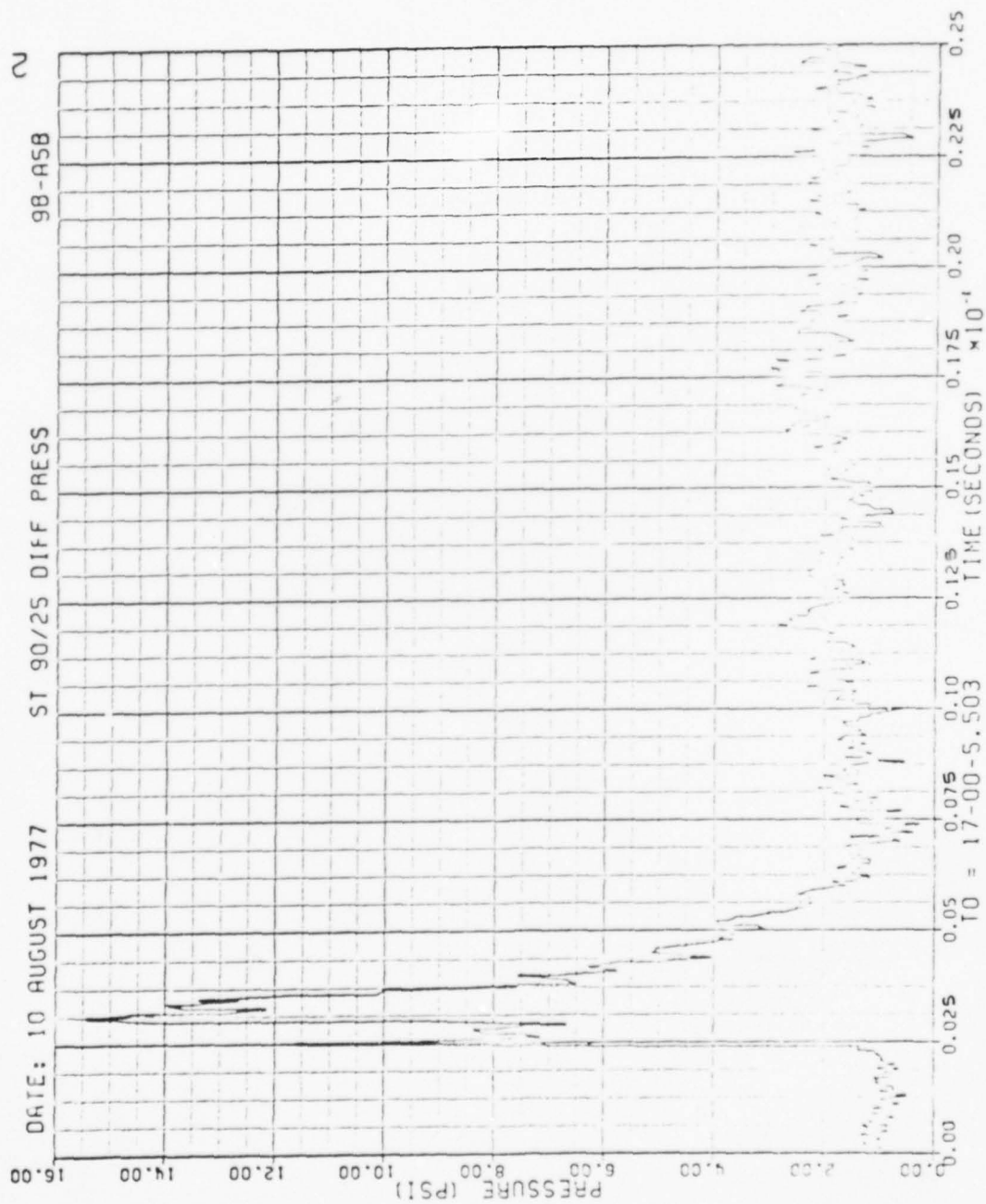


Figure 58. Continued

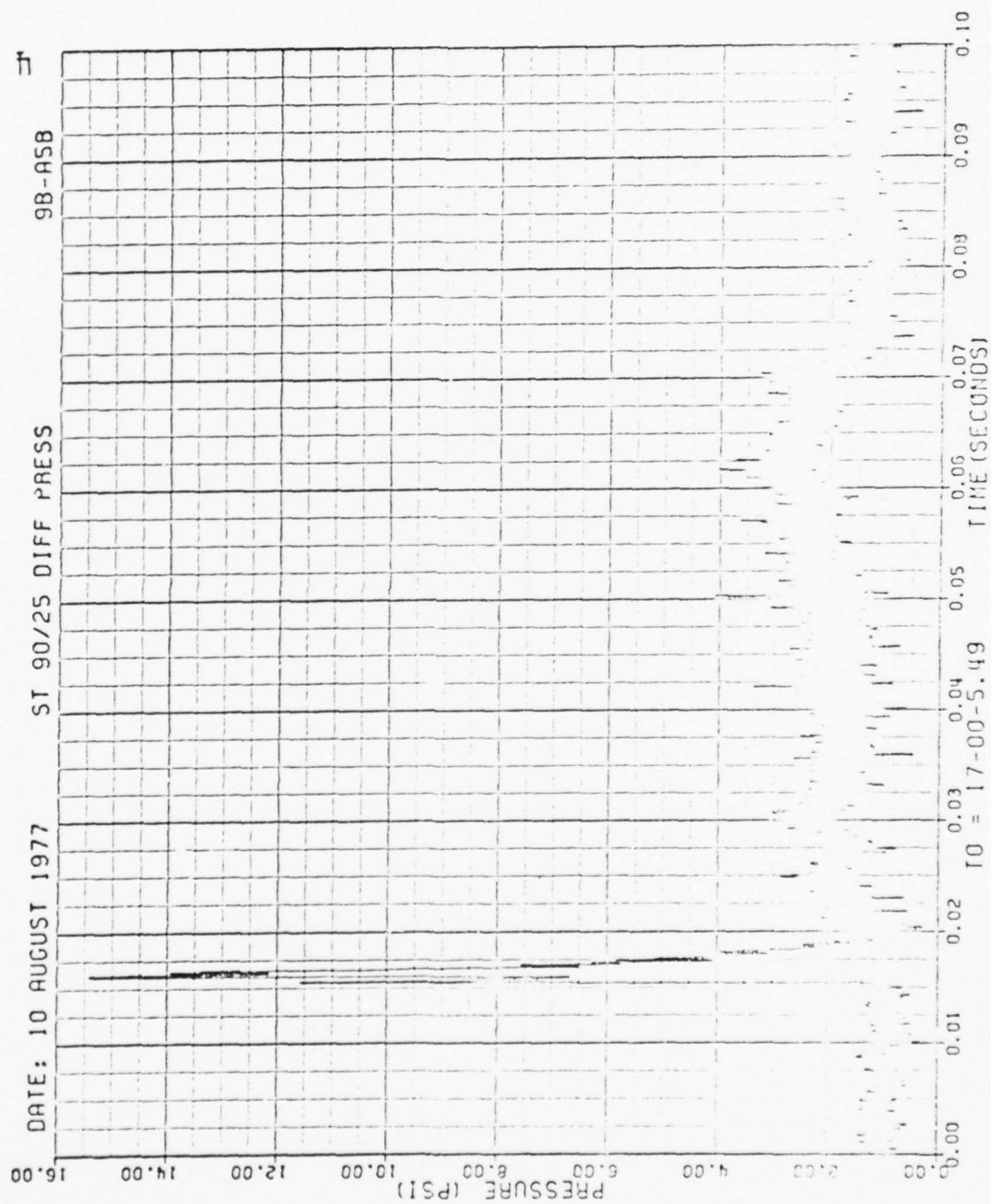


Figure 58. Concluded

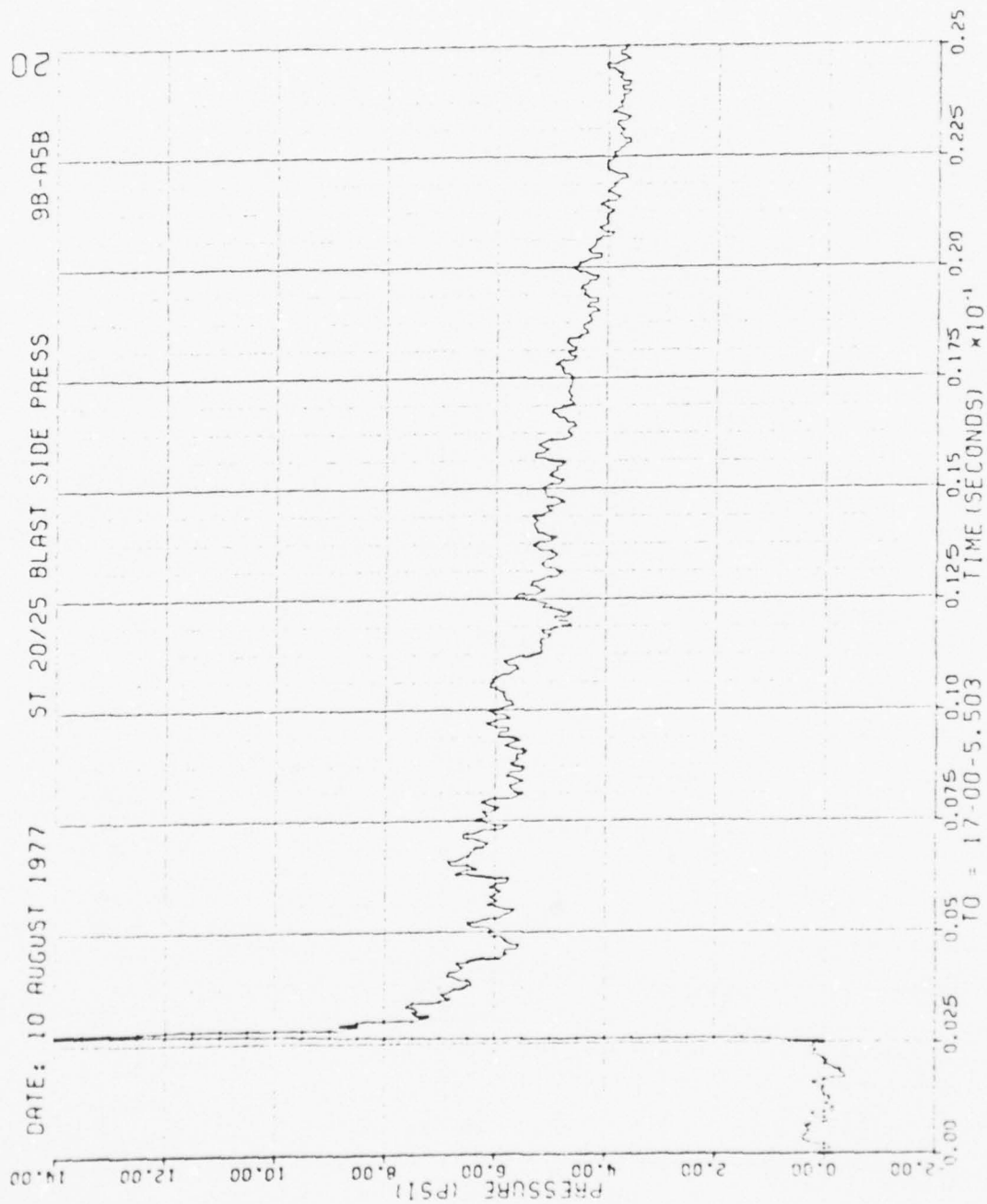


Figure 59. Blastward and Leeward Wing Pressures, Run 9B-A5, Intercept 2.

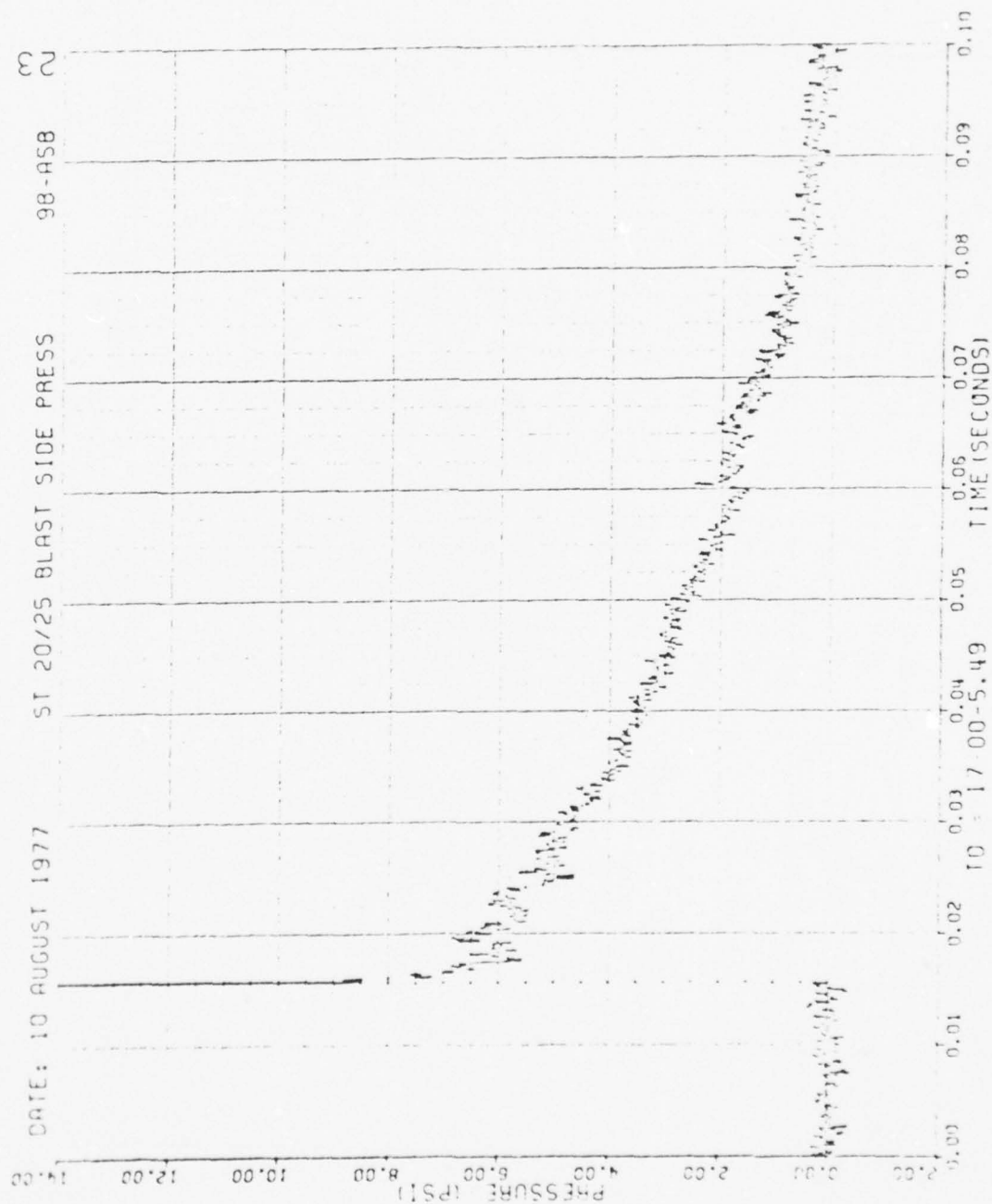


Figure 59. Continued

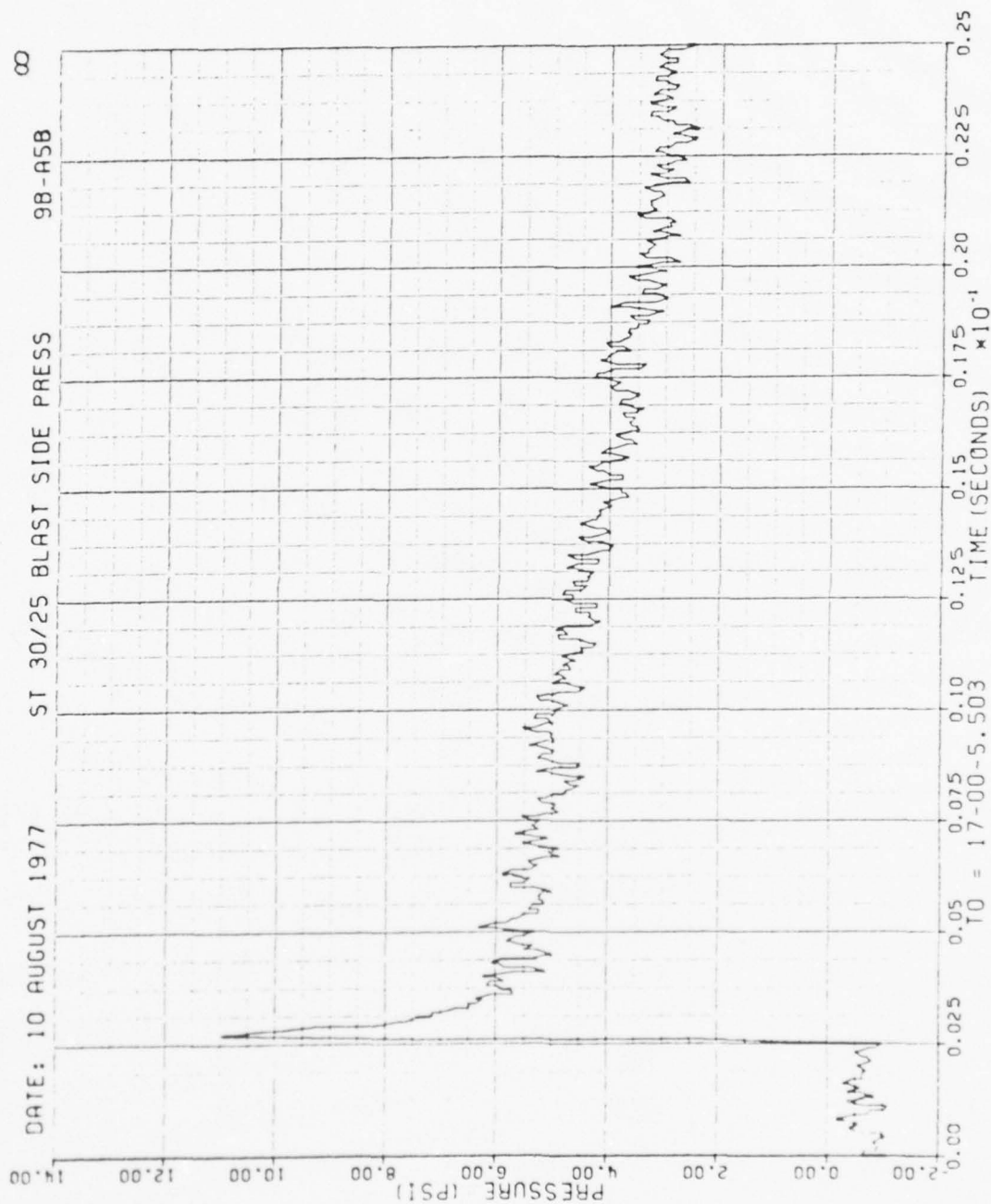


Figure 59. Continued

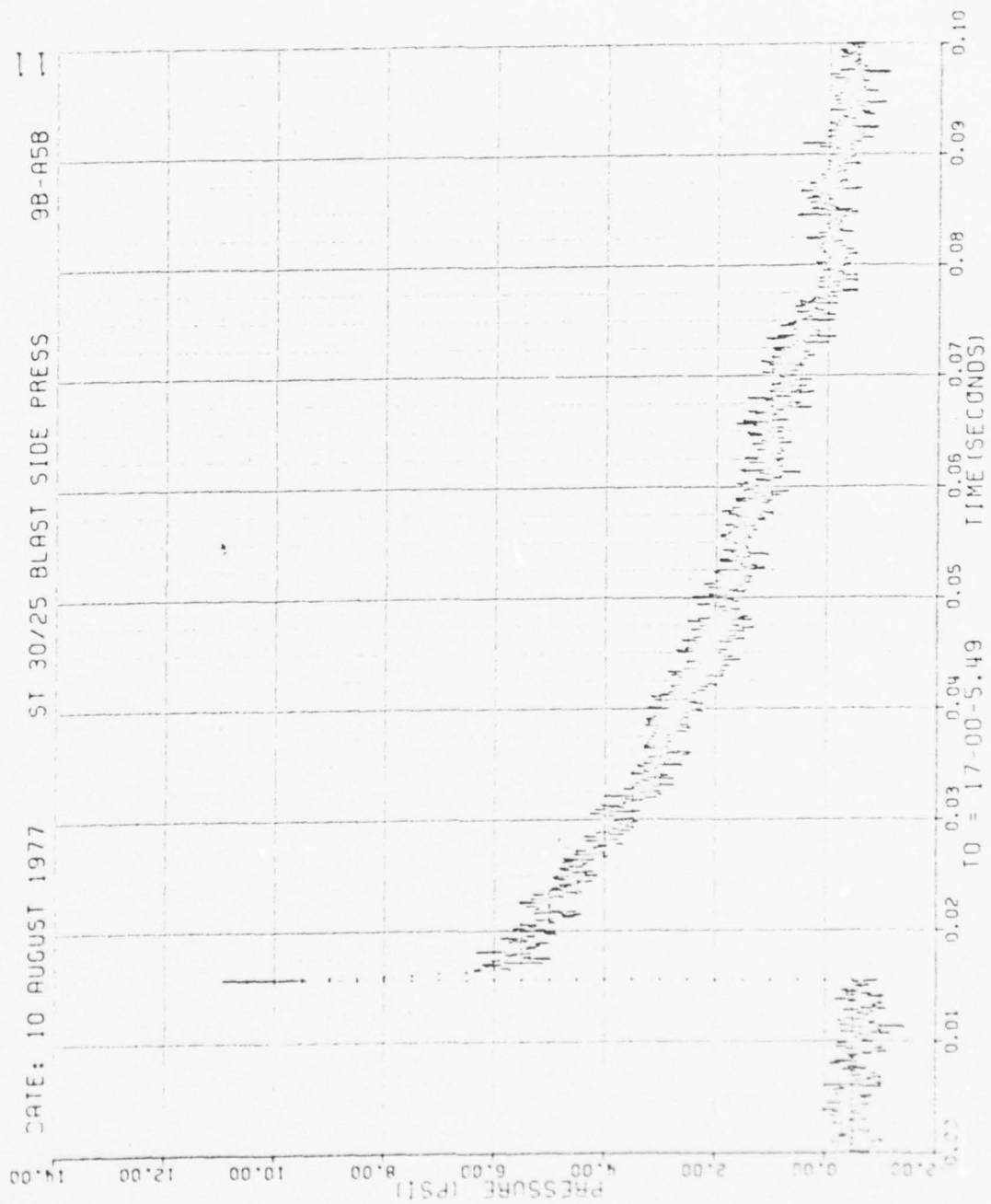


Figure 59. Continued

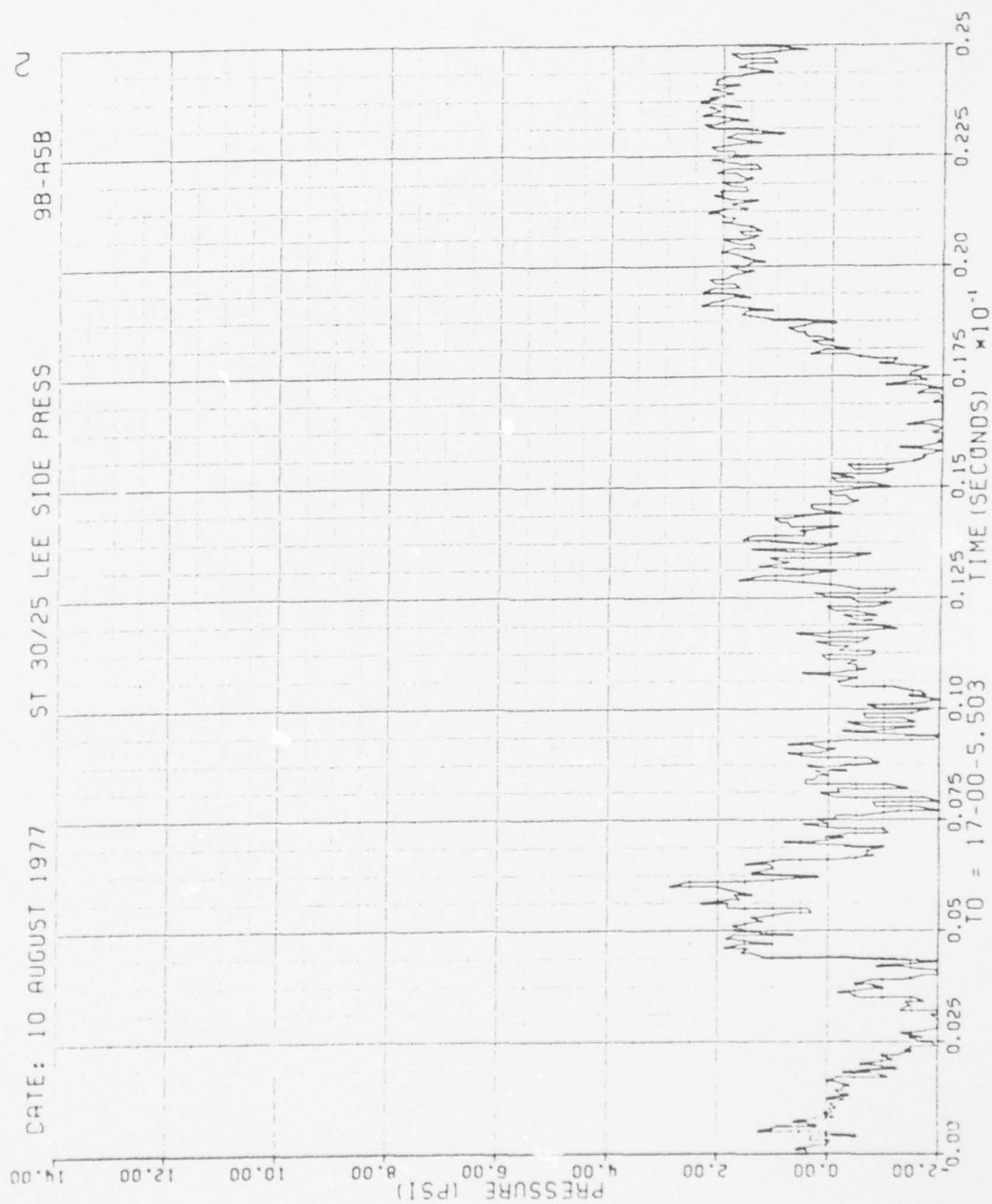


Figure 59. Continued

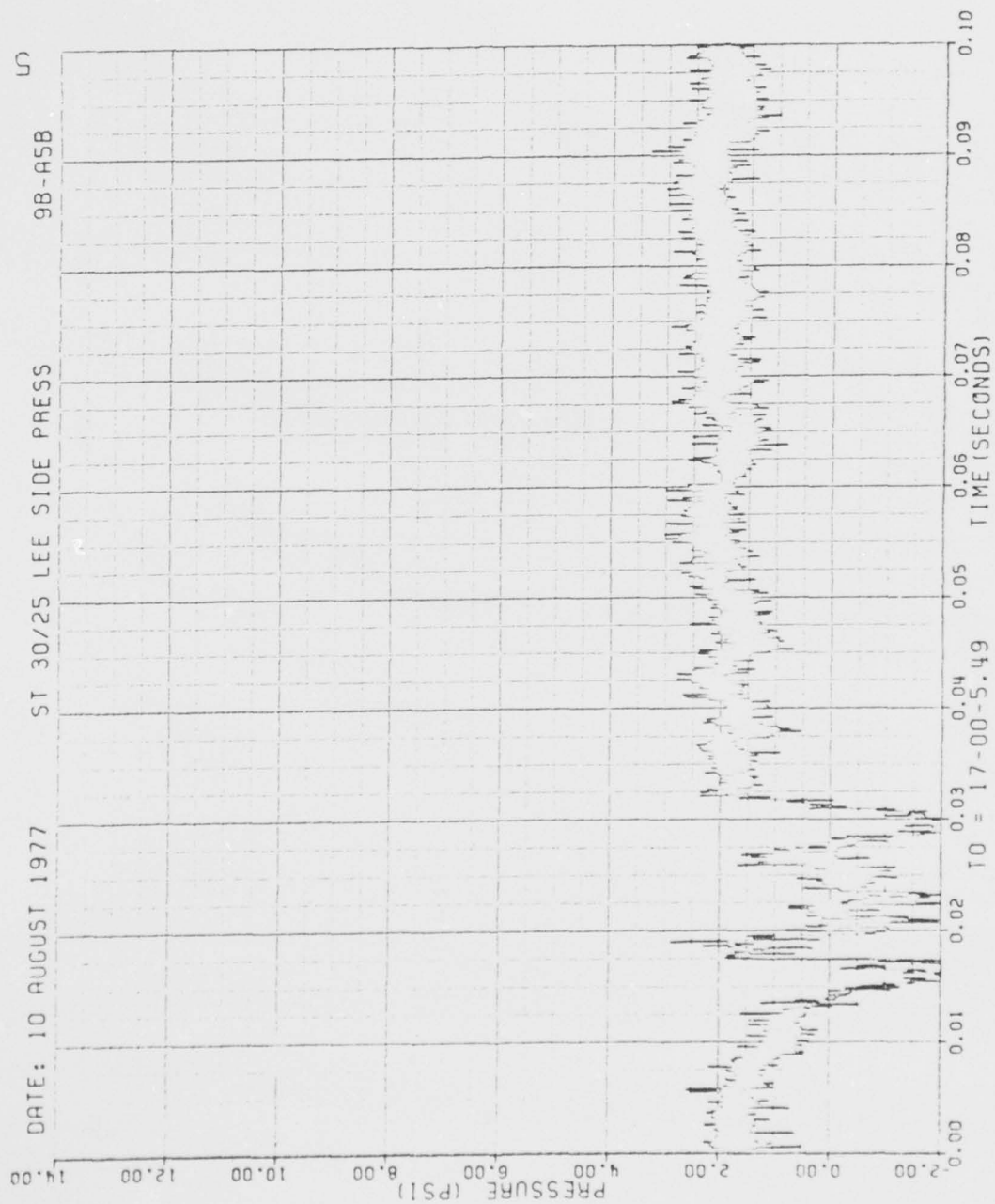


Figure 59. Continued

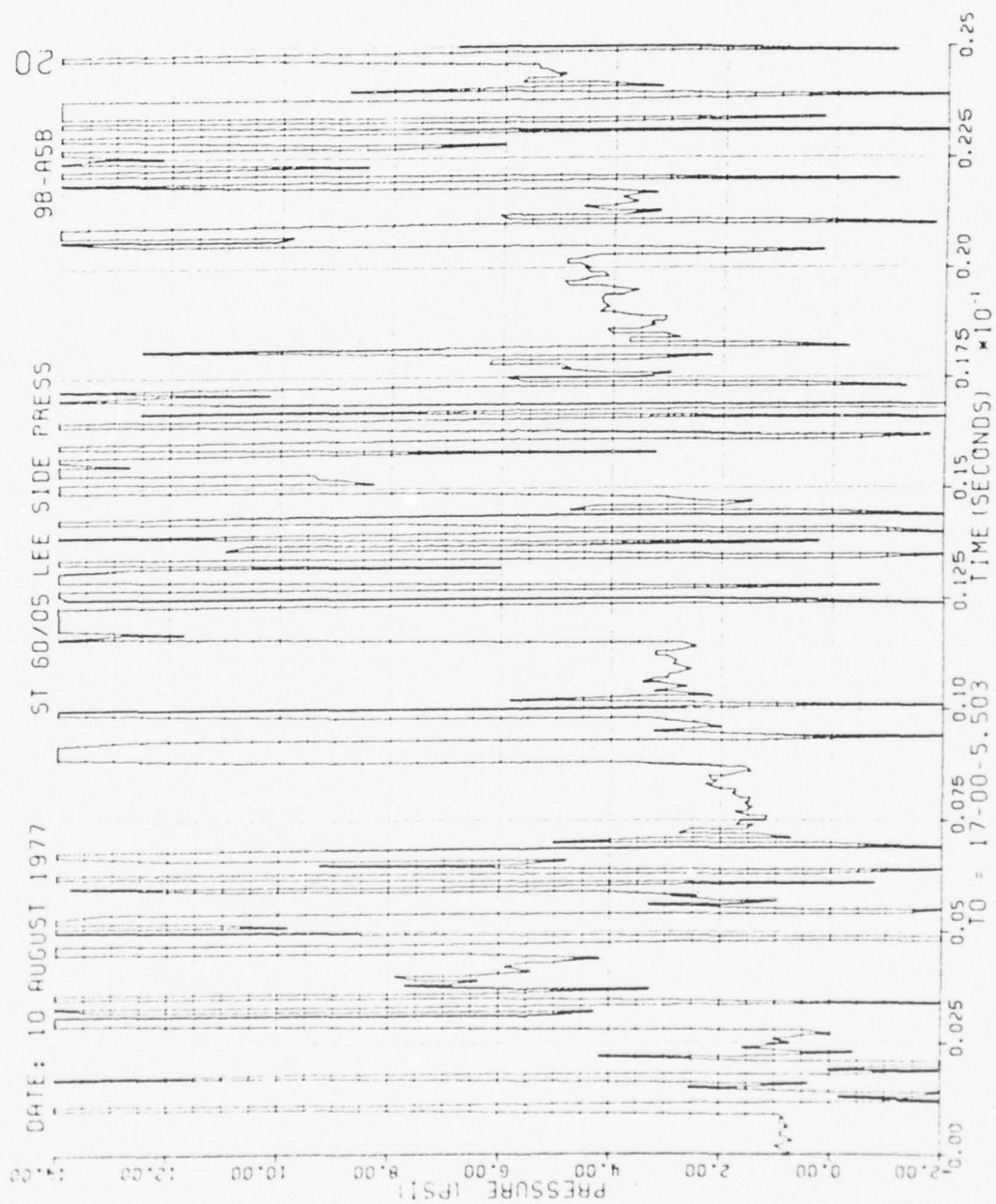


Figure 59. Continued

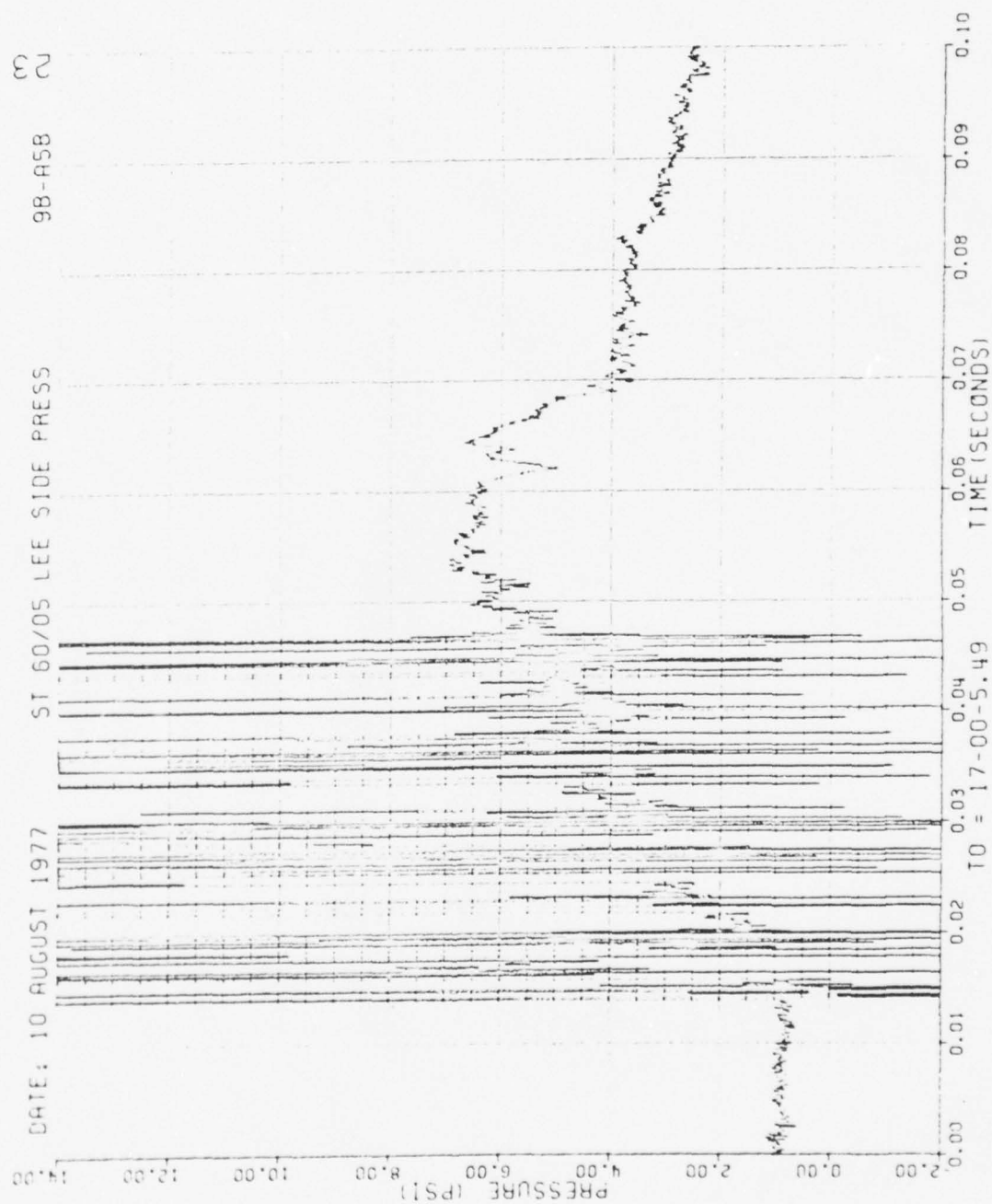


Figure 59. Concluded

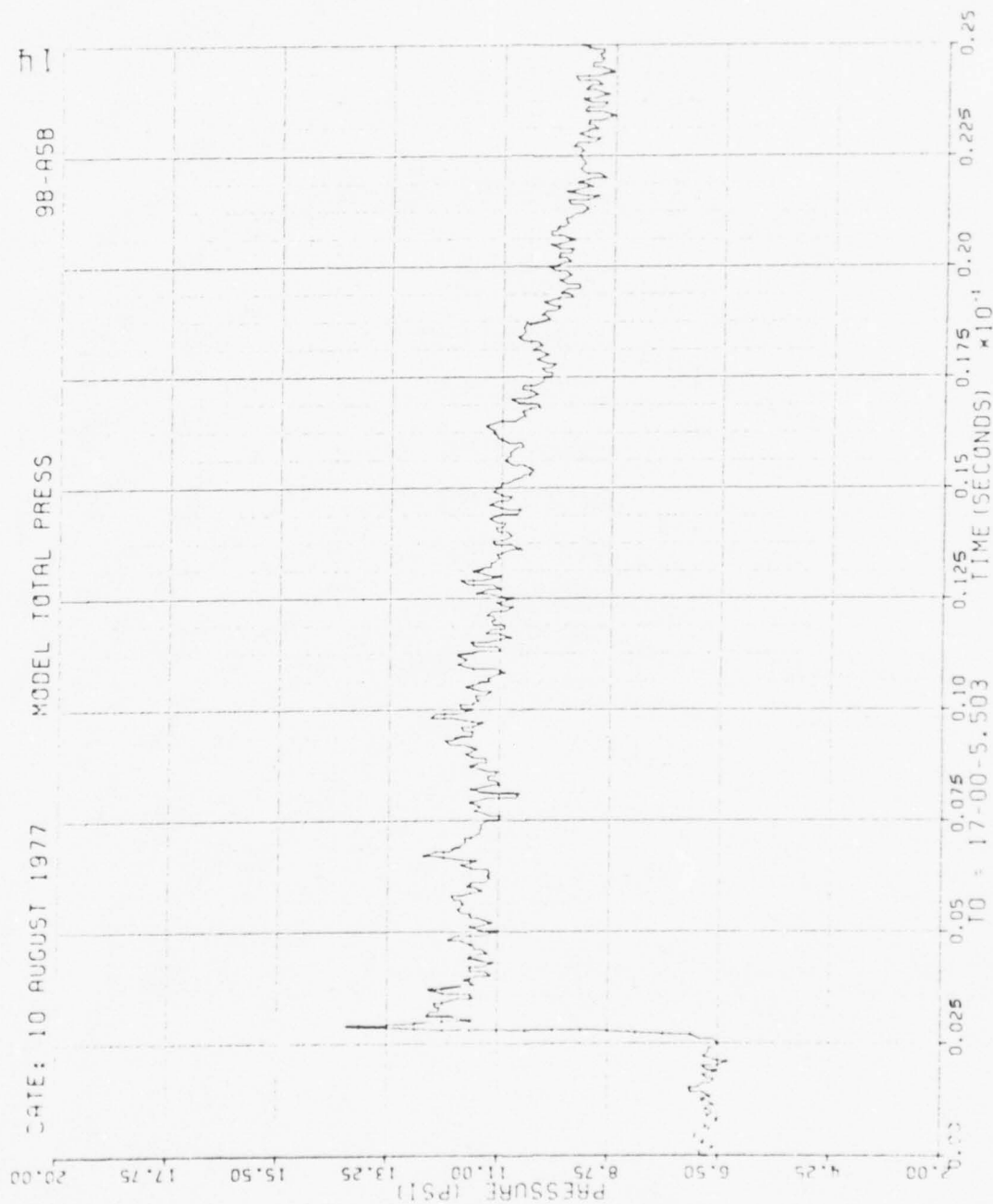


Figure 60. Total Pressure at Model, Run 9B-A5, Intercept 2.

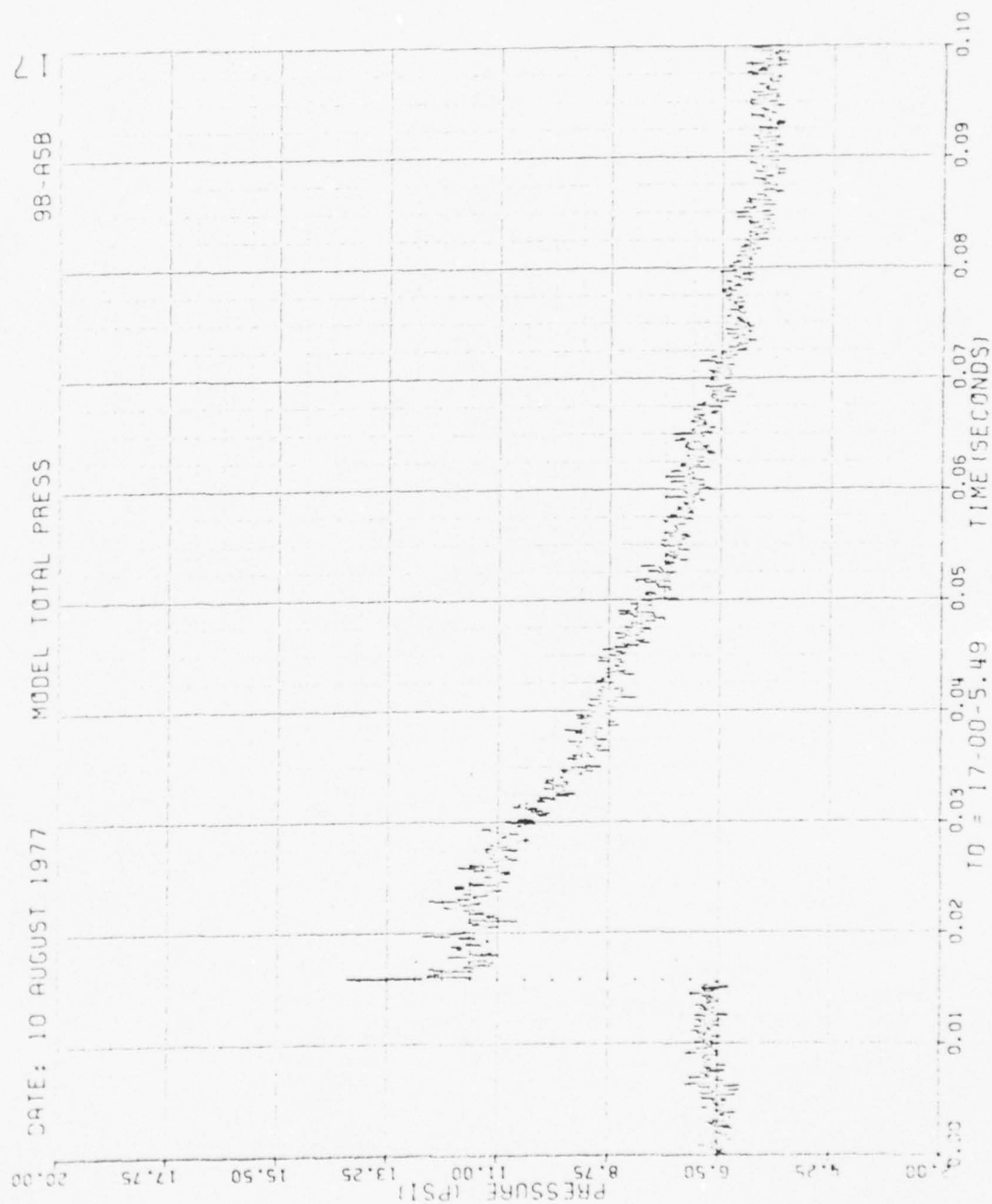


Figure 60. Concluded

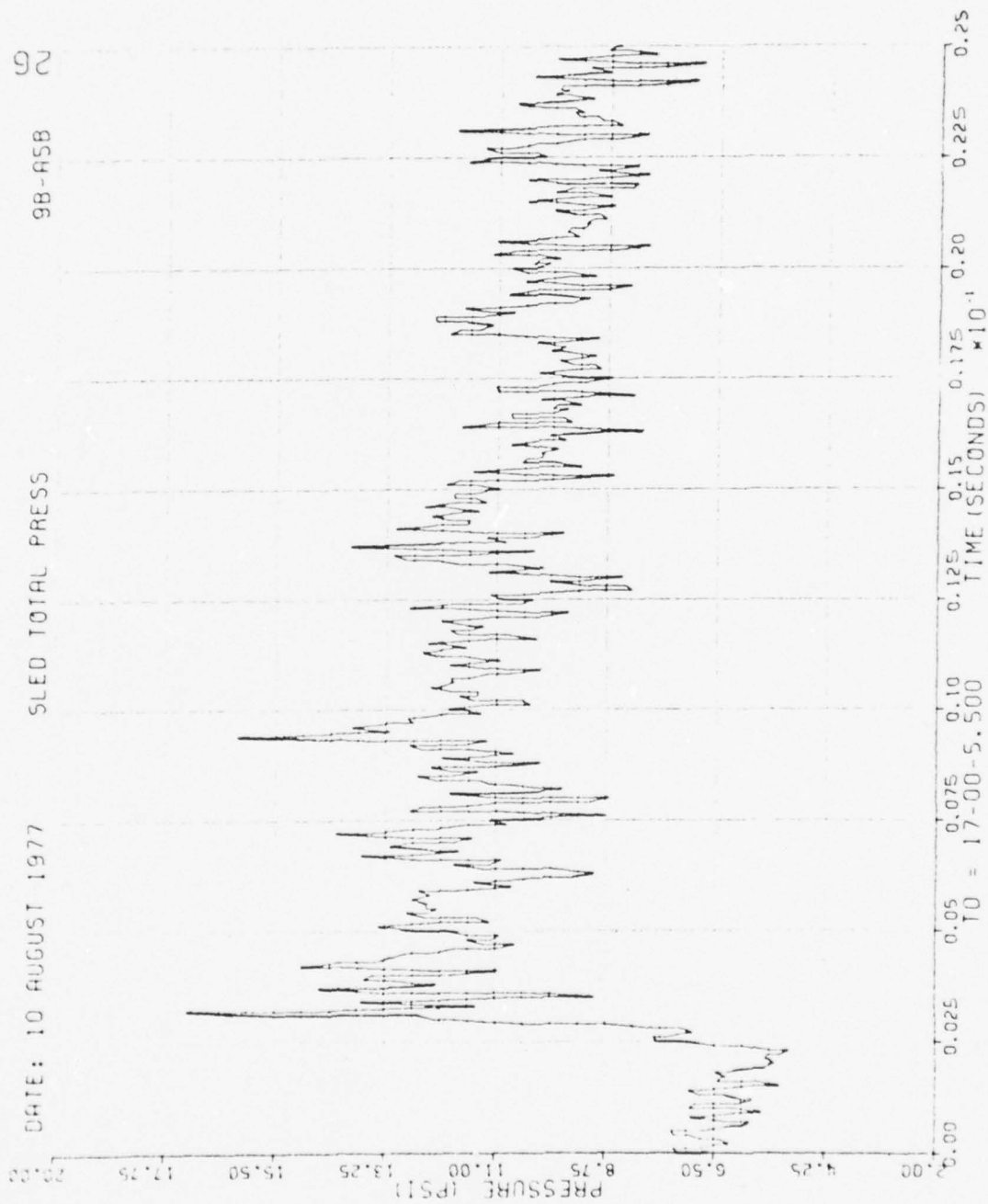


Figure 61. Total Pressure at Sled, Run 9B-A5, Intercept 2.

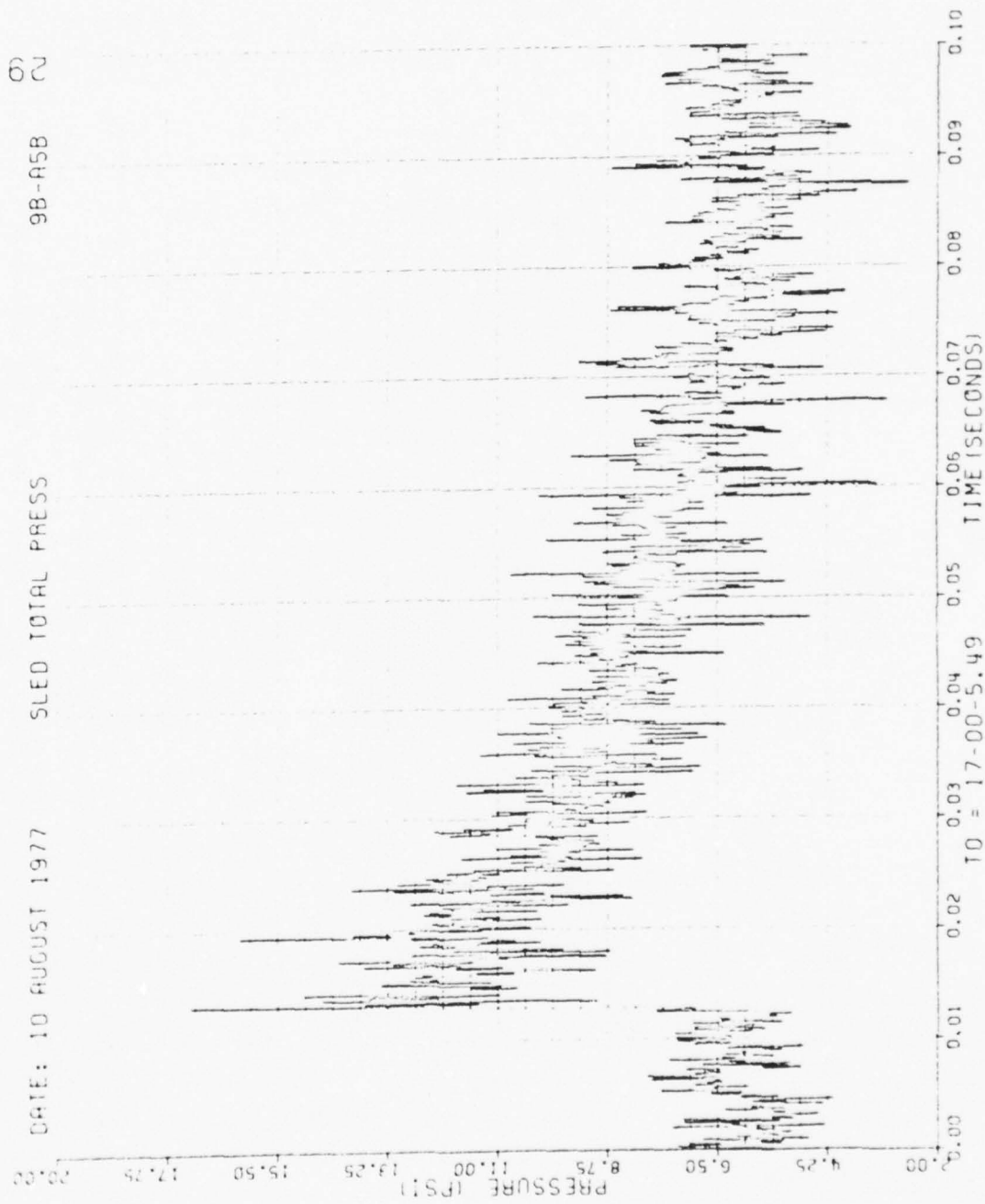


Figure 61. Concluded

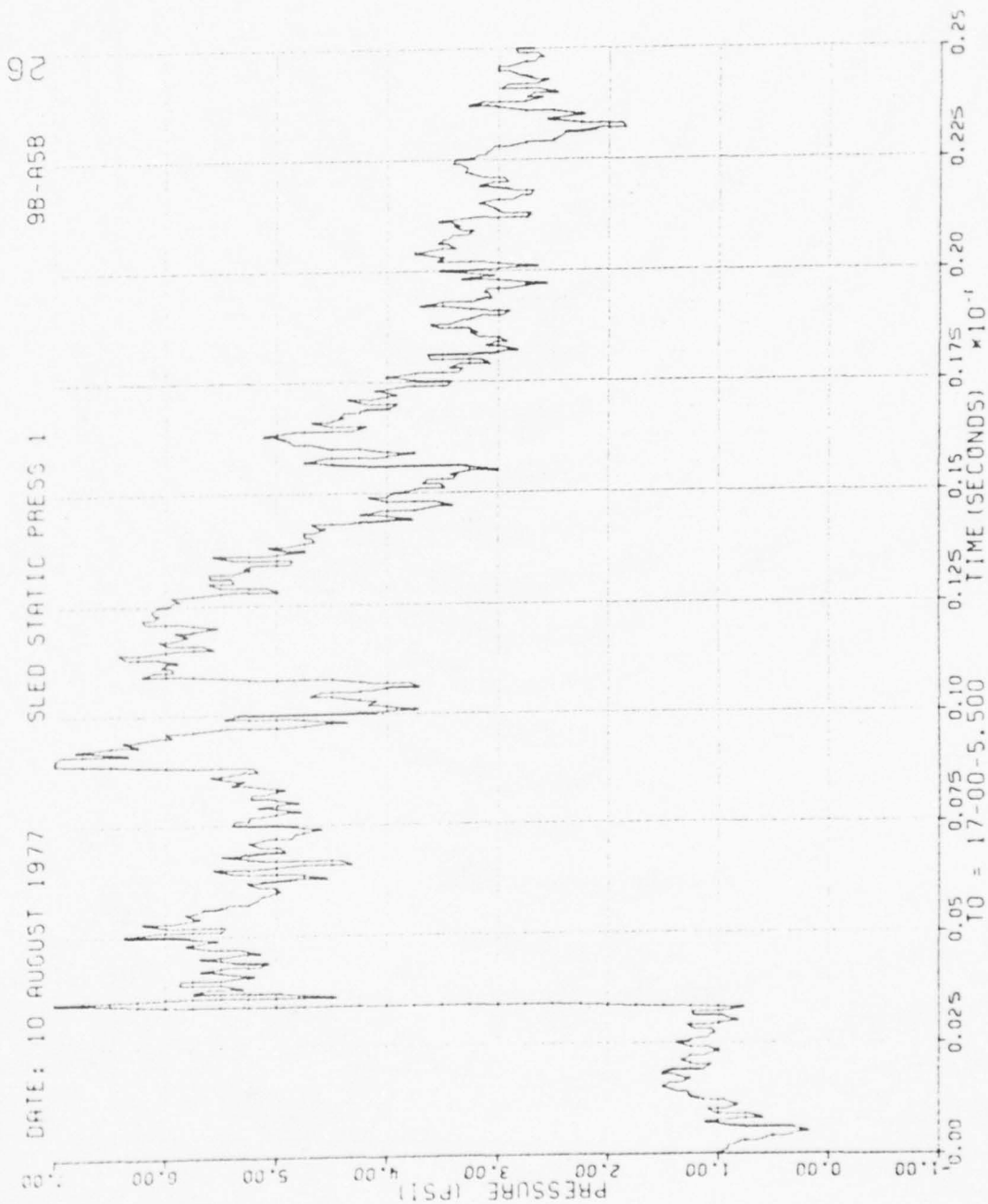


Figure 62. Static Pressure 1 at Sled, Run 9B-A5, Intercept 2.

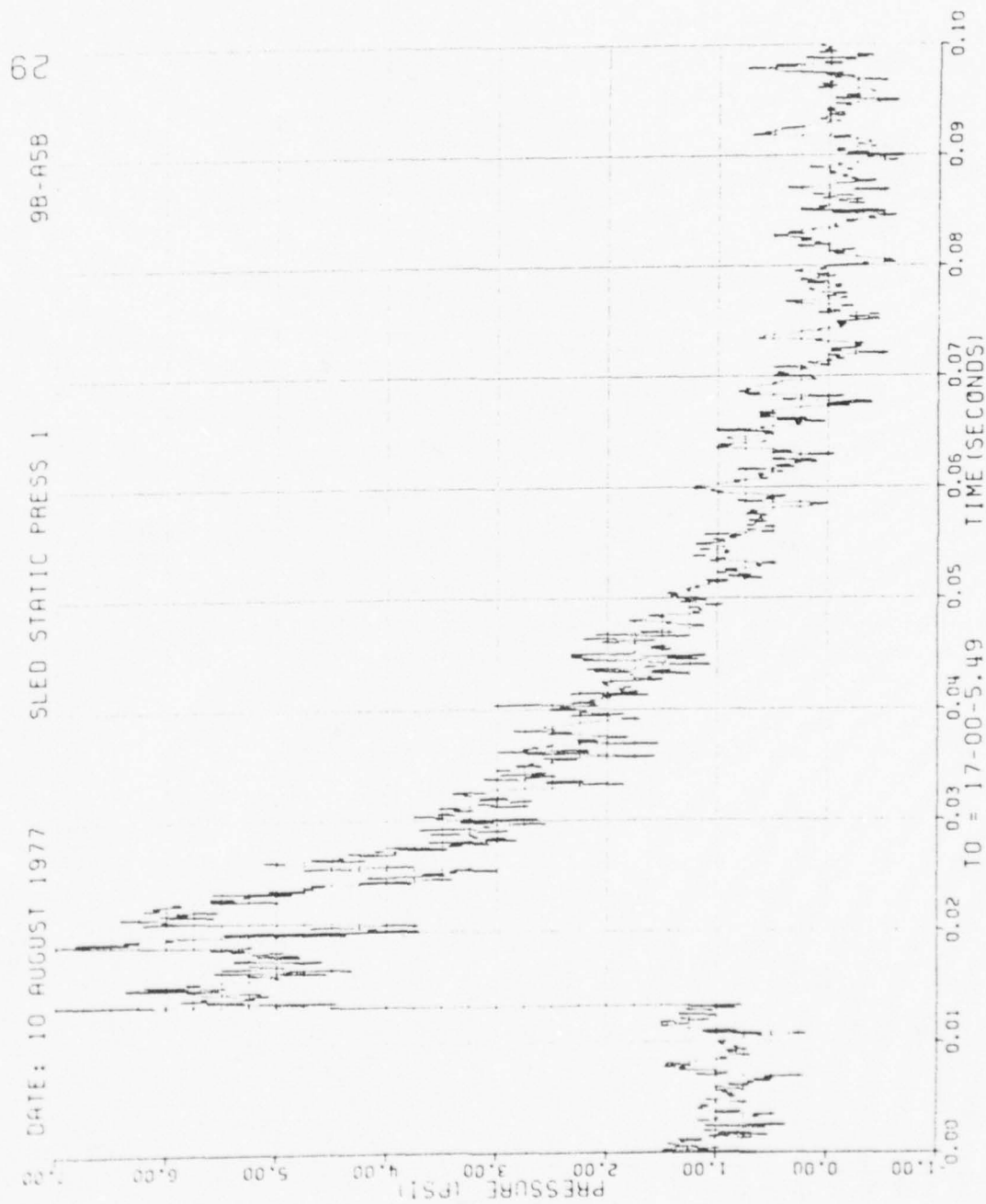


Figure 62. Concluded

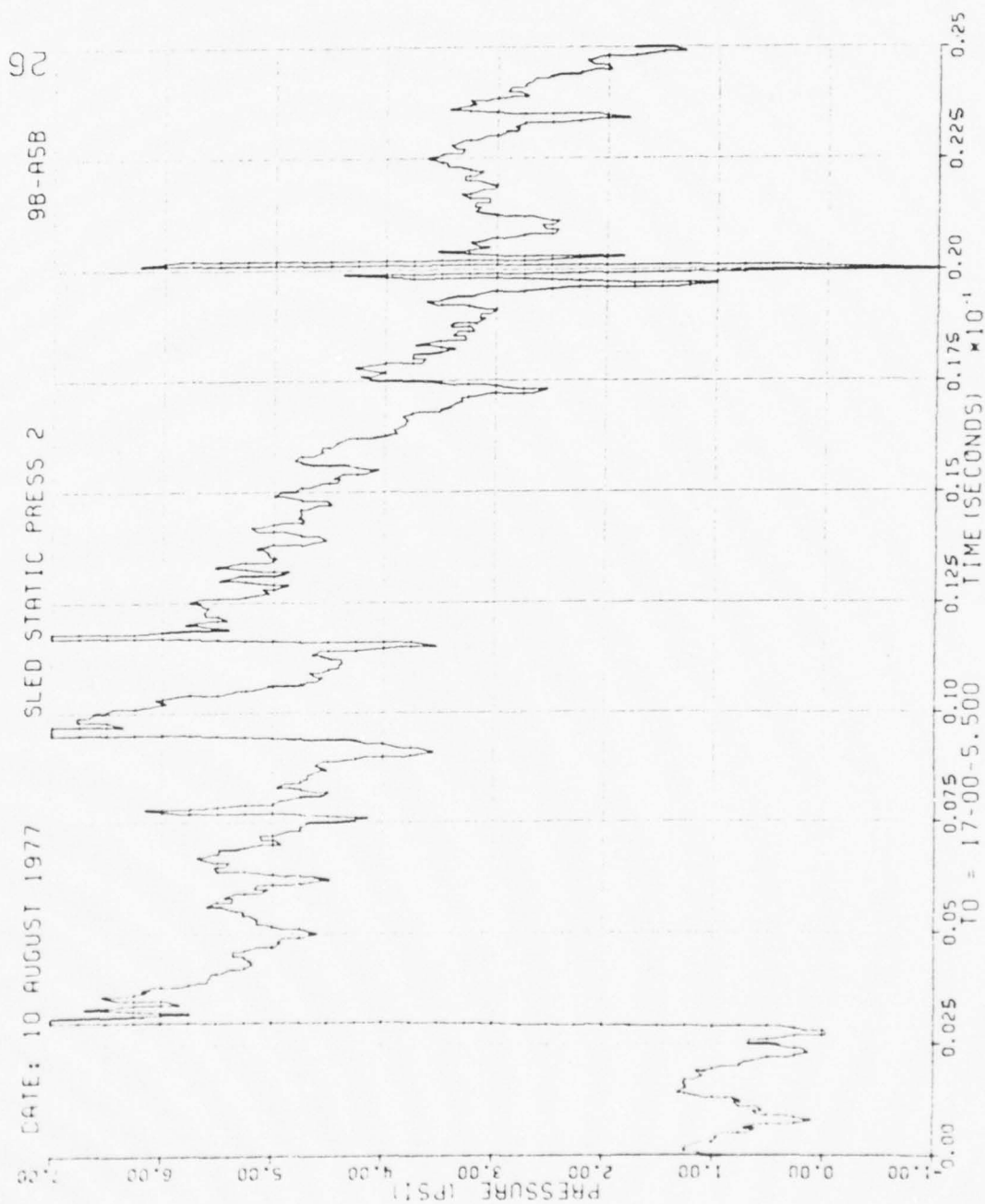


Figure 63. Static Pressure 2 at Sled, Run 9B-A5, Intercept 2.

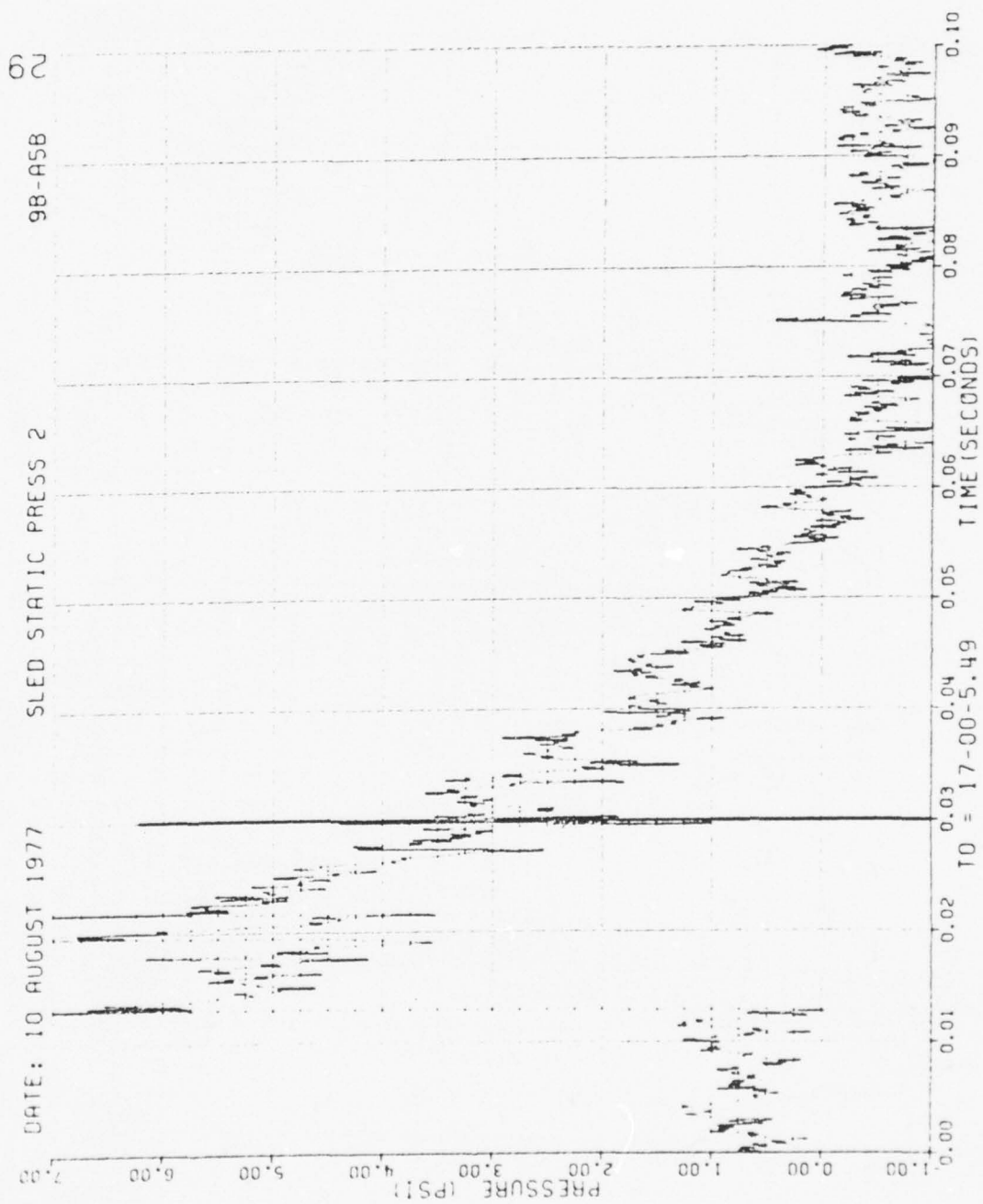


Figure 63. Concluded

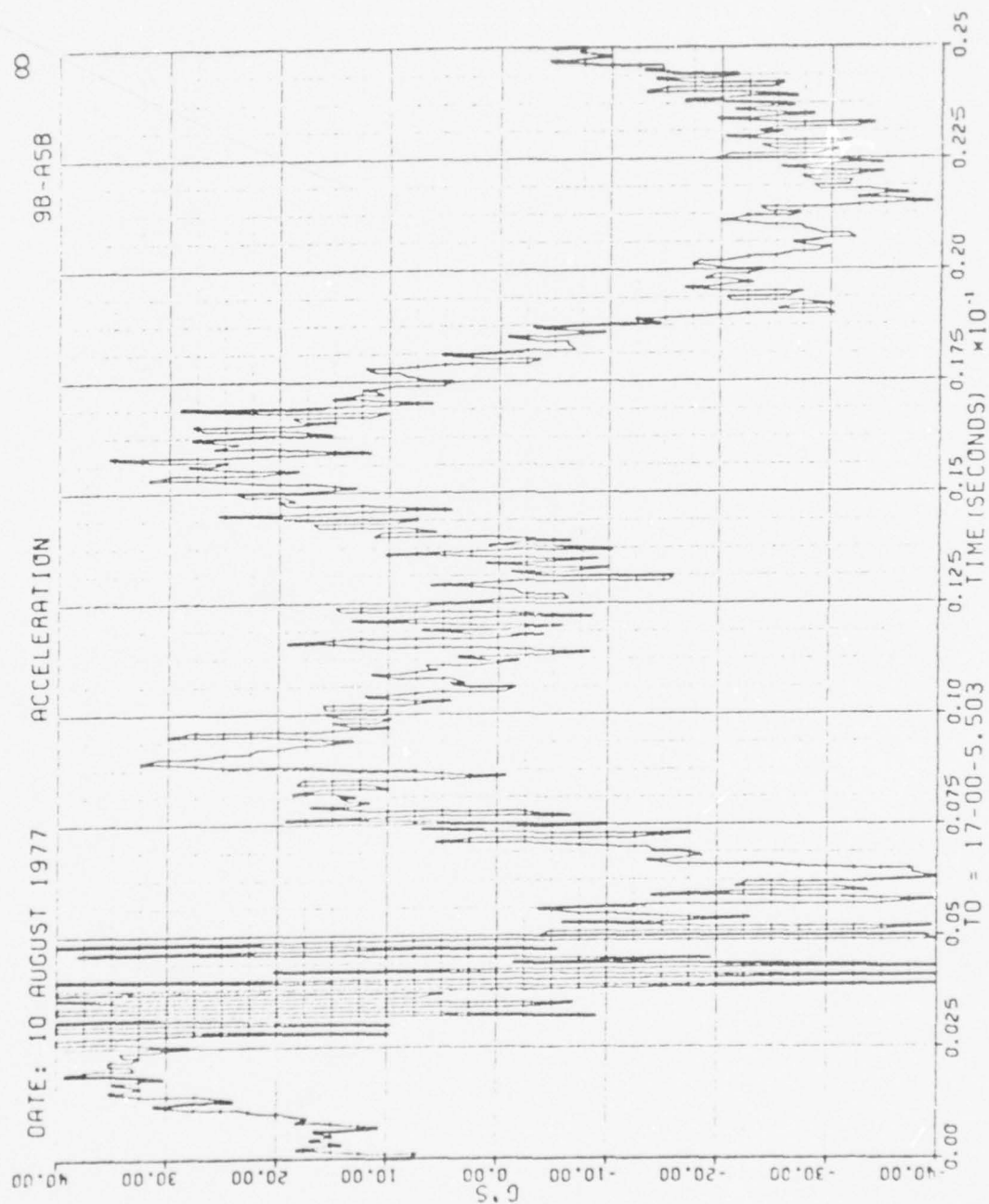


Figure 64. Wing Acceleration, Run 9B-A5, Intercept 2.

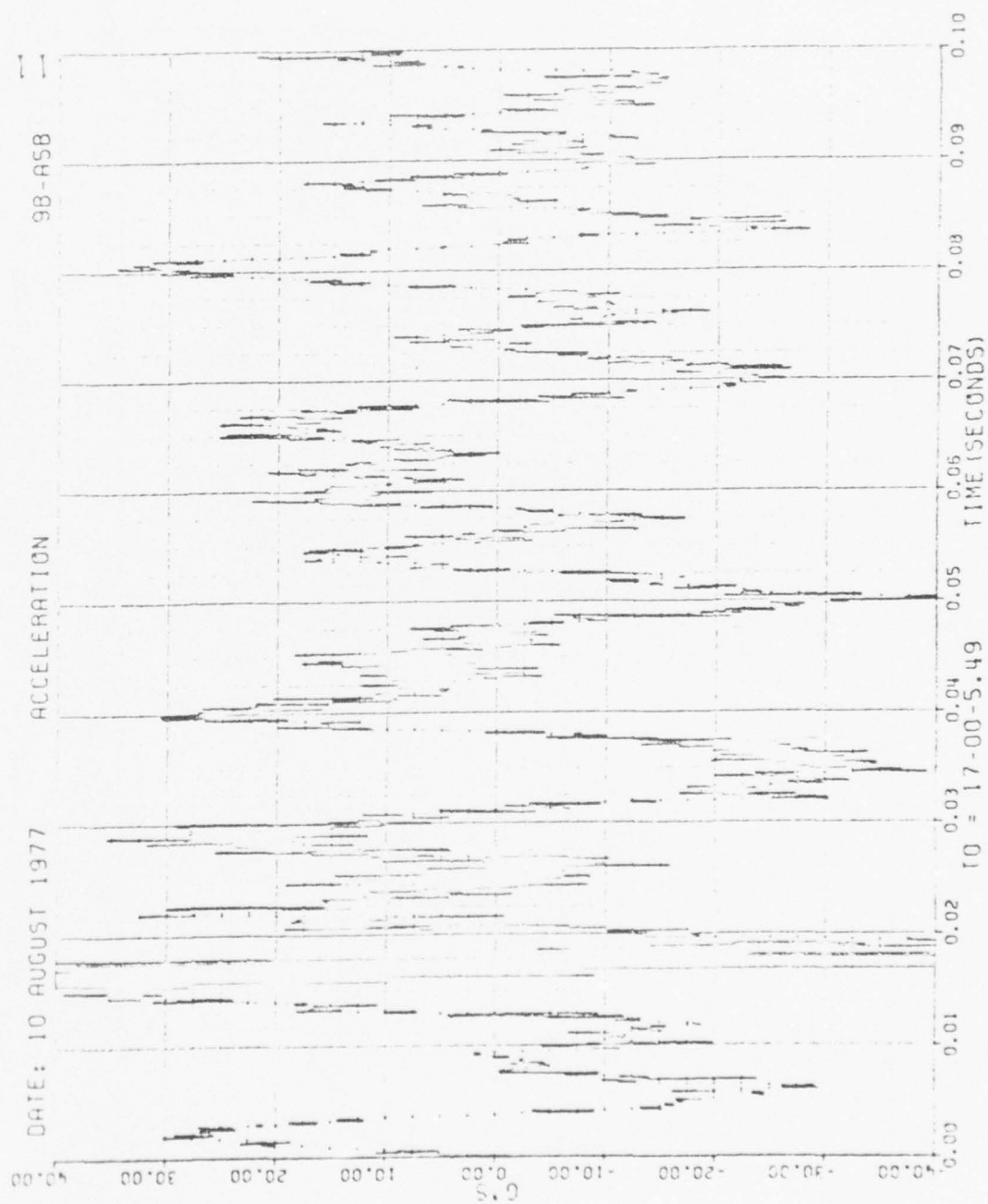


Figure 64. Concluded

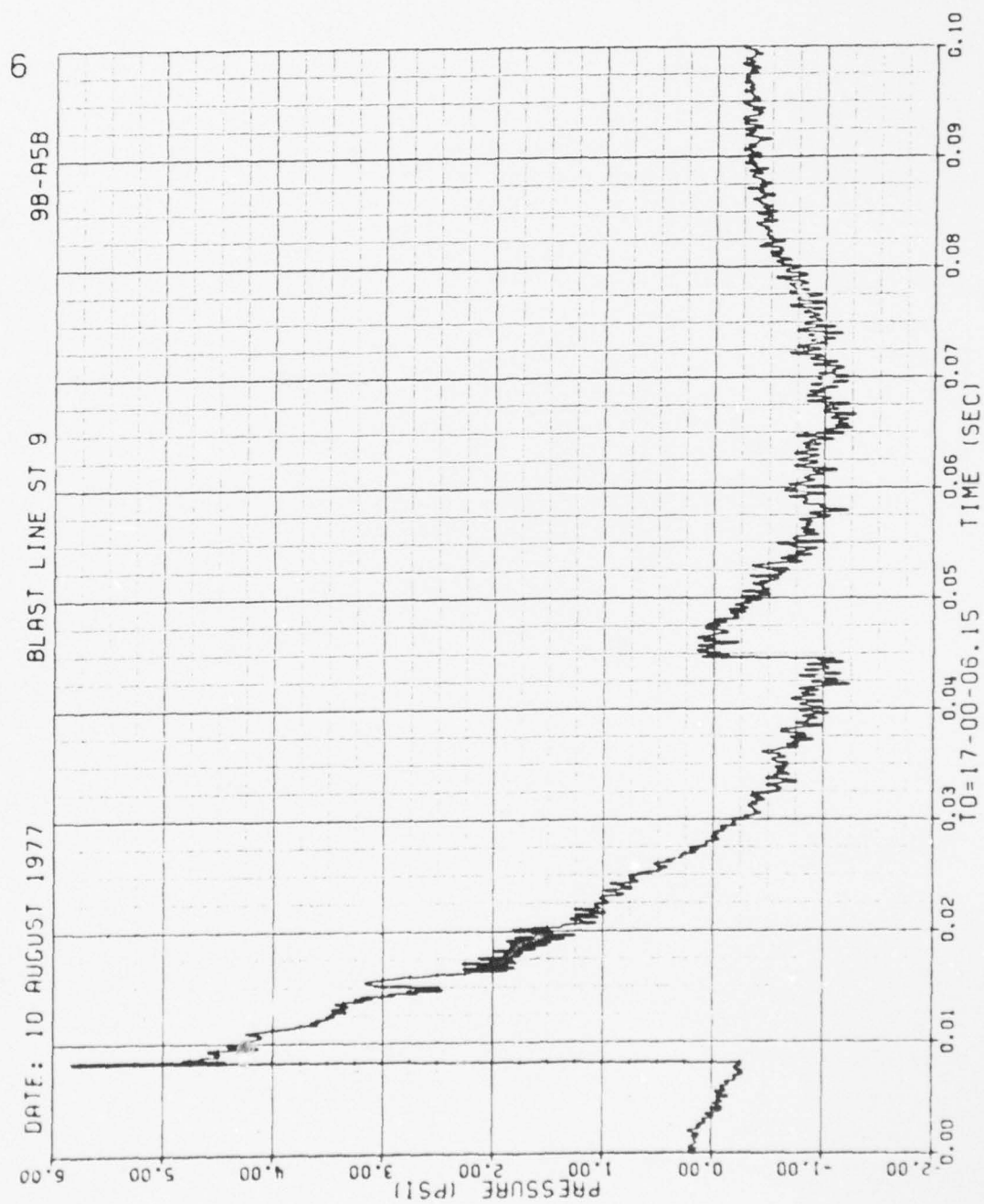


Figure 65. Blast-line Overpressures, Run 9B-A5, Intercept 3.

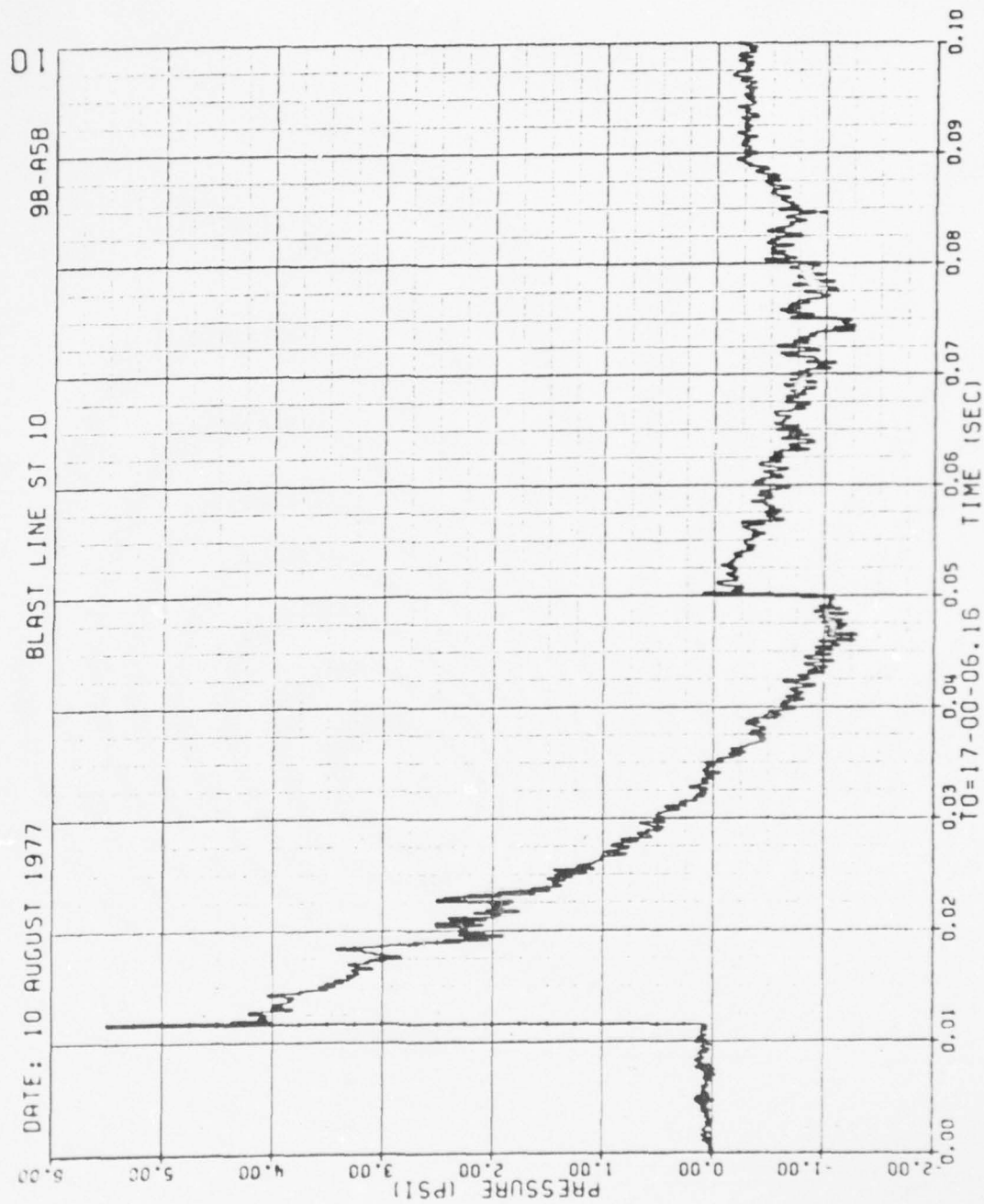


Figure 65. Continued

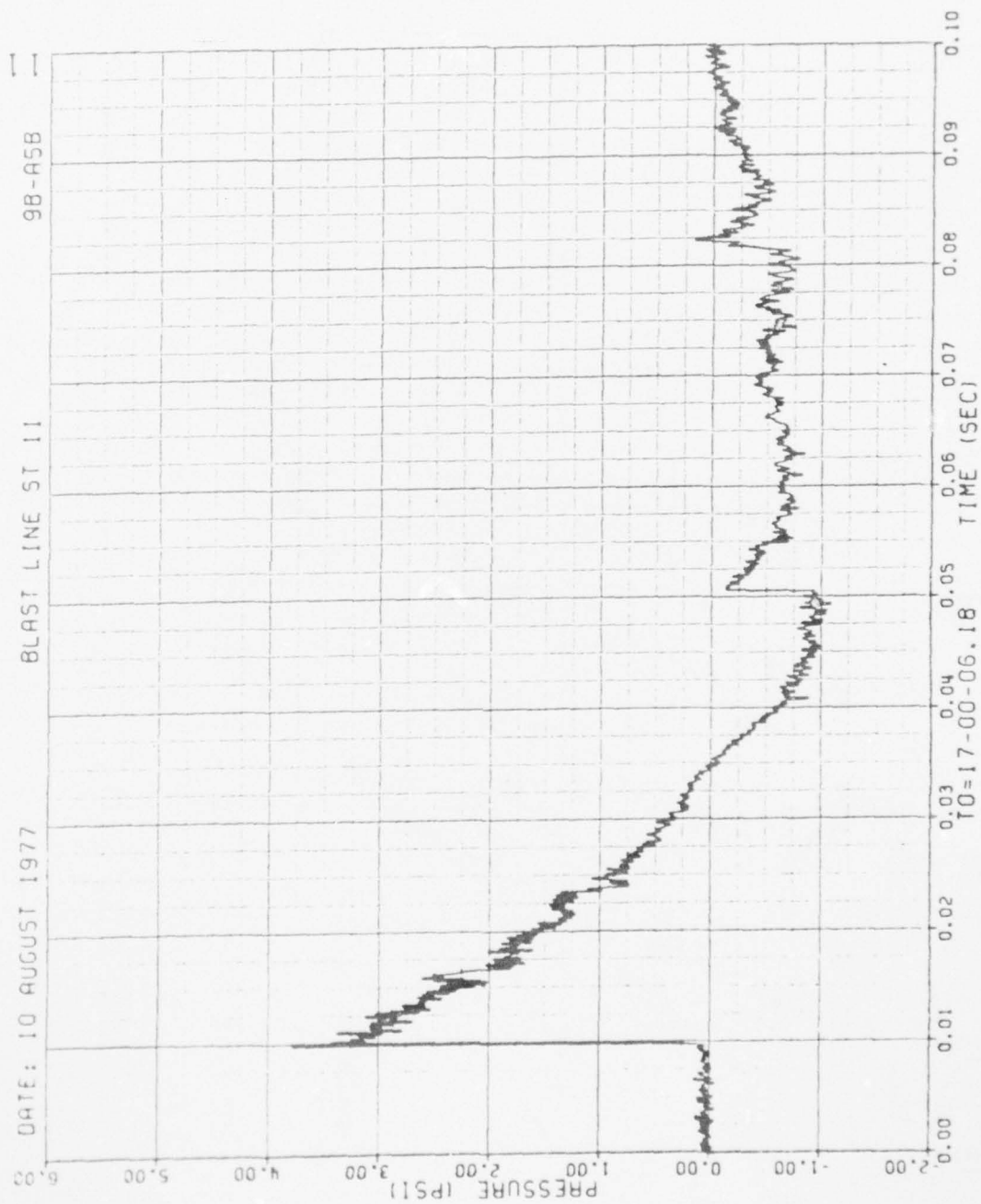


Figure 65. Continued

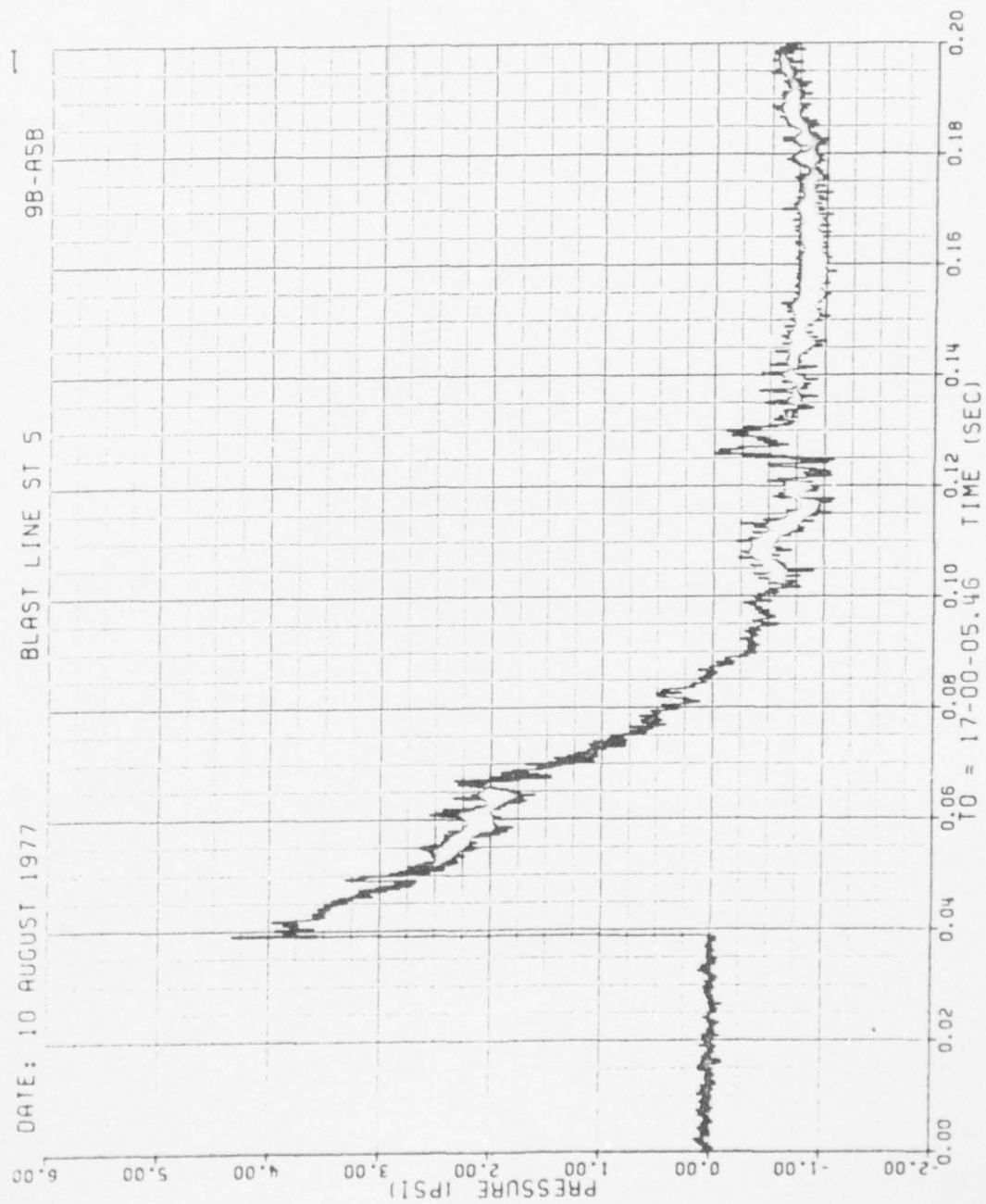


Figure 65. Concluded

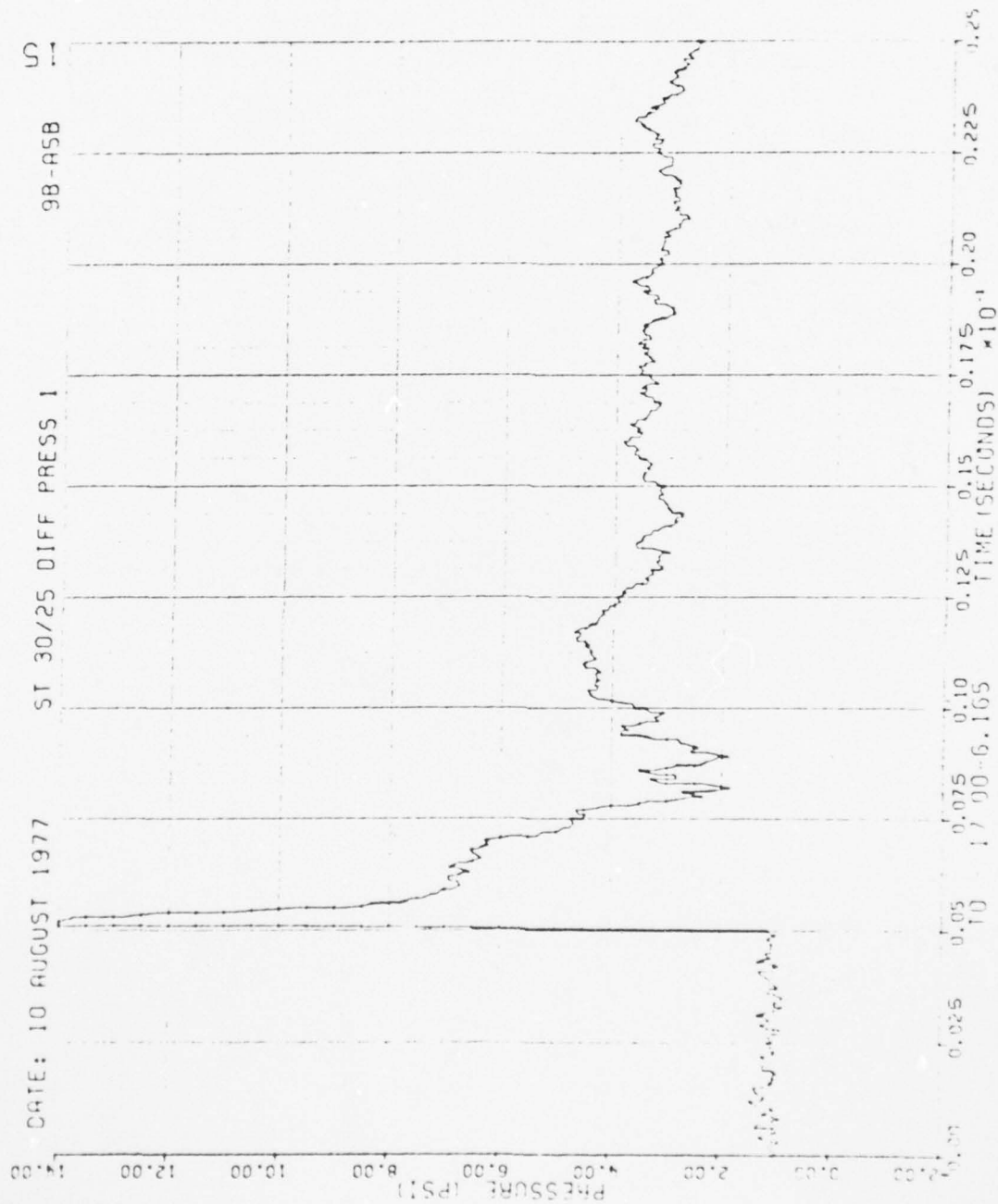


Figure 66. Differential Wing Pressures, Run 9B-A5, Intercept 3.

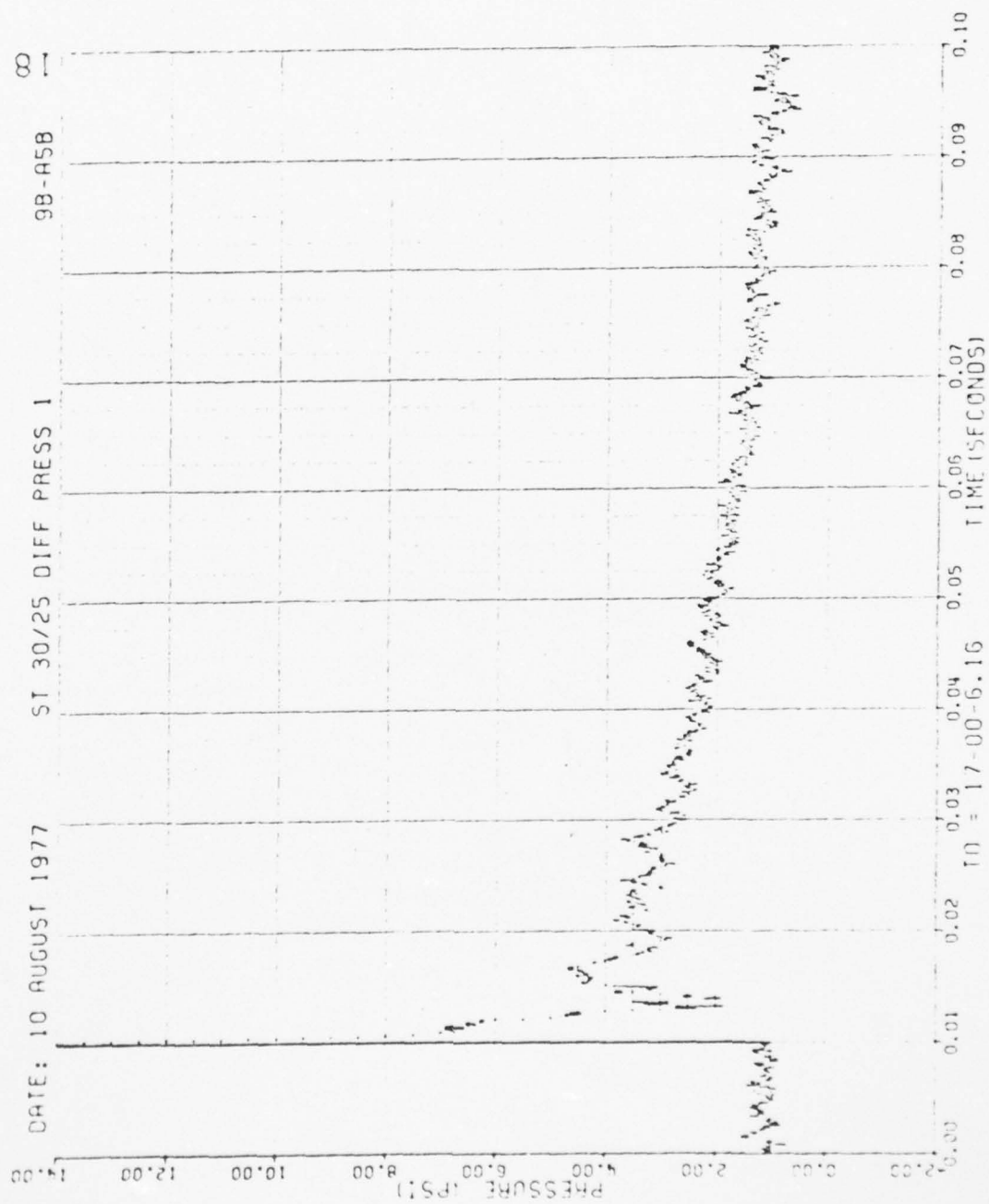


Figure 66. Continued

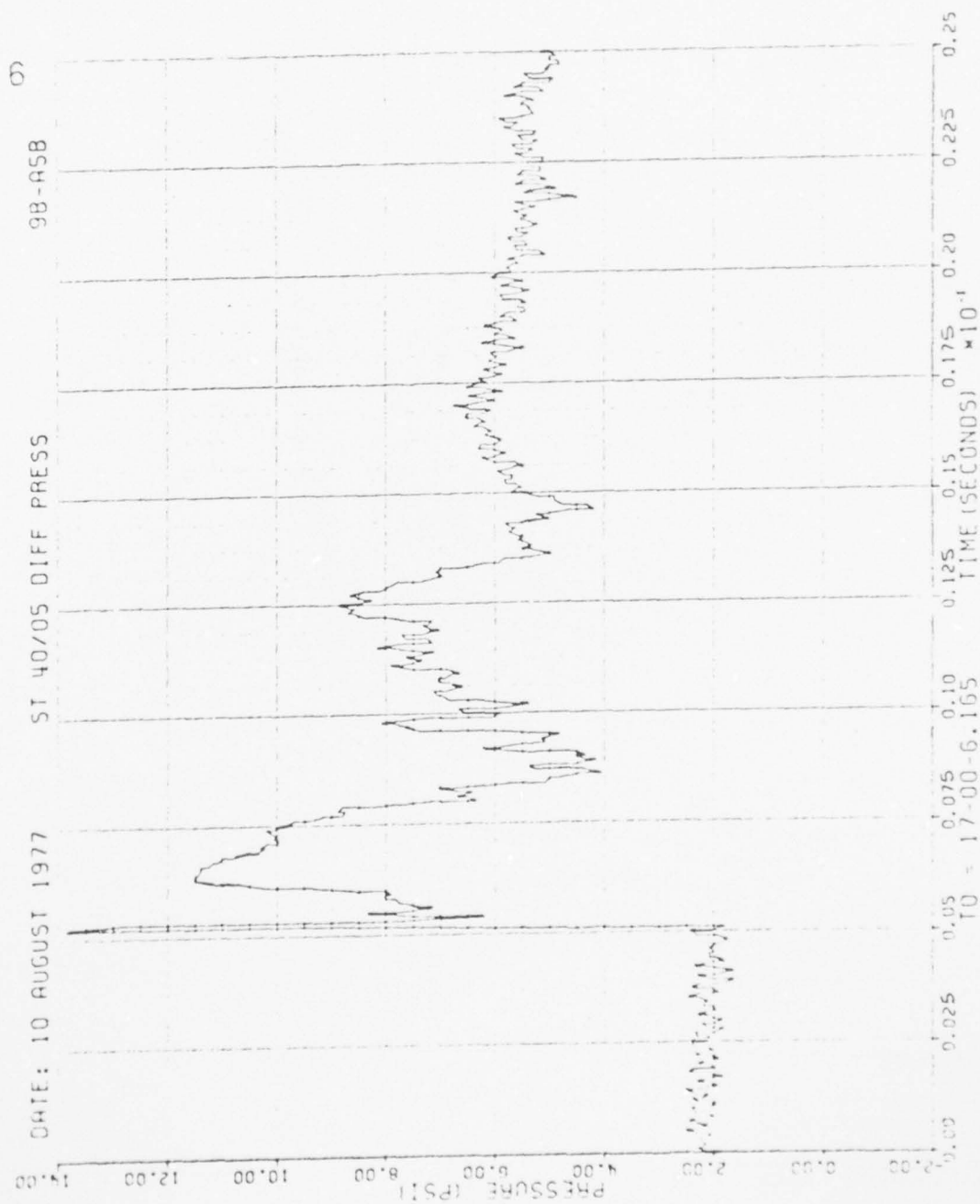


Figure 66. Continued

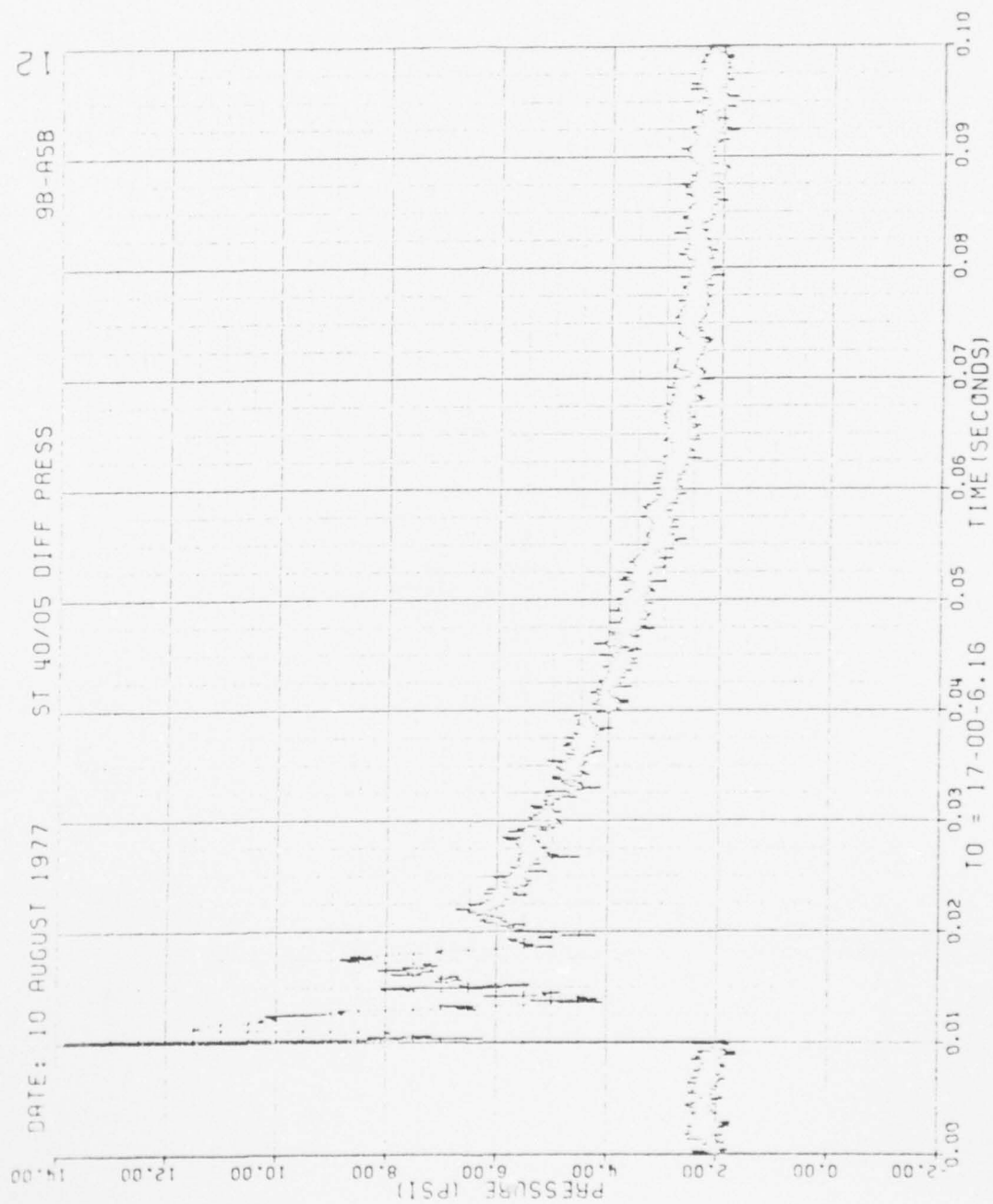


Figure 66. Continued

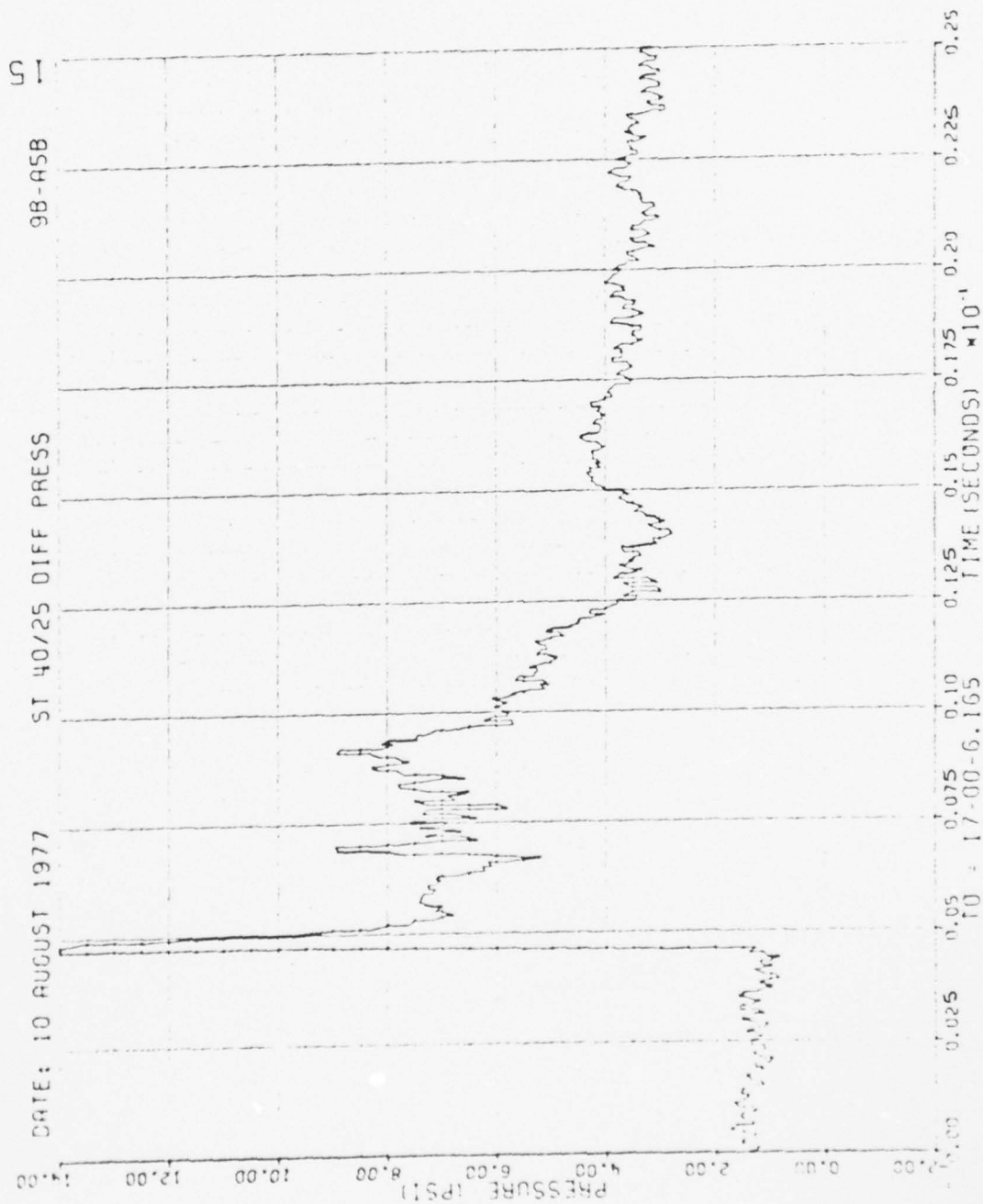


Figure 66. Continued

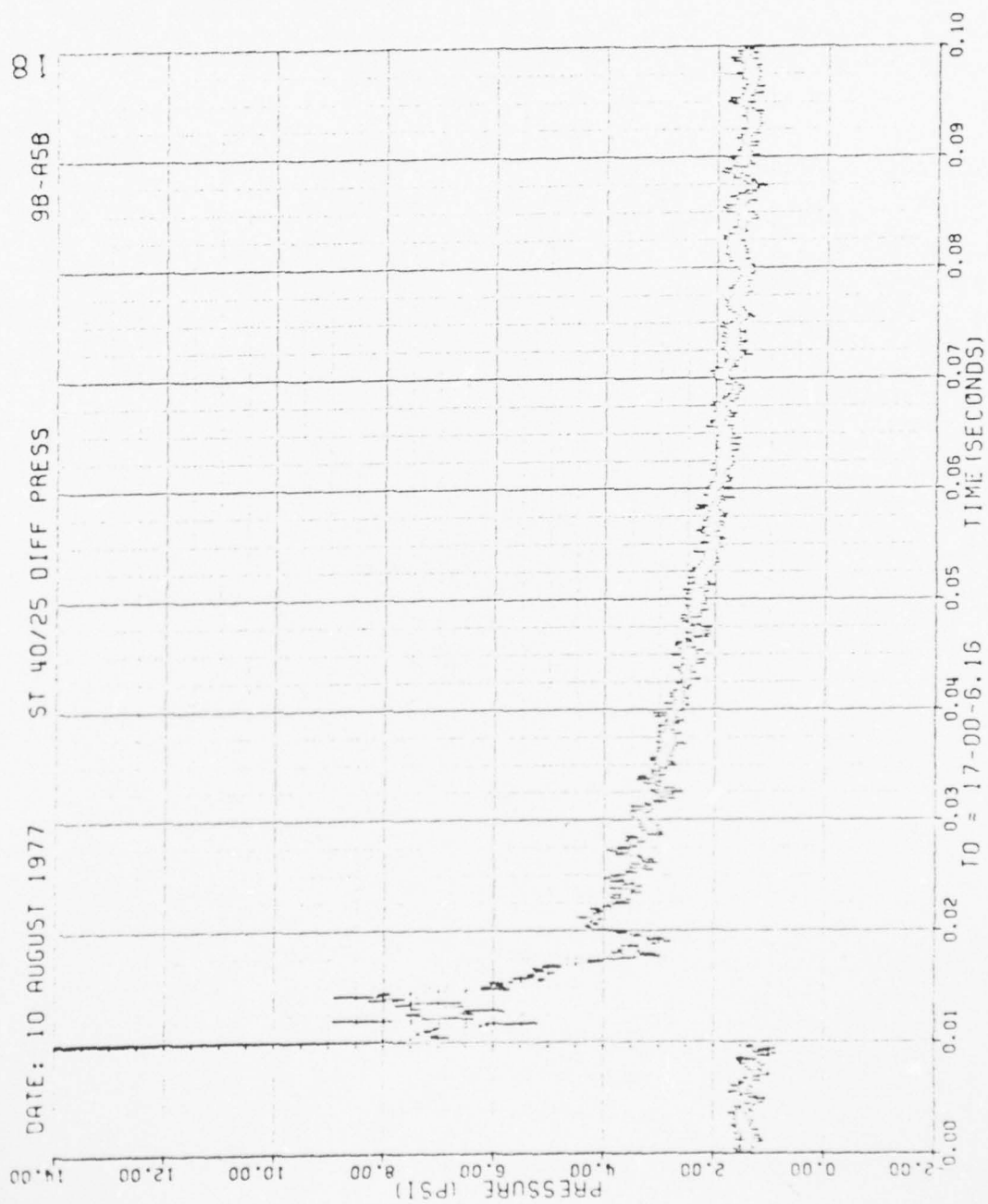


Figure 66. Continued

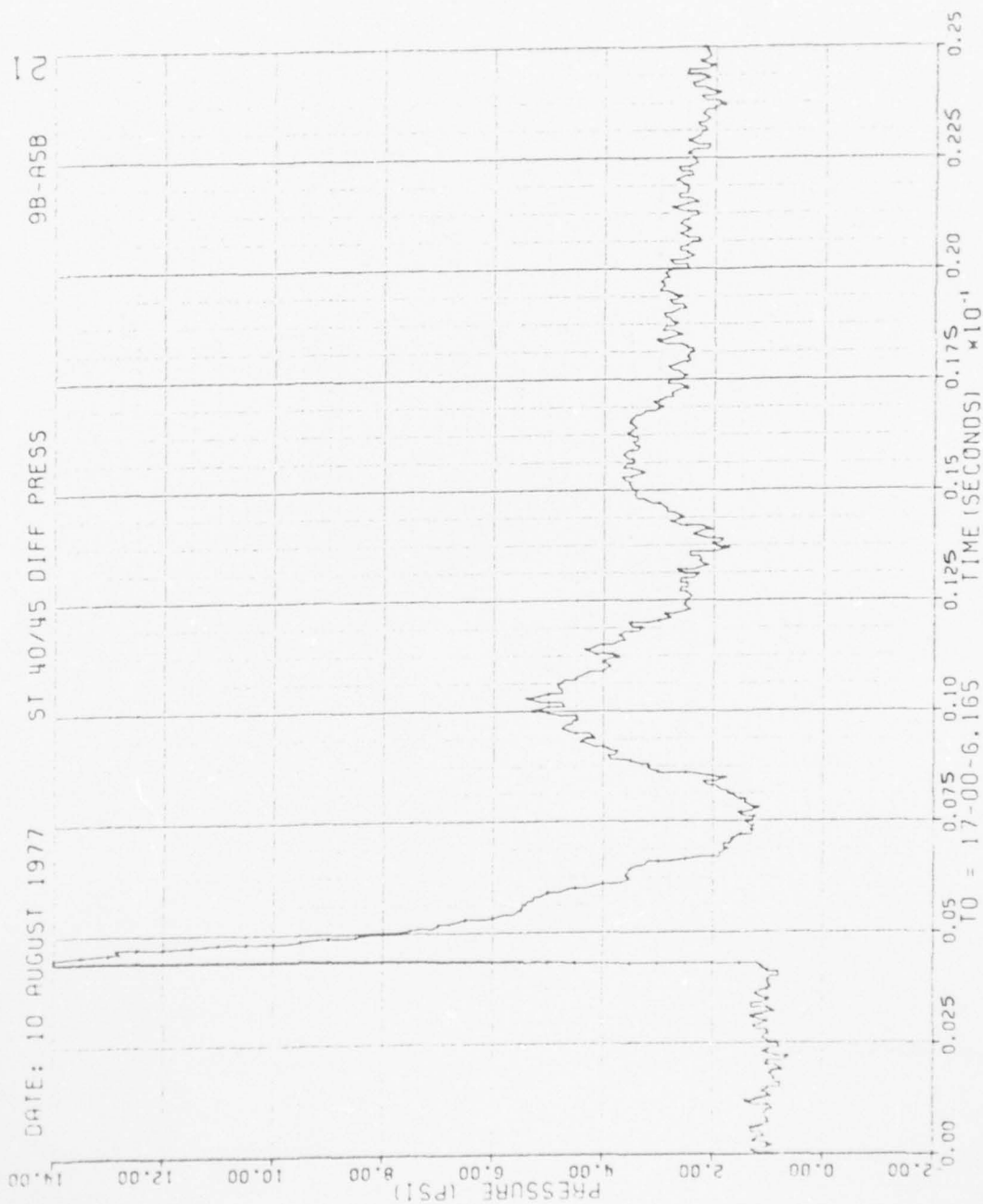


Figure 66. Continued

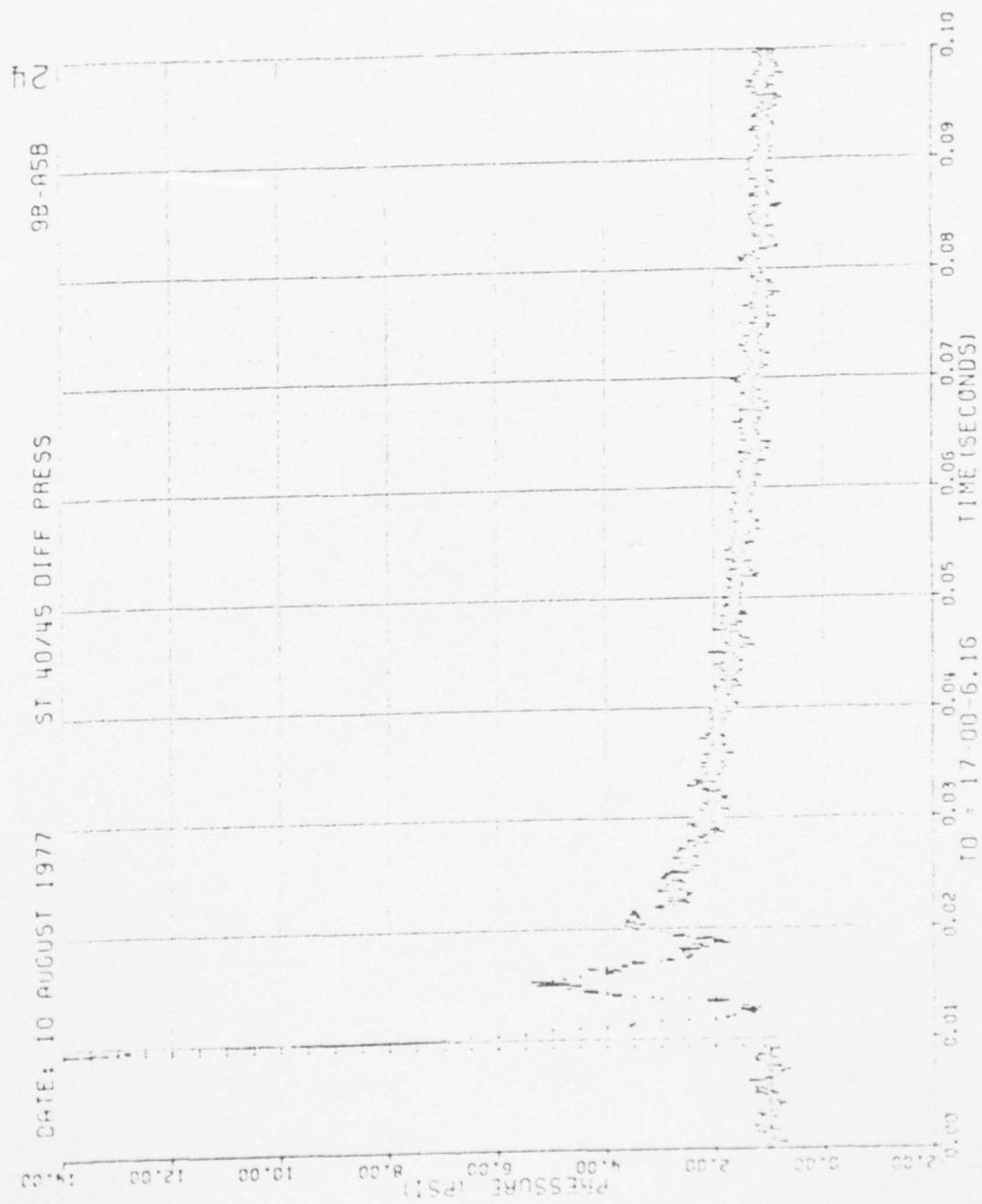


Figure 66. Continued

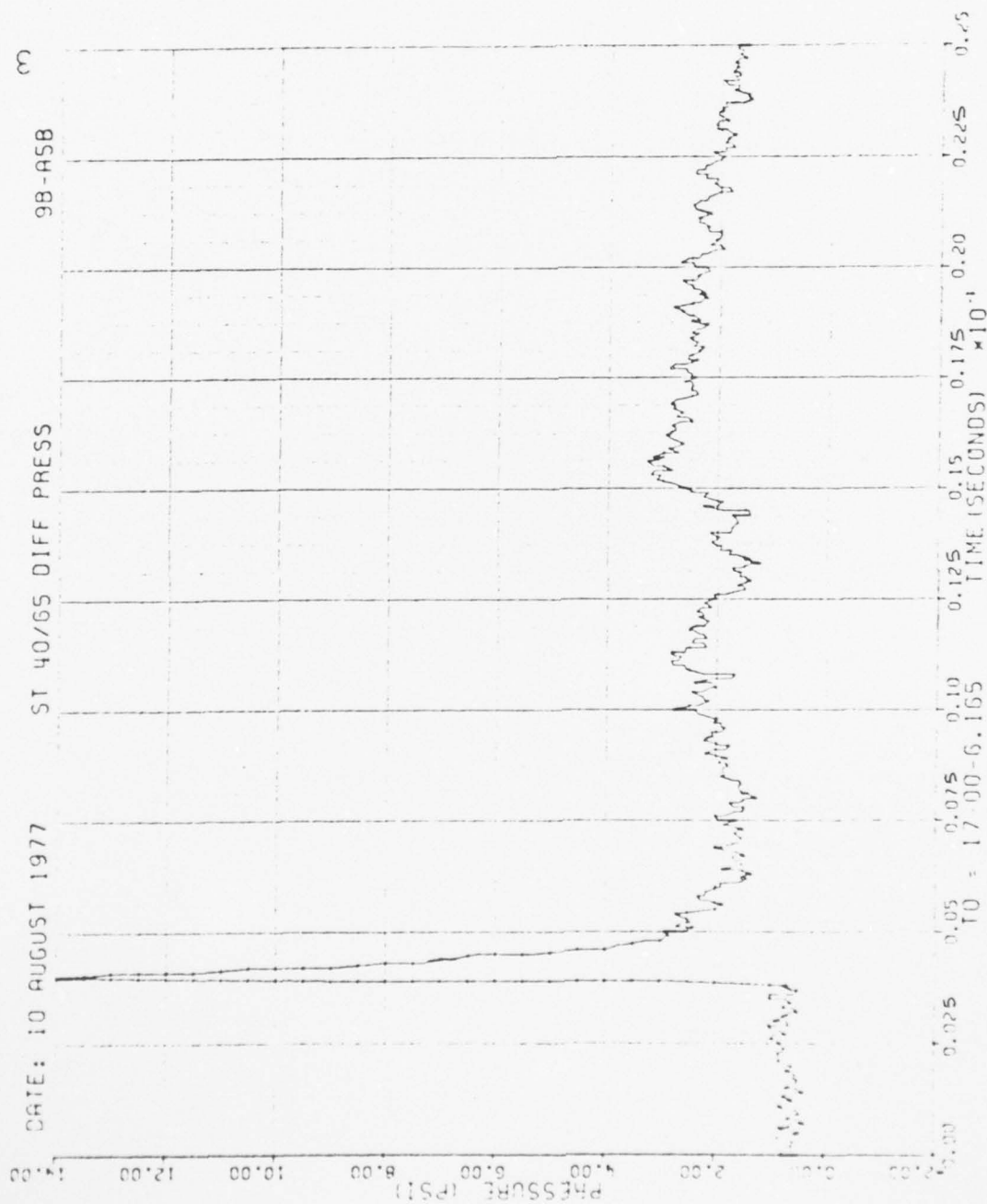


Figure 66. Continued

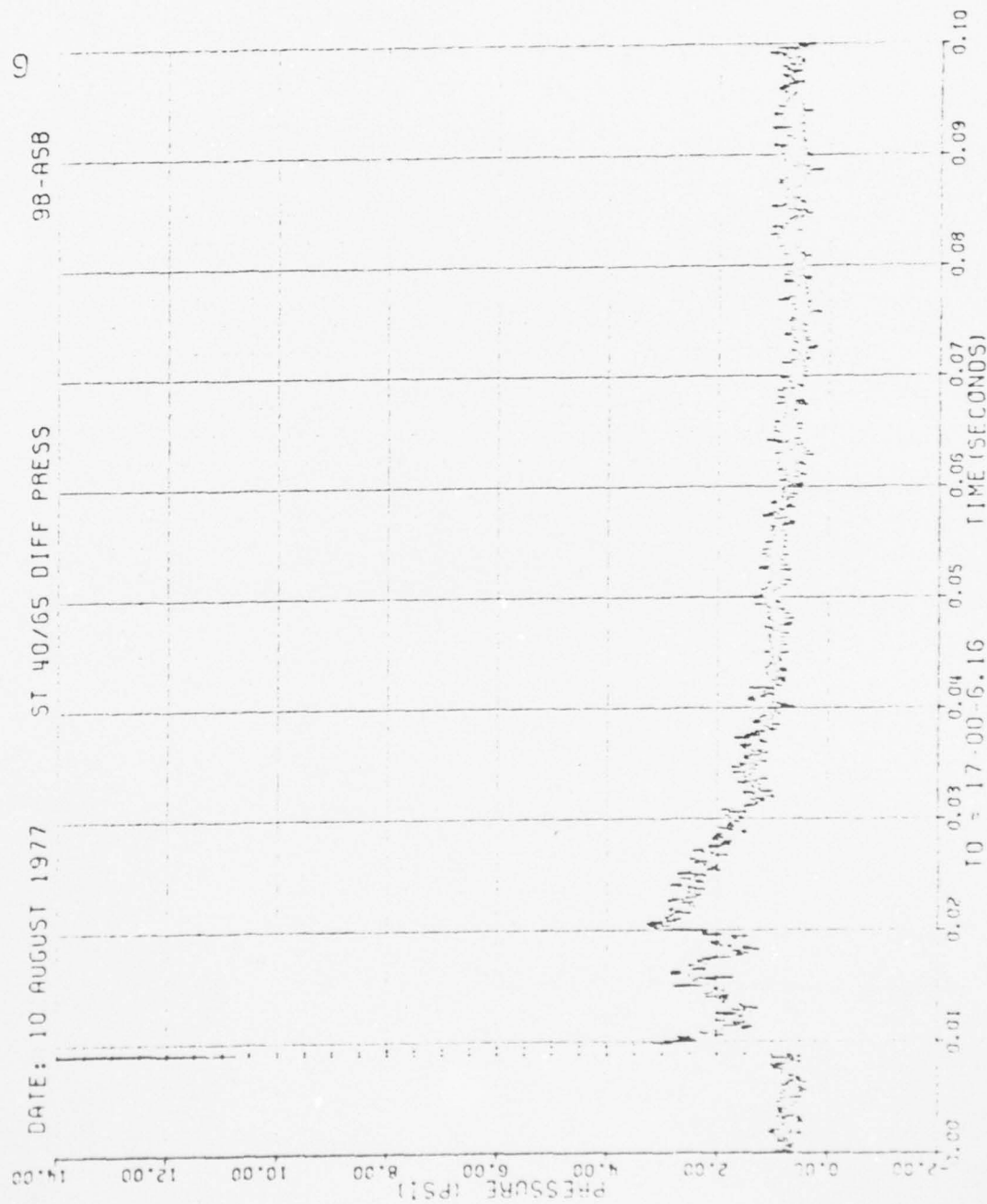


Figure 66. Continued

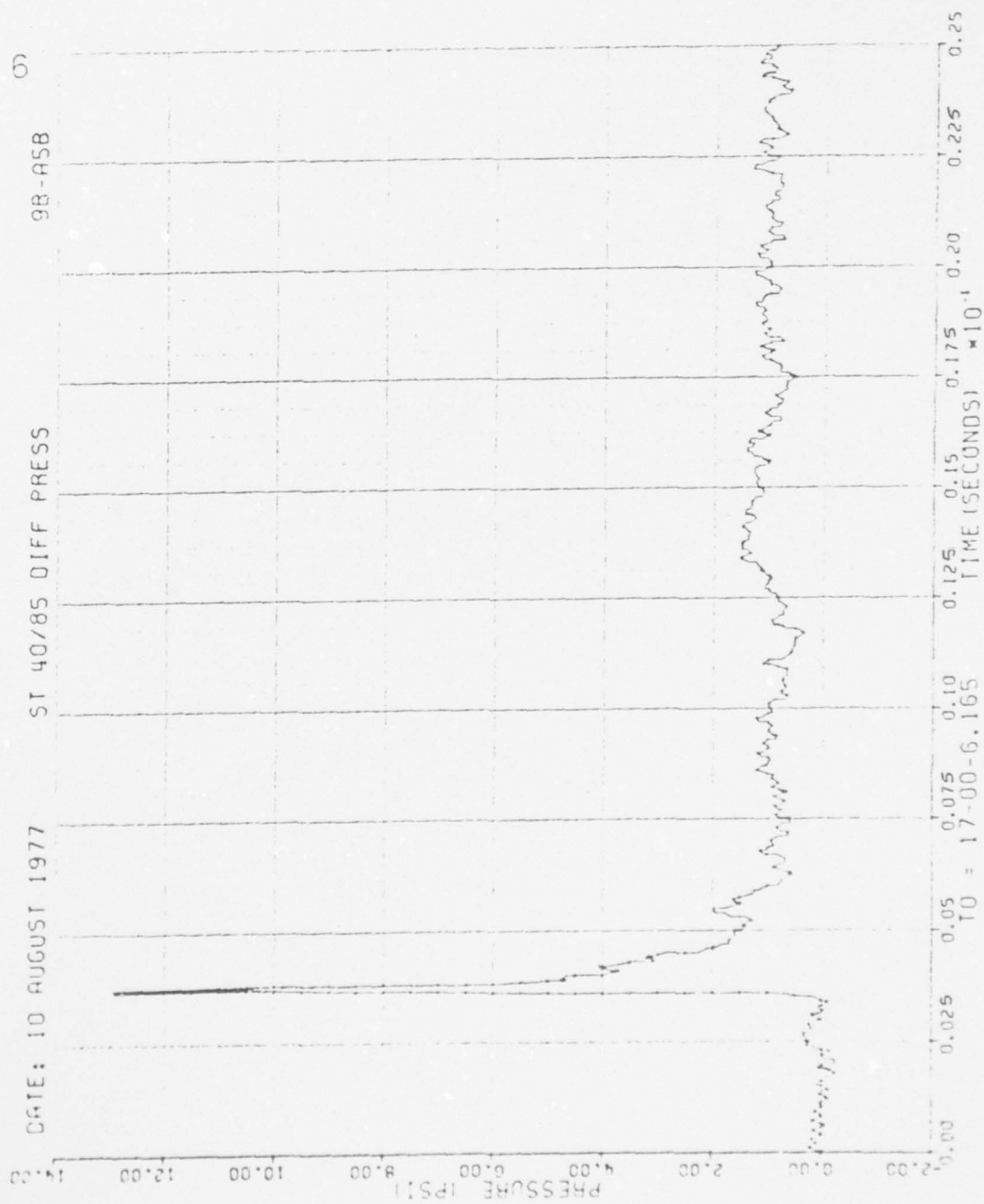


Figure 66. Continued

AD-A062 408

KAMAN AVIDYNE BURLINGTON MASS

F/G 1/3

MEASUREMENTS OF BLAST PRESSURES ON A RIGID 65 DEG SWEEPBACK WIN--ETC(U)

JAN 78 J R RUETENIK, R F SMILEY

DNA001-76-C-0106

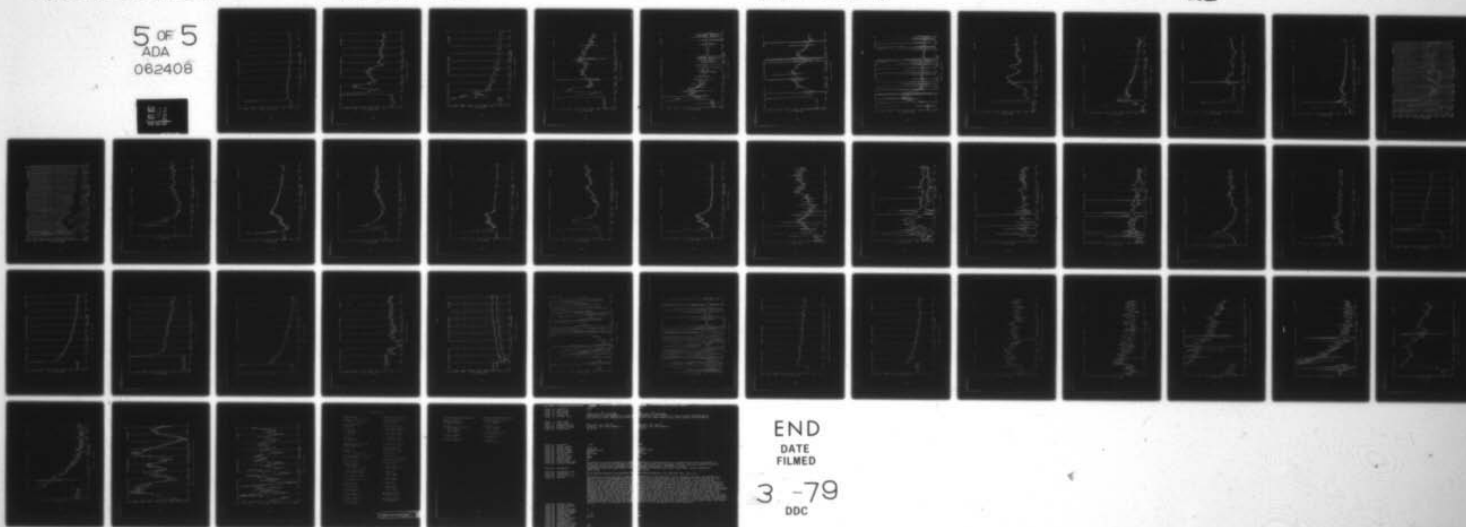
UNCLASSIFIED

KA-TR-145

DNA-4504F

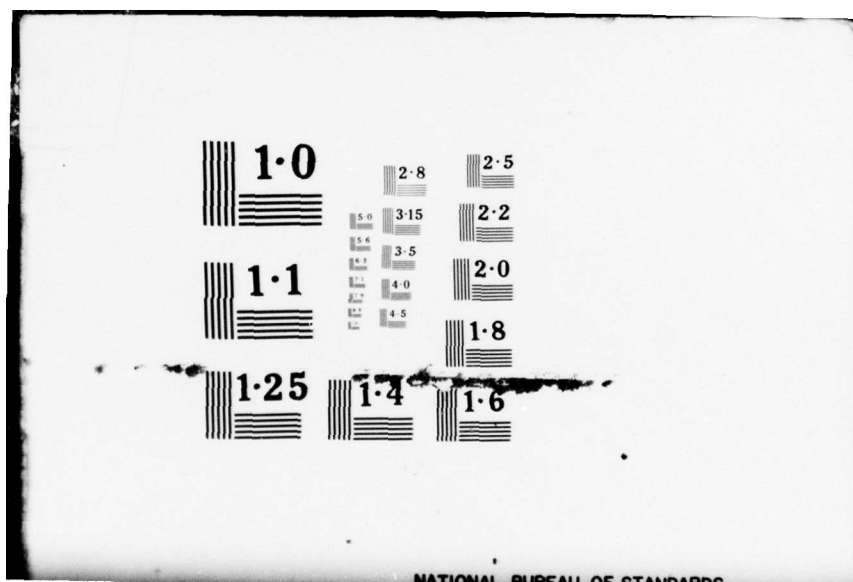
NL

5 OF 5
ADA
062408



END
DATE
FILMED

3 -79
DDC



NATIONAL BUREAU OF STANDARDS

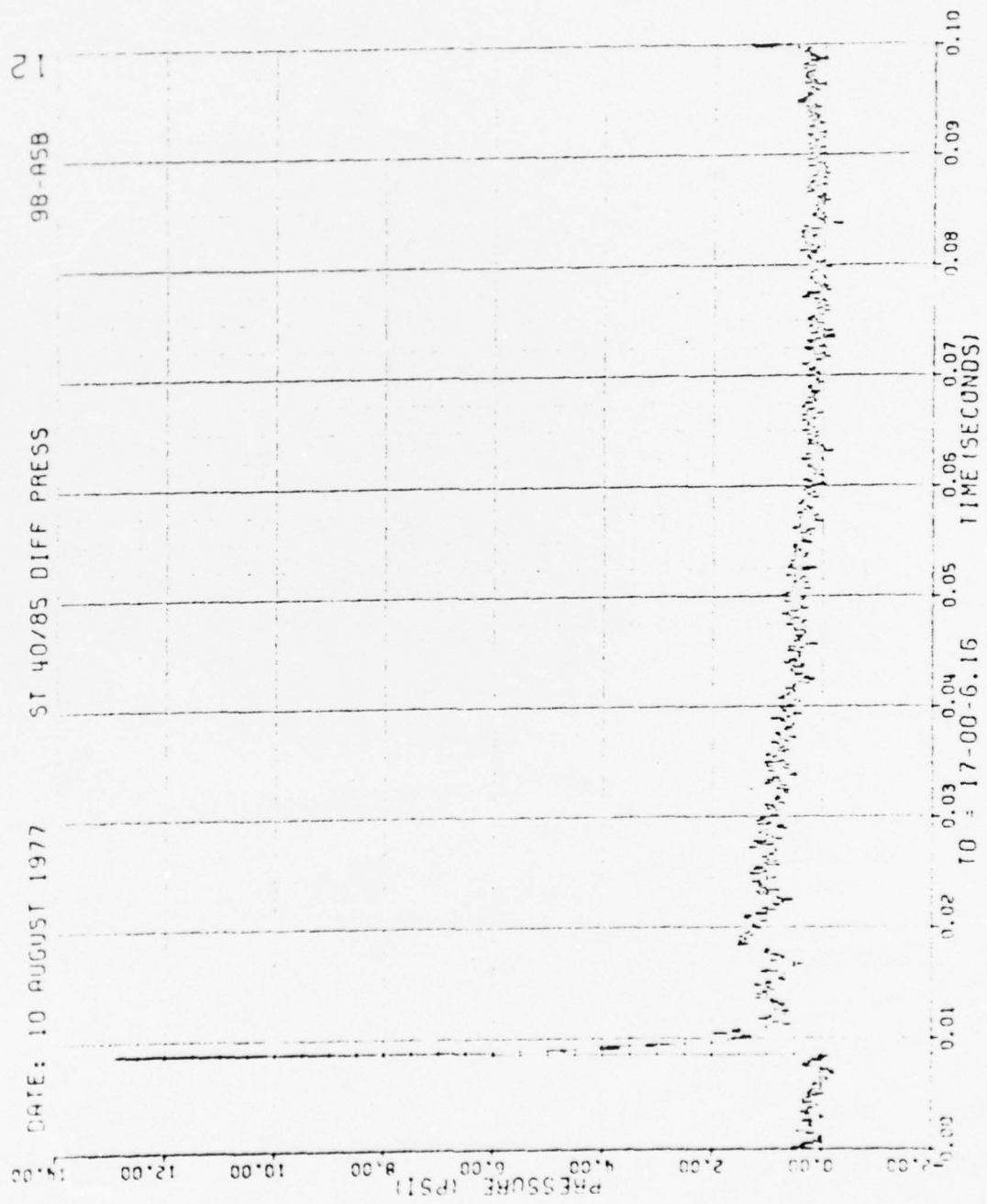


Figure 66. Continued

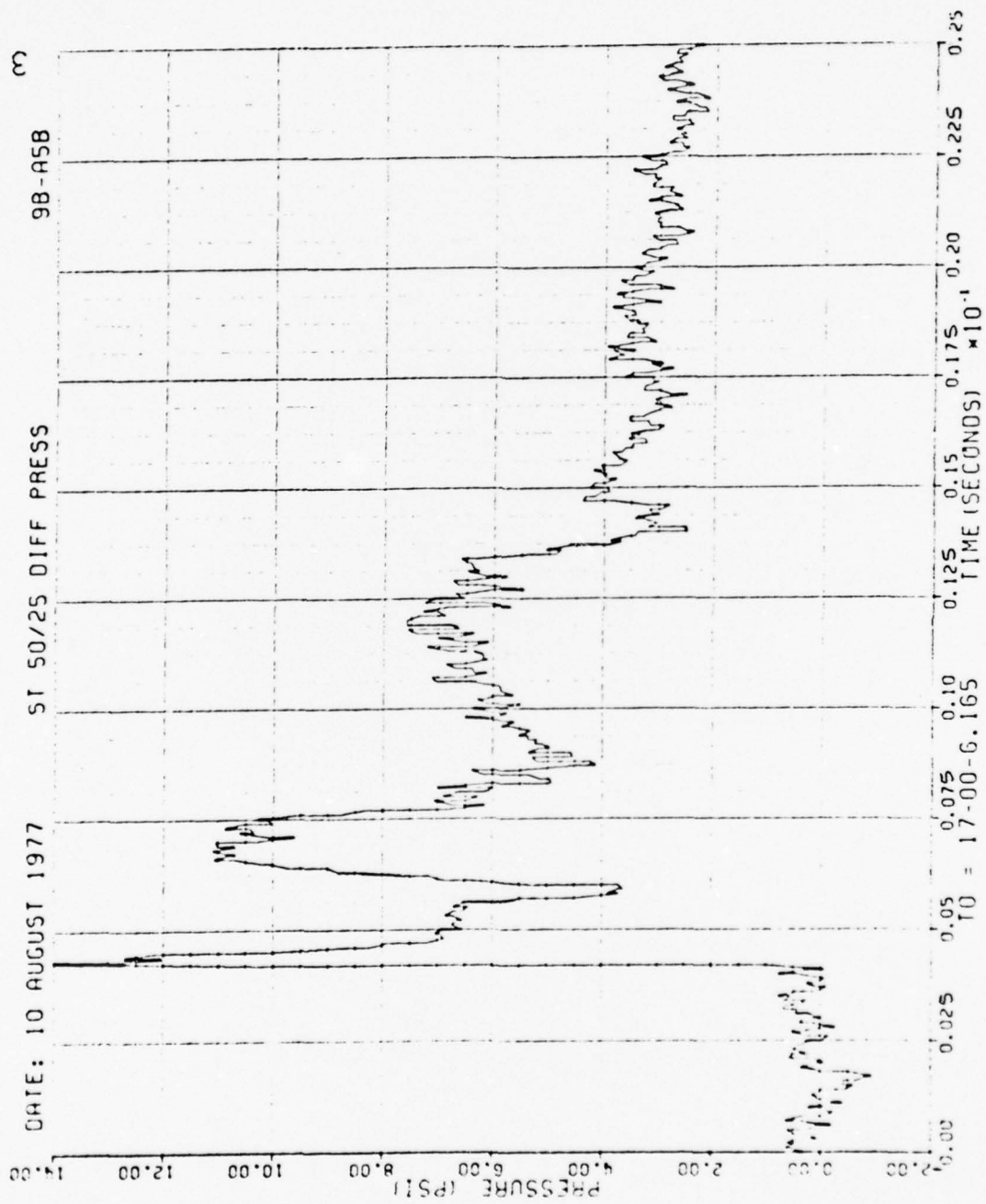


Figure 66. Continued

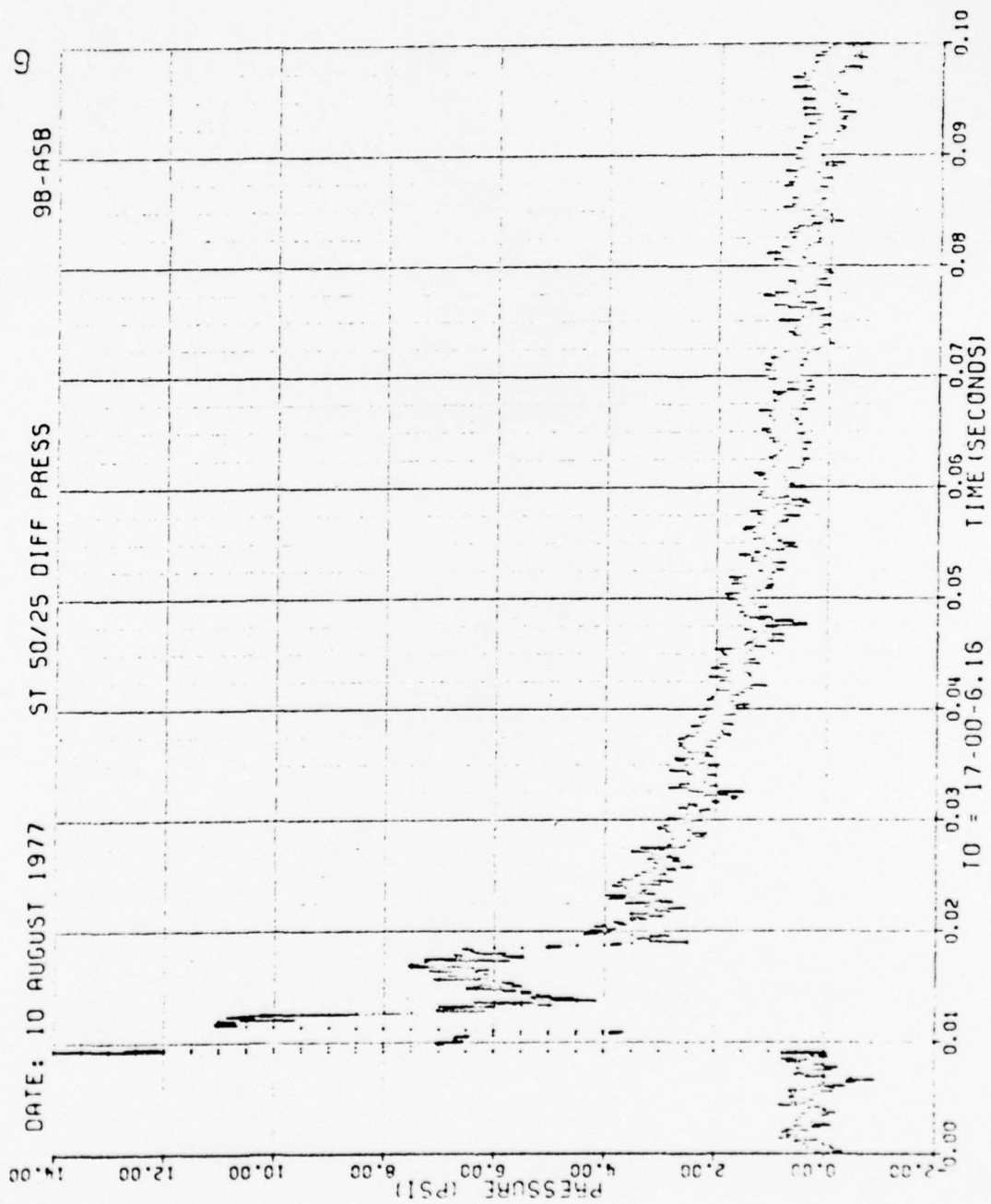


Figure 66. Continued

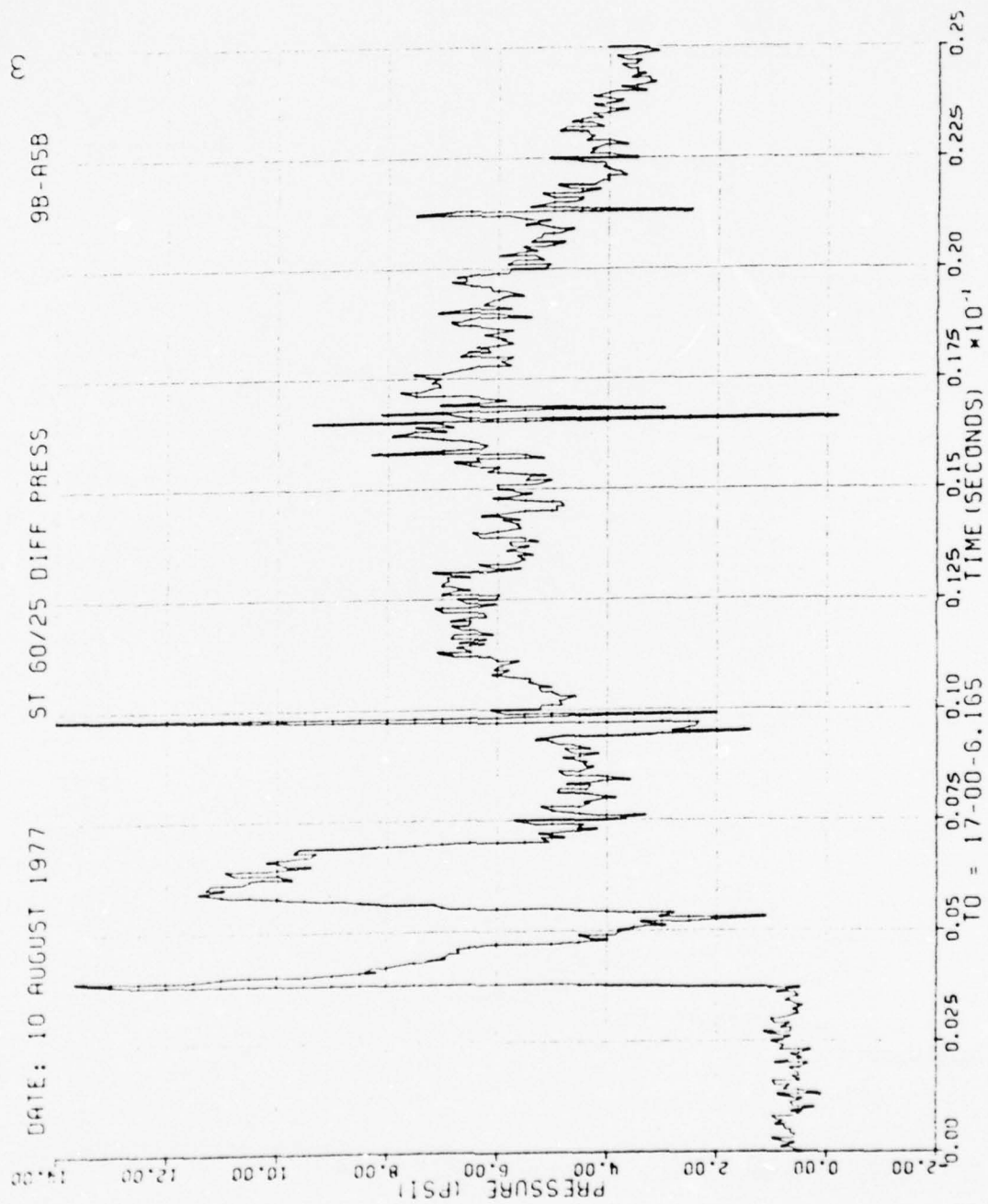


Figure 66. Continued

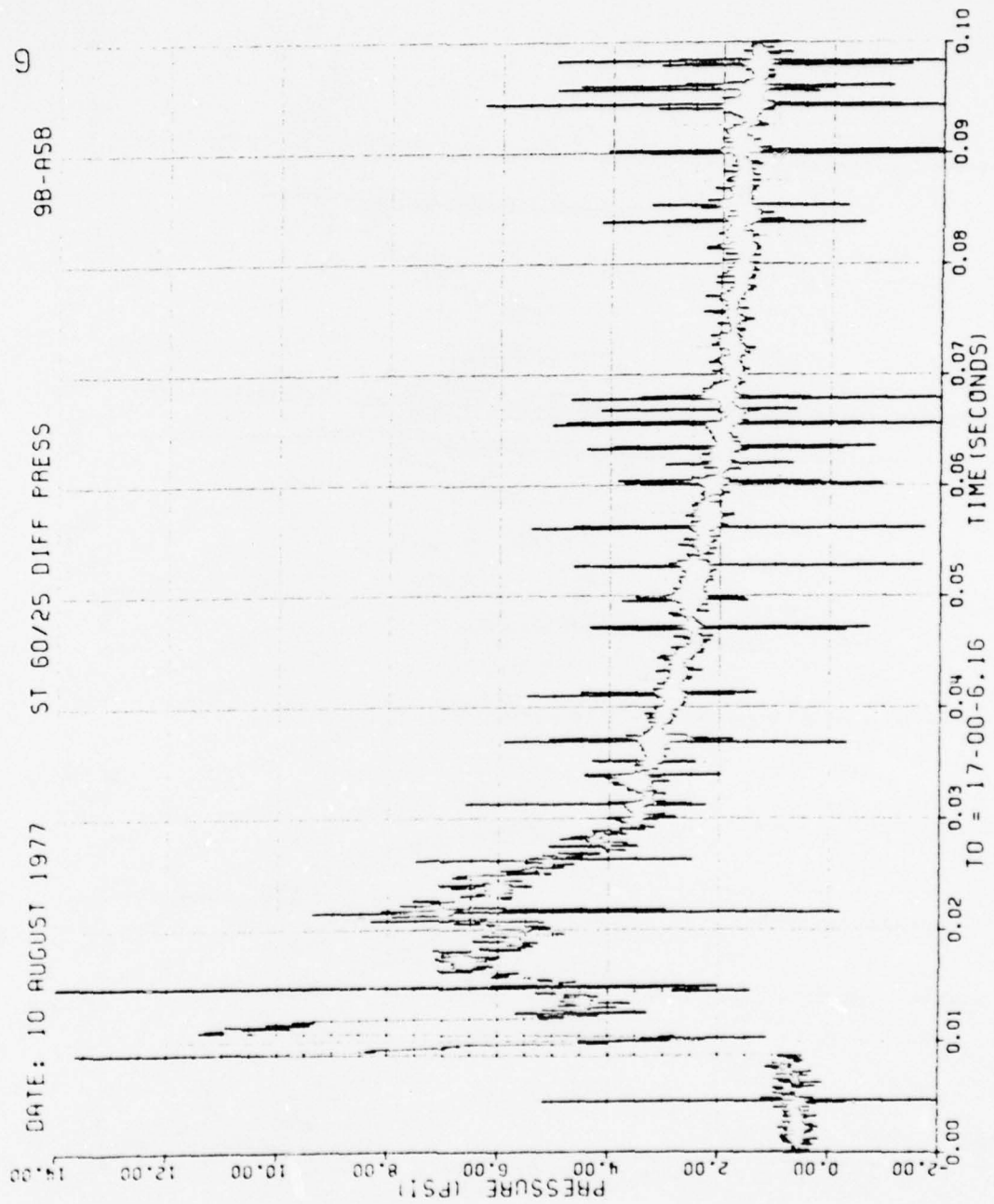


Figure 66. Continued

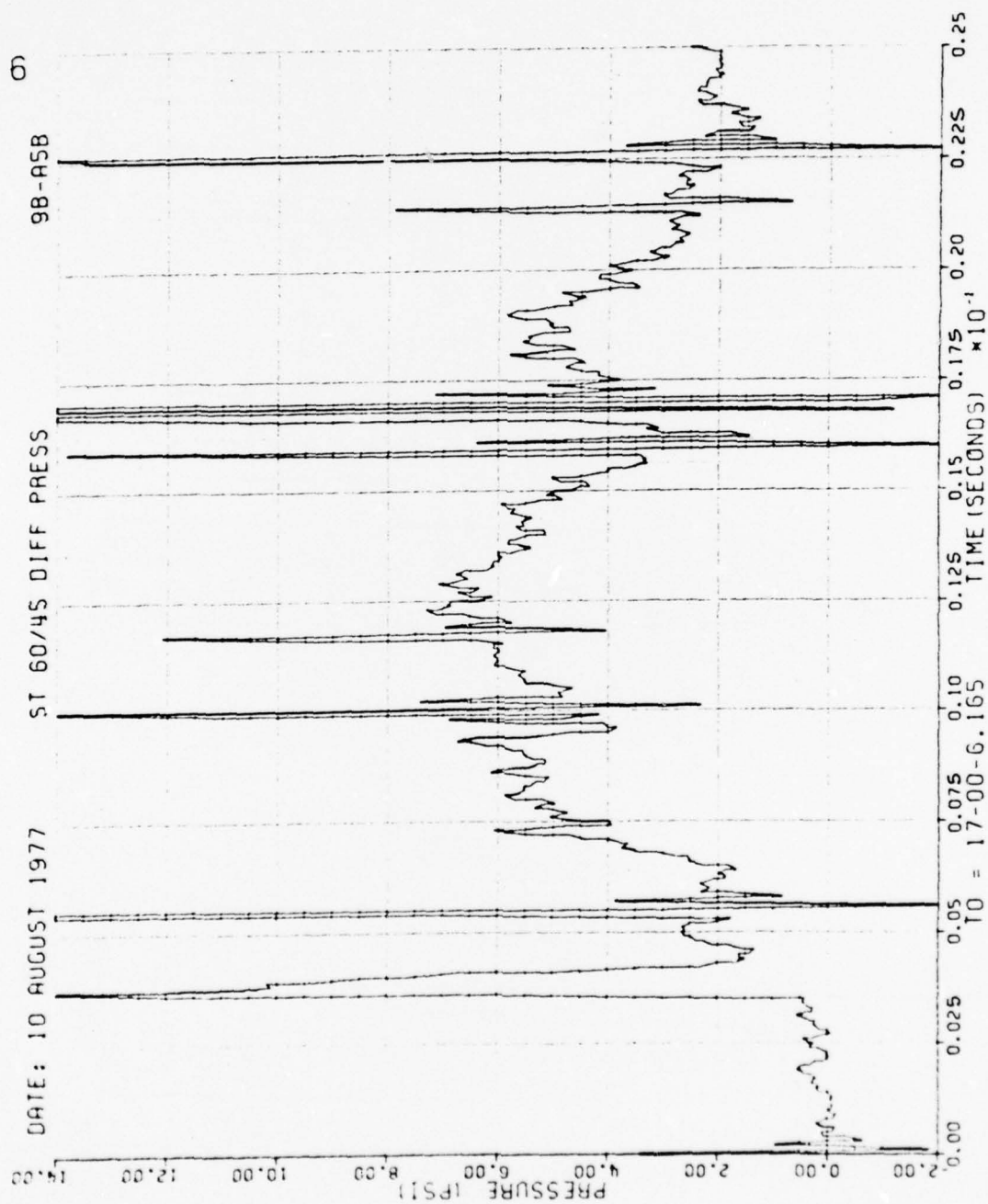


Figure 66. Continued

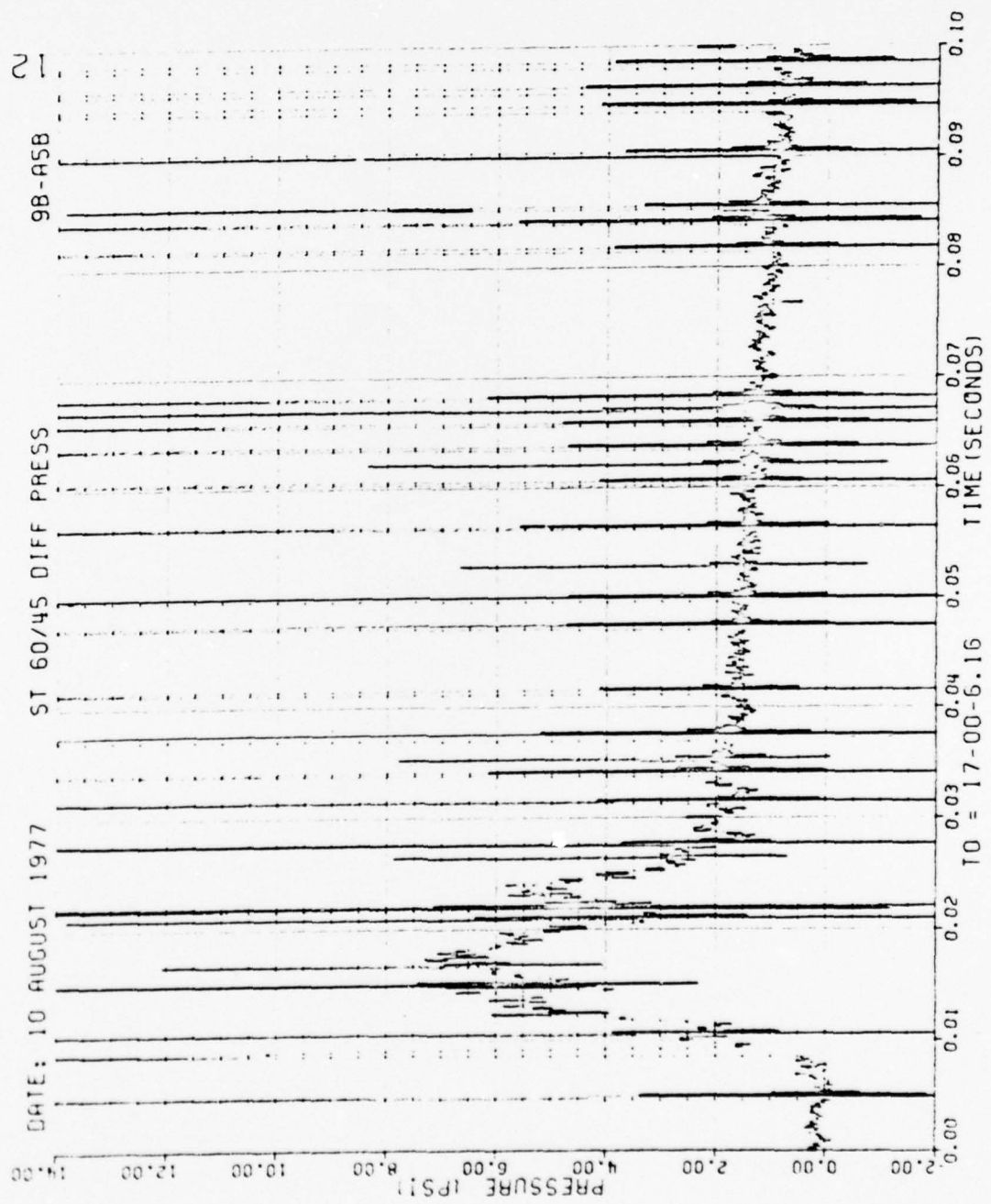


Figure 66. Continued

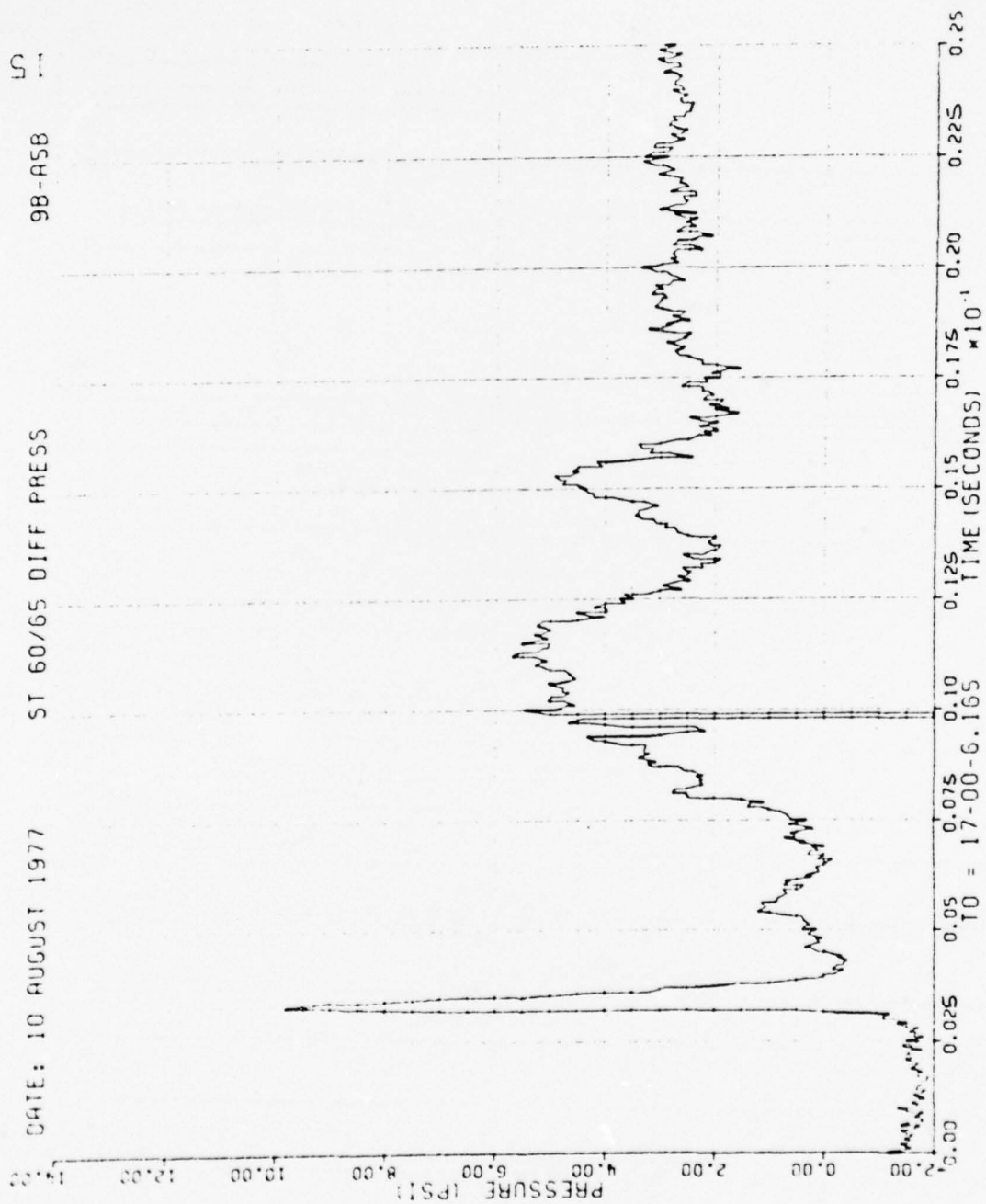


Figure 66. Continued

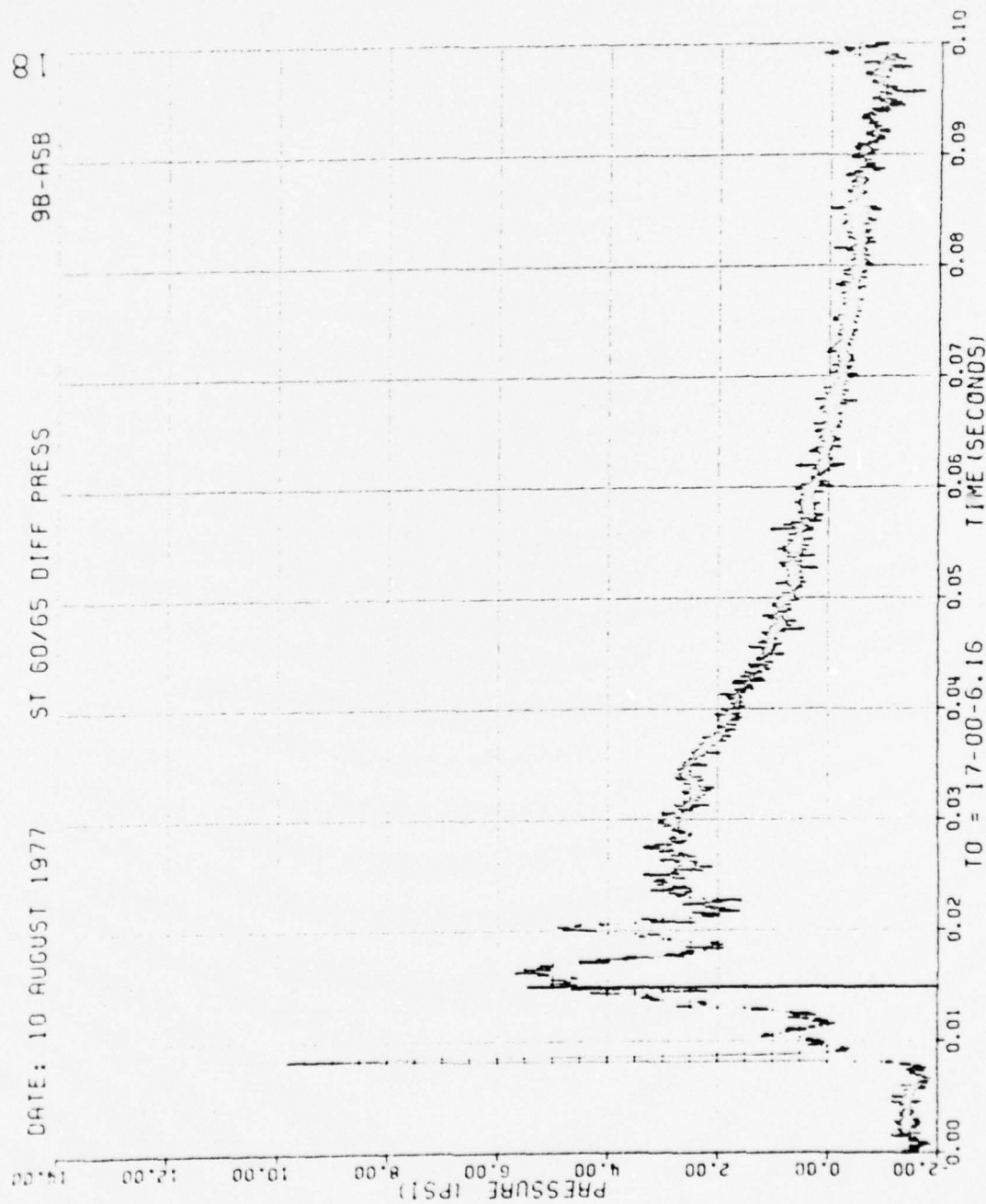


Figure 66. Continued

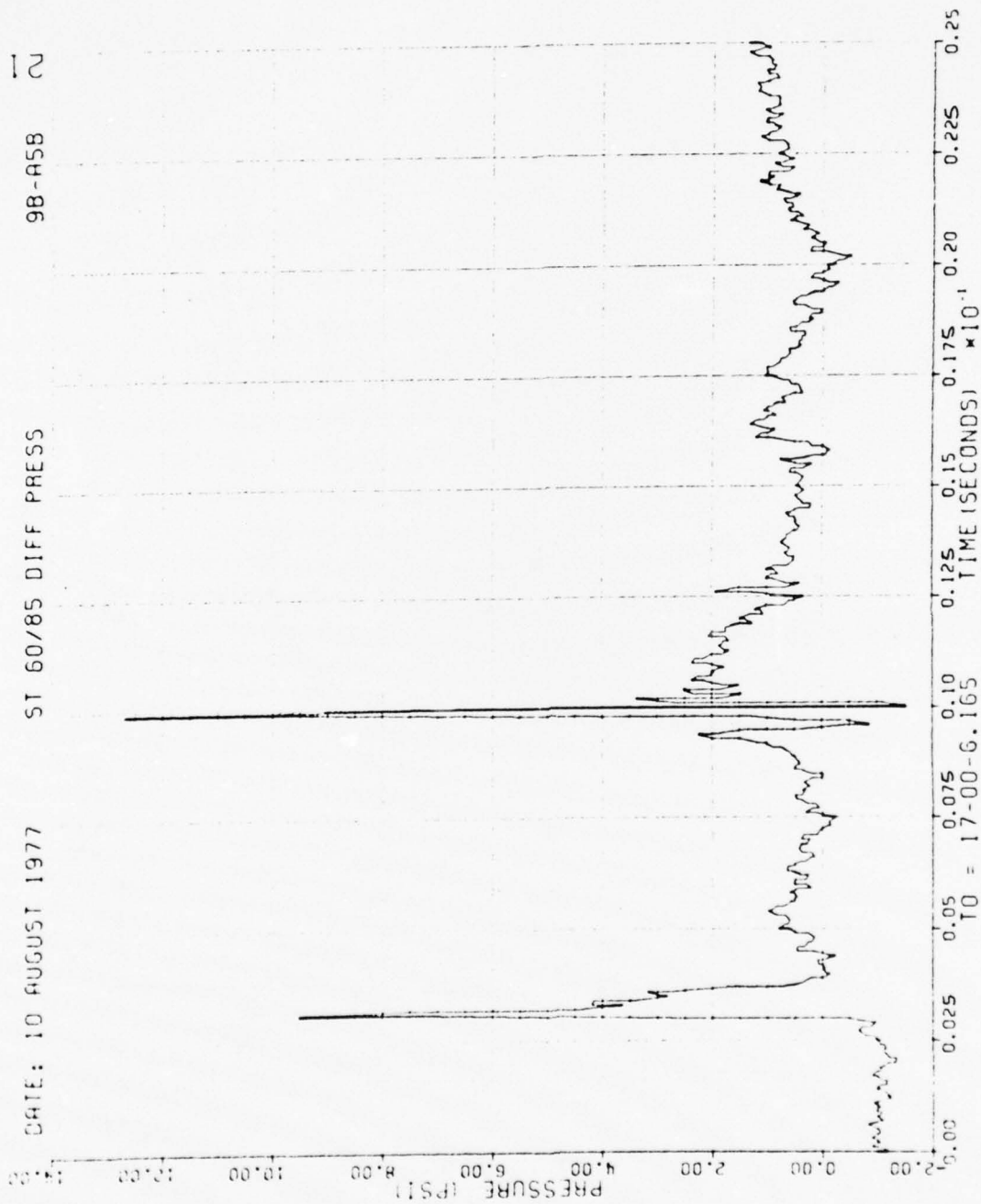


Figure 66. Continued

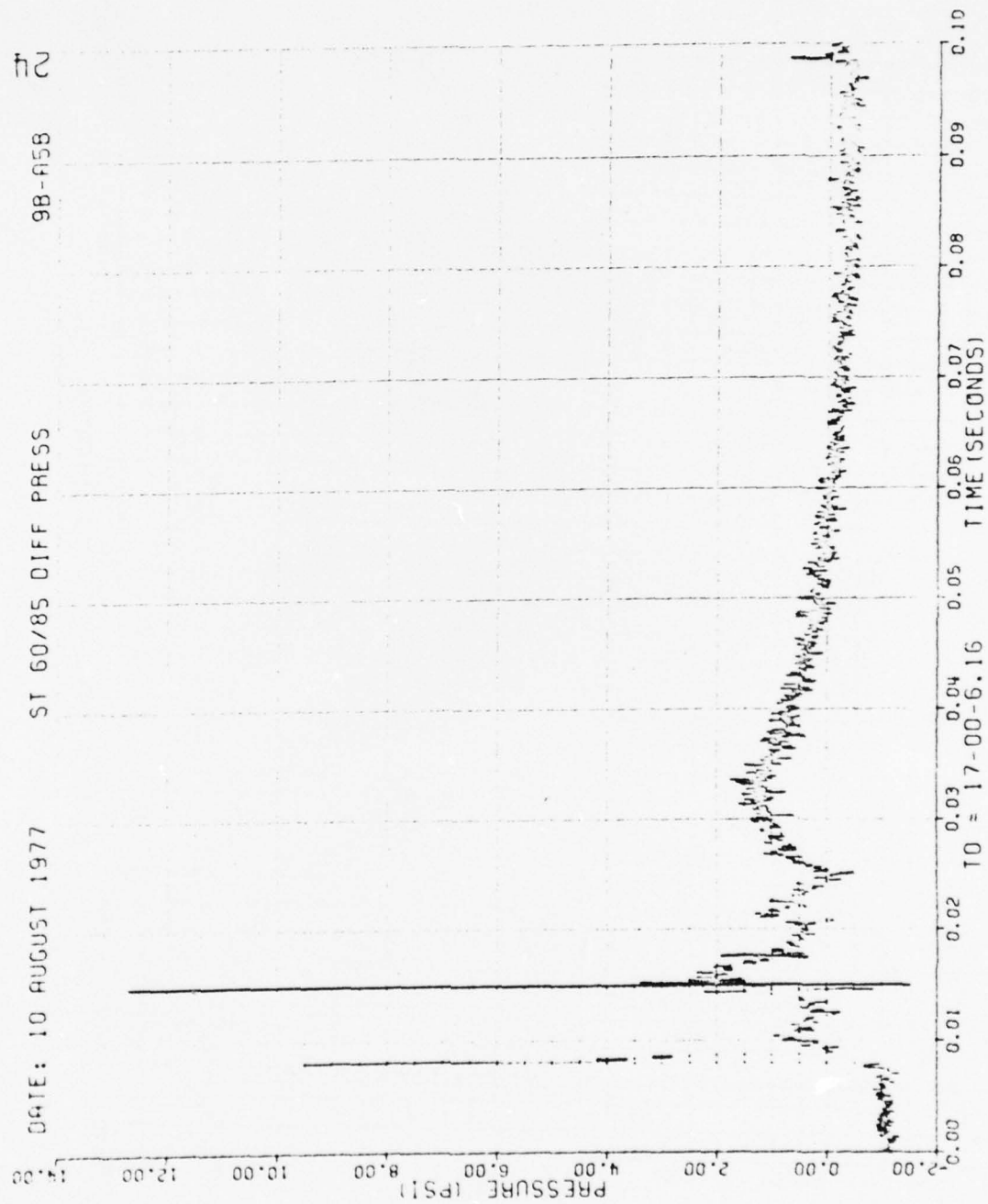


Figure 66. Continued

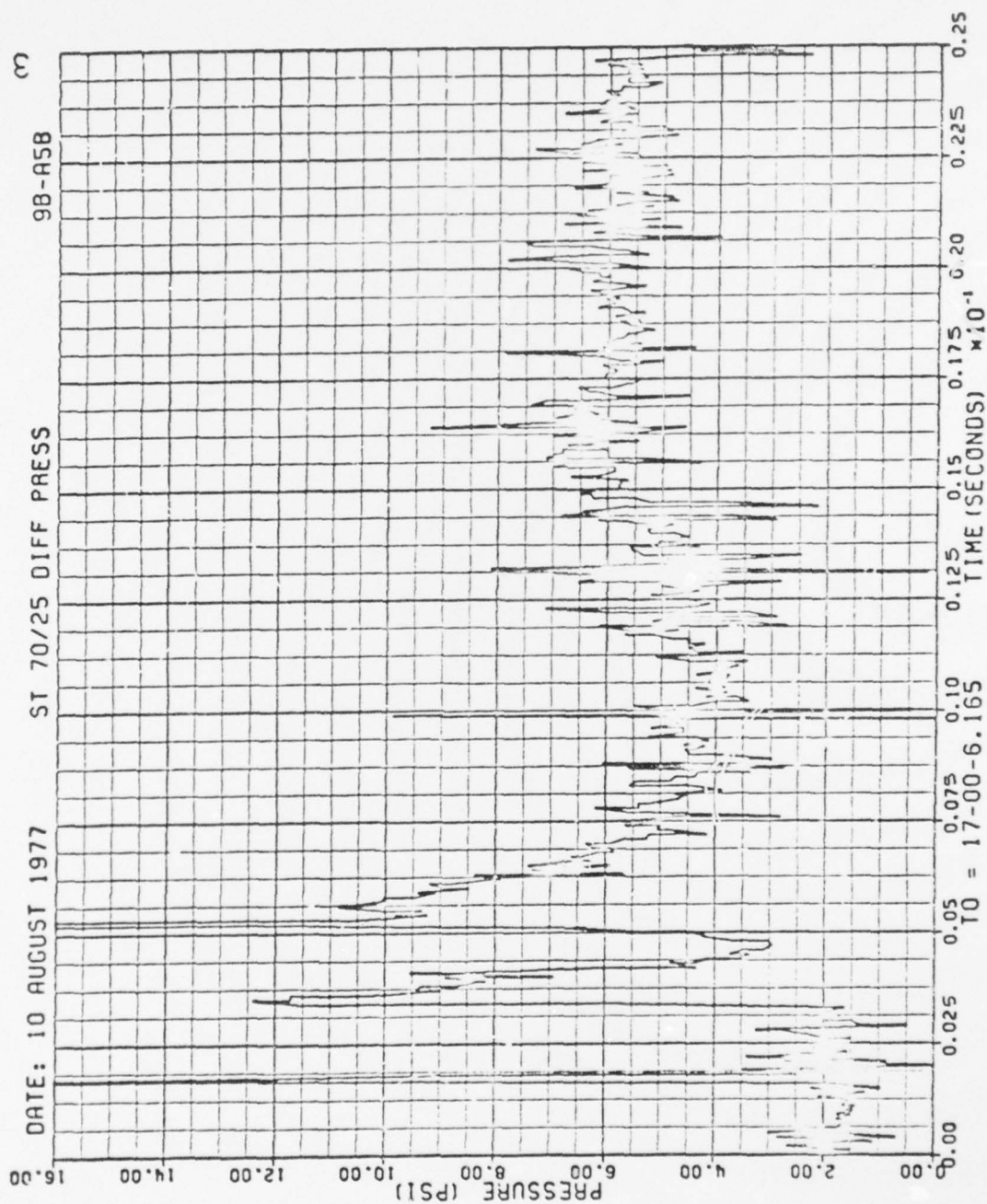


Figure 66. Continued

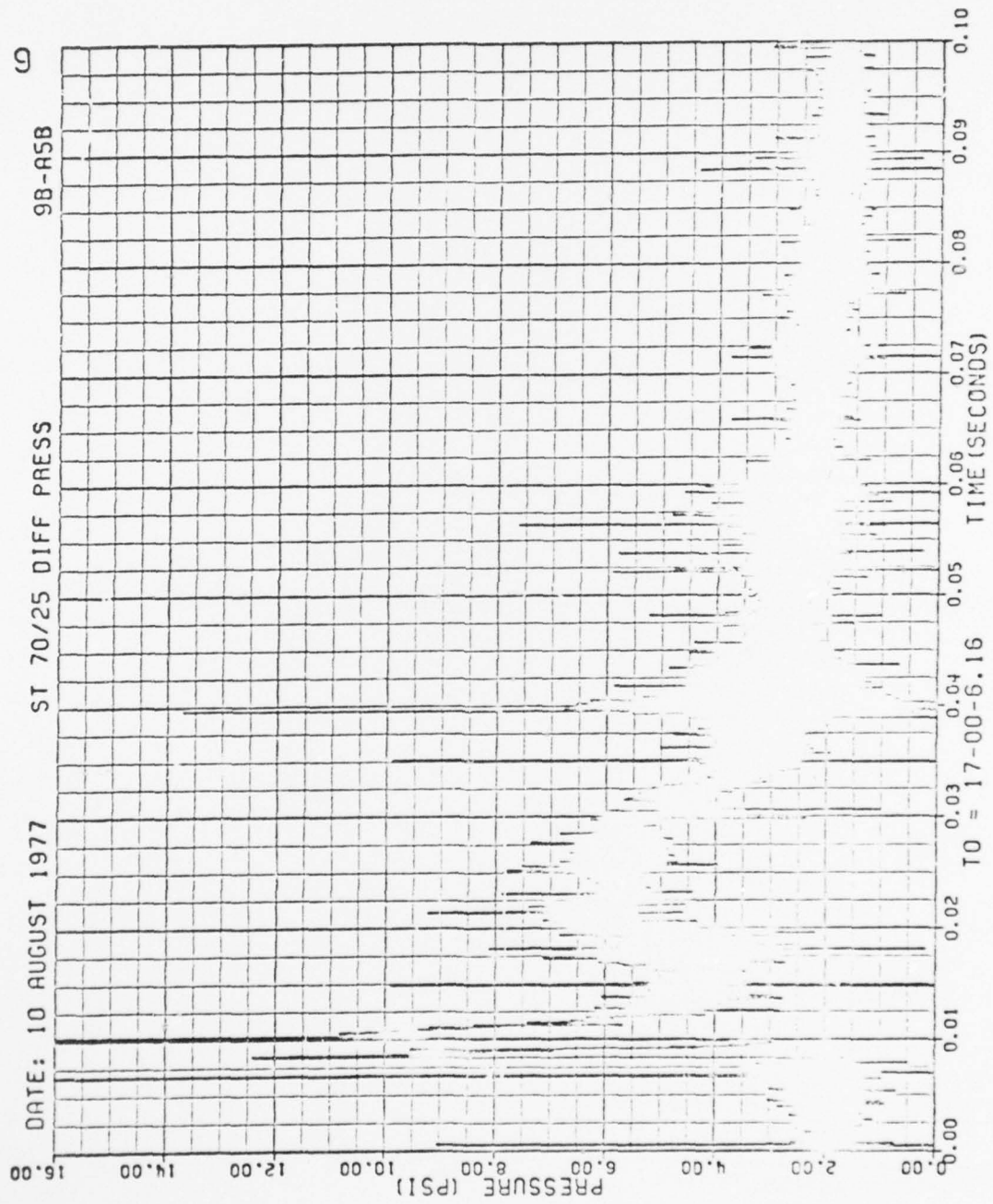


Figure 66. Continued

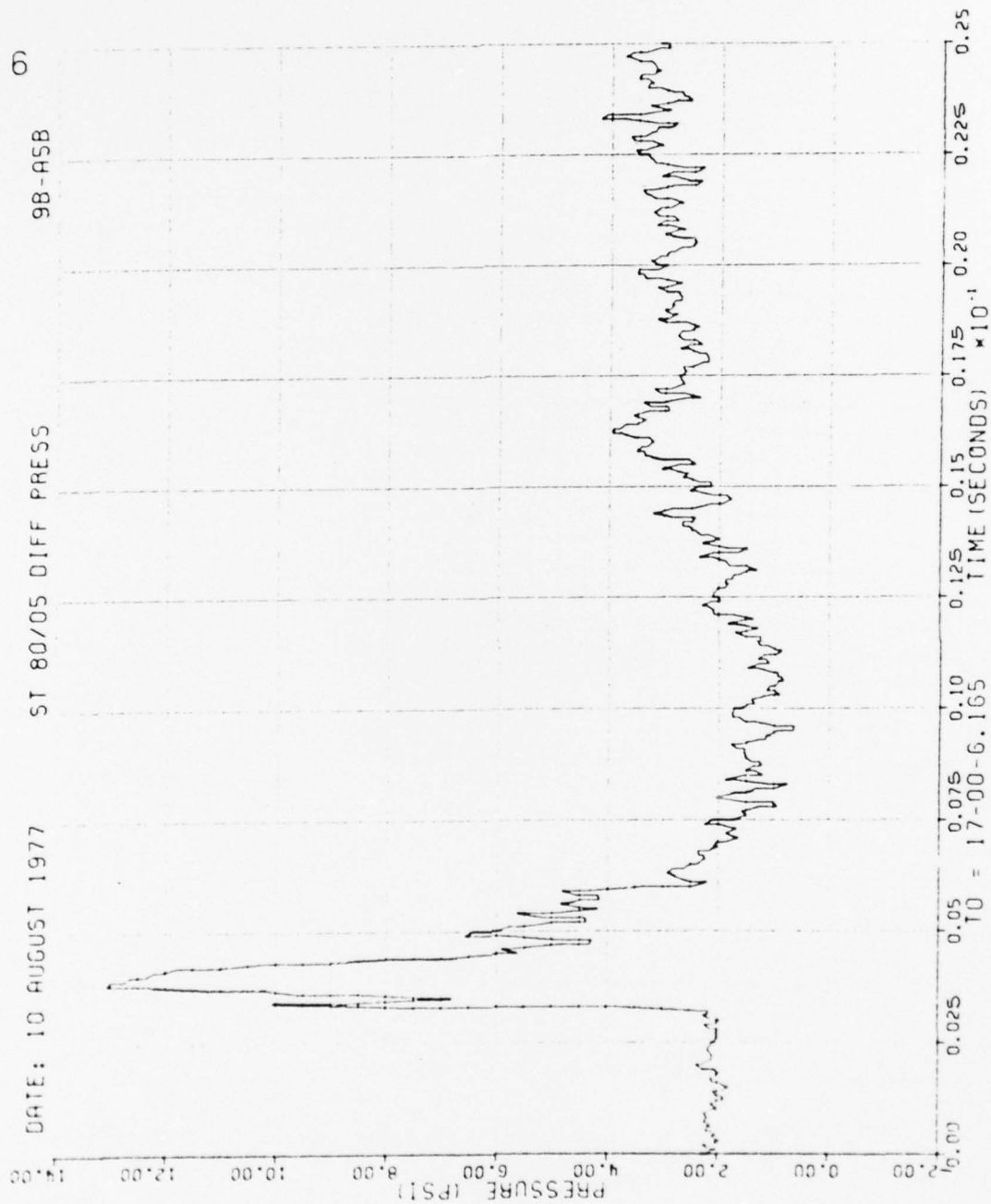


Figure 66. Continued

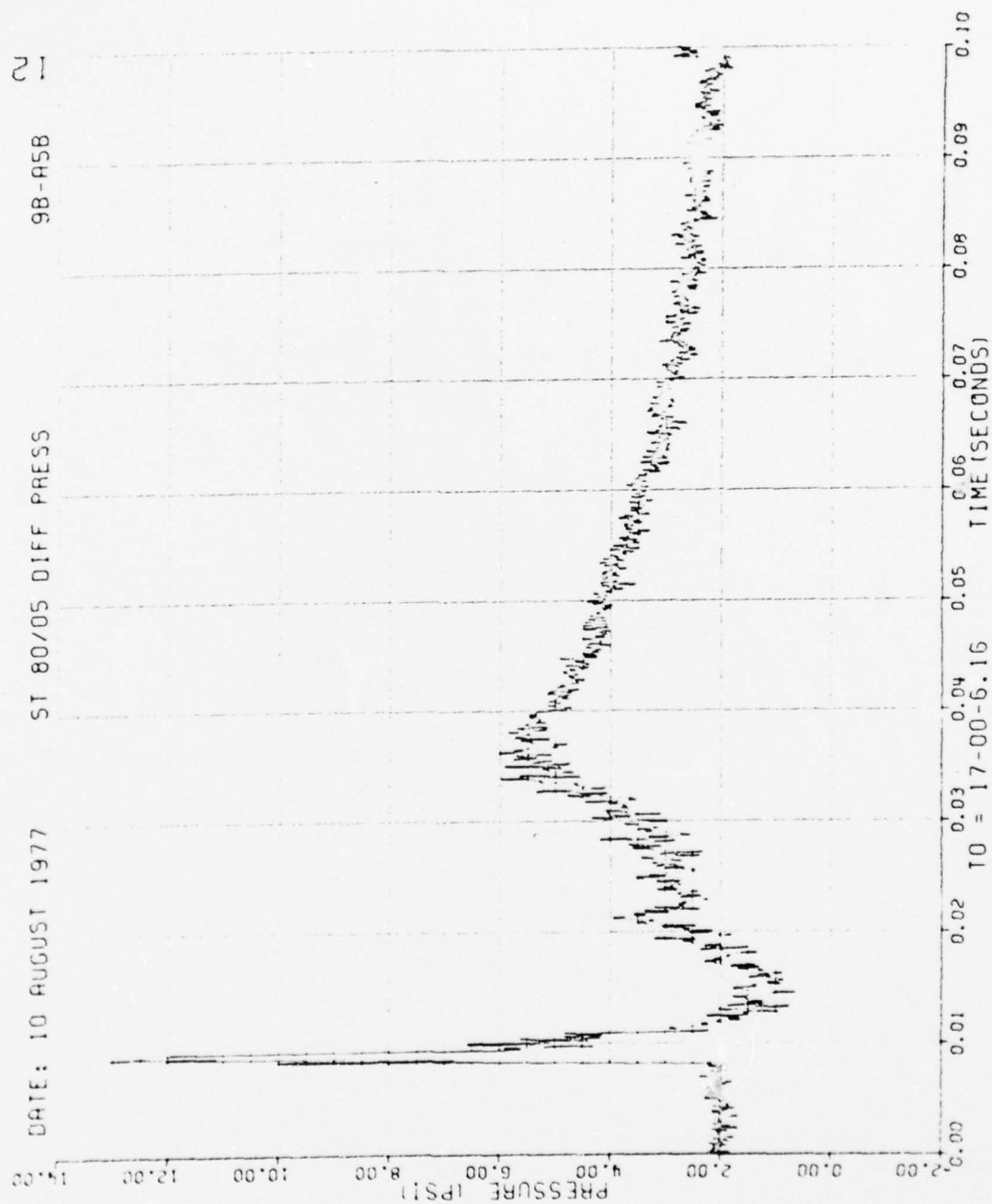


Figure 66. Continued

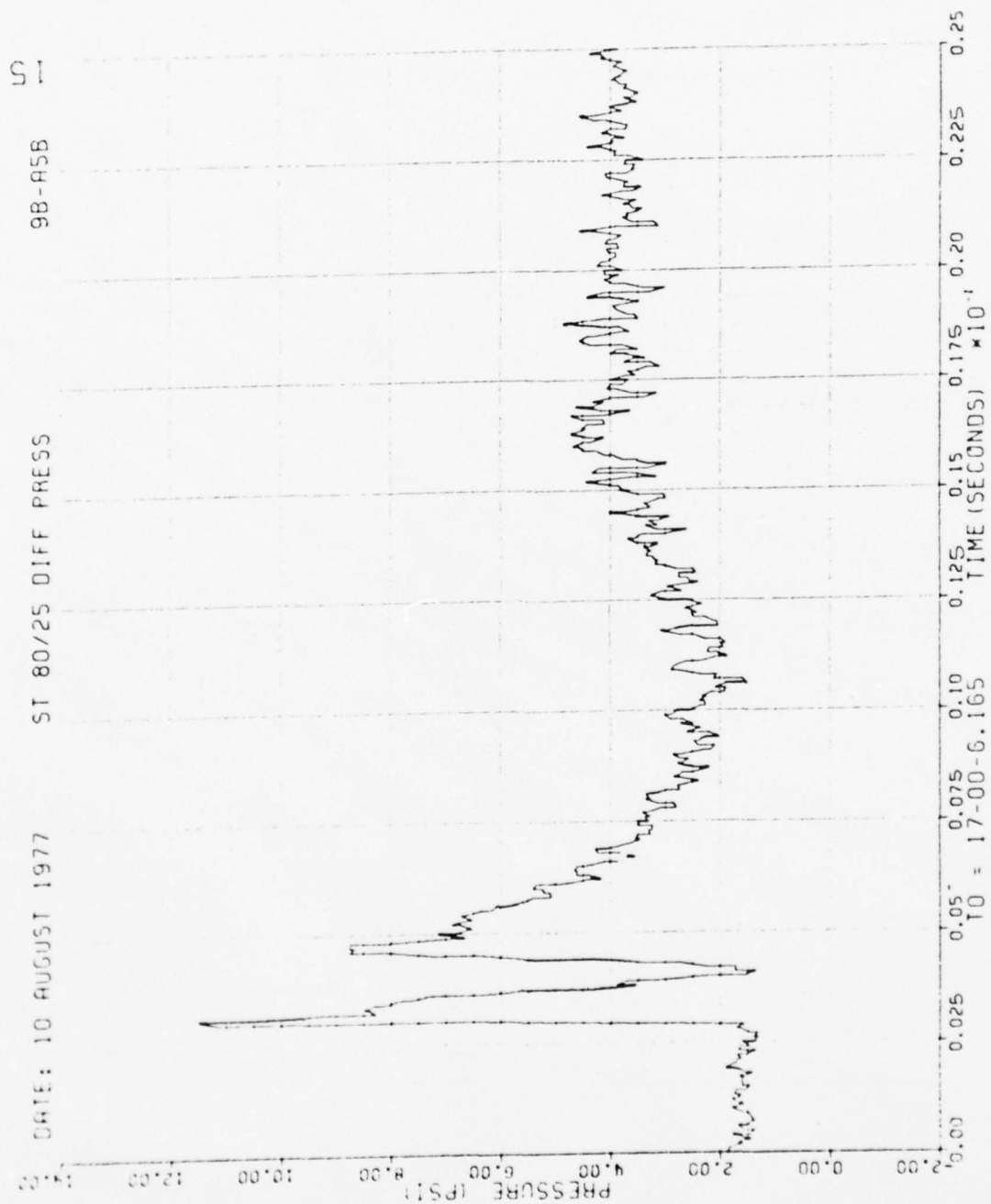


Figure 66. Continued

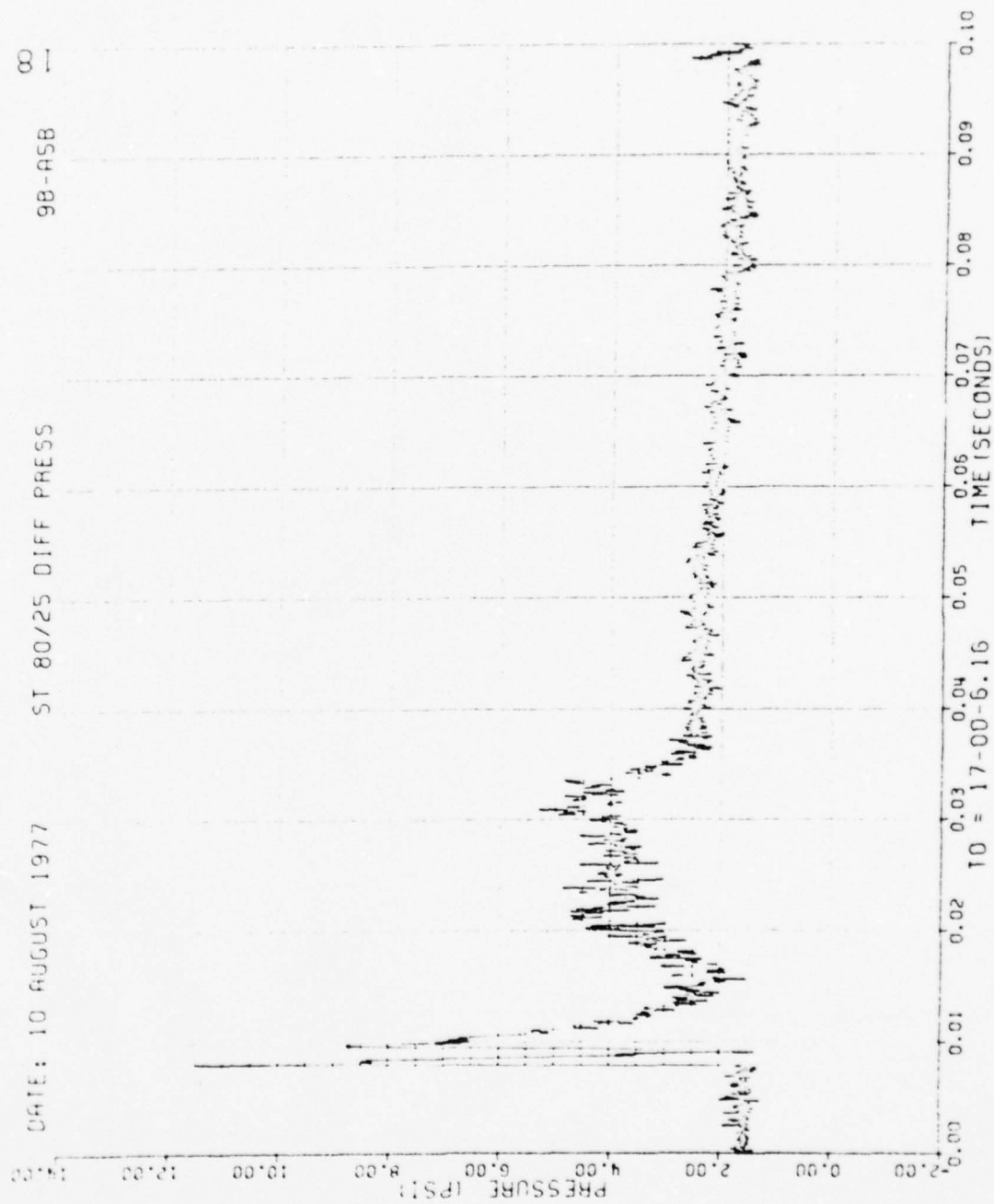


Figure 66. Continued

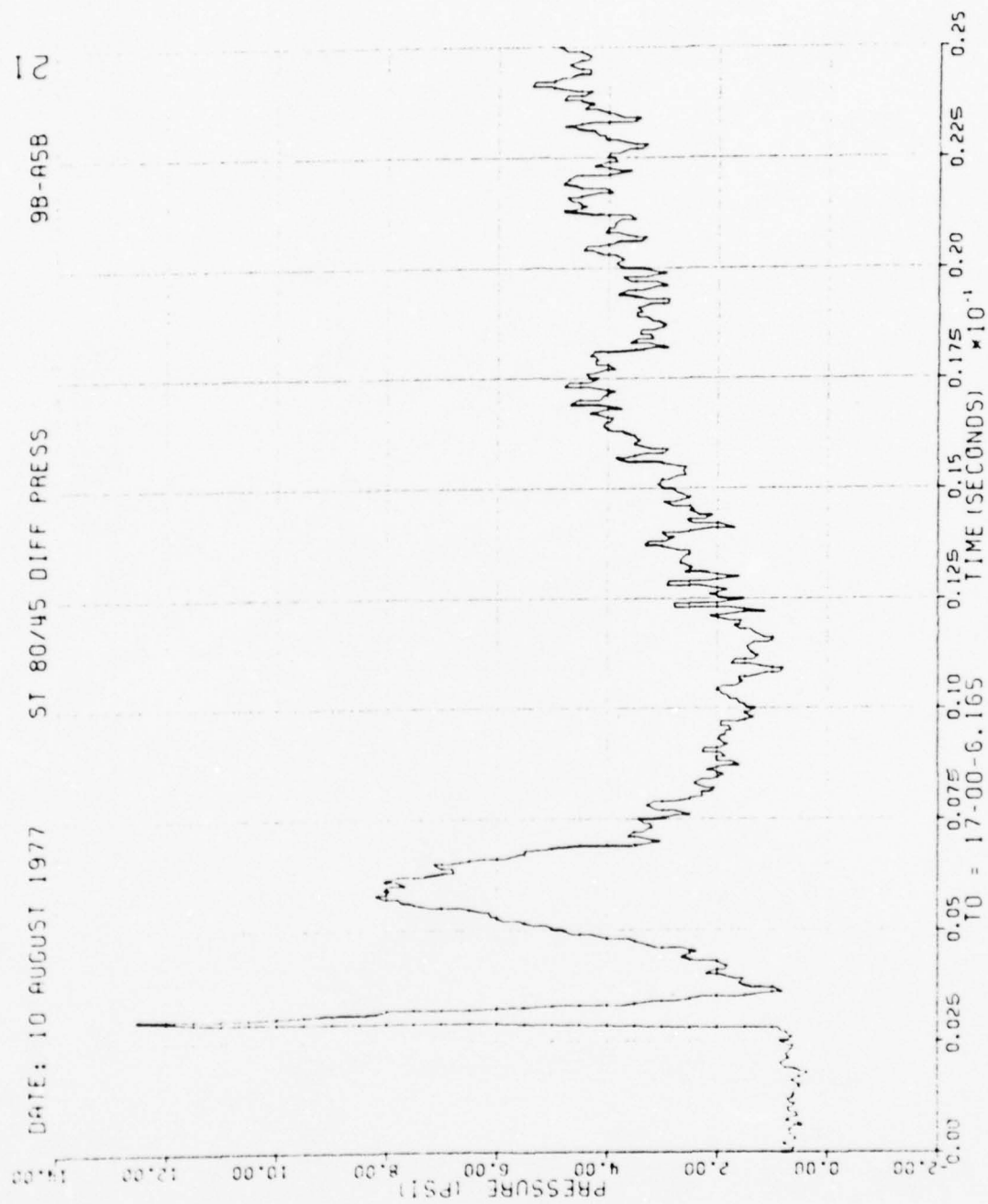


Figure 66. Continued

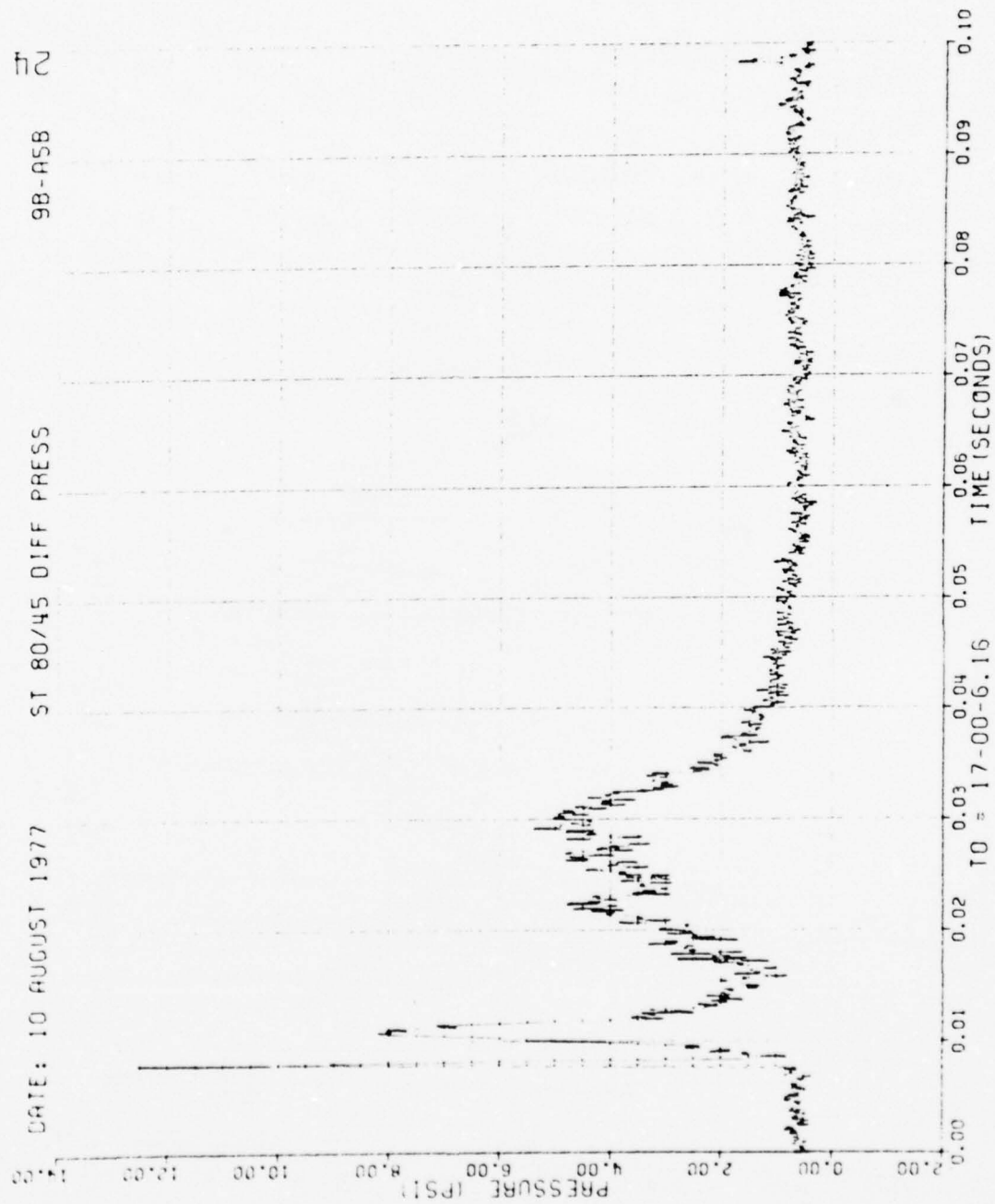


Figure 66. Continued

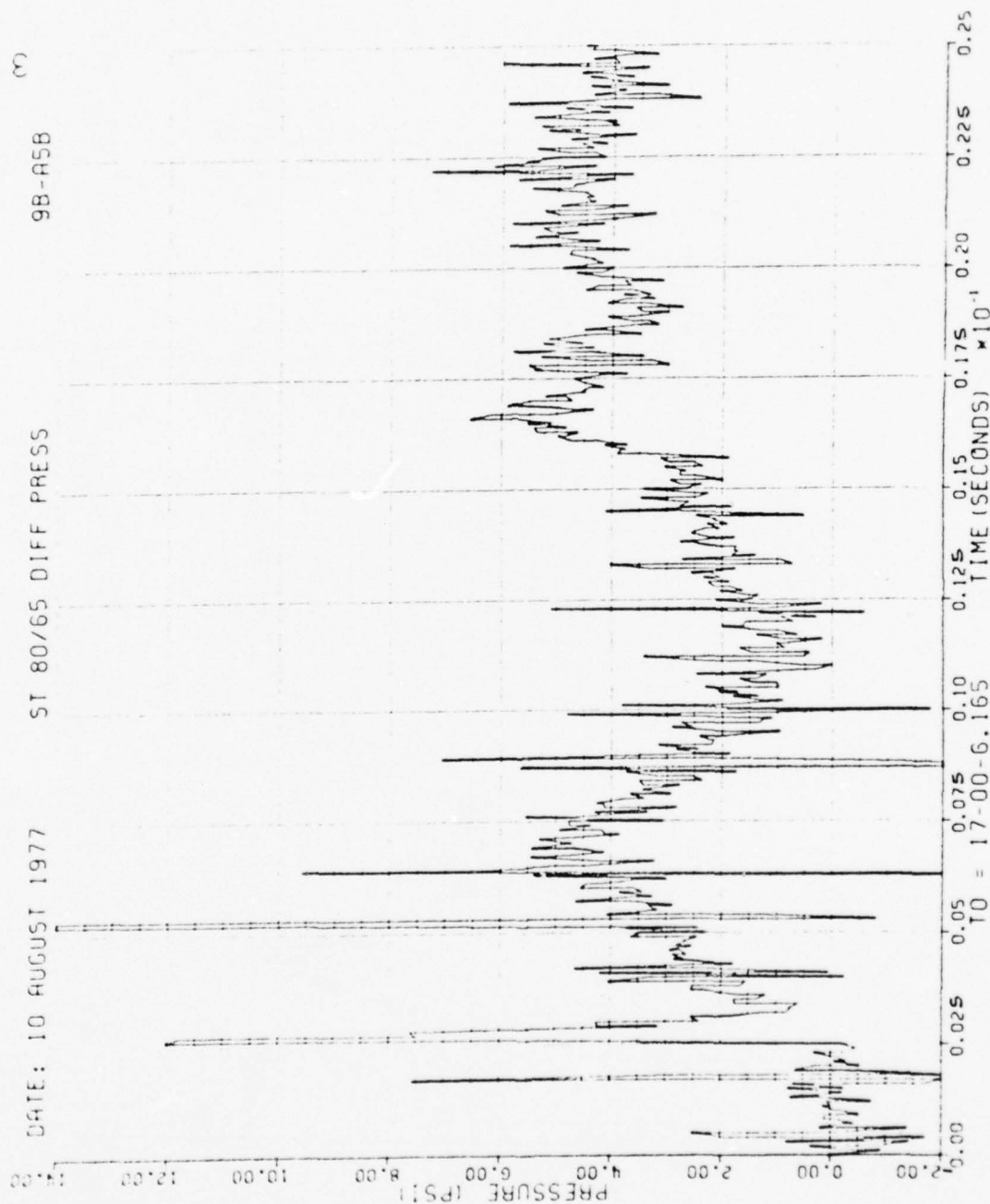


Figure 66. Continued

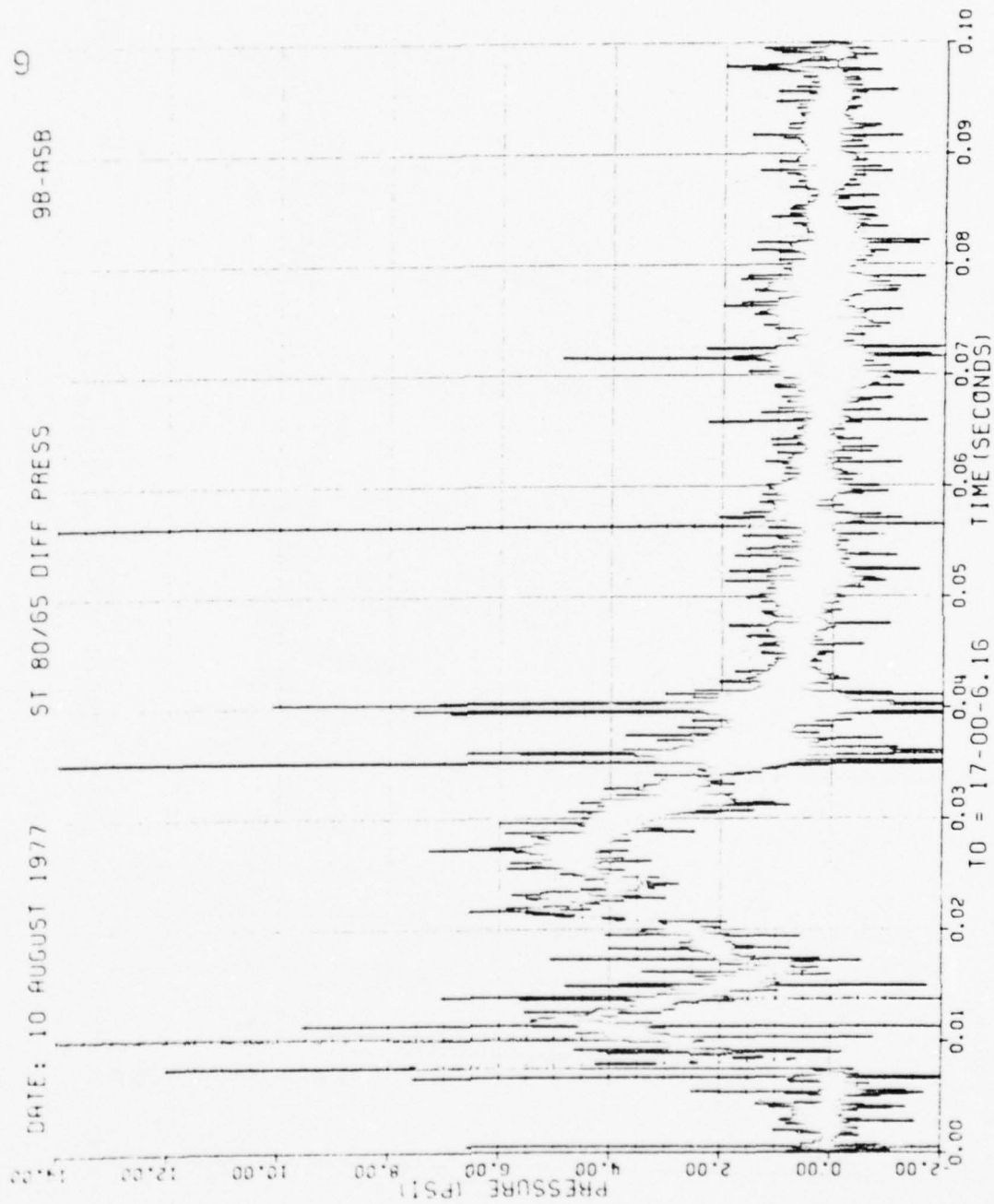


Figure 66. Continued

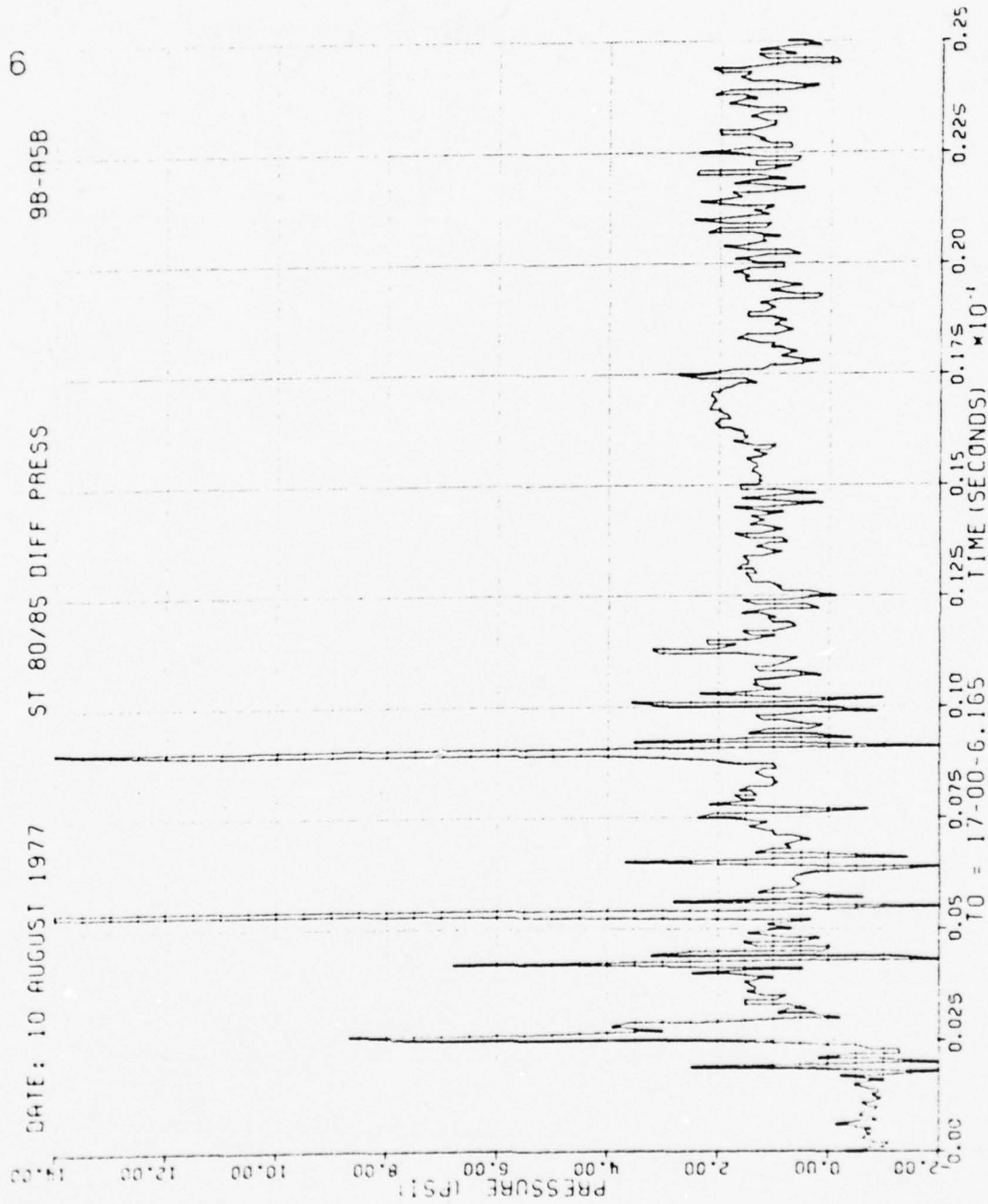


Figure 66. Continued

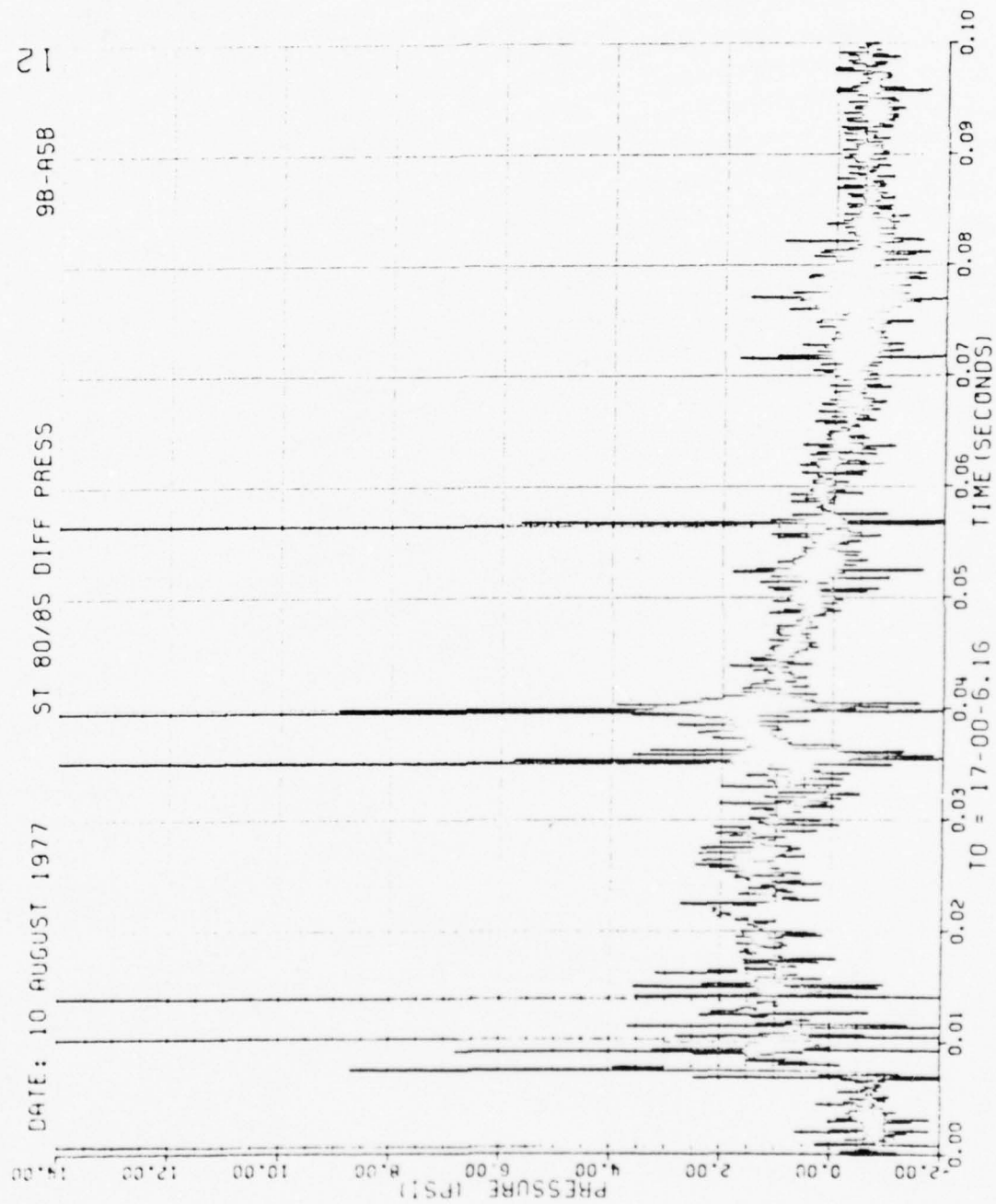


Figure 66. Continued

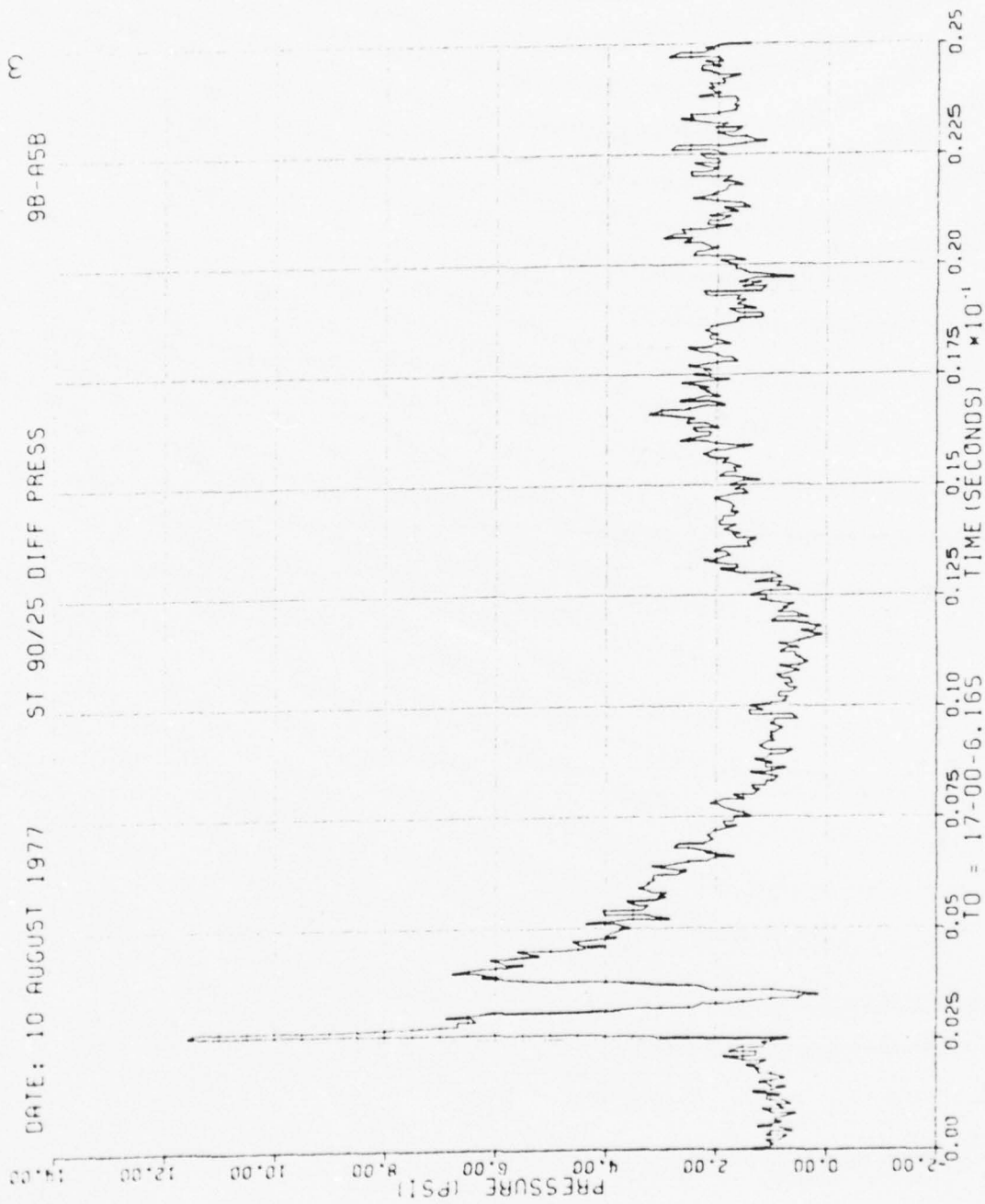


Figure 66. Continued

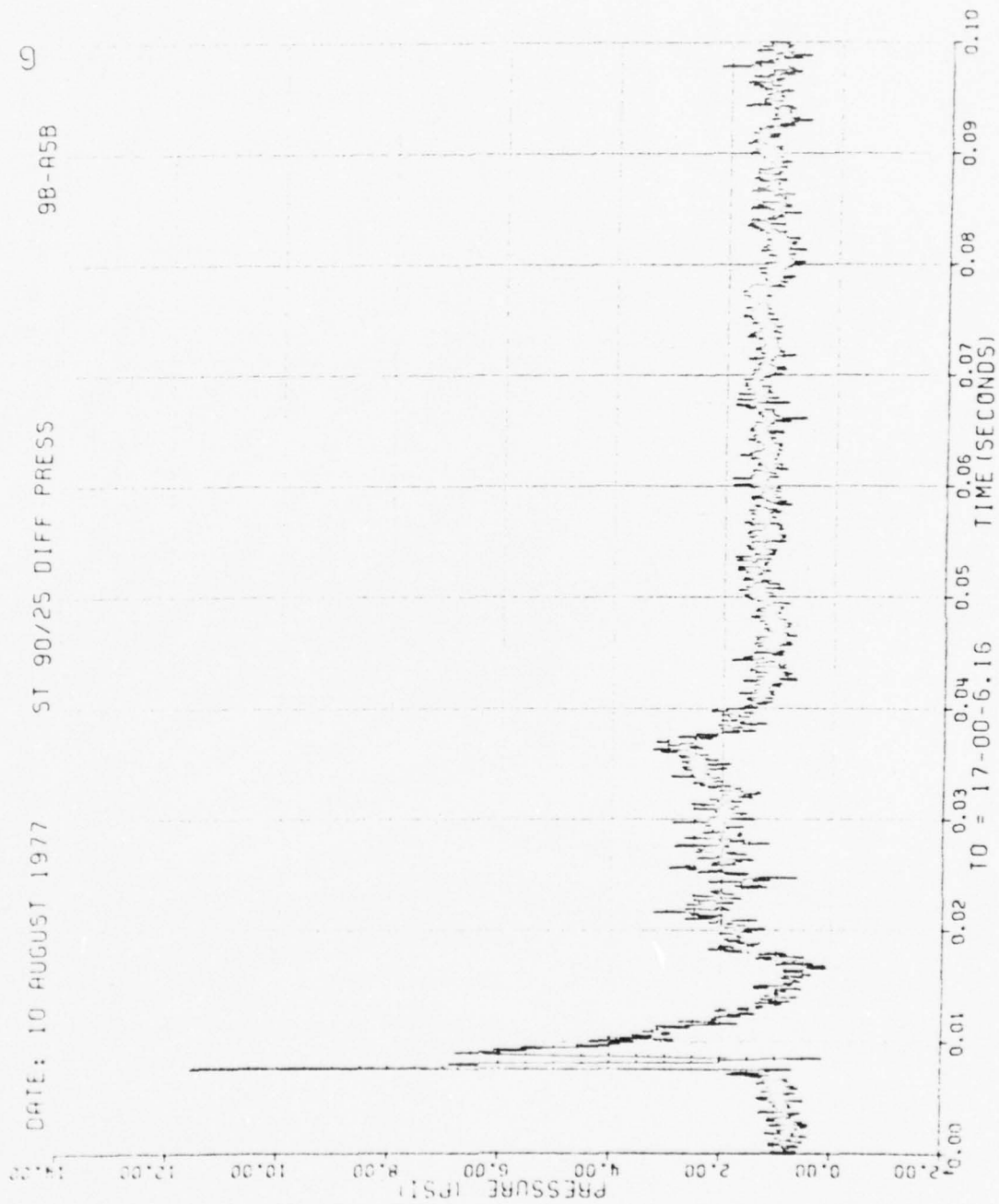


Figure 66. Concluded

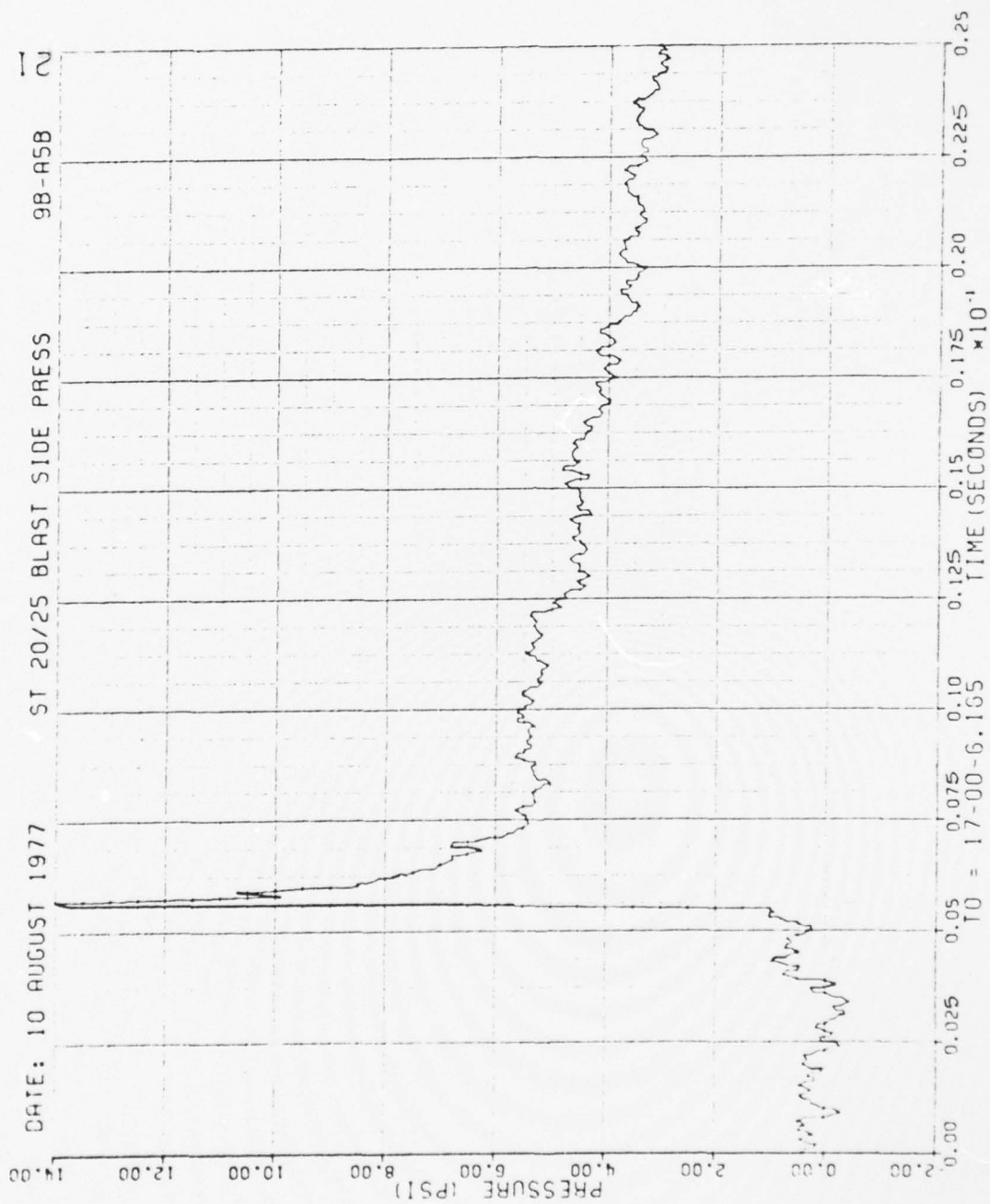


Figure 67. Blastward and Leeward Wing Pressures, Run 9B-A5, Intercept 3.

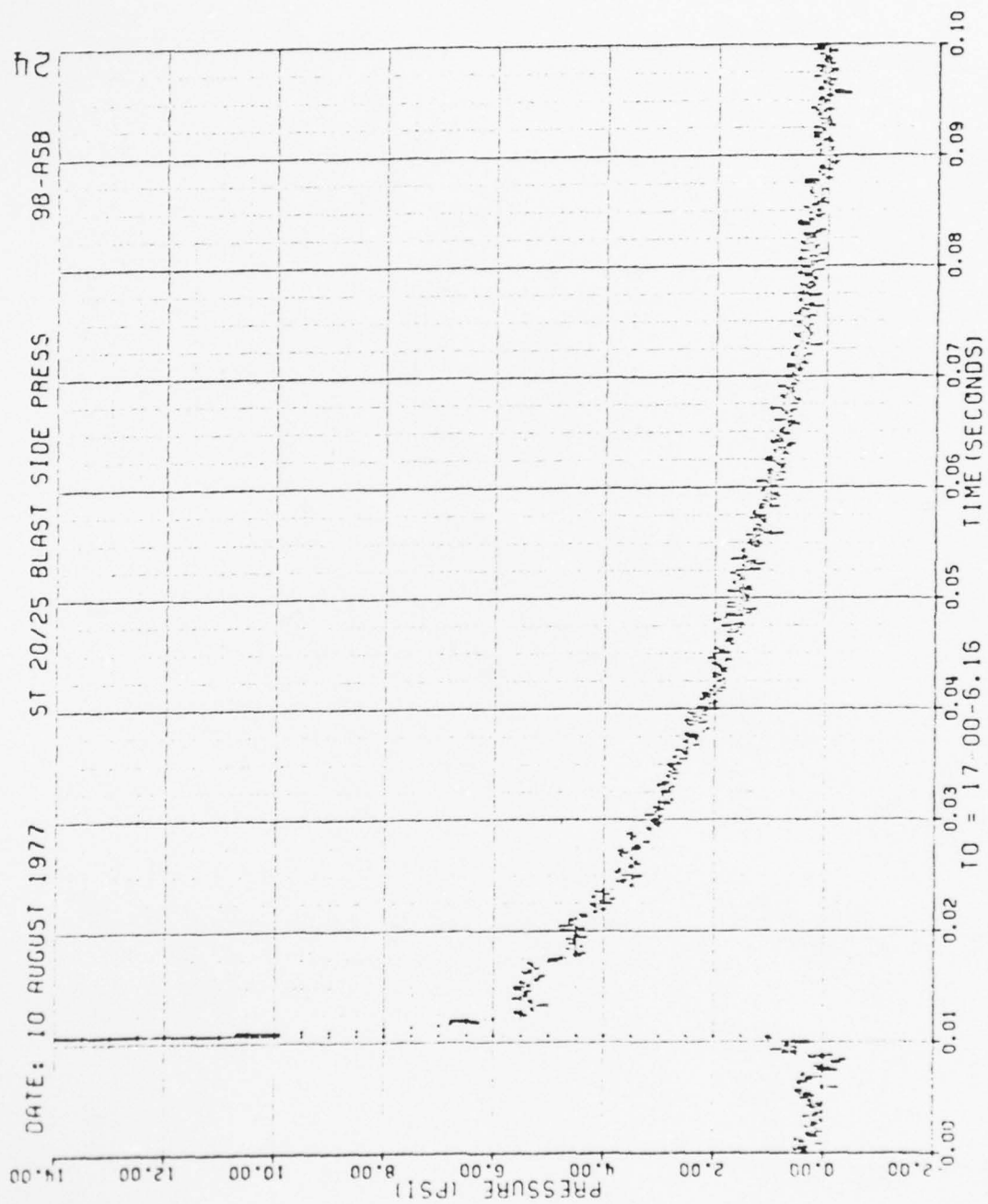


Figure 67. Continued

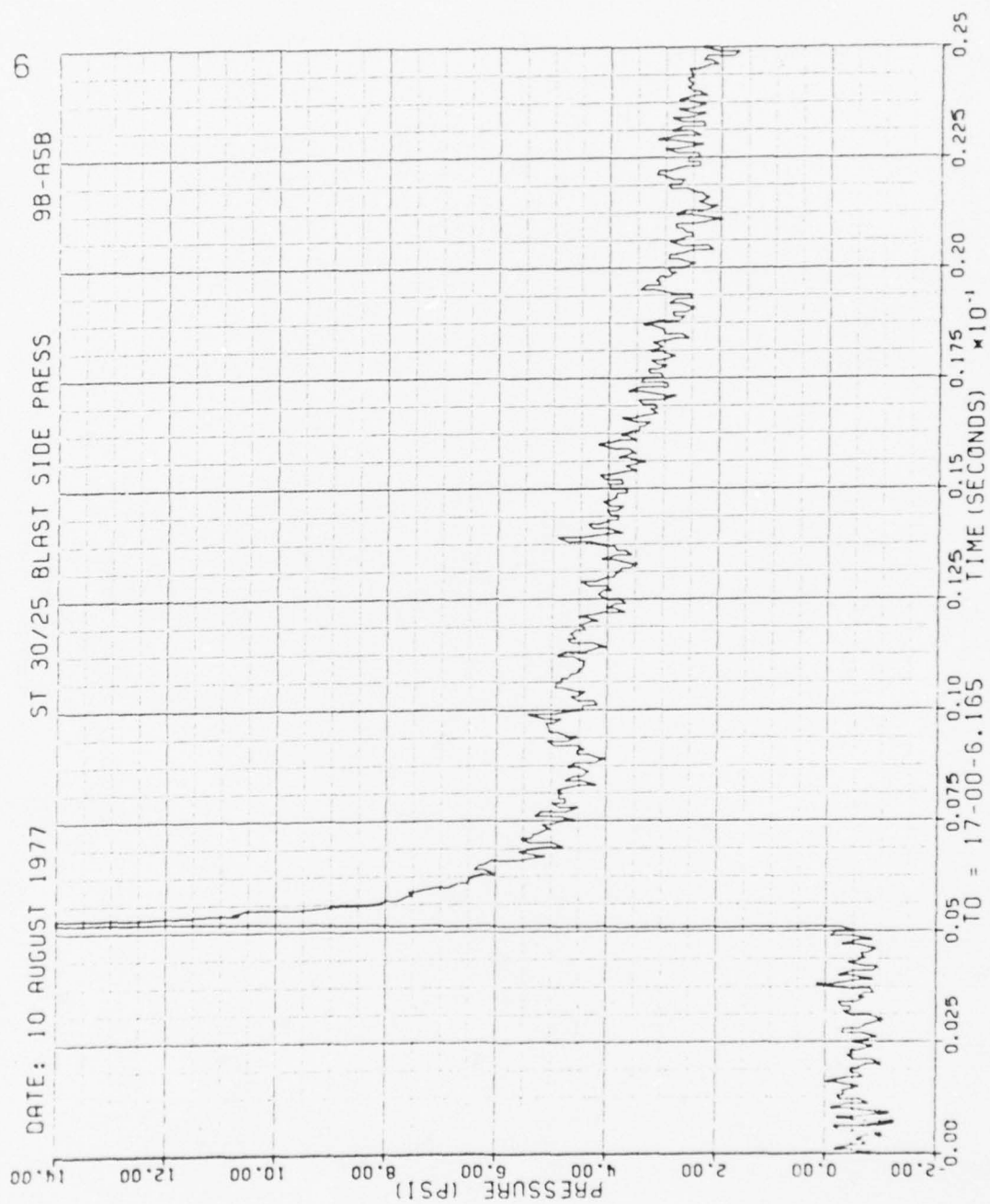


Figure 67. Continued

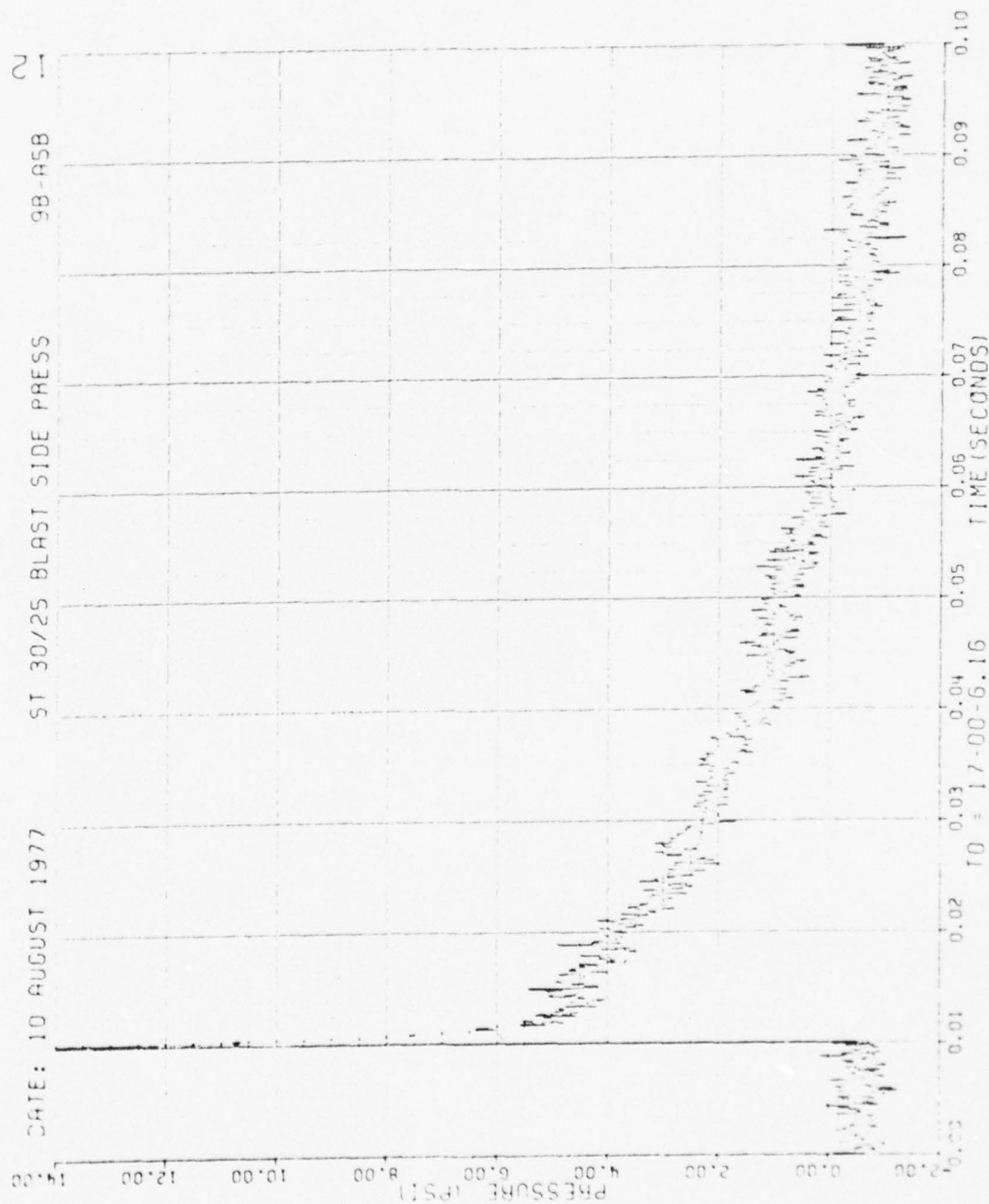


Figure 67. Continued

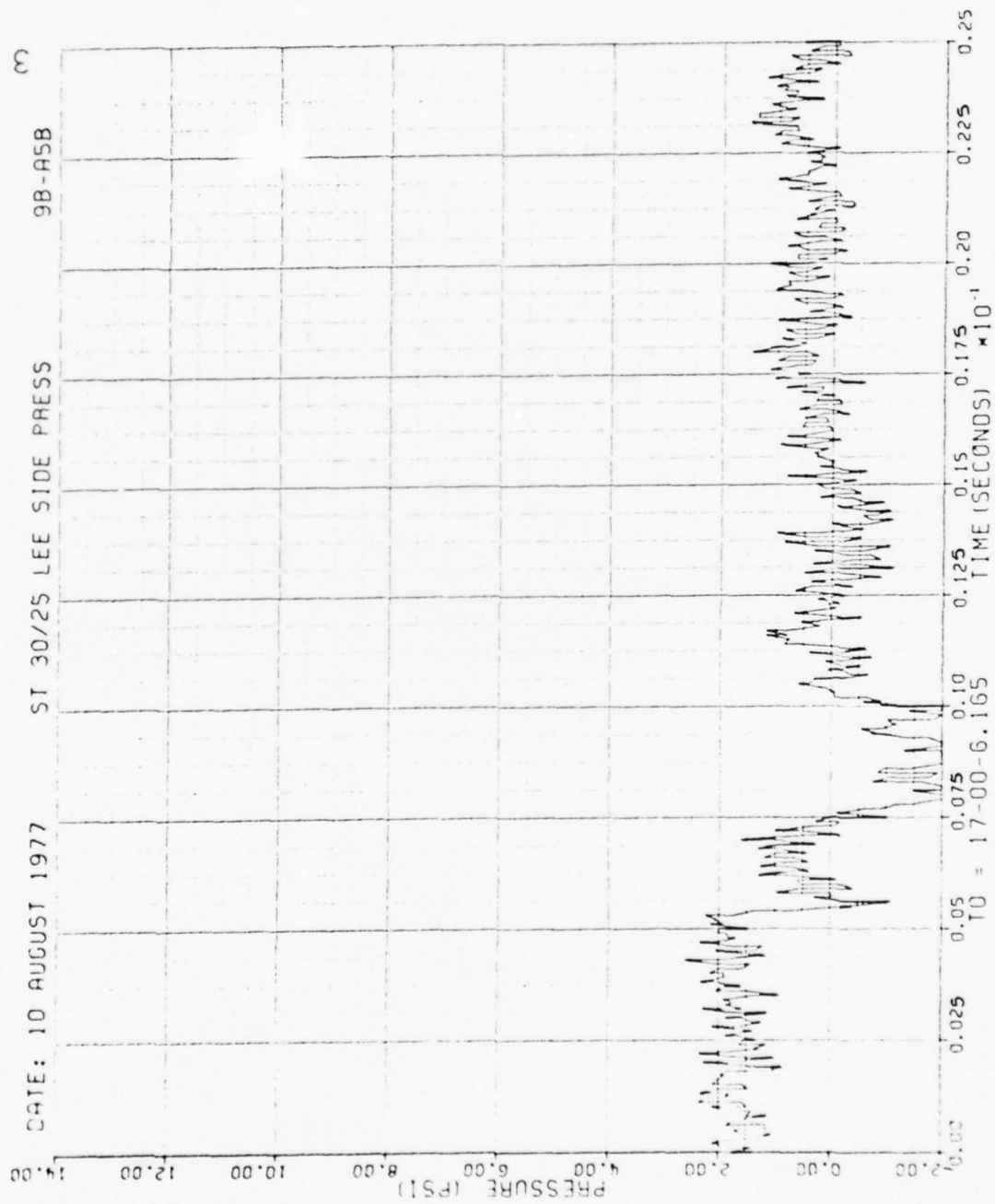


Figure 67. Continued

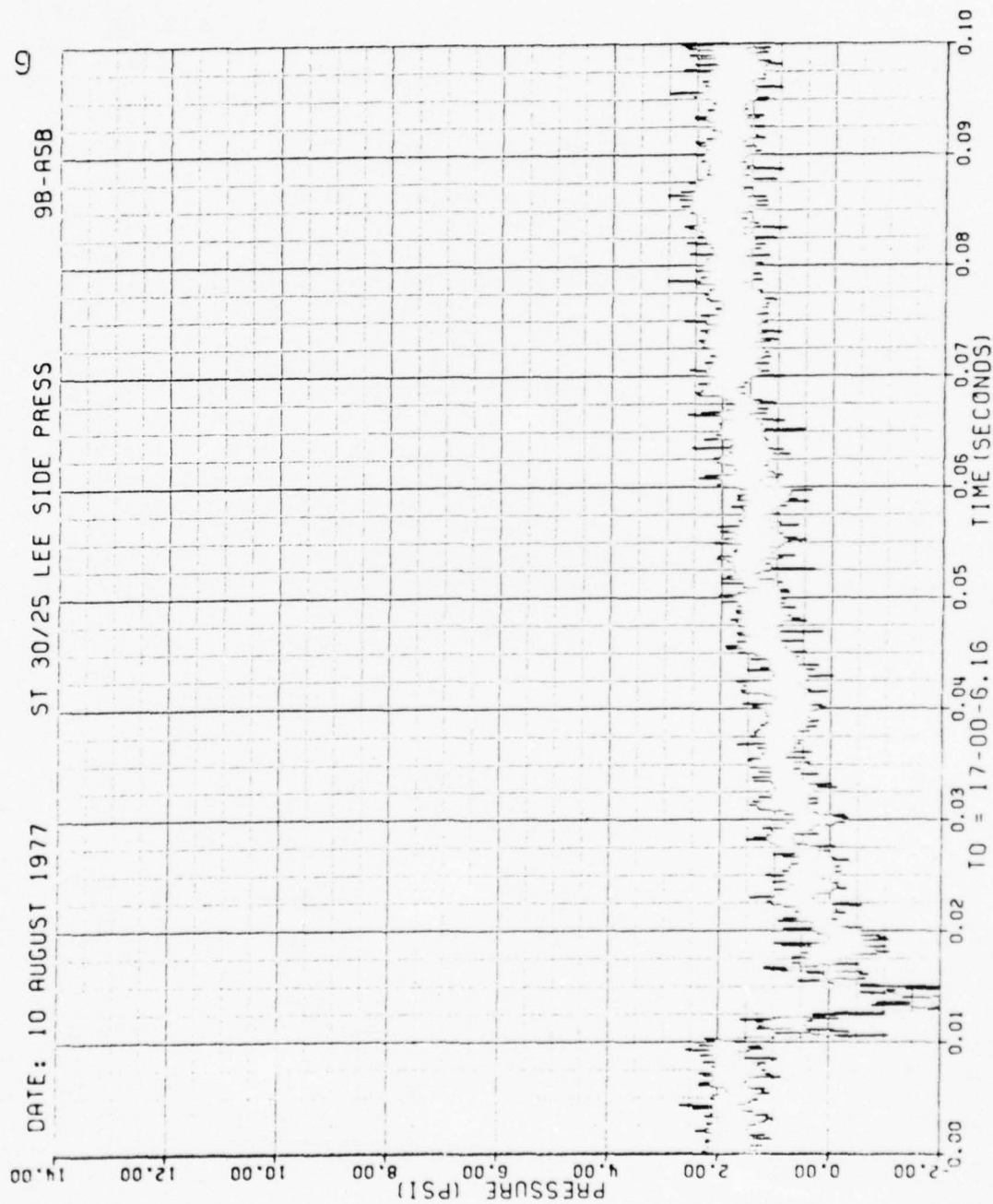


Figure 67. Continued

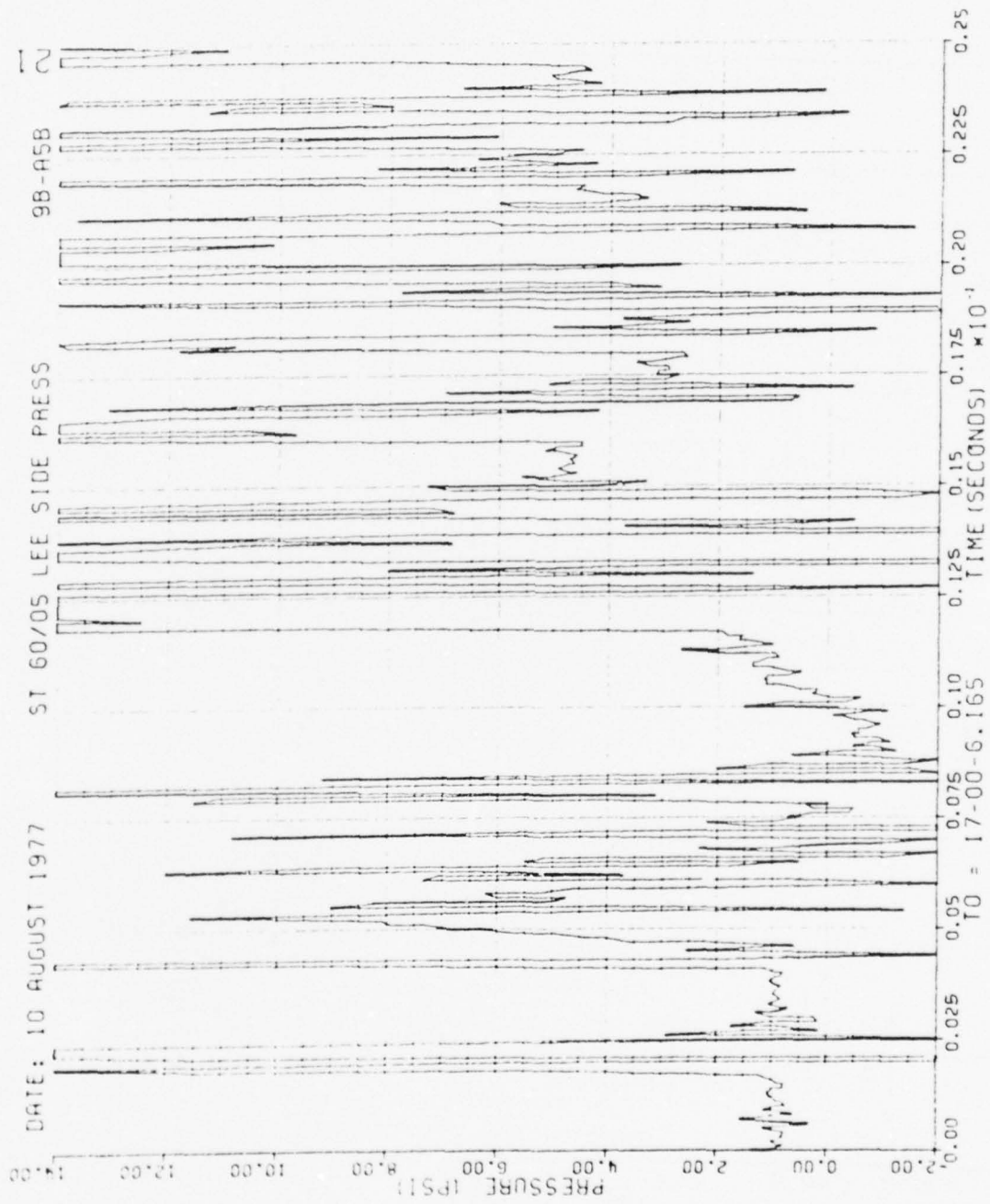


Figure 67. Continued

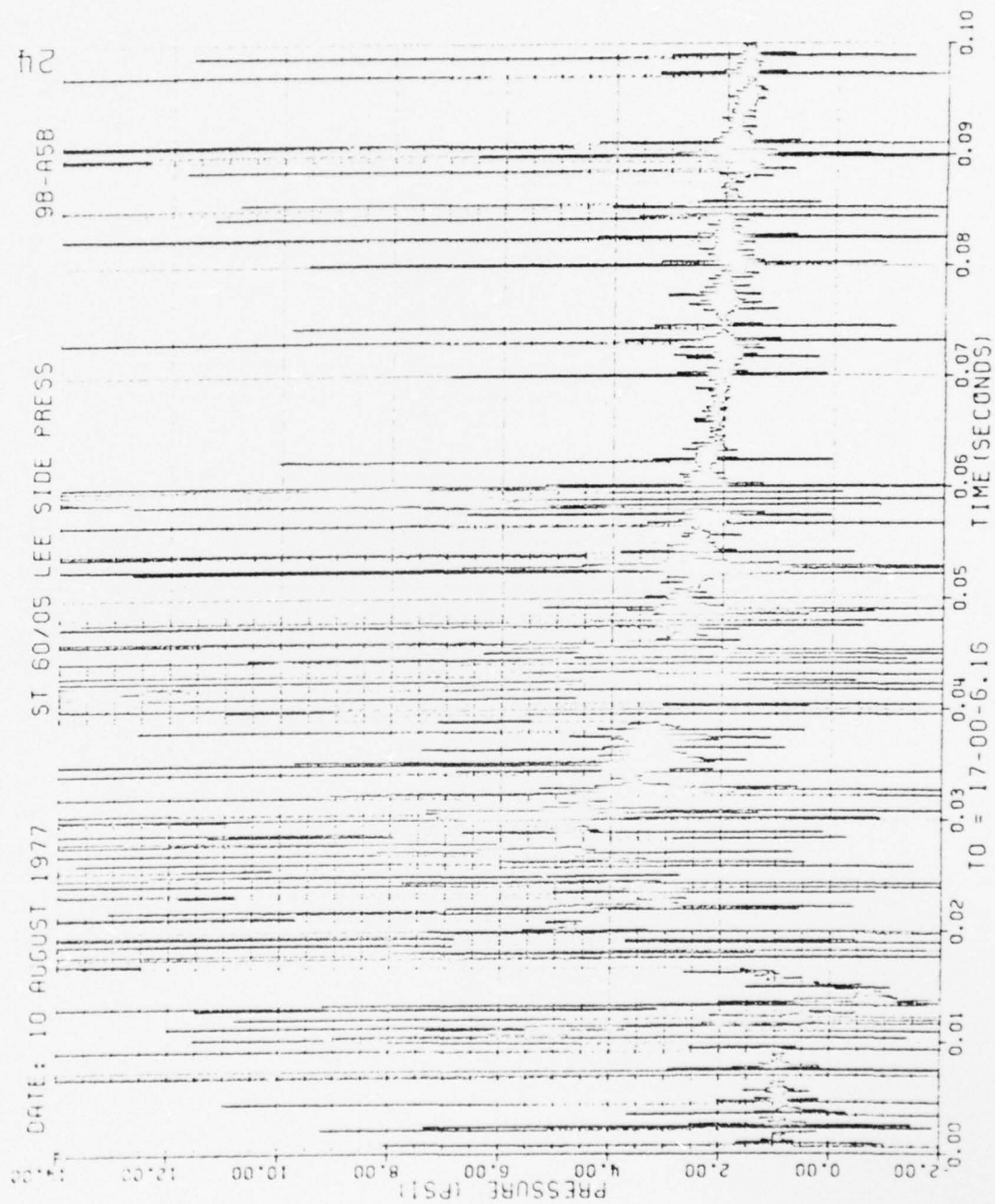


Figure 67. Concluded

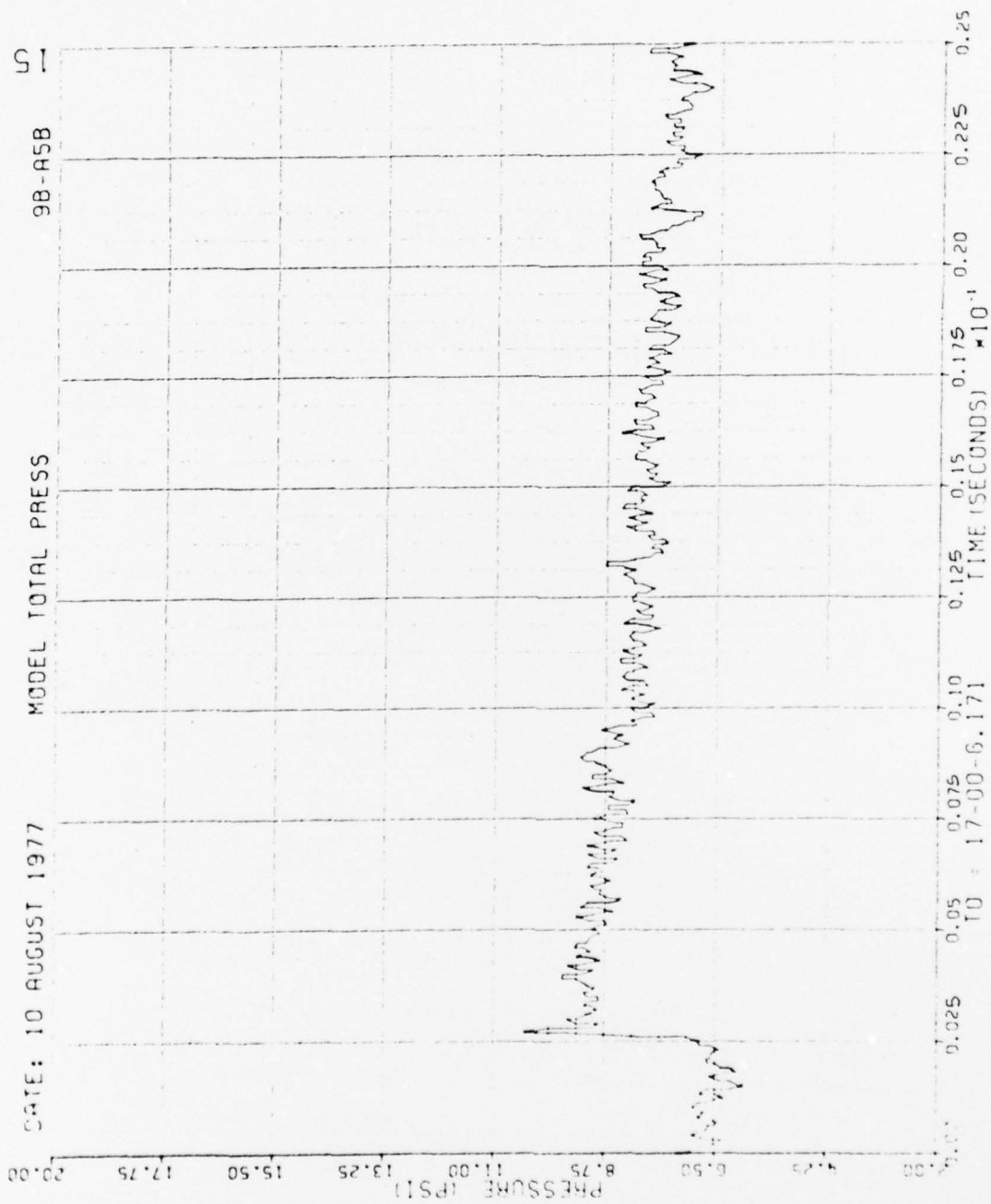


Figure 68. Total Pressure at Model, Run 9B-A5, Intercept 3.

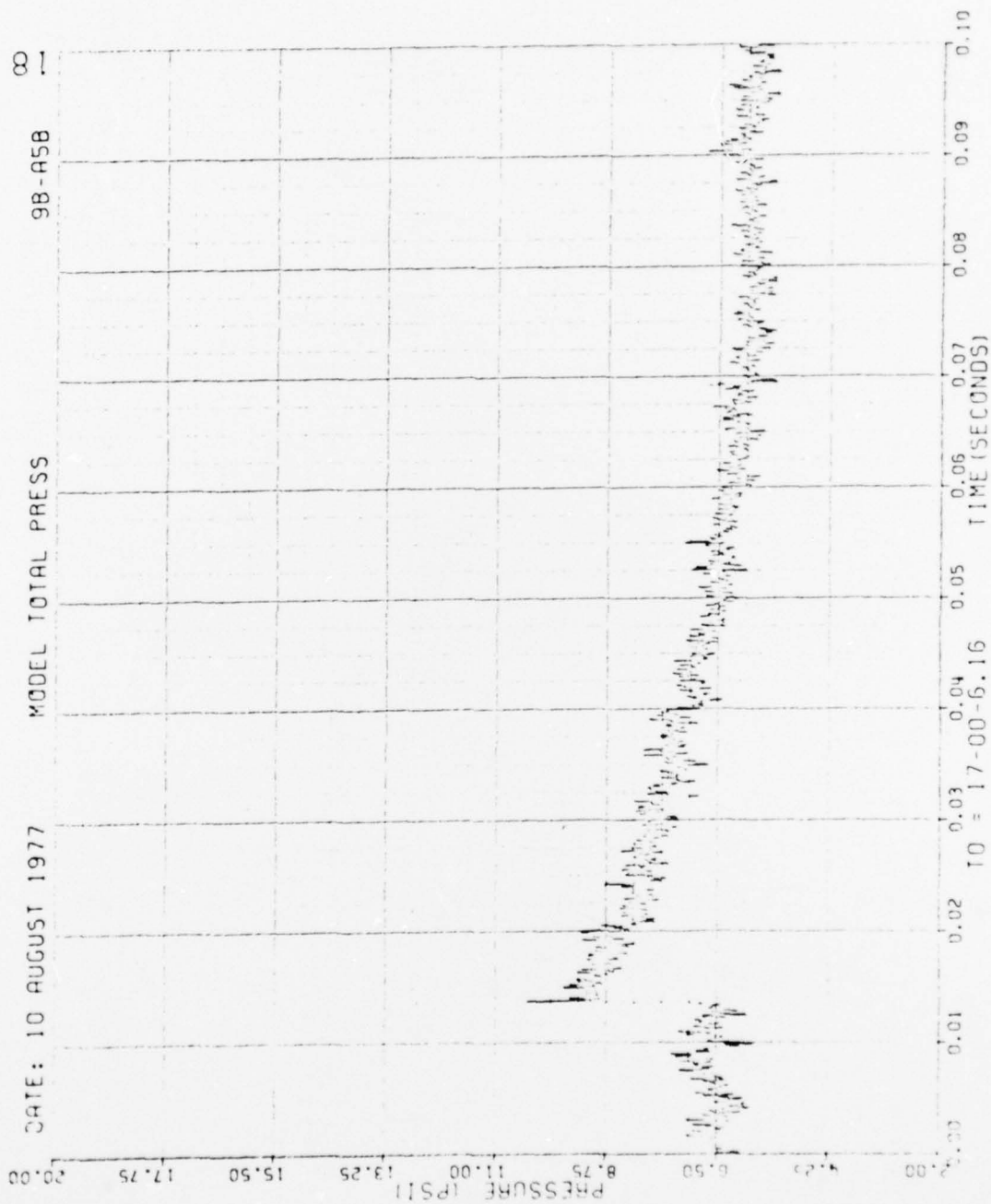


Figure 68. Concluded

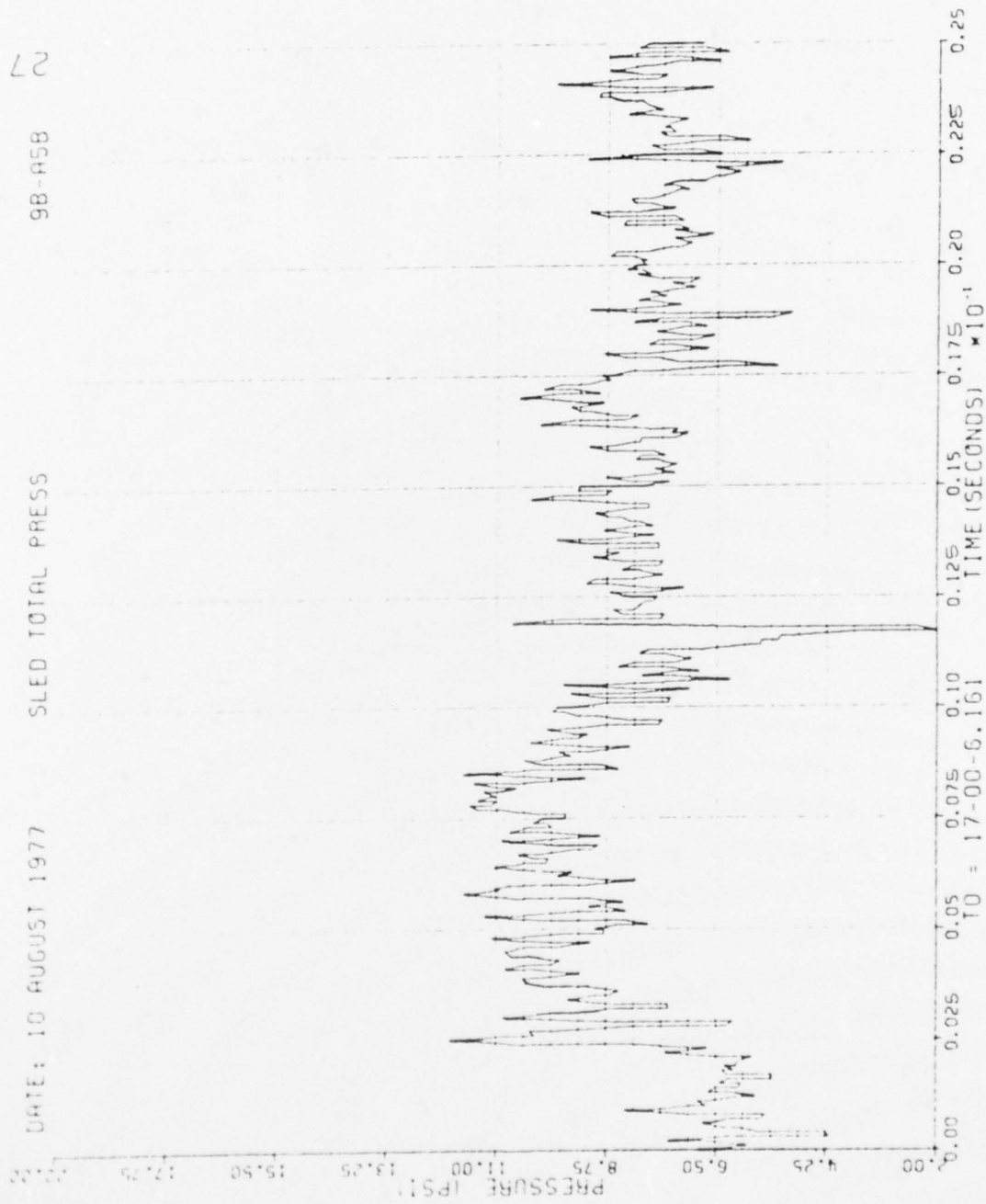


Figure 69. Total Pressure at Sled, Run 98-A5, Intercept 3.

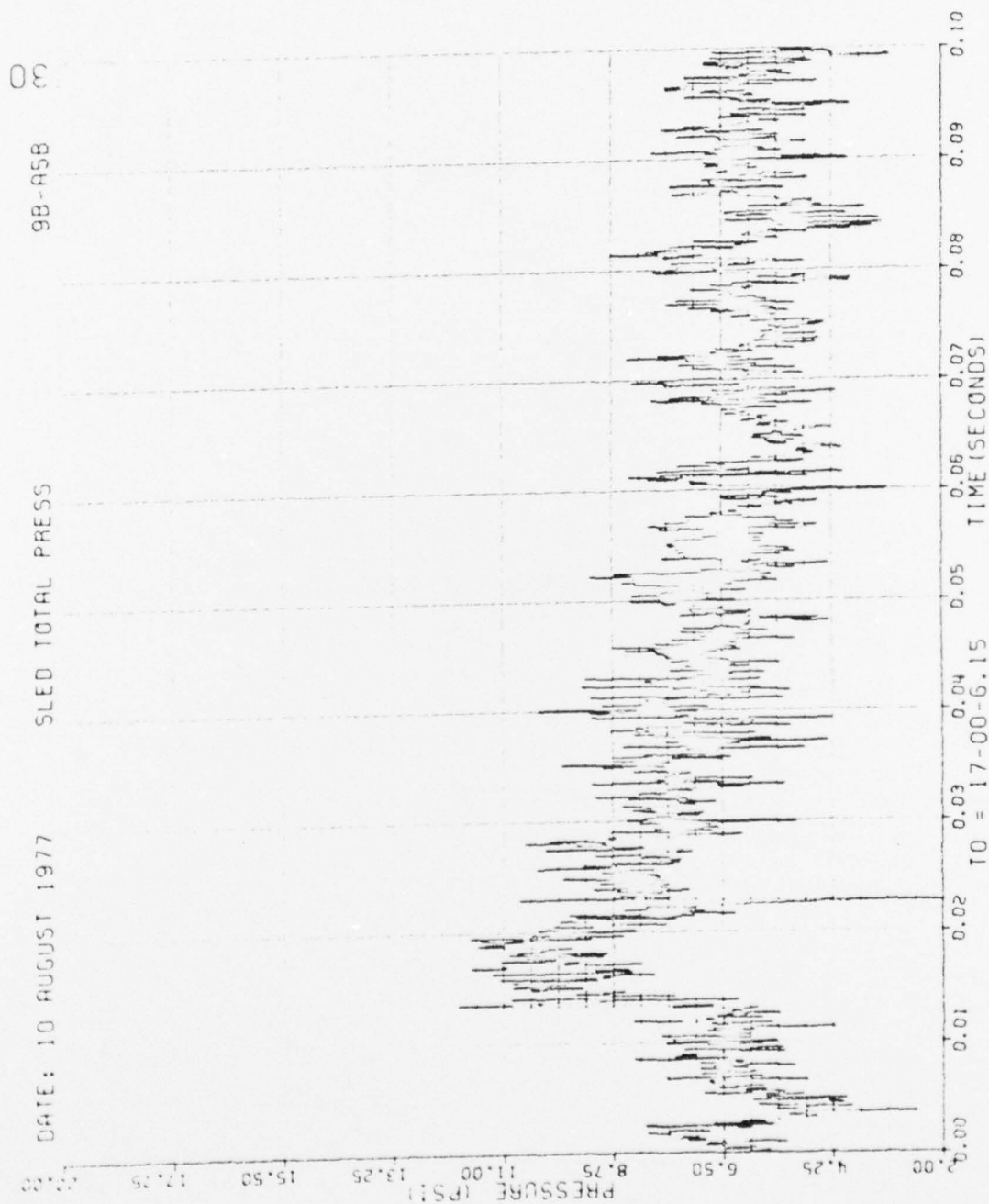


Figure 69. Concluded

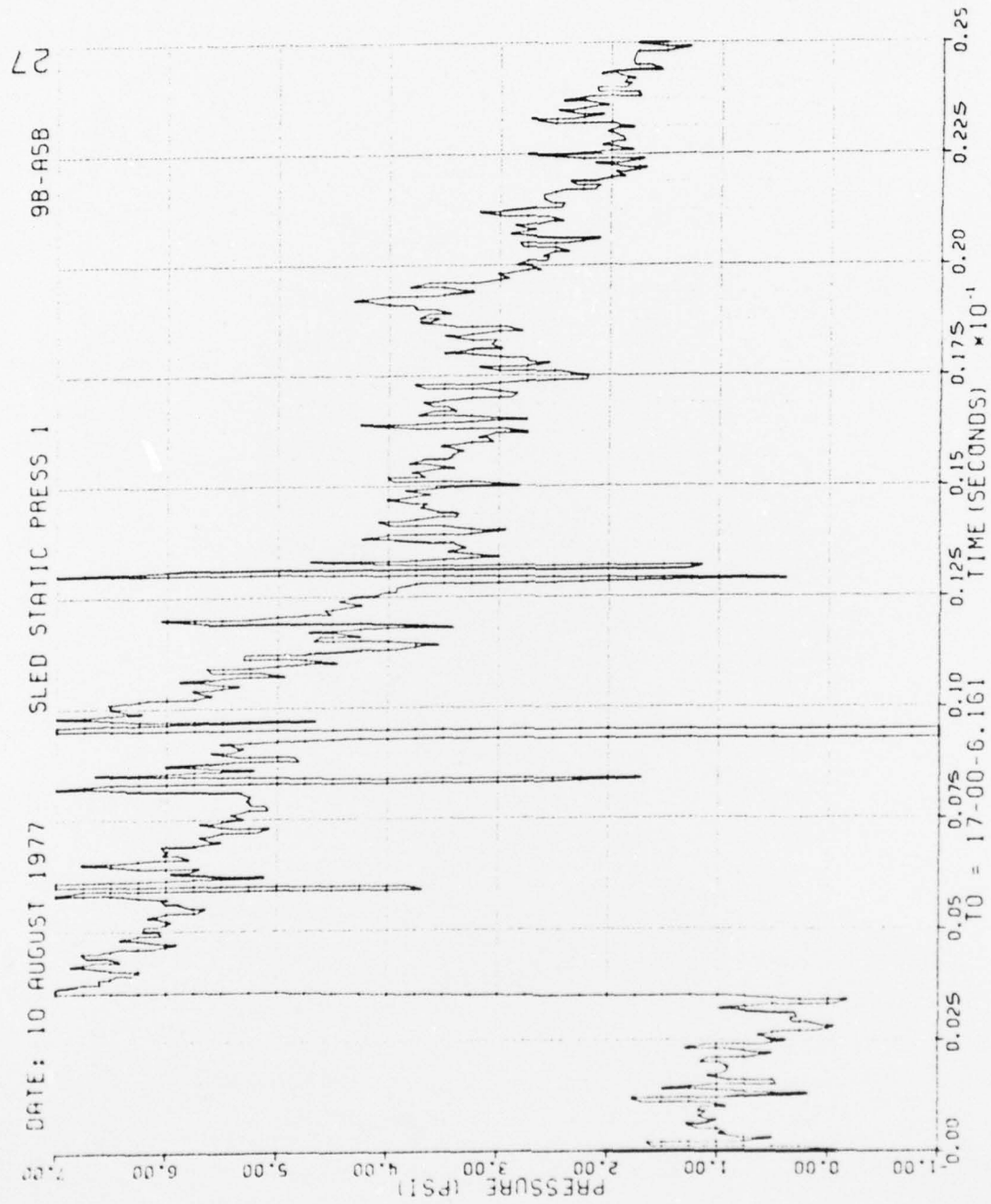


Figure 70. Static Pressure 1 at Sled, Run 9B-A5, Intercept 3.

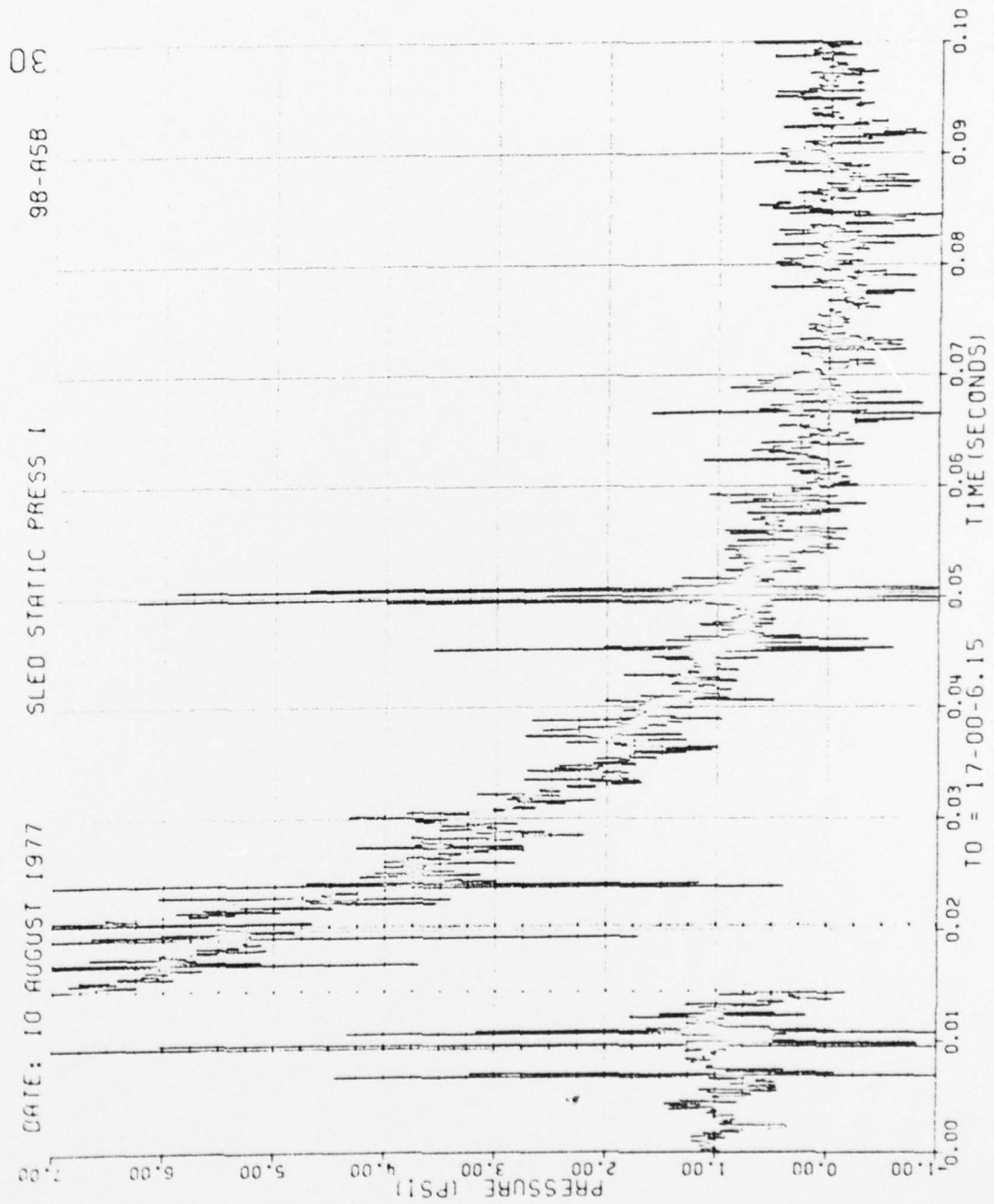


Figure 70. Concluded

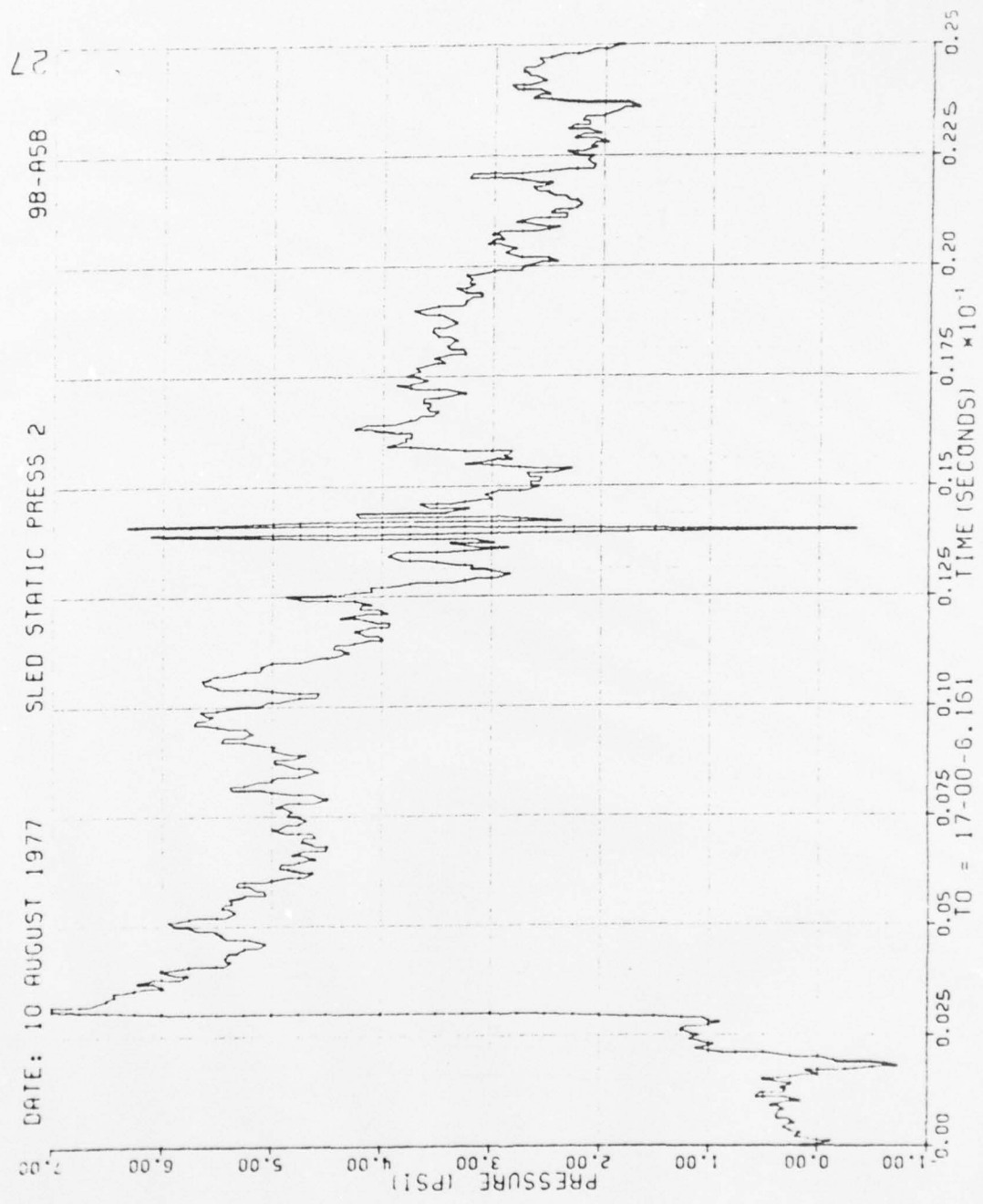


Figure 71. Static Pressure 2 at Sled, Run 9B-A5, Intercept 3.

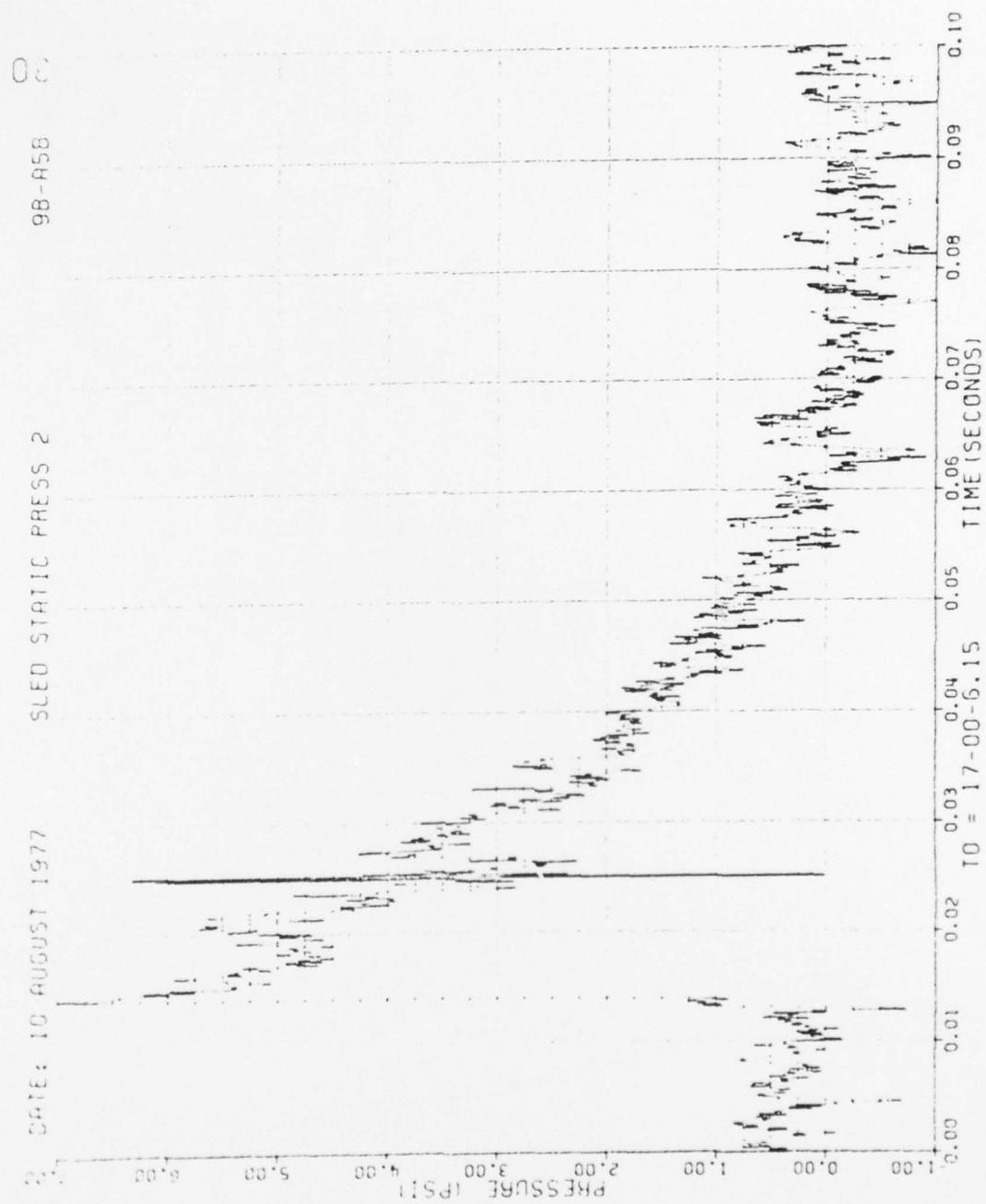


Figure 71. Concluded

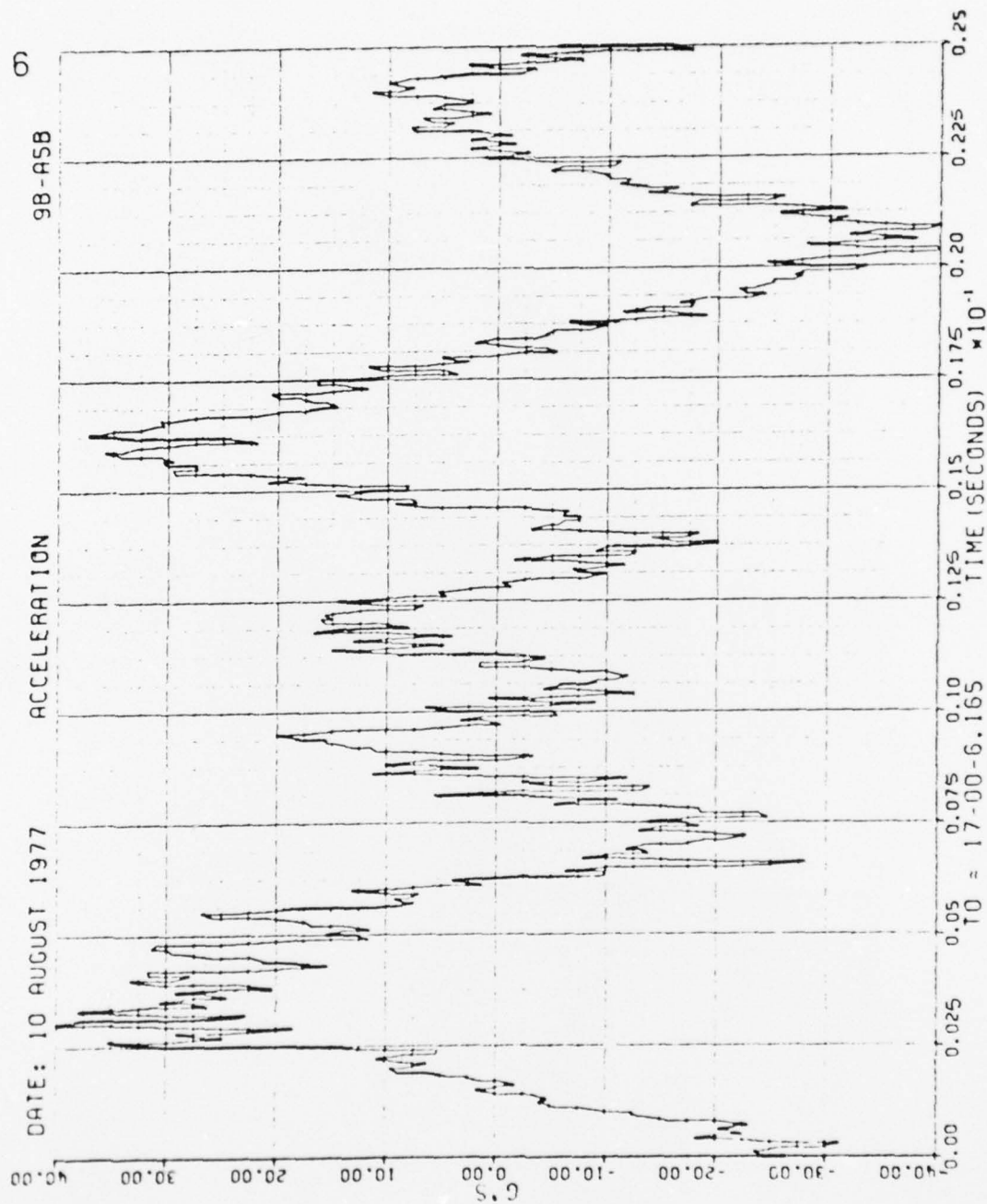


Figure 72. Wing Acceleration, Run 9B-A5, Intercept 3.

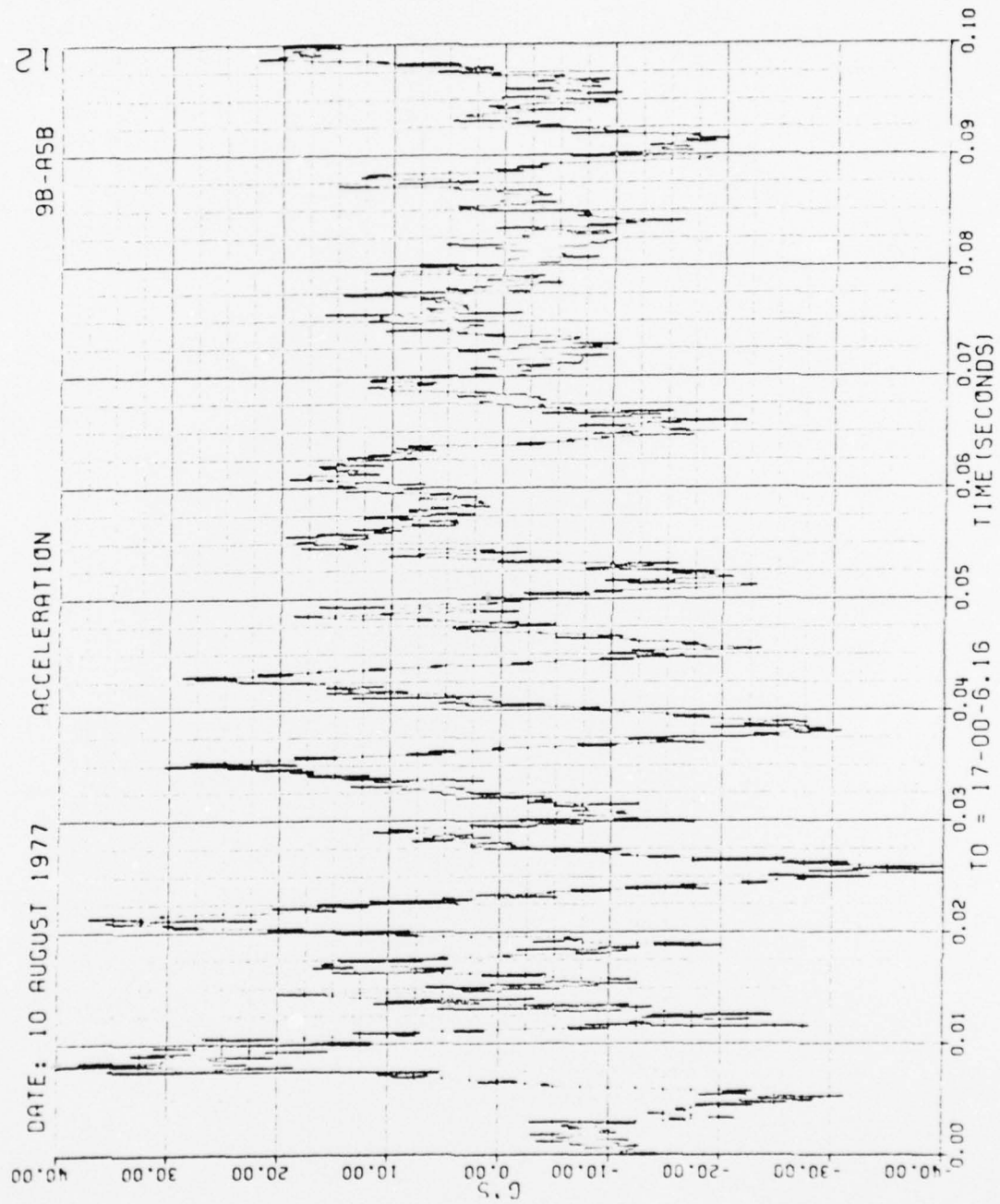


Figure 72. Concluded

DISTRIBUTION LIST

DEPARTMENT OF DEFENSE

Assistant to the Secretary of Defense
Atomic Energy
ATTN: Executive Assistant

Defense Documentation Center
Cameron Station
12 cy ATTN: DD

Defense Nuclear Agency
ATTN: SPAS
ATTN: DDST
ATTN: STSP
4 cy ATTN: TITL

Field Command
Defense Nuclear Agency
ATTN: FCPR

Livermore Division, Field Command, DNA
Department of Defense
Lawrence Livermore Laboratory
ATTN: FCPRL

Commandant
NATO School (SHAPE)
ATTN: U.S. Documents Officer

Under Secretary of Defense for Rsch. & Engrg.
Department of Defense
ATTN: Strategic & Space Systems (OS)

DEPARTMENT OF THE ARMY

Harry Diamond Laboratories
Department of the Army
ATTN: DELHD-NP
ATTN: DELHD-RBH, J. Gwaltney

U.S. Army Ballistic Research Labs
ATTN: DRXBR-BLE, W. Taylor
ATTN: DRXBR-X, J. Meszaros

U.S. Army Materiel Dev. & Readiness Cmd.
ATTN: DRCDE-D, L. Flynn

U.S. Army Nuclear & Chemical Agency
ATTN: Library

DEPARTMENT OF THE NAVY

Naval Material Command
ATTN: MAT O8T-22

Naval Research Laboratory
ATTN: Code 2627

Naval Surface Weapons Center
ATTN: K. Caudle

Naval Weapons Evaluation Facility
ATTN: L. Oliver

Office of Naval Research
ATTN: Code 464

DEPARTMENT OF THE NAVY (Continued)

Strategic Systems Project Office
Department of the Navy
ATTN: NSP-272

DEPARTMENT OF THE AIR FORCE

Aeronautical Systems Division, AFSC
ATTN: ENFT, R. Bachman
4 cy ATTN: ENFTV, D. Ward

Air Force Materials Laboratory
ATTN: MBE, G. Schmitt

Air Force Weapons Laboratory
ATTN: DYV, A. Sharp
ATTN: SUL
ATTN: DYV, G. Campbell

Foreign Technology Division, AFSC
ATTN: PDBF, Mr. Spring

Strategic Air Command/XPFS
Department of the Air Force
ATTN: XPFS, B. Stephan

DEPARTMENT OF ENERGY

Sandia Laboratories
ATTN: Doc. Con. for A. Lieber

DEPARTMENT OF DEFENSE CONTRACTORS

Aerospace Corporation
ATTN: W. Barry

Avco Research & Systems Group
ATTN: J. Patrick
ATTN: P. Grady

The Boeing Company
ATTN: S. Strack
ATTN: R. Dyrdahl
ATTN: E. York

Boeing Wichita Company
ATTN: R. Syring

Calspan Corporation
ATTN: M. Dunn

Effects Technology, Inc.
ATTN: E. Bick
ATTN: R. Wengler
ATTN: R. Parisse

General Dynamics Corporation
Pomona Division
ATTN: R. Shemensky

General Electric Co.-TEMPO
Center for Advanced Studies
ATTN: DASIA

DEPARTMENT OF DEFENSE CONTRACTORS (Continued)

General Research Corporation
Santa Barbara Division
ATTN: T. Stathacopoulos

Kaman AvIDyne
Division of Kaman Sciences Corporation
ATTN: N. Hobbs
ATTN: E. Criscione
ATTN: R. Ruetenik
ATTN: R. Smiley

Kaman Sciences Corporation
ATTN: D. Sachs

McDonnell Douglas Corporation
ATTN: J. McGrew

DEPARTMENT OF DEFENSE CONTRACTORS (Continued)

Prototype Development Associates, Inc.
ATTN: J. McDonald
ATTN: C. Thacker

R&D Associates
ATTN: C. MacDonald
ATTN: F. Field
ATTN: J. Carpenter

Rockwell International Corporation
ATTN: R. Sparling

Science Applications, Inc.
ATTN: D. Hove

SRI International
ATTN: G. Abrahamson

FIELD 2: FLD/GRP(S) 01030
FIELD 3: ENTRY CLASS U
FIELD 4: NTIS PRICES HC MF
FIELD 5: SOURCE NAME KAMAN AVIDYNE BURLINGTON MASS
FIELD 6: UNCLASS. TITLE MEASUREMENTS OF BLAST PRESSURES ON A RIGID 6
MACH 0.76 FROM ROCKET PROPELLED SLED TESTS,

FIELD 7: CLASS. TITLE
FIELD 8: TITLE CLASS. U
FIELD 9: DESCRIPTIVE NOTE FINAL REPT. JAN - DEC 77,
FIELD 10: PERSONAL AUTHORS RUETENIK, J. RAY ; SMILEY, ROBERT F. ;
FIELD 11: REPORT DATE 24 JAN 78

H

FIELD 12: PAGINATION 434P
FIELD 13: SOURCE ACRONYM
FIELD 14: REPORT NUMBER KA-TR-145
FIELD 15: CONTRACT NUMBER DNA001-76-C-0106
FIELD 16: PROJECT NUMBER N99QAXA
FIELD 17: TASK NUMBER E5L0, E501
FIELD 18: MONITOR SOURCE DNA
FIELD 19: MONITOR SERIES 4504F
FIELD 20: REPORT CLASS U
FIELD 21: SUPPLEMENTARY NOTE
FIELD 22: ALPHA LIMITATIONS

FIELD 23: DESCRIPTORS

FIELD 24: DESCRIPTOR CLASS.
FIELD 25: IDENTIFIERS
FIELD 26: IDENTIFIER CLASS.
FIELD 27: ABSTRACT

DISTRIBUTION OF DOCUMENT CONTROLLED BY DEFENSE
20305. THIS DOCUMENT IS NOT AVAILABLE FROM
BY DEFENSE NUCLEAR AGENCY, WASHINGTON, DC 20
AERODYNAMICS, *AIRCRAFT, BLAST LOADS, BLAST
ROCKET SLEDS

U
BLAST EFFECTS(AEROSPACE), HIGH EXPLOSIVE TESTS
U

INTERACTION OF A BLAST WAVE WITH A HIGHLY
SERIES OF TWO SLED TESTS PERFORMED ON THE 50
BASE IN JUNE AND AUGUST OF 1977. THESE TWO
PROGRAM OF THREE TESTS CARRIED OUT DURING THE
MACH 0.76, WAS INTERCEPTED SUCCESSIVELY BY THE
DETONATION OF THREE CHARGES OF TNT. THE MODEL
FUSELAGE COMBINATION. WING PROPERTIES WERE:
ASPECT RATIO, 0.29 TAPER RATIO, 67 DEG. LEAN
SWEEPBACK, AND A 64A012 WING SECTION. BLAST
LOCATIONS ON THE WING FOR BLAST INTERCEPT OF
INTERCEPT ANGLES OF ABOUT 50, 90 AND 135 DEG.
INTERCEPTS FROM BURSTS 45 DEGREES OUT OF THE
BY MOUNTING THE MODEL AT A ROLL ANGLE OF 45
CHARGE WAS EMPLOYED FOR ONE BURST FOR STUDY
DESCRIBES THE TESTS AND PRESENTS THE REDUCED

U

0

a

1 21

F

194970

7

FIELD 28: ABSTRACT CLASS.
FIELD 29: INITIAL INVENTORY
FIELD 30: ANNOTATION
FIELD 31: SPECIAL INDICATOR
FIELD 32: REGRADING CATEGORY
FIELD 33: LIMITATION CODES
FIELD 34: SOURCE SERIAL
FIELD 35: SOURCE CODE
FIELD 36: DOCUMENT LOCATION
FIELD 37: CLASSIFIED BY
FIELD 38: DECLASSIFIED ON
FIELD 39: DOWNGRADED TO CONF.
FIELD 40: GEOPOLITICAL CODE
FIELD 41: SOURCE TYPE CODE
FIELD 42: TAB ISSUE NUMBER

2507

4

00--00

030

HC MF
MAN AVIDYNE BURLINGTON MASS
MEASUREMENTS OF BLAST PRESSURES ON A RIGID 65 DEGREE SWEEPBACK WING AT
CH 0.76 FROM ROCKET PROPELLED SLED TESTS, PHASE 2 TEST DOCUMENTATION

NAL REPT. JAN - DEC 77,
ETENIK, J. RAY ; SMILEY, ROBERT F. ;
JAN 78

434P

-TR-145
A001-76-C-0106
9QAXA
L0, E501
A
04F

DISTRIBUTION OF DOCUMENT CONTROLLED BY DEFENSE NUCLEAR AGENCY, WASHINGTON, DC
20305. THIS DOCUMENT IS NOT AVAILABLE FROM DDC. CATALOGING INFORMATION SUPPLIED
DEFENSE NUCLEAR AGENCY, WASHINGTON, DC 20305.
AERODYNAMICS, *AIRCRAFT, BLAST LOADS, BLAST WAVES, PRESSURE MEASUREMENT,
ROCKET SLEDS

BLAST EFFECTS (AEROSPACE), HIGH EXPLOSIVE TESTS, WU01, WU14

INTERACTION OF A BLAST WAVE WITH A HIGHLY SWEEPBACK WING MODEL WAS MEASURED IN A
SERIES OF TWO SLED TESTS PERFORMED ON THE 50,788-FOOT TRACT AT HOLLOMAN AIR FORCE
BASE IN JUNE AND AUGUST OF 1977. THESE TWO TESTS WERE A CONTINUATION OF THE
PROGRAM OF THREE TESTS CARRIED OUT DURING THE SUMMER OF 1976. THE SLED, TRAVELING AT
CH 0.76, WAS INTERCEPTED SUCCESSIVELY BY BLAST WAVES PRODUCED FROM THE SEQUENTIAL
IGNITION OF THREE CHARGES OF TNT. THE MODEL CONSISTED OF A STING-MOUNTED WING AND
RELAGE COMBINATION. WING PROPERTIES WERE: 46.80-IN. SPAN, 18.95-IN. MEAN CHORD, 2.47
PECT RATIO, 0.29 TAPER RATIO, 67 DEG. LEADING EDGE SWEEPBACK, 64.8 DEG. QUARTER-CHORD
SWEEPBACK, AND A 64A012 WING SECTION. BLAST INDUCED LOADINGS WERE MEASURED AT 20
LOCATIONS ON THE WING FOR BLAST INTERCEPT OVERPRESSURES OF ABOUT 4 PSI FOR BLAST
INTERCEPT ANGLES OF ABOUT 50, 90 AND 135 DEGREES FROM HEAD-ON. IN THE FIRST TEST BLAST
INTERCEPTS FROM BURSTS 45 DEGREES OUT OF THE PLANE OF AIRPLANE SYMMETRY WERE SIMULATED
BY MOUNTING THE MODEL AT A ROLL ANGLE OF 45 DEGREES. IN THE SECOND TEST A 10,000 POUND
BURGE WAS EMPLOYED FOR ONE BURST FOR STUDYING THE EFFECT OF BLAST YIELD. THIS REPORT
DESCRIBES THE TESTS AND PRESENTS THE REDUCED TEST DATA.

0

21

970

7

000

20

